UAM Universidad Autónoma de Madrid

FACULTAD DE CIENCIAS
UNIVERSIDAD AUTÓNOMA DE MADRID

UNIVERSIDAD AUTÓNOMA DE MADRID

Synthesis, characterization and application of anion exchange membranes in fuel cells and electrolysers

Tesis Doctoral

Daniel Herranz González

Dirigida por

Pilar Ocón Esteban

A las personas que quiero,
por hacer que la vida sea tan maravillosa

Acknowledgement - Agradecimientos

Por fin acabo de sentarme a plantearme seriamente el escribir la Tesis Doctoral (parece adecuado que lleve mayúsculas, aunque sólo sea por lo que veo que me va a costar) y me ha parecido buena idea empezar por los agradecimientos. Gracias a todos los que han compartido mi tiempo y me han apoyado durante estos años (y espero que sigan haciendo mientras esto se escribe o me va a dar algo jaja), especialmente a Liber, mis padres, mi hermano, mi familia, mis compañeros de laboratorio, mis amigos y mi directora Pilar. Es maravilloso compartir la vida con gente tan espléndida y que te llena tanto, así se hace con ilusión cualquier cosa que se ponga por delante.

En las fases finales de escribir hay que volver a esta sección tan importante, pues todo hubiera sido muy distinto si la gente que me ha acompañado a lo largo de estos años no hubiera sido tan fantástica. Como digo, han sido varios años de trabajo, así que lo primero pedir disculpas si me dejo a alguien en el tintero, sabéis que os aprecio igualmente aunque ahora con tanto lío no ponga el nombre por aquí.

Quiero agradecer a Pilar, mi directora de la Tesis, por su apoyo y sus enseñanzas a lo largo de todo el proceso y especialmente por su sinceridad, porque siempre me he entendido muy bien con las personas sinceras. También quiero agradecer enormemente su aprecio al resto de personas que han compartido su tiempo conmigo en el laboratorio, pues han hecho que fuese un gusto ir a trabajar todos los días y eso es algo que no tiene precio. Por un lado, a la gente que estaba en el laboratorio cuando llegué y estuve haciendo el trabajo de fin de máster: Mikel, Manu, Alberto, Sandra, Pedro, Alicia y muy especialmente a Ricardo, con quien más tiempo he compartido a lo largo de estos años, tan bien lo he pasado y tanto me ha ayudado. Ellos fueron una razón importante de que decidiera empezar la Tesis Doctoral. Como no, agradecer también su cariño a los compañeros de laboratorio que están estos días conmigo y con quien tan buenos ratos paso: Kerly, Laura, Carlos, Guille, Victor, Lorenzo, Oxel y los que han ido pasando por nuestro amigable lugar de trabajo: Mateu, Javi, Dani, Simón, María, Ming, Joaquín, Luigi y seguro que me estoy dejando a alguien, que ya van varios nombres y lo mío no es la memoria.

During my stay in the University of Surrey I also met wonderful people that made me so comfortable in their group that the experience couldn't be better. I want to thank first John Varcoe for accepting me in his group during those 3 months and being so kind. I also want to thank the nice girls of the group: Ana Laura, Julia, Lian and Rachida. They made me feel part of the group as soon as I was there and I will never forget the good times together in the lab and out in Guildford. Special mention to the hen party of Lian! From the people I met out of the university, I want to thank Yasser for the nice times in the sport park together.

Dentro de la Universidad Autónoma ha habido también mucha gente con quien he compartido mi tiempo y quiero mencionar: Carlos Palacio, la gente del módulo 4 (Fabrice, Andrés y Edu), gente del ICP (Sergio Rojas y Jorge), Jorge Sánchez, Alfonso, Sonia, Ángela, Desi y Enrique Fatás, quien siempre tiene algún buen consejo o nos hace reír cuando pasa por el laboratorio.

También quiero agradecer el tiempo que he pasado con ellas a las personas de la juve, ya que ha sido una novedad el empezar a participar en algo así y a las personas de la Asamblea de Dignidad Investigadora de la UAM. Han sido otra faceta de la investigación, centrada en el esfuerzo por mejorar las condiciones de las investigadoras y de las personas en general.

Fuera de la universidad hay muchas amigas y amigos a quienes quiero agradecer su amistad y apoyo, aunque les haya podido ver más o menos, pero son muy importantes para mí. Sus ánimos y los buenos ratos juntos han sido de gran ayuda para seguir adelante.

Also my thanks to the friends out of the university, that have shared with me so good times and are so important to me.

A mi hermano, Lore y al resto de mi familia quiero agradecerles también su apoyo y sus ánimos. Esperemos que después de estos meses pueda sacar algo más de tiempo libre (esto de escribir se lleva mucho).

A Liber le quiero agradecer ser tan maravillosa y su apoyo incondicional, sin el cual esto no hubiera sido posible. Gracias a ella soy tan feliz. Además, es la que más me aguanta.

A mis padres decirles que no pueden hacerse idea de lo importantes que son para mí y lo agradecido que les estoy. Quiero acordarme por último de mis abuelas y abuelos, a quienes sé que les haría mucha ilusión verme avanzar en la vida.

Dani

Index

ABSTRACT

Abstract

This Doctoral Thesis has been developed around the need of high performance and stable materials to be used as anion exchange materials in alkaline media for electrochemical devices like low temperature alkaline fuel cells and zero gap liquid alkaline water electrolysers. This is a relevant topic for these technologies, which can allow to reduce the costs of the devices and improve their performance and thus help to extend their use. Both devices are related with the use of H_2 (and in the case of the fuel cells other renewable fuels like bio-ethanol) and so will be highly helpful in the sustainable energy system needed for the future.

With this main objective in mind, different strategies and polymeric materials have been used. Polybenzimidazole polymers (PBI and ABPBI) have been selected as the core materials for most of the anion exchange membranes synthesised in this Thesis due to their high mechanical, thermal and chemical stability, which are mayor requirements to obtain durable anion exchange electrolytes.

To enhance the ionic conductivity of the membrane and as a first strategy, polybenzimidazoles have been blended with poly (vinylalcohol) (PVA), a polymer that presents very good conductivity of the OH^- ions but has important structural problems when membranes are only prepared with it. The idea was to combine the best features of each polymer in a blend membrane to improve the final performance. The synthesis of the membranes was performed by mixing the solutions of both polymers and the membrane was obtained after the casting process (evaporation of the solvents under controlled conditions). Homogeneous and flexible membranes were obtained and then fully characterized. The presence of the polymers in the membrane was confirmed by IR and Raman spectroscopy as well as by NMR spectroscopy. The last also gave insights of the hydrogen bonds stablished between the polymers. This interaction between the polymers explains the good visual homogeneity of the membranes even without covalent bonds between them. The membranes were doped with KOH solution and the ionic conductivity was measured, obtaining

high values, between 20 and 100 mS cm^{-1}. All the membranes with PVA reached higher conductivities than the measured pristine PBI membrane, which was one of the objectives. It was observed that the alkali solution removed part of the superficial PVA; so, in order to enhance the retention of the polymer, crosslinking of the PVA with glutaraldehyde (GA) was performed in some membranes. This yielded not only better PVA retention but also KOH, which helped to retain the high conductivity properties. The thermal and mechanical stabilities of the membranes were demonstrated by the corresponding analysis, being especially the thermal one far beyond the required needs for the applications (the temperatures used in this fuel cells or electrolysers are below 100 ºC). Elevated and adequate KOH and water uptakes were found in the membranes, as well as the swelling increase after doping. The membranes based in different polymers (PBI or ABPBI) showed different behaviour due to the higher hydrophilicity of ABPBI. The doping of the membranes was confirmed also by XPS, which was very useful to follow the process with increasing time and confirmed the stability of the nitrogens of the polybenzimidazole molecules during the process. Finally the membranes were tested in the final devices. In the alkaline direct ethanol fuel cell, using PBI-based electrolytes the membranes of L- PVA:PBI 4:1 ratio presented the best performance, reaching 76 mW cm^{-2} maximum power density, 43 % better than the commercial tested PBI membrane. This good result was improved with the ABPBI-based membranes, since the L-PVA:ABPBI of 2:1 ratio obtained 124 mW cm^{-2}. The crosslinked membranes with PVA:ABPBI 2:1 were also tested and the best results were obtained with the membranes crosslinked with 0.25 vol.% GA crosslinking solution, that yielded 93 mW cm^{-2} maximum power density, below the linear membrane but probably much more stable in the long-term. The electrolyser results showed that the membranes with best performance were with 4:1 ratio both for PBI and ABPBI-based ones, obtaining around 150 mA cm^{-2} at 1.95 V and 50 ºC with 15 wt.% KOH, slightly better than the commercial normally used Zirfon® porous diaphragm. When the temperature was raised to 70 ºC the conductivity was improved and a very high current density of 360 mA cm^{-2} at 1.9 V was achieved, which would reach 900 mA cm^{-2} at 2 V.

Other type of membranes were prepared by crosslinking of the polybenzimidazole molecules with poly (vinylbenzyl chloride) (PVBC). The reaction was done between the CH_2-Cl groups of PVBC and the nitrogens in the imidazole rings of the polybenzimidazoles. When the crosslinking degree was optimal the membranes were obtained using the casting method, similar to the previous ones. After the crosslinking the membranes presented abundancy of unreacted CH_2-Cl groups that were used to react with a tertiary amine, DABCO, doing the quaternization step. This amine was selected due to the reported very

good stability in alkaline media. The reaction formed the quaternary ammonium (QA) groups that help to conduct the OH^- ions through the membrane. Since the quaternization was done with the already casted membrane, only one nitrogen of DABCO reacted (confirmed by solid NMR spectroscopy), as desired, due to the reported improved alkali stability of this conformation. The presence of both polymers in the membranes was corroborated by IR spectroscopy and the effectiveness of the crosslinking was probed by gel fraction measurements, which showed that the ABPBI-based membranes had a higher crosslinking degree than the PBI-c-PVBC 1:2 and 1:3 (in this order). The surface and cross-section analysis by SEM/EDX showed the homogeneous microstructure of the membranes and the equal distribution of the quaternary ammonium groups. The mechanical properties of the membranes were also tested as well as the thermal stability, which was superior to the temperatures of use and allowed to observe the degradation of the single and double crosslinking points that are formed. Similarly to the blend membranes with PVA, the water and KOH uptake and the swelling behaviour presented different values depending on the use of PBI or ABPBI, being in this case also very important the degree of crosslinking and the presence of the QA groups. The amount of quaternary ammonium groups was evaluated by the ion exchange capacity (IEC) measurements, showing the higher presence of them in the PBI-c-PVBC 1:3 membrane. The OH^- conductivity of the membranes with temperature showed values between 20 and 60 mS cm^{-1}, very adequate for the use in the fuel cells and electrolysers. The degradation of these membranes was investigated in alkaline and oxidative media by various techniques, concluding their good durability under both conditions. Finally the performance in the alkaline direct ethanol fuel cell and the electrolyser were tested. In the fuel cell the best result was obtained with the PBI-c-PVBC 1:2 membrane (66 mW cm^{-2} peak power density), higher than pristine PBI (53 mw cm^{-2}) but lower than the previous membranes with PVA. However better durability of these membranes could be expected due to their enhanced structure. The electrolyser results were very promising since similar performance than the previous membranes or commercial units was achieved (around 450 mA cm^{-2} current density at 2 V) but using milder conditions, which is highly beneficial for the durability of the system.

Finally, in order to study different quaternary ammonium head groups with good alkaline stability, membranes and ionomers based in ethylene tetrafluoroethylene (ETFE) were synthesised, characterized and evaluated in alkaline fuel cell with H_2 vs O_2. The tertiary amine selected for these study was N-methylpiperidine (MPRD), due to the previous reports of membranes with good performances. In the synthesis of the membranes the quaternization step was optimised so only 15 % of amine in the solution at 60 ºC was needed and these conditions were

applied for the synthesis of the ionomers. The analysis done with Raman spectroscopy probed the adequate and homogeneous grafting of vynilbenzyl chloride (VBC) into the precursor ETFE film and the amination with MPRD. To analyse the size and distribution of the ionomer powders, both alone and when dispersed with the catalyst in the electrodes, SEM/EDX measurements were performed. Aggregation of the particles was observed after the amination, even though they passed a vibromilling step. The components of the electrodes (carbon fibres, catalyst and ionomer particles) were clearly identified and the higher loading of the electrodes with 30 % of ionomer was observed. The IEC, water uptake and ionic conductivity of the membranes were also evaluated and compared with membranes aminated with TMA and MPY. It was found that membranes with TMA and MPY (in this order) presented higher IEC than membranes aminated with MPRD and thus the ionic conductivity followed the same order. However, the order of water uptake was the opposite, with the MPRD membrane showing the highest. This was explained by the higher hydrophilicity of the QA group formed with MPRD, which demonstrated to play an important role in the fuel cell performance at high current. For the fuel cell performance, first different loadings of ionomer (20 and 30 %) were tried, obtaining similar values (which was not the case for TMA and MPY ionomers). Then symmetrical combinations of ionomer / membrane / ionomer (same ionomer in both electrodes) were tested in the fuel cell. From the obtained results it was clear that more research is needed to understand better the effect of the ionomers at high current densities and that different ionomers clearly influence the final performance. The high hydrophilicity of MPRD probably allowed an improved water management, that prevented flooding at these current densities and therefore higher maximum power densities could be reached. The best result was obtained with the combination of TMA ionomers in the electrodes and MPRD membrane, yielding 1424 mW cm^{-2} maximum power density at 60 ºC.

RESUMEN

Resumen

Esta Tesis Doctoral se ha realizado en base a la necesidad de materiales con buenas prestaciones y estabilidad para ser usados como intercambiadores aniónicos en dispositivos electroquímicos como celdas de combustible o electrolizadores de medio alcalino. El desarrollo de estos materiales es importante para estas tecnologías ya que puede reducir el coste de estos dispositivos a la vez que se mejoran las prestaciones, permitiendo que se extienda su uso. Tanto las celdas de combustible como los electrolizadores están relacionados con el uso del hidrógeno (H_2) y además en el caso de las primeras también con otros combustibles renovables como el bio-etanol, por tanto serían muy útiles en el sistema de energía sostenible que necesitamos para el futuro. Teniendo en mente este objetivo, se ha investigado en distintas estrategias de síntesis y materiales poliméricos. Los polímeros basados en polibencimidazol (en concreto PBI y ABPBI) han sido seleccionados como los materiales principales para el desarrollo de la mayoría de las membranas, debido a su alta estabilidad mecánica, térmica y química, propiedades esenciales para conseguir membranas intercambiadoras de iones resistentes.

Como primera estrategia para mejorar la conductividad iónica de las membranas, los polímeros de polibencimidazol fueron combinados con polivinilalcohol (PVA), un polímero que presenta alta conductividad de iones OH^- pero tiene importantes problemas estructurales cuando es utilizado en solitario para preparar membranas. La idea es combinar las mejores características de ambos materiales en una membrana combinada para tener mejores prestaciones. La síntesis de las membranas se llevó a cabo mezclando las disoluciones de ambos polímeros y a continuación efectuando un proceso de casting (evaporación de los disolventes en condiciones controladas). Las membranas obtenidas, homogéneas y flexibles, fueron a continuación caracterizadas. La presencia de ambos polímeros en la membrana fue confirmada por espectroscopía IR y Raman y también a través de espectroscopía NMR. Esta última permitió también detectar los enlaces por puente de hidrógeno establecidos entre ambos polímeros. Esta interacción explica la homogeneidad de las membranas a pesar de no haber enlaces covalentes. Las membranas fueron dopadas con disolución de KOH y se

midió su conductividad iónica, obteniéndose valores en el rango de 20 a 100 mS cm^{-1}. Todas las membranas con PVA obtuvieron mejores valores de conductividad que la de PBI puro, alcanzándose uno de los objetivos planteados. Se observó que la disolución alcalina retiraba parte del PVA superficial, así que para no tener estas pérdidas se entrecruzó el PVA usando glutaraldehido (GA) en algunas de las membranas. Esto permitió no solo retener mejor el PVA sino también el KOH dentro de la estructura y por tanto las buenas propiedades conductoras. La estabilidad térmica y mecánica de las membranas fue demostrada con los ensayos correspondientes, siendo especialmente buena la térmica ya que las membranas soportan temperaturas bastante superiores a los 100 ºC (temperatura por debajo de la cual son utilizadas en la pila de combustible o electrolizador). Se han determinado valores elevados y adecuados de absorción de KOH y de agua, junto con el hinchamiento asociado a estos procesos durante el dopaje. Las membranas basadas en distintos polímeros (PBI o ABPBI) mostraron un comportamiento diferente debido a la mayor hidrofilicidad del ABPBI. El proceso de dopado de las membranas fue confirmado también por XPS, que además fue muy útil para seguir el proceso al aumentar el tiempo de dopado y confirmo la estabilidad de los nitrógenos del polibencimidazol a lo largo del mismo. Finalmente, las membranas fueron evaluadas en los dispositivos electroquímicos. En la celda de combustible alcalina de etanol directo, con las membranas basadas en PBI el mejor resultado se obtuvo con la membrana L-PVA:PBI 4:1, que alcanzó una densidad de potencia de 76 mW cm^{-2}, un 43 % mejor que la membrana de PBI comercial. Este buen resultado fue superado con las membranas basadas en ABPBI, en concreto la membrana L-PVA:ABPBI 2:1 alcanzó 124 mW cm^{-2}. Las membranas entrecruzadas de PVA:ABPBI fueron también probadas, obteniéndose los mejores resultados con las membranas entrecruzadas con disolución de GA de 0.25 vol. %. Éstas alcanzaron valores de densidad de potencia de 93 mW cm^{-2}, por debajo de las membranas lineales, pero probablemente mucho más estables a largo plazo. En las medidas en electrolizador, los resultados mostraron que las membranas con mejores prestaciones fueron las de ratio 4:1 basadas tanto en PBI como en ABPBI, obteniendo valores en torno a 150 mA cm^{-2} a 1.95 V y 50 ºC con KOH 15 wt.%, ligeramente mejores que el diafragma poroso comercial de Zirfon® que se usa normalmente. Cuando la temperatura fue elevada a 70 ºC la conductividad mejoró y se obtuvieron densidades de corriente aún más altas, en torno a 360 mA cm^{-2} a 1.9 V que alcanzarían 900 mA cm^{-2} a 2 V.

Se preparó también otro tipo de membranas a través del entrecruzamiento de las cadenas de polibencimidazol con el polímero cloruro de polivinilbencilo (PVBC). La reacción se llevó a cabo entre los grupos CH_2-Cl del PVBC y los nitrógenos en los anillos imidazol de los polibencimidazoles. Cuando se alcanzó un grado de

entrecruzamiento adecuado las membranas fueron obtenidas a través del método de casting mencionado anteriormente. Después del entrecruzamiento las membranas tienen muchos grupos CH_2-Cl que no han reaccionado, los cuales son usados para reaccionar con una amina terciaria, el DABCO, dándose el proceso de cuaternización. Esta amina fue seleccionada debido a su alta estabilidad en medio alcalino. La reacción de cuaternización formó los grupos de amonio cuaternario (QA) que ayudan a la conducción de los iones OH^- a través de la membrana. Como el paso de la cuaternización se hizo una vez la membrana ya estaba formada tras el casting, sólo uno de los dos nitrógenos del DABCO reaccionó (como se confirmó por NMR). Este era el objetivo deseado ya que en esta conformación la estabilidad alcalina es superior. La presencia de ambos polímeros en la membrana fue confirmada por espectroscopía IR y la efectividad del entrecruzamiento se estudió por medidas de fracción de gel, las cuales mostraron un mayor grado de entrecruzamiento en las membranas de ABPBI-c-PVBC 1:2 que en las de PBI-c-PVBC 1:2 y 1:3 (en este orden). La superficie y la sección transversal de las membranas fue estudiada con SEM/EDX, observándose una alta homogeneidad en su microestructura y una distribución igualitaria de los grupos de amonio cuaternario. Las propiedades mecánicas fueron evaluadas, así como la estabilidad térmica; en la última se vio la más que suficiente resistencia de las membranas a la temperatura y se pudo observar la degradación de los puntos simples y dobles de entrecruzamiento. Al igual que en las membranas con PVA, los valores de absorción de agua y KOH, así como los cambios dimensionales fueron distintos dependiendo del uso de PBI o ABPBI, siendo además en este caso también importante el grado de entrecruzamiento y la presencia de los grupos de amonio cuaternario. La cantidad de grupos de amonio cuaternario fue determinada a través de la medida de capacidad de intercambio iónico (IEC), encontrando mayor abundancia en las membranas de PBI-c-PVBC 1:3. La conductividad iónica de estas membranas a distintas temperaturas dio valores entre 20 y 60 mS cm^{-1}, adecuados para su uso en los dispositivos finales. Se investigó la degradación de las membranas en medio alcalino y oxidativo con varias técnicas, concluyéndose que presentan buena durabilidad en ambas condiciones. Finalmente, las membranas fueron probadas en la celda de combustible alcalina de etanol directo y en el electrolizador. En la celda de combustible el mejor resultado se obtuvo con la membrana de PBI-c-PVBC 1:2 (66 mW cm^{-2} máxima densidad de potencia), mejor que el PBI puro (53 mW cm^{-2}) aunque inferior que las anteriores membranas con PVA. Aun así, es de esperar mejor durabilidad debido a su estructura entrecruzada. Los resultados en el electrolizador han sido muy prometedores, ya que se obtuvieron prestaciones similares a las membranas anteriores o unidades comerciales, pero en unas condiciones de medida más suaves, las cuales son altamente beneficiosas para la durabilidad del sistema.

Por último, para estudiar otros grupos de amonio cuaternario con buena estabilidad alcalina, se prepararon membranas e ionómeros basados en etileno tetrafluoroetileno (ETFE), los cuales fueron sintetizados, caracterizados y evaluados en celda de combustible alcalina usando H_2 y O_2. La amina terciaria seleccionada para este estudio fue la N-metilpirrolidona (MPRD), debido a estudios anteriores que obtenían buenos resultados. En la síntesis de las membranas se optimizó el proceso de cuaternización de forma que sólo hacía falta un 15 vol.% de amina en la disolución y 60 ºC. Estas mismas condiciones fueron usadas para la síntesis de los ionómeros. El análisis realizado por Raman probó el grado adecuado y la homogeneidad del injerto del cloruro de vinilbencilo (VBC) en la película precursora de ETFE, además de la correcta aminación con MPRD. Para analizar el tamaño y distribución de los polvos de ionómero, tanto solos como dispersos junto con el catalizador en el electrodo, se realizaron medidas de SEM/EDX. Se observó que las partículas estaban agregadas después del proceso de cuaternización, a pesar de haber sido tratadas con un proceso de molienda. Los componentes de los electrodos (fibras de carbón, catalizador y partículas de ionómero) fueron claramente identificados y se distinguió la mayor carga de ionómero en los electrodos que tenían un 30 % de éste. El IEC, la absorción de agua y la conductividad iónica de las membranas fueron medidas y comparadas con membranas aminadas con TMA y MPY. Se observó que las membranas con TMA y MPY (en este orden) presentaban mayores valores de IEC que aquellas aminadas con MPRD y por tanto los valores de conductividad seguían la misma tendencia. Sin embargo, los valores de absorción de agua presentaban el orden inverso, siendo la membrana de MPRD la que tenía el mayor. Esto se explica por la mayor hidrofilicidad del grupo de amonio cuaternario formado con el MPRD, lo cual demostró jugar un papel importante en los resultados de celda de combustible al llegar a altas densidades de corriente. En las medidas en celda de combustible, primero se probaron distintas cargas de ionómero en los electrodos (20 y 30 %), obteniéndose valores similares en ambos casos. Este no fue el caso para los ionómeros con TMA y MPY. Después, combinaciones simétricas de ionómero /membrana / ionómero (mismo ionómero en ambos electrodos) fueron evaluadas en la celda de combustible. Los resultados obtenidos dejan claro que más investigación será necesaria para entender mejor el efecto de los ionómeros a altas densidades de corriente, pero su influencia es apreciable. La alta hidrofilicidad del MPRD probablemente permitió un mejor control del agua en los electrodos, previniendo su inundación y por tanto pudiéndose alcanzar mayores máximos de densidad de potencia. El mejor resultado fue obtenido con la combinación de ionómeros con TMA en los electrodos y membrana con MPRD, llegando a obtener una densidad de potencia de 1424 mW cm^{-2} a 60 ºC.

List of abbreviations

ABPBI	Poly (2,5-benzimidazole)
AEI	Anion exchange ionomer
AEM	Anion exchange membrane
AEMFC	Anion exchange membrane fuel cell
AFC	Alkaline fuel cell
CL	Catalytic layer
DABCO	1,4-diazabicyclo [2.2.2] octane
DEFC	Direct ethanol fuel cell
EDX	Energy dispersive X-ray spectroscopy
ETFE	Ethylene tetrafluoroethylene
GDE	Gas diffusion electrode
IEC	Ion exchange capacity
IR (or FT-IR)	Infra red (or Fourier transform Infra red) spectroscopy
LAWE	Liquid alkaline water electrolyser
MEA	Membrane-electrode assembly
MPRD	N-methylpiperidine
MPY	N-methylpirrolidine
ORR	Oxygen reduction reaction
PBI	Poly (2,2'-(*m*-phenylene)-5,5'-bibenzimidazole
PEM	Proton exchange membrane
PEMFC	Proton exchange membrane fuel cell or Polymer electrolyte membrane fuel cell
PVA	Poly (vinylalcohol)
PVBC	Poly (vinylbenzyl chloride)
TMA	Trimethylamine
UP	Ultra pure water
VBC	Vinylbenzyl chloride
WU	Water uptake
XPS	X-ray photoelectron spectroscopy

CHAPTER 1. Introduction

INTRODUCTION

1 Use of energy and its consequences

Energy is needed for every activity we do, it has multiple forms such as mechanical, electromagnetic, thermal, chemical and nuclear and can be produced, stored and used in different ways. How we do the whole process will have an impact in our lives and environment, which are intrinsically connected. In the last century there has been a huge increase in the energy production and consumption, mainly from the use of fossil fuels as coal, oil and gas. The result is that in 2017 the 81% of the energy production was from fossil fuels, as showed in Figure 1.1.

The consumption of the energy is also mainly done with fossil fuels. Renewables are increasing but still play a minor percentage in the total energy landscape. As Figure 1.2 reveals, primary energy world consumption is increasing every year at fast pace. This energy system we have is creating tremendous impact on the environment, since it is not planned to be sustainable but just to continue growing. It is also not equal in all the countries and the social differences between the few rich people that control international companies and the huge population that lives in poverty is dramatic.

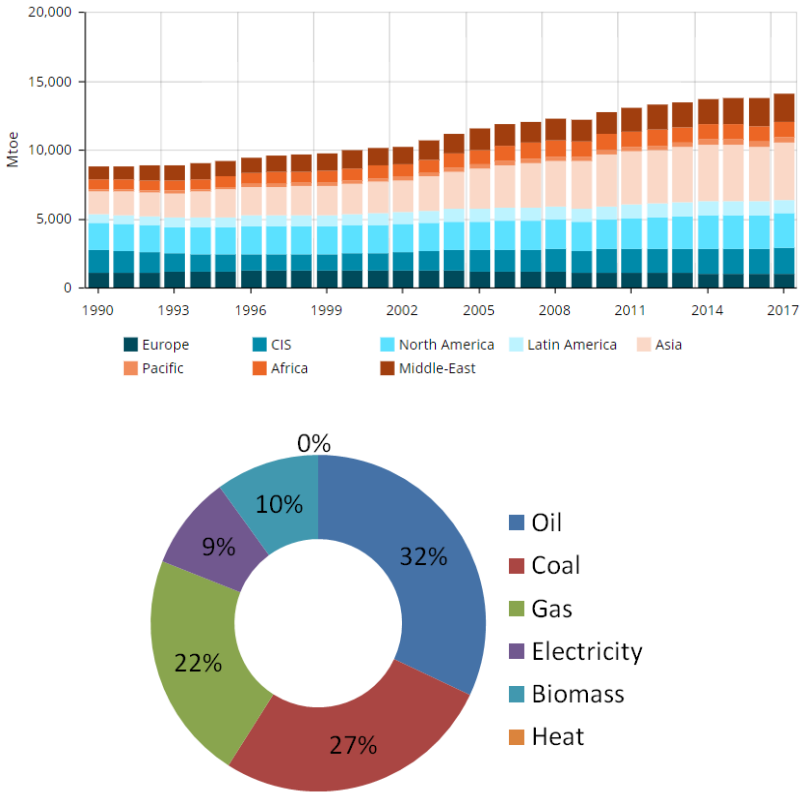

Figure 1.1. Total world energy production by regions (1990-2017) and by energy sources (2017). (Source: Enerdata [1])

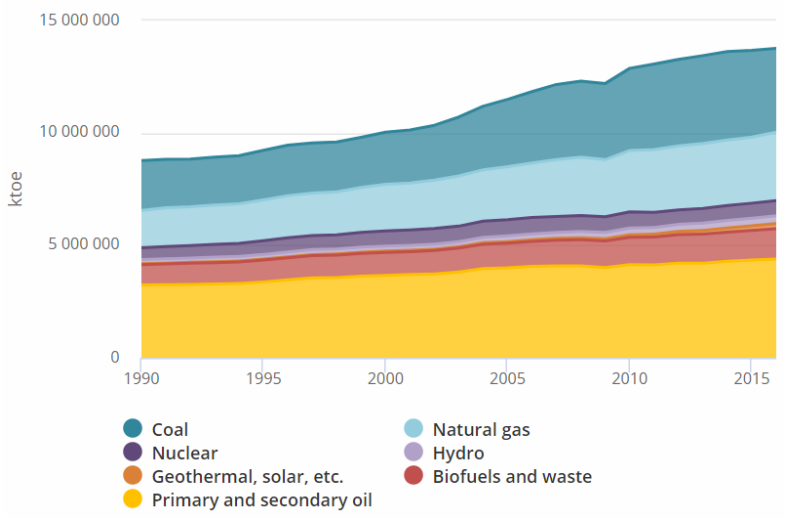

Figure 1.2. Total Primary Energy World Supply by source of energy. (Source: International Energy Agency [2])

In 1992 "World Scientists' Warning to Humanity" was written by the Union of Concerned Scientists and more than 1700 independent scientists. They called to realise the deep and long term effects of the pollution and destruction of the environment that humans were been responsible. The final consequence would be a great misery to earth living conditions and humanity if urgent changes were not done, since the limits biosphere can tolerate were near to be surpassed with the substantial and irreversible harm that would produce. 25 years later, the "World Scientists' Warning to Humanity: A Second Notice" again analyses important parameters as ozone depletion, fresh water availability, total marine catch, ocean dead zones, forest loss, vertebrate species abundance (biodiversity), CO_2 emissions, temperature change, and human and livestock population. With the exception of the first one, humanity has continued to make worse the rest of environmental problems. Efforts have been done to make international agreements to solve this problem, some of the most important have been the 1992 United Nations Framework Convention on Climate Change (UNFCCC) adopted at Rio Earth Summit, which determines the general frame to specify the tools to fix the emissions limits and the international cooperation; the Kyoto Protocol of COP 3 in 1997, the legal instrument with binding agreements about the reduction of emissions for developed countries; the Copenhage COP 15 in 2009, which was a failure to adopt a new binding global agreement to substitute Kyoto Protocol when it ends at 2013 and no compromise is reached to avoid global warming over 2ºC and the Paris Agreement in 2015, that is the largest one achieved at global level and has compromised the majority of countries to set concrete climate actions to avoid reaching 2ºC by the end of this century. The last one has been the COP 24 in Katowice in December 2018, in which urgent advise has been made to increase the climate objectives to 2020 and there is a climate summit announced to September 2019 where these new objectives will be announced.

Some of the main actions needed to correct the actual path are to cut green house gas (GHG) emissions and stop using fossil fuels. In order to do this other actions are needed to continue producing energy. It is also necessary to consider the educational change in order to teach people the need of a sustainable energy and economy system with the considerations that implies in our daily lives. If the population is not conscious of these needs, they won't apply the actions needed nor will demand the politicians to do it. In the search of other ways to produce and use energy new technologies are being developed. Some of them are the renewable energies, as for example solar, wind, geothermal and biomass. Thanks to the boost they have experimented in the last decades, renewables have contributed to 19.3% of global energy consumption and 24.5% of the electricity generation in 2015 and 2016 respectively, based on REN21's 2017 report. However, fast increase of renewables and associated technologies is needed to

mitigate climate change and reach a sustainable energy system, as was previously discussed.

In the search of alternatives to oil, fuels as hydrogen and short chain alcohols can play a key role. Hydrogen has the great advantage of its abundance in nature (while not free) and in the long term it could be developed an energy system based on it which would have almost no pollution associated by obtaining the hydrogen from water using renewable energy power and then using it as fuel in thermal or electrochemical devices. Something similar is applicable to short chain alcohols which can be produced from sustainable biomass production and then used as fuels, with the CO_2 produced in this process assimilated by the forests that would be used for the next biomass, making a closed cycle with overall zero emissions. Alcohols also have the advantage of their liquid state, which makes them easier to transport and manage and to adapt to the previous existing technology. Hydrogen can also be managed as a liquid but with the drawback of the very low temperatures needed. The most common ones are methanol and ethanol, the first has been more investigated and good conversion efficiencies have been obtained, however not as much as hydrogen nor the power densities are yet near. Also, the electro-oxidation mechanism of methanol is better understood. One of the main drawbacks on methanol is its toxicity while on the other hand ethanol doesn't have that problem. Ethanol also have higher energy density, being able to give 12 electrons theoretically per ethanol molecule, which is believed to be not that much since the C-C bond is very difficult to break. This means that fewer electrons are obtained but also that no CO_2 is produced, with the evident advantage for reducing green house gas emissions. Ethanol is also easily obtained from biomass and is probably the main alternative to methanol in direct alcohol fuel cells [3].

2 Fuel cells and electrolysers

2.1 Fuel cells

Fuel cells and electrolysers are emerging technologies with wonderful potential. In these technologies, an electrolyte is needed to separate two electrodes where electrochemical reactions occur. The separation must be physical and electrical but the electrolyte allows the ionic conduction of ions in order to close the circuit (so the current goes through the external circuit and can be used) and to make possible the continuity of the reactions at the electrodes.

But, what is a fuel cell? What do we understand for membranes in this field? Fuel cells are electrochemical devices that convert directly the chemical energy of the reagents into electrical energy and side-products via an electrochemical reaction. This process allows theoretical efficiencies as high as 80% [4], which is a wonderful advantage compared to the thermal machines limited thermodynamically by the Carnot Cycle. There are many types of fuel cells, the most relevant are: alkaline fuel cells (AFCs), polymer electrolyte membrane fuel cells (PEMFCs), phosphoric acid fuel cells (PAFCs), molten carbonate fuel cells (MCFCs) and solid oxide fuel cells (SOFCs).

Polymer electrolyte membrane fuel cells have as principal characteristics the low operation temperature (<120ºC), high power density and easily scale-up, making them a promising technology for power generation. Their main application fields are backup power, portable power, distributed generation and transportation [4]. It is relevant to note the role of transition energy technology, since they can play an important function in the near future in order to overcome the fossil fuel depletion and mitigate the climate change. The reason is that fuels like hydrogen or alcohols, which are produced by unsustainable ways, could be produced with renewable energies. An example of this is the actual production of hydrogen mainly from catalytic reforming of methane and just some from electrolysis [5]. The hydrogen can be produced from electrolysis powered with electricity coming from renewables. This should be done when production is higher than the demand, allowing to store chemically the energy and later use it when needed with a PEMFC; this is known as the "hydrogen economy system". It is also possible to accumulate energy in short chain alcohols like methanol or ethanol and use them to power PEMFCs [3,6], mainly used in the portable applications. A great advantage of this technology is the low pollution associated with the process. For

example, when hydrogen is used as fuel the only products are electricity and water. The potential of PEMFCs is really promising but still drawbacks as high cost (mainly from the expensive catalysts based in Pt) and low durability have to be overcome for a general commercialization [4].

In PEMFCs one of the most important components is the polymeric ion exchange membrane (IEM) that works as electrolyte. It has to be an electrical insulator to force the produced electrons to go through the external circuit, it also has to avoid the mixture of the reagents supplied in anode and cathode and it is responsible of the adequate ionic conductivity of the ions travelling through it. Depending on the ions movement two types of IEMs can be distinguished: anion exchange membranes (AEMs), where the ionic charge carriers are the hydroxide ions (OH^-) that travel from cathode to anode and cation exchange membranes (CEMs) where generally the proton ion (H^+) moves from anode to cathode in the fuel cell. For that reason, the last ones are also called proton exchange membranes (PEMs). The AEMs are used in alkaline media and the others in acid media. The proton exchange membrane fuel cells (PEMFCs) have been historically more used because the discovery of the Nafion® membrane that has good ionic conductivity and durability and has been the standard so far [7]. The higher mobility of the H^+ ion compared to OH^- in aqueous media has also been a relevant factor [8]. The alkaline media in the other hand doesn't have a standard membrane and presents relevant advantages that have produced high interest in the last years. Some of them are the faster electrochemical kinetics in the alkaline media, possible absence of noble metals as catalysts, minimized corrosion problems and cogeneration of electricity and valuable chemicals [9].

Independently of the media, membranes are expected to have good ionic conductivity, long term chemical and electrochemical stability, adequate mechanical strength, good moisture control, low fuel or oxygen crossover and production costs compatible with intended application [7,8].

In the FCs, the active materials (fuel and oxidant) are continuously fed and extracted. The fuel cell, Figure 1.3, is made up of two electrodes: the anode, where the fuel is oxidized, and the cathode, where the oxidant (O_2) is reduced. It also involves an electrolyte, which acts as an ionic conductor and electrical insulator. The electrons obtained in the anode are addressed direct to the cathode through the external circuit, generating an electric current directly usable. In addition, the protons produced in the anode, go through the electrolyte, up to the cathode to reduce O_2, generating water as the only product of the reaction. The reaction is exothermic and has a value of ΔH^0_r= -285.83 kJ/mol for H_2O (l) and -241.862 kJ/mol for H_2O (v). Although this is a spontaneous reaction, it needs to be catalysed to be operational, since the kinetics of the process are too slow otherwise.

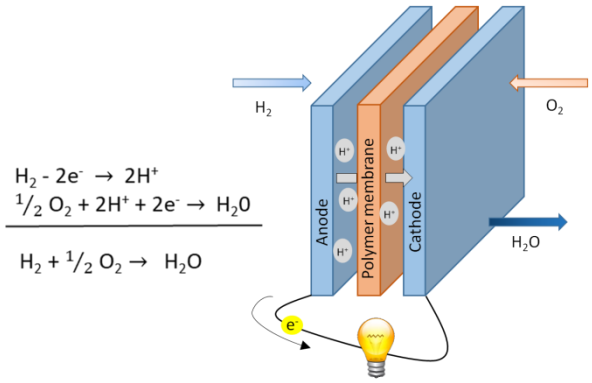

Figure 1.3. Polymer exchange membrane fuel cell working with H_2 and O_2.

At atmospheric pressure, the maximum potential difference obtained by the fuel cell will be determined by the difference of energy between the initial and final state of the system. The Gibbs free energy variation of the process, ΔG, can be calculated from the operation temperature (T) and changes with both enthalpy (ΔH) and entropy (ΔS) of the reaction. Under standard conditions:

$$\Delta G^0 = \Delta H^0 - T\,\Delta S^0 \quad (1)$$

and the maximum potential difference, obtained in the fuel cell, $E^0_{theoric}$, will be:

$$E^0 = \frac{-\Delta G^0}{nF} = 1,23V \quad (2)$$

where n is the number of electrons exchanged and F, the Faraday's constant. At 298 K and 1 atm, ΔG^0 = -237.340 J/mol and therefore E^0= 1.23 V. For an operating temperature of 80ºC, the values of ΔH and ΔS change, but slightly, and the decrease in ΔG will be mainly due to the temperature, resulting in a theoretical potential difference of 1,18 V approximately. However, in practice this potential, called the open circuit potential, is significantly lower than this potential value, usually less than 1V. This suggests that some losses appear in the fuel cell even when no external current is generated. The potential difference of the fuel cell in operation, that is, when the current is passing through the system, $E_{fuel\ cell\ (I)}$, will be given by the sum of thermodynamic or reversible value (I=0), minus the anode and cathode activation overvoltage and the ohmic losses or overvoltage. The electrode kinetics were represented by the Butler-Volmer equation and the mass transport process was described by the multi-component Stefan Maxwell equations and Fick´s law, and the ionic and electronic resistances described by Ohm´s law. The $E_{fuel\ cell\ (I)}$ value could be obtained by:

$$E_{fuel\ cell\ (I)} = E_{Reversible\ (I=0)} - \eta_{activation} - \eta_{ohmic} \quad (3)$$

The losses considered are in relation to the activation overvoltages and they are dependent on the kinetics of the processes involved and therefore directly related to the goodness of catalyst used for the process. Thus, $\eta_{activation}$ is related directly with both the oxidation kinetic reaction and the reduction kinetic reaction of the reagent involved on the catalysts surface materials. The $\eta_{activation}$ for an H_2/O_2 fed in PEMFC will come mainly determined by the slow kinetics of oxygen reduction reaction (ORR) on the catalyst material in comparison to H_2 oxidation, while $\eta_{activation\ (transport)}$ is consequence of material transport. This overpotential considers the combination of the flow of reactants and products in the fuel cell. The polarization from concentration gradients occurs when a reactant is rapidly consumed at the electrode by the electrochemical reaction so that gradients are established. The η_{ohmic} = iR will be due to the combination of resistors provided by internal/external electrical contacts and ionic resistance due to ions motion trough the membrane. Therefore, the fuel cell when current is not cero has an $E_{fuel\ cell(I)}$ expression like this:

$$\boldsymbol{E_{fuel\ cell\ (I)} = E_{rever\ (I=0)} - \frac{RT}{\alpha_c} ln\left(\frac{i}{i_{0,c}}\right) - \frac{RT}{\alpha_a} ln\left(\frac{i}{i_{0,a}}\right) - \frac{RT}{\alpha_c} ln\left(\frac{i_{I,c}}{i_{I,c}-i}\right) - \frac{RT}{\alpha_a} ln\left(\frac{i_{I,a}}{i_{I,a}-i}\right)} \quad (4)$$

$$\boldsymbol{E_{rev\ (I=0)} = 1,229 - (8,5\ 10^{-4})(T - 298,15) + (4,308\ 10^{-5})T[\ln\ (P_{H2}) + 0,5\ln(P_{O2})]} \quad (5)$$

Being i_{oc}, α_c, i_{Lc} and i_{oa}, α_a ,i_{La} the exchange current density, transfer coefficient and limit current density of the cathodic and anodic processes respectively [10]. The polarization curve of the device can be found at in Figure 1.4, where the different losses mentioned above are indicated.

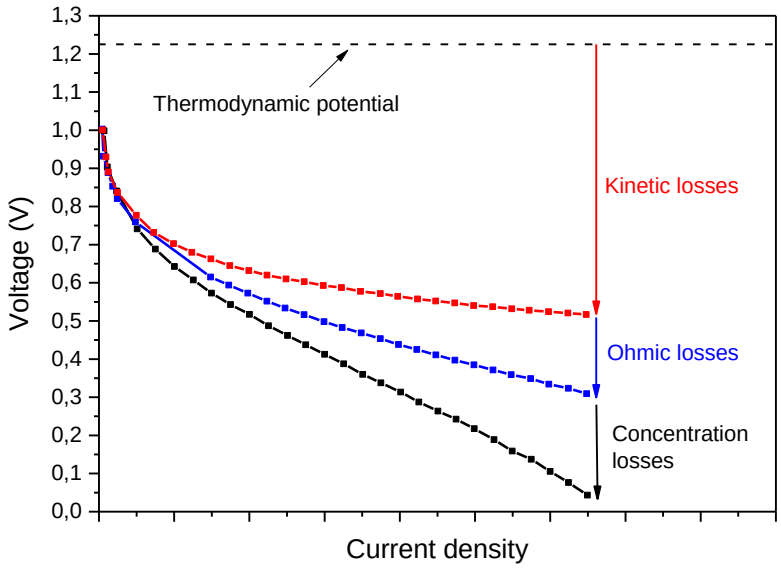

Figure 1.4. Polarization curves with voltage losses of a fuel cell.

It was previously stated that the ion exchange polymer membrane is electrically insulator and practically impermeable to reactant gases, but some small amount of mainly H_2 will crossover from anode to cathode. Hydrogen that permeates through the membrane does not participate in the electrochemical reaction on the anode side. Each hydrogen molecule on the cathode side reacts with oxygen on the surface of the catalyst resulting in two fewer electrons in the generated current that travels through the external circuit, and thus in a lowering of cathode and the overall fuel cell potential. These losses are not big in fuel cell operation, but when the fuel cell is at open circuit potential or at very low current densities, this situation may have a dramatic effect on fuel cell potential. At least, all these losses have to be taken into account when the device works and have a lot to do with good fuel cell performance.

The same effects are presented when other fuels are used, with the differences due to the chemical composition they present respectively. Ethanol is one of the most interesting alternative fuels. It has the advantage of the liquid state, making it more easy to handle than hydrogen and similar to oil. This is an important advantage since it allows to adapt easily all the industrial knowledge and facilities designed for liquid oil to the liquid ethanol. Similar to hydrogen, it can be considered a renewable fuel if it comes from renewable sources like reforming of biomass residues. Many of these advantages are shared with methanol, the other most studied alcohol for fuel cells, but the last is very toxic with the environmental and safety issues that implies. The reactions taking place in an alkaline fuel cell using ethanol are presented in Figure 1.5.

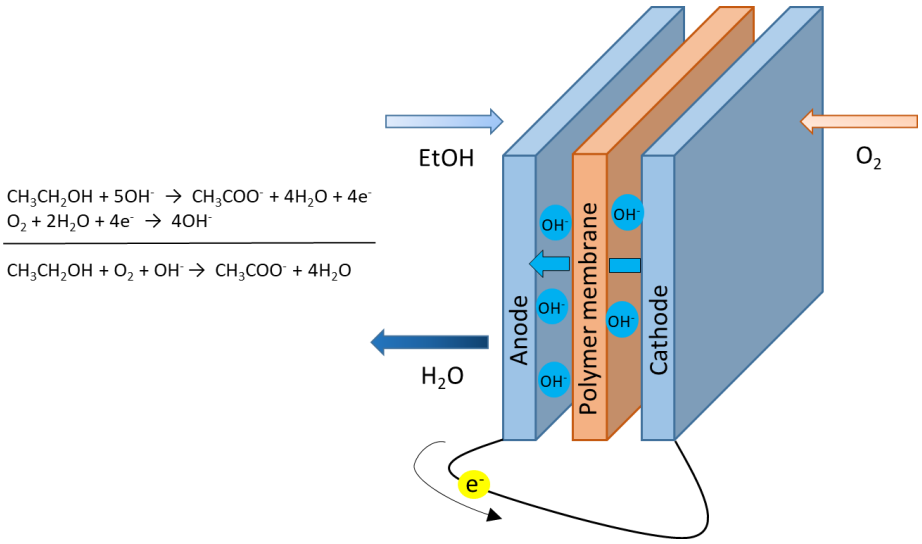

Figure 1.5. Alkaline polymer exchange membrane fuel cell working with EtOH and O_2.

Due to this advantages, the performance of most of the synthesised materials were evaluated in an alkaline direct ethanol fuel cell (DEFC).

2.2 Electrolysers

Hydrogen is a promising energy carrier and a sustainable energy system can be built around it as it has been previously explained. This "Hydrogen economy" will be based in the power generation of electricity with renewable energies that, in case of excess, would be used in water electrolisers to produce high purity hydrogen so the energy is chemically stored until needed, when a fuel cell would produce electrical power again. Water electrolysis (WE) is a viable process to produce high purity hydrogen, but further development is needed to reduce the operational costs and investment so a widespread utilization can be achieved. The most common current technologies used are proton exchange membrane WE (PEMWE) and liquid alkaline WE (LAWE). LAWE is already a well established technology in which cheap nickel electrodes are separated by a porous diaphragm and a liquid electrolyte is used (typically 30 wt.% KOH) at temperatures around 80-90 ºC. These conditions are aggressive to the materials but the high temperature and the concentrated solution allow to decrease the ohmic drop in the cell and operate it at voltages ranging around 1.9 or 2.1 V. The introduction of the zero gap configuration, in which a solid electrolyte is placed directly in contact with anode and cathode between them, allows to reduce the voltage drop and the energy required to produce H_2 and therefore improves the energy efficiency. The use of a solid polymer electrolyte membrane has the advantages of lower voltage drop than a porous separator, the electrodes can be fabricated directly into the membrane surface and the cell feed can be pure water rather than aqueous alkali [11]. Large development has been done in the acidic media but the cost of the expensive noble metal catalysts and the membranes have hindered a higher commercialization. On the other side, the alkaline media opens the possibility of using cheaper metal electrocatalysts as anode materials as well as lower overpotential for oxygen evolution, making the overall process cheaper. These reasons have made attractive the design of zero gap electrolysers with hydroxide conductive membranes. As it can be observed, the mayor development of the acidic media and the later research in the alkaline media looking for cheaper alternatives has been very similar to the fuel cell technology. Also for both technologies, stable anion conductive membranes with adequate properties have not been sufficiently developed yet and the advancements done for one of the technologies can be easily applicable to the other.

The reactions and the scheme of a zero gap liquid alkaline water electrolyser are presented in Figure 1.6.

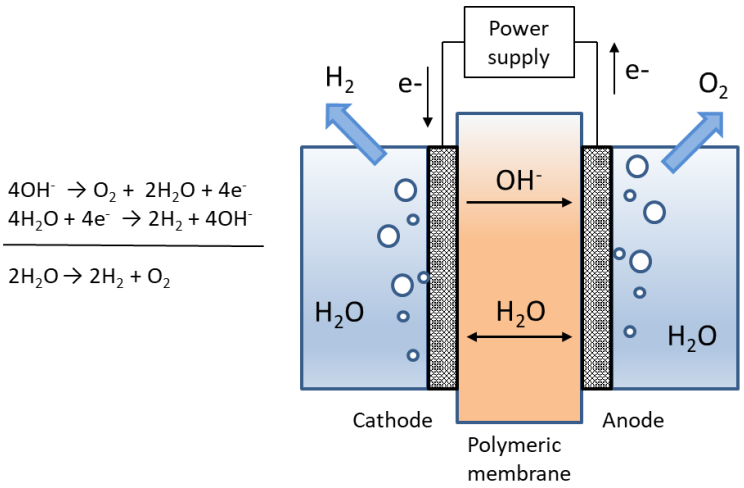

Figure 1.6. Reactions and scheme of a zero gap liquid alkaline water electrolyser.

The traditional alkaline water electrolysers use a porous diaphragm to separate the produced gases (O_2 and H_2), preventing as much as possible the mix since it could be explosive at certain percentages and also to obtain high purity of the gases and elevated current efficiencies. It also should minimize the formation of the "courtain" of gas bubbles. Some of the materials that have been used to work as separators (organic and inorganic) are: niquel oxide, asbestos, polymeric materials, polyantimonic acid and polysulfone/zirconium oxide (Zirfon®) [5]. The replace of the separator/diaphragm with an ion exchange membrane offers the advantage of better gas separation and lower area resistances. In conclusion, the application of advanced anion exchange membranes in water electrolysers can lead to enhanced performance by taking advantage of the properties of the two traditional electrolysis types. The cost can be reduced by using cheap electrode materials and catalysts due to the alkaline media and the efficiency improved with the lower ohmic drop and better gas separation of the thin polymeric anion exchange electrolyte membranes.

3 Polymeric materials in alkaline media

Polymers are the core materials in the polymer electrolyte membrane fuel cells (PEMFCs) and zero gap liquid alkaline water electrolyzers (LAWEs). Sometimes a polymer alone functionalized, sometimes different polymers combined and other times polymers combined with other materials. The polymers used must fulfil the following properties: being an electrical insulator, a good ionic conductor (of the ions required in each case), separate effectively the reactants of both electrodes and be stable in the conditions of performance. In the case of the ionomers, it is also helpful that they have some binding ability with the catalyst particles. Many polymers have these properties and different chemistries have been investigated. In the field of alkaline applications a great review was done by Varcoe et al. [5] where they explain deeply the use of these materials. They review the most common polymer backbones like "poly(arylene ethers) such as poly(ether ketones), poly(ether imides), poly(ether oxadiazoles) and poly(phenylene oxides) [PPO]; polyphenylenes, perfluorinated types, polybenzimidazole (PBI), poly(epichlorohydrins) [PECH], unsaturated polypropylene and polyethylene types, those based on polystyrene and poly(vinylbenzyl chloride) [PVBC], polyphosphazenes, radiation-grafted types, those synthesised using plasma techniques, pore-filled types, electrospun fibre types, PTFE-reinforced types, and those based on poly(vinyl alcohol) [PVA]." They also describe the different cationic head group chemistries generally used: Quaternary ammoniums (QA), heterocyclic systems, guanidinium systems, P-based systems types, sulfonium types and metal-based systems.

From all these possibilities, and because of the reasons that will be explained, polybenzimidazoles were selected as a promising family of polymers to further investigate its applicability for fuel cells and electrolyzers. To improve its properties it was decided to be combined with other polymers to synthesise the membranes. Two strategies were followed: blend membranes of polybenzimidazole with poly(vinyl alcohol) (PVA) and crosslinked membranes of polybenzimidazole with poly(vinylbenzyl chloride). In the last ones the selected amine to form the quaternary ammonium group was 1,4-diazabicyclo[2.2.2]octane (DABCO). In the search of another stable cationic head group, the benzyl-N-methylpiperidinium (MPRD) was investigated in membranes and ionomers of well known ethylene tetrafluoroethylene (ETFE) based materials radiated and grafted with vinylbenzyl chloride (VBC).

3.1 Membranes based in polybenzimidazoles

Benzimidazole and its family can be used in the energy world easily in the form of polymers, since these materials have the possibility to create designed structures for many applications. As it has been previously explained, the membrane is a key component of the fuel cell or the electrolyzer, here is where benzimidazoles (in the form of polybenzimidazole for example) play a key role, in the conformation of a solid polymer electrolyte membrane, alone or with other chemical materials.

a) Synthesis of polybenzimidazole materials

Polibenzimidazoles are synthesised by the repetitive reaction of aromatic amino groups with carboxyl groups using a 1:2 molar ratio by the process of step-grow polymerization [12]. Usually the monomer reagents are a diacid and a tetra-amine, like the example in Figure 1.7. There are many polybezimidazoles but the ones that have presented better application and have been more studied are poly(2,2'-(*m*-phenylene)-5,5'-bibenzimidazole), known as PBI and poly(2,5-benzimidazole), known as ABPBI. Both were first synthesised by Vogel and Marvel in 1961 [13]. For PBI the synthesis was a two step process with an intermediate prepolymer that prevented the production of high molecular weight polymer. Cho et al. [14,15] discovered a process with 3,3',4,4'-tetraaminobiphenyl (TAB) and isophthalic acid (IPA) to do the synthesis in a single step obtaining high molecular weight, in the presence of catalysers and at temperatures higher than 350ºC. It is important to know the molecular weight of the polymer, which is obtained by the measurement of the inherent viscosity (IV, in dLg^{-1}) of the polymer dissolved in concentrated sulphuric acid. For membrane application, usually casted from solution, it is interesting to have high molecular weight in order to achieve mechanical stable membranes that can support higher doping and thus obtain better ionic conductivity. The previously described method of Vogel and Marvel and Cho et al can be classified in the heterogeneous molten/solid state synthesis [16,17]. The other synthesis method used is the homogeneous solution synthesis, using solvents as polyphosphoric acid (PPA) [18], this method allows to use moderate temperature and more stable monomers and is excellent to synthesise linear high molecular weight polymers at laboratory or small batch scale. These advantages make this synthesis method the most commonly used. Another example of solvent is Eaton's reagent, a mixture of phosphorus pentoxide (P_2O_5) and methanesulphonic acid (MSA) proposed by Eaton et al. [19], which has low viscosity making it suitable for the homogeneous solution synthesis and the acid

washing after it [20,21]. A shorter reaction time with high molecular weight has been obtained using homogeneous solution microwave-assisted synthesis recently, both for PBI and ABPBI [17].

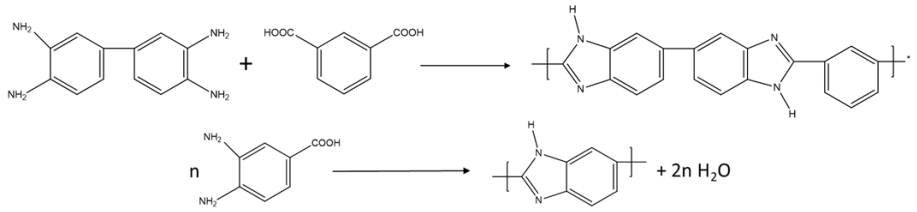

Figure 1.7. Example synthesis of (top) poly(2,2'-(*m*-phenylene)-5,5'-bibenzimidazole), abbreviated as PBI, and (bottom) poly(2,5-benzimidazole) (ABPBI).

ABPBI is synthesised from a single monomer, (3,4-diaminobenzoic acid) (DABA), which as the advantages of being less expensive, commercially available and non-carcinogenic. The scheme is showed in Figure 1.7. Different synthesis have been done by the homogeneous solution method in PPA or Eaton's reagent, and inherent viscosity values as high as 7.33 have been reached, as reported by Li et al. by using recrystallized DABA [22]. This is essential for the direct casting of ABPBI membranes since it has been suggested by Asensio and Gómez-Romero that values of at least 2.3 dL g^{-1} are necessary to cast good membranes [16].

In the case of ABPBI, since there is only a monomer, its purity is not as critical as in PBI, however, the use of high purity monomer produces polymers of high molecular weight [23]. Since polybenzimidazoles have to be doped in order to become ionic conductors, two methods are used to prepare the membranes: direct casting from the polymerization solution, as the work developed by Asensio et al. [24] or dissolving the previously synthesized polymer and then do the casting of the membrane. The casting process consist in the formation of a thin film by the deposition of the polymer by evaporation of the solvent in the solution. To solubilize PBI or ABPBI usually strong bases or acids are needed, only a few organic solvents can also do it, one of them is the N,N-dimethylacetamide (DMAc) [16,25]. There is also an alternative way to cast ABPBI membranes from a mixture of NaOH and ethanol [26].

b) Properties and characterization of benzimidazole materials

The structure of polybenzimidazoles has a good degree of flexibility and chemical and thermal resistance compared to other polymers with more single bonds in

their main chain between aromatic units. The presence of aromatic units in the main chain helps to have higher thermal stability than the aliphatic counterparts, which is also important [12]. In order to characterize polybenzimidazoles, one of the most important parameters is the molecular weight of the polymer, which will be highly related with the final membranes properties. The common way to obtain the molecular weight is by measurement of the intrinsic viscosity of the polymer (η_{IV}) at a certain temperature (normally 25-30ºC). From the plotting of the specific viscosity (η_{sp}) as function of the polymer concentration, the intrinsic viscosity is calculated extrapolating to zero concentration. A simpler measurement process was proposed to do the calculation with a single-point method using Eq. (6), where C is the polymer concentration in a concentrated acid like 96 wt% H_2SO_4.

$$\eta_{IV} = (\eta_{SP} + 3\ln(1 + \eta_{SP}))/4C \qquad (6)$$

The protocol test is to calculate the η_{sp} of a polymer solution 5 g L^{-1} in concentrated sulfuric acid at 30ºC using an Ubbelohde viscometer. From the η_{IV} value the average molecular weight is calculated with the Mark–Houwink–Sakurada expression:

$$\eta_{IV} = K * M_W^{\alpha} \qquad (7)$$

were the Mark-Houwink constants depend on the molecular weight range and distribution. Values often used for this constants are $K = 1.94\times10^{-4}$ dL g^{-1} and $\alpha = 0.791$, obtained from Buckley et al. by light scattering measurements. Other solvents as formic acid or MSA can also be used to measure the viscosity of polybenzimidazoles [17].

There are various techniques in order to investigate the structure of polybenzimidazoles. Nuclear magnetic resonance is very powerful for pure organic compounds or the repeating unit of a polymer. Solvents that can be used include deuterated dimethyl sulfoxide (DMSO- d_6) and deuterated sulfuric acid (D_2SO_4). The most commonly used to record ^{1}H-NMR spectra is DMSO- d_6 because with D_2SO_4 the fast exchange interaction with the proton in the imine of the imidazole rings (-NH-) causes the chemical shift of that hydrogen to be often indiscernible [27]. ^{1}H-NMR PBI characteristic signals in DMSO- d_6 are at 13.2 (2H), 9.1 (1H),

8.3 (2H) and 8.0–7.6 (7H) ppm, the first of them attributed to the imidazole protons and the others to the aromatic protons [28,29]. IR and Raman spectroscopy are also used, mainly to identify different functional groups and obtain or corroborate the chemical structure of the polymers [27,30,31]. In PBI, the IR spectrum region from 2000 to 4000 cm^{-1} is interesting since N–H stretching modes occur in this range, showing three typical bands at 3415, 3145, and 3063 cm^{-1}. The broad band around 3145 cm^{-1} has been attributed to the stretching vibrations of N–H groups self-associated by hydrogen bonds, and the peak at 3145 cm^{-1} is assigned to the N–H groups stretching vibration. In the region from 1630 to 1500 cm^{-1}, the peaks observed come from the vibration of C=C and C=N bonds [32]. In the Raman spectra of PBI the most significant absorption band comes from the benzene ring vibration and is located around 1000 cm^{-1} [31]. For the measurement of the Raman spectra it is relevant to use an excitation wavelength of 785 nm (red laser) since it gives much less fluorescence than the 532 nm (green laser) [33]. Because the structure and functional groups are the same, ABPBI presents the same IR peaks than PBI, as reported by Asensio et al. [34]. They also investigated the bands appearing when the polymer membrane is doped with phosphoric acid: in the N-H stretching zone they found the evolution of nitrogen protonation by the acid, and in the medium and high doped samples the broad band of N^{+}-H vibration becomes stronger while the non-associated imidazole protons decrease. In polybenzimidazoles doped with alkaline media for anion conductivity purposes the structure changes are also clearly identified. Aili et al. [35] investigated PBI with different degrees of KOH doping and found that in the IR spectra, at KOH concentrations higher than 15 wt.% the N-H stretching band at 3415 cm^{-1} disappear as well as the broad band around 3100cm^{-1} of shelf-associated hydrogen bonded N-H groups. They concluded that the IR data indicated the predominance of the deprotonated form of PBI with KOH concentrations of the bulk solution around 15-20 wt.%. In the ^{1}H-NMR spectrum the signal at 13.3 ppm of the N-H proton disappeared at high bulk KOH concentration and most signals from the aromatic protons showed upfield shift compared to pristine PBI, indicating complete ionization. This full ionization of the polymer releases the extensive intermolecular hydrogen bonding allowing for high swelling behaviour and water and KOH uptake and therefore enhanced ion conductivity. This study corroborates the knowledge that the introduction of species that interact with imidazole groups by hydrogen bonding decreases the intermolecular polybenzimidazole cohesion, causing a strong plasticizing effect observed in the great decay of the tensile strength and enhanced elongation at break when the doping level increases, specially when full ionization of the polymer is reached. Using an even higher concentration doping solution, they found that a higher crystallinity structure was obtained, as observed by XRD, mechanical test and swelling behaviour measurements. X-ray photoelectron

spectroscopy (XPS) is also a helpful technique for the characterization of polybenzimidazoles, concretely for the capacity to distinguish the oxidation states of the elements present and allow their quantification in the surface of the membrane [33]. Other fundamental measurements usually performed on the synthesised membranes are the determination of the ionic conductivity, the swelling behaviour with water and in acidic/alkaline media or the thermogravimetric analysis (TGA). In conclusion, a full set of characterization analysis have been studied and are used to identify and test the properties of the synthesised polybenzimidazoles and the membranes prepared with them.

c) Commercial availability

There have been different companies relevant in the fuel cell membrane field, probably the most known one is DuPont for developing the Nafion® membrane made of a sulfonated tetrafluoroethylene based fluoropolymer-copolymer with excellent thermal and mechanical stability as well as high proton conductivity in low temperature fuel cells. Companies like Solvay, Gore and others have also commercialized membranes with this chemistry. This membrane has been the standard for fuel cells used in low temperature and acidic media, but at temperatures higher than 100 ºC Nafion® performance drops dramatically due to the lower hydration level. It is in these conditions where membranes made of polybenzimidazoles have showed good performance and promising applicability and production for commercialization has occurred. BASF Fuel Cell (formerly PEMEAS Fuel Cell), part of one of the larger chemistry industries, has developed a product line about a membrane electrode assembly (MEA) based in a PBI membrane: Celtec® [36,37]. These MEAs optimal operation conditions are between 120 and 180ºC, doped in phosphoric acid. They have showed relevant advantages working as high temperature PMFCs, like high tolerance to fuel gas impurities such as CO (up to 3%), H_2S (up to 10 ppm), NH_3, or methanol, no humidification required, far simpler system due to elimination of water and a less complex reformer technology. In addition, several advantages can be obtained for the electrocatalysis, but it is necessary to be especially careful at the high stability towards corrosion needed to ensure long fuel cell lifetimes, apart from high activity for the oxidation of the fuels and the oxygen reduction reaction. Other companies that commercializes PBI and PBI based membranes are "PBI Performance Products" with their Celazole® PBI PEM [25,38] and Danish Power System with their Dapozol® membranes and MEAs [39]. Membranes based on PBI are of high applicability as it can be observed, both for the fuel cell technology in development and also for other applications as carbon capture, pervaporation dehydration processes or electrochemical hydrogen separation among others.

d) Proton exchange membrane fuel cells (PEMFCs)

Polybenzimidazole (PBI) as ionic exchange membrane can be used as proton exchange if the material is doped with phosphoric acid (H_3PO_4), sulphuric acid (H_2SO_4) and nitric acid (HNO_3) solvent media. The PBI has benzimidazole units in the polymer chain which have the pKa = 5.5 that is responsible for the weak acid character and present excellent oxidative and thermal stability [40]. The acid molecules penetrate the membranes during doping process, due to the acid-base interaction between them and gradually swelling of PBI membrane. Therefore, PBI can be easily doped with different type strong acids, which act predominantly protonating through the PBI membranes.

In these circumstances, the material can work as solid electrolyte in a fuel cell in temperature range between (100-200ºC), overcome the dehydration problem that the Nafion@ membrane has in operation condition at around 100ºC and in consequence solve the dramatic reduction of its proton conductivity, presenting a near zero electro-osmotic drag [41]. High temperature makes HT-PEMFC more tolerant to impurities in feed gases (CO e.g.) and simplifies elimination of waste heat with a simpler cooling system. If the fuel cell is working with reformed natural gas as a power source, the device does not require humidification of reactants due to the simple water management; all these features greatly simplify design of HT-PEMFC stack [42].

In the PBI/H_3PO_4 system, the polybenzimidazole acts not only as a matrix polymer but also as proton acceptor [43]. For HT-PEMFCs, PBI/H_3PO_4 is considered a reasonably successful solid electrolyte because the excellent conductivity and thermo-chemical stability. Phosphoric acid has been widely employed as an anhydrous proton conductor because of its high proton conductivity, low cost, and thermal stability. At temperatures above 150ºC, the dehydration of the acid occurs and yields pyro-phosphoric acid or higher oligomers, which exhibit worse proton conductivity. On the other hand, the long-running operation leads to the release and dilution of H_3PO_4 from the membranes, which results in a loss of the acid into the fuel cell gas/vapour exhaust streams, the decrease of membrane ionic conductivity and thus a lower fuel cell performance occurs. The high proton conductivity of the membranes was proved only when the polymer holds a large excess of phosphoric acid [44]. The optimum doping level is around 5 moles H_3PO_4 per PBI repeat unit, where a compromise between conductivity and mechanical properties is achieved.

A thick membrane it is not usually advantageous because it is the main responsible of the large ohmic polarization and modest power performance of HT-MEA. However, approx. 100 μm has been implemented with the intention of improving

their mechanical properties [45]. The acid doping is an essential process, but it softens the PBI membrane, causing membrane ripping in MEA fabrication. The mechanical stability of the doped PBI membrane can be improved by lowering the H_3PO_4 doping level, however, the proton conductivity is reduced [46].

The problems of HT-PEMFCs operating at temperatures up to 100ºC are not solved yet, and demonstrate the necessity of research on new and more satisfactory alternatives. In this context, the ionic liquids (ILs) have been used as non-aqueous and low volatility proton carriers replacement of aqueous electrolytes. The protic ILs for example are able to transport protons due to their acid-base character and their capability to form complex or intermolecular hydrogen bonds [47] even in non-aqueous conditions. This type of materials tries to overcome the formation of unstable materials in the operating conditions and then to improve the performance of the PEMFC at high temperatures. The first research team working in this subject was Watanabe and colleagues, who identified the potential electroactive use of ILs in fuel cell reactions [48]. Sometimes, polymer phase substrate and the IL result in non-homogeneous and unmanageable membranes when both components are integrated together. In general, ILs and polymers dissolved in a common solvent and later are casted as a film. In this way hybrid membranes are obtained and the materials may be studied once the solvent has been removed. PBI-based hybrid membranes holding ILs are examples of this methodology.

Some of the authors that have investigated this field with membranes using polybenzimidazoles are Greenbaum et al. [49], Schauer et al. [50], Wang et al. [51], Savinell et al. [52] and Ocón et al. [53]. The composite membranes prepared were generally homogeneous and chemically and thermally stable at wide temperature range. However, phase separation between the components when mixing with a strong acid or under operation is a general problem difficult to solve. The ILs help to reach good conductivity values, above 10 mS cm^{-2}, but usually plasticiser hindering the mechanical properties of the membranes. Another problem is that it has been observed that ILs tend to migrate out of the membrane under performance at high temperatures. In general, more research it still needed before ILs and in general HT-PEMFCs can have a widespread commercialization.

e) Anion exchange membrane fuel cells (AEMFCs)

Many electrochemical systems use ion-exchange membranes, such as fuel cells, electrolysers or redox flow batteries. Traditionally cation exchange membranes have been used in these systems due to the idea that anion exchange membranes had too low conductivity and stability. However, in the last years many advances have been made and anion exchange membranes (AEMs) are demonstrating to

have performances comparable to acid ones, showing promising application in several technologies [5]. These membranes conduct negatively charged ions like OH^- or Cl^- and usually have positive charged groups in the polymer structure, which could be directly present in the polymer backbone or more commonly fixed to it by extended side chains of varying lengths and chemistries. Varcoe et al. [5] investigated a deep review about the different chemistries of polymer backbones and head groups and their current state of research. The use of alkaline media, compared to acid media, has some advantages like the better electrochemical kinetics of the oxygen reduction reaction (ORR). This allows the possibility of using non-noble metals in the electro-catalysts reducing the fuel cell system cost. Other advantages are the minimized corrosion problems and the cogeneration of electricity and valuable chemicals [9,54]. Compared to classical alkaline fuel cells (AFCs) where the electrolyte is an aqueous phase, the use of AEMs solves the carbonation problems and the difficulties of the liquid electrolyte management. The fuels commonly used in anion exchange membrane fuel cells (AEMFCs) are hydrogen and alcohols. Hydrogen is the common fuel in commercialization and research and gives the higher power densities. On the other hand, alcohols like methanol or ethanol have the advantages of easier handle, store and transport and can be acquired from abundant biomass, which is environmental friendly considering the process is carbon-neutral.

Among all the polymers available and tested for AEMFCs, polybenzimidazoles have demonstrated good applicability and the most commonly used and studied are PBI and ABPBI. Some of their advantages remain in the properties previously described, as excellent thermal stability, which allows to use them at higher temperatures, superior mechanical properties that can withstand the performance conditions and presence of amine and imine groups which form strong hydrogen bonding interactions and can be further functionalized. The great stability properties have also encouraged many studies combining polybenzimidazoles with other polymers, creating blend or crosslinked membranes with excellent performances. Membranes based on polybenzimidazoles alone or with other polymers have also demonstrated low alcohols crossover, making them adequate electrolytes in alcohol fuel cells. In the alkaline media, the pristine form of PBI can be equilibrated in aqueous solutions of alkali metal hydroxides forming homogeneous systems with the hydroxide salt and water dissolved in the polymer matrix. These materials have showed high ion conductivity, great chemical stability at low alkali concentrations and have been tested as anion conducting electrolytes in fuel cells with hydrogen or alcohol and in water electrolysers. In order to understand the physical and chemical properties of polybenzimidazoles in alkaline media Aili et al. have made a study with thin films of PBI in aqueous KOH solution with concentrations from 0 to 50 wt.% [35]. They observed by the EDS

cross-sectional maps, that the dissolved KOH is evenly distributed in the electrolyte membrane. The polymer has strong water affinity through hydrogen bonding with the imidazole groups, absorbing around 3 water molecules per repeating unit (r.u.) and KOH forms various hydrated complexes when dissolved in water. The degree of ionization of the polymer is determined by the position of the acid-base equilibrium presented in Figure 1.8. They observed that it depends on the KOH concentration as was expected, increasing the KOH content per PBI r.u. with the higher concentration of the bulk solution, reaching 2.6 KOH molecules/r.u. at bulk concentration of 25 wt.%.

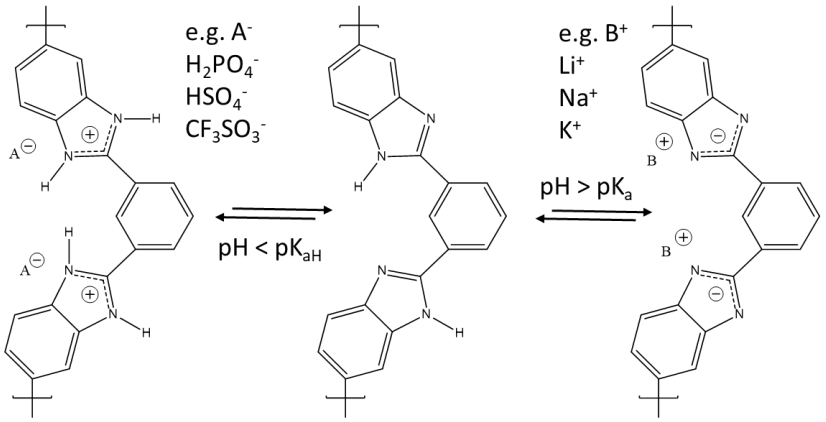

Figure 1.8. Scheme showing the amphoteric nature of PBI in acidic (left) and alkaline (right) environments.

A similar trend was observed for the water molecules, reaching more than 20 H_2O molecules/r.u. at KOH concentration around 20-25 wt.% in the bulk solution. In the polymer phase, the number of water molecules per KOH decreased while increasing the bulk solution concentration, showing a concentrating effect of KOH in the polymer. They did the measurements by titration and gravimetrically, getting consistent results that corroborate previous knowledge. They also observed the anisotropic swelling behaviour of the polymer at different KOH concentrations that had been previously reported and performed X-ray diffraction (XRD) measurements to explain it. The explanation they found was that the increasing of surface area and thickness up to 15 wt.% concentration was due to the uptake of water and KOH, but further increasing the concentration lead to full ionization of the polymer is approached, breaking many of the hydrogen bonds and separating the layered structure. This separation is easier in the interlayer dimension than in the intra-layer one, causing the high thickness increase and area decrease. When KOH bulk solution concentration reached 50 wt.% sharp peaks appeared in the XRD and were attributed to a crystalline phase of a poly(potassium benzimidazolide) hydrate with a symmetric and highly regular structure with

crystallite size in the range of 70 to 120 nm. These crystalline peaks were vanished after washing in water until neutral pH. They also observed that the previously described effect of the introduction of water and KOH that disturb the polymer hydrogen bonding of imidazole groups affected the mechanical properties, causing great decay in the tensile strength and enhanced elongation at break. When full ionization of the polymer was reached, at 20-25 wt.%, more than 200% elongation at break and 0.3 GPa elastic modulus were obtained, which compared with the 80% elongation at break and 3.0 GPa in pure water show the great differences. The IR measurements showed clearly that the chemical environment of the benzimidazole moieties changed greatly from the dissociation of the acidic proton. The result was that the deprotonated form of PBI predominates when the KOH concentration of the bulk solution is around 15-20%.

In order to discuss the different membranes based on polybenzimidazoles the classification of anion exchange membranes made by Merle et al. will be useful [8]. Membranes are classified in three main groups: heterogeneous membranes, interpenetrating polymer networks and homogeneous membranes. The heterogeneous membranes are composed by an anion exchange material embedded in an inert compound and can be divided in ion-solvating polymers if the inert compound is a salt or hybrid membranes in it is an inorganic segment. Polybenzimidazoles alone or blended with other polymers would fall into the category of ion-solvating polymers. The interpenetrating polymer network is a combination of two polymers in which one or both are synthesised or crosslinked in the presence of the other without any covalent bonds between them. The homogeneous membranes are composed only by the anion exchange material, forming a one-phase system, where the cationic charges are covalently bond to the polymer backbone. Mobile counter ions are associated with the ionic sites to preserve the electro-neutrality of the polymer. Example of the cationic sites are the quaternary ammonium (QA) groups commonly used in AEMs. Depending on the production method and the starting materials, homogeneous membranes are divided into three types: (co)polymerization of monomers, modification into a polymer and modification on a preformed film.

Alkali doped PBI was investigated by Xing et al. for use in AEMFCs [55]. They obtained very interesting results, like conductivity as high as 9×10^{-2} S cm^{-1} at 25 ºC, higher than 2×10^{-2} S cm^{-1} of a H_2SO_4-doped PBI membrane, or the similar performance in hydrogen/oxygen fuel cells with alkali doped PBI membrane and Nafion 117 membrane. Since that pioneering work extensive attention has been paid to the alkali doped PBI membranes and thus great progress has been made. However, relevant issues are still remaining such as alkali leakage, fuel permeability and mechanical stability. The single cell performance of alkali doped PBIs have

been extensively studied with various fuels [56], such us hydrogen, methanol, ethanol, ethylene glycol, glycerol, formate and borohydrides.

Using hydrogen as fuel, Zarrin et al. [57] have developed a stable and highly ion conductive porous membrane doped with KOH. They found enhanced ionic conductivity by introducing the porosity in the membrane and obtained around twice better cell performance and conductivity compared with a commercial Fumapem® FAA membrane. Moreover, the KOH doped PBI membrane maintained the ionic conductivity after 14 days of stability test, far more than the 3h of the commercial one. The peak power density obtained with the porous PBI membrane of porosity 0.7 was 72 mW cm^{-2}, better than the 41 and 45 mW cm^{-2} obtained with a dense PBI membrane and the commercial FAA membrane respectively. This better performance was demonstrated to be ascribed to the fact that the porous structure offered a higher ion transport rate through the membrane. One of the previously mentioned issues is the gradual alkali leakage during the cell operation. To solve it Zeng et al. [58] synthesized a sandwiched porous PBI membrane doped with KOH. The pore-forming method rendered numerous sponge-like walls and interconnected macropores, improving the interaction between the PBI and the doping alkali, indicating that both anionic conductivity and alkali retention could be enhanced by this method. Using this sandwiched porous PBI membrane doped with KOH in an AEMFC they obtained an open-circuit voltage (OCV) of 1.0 V and a peak power density of 544 mW cm^{-2} at 90ºC, which was higher than using the conventional membrane structure. They also investigated the durability of the fuel cell at a constant current density of 700 mW cm^{-2} and found that the conventional fuel cell had a dramatic voltage drop after short operation time, which was ascribed to the progressive release of the alkali solution. On the other hand, the sandwiched porous membranes performed with improved stability, the voltages reduced gradually to 0.1 V and remained there for another 25 h approximately. They explained that the performance enhancement was attributed to the retarding in the release of the alkali solution from the sponge-shaped wall, maintaining the high conductivity of the membrane. However, finally the leakage occurred but as the authors indicated, the membrane could be reused after doping with KOH solution again.

Other approach was the used by Lu et al. [59]. They used PBI to react with poly(vinylbenzyl chloride) (PVBC), a polymer commonly used by other groups as for example Varcoe et al. in their grafted PTFE membranes [60,61]. PVBC has the advantage of reacting with the imidazole rings of PBI creating a crosslinking connection with remaining -CH_2Cl groups unreacted that can be later functionalized as desired. For the functionalization of these groups they decided to use the diamine 1,4-diazabicyclo[2.2.2]octane (DABCO), a very stable amine in

alkaline media specially when only one of the two nitrogen is quaternized as previously reported [5,8]. This method had the advantage that quaternization is done in the already casted membrane so it can be ensured that only one of the nitrogens react with PVBC obtaining the stability desired. Thanks to the good mechanical properties of PBI they obtained membranes with good flexibility and strength both in dry conditions and saturated in water as well as high hydroxide conductivity (>25 mS cm^{-1} at room temperature) and superior chemical stability in alkaline environment. They tested the membrane in the H_2/O_2 fuel cell obtaining a peak power density of 230mWcm^{-2} at 50 ºC and performed stability test, which showed high durability both in the constant current and continuous open circuit voltage.

In addition to be used anion exchange membrane, alkali doped PBI can work as ionomer, serving as ion-conductive pathway in the catalyst layer as well as a binder. Matsumoto et al. [62] developed a well-structured electrocatalyst for AEMFCs composed of carbon nanotubes (CNT), KOH doped PBI ionomer and platinum nanoparticles. This allowed them to obtain high effective diffusivity and improved electrochemical activity and they obtained a peak power density of 256mWcm^{-2} at 50 °C when tested in a H_2/O_2 fuel cell.

For fuel cells running on methanol, Hou et al. [63] tested a direct methanol fuel cell with a KOH doped PBI membrane and observed that when a mixed solution of 2.0M methanol and 2.0M KOH was used as fuel the OCV was around 1.0 V and the peak power density was 31 mW cm^{-2} at 90ºC. Wu et al. [64] prepared a membrane of KOH doped PBI with CNT nanocomposites and obtained maximum power densities of 67mWcm^{-2} and 104mWcm^{-2} at 60 and 90ºC respectively with a fuel composition of 2.0M methanol + 6.0M KOH and humidified oxygen. Li et al. [65] worked with pristine PBI membrane synthesised by solution casting method and treated it separately with 2.0M $H_3PO_4$and 6.0M KOH to prepare a PEM and an AEM respectively. They also studied several parameters of the structure design and operating parameters. They found that the conductivity of the KOH doped PBI membrane was higher than the phosphoric acid membrane, 21.6 and 7.9 mS cm^{-1} respectively. They also obtained a higher peak power density with the KOH doped PBI membrane, 117.9mWcm^{-2} at 90 °C, than with the acid one, 46.5mWcm^{-2}. They even reached a peak power density of 158.9mWcm^{-2} at 90 °C when using a free-microporous layer electrodes and tripled the fuel flow rate.

In fuel cells running on ethanol, Hou et al. [66] developed a KOH doped PBI membrane and found that with fuel composition of 2.0M ethanol +2.0M KOH they obtained OCV of 0.92 V and maximum power density of 42.9 mW cm^{-2} at 75ºC and 0.97 V and 60.9 mW cm^{-2} at 90ºC. Modestov et al. [67] fabricated a

membrane electrode assembly (MEA) employing non-platinum electrocatalysts and a KOH doped membrane. In the anode they used a mixed solution of 3.0M KOH +2.0 M ethanol as fuel while in the cathode they used air flow. With these conditions and at temperature of 80 ºC a peak power density of 100 mW cm^{-2} was obtained at a voltage of 0.4 V. It was also found that by operating the fuel cell with pure oxygen the current density was improved by 10%. Also using ethanol as fuel, recently Herranz et al. [33] tested the fuel cell performance of membranes synthesised with PBI and poly(vinyl alcohol) (PVA) with different weight ratios. PVA alcohol groups interacted with PBI by hydrogen bonding as well as allowing enhanced conductivity of the hydroxyl anion through the membranes. The increasing content in the PVA blend membrane lead to higher conductivities but if excessive could bring structural problems since PBI demonstrated to be essential for the membrane integrity. PVA:PBI 4:1 membrane obtained the best performance with a peak power density of 76 mW cm^{-2} at 90ºC, 50% higher than a pristine KOH doped PBI tested in the same conditions.

ABPBI has also been widely investigated for AEMs synthesis and application. Luo et al. [68] synthesised ABPBI and prepared the pristine membranes by the solution casting method. They studied the conductivity of the membranes at various alkali doping levels. They found high conductivity values for the membranes as 2.3×10^{-2} Scm^{-1} at 25ºC and 7.3×10^{-2} Scm^{-1} at 100 °C in the ABPBI membrane with alkali doping level of 0.37. They also founded the membranes have great thermal stability and excellent chemical stability, demonstrated by maintaining the conductivity values in alkaline media at 100ºC for more than 1000h.

Other alcohols and fuels have also been tested in AEMFCs using polybenzimidazoles in the membrane structure, showing promising results [69,70]. Overall, the applicability and interest of benzimidazoles as AEMs are actual and will continue increasing due to their excellent properties.

f) Conclusions polybenzimidazoles

Polybenzimidazoles have been deeply studied in the last decades and great advancements have been done in their synthesis, making them economical materials with excellent thermal and mechanical properties as well as high chemical resistance in acidic and alkaline media. Their special structure with imidazole moieties and high intermolecular hydrogen bonding makes them excellent materials to be used and ion exchange membranes for fuel cells. They can be used alone or in combination with other polymers or compounds, like the ionic liquids, as has been demonstrated many times. With them, it is possible to reach performances similar to other fuel cells and allow the application at higher temperatures, with all the benefits that implies. In the acidic media temperatures

in the range of 120 to 200ºC are used with good performances and easier water management but still issues like structural stability with high doping level have to be solved. In order to help with the conductivity ionic liquids have been investigated because of their non aqueous and low volatility properties as proton carriers. Interesting developments have been done but further research is necessary. In the alkaline media their application has also attracted great interest. The ionization of the structure has been clearly identified at certain doping levels and the plasticizing effects it has. Pristine polybenzimidazole membranes have been directly doped with alkali solutions obtaining very good conductivity values and other strategies like crosslinking with other polymers or synthesis of blend membranes have reported also promising results. The fuel cell performance is not yet as good as in the acidic media but good results around 100 mW cm^{-2} have been obtained. Commercialization of membranes and MEAs based of PBI shows the potential they have and research continues nowadays to develop them even more and better understand the possibilities of these wonderful materials in the fuel cell technology and the energy applications.

3.2 Other polymers used to synthesise membranes

Polybenzimidazoles have been at the core of the studied membranes in this research, but always combined with other polymeric materials. The most important used were poly(vinyl alcohol) (PVA) and poly(vinylbenzyl chloride) (PVBC), which properties and contribution to the membranes will be explained in the relevant chapters. Ethylene tetrafluoroethylene (ETFE) will be also further commented since membranes and ionomers based on this material were used to study new chemistries of quaternary ammonium head groups, as well as the properties of the tertiary amines used for quaternization: 1,4-diazabicyclo[2.2.2]octane (DABCO) and N-methylpiperidine (MPRD).

3.3 Ionomers

The ionomers are the polymeric materials used, in solution or dispersion form, to work as binder between the catalyst particles and with the support and the membrane. They also have the important functionality of introducing ionic conductivity in the electrode, since they are ion exchange materials as well as the membranes. The use of the ionomers can greatly enhance the performance of the fuel cell by maximizing the catalyst utilization, this effect is based in the

optimization of the tri-phase interface between the fuel diffusion, the ionic conduction and the electronic conduction pathways, making these places available to the maximum extent of catalyst surface (a descriptive illustration is presented in Figure 3.13 in the Experimental chapter). The ionomers have been used extensively in the proton exchange membrane fuel cells and more recently they are being also extensively studied for the alkaline polymer electrolyte membrane fuel cell application. The acidic ionomers most studied, used and commercially available are the Nafion® dispersions representing the state of the art [71]. In the alkaline media there are not yet well stablished ionomer materials, commercial anion exchange ionomers have been developed by Tokuyama [72] or Fumatech [73] but many groups use the Nafion® ones, mainly for the very good binder properties even if no better hydroxide conductivity is obtained.

Other interesting aspect is the effect of the cationic head groups of the anion exchange ionomers in the electrode reactions, since they are in such close contact. From the studies made so far, some conclusions can be made like the almost no effect of the Cl^- ion in the ORR over Pt, contrary to the observations in acidic media or the oxidation of organic cations by Pt at high potentials and the possible impact of the degradation products on the ORR performance. It has also been formulated that for further study the reactions taking place in these conditions, a good strategy would be to compare anion exchange ionomers with different head groups but similar backbone. It should also be considered the use of Nafion®-ionomer free systems and the use of electrolyte solutions without fully solubilized cationic molecules [5].

It can be concluded that the study of different anion exchange ionomer chemistries is still in development and great advances in fuel cell performance and stability can be obtained by using them.

4 References of the chapter: Introduction

[1] ENERDATA, Global Energy Estatistical Yearbook 2018, (n.d.). https://yearbook.enerdata.net/total-energy/world-energy-production.html (accessed April 13, 2019).

[2] International Energy Agency, (n.d.). https://www.iea.org/statistics/?country=WORLD&year=2016&category=Energy supply&indicator=TPESbySource&mode=chart&dataTable=BALANCES (accessed April 13, 2019).

[3] H.R. Corti, E.R. Gonzalez, Direct Alcohol Fuel Cells, Springer, Dordrech, 2014. doi:10.1007/978-94-007-7708-8.

[4] Y. Wang, K.S. Chen, J. Mishler, S.C. Cho, X.C. Adroher, A review of polymer electrolyte membrane fuel cells: Technology, applications, and needs on fundamental research, Appl. Energy. 88 (2011) 981–1007. doi:10.1016/j.apenergy.2010.09.030.

[5] J.R. Varcoe, P. Atanassov, D.R. Dekel, A.M. Herring, M. a. Hickner, P. a. Kohl, A.R. Kucernak, W.E. Mustain, K. Nijmeijer, K. Scott, T. Xu, L. Zhuang, Anion-exchange membranes in electrochemical energy systems, Energy Environ. Sci. 7 (2014) 3135–3191. doi:10.1039/b000000x.

[6] Z. Zakaria, S.K. Kamarudin, S.N. Timmiati, Membranes for direct ethanol fuel cells: An overview, Appl. Energy. 163 (2016) 334–342. doi:10.1016/j.apenergy.2015.10.124.

[7] B. Smitha, S. Sridhar, a. a. Khan, Solid polymer electrolyte membranes for fuel cell applications - A review, J. Memb. Sci. 259 (2005) 10–26. doi:10.1016/j.memsci.2005.01.035.

[8] G. Merle, M. Wessling, K. Nijmeijer, Anion exchange membranes for alkaline fuel cells: A review, J. Memb. Sci. 377 (2011) 1–35. doi:10.1016/j.memsci.2011.04.043.

[9] Z.F. Pan, L. An, T.S. Zhao, Z.K. Tang, Advances and challenges in alkaline anion exchange membrane fuel cells, Prog. Energy Combust. Sci. 66 (2018) 141–175. doi:10.1016/j.pecs.2018.01.001.

[10] R.P. O'Hayre, S.-W. Cha, W. COLELLA, F.B. PRINZ, eds., Fuel cell fundamentals, 3th ed., John Wiley & Sons, Hoboken, New Jersey, 2016. doi:10.1002/9781119191766.

[11] D. Pletcher, X. Li, Prospects for alkaline zero gap water electrolysers for hydrogen production, Int. J. Hydrogen Energy. 36 (2011) 15089–15104. doi:10.1016/j.ijhydene.2011.08.080.

[12] Robert O. Ebewele, Polymer Science and Technology, CRC Press LLC, Boca Raton, New York, 1985. doi:10.1016/0025-5416(85)90434-3.

[13] H. Vogel, C.S. Marvel, Polybenzimidazoles, New Thermally Stable

Polymers, J. Polym. Sci. 50 (1961) 511–539. doi:https://doi.org/10.1002/pol.1961.1205015419.

[14] E. Choe, Catalysts for the Preparation of Polybenzimidazoles, J. Appl. Polym. Sci. 53 (1994) 497–506. doi:https://doi.org/10.1002/app.1994.070530504.

[15] C. EW, Single-stage melt polymerization process for the production of high molecular weight polybenzimidazole, US patent 4,312,976, 1982.

[16] Q. Li, J.O. Jensen, R.F. Savinell, N.J. Bjerrum, High temperature proton exchange membranes based on polybenzimidazoles for fuel cells, Prog. Polym. Sci. 34 (2009) 449–477. doi:10.1016/j.progpolymsci.2008.12.003.

[17] J. Yang, R. He, D. Aili, Synthesis of Polybenzimidazoles, in: High Temp. Polym. Electrolyte Membr. Fuel Cells, Springer Switzerland, 2016. doi:10.1007/978-3-319-17082-4_7.

[18] Y. Iwakura, K. Uno, Y. Imai, Polyphenylenebenzimidazoles, J. Polym. Sci. 2 (1964) 2605–2615. doi:https://doi.org/10.1002/pol.1964.100020611.

[19] P.E. Eaton, G.R. Carlson, J.T. Lee, Phosphorus pentoxide-methanesulfonic acid. Convenient alternative to polyphosphoric acid, J. Org. Chem. 38 (1973) 4071–4073. doi:10.1021/jo00987a028.

[20] H. Kim, S.Y. Cho, S.J. An, Y.C. Eun, J. Kim, H. Yoon, H. Kweon, K.H. Yew, Synthesis of Poly (2,5-benzimidazole) for use as a Fuel-Cell Membrane, Macromolecurar Rapid Commun. 25 (2004) 894–897. doi:10.1002/marc.200300288.

[21] J. Jouanneau, R. Mercier, L. Gonon, G. Gebel, Synthesis of Sulfonated Polybenzimidazoles from Functionalized Monomers : Preparation of Ionic Conducting Membranes, Macromolecules. 40 (2007) 983–990. doi:10.1021/ma0614139.

[22] W. JS, L. MH, S. RF, High temperature membranes, in: V. W, L. A, G. HA (Eds.), Handb. Fuel Cells, Vol. 3, John Wiley & Sons Ltd, United States, 2003: pp. 436–446.

[23] J.A. Asensio, S. Borro, P. Gómez-Romero, Polymer Electrolyte Fuel Cells Based on Phosphoric Acid-Impregnated Poly(2,5-benzimidazole) Membranes, J. Electrochem. Soc. 151 (2004) 304–310. doi:10.1149/1.1640628.

[24] J.A. Asensio, S. Borrós, P. Gómez-Romero, Proton-conducting membranes based on poly (2,5-benzimidazole) (ABPBI) and phosphoric acid prepared by direct acid casting, J. Memb. Sci. 241 (2004) 89–93. doi:10.1016/j.memsci.2004.03.044.

[25] K.J. Fishel, A.L. Gulledge, A.T. Pingitore, J.P. Hoffman, W.P. Steckle, B.C. Benicewicz, Solution Polymerization of Polybenzimidazole, J. Polym. Sci. Part A Polym. Chem. 54 (2016) 1795–1802. doi:10.1002/pola.28041.

[26] M. Litt, R. Ameri, Y. Wang, R. Savinell, J. Wainwright, Polybenzimidazoles/phosphoric acid solid polymer electrolytes:

mechanical and electrical properties, Mater Res Soc Symp Proc. 548 (1999) 313–323. doi:10.1557/PROC-548-313.

[27] R.H. He, B.Y. Sun, J.S. Yang, Q.T. Che, Synthesis of poly[2,2'-(m-phenylene)-5,5'-bibenzimidazole] and poly(2,5-benzimidazole) by microwave irradiation, Chem. Res. Chinese Univ. 25 (2009) 585–589. https://www.scopus.com/record/display.uri?eid=2-s2.0-78349266007&origin=resultslist&sort=plf-f&src=s&st1=yang&st2=microwave+irradiation&nlo=&nlr=&nls=&sid=d064d47c88ea37b8ad94d286d431cc59&sot=b&sdt=cl&cluster=scopubyr%2C%222009%22%2Ct&sl=60&s=%28AUTHOR-NA.

[28] J. Yang, R. He, Q. Che, X. Gao, L. Shi, A copolymer of poly[2,2'-(m-phenylene)-5,5'- bibenzimidazole] and poly(2,5-benzimidazole) for high-temperature proton-conducting membranes, Polym. Int. 59 (2010) 1695–1700. doi:10.1002/pi.2906.

[29] F. Conti, S. Willbold, S. Mammi, C. Korte, W. Lehnert, D. Stolten, Carbon NMR investigation of the polybenzimidazole–dimethylacetamide interactions in membranes for fuel cells, New J. Chem. 37 (2013) 152. doi:10.1039/c2nj40728k.

[30] P. Musto, F.E. Karasz, W.J. MacKnight, Hydrogen bonding in polybenzimidazole/polyimide systems: a Fourier-transform infra-red investigation using low-molecular-weight monofunctional probes, Polymer (Guildf). 30 (1989) 1012–1021. doi:10.1016/0032-3861(89)90072-4.

[31] Q. Li, R. He, R.W. Berg, H.A. Hjuler, N.J. Bjerrum, Water uptake and acid doping of polybenzimidazoles as electrolyte membranes for fuel cells, Solid State Ionics. 168 (2004) 177–185. doi:10.1016/j.ssi.2004.02.013.

[32] L.A. Diaz, J. Hnat, N. Heredia, M.M. Bruno, F.A. Viva, M. Paidar, H.R. Corti, K. Bouzek, G.C. Abuin, Alkali doped poly (2,5-benzimidazole) membrane for alkaline water electrolysis: Characterization and performance, J. Power Sources. 312 (2016) 128–136. doi:10.1016/j.jpowsour.2016.02.032.

[33] D. Herranz, R. Escudero-Cid, M. Montiel, C. Palacio, E. Fatás, P. Ocón, Poly (vinyl alcohol) and poly (benzimidazole) blend membranes for high performance alkaline direct ethanol fuel cells, Renew. Energy. 127 (2018) 883–895. doi:10.1007/978-3-642-20487-6.

[34] J.A. Asensio, S. Borrós, P. Gómez-Romero, Proton-conducting polymers based on benzimidazoles and sulfonated benzimidazoles, J. Polym. Sci. Part A Polym. Chem. 40 (2002) 3703–3710. doi:10.1002/pola.10451.

[35] D. Aili, K. Jankova, J. Han, N.J. Bjerrum, J.O. Jensen, Q. Li, Understanding ternary poly(potassium benzimidazolide)-based polymer electrolytes, Polymer (Guildf). 84 (2016) 304–310. doi:10.1016/j.polymer.2016.01.011.

[36] J. Mader, L. Xiao, T.J. Schmidt, B. Fuel, V. Ave, Polybenzimidazole/Acid

Complexes as High-Temperature Membranes, Adv Polym Sci. 216 (2008) 63–124. doi:10.1007/12.

[37] BASF Proton-Conductive Membrane, (n.d.). https://www.basf.com/global/en/who-we-are/organization/locations/europe/german-companies/BASF_New-Business-GmbH/our-solutions/proton-conductive-membrane.html (accessed February 10, 2019).

[38] PBI products. Celazole PBI, (n.d.). https://pbipolymer.com/markets/membrane/ (accessed February 10, 2019).

[39] Danish Power Systems High Temperature PEM Fuel Cells, (n.d.). http://daposy.com/fuel-cells (accessed February 10, 2019).

[40] J.S. Wainright, J.-T. Wang, D. Weng, R.F. Savinell, M. Litt, Acid-Doped Polybenzimidazoles: A New Polymer Electrolyte, J. Electrochem. Soc. 142 (1995) L121–L123. doi:10.1149/1.2044337.

[41] D. Weng, J.S. Wainright, U. Landau, R.F. Savinell, Electro-osmotic Drag Coefficient of Water and Methanol in Polymer Electrolytes at Elevated Temperatures, J. Electrochem. Soc. 143 (1996) 1260–1263. doi:10.1149/1.1836626.

[42] A. Chandan, M. Hattenberger, A. El-Kharouf, S. Du, A. Dhir, V. Self, B.G. Pollet, A. Ingram, W. Bujalski, High temperature (HT) polymer electrolyte membrane fuel cells (PEMFC)-A review, J. Power Sources. 231 (2013) 264–278. doi:10.1016/j.jpowsour.2012.11.126.

[43] K.D. Kreuer, A. Fuchs, M. Ise, M. Spaeth, J. Maier, Imidazole and pyrazole-based proton conducting polymers and liquids, Electrochim. Acta. 43 (1998) 1281–1288. doi:10.1016/S0013-4686(97)10031-7.

[44] Y.-L. Ma, J.S. Wainright, M.H. Litt, R.F. Savinell, Conductivity of PBI Membranes for High-Temperature Polymer Electrolyte Fuel Cells, J. Electrochem. Soc. 151 (2004) A8–A16. doi:10.1149/1.1630037.

[45] W. Vielstich, A. Lamm, H.A. Gasteiger, H. Yokokawa, eds., Handbook of Fuel Cells: Fundamentals, Technology, Applications, John Wiley & Sons, Ltd., United States, 2009.

[46] D. Aili, T. Allward, S.M. Alfaro, C. Hartmann-Thompson, T. Steenberg, H.A. Hjuler, Q. Li, J.O. Jensen, E.J. Stark, Polybenzimidazole and sulfonated polyhedral oligosilsesquioxane composite membranes for high temperature polymer electrolyte membrane fuel cells, Electrochim. Acta. 140 (2014) 182–190. doi:10.1016/j.electacta.2014.03.047.

[47] J. Wu, X.Z. Yuan, J.J. Martin, H. Wang, J. Zhang, J. Shen, S. Wu, W. Merida, A review of PEM fuel cell durability: Degradation mechanisms and mitigation strategies, J. Power Sources. 184 (2008) 104–119. doi:10.1016/j.jpowsour.2008.06.006.

[48] M.A.B.H. Susan, A. Noda, S. Mitsushima, M. Watanabe, Brønsted acid–base ionic liquids and their use as new materials for anhydrous proton conductors, Chem. Commun. 3 (2003) 938–939. doi:10.1039/b300959a.

[49] H. Ye, J. Huang, J.J. Xu, N.K.A.C. Kodiweera, J.R.P. Jayakody, S.G. Greenbaum, New membranes based on ionic liquids for PEM fuel cells at elevated temperatures, J. Power Sources. 178 (2008) 651–660. doi:10.1016/j.jpowsour.2007.07.074.

[50] J. Schauer, A. Sikora, M. Plíšková, J. Mališ, P. Mazúr, M. Paidar, K. Bouzek, Ion-conductive polymer membranes containing 1-butyl-3-methylimidazolium trifluoromethanesulfonate and 1-ethylimidazolium trifluoromethanesulfonate, J. Memb. Sci. 367 (2011) 332–339. doi:10.1016/j.memsci.2010.11.018.

[51] J.T.W. Wang, S.L.C. Hsu, Enhanced high-temperature polymer electrolyte membrane for fuel cells based on polybenzimidazole and ionic liquids, Electrochim. Acta. 56 (2011) 2842–2846. doi:10.1016/j.electacta.2010.12.069.

[52] Q. Che, R. He, J. Yang, L. Feng, R.F. Savinell, Phosphoric acid doped high temperature proton exchange membranes based on sulfonated polyetheretherketone incorporated with ionic liquids, Electrochem. Commun. 12 (2010) 647–649. doi:10.1016/j.elecom.2010.02.021.

[53] M. Mamlouk, P. Ocon, K. Scott, Preparation and characterization of polybenzimidazole/diethylamine hydrogen sulphate for medium temperature proton exchange membrane fuel cells, J. Power Sources. 245 (2014) 915–926. doi:10.1016/j.jpowsour.2013.07.050.

[54] V. Vijayakumar, S.Y. Nam, Recent advancements in applications of alkaline anion exchange membranes for polymer electrolyte fuel cells, J. Ind. Eng. Chem. 70 (2019) 70–86. doi:10.1016/j.jiec.2018.10.026.

[55] B. Xing, O. Savadogo, Hydrogen/oxygen polymer electrolyte membrane fuel cells (PEMFCs) based on alkaline-doped polybenzimidazole (PBI), Electrochem. Commun. 2 (2000) 697–702. doi:10.1016/S1388-2481(00)00107-7.

[56] Q.X. Wu, Z.F. Pan, L. An, Recent advances in alkali-doped polybenzimidazole membranes for fuel cell applications, Renew. Sustain. Energy Rev. 89 (2018) 168–183. doi:10.1016/j.rser.2018.03.024.

[57] H. Zarrin, G. Jiang, G.Y.-Y. Lam, M. Fowler, Z. Chen, High performance porous polybenzimidazole membrane for alkaline fuel cells, Int. J. Hydrogen Energy. 39 (2014) 18405–18415. doi:10.1016/j.ijhydene.2014.08.134.

[58] L. Zeng, T.S. Zhao, L. An, G. Zhao, X.H. Yan, A high-performance sandwiched-porous polybenzimidazole membrane with enhanced alkaline retention for anion exchange membrane fuel cells, Energy Environ. Sci. 8 (2015) 2768–2774. doi:10.1039/c5ee02047f.

[59] W. Lu, G. Zhang, J. Li, J. Hao, F. Wei, W. Li, J. Zhang, Z.-G. Shao, B. Yi, Polybenzimidazole-crosslinked poly(vinylbenzyl chloride) with quaternary 1,4-diazabicyclo (2.2.2) octane groups as high-performance anion exchange membrane for fuel cells, J. Power Sources. 296 (2015) 204–214. doi:10.1016/j.jpowsour.2015.07.048.

[60] H. Herman, R.C.T. Slade, J.R. Varcoe, The radiation-grafting of vinylbenzyl chloride onto poly(hexafluoropropylene-co-tetrafluoroethylene) films with subsequent conversion to alkaline anion-exchange membranes: Optimisation of the experimental conditions and characterisation, J. Memb. Sci. 218 (2003) 147–163. doi:10.1016/S0376-7388(03)00167-4.

[61] S.D. Poynton, R.C.T. Slade, T.J. Omasta, W.E. Mustain, R. Escudero-Cid, P. Ocón, J.R. Varcoe, Preparation of radiation-grafted powders for use as anion exchange ionomers in alkaline polymer electrolyte fuel cells, J. Mater. Chem. A. 2 (2014) 5124–5130. doi:10.1039/c4ta00558a.

[62] K. Matsumoto, T. Fujigaya, H. Yanagi, N. Nakashima, Very high performance alkali anion-exchange membrane fuel cells, Adv. Funct. Mater. 21 (2011) 1089–1094. doi:10.1002/adfm.201001806.

[63] H. Hou, G. Sun, R. He, B. Sun, W. Jin, H. Liu, Q. Xin, Alkali doped polybenzimidazole membrane for alkaline direct methanol fuel cell, Int. J. Hydrogen Energy. 33 (2008) 7172–7176. doi:10.1016/j.ijhydene.2008.09.023.

[64] J.F. Wu, C.F. Lo, L.Y. Li, H.Y. Li, C.M. Chang, K.S. Liao, C.C. Hu, Y.L. Liu, S.J. Lue, Thermally stable polybenzimidazole/carbon nano-tube composites for alkaline direct methanol fuel cell applications, J. Power Sources. 246 (2014) 39–48. doi:10.1016/j.jpowsour.2013.05.171.

[65] L.-Y. Li, B.-C. Yu, C.-M. Shih, S.J. Lue, Polybenzimidazole membranes for direct methanol fuel cell: Acid-doped or alkali-doped?, J. Power Sources. 287 (2015) 386–395. doi:10.1016/j.jpowsour.2015.04.018.

[66] H. Hou, G. Sun, R. He, Z. Wu, B. Sun, Alkali doped polybenzimidazole membrane for high performance alkaline direct ethanol fuel cell, J. Power Sources. 182 (2008) 95–99. doi:10.1016/j.jpowsour.2008.04.010.

[67] A.D. Modestov, M.R. Tarasevich, A.Y. Leykin, V.Y. Filimonov, MEA for alkaline direct ethanol fuel cell with alkali doped PBI membrane and non-platinum electrodes, J. Power Sources. 188 (2009) 502–506. doi:10.1016/j.jpowsour.2008.11.118.

[68] H. Luo, G. Vaivars, B. Agboola, S. Mu, M. Mathe, Anion exchange membrane based on alkali doped poly(2,5-benzimidazole) for fuel cell, Solid State Ionics. 208 (2012) 52–55. doi:10.1016/j.ssi.2011.11.029.

[69] R.N. Couto, J.J. Linares, KOH-doped polybenzimidazole for alkaline direct glycerol fuel cells, J. Memb. Sci. 486 (2015) 239–247. doi:10.1016/j.memsci.2015.03.031.

[70] L. Zeng, T.S. Zhao, L. An, G. Zhao, X.H. Yan, Physicochemical properties of alkaline doped polybenzimidazole membranes for anion exchange membrane fuel cells, J. Memb. Sci. 493 (2015) 340–348. doi:10.1016/j.memsci.2015.06.013.

[71] K.A. Mauritz, R.B. Moore, State of Understanding of Nafion, Chem. Rev. 104 (2004) 4535–4586. doi:10.1021/cr0207123.

[72] G.K.S. Prakash, F.C. Krause, F.A. Viva, S.R. Narayanan, G.A. Olah,

Study of operating conditions and cell design on the performance of alkaline anion exchange membrane based direct methanol fuel cells, J. Power Sources. 196 (2011) 7967–7972. doi:10.1016/j.jpowsour.2011.05.056.

[73] M.S. Naughton, G.H. Gu, A.A. Moradia, P.J.A. Kenis, Tailoring electrode hydrophobicity to improve anode performance in alkaline media, J. Power Sources. 242 (2013) 581–588. doi:10.1016/j.jpowsour.2013.05.054.

CHAPTER 2. Objectives

Objectives

The work of this Thesis is based in the search of optimised anion exchange materials for working in low temperature alkaline fuel cells and electrolysers. Different strategies must be used in order to combine polybenzimidazoles with other polymers and also different quaternary ammonium groups have been utilized in the synthesis and tested in operation. The following main objectives are suggested to achieve the good development of anionic exchange membranes for use in the above devices:

- Synthesise blend membranes with different ratios of polybenzimidazoles with poly (vinylalcohol) (PVA) using the casting method. Perform a complete characterization to understand the properties of the membranes.

- Study the performance of PVA:polybenzimidazole membranes in a single cell alkaline direct ethanol fuel cell (DEFC) and in a zero gap liquid alkaline water electrolyser (LAWE).

- Develop membranes based on polybenzimidazoles crosslinked with poly (vinylbenzyl chloride) (PVBC) in different ratios. Form quaternary ammonium groups by reaction with 1,4-diazabicyclo [2.2.2] octane (DABCO) and characterize the membrane composition and properties.

- Test the polybenzimidazole-c-PVBC membranes in the alkaline DEFC and the zero gap LAWE to evaluate their performance in these electrochemical devices.

- Prepare membranes based in ethylene tetrafluoroethylene (ETFE) and aminate them with different amines to obtain stable quaternary ammonium head groups and finally evaluate these membranes in an alkaline polymer anion exchange electrolyte fuel cell.

CHAPTER 3. Experimental

Experimental

1 Synthesis of anion exchange membranes and ionomers

The description of the synthesis of the materials used in this Thesis is described below. Special emphasis and details are given since it represents a relevant part of the work done in the laboratory.

1.1 PVA:polybenzimidazole membranes

The synthesis of these membranes has been done using the casting method [1], which consist in the controlled evaporation of a solution containing the polymeric materials to form a film when all the solvent is removed. The advantage of this method is the good homogeneity that can be achieved and the control of the thickness of the membranes after a few test experiments. The surface where the casting is done is very important in terms of affinity to the solution. A surface that repels the solution will make difficult to form thin membranes but a surface that interacts too much will make very hard to peel off the membrane after the casting. It is also important the complete flatness of the surface so the thickness of the resulting membrane is homogeneous at every spot of the area.

Two series of membranes were prepared, one with poly(2,2'-(*m*-phenylene)-5,5'-bibenzimidazole) (PBI) and poly(vinyl alcohol) alcohol (PVA) and the other with poly(2,5-benzimidazole) (ABPBI) and PVA.

For the PVA:PBI membranes, a solution of 3,5 wt.% PBI in N,N-dimethylacetamide (DMAc) was prepared with 3.5 g of PBI powder (BETWEEN, LizenzGMBH, density 0.7-0.9 dL g^{-1}) in 96.5 g of DMAc (99.5%, Sigma Aldrich) by heating at 80 ºC for 48 h, another solution was prepared of 5 wt.% PVA in dimethyl sulfoxide (DMSO) by heating at 85 ºC for 30 min, 1 g of PVA

(hydrolysed, powder of MW 89.000-98.000, 99 %, Sigma Aldrich) in 20 g of DMSO (99.9%, Sigma Aldrich), both under continuous stirring. To prepare membranes with different weight ratios, the appropriate amounts of each solution were mixed in a glass baker and stirred at 500 rpm 40 min at room temperature. Then the solution was placed in Petri dishes with PTFE liner of 50 mm diameter (Welch Fluorocarbon) (approximately 5 mg of solution for the PVA:PBI 4:1 membrane). For the casting process the Petri dishes were introduced into a vacuum oven (Memert VO200, see Figure 3.1b) were a first ramp was done to reduce the pressure from ambient pressure to 10 mbar and raise the temperature to 40 ºC in 1 h. Then the pressure and temperature were maintained at 10 mbar and 40 ºC overnight. After the casting the membranes were easily peeled off the ETFE liner and stored in sealed inert plastic bags until needed.

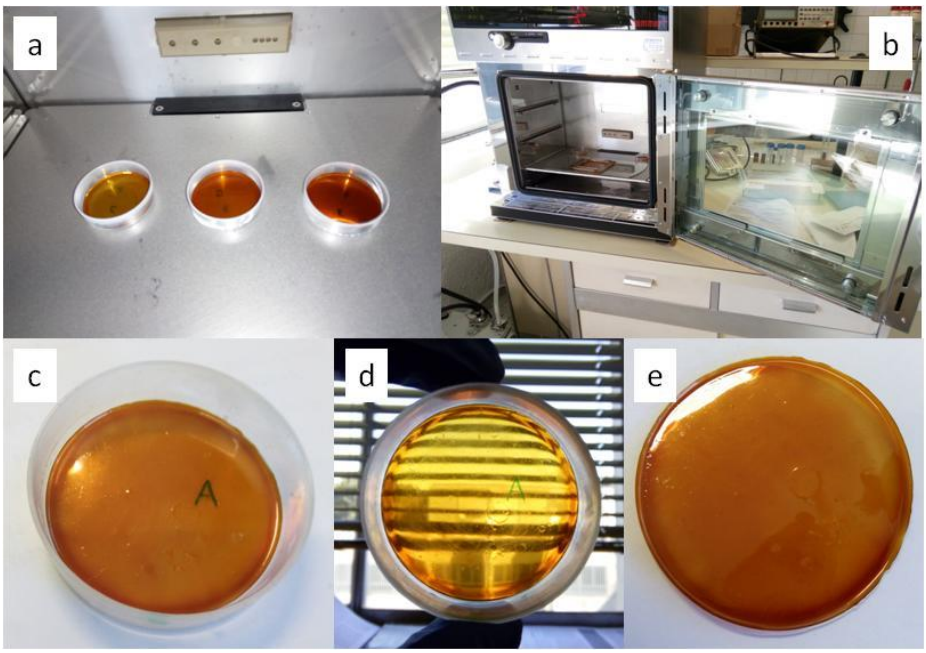

Figure 3.1. Casting process in vacuum oven of PVA:PBI membranes.

In the case of the PVA:ABPBI membranes, first the ABPBI polymer was synthesised via condensation of 3,4-diaminobenzoic acid monomer (DABA, 97 wt%) in polyphosphoric acid (PPA, 85 wt%, Aldrich), subsequently it was neutralised, washed, dried and milled following the procedure reported by Abuin et al. [2]. The measured intrinsic viscosity of the polymer solution in 96 wt.% H_2SO_4 at 30 °C was 2.96 dL g^{-1}, from this value the averaged molecular weight was calculated according to the Mark-Houwink equation [3], obtaining 23,200 g mol^{-1}.

Then, a solution of 1 wt.% PVA in DMSO was prepared by heating at 80 ºC for 30 min under continuous stirring and then cooling down naturally to room temperature. Dissolution of ABPBI was done in a mixture of absolute ethanol/NaOH according to a previously reported method [4]. To achieve complete dissolution of ABPBI the mixture was refluxed at 50 ºC. The final solution contained 1 wt.% of ABPBI and 1 wt.% of NaOH. Depending of the desired ratio of the polymers, the corresponding quantities of solutions, previously heated at 50 ºC, were mixed in a glass beaker by gently stirring. For the casting process the mixture was placed in glass Petri dishes of 70 mm diameter (Duran™ Steriplan Soda-lime Petri dishes) in an air convection oven (San Jor SE60DF) and maintained overnight at 50ºC. The mixture of both hot solutions is important in order to obtain a homogeneous final solution and membranes. After the casting, immersion in ultrapure water (UPW) was used to help peeling off the membranes from the Petri dishes and they were finally stored in sealed inert plastic bags until used.

These membranes are denoted as "linear" (L-): L-PVA:PBI and L-PVA:ABPBI in contrast to the "crosslinked" (C-) ones: C-PVA:PBI and C-PVA:ABPBI.

The C-PVA:PBI and C-PVA:ABPBI crosslinked membranes were prepared by a procedure previously reported by Yeom et al. [5]. The crosslinking was done by heating the dry linear membranes in different reaction solutions for varying the degree of crosslinking. The reaction solutions contained different amounts of aqueous glutaraldehide solution (GA, 25% aqueous solution, Aldrich), acetone and HCl (35–36 wt%, Biopack).The GA solution content varied from 0.5 vol.% to 50 vol.% and the HCl content was maintained at 0.12 vol.%. When the process was finished, the membranes were washed several times in UPW and immersed in UPW for 24 h at 40 ºC to remove any residual HCl and GA. Finally they were dried in and oven at 50 ºC overnight and stored.

Also membranes composed only of PVA or ABPBI were prepared. L-PVA membranes were prepared from a solution of 1 wt.% PVA in DMSO and L-ABPBI membranes from a solution of 1 wt.% ABPBI in ethanol/NaOH, both by the casting method as previously described. Some of these membranes were also crosslinked by the described crosslinking method with GA. Commercial PBI membranes (Dapozol M-40) from the company Danish Power Systems were used for comparison purposes.

The thickness of the synthesised membranes ranged from 40 to 120 μm (measured with a Mitutoyo Digital Micrometer). When conduction of the hydroxide anions was required, the membranes were doped in aqueous KOH solution. The doping time was done in order to finish just before use. Prior to use, the doped

membranes were rinsed with UPW three or four times to remove the residual superficial KOH.

1.2 Polybenzimidazole-c-PVBC crosslinked membranes quaternized with DABCO

Membranes of polybenzimidazole-c-PVBC were also synthesised by the crosslinking method explained in the previous section. In this case, however, there is an important difference: the crosslinking reaction between PBI or ABPBI with PVBC in solution. Similarly to the PVA:polybenzimidazole membranes, two series of membranes were synthesised: one with different ratios of PBI-c-PVBC and the other with ABPBI-c-PVBC.

In the PBI-c-PVBC membranes, first the desired quantity of solid PVBC (60/40 mixture of 3- and 4- isomers respectively with average molecular weight Mn ~55,000 and Mw~100,000, Sigma Aldrich) was weighted and introduced in a glass vial with the desired quantity of 3.5 wt.% PBI solution in DMAc in order to have the target molar ratio. The ratios of PBI-c-PVBC synthesised ranged from 1:1 to 1:4. Then the mixture was stirred with an ultrasonic homogenizer (UP50H Hielscher) until complete dissolution of PVBC was observed. The solution was so dark that a backlight lantern was needed to observe the solid PVBC. With the solution completely homogeneous, a stirring magnet was introduced and the vial closed for heating at 80 ºC various hours under continuous stirring at 350 rpm. The synthesis method was based in the procedure reported by Lu et al. [6]. In the previous step of heating at 80 ºC is where the crosslinking reaction occurs, since it needs a high activation energy reached with the help of the temperature. The reaction is very temperature dependent and small variations lead to important differences in the final membrane, for this reason good control of the temperature was done by a digital heating plate (Ibx Instruments, H03D Series) and other sources of heating/cooling like air streams were avoided. When the crosslinking step was done, the solution was naturally cooled down under stirring and placed in glass Petri dishes of 70 mm diameter (see Figure 3.2b). These Petri dishes were used because of the good inner flat surface compared to the normal glass ones. The quantity of solution on each Petri dish depended on the polymer ratio and the final thickness but it was between 2.5 and 3 g to obtain membranes approximately around 50 μm thickness. For the casting process the Petri dishes were directly placed in a vacuum oven (Memert VO200) and two steps were performed: the first to lower the pressure from ambient pressure to 100 mbar and raise the temperature to 40 ºC in 1 h and the second to maintain these conditions (100 mbar

and 40 ºC) overnight. When the casting was ended the pressure was restored manually to ambient conditions and the Petri dishes were taken from the oven (see Figure 3.2c and d). Following covering the Petri dishes for around 10 min was done to help peel off the membranes, they were then dried with filter paper, the thickness was measured (Mitutoyo Digital Micrometer) and they were finally stored in sealed inert plastic bags until required. These membranes were denoted as PBI-c-PVBC.

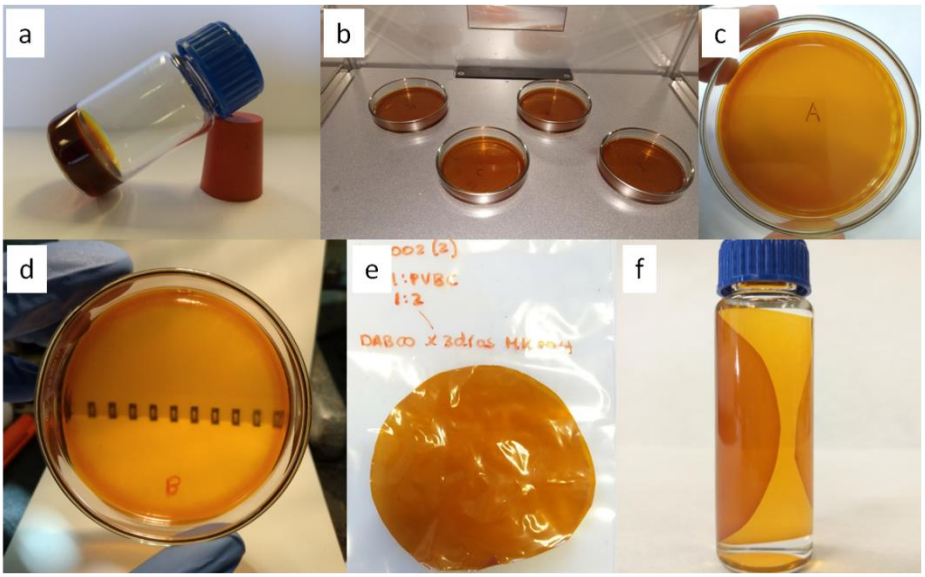

Figure 3.2. Synthesis process of PBI-c-PVBC membranes. a) Example of too long crosslinking time, b) solutions on the Petri dishes in the oven prior to casting, c) and d) membranes after casting, e) membrane after 3 days quaternization with DABCO and f) doping of membrane in KOH solution.

The ABPBI-c-PVBC membranes were prepared following the same idea. First a desired amount of PVBC was introduced in a solution of 1 wt.% ABPBI and 1 wt.% $LiNO_3$ (95 wt.%, Sigma Aldrich) in N-methyl-2-pyrrolidone (NMP, 99.8 wt.%, Carlo Erba) and the mixture was stirred until it was completely homogeneous. The molar ratios studied ranged from 1:1 to 1:3 of ABPBI-c-PVBC. For the crosslinking and casting the mixture was placed in a Petri dish and dried in an oven at 100 ºC for 48 h. Similar to the previous ones, the membranes were peeled off with the help of immersion in UPW, dried, the thickness measured and stored. The obtained membranes were denoted as ABPBI-c-PVBC.

The polybenzimidazole-c-PVBC membranes were quaternized by reaction of the $-CH_2-Cl$ group of PVBC with a tertiary amine, 1,4-diazabicyclo [2.2.2] octane (DABCO, 99 wt.%, Sigma Aldrich), to form positively charged quaternary

ammonium (QA) groups. A solution of DABCO 0.5 mol L^{-1} in ethanol was prepared and the crosslinked membranes were introduced in a sealed glass bottle (around 30 mL volume) with the solution and kept at 60 ºC for 24 h and 72 h in the cases of ABPBI and PBI membranes, respectively. Then the membranes were washed several times with UPW and dried with filter paper prior to storage in sealed inert plastic bags (Figure 3.2e). These membranes were denoted as PBI-c-PVBC/Cl and ABPBI-c-PVBC/Cl since the Cl^- ion is the remaining counter ion of the QA groups.

For the membranes to be finally converted to the OH^- form by exchanging the Cl^- ions, they were introduced in KOH 1M aqueous solution (Figure 3.2f). These membranes were denoted as PBI-c-PVBC/OH and ABPBI-c-PVBC/OH. The complete process of synthesis is showed in Figure 3.3.

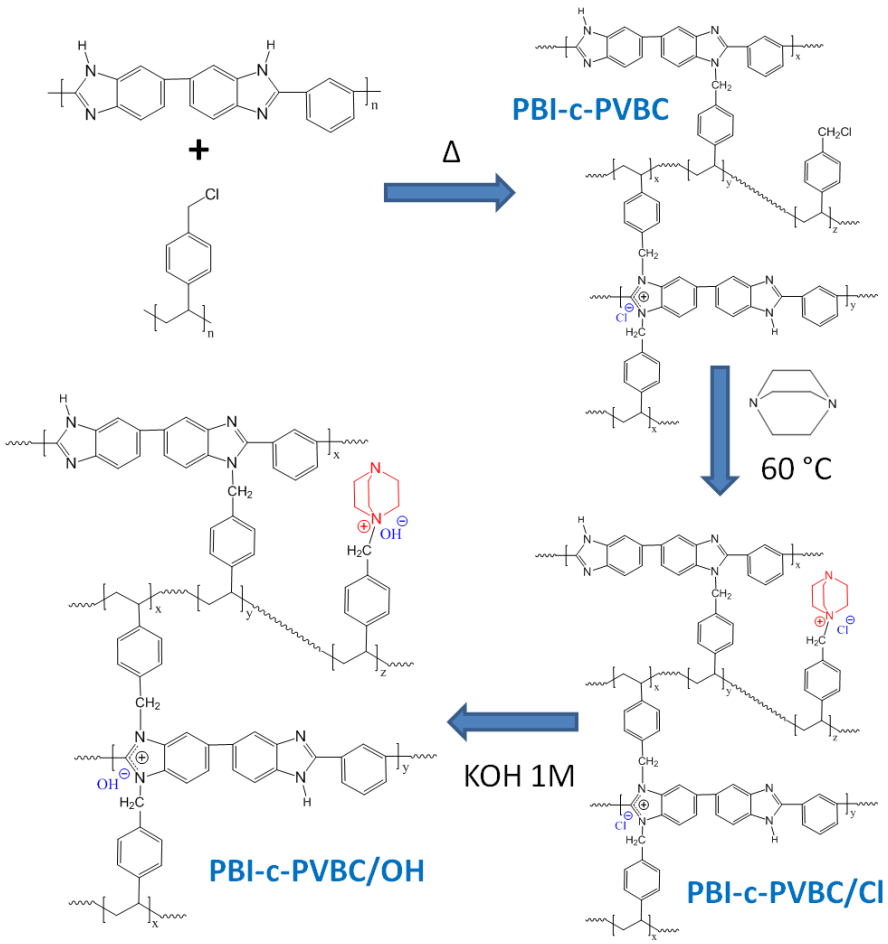

Figure 3.3. Scheme of the synthesis of PBI-c-PVBC crosslinked structure, quaternized in Cl^- form and converted to OH^- form.

1.3 Membranes and ionomers based on radiation grafted ETFE-VBC aminated with TMA and MPRD

These materials synthesis consisted in a two-step process. First is the radiation-grafting technique: an already prepared commercial material (powder or film) of poly(ethylene-*co*-tetrafluoroethylene) (ETFE) was radiated with e-beam radiation to create reactive sites on the polymer chains where grafted polymeric side-chains can be attached when there is presence of suitable monomers. This method has the advantage of using already homogeneously prepared based materials and that different chemistries can be tested in grafted materials with the same ion exchange capacity (IEC). On the other hand the radiation may produce some undesirable effects as formation of covalent crosslinking, scission of the backbone chain (weakening mechanically the material) or introduction of reactive unsaturated chemical groups [7]. After the radiation grafting, the materials were reacted via the side-chains with different amines to form quaternary ammonium groups (the quaternization process previously described in the polybenzimidazole-c-PVBC membranes). In this section, the synthesis of both anion exchange membranes (AEMs) and anion exchange ionomers (AEI) is described.

For the synthesis of the membranes, ETFE films (Nowofol, thickness of 25 μm) were electron beamed in the presence of air (4.5 MeV Dynamatron Continuous Electron Beam Unit, STERIS Synergy Health, SouthMarston, UK), the number of passes were used to control the total absorbed dose (10 kGy per pass). The films were exposed to 30 (final membranes with TMA) or 40 kGy (final membranes with MPRD) and then stored at -40 ºC. For the grafting, the e-beam treated ETFE films were submerged in aqueous solution with 5 vol.% of vynilbenzyl chloride monomer (VBC, 97% Sigma Aldrich, used without any purification treatment) and 1 vol.% 1-octyl-2-pyrrolidone dispersant (Sigma Aldrich) in glass vessels. The grafting solutions were purged with N_2 for 2 h and then the vessels were sealed and they were heated at 70 ºC for 16 h under continuous stirring (see Figure 3.4a). After the grafting, the films were washed multiple times with toluene to remove any excess of present VBC monomer or homopolymer. The VBC-grafted films were then dried at 70 ºC in a vacuum oven for 5 h (Figure 3.4b). Subsequently it was done the amination of the membranes. Two amines were used: trimethylamine (TMA) and N-methylpiperidine (MPRD). For amination with TMA, the VBC-grafted films were immersed in TMA 45 vol.% aqueous solution for 24 h at room temperature, while for amination with MPRD, the membranes were submerged in different percentages of amine in aqueous solution (100, 25 and 15 vol.%) at different temperatures (60 and 70 ºC) for 18 h (see Figure 3.4c). After the amination the membranes, which were mostly in Cl^-

anion form (with Cl^- anions as counter-ions of the positive quaternary ammonium groups), were washed multiple times with ultrapure water (UPW) and boiled in UPW at 70 ºC for 4 h (TMA-membrane) or 60 ºC for 1 h (MPRD membrane) to remove any excess of amine. In order to convert them to fully Cl^- form, they were immersed in aqueous NaCl 1 M at room temperature overnight with at least two replacements of the solution during that period of time. Finally they were thoroughly washed with UPW to remove any excess of Cl^- and Na^+ ions to obtain the Cl^- form AEMs and stored in UPW in sealed plastic bags (Figure 3.4d).

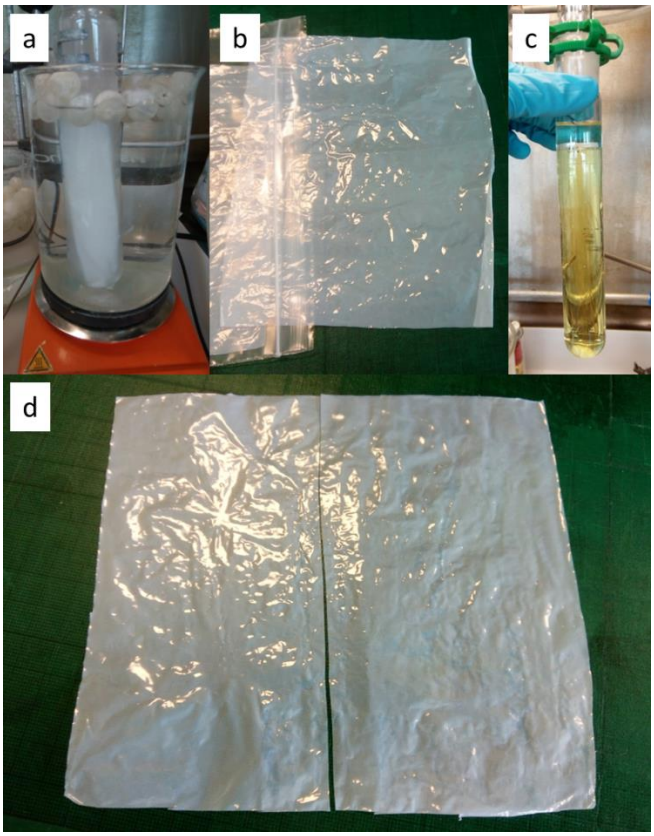

Figure 3.4. Process of synthesis of ETFE-VBC-MPRD membranes. a) Grafting of VBC, b) VBC-grafted membrane, c) Amination with MPRD and d) ETFE-VBC-MPRD final membrane in Cl^- form.

In the synthesis of the ionomers, the process used was overall the same than for the membranes. The differences are summarized in the next paragraph: The base materials were ETFE powders (Fluon® Z-8820X, AGC Europe, particle diameters 20–30 mm), which were irradiated using the same electron-beam facility to a total dose of 100 kGy. Batches up to 20 g of e-beamed powders were grafted with aqueous solutions similar to the AEMs but at 60 ºC for 24 h (Figure 3.5a).

The VBC-grafted powders were filtrated, washed with toluene and then dried in a vacuum oven at 50 ºC for 5 h (Figure 3.5b). For the amination with TMA or MPRD, similar conditions were used than for the membranes: 45 vol.% aqueous solution, 24 h and room temperature for TMA and 15 vol.% 18 h and 60 ºC for MPRD (Figure 3.5c). After the amination the solution was filtered (Figure 3.5d) and the powders washed with UPW thoroughly, the powders were kept in UPW overnight at 50 ºC and then filtered again and divided in smaller portions in plastic bottles. They were kept in NaCl 1 M solution overnight under continuous stirring and then centrifuged (Thermo Scientific, Megafuge 16, see Figure 3.5e) to take out the NaCl solution. New NaCl 1 M solution was introduced and the powders stirred for 30 min. This short cycle of "centrifuge/ take out solution/ introduce new solution/ stirring" was repeated several times with NaCl 1M solution to achieve full Cl^- form of the ionomer powders and then with UPW to remove any excess of Cl^- and Na^+ ions. The powders were then dried in the vacuum oven overnight at 50 ºC and ball milled (in a vibromilling Fritsch equipment, see Figure 3.5f) for 8 h to deagglomerate the particles. The final ionomer powders were stored dry in plastic bags until use.

Figure 3.5. Synthesis of ETFE-VBC-MPRD ionomer powders. a) Grafting with VBC, b) Grafted powders, c) Amination with MPRD, d) Filtration of aminated powders, e) Centrifuge and washing and f) Vibromilling of final ionomer powders for deaglomeration.

The grafting process of the films and powders was developed by the group of John Varcoe, as well as the amination with TMA [8]. The contribution done here was mostly in the test and optimization of the synthesis with MPRD, which had been previously tested [9] but in different conditions.

2 Structural characterization

2.1 Infra-red (IR) and Raman spectroscopy

IR and Raman spectroscopy are useful characterization techniques to identify the structure of molecules, especially if characteristic functional groups are present. For this reason they were used extensively to identify the components present in the synthesised materials.

Both are based in detecting the photons emitted by the transition between vibrational energy levels of molecules, when the electrons go from an excited state to lower vibrational energy levels. In order to have the electrons in excited states they have to be first beamed with a source of photons. The vibrations a molecule can undergo can be classified depending on the movements involved (vibrational modes) in basically, stretching vibrations (symmetric and asymmetric) and bending vibrations (in-plane and out-of plane). Depending on the structure and composition of the molecule, the vibrations may change or not the polarizability (position of the electron cloud of the molecule) and/or the dipole moment. Usually molecules with strong dipole moment are difficult to polarize. In order to be IR active (able to be detected by IR spectroscopy) a vibrational mode must change the dipole moment, and in order to be Raman active the vibrational mode must change the polarizability. For this reason there are some vibrational modes that can be detected by both techniques and others that can only be detected by one of them, so in many cases they complement each other[10].

The equipments used in these techniques were the following: the IR spectroscopy was done with Perkin Elmer Spectrum Two spectrometer with an attenuated total reflectance accessory (ATR) between 4500 and 450 cm^{-1} and a resolution of 2 cm^{-1}. The Raman spectra were acquired with a Via Raman spectrometer (Renishaw) with an excitation wavelength of 785 nm (red laser). It was used the red laser (785

nm) instead of green (532 nm) because the last one produced much more fluorescence (from polybenzimidazole molecules). In the Raman spectra 10 scans were employed with 10 s of exposure time per measurement. The reference of the Raman shift scale was the sharp silicon line located at 520 cm^{-1}.

With the samples of membranes and ionomers based of ETFE, it was used a Renishaw InViaRaman Spectrometer (laser λ=785 nm) equipped with CCD and Leica microscope.

2.2 Nuclear magnetic resonance (NMR)

NMR spectroscopy is commonly used in organic chemistry to identify and study the structure of organic molecules since it gives very precise information about the present atoms and their environment (neighbours) allowing to define the differences and bonds between them. It has been used in this work to further study the structure and composition of the synthesised materials, having special attention in the interactions between them.

NMR spectroscopy observes the local magnetic fields around atomic nuclei (related to their spin) by placing the samples in a magnetic field and exciting the nuclei with radio waves into nuclear magnetic resonance, this produces a signal that is detected by sensitive radio receivers. The intramolecular magnetic field around an atom changes significantly depending on the chemical environment giving characteristic values depending on the concrete situation. This influence of the chemical environment determines the position in the spectra, how much the atom is shifted (in ppm units) from a reference, by "shielding" (giving more near electron cloud) and so shifting "downfield" to higher ppms or "deshielding"(taking again electron cloud) and thus shifting "upfield" to lower ppms. The nuclear magnetic resonance depends on the isotope studied, the most common types are the ^{1}H and the ^{13}C-NMR spectroscopy and both of them have been used in this work.

Usually liquid NMR spectroscopy (with the sample dissolved in a solvent) is performed since the random movement of the molecules helps to obtain very define and clear peaks, which can be quantified to know relatively how many atoms correspond to that signal.

Due to the difficulty to dissolve some of the samples and also in order to study them without alteration, solid-state NMR spectroscopy was also used. For this technique the material is densely packed into a ZrO_2 rotor (the sample vessel). The

rotor is placed into the strong magnetic field, tilted with a direction respect to it known as the Magic Angle (54.7 º). This Magic Angle Spinning (MAS) helps to obtain narrower signals by reducing some anisotropic interactions present in the solid state. To improve the signal to noise ratio, cross polarization (CP) of the magnetization is done from the abundant protons to the measured nuclei (^{13}C in our work). The cross polarization however makes very uncertain the relative quantification of the signals, so qualitative rather than quantitative analysis has to be done.

The ^{1}H-NMR spectra of this work have been measured with a Bruker DRX 500 MHz spectrometer at 298K, with chemical shifts relative to the TMS. The samples were first dried in an oven and then dissolved (not completely in all the cases) in DMSO-d_6 (deuterated).

The solid-state ^{13}C CP NMR spectra were recorder in a Bruker AV-400- WB spectrometer at ambient temperature working at 13C resonance frequency of 100.61 MHz. The samples were introduced and compacted in ZrO_2 rotors with Kel-F end caps. Spin-lock cross polarization with magic angle sample spinning (CPMAS) was used to obtain the spectra and all samples were accumulated one night. Chemical shifts were reference relative to the CH_2 signal of adamantane (29.5 ppm) as secondary reference and the TMS (tetramethylsilane) as primary reference.

2.3 X-ray photoelectron spectroscopy (XPS)

This technique is used for the characterization of the surface of the membranes at different stages of the synthesis or after different treatments (like alkali doping). The X-ray photoelectron spectroscopy is based in the photoelectric effect, observing the emission of electrons coming from the inner levels of the atoms when they are irradiated with an X-ray beam of high energy [11]. The electrons collected are those who didn't lose kinetic energy with atoms or other electrons and thus only come from the very surface of the material (0.5-4 nm), giving information only about the first layers (5-10) [12]. The information that can be obtained is the chemical composition, the relative ratio between the present elements, the different binding energies of the same element with different bonds and semi-quantitatively the ratio between these species.

Our measurements were performed in an ultrahigh vacuum system (UHV) with base pressure of 1 x 10^{-9} mbar using a hemispherical analyzer (SPECS Phoibos 100 MCD-5) (Figure 3.6a). A constant resolution of 0.9 eV was obtained using a

pass energy of 9 eV, accumulating spectra until a good ratio signal to noise was obtained. The binding energies were calibrated using the Au $4f_{7/2}$, Ag $3d_{5/2}$ and Cu $2p_{3/2}$ lines of reference samples at 84.0, 368.3 and 932.7 eV, respectively. Twin anode (Mg and Al) X-ray source was operated at a constant power of 300W using Mg Kα radiation (hν = 1253.6 eV). The insulating character of the samples produced some charging effect, which was corrected by peaking the C 1s band attributed to C-C bonds at 285.0 eV and shifting accordingly all other core levels. The samples were previously dried in the vacuum oven (Memert VO200) at 60 ºC and 10 mbar for at least 3 h. In order to have a flat surface membrane for the XPS they were dried using the set up presented in Figure 3.6b.

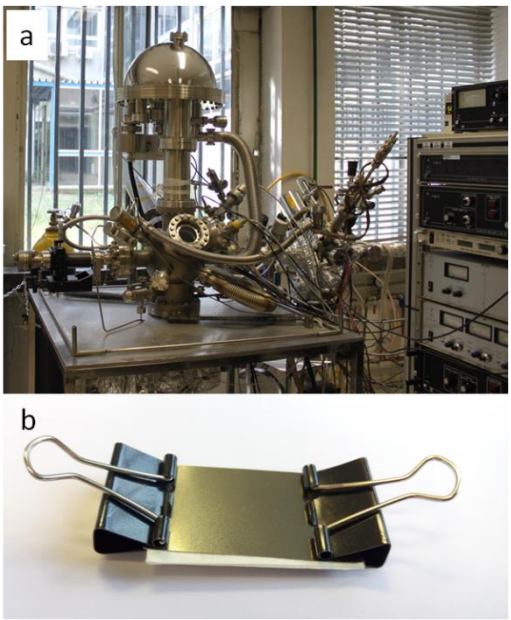

Figure 3.6. a) UHV system with hemispherical analyzer SPECS Phoibos 100 MCD-5 for XPS measurements and b) set up with tweezers, thin stainless steel plates and filter paper to dry the membrane pieces flat in the vacuum oven prior to take them to the XPS.

2.4 Scanning electron microscopy (SEM) and energy dispersive X-ray spectroscopy (EDX)

The scanning electron microscopy (SEM) allows to observe the superficial aspect of the samples with a great range magnification and degree of resolution. It helps to know how homogeneous is the surface and cross-section of the membranes and the particle size of ionomer powders, as well as the aspect of the electrodes. Energy dispersive X-ray spectroscopy (EDX) gives information about the

chemical elements present in the selected area of the sample, allowing to know approximately the atomic or weight ratio between different elements and thus the composition of the area.

In the SEM, electrons are accelerated in a magnetic field and collide with the sample. When the beam of electrons hit the sample, the kinetic energy carried is dissipated in different ways that produce a variety of signals depending on the electron-sample interaction: secondary electrons, backscattered electrons, diffracted backscattered electrons, photons (characteristic X-rays of the element), visible light and heat. For imaging the samples commonly secondary electrons and backscattered electrons are used, the first for showing morphology and topography and the second for illustrating contrast in composition in multiphase samples. Their energy is also related with the atomic number of the element, so the higher the atomic number, the brighter the spot. When the incident electrons have inelastic collisions with electrons in concrete orbitals in an atom of the sample, they transfer the energy they carry and excite the electron to a higher energy orbital. When the excited electrons return to lower energy orbitals, they emit X-rays of a fixed wavelengths characteristic of the element, allowing to determine the chemical composition of elements by the EDX.

Depending on the samples sometimes metallization (coating the sample surface with a few atoms layer of metal) is needed for conductivity requirements. For the membranes and ionomers studied it was done since they are electrical insulators, but it was not necessary in the case of the electrodes analysed.

The instrument used was a Hitachi S-300 scanning electron microscope, equipped with an INCAx-sight (Oxford Instruments) system for the EDX analysis. Images and analysis were taken for the samples at representative areas and with different magnifications.

Some of the samples, ionomers based in ETFE and the electrodes used with them, were analysed with a Field Emission Scanning Electron Microscopy (FE-SEM) JEOL JSM-7100F instrument. To analyse the ionomers or the grafted precursor, small amounts of powders were deposited in the sample holder using epoxy resin and then coated with Au.

3 Fundamental properties of the materials

Anion exchange membranes (AEMs) have different properties or parameters that influence the final performance for the desired application. It is very important to determine them in order to know if the membranes under study will work well under the final conditions. Depending on the concrete property it is measured and different stages of the membrane fabrication process as it will be explained.

3.1 Degree of grafting

The degree of grafting was calculated in the materials (membranes and ionomers) based on ETFE, since they were the only ones first irradiated with an e-beam and the grafted with VBC. The calculation was done according to the following formula[8]:

$$DoG = \frac{m_g - m_i}{m_i} \, x \, 100\% \qquad (3.1)$$

were m_g is the mass of the grafted sample and m_i is the initial mass of the sample before grafting. This was calculated with good accuracy for membranes, but in the case of the powders for ionomers it is very easy to suffer some losses in the filtration processes and so the previous calculation can give us an idea but not a very accurate DoG. This parameter tells us if the grafting process was successful and the extension, allowing to predict if the IEC will be good when the material is quaternized. To give a very broad idea, a DoG around 65 % can give an IEC about 2 mmol/g approximately with the membranes and ionomers used in this work.

3.2 Gel fraction

Gel fraction measurements were performed to know the quantity of polymer remaining in the membrane after trying to dissolve it. The pieces of membrane were immersed in the corresponding solvents in sealed bottles at 70 ºC inside and oven during different consecutive times (for example first step during 2 h, then 8 h and so on). After each step of time, the membranes were gently washed with ultrapure water and dried until constant weight was obtained (which was the

recorded weight for that time). Then they were immersed in new solvent solution inside the sealed bottle and placed again in the oven. This process was repeated until a constant weight is obtained. This final weight is indicative of the crosslinking degree between the polymers of the membrane.

3.3 Thermal and chemical stability

3.3.1 Thermal stability

The thermal stability of the membranes was evaluated by thermogravimetric analysis (TGA) in order to investigate the temperature at which the membranes start to degrade and have a better understanding of the degradation processes at higher temperatures for the structural information that can give us. Since the final application is a low temperature polymer electrolyte membrane fuel cell or an electrolyser, the maximum temperature at which the membranes might be exposed is below 100 ºC, so if the membrane thermal stability is above that value with some margin there shouldn't be degradation due to the temperature. Differential scanning calorimetry (DSC) or derivative weight calculation were also used in the TGA experiments to identify clearly each degradation step and the extension.

The thermogravimetric analysis were performed in a TA Instrument 20, heating the samples from 25 to 900 ºC at a heating rate of 10 ºC min^{-1} under nitrogen atmosphere. The differential scanning calorimetry was measured in a TA Instrument 10, with the samples sealed in aluminium pans and heating from 25 to 300 ºC at a heating rate of 10 ºC min^{-1}.

3.3.2 Stability in alkaline and oxidative media

Membranes and ionomers need to have sufficient stability in the media where they have to perform, and the main characteristics in the alkaline fuel cells and electrolysers are, of course, the presence of a high pH media due to the hydroxide ions and the presence of O_2 molecules (as reactant in the fuel cell and product in the electrolyser). These species produce degradation in the functional groups (as the quaternary ammonium groups of some membranes) and/or the backbone structure of the polymeric materials. For this reason, some preliminary ex-situ study of the stability of these groups is recommended in order to know how long the materials could work before the degradation process in too advanced.

In the alkaline media, the typical degradation process consists on storing a weighted sample in 1 M KOH solution at elevated temperature (typically 60 ºC) for some time and then measure different properties like the ionic conductivity, IEC or swelling behaviour to determine the changes occurred[6,13].

a) Degradation in alkaline media

There are many methods to study the degradation the alkali media produces in the membranes. They basically consist in introducing the membranes in a sealed container with KOH solution at elevated temperature over a certain period of time. Some of the membranes in which the alkali degradation was studied were cut in pieces and each piece was introduced in crystal vial completely filled with KOH 1M solution. The vial was closed and placed in an oven (Memert VO200) for different durations. When the desired time was finished, the piece of membrane was taken out of the solution, rinsed with ultrapure water (UPW) and the different evaluations could be done: for example measure the ionic conductivity, the IEC, the WU and swelling behaviour or the fragility.

b) Degradation in oxidative media

The degradation in oxidative media was done with Fenton's reagent: a solution of $FeSO_4$ $4x10^{-6}$ M with H_2O_2 3 vol.%. In this solution the H_2O_2 reacts with the Fe (II) to form hydroxyl radicals that attack the polymer structure. This test is much more aggressive than the real conditions in for example fuel cell operation, but can help to give an idea of the oxidative stability of the membranes [14,15].

In our measurements, first the membranes were introduced in UPW for 24 h so complete hydration was achieved, then they were soaked in Fenton's reagent solution for 24 h at 40 ºC in an oven (Figure 3.7b). When that step was done, they were rinsed with UPW (Figure 3.7d) and the superficial liquid removed with filter paper just before weighting them. After this process they were introduced again in fresh Fenton's reagent solution for another 24 h at 40 ºC. This process was repeated for a total of 8 days test. Since the membranes are significantly weakened in the process, special care was taken to handle them as little as possible, using for immersion and moving a plastic Petri dish, as showed in Figure 3.7a.

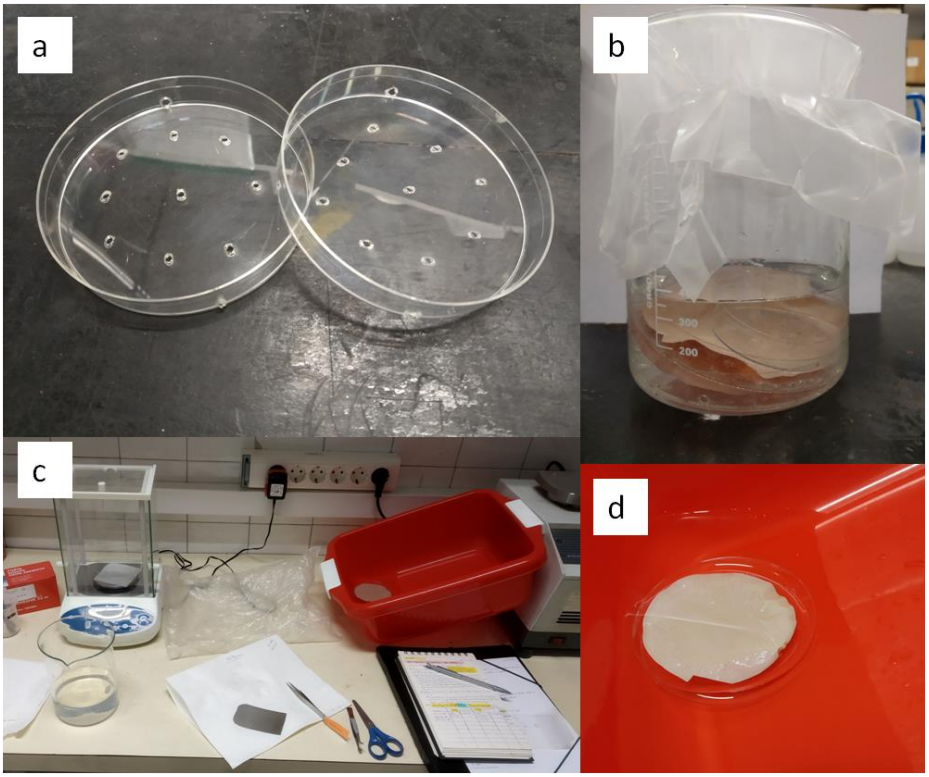

Figure 3.7. a) Petri dishes used to hold and transport the membrane, b) crystal beaker with membranes and Fenton's reagent (out of the oven), c) set up for weighting after each day degradation process and d) detail of membrane rinsed in UPW on the Petri dish.

3.4 Mechanical stability

Mechanical stability tests are performed to have a better idea of the resistance of the membranes under mechanical stress. It is relevant to know the mechanical stability of the synthesised films since they have to suffer high pressure when the MEA is compressed in the final cell of a fuel cell or in the electrolyser. Usually an approximate idea can be done from the direct handling of the films, being easy to know if they can be folded and stretched without trouble or if they are very brittle or too soft and disintegrate. This test allows us to quantitatively compare between different membranes. However the error margin in the results is considerable since the membranes are never 100 % perfect and even more when they are synthesised in the laboratory and very small physical differences may produce differences in the elongation and maximum stress they can support. The scheme of the test and a testing machine are showed in Figure 3.8.

The mechanical tensile stress tests were performed using a MTS® QTest1/L Elite testing machine equipped with a 100 N load cell. The membranes were cut to Type 4 dumbbell test pieces (according to ISO 37) and the initial dimensions of the samples were 2 mm width and 20 mm gauge length. The crosshead speed used was 10 mm min^{-1}. At least three pieces were used for each different sample.

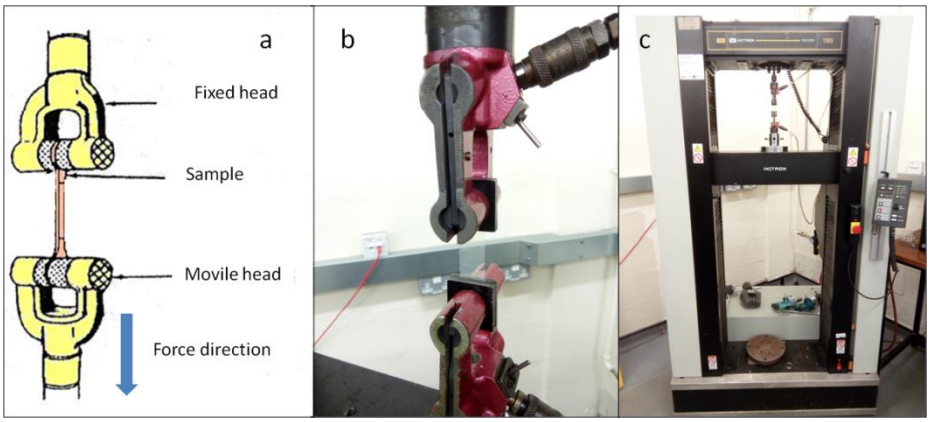

Figure 3.8. a) Scheme of the test, b) detail of the testing machine showing heads and sample and c) testing machine.

3.5 Ion exchange capacity (IEC)

The ion exchange capacity (IEC) is one of the main properties of the anion exchange membranes and ionomers that have fixed positively charged groups, like the quaternary ammonium groups (QA). It is defined as the mmols of ion exchanged in every per gram of membrane, as expressed in this formula:

$$IEC\ (ion) = \frac{n_{ion}}{M_{dry\ membrane}} \qquad (3.2)$$

were n_{ion} are the mols of the ion and $M_{dry\ membrane}$ is the dry weight of the membrane in grams. So the units are usually expressed in "mmols g^{-1}".

It can be made with different ions but the most common are OH^- and Cl^-, the first because it is usually the final counter-ion present in the membrane under operation and the second because is commonly the ion present in membranes that had C-Cl groups and were quaternized with a tertiary amine, remaining the Cl^- as counter-ion before the final exchange to OH^- form prior to operation.

IEC is directly associated with other important properties like the ionic conductivity and the water uptake, since the QA groups are responsible of the good conductivity through the membrane and they are highly hydrophilic. A very low IEC will rend low conductivity, but if it is very high the water uptake and swelling behaviour might increase too much weakening in excess the membrane and allowing it to break under operation and flooding the electrodes with water.

Different methods can be used to determine the IEC, depending on the ion chosen and the process used, but mainly consist in titrations of a solution in which we can measure either the ions exchanged and taken out from the membrane or the rest of the ions in the solution from an already know quantity and determine how many have been introduced in the membrane.

With the membranes and ionomers based on ETFE, the ion determined was the Cl^-, following the process established in Varcoe's group[8]. In this process, the materials in Cl^- form (just recovered from the WU measurement, so the dried mass of the samples was known) were immersed in aqueous $NaNO_3$ solution 2.4 M (20 mL) for 5 h. Subsequently the solutions were acidified with aqueous HNO_3 2 M (2 mL) and titrated with a standardized solution of aqueous $AgNO_3$ (20.00 ± 0.06 M). For the titrations it was used a Metrohm 848 Titrino Plus autotitrator equipped with an Ag Titrode (Cl^- anion selective electrode). The IEC (mmols g^{-1}) was calculated with the end point of the titration (Ep, in mL), which is the maxima in the first differential plot of the Ag Titrode potential *vs.* volume representation.

$$IEC\ (Cl^-) = \frac{Ep\ x\ 0.02}{M_{dry}} \qquad (3.3)$$

For the membranes based on polybenzimidazole-c-PVBC quaternized with DABCO, the IEC of OH^- ions was measured, based on the process of Scott et al. [16]. First the pieces of membranes were dried in a vacuum oven at 40 ºC and 100 mbar until constant weight was observed, then the membranes were immersed in ultrapure water (UPW) 24 h at room temperature in plastic bottles in order to fully hydrate them (explained in the WU and swelling behaviour sections), the water is then replaced with KOH 1 M aqueous solution and membranes are maintained there at room temperature 20 min, subsequently the KOH solution is replaced with new one and this process is repeated until the membrane pieces have been a total time of 1 h in KOH 1 M. This step ensures the complete exchange of the Cl^- ions next to the QA groups with OH^- ions. Then the membranes are washed repeatedly with UPW until neutral pH is observed with pH paper to ensure the "free" (not fixed to QA groups) OH^- ions have been removed from the membrane. After this step, each membrane piece is immersed in exactly 50 mL of NaCl 1 M aqueous solution in their corresponding plastic bottles, and maintained there for

24 h to ensure exchange of the ions so the OH^- ions that were on the membrane go to the solution. Finally a known volume of each solution is titrated with aqueous H_2SO_4 0.02M (previously titrated itself to know the exact concentration) using methyl red as visual indicator of the end point (Ep, in mL) using a Titrette GMBH bottle-top digital burette. At least three fractions of each solution were titrated. The IEC (mmol g^{-1}) was calculated with the volume of the end point and the dry mass of the membrane (g) according to the following formula:

$$IEC\ (OH^-) = \frac{Ep\ x\ 0.02}{M_{dry}} \qquad (3.4)$$

3.6 KOH, water uptake (WU) and swelling ratio

All these properties are relevant parameters of the prepared membranes since the dimensional changes (swelling ratio) can affect the membrane-electrode assembly (MEA) if the membrane is dried and hydrated multiple times, as well as the important influence of the capacity the membrane has to absorb water (WU), which is necessary for the good ionic conductivity of the polymeric materials as well as for the stability of the functional groups [17]. KOH uptake gives an idea of how much free KOH is within the membrane structure and may contribute to the conductivity. However too high WU and dimensional changes can weak the membrane in excess and flood the electrodes reducing the performance output as previously explained. Usually WU and swelling ratio are measured together, and KOH uptake can be easily done at the same time using KOH solution instead of putting the membrane in water.

Experimentally these properties were determined using the following process: the membrane was dried in the vacuum oven, then rectangular pieces of approximately 10 x 15 mm were cut, weighted, the thickness measured with a digital calibre (Mitutoyo, accuracy of 0.001 mm) and the length width a digital micrometer (Metrica, accuracy of 0.01 mm) (both in Figure 3.9) to obtain the initial values (X_0: M_0, T_0, L_0, W_0 for mass, thickness, length and width respectively). Subsequently they were introduced in ultrapure water (UPW) (for just WU) or in KOH solution (for also KOH uptake, concentration and time depending on the membrane) until complete hydration and doping were achieved. Then the pieces were rinsed with UPW, the superficial liquid removed with filter paper and they were weighted and the dimensions were measured to obtain the hydrated values (X_H) or hydrated and doped values (X_{H+KOH}). If the membranes had been doped, finally they were dried again in the vacuum oven and weighted to obtain the weight of the membrane with only KOH (X_{KOH}).

Figure 3.9. Digital calibres used for measure a) thickness and b) length and width.

Based on these data, the swelling or increment (in % respect to the initial values) in volume (S_V), in thickness (S_T), in length (S_L), in width (S_W), in mass due to water uptake (WU) and in mass due to KOH uptake were calculated:

Volume swelling: $$S_V(\%) = \frac{T_H * L_H * W_H - T_0 * L_0 * W_0}{T_0 * L_0 * W_0} * 100 \quad (3.5)$$

Thickness increase: $$S_T(\%) = \frac{T_H - T_0}{T_0} * 100 \quad (3.6)$$

Length increase: $$S_L(\%) = \frac{L_H - L_0}{L_0} * 100 \quad (3.7)$$

Width increase: $$S_W(\%) = \frac{W_H - W_0}{W_0} * 100 \quad (3.8)$$

Water uptake: $$WU\ (\%) = \frac{M_H - M_0}{M_0} * 100 \quad (3.9)$$

Water uptake (with doping): $$WU\ (\%) = \frac{M_{H+KOH} - M_{KOH}}{M_0} * 100 \quad (3.10)$$

$$KOH\ uptake\ (\%) = \frac{M_{KOH} - M_0}{M_0} * 100 \quad (3.11)$$

3.7 Ionic conductivity

The ionic conductivity is one of the most important property of the membranes measured before the single cell test, in order to know how good the final performance will be. The ionic conductivity express how easily can the ions move through the membrane and thus how well does the membrane work as an ion exchange polymer [18]. To obtain the experimental measurement the electrochemical impedance spectroscopy (EIS) is used [19,20], working under open circuit conditions. The membrane is placed between two electronic conducting electrodes and a sinusoidal voltage is applied between them, in such way that the impedance of the system can be obtained. The intersection of the plotted data with the real axis of the impedance will be the value corresponding to the resistance (R, in ohms Ω) of the membrane. From this value the ionic conductivity is calculated with the following formula:

$$\sigma = \frac{l}{R*A} \qquad (3.12)$$

were l is the thickness of the membrane (cm), R the resistance value (Ω) and A the area of membrane between the electrodes (cm^2). So the final units of the conductivity are S cm^{-1}.

The system used to measure the conductivity consists in a cell (Figure 3.10) with two stainless steel plates in the extremes which can be heated by external temperature controllers, between these plates two Teflon® plates are prevent direct contact of the hot steel plates with the membrane and finally in the middle is placed the membrane, with two stainless steel rectangular thin electrodes, one at each side, placed perpendicularly so the area covered by the membrane between them is a square on known area value (0.36 cm^2) (see Figure 3.10b). The cell has inlets and outlets for gases in the steel plates that allow for humidification of the system with an external heated tubular humidifier. The Teflon® plates have also openings for the humidified gases to reach me membrane. This system was used to measure the through-plane OH^- conductivity of the membranes. The EIS measurements were done with an AUTOLAB equipment (PGSTAT 302 N) equipped with a Frequency Response Analyzer (FRA) and controlled with NOVA software. The frequency range used was from 100 kHz to 1 Hz and the measurements were recorded with AC signal amplitude of 10 mV around the open circuit potential. The membranes were usually doped/exchanged with KOH, so in OH^- form. Previous to the measurement the membrane pieces were rinsed with UPW and superficially dried with filter paper to remove any excess of KOH and liquid.

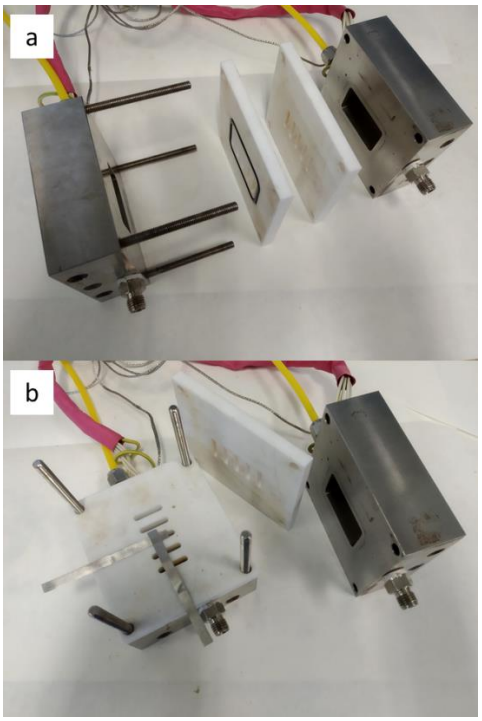

Figure 3.10. Cell used for the ionic conductivity measurements.

For membranes based on ETFE, the measurement process was different, based in the procedure used by Varcoe's group [8]. It was measured the in-plane Cl^- conductivity of the membranes. The fully hydrated membranes, in Cl^- form, were cut in rectangular pieces and mounted in a 4-probe BekkTech BT-112 test cell (supplied by Alvatek, UK), which were submerged in UPW at controlled temperatures (see Figure 3.11). The impedance was recorded with a Solartron 1260/1287 combination controlled by ZPlot/ZView software (Scribner Associates, USA) and the spectra were collected over a frequency range of 100 kHz to 0.3 Hz with 10 mV amplitude. The conductivity was calculated with this formula:

$$\sigma = \frac{l}{R*w*t} \qquad (3.13)$$

were w is the width of the membrane and t is the distance between the Pt sense electrodes (0.425 cm). This is basically the previous formula but with the area of the cross-section of the membrane, since the measurement is in-plane.

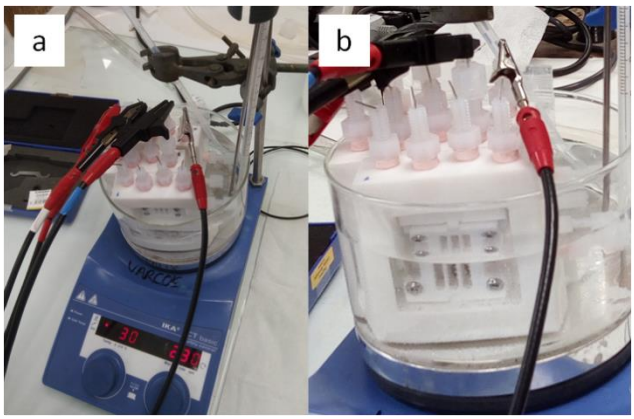

Figure 3.11. a) Test cells 4-probe BekkTech BT-112 immersed in water used to determine the in-plane Cl^- conductivity of ETFE-based membranes and b) detail of the test cells.

The activation energy(Ea) is an interesting property of the membranes directly related with the conductivity, it measures how the conductivity changes with the temperature and the obtained value is related with the possible processes involved in the transportation of the ionic charges through the membrane. It is based in the Arrhenius law:

$$\sigma = \sigma_0 * e^{\frac{-Ea}{R*T}} \qquad (3.14)$$

were σ_0 is the conductivity at infinite temperature, Ea is the activation energy (kJ mol^{-1}), R is the ideal gas constant (8.314 kJ mol^{-1} K^{-1}) and T is the temperature (K). The value of Ea is obtained from the slope of plotting ln(σ) *vs.* 1/T.

4 Performance in single cell

With the information of the previous study of structural characterization, chemical composition and functional groups, most relevant properties and stability of the materials prepared, the most promising materials are selected to be used in the single cell. This is actually the final application of the materials in conditions quite similar to a possible use in a final device under real operation conditions. The procedure to prepare the complete set up and the measurements performed will be explained. The first focus of the measurements will be to know how much power density the system is able to reach using the synthesised materials at certain

conditions, since it is a very good parameter to know if the system is working well altogether.

Three different systems have been used for different purposes: a fuel cell fuelled with EtOH/KOH and O_2 to measure the membranes of PVA:polybenzimidazole and polybenzimidazole-c-PVBC, a zero gap liquid alkaline water electrolyser (LAWE) to measure the same membranes and a fuel cell fuelled with H_2 and O_2 to measure the materials based in ETFE.

4.1 Fuel cell

In order to measure the performance in the single cell, first the anion exchange membrane has to be transformed to the OH^- form and then it has to be placed between the electrodes (anode and cathode) to form the membrane-electrode assembly (MEA), which is the heart of the single cell system, the place where the reactants arrive to the catalysts surface, the electrochemical reactions take place in the electrodes and the ions are conducted through the membrane. The electrodes were also previously prepared as it will be explained.

The overall system and components are presented in Figure 3.12a. The bipolar plates conduct the electrons produced/consumed to the external circuit and have the inlets and outlets for the fuel and oxidant, they usually have carved in their surface the channels that distribute the fuel or oxidant homogeneously to the electrode. The gaskets help to avoid escape of the reactants and prevent the contact between the bipolar plates, which would cause the short-circuit and thus the cell wouldn't work. Finally the membrane electrode assembly (MEA) is in the middle (as showed in Figure 3.12c before closing the cell) and its function is the correct performance of the electrochemical reactions and conduction of the ions as it has been explained.

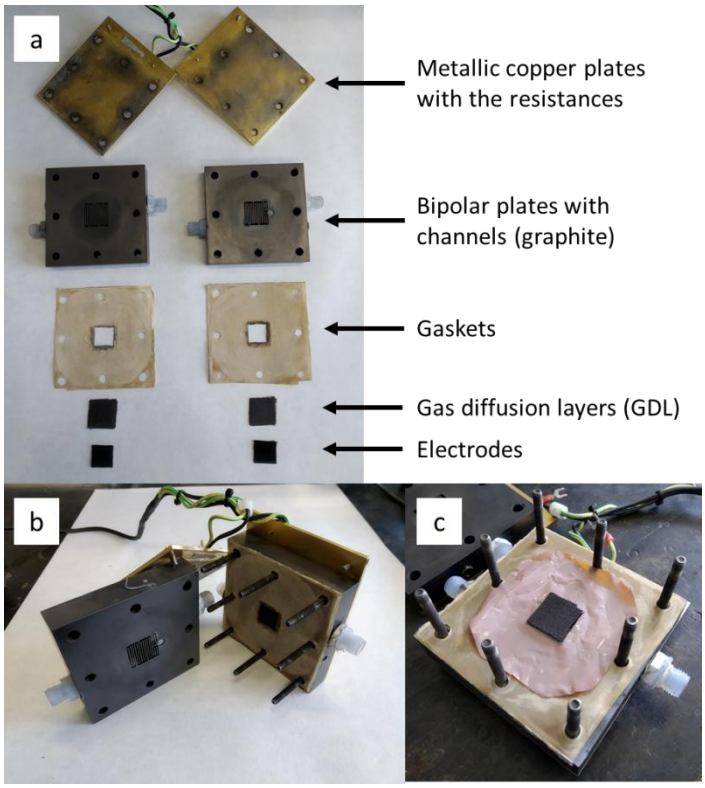

Figure 3.12. a) Components of the single cell used for fuel cell measurements, b) intermediate step of assembly of the cell and c) Membrane-electrode assembly (MEA) prepared and placed in the single cell before closing.

The membrane electrode assembly (MEA) is formed by the anion exchange membrane placed in the middle of the two electrodes. Each electrode has two different layers: the gas diffusion layer which allows the gases to diffuse through it and also works as electron conductor, transporting the electrons to/from the bipolar plates; the other is the catalytic layer, formed by the catalyst support (normally paper or carbon cloth), the catalyst particles and the ionomer particles; in this layer the reagents reach the catalyst surface and the oxidation/reduction occurs generating or consuming the electrons. The ions (OH^- since we are working in alkaline media) are transported through the electrolyte membrane, from the cathode were they are produced to the anode where they are consumed. The ionomers work as binder of the catalyst particles and also can help to conduct the ions to the catalyst surface. The complete scheme is showed in Figure 3.13.

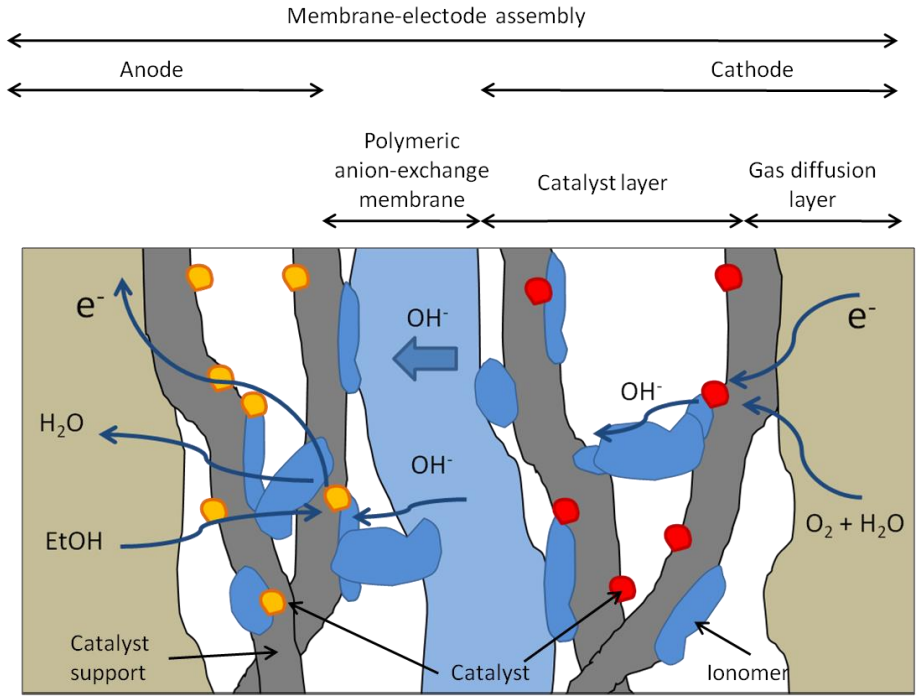

Figure 3.13. Scheme of the membrane-electrode assembly (MEA) and the transport of the species in an alkaline fuel cell with EtOH as fuel. (Relative dimensions are just for illustration purpose, they do not represent real ones).

4.1.1 Fuel cell with EtOH/KOH *vs.* pure O_2

The main difference of this system is the liquid state of the fuel at the anode, an aqueous solution of EtOH 2 M and KOH 2 M, which ensures the complete hydration of the system under performance.

a) MEA preparation

For the preparation of the MEA, first the electrodes were prepared separately and then put together with the membrane. To prepare the membrane, it was in kept in KOH solution (concentration and time depending on the membrane) at room temperature, after this process it was rinsed with ultrapure water (UPW) and placed between the electrodes.

The electrodes were prepared following this procedure: an ink was made mixing in a crystal vial the required quantity of catalyst with UPW (150 μL), isopropyl alcohol (380 μL) and the corresponding quantity of 5 wt.% Nafion® solution,

which has been previously optimised and is calculated according to this proportion:

$$0.55 = \frac{mg_{(C+catalyst)}}{mg_{(C+catalyst)}+mg_{ionomer}} \qquad (3.15)$$

were the $mg_{(C+catalyst)}$ is the mass of carbon and catalyst and the $mg_{ionomer}$ is the mass of Nafion® in the 5 wt.% solution. The density of the Nafion® solution is 0.924 mg μL^{-1}.

The volumes previously described are for preparing an electrode of 4 cm^2, being necessary to multiple them and all the quantities by the adequate factor if larger areas are prepared. Also a small factor should be used to increment the quantities since normally some losses occur in the process of preparing the electrodes. For the anode the catalyst used was commercial PtRu/C (30 wt.% Pt, 15% Ru, 55% C, from Alfa Aesar - Johnson Matthey), to deposit 1.33 mg Pt cm^{-2} of electrode. For the cathode the catalyst used was commercial Pt/C (40 wt.% Pt, 60% C) from the same company, to deposit 1 mg Pt cm^{-2}. Once all the components of the ink were together, they were mixed using an ultrasonic homogenizer until homogeneous mixture was observed. Then the ink was sprayed with an airbrush over the diffusion layer, a commercial carbon cloth (ELAT GDL-LT 1200W). During the spraying, every short time the electrode was dried on a metal surface over a heating plate and then weighted in an electronic balance to calculate how much catalyst and ionomer have been placed, this method allowed to deposit very precisely the exact quantity of desired catalyst over the electrode.

When the electrodes are prepared they are stored in plastic boxes until the MEA is prepared. To conclude the preparation of the MEA, the electrodes are placed in each side of the membrane (with the catalyst layer facing the membrane, see Figure 3.12c) and sandwiched with the gaskets and bipolar plates previously explained. Not hot-pressing was necessary since the pressure and hot at the beginning of operation were enough to achieve good superficial contact between the membrane and the catalyst layer.

b) Single cell test

Once the single cell (ElectroChem) is closed, it is placed next to the station and the fuel and oxidant inlets and outlets are connected, as well as the equipment that heats the cell and controls the temperature and the electrical contacts to control current and voltage from the station. An overview is presented in Figure 3.14.

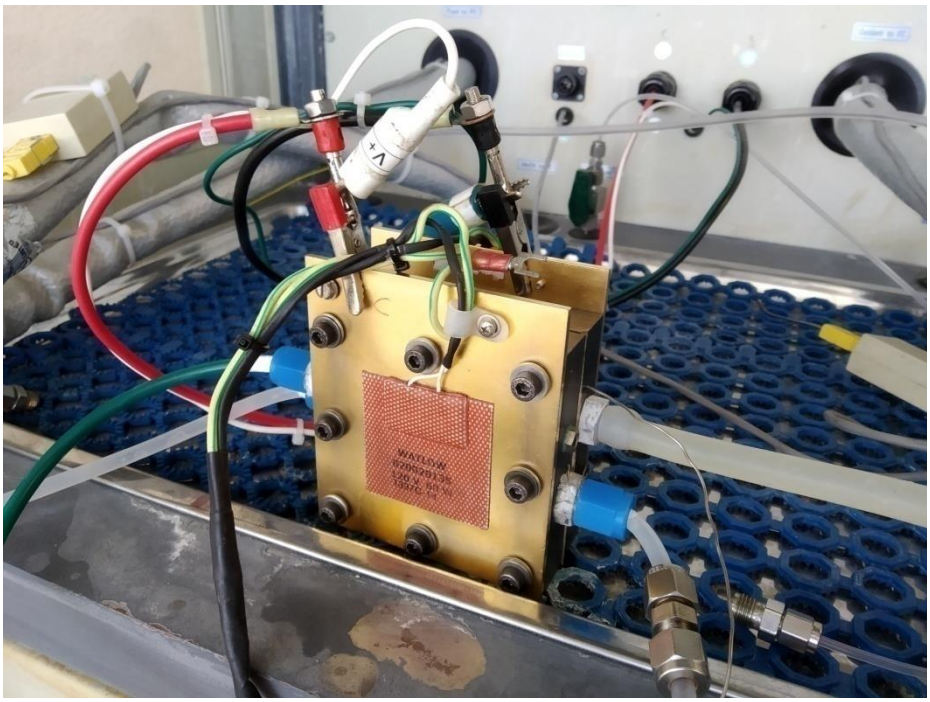

Figure 3.14. Single cell prepared to start operation in the Arbin FCTS station.

The characterization of the fuel cell performance was mainly done with the polarization and power density curves. This data is very relevant because it directly shows how the system converts the chemical energy of the reactant to electrical energy. The polarization curve is obtained as follows: starting at open circuit voltage (OCV), a current is imposed and the corresponding voltage is observed, the imposed current increases until values near the short circuit (by a linear voltametry) where it stops. This gives us the measurement of the voltage *vs.* the current (the polarization curve), from which the power density curve (power density *vs.* current) is easily calculated from the formula (P = V * I). The system has a reference electrode connected with the counter-electrode and both connected to the negative electrode, the anode. The working electrode, positive, is connected to the cathode.

These measurements are recorded using a test station FCTS (Arbin) and the MITS PRO software. Polarization and power density curves are measured with the fuel cell under operation, this means with fuel and oxidant running in their corresponding sides. The flows used were 0.2 L min^{-1} of pure O_2 in the cathode and 1 mL min^{-1} of aqueous EtOH 2 M and KOH 2 M in the anode. The back-pressure in the cathode and the temperature were set depending on the experiment. Previously to the final polarization measurements, the MEAs were activated by different processes like first trials polarization curves, imposing high

currents to generate water and hydrate better the membrane or doing impedance spectroscopy (EIS) measurements, in order to achieve a stable state of the system. When reproducible results were obtained, the final polarization and power density curves were recorded. The polarization curves were done at a voltage ramp rate of 10 mV s^{-1} to have a velocity slow enough to observe clearly the different processes but fast enough so the system was not considerably modified during data acquisition.

4.1.2 Fuel cell with pure H_2 *vs.* pure O_2

In this system fuel and oxidant are supplied to the cell in gaseous state, requiring special care so no H_2 escapes due to its danger in ignition. The scheme of the reactions taking place in the MEA is similar to that of Figure 3.13 just changing the EtOH with H_2 and taking into account that no other reaction products apart of water and the produced electrons are present. In the case of EtOH the rest of possible reaction products are not presented for clarity of the illustration.

a) MEA preparation

The process to prepare the MEA is mainly similar to the previous one, the steps of the spraying are illustrated in Figure 3.15, and the differences are explained here. The inks are prepared with 1 mL of UPW and 9 mL of isopropyl alcohol, the ionomer (AEI) represented a percentage of the total solid mass deposited: 20 % with AEI (TMA) and 20 or 30 % with AEI(MPRD), the gas diffusion layer used was commercial Toray TGP-H-60 carbon paper, the catalysts used were Pt/C for the cathode (Alfa Aesar, Johnson Matthey, 40 wt.% Pt and 60% C) and PtRu/C for the anode (Alfa Aesar, Johnson Matthey, 50 wt.% Pt, 25% Ru and 25% C), the area of the gas diffusion layers sprayed was 5 cm^2 and the Pt loadings for anodes and cathodes were 0.40 and 0.03 mg Pt cm^{-2} respectively. This was done following the procedure used in Varcoe's group [21]. Since the catalyst layers contained AEI particles in Cl^- form and the membrane is also stored in Cl^- form, the electrodes and the membrane were placed in KOH 1 M solution for 1 h and then washed with UPWprior to assembling the MEA and sandwiching it in the single cell (see Figure 3.15f).

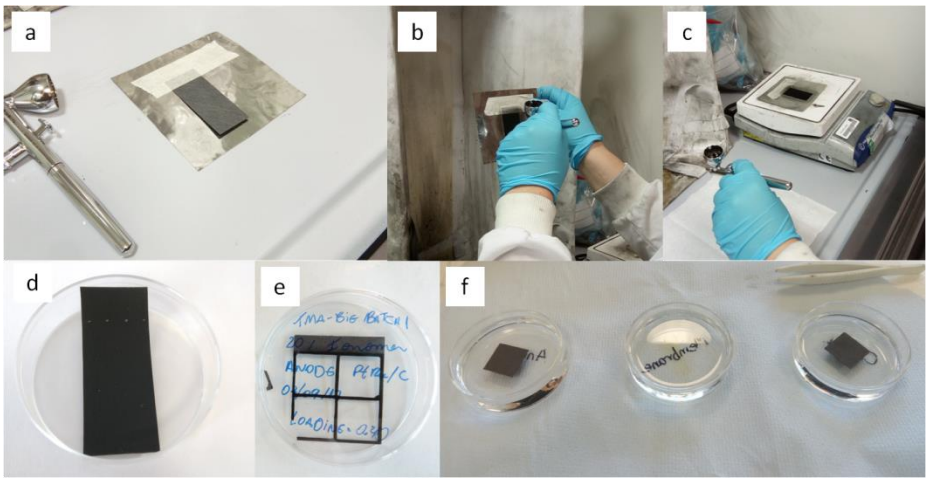

Figure 3.15. Steps of spraying and final use of the electrodes. a) Preparation of the gas diffusion layer to be sprayed, b) spraying process, c) drying to weight during spraying, d) sprayed gas diffusion layer, e) rests of cutting the electrodes from the sprayed area and f) electrodes in KOH solution prior to MEA final assembly.

b) Single cell test

The same explanation of the general method explained before applies here. The differences are resumed in the following lines. The single cell fixture was from Scribner Associates, USA, as well as the fuel cell station, the test were conducted at 60 ºC and the gases flows were set to 1 L min^{-1}, without back-pressurization, the MEAs were activated by operation at 0.5 V until a stable current was observed (minimum 1 h) and *in situ* area specific resistances were obtained using the 850C's internal current interrupt method.

4.2 Electrolyser

The zero gap liquid alkaline water electrolyser (LAWE) measurements were the other final application device where some of the membranes were tested. They were performed using a zero gap configuration, which is essentially similar to that of the fuel cell and is well explained and illustrated by Abuin et al. [2]. The experiments were performed in the laboratory of G. C. Abuin in Buenos in the Instituto Nacional de Tecnología Industrial (INTI) of Argentina. Two Ni foam electrodes (Sigma Aldrich, thickness 1.6 mm, bulk density 0.45 g cm^{-3}, porosity 95%) of 3.61 cm^2 geometric area were attached directly to membrane surfaces, giving an active electrode geometric surface area of 4.40 cm^2. The current feeders were gold plated Ni sheets which also acted as electrolyte distributors. The cell

was connected to a system, in which the KOH solution was recirculated from a reservoir tank by a peristaltic dual head pump (MasterFlex) and heated prior to be introduced in the cell (which was also heated at controlled temperature).

The main characterization tests performed were the electrolysis load curves and the chronopotenciometric measurements. The first ones are very similar to the polarization curves previously explained, so the current is imposed to the system and the corresponding voltage is measured, in the range of 1.5 to 2 V, plotting in this case the current density *vs.* the voltage. In the chronopotenciometric measurement, a constant current density is imposed for a determined time to observe the variation in the voltage of the system. A picture of the cell is presented in Figure 3.16.

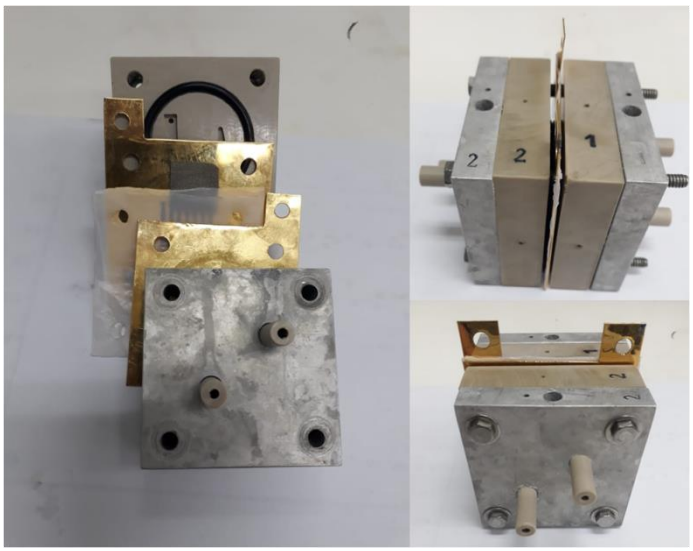

Figure 3.16. Configuration of the zero gap liquid alkaline water electrolysis (LAWE) cell.

5 References of the chapter: Experimental

[1] J. Ran, L. Wu, Y. He, Z. Yang, Y. Wang, C. Jiang, L. Ge, E. Bakangura, T. Xu, Ion exchange membranes: New developments and applications, J. Memb. Sci. 522 (2017) 267–291. doi:10.1016/j.memsci.2016.09.033.

[2] L.A. Diaz, J. Hnat, N. Heredia, M.M. Bruno, F.A. Viva, M. Paidar, H.R. Corti, K. Bouzek, G.C. Abuin, Alkali doped poly (2,5-benzimidazole) membrane for alkaline water electrolysis: Characterization and performance, J. Power Sources. 312 (2016) 128–136. doi:10.1016/j.jpowsour.2016.02.032.

[3] J. Yang, R. He, D. Aili, Synthesis of Polybenzimidazoles, in: High Temp. Polym. Electrolyte Membr. Fuel Cells, Springer Switzerland, 2016. doi:10.1007/978-3-319-17082-4_7.

[4] L.A. Diaz, G.C. Abuin, H.R. Corti, Methanol sorption and permeability in Nafion and acid-doped PBI and ABPBI membranes, J. Memb. Sci. 411–412 (2012) 35–44. doi:10.1016/j.memsci.2012.04.013.

[5] C.-K. Yeom, K.-H. Lee, Pervaporation separation of water-acetic acid mixtures through poly(vinyl alcohol) membranes crosslinked with glutaraldehyde, J. Memb. Sci. 109 (1996) 257–265. doi:10.1016/0376-7388(95)00196-4.

[6] W. Lu, G. Zhang, J. Li, J. Hao, F. Wei, W. Li, J. Zhang, Z.-G. Shao, B. Yi, Polybenzimidazole-crosslinked poly(vinylbenzyl chloride) with quaternary 1,4-diazabicyclo (2.2.2) octane groups as high-performance anion exchange membrane for fuel cells, J. Power Sources. 296 (2015) 204–214. doi:10.1016/j.jpowsour.2015.07.048.

[7] L. Gubler, Polymer design strategies for radiation-grafted fuel cell membranes, Adv. Energy Mater. 4 (2014) 1300827. doi:10.1002/aenm.201300827.

[8] L. Wang, E. Magliocca, E.L. Cunningham, W.E. Mustain, S.D. Poynton, R. Escudero-cid, M.M. Nasef, J. Ponce-gonzález, R. Bance-souahli, R. C. T. Slade, D. K. Whelligan, J.R. Varcoe, An optimised synthesis of high performance radiation-grafted anion-exchange membranes, Green Chem. 19 (2017) 831–843. doi:10.1039/c6gc02526a.

[9] J. Ponce-González, D.K. Whelligan, L. Wang, R. Bance-Soualhi, Y. Wang, Y. Peng, H. Peng, D.C. Apperley, H.N. Sarode, T.P. Pandey, A.G. Divekar, S. Seifert, A.M. Herring, L. Zhuang, J.R. Varcoe, High performance aliphatic-heterocyclic benzyl-quaternary ammonium radiation-grafted anion-exchange membranes, Energy Environ. Sci. 9 (2016) 3724–3735. doi:10.1039/C6EE01958G.

[10] P.J. Larkin, IR and Raman Spectroscopy, Elsevier, Amsterdam, 2011. doi:10.3390/rel9100297.

[11] M.P. Seah, D. Briggs, eds., Practical surface analysis by Auger and X-ray Photoelectron spectroscopy, John Wiley and Sons Ltd, Chichester, 1983.

[12] S. Tanuma, C.J. Powell, D.R. Penn, Calculations of electron inelastic mean free paths. V. Data for 14 organic compounds over the 50–2000 eV range, Surf. Interface Anal. 21 (1993) 165–176. doi:10.1002/sia.740210302.

[13] D. Aili, K. Jankova, Q. Li, N.J. Bjerrum, J.O. Jensen, The stability of poly(2,2'-(m-phenylene)-5,5'-bibenzimidazole) membranes in aqueous potassium hydroxide, J. Memb. Sci. 492 (2015) 422–429. doi:10.1016/j.memsci.2015.06.001.

[14] P. Taylor, Y.S. Kim, K. Lee, Fuel Cell Membrane Characterizations, (2015) 37–41. doi:10.1080/15583724.2015.1011275.

[15] Y.S. Guan, H.T. Pu, M. Jin, Z.H. Chang, D.C. Wan, Preparation and characterisation of proton exchange membranes based on crosslinked polybenzimidazole and phosphoric acid, Fuel Cells. 10 (2010) 973–982. doi:10.1002/fuce.201000071.

[16] R. Espiritu, B.T. Golding, K. Scott, M. Mamlouk, Degradation of radiation grafted hydroxide anion exchange membrane immersed in neutral pH: removal of vinylbenzyl trimethylammonium hydroxide due to oxidation, J. Mater. Chem. A. 5 (2017) 1248–1267. doi:10.1039/C6TA08232G.

[17] K.F.L. Hagesteijn, S. Jiang, B.P. Ladewig, A review of the synthesis and characterization of anion exchange membranes, J. Mater. Sci. 53 (2018) 11131–11150. doi:10.1007/s10853-018-2409-y.

[18] R.C.T. Slade, J.R. Varcoe, Investigations of conductivity in FEP-based radiation-grafted alkaline anion-exchange membranes, Solid State Ionics. 176 (2005) 585–597. doi:10.1016/j.ssi.2004.09.044.

[19] A.J. Bard, L.R. Faulkner, Electrochemical methods, 2nd ed., John Wiley & Sons, New York, 2001. doi:10.1021/ed060pa25.1.

[20] X.-Z. Yuan, C. Song, H. Wang, J. Zhang, Electrochemical Impedance Spectroscopy in PEM Fuel Cells, Springer London Dordrecht Heidelberg New York, 2010. doi:10.1007/978-1-84882-846-9.

[21] A.L. Gonçalves Biancolli, D. Herranz, L. Wang, G. Stehlíková, R. Bance-Soualhi, J. Ponce-González, P. Ocón, E.A. Ticianelli, D.K. Whelligan, J.R. Varcoe, E.I. Santiago, ETFE-based anion-exchange membrane ionomer powders for alkaline membrane fuel cells: a first performance comparison of head-group chemistry, J. Mater. Chem. A. 6 (2018) 24330–24341. doi:10.1039/C8TA08309F.

CHAPTER 4. Blend membranes of PVA:polybenzimidazole

Blend membranes of PVA:polybenzimidazole

1 Introduction

The classification made by Merle et al. [1] is very adequate to differentiate the non-commercial anion exchange membranes (AEMs) depending mainly on their final structure and their synthesis procedure. The membranes are divided in heterogeneous membranes (subdivided in ion solvating polymers and hybrid membranes), interpenetrated polymer networks (IPNs) and homogeneous membranes. The last ones are divided depending on the preparation method: (co)polymerization of monomer, modification into a polymer and modification on a preformed film. It is very common, especially in the homogeneous membranes, to have functionalization in order to present positive cationic charges covalently bound to the polymer backbone [2–5]. These groups (usually quaternary ammonium groups) have associated counter-ions, which are OH^-s that move from one group to another and with the help of water to give the anionic conductivity necessary for the device to work. These membranes present good conductivity and adequate thermal stability but many of them suffer greatly from chemical degradation of the quaternary ammonium groups by the attack of the hydroxide ions, reducing the ion exchange capacity (IEC) and conductivity [6].

This problem is avoided using heterogeneous membranes with a doping solution responsible of the conductivity, instead of directly the functional groups of the polymer. Poly (2,2'-(*m*-phenylene)-5,5'-bibenzimidazole (PBI), poly (2,5-benzimidazole) (ABPBI) and other polybenzimidazole-based materials are well known to have satisfactory thermal, chemical and mechanical properties when they are alkali doped, as it has been discussed in the introduction of the Thesis. In order to enhance the conductivity of the membrane, blending the polybenzimidazole polymer with another polymer was chosen as an adequate strategy since it is commonly used with good results [1,7]. The other polymer chosen was poly (vinyl alcohol) (PVA), which has been previously studied for multiple applications and in different kinds of membrane. This polymer structure

presents an aliphatic chain with abundant alcohol pending groups, which are responsible of its highly hydrophilic nature and its very good HO^- transport property. Its structure becomes amorphous with the incorporation of KOH, being the ionic conductivity mainly localized in the amorphous phase [8]. Other advantages of PVA are the film forming ability, being inexpensive, biodegradable and thermally and chemically stable.

Some relevant examples of the use of PVA in ion exchange membranes are presented here: Lewandoski et al. [9] studied the system of PVA/KOH/H_2O and found that the ionic conductivity of the polymer electrolyte was in the range of 10^{-3} S cm^{-1}. Since the ionic conductivity depends highly in the content of KOH and water in the membrane, Yang et al. [8] synthesised an anion exchange membrane with higher contents of both in the PVA matrix, reaching 47 x 10^{-3} S cm^{-1} but affecting too much the mechanical strength. Acrylic acid was used to reinforce the membrane and keep the KOH inside by Yang et al. [10], they synthesised a solid polymer electrolyte system of PVA/PAA/KOH that reached a high conductivity of 30 x 10^{-2} S cm^{-1} and exhibited good mechanical and thermal properties. Nijmeijer et al. [11] prepared membranes of PVA crosslinked with itself using PEGDGE at various degrees and doped with KOH solution, they found that the introduction of PEGDGE enhanced the conductivity of the membrane, probably acting as a plasticizer improving the flexibility of the polymer chains and maybe by increasing the number of charge carriers. However too high proportion of crosslinking agent reduces the conductivity of the membranes. Some of these studies and other can be found in the review of Merle et al. [1]. PVA has also been used in membranes for alkaline batteries or alkaline direct borohydride fuel cells [6].

One of the main problems of PVA is the too high swelling capacity of the membranes in water, this causes the mechanical stability to decrease so much that the membranes are not useful for the final application. Also membranes of PVA tend to be very rigid as synthesised, before any alkali treatment and thus fragile and easy to break. To solve these problems different strategies have been carried out as described. In our case the strategy has been blending PVA with polybenzimidazoles to stabilize mechanically the membrane and make it more flexible, while PVA enhances the conductivity of the mixture.

2 Synthesis, characterization and properties

First, a mention should be done about the development of this work. The research of this chapter of PVA:polybenzimidazole membranes and the next one (polybenzimidazole-c-PVBC membranes) has been done in close collaboration between our group, directed by Professor Pilar Ocón in Madrid (Spain) and the group of Graciela Abuin in Buenos Aires (Argentina). More detailed explanation in the end of the Appendix.

The experimental procedure has been explained in detail in the previous chapter, so here just some considerations about it will be explained shortly. The temperature and vacuum (in case of vacuum oven) are critical to be controlled during the casting process, as well as level the surface where the casting is going to be performed. The membranes obtained had different depending on the thickness and components. Since PVA is a white powder that would lead to transparent membranes and the polybenzimidazoles used (PBI and ABPBI) are brown, the brownish colour of the membranes come from the last ones. Slight difference can be appreciated between different weight ratios of PVA:polybenzimidazole, not being obvious the composition of the membrane by direct observation. To peel out the membranes from the Petri dish, the addition of water filling the Petri dish and remaining there for at least 10 min was very useful. The obtained membranes had brownish colour and were very flexible, specially the PVA:PBI ones. The PVA:ABPBI were more rigid but still easy to handle. After the crosslinking both kind of membranes became stiffer but were manipulated without trouble.

2.1 Determination of the presence of polymers in the membrane and interactions between them

In order to verify experimentally the presence of both polymers in the membrane and the possible interactions different techniques were used.

2.1.1 Nuclear magnetic resonance (NMR)

The linear (not crosslinked) membrane of weight ratio PVA:PBI 4:1 (L-PVA:PBI 4:1) was chosen to perform the NMR analysis. Two techniques were used: solid

NMR to obtain the ^{13}C spectra and liquid NMR to obtain the ^{1}H NMR spectra. Pure PVA and PBI were also analysed for comparison.

For the solid ^{13}C NMR spectroscopy, Figure 4.1 shows the chemical structure of PVA and PBI with numbered carbons, a relevant part of the NMR spectra and the general spectra of the samples. Assignment of the peaks was done according to bibliography [12–15].

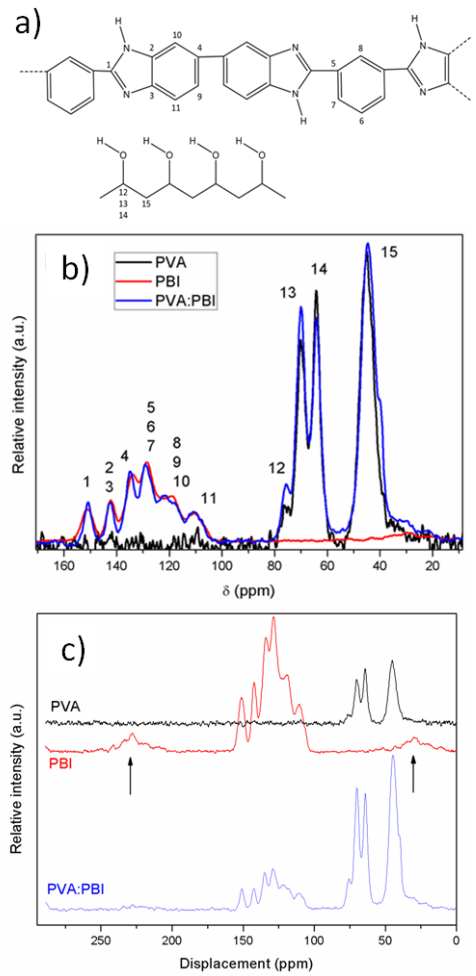

Figure 4.1. a) Structure of PBI and PVA molecules with numbered carbons, b) partial ^{13}C NMR spectrum of PVA, PBI and PVA:PBI membranes with numbers of ascribed carbons and c) complete solid ^{13}C-NMR spectra of PVA, PBI and PVA:PBI membranes. Displacement by offset was done to appreciate them separately. Rotational side bands observed in the PBI spectrum are marked with arrows.

For comparison between the different spectra, the intensity of the peaks was normalized. In the range were PBI signals are present (170-100 ppm) normalization was done with to peak at 128.5 ppm, assigned to carbons 5, 6 and 7, which as Figure 4.1a describes, belong to the solitary aromatic ring and shouldn't be influenced by the mixture with PVA. In the region where PVA peaks appear (90-30 ppm), normalization was done to the peak at 45 ppm, assigned to carbon 15, which comes from the CH_2 of PVA and is not expected to be influenced. The peaks numbered 12, 13 and 14 were assigned to carbons corresponding to the alcohol groups (CHOH) when the alcohol group presented two, one or none hydrogen bond with neighbours respectively. These signals from carbon 12, 13 and 14 are also called respectively isotactic, heterotactic (or atactic) and syndiotactic [16]. From the comparison of the pure polymers and the spectrum of the membrane, the presence of PVA and PBI can be clearly deduced. Some small differences presented in the spectra, respect to the pure ones, can give information about the interaction between them in the membrane. In the PVA region, the peaks 12 and 13 increase in intensity while the peak 14 decreases, meaning a higher proportion of OH groups of PVA forming hydrogen bonds, probably with PBI. In the PBI region, carbon 1 presents a sharper and taller signal in the 4:1 membrane and signals of 4 and 8, 9 and 10 move slightly downfield; all of them but 8 belong to the imidazole structure near the nitrogens and may present these variations due to the hydrogen bonds with PVA. The signals that appear in 227 and 30 ppm in Figure 4.1c are attributed to the rotational side-bands of PBI [15].

In the ^{1}H NMR study the results are presented in Figure 4.2. Assignments of the peaks were done according to bibliography [12,14,16].

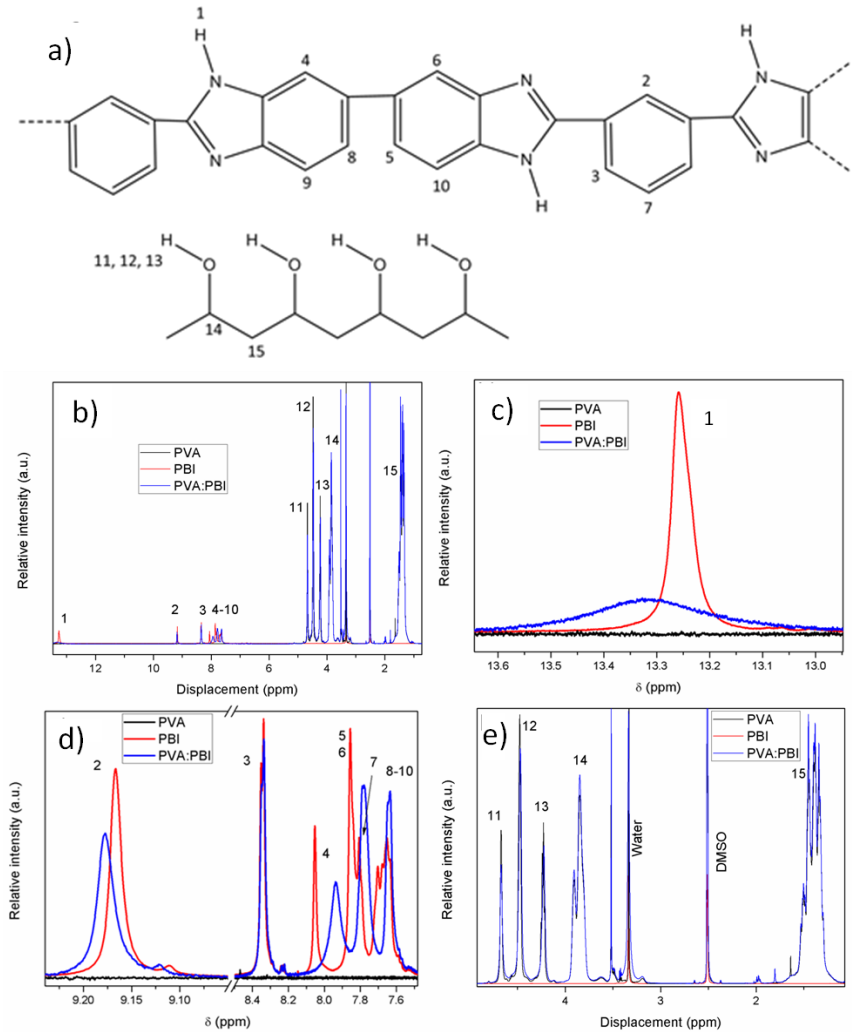

Figure 4.2. a) Structure of PBI and PVA molecules with numbered hydrogens, b) complete ^{1}H-NMR spectra of PVA, PBI and PVA:PBI solutions in DMSO-d_6, c) and d) regions with the signals coming from PBI hydrogens and e) region with signals from PVA hydrogens.

Table 4.1. Numbered protons with their respective chemical shift (δ) and integration values. [a]Atom labelling is referred to Figure 4.2a. [b] The number of equivalent protons in showed in parenthesis.

Atom[a]	^{1}H δ (ppm)[b]
1	13.3 (1H)
2	9.16 (1H)
3	8.34 (2H)
4	8.05 (1H)
5, 6	7.85 (2H)
7	7.81 (1H)
8-10	7.70-7.63 (3H)
11-13	4.67-4.22 (1H)
14	3.85 (1H)
15	1.40 (2H)

The L-PVA:PBI 4:1 result presented in Figure 4.2 corresponds to a mixture of the solution of PVA in DMSO-d_6 with PBI in DMSO-d6 with approximately 4:1 ratio. A membrane of L-PVA:PBI 4:1 was also dissolved and the comparison between both spectra is presented in Figure 4.3. No relevant differences can be appreciated. The spectra of the mixture was used for the previous comparison because of the better definition of the spectrum.

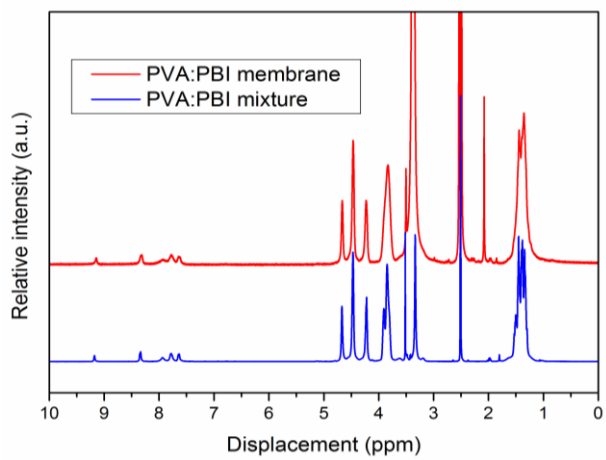

Figure 4.3. Spectra of L-PVA:PBI 4:1 membrane and mixture of DMSO-d_6 solutions of PVA and PBI with approximately 4:1 ratio.

Comparing the PVA:PBI mixture with the pure polymers (Figure 4.2), some relevant differences can be appreciated. The interaction between the polymers is

with both dissolved in solution, so it is not expected to be as intense as when they are in intimate contact in the membrane. The signal at 13.25 ppm, ascribed to the N-H proton (number 1), suffers in the PVA:PBI mixture a decrease in height, expansion of the width and slight shift downfield of 0.06 ppm. This could be explained as a clear sign of the interaction of these protons with PVA via hydrogen bonds [12]. Another change present in the PBI region is the small shift downfield of 0.01 ppm of the signal at 9.16 ppm (number 2, in Figure 4.2c), this signal is ascribed to the solitary proton in the aromatic ring and the shift could be produced by the hydrogen bonds of the near nitrogens in the imidazole rings. In the same region, changes are also observed in the signals between 8.1 and 7.6 ppm (numbers 4-10). They belong to the hydrogens in aromatic rings and probably the hydrogen bonds of NH groups modify the electron cloud producing these shiftings and modifications. Figure 4.2e shows the region where PVA signals appear. The signals not marked come from impurities and the signals at 3.3 and 2.5 ppm come from the protons of residual water presented in the solution and the DMSO used as solvent respectively [12]. The signals at 4.67, 4.47 and 4.22 ppm are ascribed to the isotactic, heterotactic and syndiotactic alcohol groups respectively (similar behaviour as the ^{13}C spectrum). No relevant differences are observed in the PVA:PBI mixture respect to pure PVA, but it makes sense since probably the ratio of "reacted" PVA (via hydrogen bonds with PBI) to the unreacted would be very low and the unreacted signals neglect the changes, even more in solution.

From the above results, it is clear the presence of both polymers in the membrane and the forming of hydrogen bonds between them, having a good chemical interaction without covalent bonds involved. This is probably the reason of the good appearance and homogeneity of the membranes, since if it was just a physical mixture probably great phase separation would occur.

2.2 Infra-red (IR) spectroscopy and Raman spectroscopy

The presence of the polymers and the functional groups were further studied using IR and Raman spectroscopy, as well as the effect of doping the membranes with KOH solution and the crosslinking with glutaraldehyde (GA).

A complete characterization of linear membranes is done first with the PBI-based ones, concretely with L-PVA:PBI ratios 2:1, 4:1 and 6:1 and compared with pristine PVA and PBI. The results are presented in Figure 4.4.

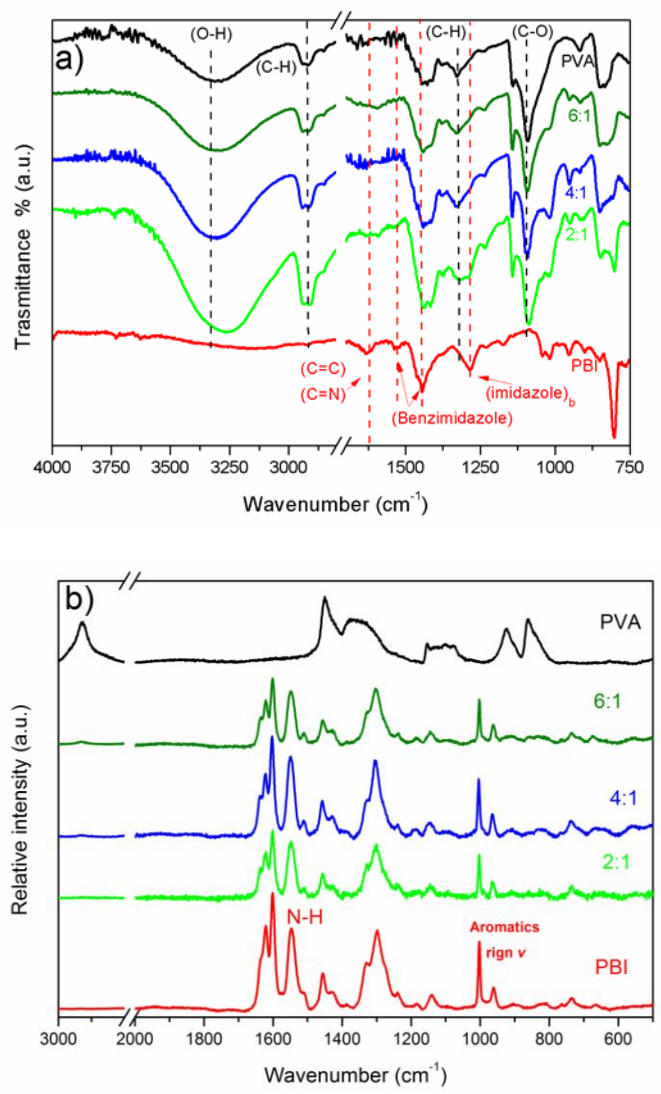

Figure 4.4. a) FT-IR/ATR and b) Raman spectra of undoped PBI, PVA and L-PVA:PBI membranes (2:1, 4:1 and 6:1).

The pristine spectrum of PVA shows a strong broad band centred at 3270 cm^{-1} due to the intermolecular hydrogen bonding and the alcohol group (O-H) stretching vibration, while the transmission peak at 1093 cm^{-1} comes from the C-O bond of PVA [17]. The asymmetrical and symmetrical C-H stretching vibrations appear at 2940 cm^{-1} and 2910 cm^{-1} respectively, and the two peaks that appear at 1425 and 1328 cm^{-1} come from the -C-H and -O-H bending, in agreement with Panero et al. [18]. As it can be observed in Figure 4.4a PVA:PBI membranes present the same characteristic peaks of PVA. Pristine PBI more important bands are in the region from 2000 to 1000 cm^{-1} and are the following: aromatic (C=C)

and (C=N) stretching modes at 1630 cm^{-1}, N-H stretching at 1536 cm^{-1}, benzimidazole in-plane deformation at 1450 cm^{-1}, and breathing mode of the imidazole rings at 1289 cm^{-1} are present in figure 4.4b [19,20]. However, the characteristic peaks of PBI are not clearly visible in the IR spectra of the blend membranes.

In the Raman spectra (see Figure 4.5) the most prominent bands come from the PBI typical ones (relative intensity in parenthesis): 1622 cm^{-1} (strong, from C=C and C=N), 1600 (strong, from C-N stretching), 1545 (strong, from N-H stretching), 1450 (medium, from benzimidazole ring), 1299 (strong, breathing mode of imidazole rings), 998 (weak) and 958 cm^{-1} (weak), both from aromatic ring vibrations [21,22]. The blend membranes with PBI presented peaks over a high broad band produced by fluorescence of the material, which was the reason of the higher intensity of the PBI peaks in PBI-based membranes, more than 20 times higher than pristine PVA even when the base-line correction was performed. The consequence was that PVA signals were masked and the Raman spectra of L-PVA:PBI membranes were similar to the PBI spectrum. As it can be observed in Figure 4.5b all PVA:PBI ratios presented similar peaks.

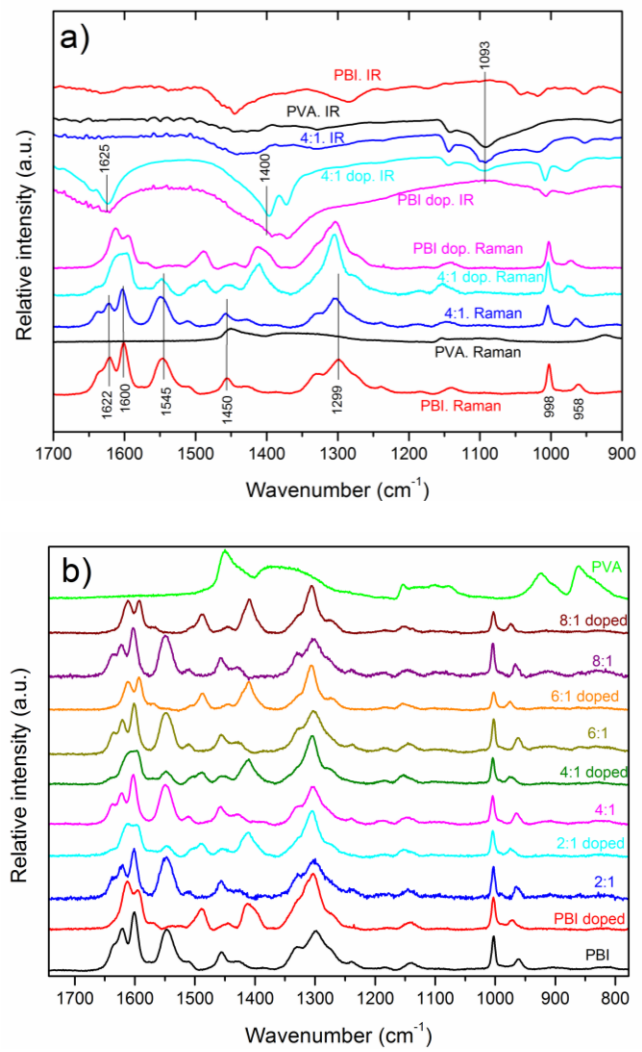

Figure 4.5. a) IR and Raman spectra of PBI and L-PVA:PBI 4:1 membranes as synthesised and doped with KOH solution as well as pristine PVA and b) Raman spectra of L-PVA:PBI weight ratios from 2:1 to 8:1 and pristine PBI with and without KOH doping and pristine PVA.

In order to check if L-PVA:ABPBI presented similar spectra, the 2:1 membrane was measured and the spectrum is presented in Figure 4.6. ABPBI presents the same relevant peaks of PBI like the peak at 1624 cm^{-1} from the C=C and C=N stretching vibrations and the peak at 1284 cm^{-1} of the breathing mode of the imidazole rings. The blend membrane shows these peaks and also typical peaks of PVA like the peaks at 2940 and 1093 cm^{-1} from C-H and C-O stretching vibrations respectively.

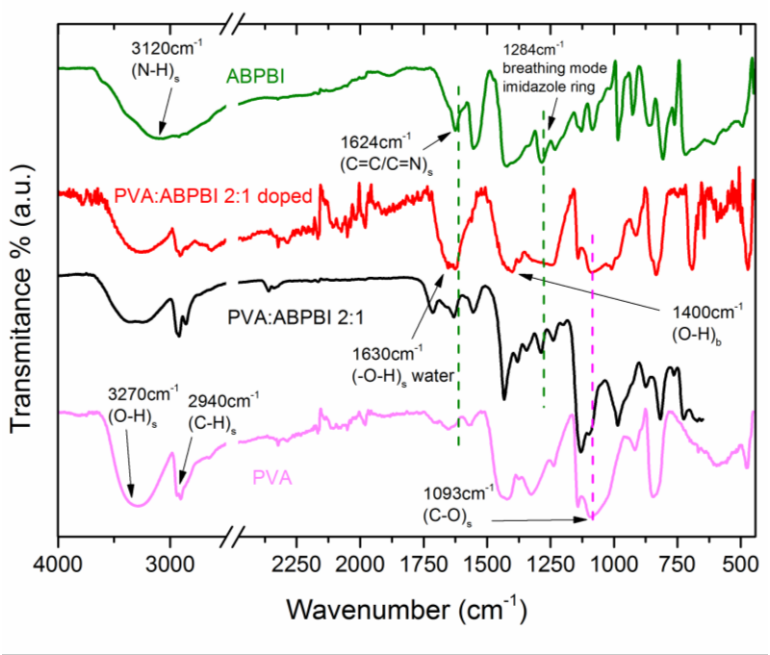

Figure 4.6. IR spectra of L-PVA:ABPBI 2:1 undoped and doped in KOH solution compared to pristine PVA and ABPBI.

Doping the membranes in KOH solution was done to enhance the ionic conductivity as it will be explained later. When the membranes are doped some changes occur in the spectra. The most relevant ones are the appearance of an intense band around 1625 cm^{-1} and another around 1400 cm^{-1}, coming from the O-H stretching of absorbed water and from the bending mode of O-H of hydroxide respectively [19,21]. Many peaks are occulted by these broad bands but others like the peak at 1093 cm^{-1} of C-O vibration are still visible. It is also interesting to note that the peak of N-H stretching at 1545 cm^{-1} in Raman is greatly reduced or even disappears after doping with KOH solution, due to the substitution of the acid H by K from KOH as described by Aili et al. [23]. These spectra can be observed in the previous Figures 4.5 and 4.6. The doping conditions were 3 days in KOH 6 M solution at room temperature.

Both IR and Raman were helpful to corroborate the presence of both polymers in the blend membranes and to check the correct doping of the membranes with KOH solution. These techniques were less time consuming than liquid or solid NMR since no dissolution or long time accumulation were needed, on the other hand they didn't allow us to observe the interactions between the polymers as the NMR did.

The process of crosslinking the PVA of the blend membranes with GA (see Figure 4.7) has been explained in the Experimental part. Some membranes are crosslinked in order to see if this process can enhance properties like mechanical, thermal or chemical stability and obtain a better performance in the PEMFC or WE, as it has been previously investigated by other groups with PVA membranes [1,17,24]. Yeom et al. [24] immersed pure PVA films in acetone with different glutaraldehyde contents (from 5 to 50 vol.% aqueous solution) using HCl as catalyst to obtain very stable PVA crosslinked membranes. Their best performance in pervaporation separation of acetic acid water mixtures was achieved with the membrane containing 5 vol.% of GA. It has to be noted that the crosslinking process between the GA molecules and the alcohol groups of PVA can affect the hydrophilic nature of the anion exchange membrane and the OH^- transport through it.

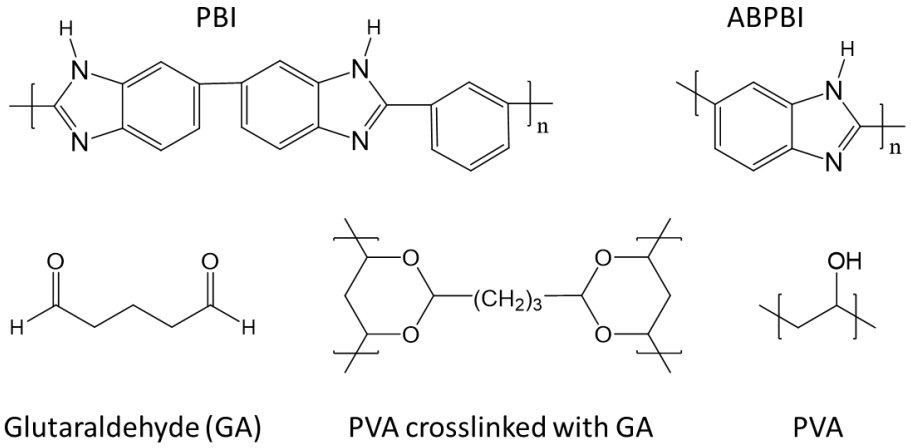

Figure 4.7. Chemical structures of the molecules and polymers used in the synthesis and the structure of the PVA chains crosslinked by GA.

To verify that the crosslinking process had been done properly, IR spectroscopy was used with the membranes C-PVA:ABPBI 4:1 and C-PVA:PBI 4:1 that were prepared with GA solution contents from 0.5 vol.% to 50 vol.%. The results are presented in Table 4.2.

Table 4.2. Absorbance ratios of hydroxyl (A_{3350}/A_{2940}) and aldehyde (A_{1720}/A_{2940}) groups of C-PVA:ABPBI membranes of 4:1 ratio crosslinked with solutions of different content of GA: 0, 0.5, 1, 5, 10, 30 and 50 vol.% and hydroxyl groups (A_{3350}/A_{2940}) absorbance ratios of membranes with pure PVA, C-PVA:PBI 4:1 and C-PVA:ABPBI 4:1.

	Aldehyde groups (absorbance ratio A_{1720}/A_{2940})	Hydroxyl groups (absorbance ratio A_{3350}/A_{2940})		
GA content (vol.% in reaction solution)	C-PVA:ABPBI 4:1	C-PVA:ABPBI 4:1	C-PVA:PBI 4:1	PVA
0	-	1,15	1,28	-
0,5	0,18	0,93	1,22	-
1	0,19	0,88	1,10	-
5	0,31	0,78	1,02	1,15
10	0,4	0,77	1,00	1
30	0,57	0,75	0,99	0,75
50	0,73	0,74	0,91	0,75

As Yeom et al.[24] observed for pure PVA membranes, in our blend membranes the IR spectra changed with the increasing content in GA. The following changes were observed:

- A decrease of the band at 3300-3400 cm^{-1} related with the reaction of PVA hydroxyl groups with GA (acetylation) and consequent loss of hydroxyl groups.

- An increase in the peaks at 1720, 2731 and 2866 cm^{-1}, which come from aldehyde groups. This could be produced by unreacted GA but this is unlikely due to the washing processes done to remove residual GA. Therefore probably the change comes from GA molecules in which only one aldehyde group has reacted with PVA and the other remains unreacted as a pendant group. This monofunctional reaction is probably favoured when the progress of the bifunctional crosslinking reaction reduces the chain mobility as postulated by Yeom et al.

- An increase in the peaks between 970 and 1385 cm^{-1} produced from the reaction of hydroxyl and aldehyde groups to form acetal carbon-oxygen bonds. This can occur with two aldehyde groups from GA with PVA hydroxyl groups (the bifunctional reaction that produces crosslinking) or with just one aldehyde group from GA reacting (monofunctional reaction previously explained).

To analyse and compare the IR spectra the peak at 2940 cm^{-1} (methylene stretching band) was used as a reference, following the strategy of Yeom et al. This reference was compared with the hydroxyl group vibration at 3350 cm^{-1} (A_{3350}/A_{2940} absorbance ratio) for association with the acetylation and the aldehyde group peak at 1720 cm^{-1} (A_{1720}/A_{2940} absorbance ratio) for the monofunctional reaction. Base line issues didn't allow to use the peaks of formed acetal carbon-oxygen bonds.

The results presented in Table 4.2 show that, as it was expected, increasing the content of GA in the reaction solution reduces the presence of hydroxyl groups due to the acetylation reaction. It also increased the monofunctional reacted GA, which makes sense due to the probably lower mobility of the chains with higher crosslinking. The trends PVA, PVA:PBI and PVA:ABPBI absorbance ratios of hydroxyl groups are also presented in the same table. PVA and PVA:ABPBI membranes have a similar trend, going to a similar absorbance ratio constant value when the GA content in the reaction solution is higher than 30 vol.%. In the case of PVA:PBI membranes the behaviour is different since it stabilizes at a higher absorbance ratio value. This is probably due to the membrane microstructure, which is less homogeneous in PVA:PBI membranes than in PVA:ABPBI ones (see SEM analysis later), hindering GA the access to some hydroxyl groups of PVA. The microstructural difference of PBI and ABPBI membranes has been reported previously by Diaz et al. [25].

It is clear that the most important changes in the absorbance ratios occur up to 5 vol.% GA content in the reaction solution. Although a higher crosslinking degree improves membrane stability, it also produces compact structures and consumption of hydroxyl hydrophilic groups of PVA and therefore lower conductivity values are expected. This is corroborated in the conductivity measurements, where the best conductivity values of crosslinked membranes were obtained with 0.5 vol.% for C-PVA:ABPBI membranes and even this low crosslinking degree produced an enormous decay in conductivity of the C-PVA:PBI membranes.

To further probe the crosslinking of the PVA in the membrane a gel content test was performed by immersion in a solution of DMSO-EtOH 5:2 with 1 wt.% NaOH at 80 ºC for 30 h. After the test the L-PVA:ABPBI membrane was completely dissolved while the C-PVA:ABPBI (GA 0.5 vol.%) had a gel fraction of 94 %.

Finally, since the imidazole/aldehyde reaction has been reported previously, the possible reaction of GA with benzimidazole was investigated by IR comparing the spectrum of L-ABPBI and the same membrane after being subject of the GA crosslinking procedure (with reaction solution of 0.5 vol.% GA). The results indicated that no reaction occurred between them since no differences were observed in the spectra.

The results obtained with IR spectroscopy in the crosslinked samples have been very useful to observe the consumption of alcohol groups from PVA in the process, obtaining mayor changes up to 5 vol.% in the relative intensities of the spectra. The effective crosslinking was also corroborated by gel fraction

measurements and the possible crosslinking of polybenzimidazole molecules was discarded from the IR results.

2.3 Thermal stability of the membranes

The thermal stability of the membranes was evaluated to know if they can be used in the final application conditions, either AEMFC or zero gap LAWE, and to obtain information about the degradation process at high temperatures. First, the behaviour of different weight ratios of L-PVA:PBI membranes were studied by thermogravimetric analysis (TGA) and differential scanning calorimetry (DSC) (2:1, 4:1 and 6:1) as well as pristine PVA and PBI membranes for comparison, the results are presented in Figure 4.8.

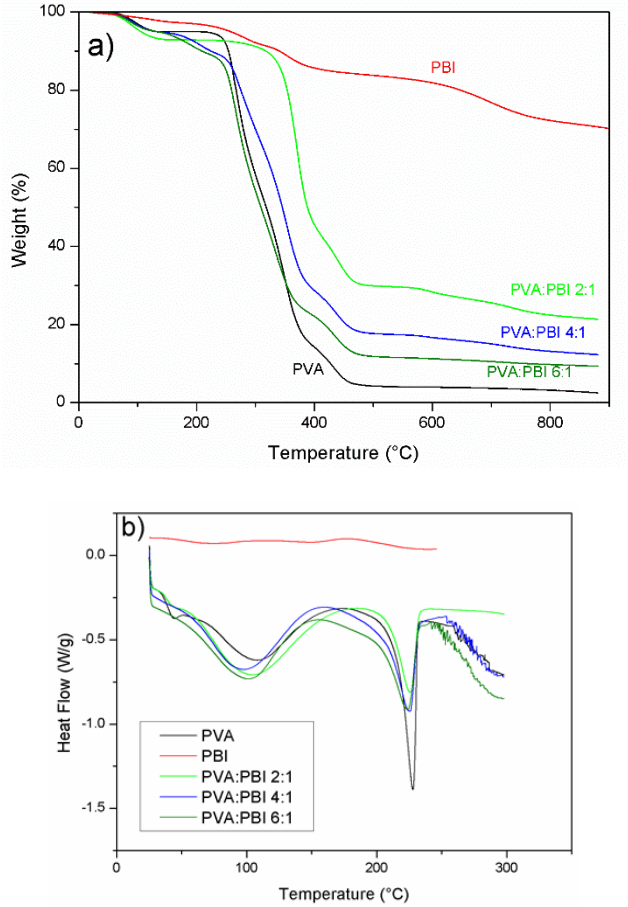

Figure 4.8. a) TGA and b) DSC measurements of blend L-PVA:PBI membranes of different ratios and pristine PVA and PBI membranes.

PBI membranes have been previously studied by many groups [19,20,26–28], in our measurements it can be observed that about 10-15 % weight loss occurs before reaching 150 ºC due to absorbed water and above that temperature no relevant weight loss is identified until reaching 500 ºC, verifying the excellent thermal stability of this polymer. From 500 to 900 ºC there is another weight loss of about 10-15 % that may come from formation of benzene and acetonitrile but most of the original mass still remains [29]. In the pure PVA membrane, three main regions of weight loss are identified. First, it losses about 5 wt.% at 96 ºC probably due to absorbed water. The second region is between 200 and 375 ºC and presents a sharp decrease of approximate weight loss of 80 wt.% from the degradation of PVA polymer membrane. It starts with the elimination of water accompanied by the formation of polyene structures in a process known as "chain stripping", after which a second loss occurs around 350 ºC were the polyene structures are converted to low-molecular weight aliphatic products, as has been described in bibliography [30–32]. The third step occurs at 400-500 ºC with a weight loss around 12 %, due to the cleavage of C-C in the backbone of PVA polymer (also called carbonation). After that the sample degrades gradually until reaching 880 ºC, remaining only 2.5 wt.% of residual ash.

In Figure 4.8a it can be observed that all the studied L-PVA:PBI samples are thermally stable at least up to 250 ºC. This is a very good result since the membranes are intended to work in the AEMFC or the zero gap LAWE at temperatures below 100 ºC and thus not temperature degradation is expected. It is interesting to note the different behaviour between membranes with different ratios, in the region from the degradation step at 350 ºC the ratios are clearly separated, with the membranes of higher content of PVA being in the lower part and presenting the lower final weight of residual ash. This result is logical because PBI still retains most of its weight in this region and thus membranes with higher PBI content show higher residual ash weight.

In the differential scanning calorimetry (DSC) results of the membranes (see Figure 4.8b) the broad endothermic band around 100 ºC is due to the evaporation of water. Blend L-PVA:PBI and pristine PVA have a clear melting transition (T_m) around 228 ºC, as it has been reported for PVA elsewhere [32,33]. The intensity of this peak is lower in the blend membranes, which can be explained by a decrease in crystallinity of PVA due to the mixture with PBI [32].

The thermogravimetric analysis of L-PVA:PBI membranes with different ratios is presented in Figure 4.9a, compared with pristine ABPBI and again with pure PVA. The general analysis is similar, with the very thermally stable polybenzimidazole polymer and the final residual ash related with the PVA content. In the same figure is also showed the TGA of a doped sample, it can be observed that the general

behaviour is similar to the undoped one but higher residual ash weight remains in the end. This effect may be related with possible removal of PVA from the blend membrane during the doping process of 3 days in KOH 6 M.

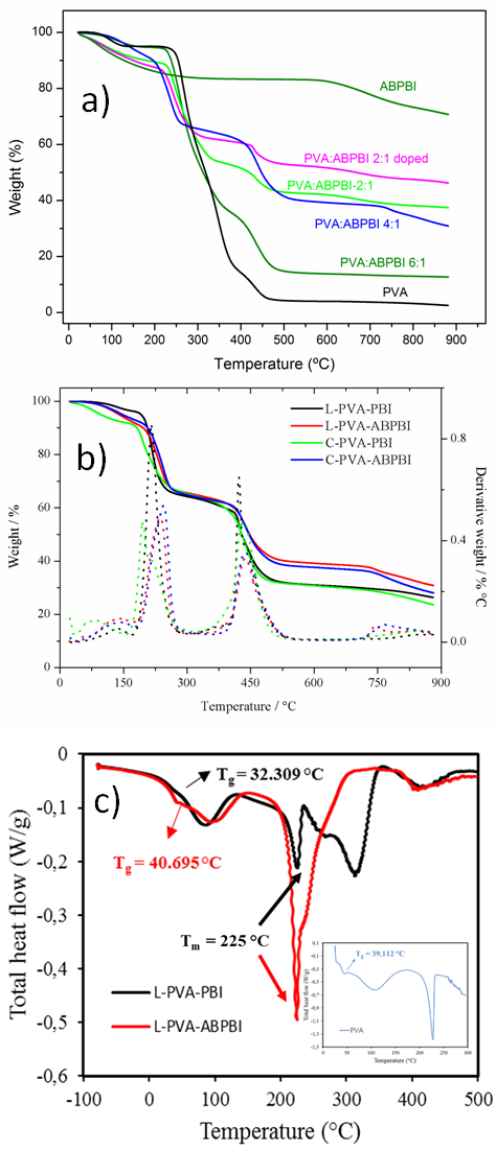

Figure 4.9. a) TGA of pristine ABPBI and PVA, blend membranes of L-PVA:ABPBI and doped L-PVA:ABPBI 2:1, b) TGA and DTG of linear and crosslinked PVA:PBI and PVA:ABPBI 4:1 membranes (0.5 vol.% GA) and c) DSC of linear PVA:PBI and PVA:ABPBI 4:1 membranes and pristine PVA (inset).

In order to investigate the effect of crosslinking, the measurements presented in Figure 4.9b were performed. Small differences are observed between the different

polybenzimidazole-based membranes, with a slightly higher weight loss around 450 ºC in the PBI ones which is probably related with differences in the microstructure. The crosslinked membranes show no difference with the respective linear ones so no thermal stability improvement is obtained. However that is not a trouble since the linear ones are already thermally stable for the application temperature range as it has been explained.

Looking at the DSC results of Figure 4.8b and Figure 4.9c it has not been detected any glass transition temperature (T_g) coming from PBI or ABPBI. The peaks of the blend membranes at 32.3 and 40.7 ºC come from the T_g of PVA (pristine one is around 39.1 ºC). The second endothermic peak is around 225 ºC and comes from the T_m of PVA as previously explained. The fact that a single T_g between both precursor polymers is not found is another probe that the membranes are blends of the polymers.

In summary, it has been observed that the higher content of PVA logically gives a lower residual ash weight at high temperatures, the degradation steps of the polymers have been studied, the mixture of PVA and PBI reduces the crystallinity of the first, the crosslinking doesn't affect the thermal stability and all blend membranes are stable at the desired operation temperature: below 100 ºC.

2.4 Ionic conductivity of the anion exchange membranes

The ionic conductivity of the membranes was measured since it is critical to know how well do they transport the OH^- anions in order to have an idea of their performance in the fuel cell or electrolyser. First, the conductivity was evaluated in L-PVA:PBI membranes with different ratios varying the days of doping with KOH 6 M solution at room temperature to investigate when adequate values were obtained. The results are presented in Table 4.3.

Table 4.3. Best conductivity (σ) and activation energy (Ea) for each L-PVA:PBI membrane at their optimum doping time and Ea for each membrane at 4 days of doping.

Membrane	σ / mS·cm^{-1} at 90 °C	Ea / kJ·mol^{-1}	Optimal doping time / days	Ea (4 days of doping) / kJ·mol^{-1}
PVA:PBI 8:1	103	9.08	1	8.75
PVA:PBI 6:1	93	9.89	2	9.73
PVA:PBI 4:1	70	6.48	3	12.66
PVA:PBI 2:1	38	4.59	3	13.18
PBI	28	6.54	5	6.47

It was observed that higher content of PVA produced a higher maximum conductivity and a shorter doping time was required to get it. The conclusion is that the presence of PVA enhances the ionic conductivity as it was expected, with higher amount of PVA more hydroxyl groups are available to absorb water and KOH by hydrogen bonds and thus easier mobility of the OH^- ions and also shorter doping time is needed since PVA is faster to dope than polybenzimidazoles. After reaching the maximum conductivity at their respective days of doping the blend membranes presented some reduction of the conductivity, this may be related with some degradation at such concentrated alkaline media, for example by removal of PVA from the blend membrane.

The best conductivity value of the L-PVA:PBI membranes was obtained with the PVA:PBI 8:1 ratio, which reached a conductivity of 103 mS cm^{-1} at 90 ºC. The other membranes obtained lower values with the decreasing in PVA content, like the 70 mS cm^{-1} obtained with PVA:PBI 4:1 at 90 ºC. Finally pristine PBI presents the lowest conductivity with 28 mS cm^{-1} at 90 ºC, which is 3.6 and 2.5 times lower than 8:1 and 4:1 membranes respectively. The obtained value for doped PBI is in the range of conductivities obtained by other authors [21,34].

To study the temperature dependence of OH^- conductivity in these membranes and the possible transport mechanisms behind that behaviour, the activation energy (E_a) was obtained from the slope of fitting the ln(σ) *vs.* 1/temperature representation, as showed in Figure 4.10.

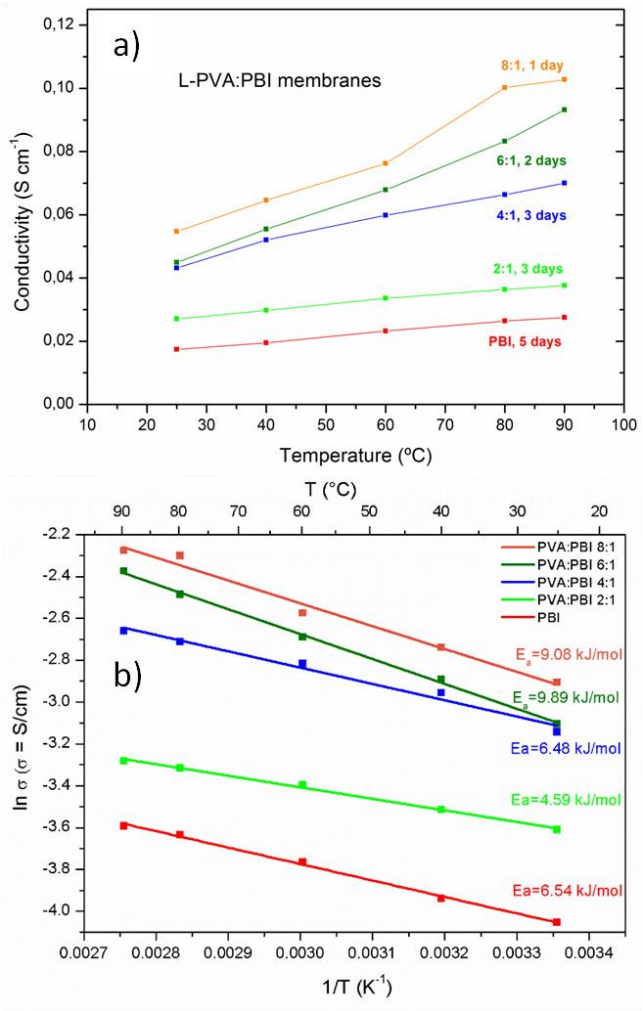

Figure 4.10. a) OH^- conductivity at different temperatures and b) associated activation energy (E_a) values obtained from the data fitting of the L-PVA:PBI membranes of different weight ratios at their corresponding best doping time with KOH 6 M.

The ionic conductivity of the membranes increases when the temperature is raised due to the enhanced mobility of the OH^- anions in the polymeric membrane. The activation energy was calculated with the Arrhenius law (equation 3.2, described in detail in the Experimental) and the obtained values are presented in Table 4.3 for each membrane's best doping time and also for every membrane with 4 days of doping. The results are similar to others previously reported in literature, like crosslinked PVA/poly (diallyldimethylammonium chloride) membranes pre-treated with 1 M KOH (Ea values of 8–10 kJ mol^{-1}) [35] or membranes of PVA/sodium alginate doped with 40 wt.% KOH (7–40 kJ mol^{-1}) [20] but have slightly lower values than some polybenzimidazole doped membranes as PBI

treated with 4 M KOH (22-23 kJ mol^{-1}) [19] or ABPBI membranes impregnated with 1 M NaOH (13.6-14-2 kJ mol^{-1}) [28]. These values have been reported to be consistent with various possible mechanisms of the anions transport. Some of the mechanisms that have been discussed to have a relevant contribution are the Grotthuss mechanism, diffusion, convection and surface site hopping. The last one wouldn't contribute in these membranes since no fixed positive quaternary ammonium groups are present. It is also important to note the relevance of humidity and temperature in these processes. Among the others, Grotthuss mechanism is considered to have an important contribution. It is based in the formation/rupture of covalent bonds of the OH^- with the water molecules through its hydrogen-bonded network to explain the transport, similarly to the situation in solution [36,37].

Since the alkali solution of the previous experiments was very concentrated (6 M), it was tried to dope these membranes with lower concentration to see if good results could be also obtained. The membranes selected to perform this study were the PVA:PBI and PVA:ABPBI 4:1. Both were also crosslinked with different amounts of GA to investigate the effect of crosslinking in the conductivity. The selected KOH aqueous concentration was 15 wt.% (2.67 M) and the membranes were immersed for 7 days to ensure complete doping. The conductivity and activation energy results obtained at different temperatures are presented in Figure 4.11a and b.

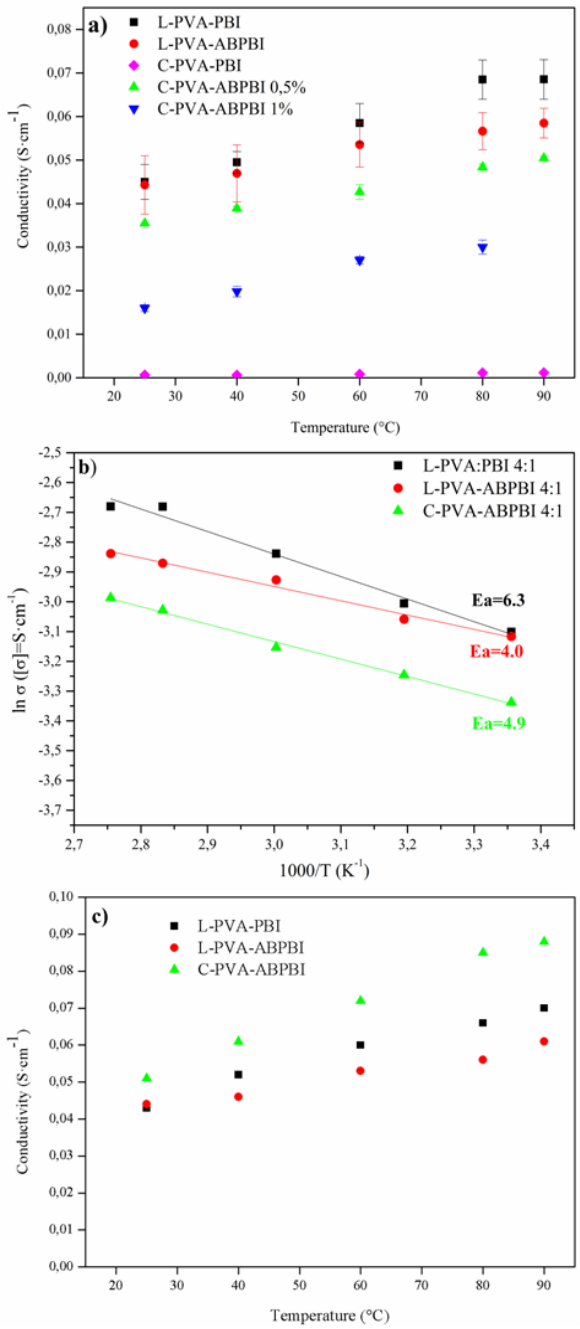

Figure 4.11. a) Ionic conductivity of the membranes L- and C-PVA:polybenzimidazole 4:1 at different temperatures doped with KOH 15 wt.%, crosslinked membranes are with 0.5 vol.% GA solution (PBI and ABPBI:PVA 4:1) and 1 vol.% GA solution (ABPBI:PVA 4:1), b) Arrhenius plot and activation energy of membranes L-PVA:PBI, L-PVA:ABPBI, C-PVA:ABPBI (0.5 vol.% GA) of 4:1 ratio doped in KOH 15 wt.% solution and c) ionic conductivity of the membranes in b) but doped in KOH 30 wt.% solution.

As it can be observed, the doped L-PVA:polybenzimidazole membranes performed high OH^- and very similar conductivities, in the range of 40-70 mS cm^{-1}, being slightly higher for the PBI based ones. These results corroborate the good ionic conductivity expected for the ABPBI based membranes and that using lower alkali concentration for a longer time is perfectly functional to obtain similar conductivity values since high doping of the membrane is reached. For the crosslinked membranes, 0.5 vol.% of GA solution produces interesting changes: in the PVA:ABPBI membrane a small decrease in the conductivity is observed, while the PVA:PBI membrane suffers a huge decrease obtaining a final conductivity lower than 1 mS cm^{-1}. These important difference between both types of membranes is probably related with the superficial or bulk microstructure, in such manner that the crosslinking in the PVA:PBI membranes entangles too much and blocks the conductive ways for the OH^- ions. Further increasing the crosslinking of the PVA:ABPBI membranes with 1 vol.% GA solution decreases more the ionic conductivity, with an important difference with the linear membranes. From these results, further study and application will only be done (for the crosslinked membranes) with PVA:ABPBI membranes crosslinked with 0.5 vol.% GA solution. The increase in the conductivity at higher temperatures is observed as in the previous results and the activation energy of showed for the best membranes in Figure 4.11b. The obtained values are in the same range of those obtained for PVA:PBI membranes doped in 6 M and thus the same transport mechanisms are involved.

A intermediate doping alkali concentration of 30 wt.% KOH solution (5.34 M) was tried with these previous membranes to see how it affects the ionic conductivity; same doping time of 7 days was used. The obtained results (see Figure 4.11c) present very similar conductivity of the linear membranes, which means that high doping is also reached and not large degradation occurs with these higher KOH concentration. However, with the C-PVA:ABPBI membrane (0.5 vol.% GA solution) a relevant increase of the conductivity is observed, this might be explained from the more entangled structure of the crosslinked membrane, which is not completely doped with the 15 wt.% KOH solution and reaches an improved doping level with the 30 wt.% one. Despite these promising results with the 30 wt.% KOH solution, finally it was decided that the 15 wt.% was better since very good conductivity values were also obtained with a much lower alkali concentration, which is expected to be an important advantage in the long term of the final device lifetime.

2.5 Mechanical properties

The membranes need to have some mechanical resistance in order to be easy to manipulate for the MEA conformation and more important, to stand the pressure in the final device under operation. In order to have an idea of the mechanical resistance to stress, two membranes of L-PVA:PBI (2:1 and 4:1) were tested in dry conditions and compared with pure PBI membrane. Moreover, to observe the effect of the doping in the mechanical strength, with the membranes having KOH inside and fully hydrated, the previous membranes were also tested in these conditions, more similar to those present in the fuel cell of electrolyser. The obtained results can be observed in Figure 4.12.

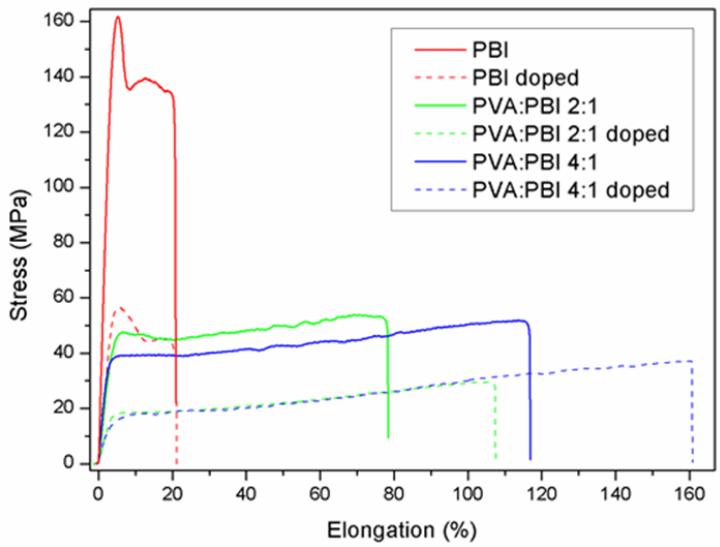

Figure 4.12. Mechanical tensile strength of PBI, L-PVA:PBI 2:1 and 4:1 membranes as synthesised and doped in KOH 6 M.

From Figure 4.12, in the not doped membranes, it is clear that pristine PBI has higher mechanical strength that the blend membranes and all of them have good mechanical properties, being very similar between the two studied blend ratios. This result makes sense since PBI membranes have always demonstrated high mechanical strength like in the studies of Zeng et al. [21,38] where values around 100 MPa are obtained for PBI, being higher in our case but in the same order of magnitude or those of Aili et al. [23,39] which are very similar to our results, around 140 MPa. On the other side, PVA usually has much lower mechanical strength values, like those reported by Yang et al. [8,10], below 4 MPa. PVA also shows higher elongation % than PBI and thus the obtained results with blend

membranes of lower tensile strength but higher elongation than PBI. When the membranes are doped it is observed a reduction in the maximum stress (especially in pure PBI) and improvement in the elongation (especially in the blend membranes). This effect is produced by the cleavage of intermolecular hydrogen bonds of the polymers due to the introduction of water and KOH molecules in the structure, making it less rigid [40]. It has been observed the same effect in the previously mentioned studies.

For the membranes based in ABPBI, the samples used to perform the tests were the L- and C-PVA:ABPBI 4:1. When these membranes are manipulated it is already observed that they are much more fragile than the PBI based one and the mechanical test corroborated it. A low value around 1.5 MPa is obtained for the linear membrane, while presenting very good elongation (around 175 %). When they are crosslinked, the membrane becomes more rigid as expected, with a higher tensile strength around 3 MPa and reduced elongation (around 30 %). Since membranes with tensile strength values near 2.5 MPa are considered acceptable for the final use [10], all the previous synthesised membranes are adequate from the mechanical properties point of view to be used in the electrolyser of fuel cell, being the ABPBI based ones near the limit.

2.6 Surface and cross-section

The surface and cross-section of the membranes were investigated by scanning electron microscopy (SEM) pictures and energy dispersive X-ray (EDX) analysis and the results are presented in the following figures. The different ratios of linear PVA:PBI membranes surface pictures are presented in Figure 4.13 and 4.14.

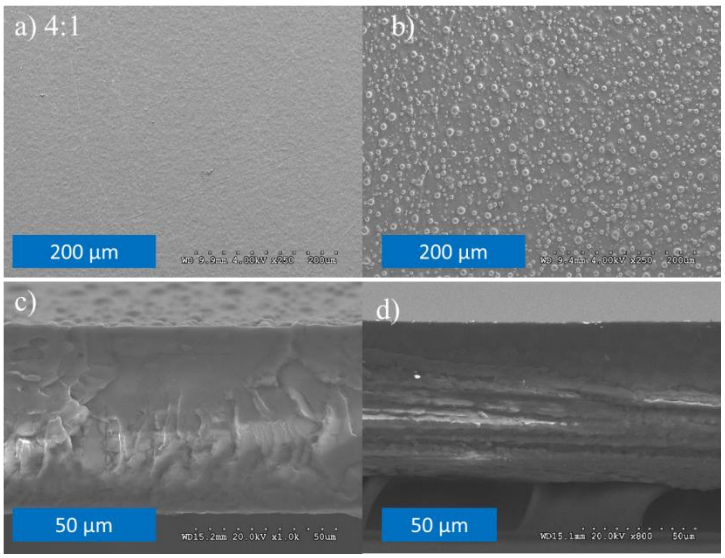

Figure 4.13. Linear PVA:PBI 4:1 membrane surface (top) and cross-section (bottom) a) and d) before doping and b) and c) after doping in KOH 6 M.

The surface of the linear PVA:PBI membranes before doping was smooth and flat in all the cases as it was expected. However, after the doping process a change is observed in the surface of the membranes, especially those with lower PVA content: small circular islands appear in the surface, probably due to the removal of some polymer by the alkali solution. As is can be observed, in the ratios with higher amount of PVA this effect is not observed, so probably the PVA is the removed component and there is still too much to clearly see its removal.

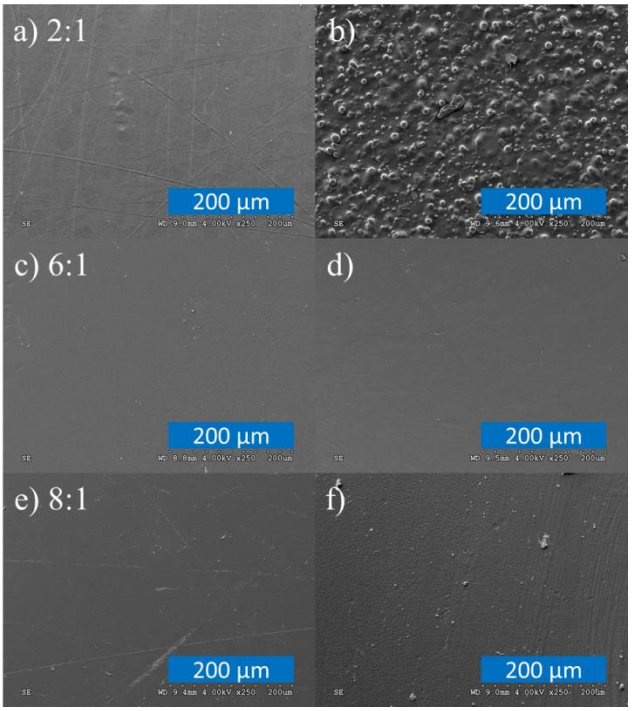

Figure 4.14. Different ratios of L-PVA:PBI membranes before (left) and after (right) doping in KOH 6 M. a) and b) are 2:1, c) and d) are 6:1, e) and f) are 8:1.

The EDX results, presented in Figure 4.15 and Table 4.4, confirm this idea since the circular islands have a much higher N/O ratio (N from PBI and O from PVA) than the undoped membrane and the dark areas of the doped one. This results would come from mainly PBI remaining in the circular islands and mostly PVA being removed from the rest of the surface. Some sulphur is observed also in the membranes, probably coming from residues of the DMSO used as solvent in the synthesis.

It is important to note that the removal of PVA apparently occurs only in the surface, no tunnel like forms are observed in the cross-section of the doped membranes (Figure 4.13c). These means that not crossover of the reactants under operation is expected due to the doping process, which is a relevant requirement.

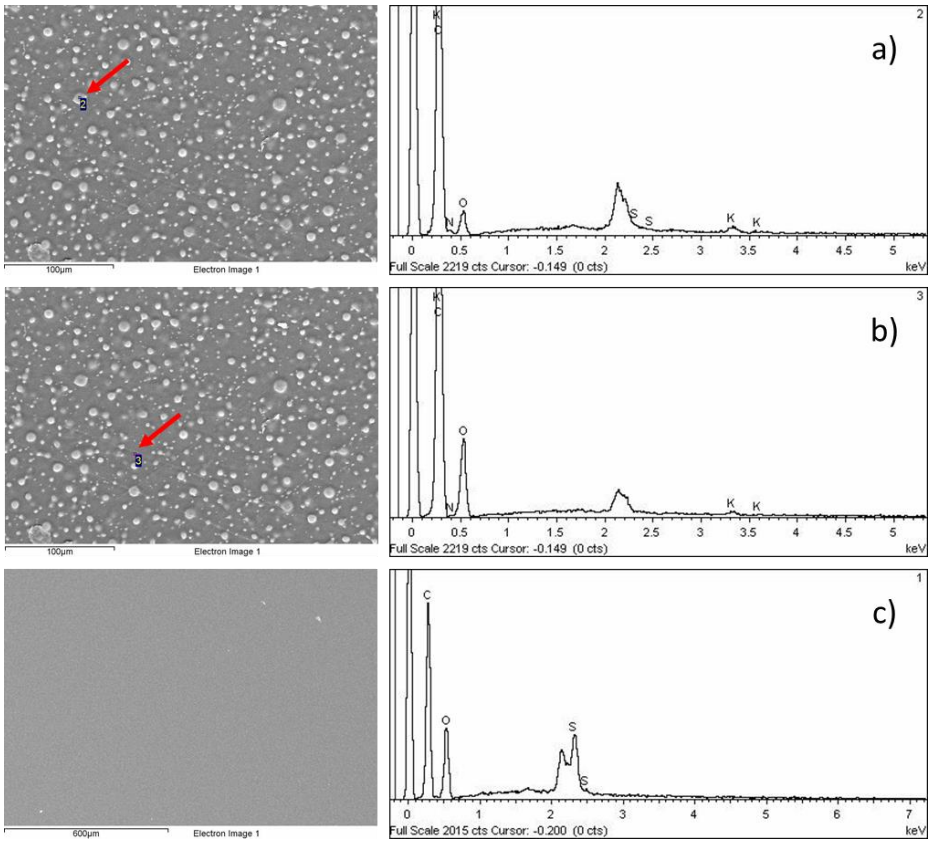

Figure 4.15. SEM pictures and EDX analysis of L-PVA:PBI 4:1 a) circular island, b) dark zone (both after doping the membrane in KOH 6 M) and c) general area of the membrane before doping.

Table 4.4. EDX analysis results from the spectra of Figure 4.15, membrane of L-PVA:PBI 4:1.

	Atomic %		
	4:1 doped		4:1 undoped
Element	Circular islands	Dark zone	General
C	77,2	75,84	65,86
N	12,16	3,32	5,08
O	10,48	20,81	28,54
K	0,08	0,04	
S	0,08		0,52
N/O	1,16	0,16	0,18

The surface and cross-section of L-PVA:ABPBI 4:1 and C-PVA:ABPBI 4:1 (0.5 vol.% GA) after being doped in KOH 15 wt.% were also studied. In contrast with the heterogeneities showed in the L-PVA:PBI membrane, the linear and C-PVA:ABPBI membranes presented a smooth and homogeneous surface which might come from a better miscibility of these polymers.

It can be concluded that the membranes have homogeneous surface before doping and are affected superficially by the alkali doping solution by removal of PVA, except the analysed PVA:ABPBI linear and crosslinked membranes which show an homogeneous appearance even after the doping process.

2.7 Water uptake, KOH uptake and swelling behaviour

The following results present in detail how the membranes change in weight and dimensions due to the incorporation of water and KOH due to the doping process. It is important to consider what these changes could produce for the MEA preparation and the final device performance. As in the previous sections, first the linear PVA:PBI membranes are studied. Their water uptake, KOH uptake and swelling results are presented in Figure 4.16.

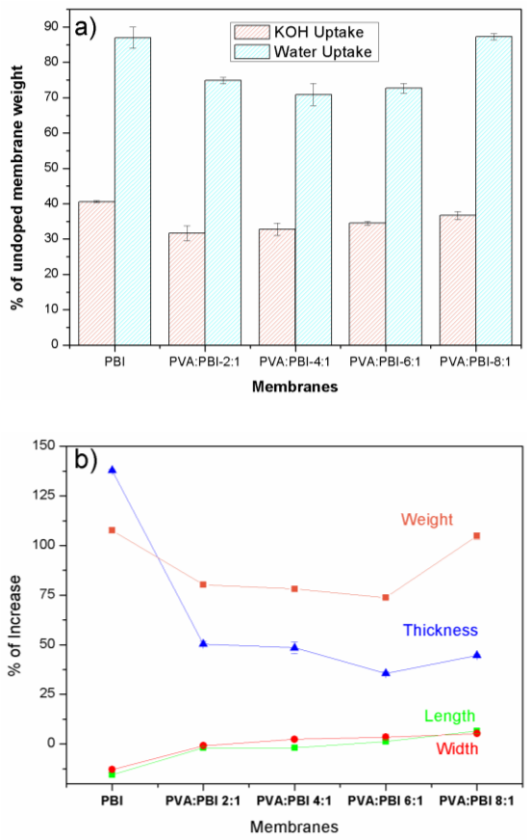

Figure 4.16. L-PVA:PBI membranes and pristine PBI membrane results of a) KOH and water uptake and b) swelling behaviour after doping in KOH 6 M solution for their corresponding best doping time (5 days PBI, 3 days 2:1 and 4:1, 2 days 6:1 and 1 day 8:1).

Both PVA and PBI show high affinity to water as it has been previously reported. For example PVA membranes gain around 36 wt.% when hydrated, which corresponds to 0.9 molecules of water per PVA r.u. (repeating unit) as investigated by Lim et al. [41], while PBI membranes gain 23 wt.% in water, which corresponds to 4 molecules of water per PBI r.u. [19]. Since PVA gains relatively more water than PBI, it would be expected than the addition of PVA to PBI to form the blend membranes will increase the amount of absorbed water and KOH. The values we obtain are much higher than those just mentioned. This is explained by the fact that the membranes increase the water uptake greatly when kept in alkaline medium due to the water molecules solvating the K^+ of OH^- ions that enter the structure, reaching values of above 10 water molecules per PBI r.u. as reported by Linares et al. [19].

From our results, pristine PBI membrane absorbs more than 85 wt.% of water and approximately 40 wt.% of KOH. The volume increase is around 75 % (volume

increases are not showed in the figure), which is in the range of the 84 % obtained by Aili et al. in similar conditions [42]. The addition of PVA, contrary to the expected behaviour, shows that low quantities of PVA reduce the KOH uptake and water uptake of the blend membranes respect to PBI. The volume swelling is also reduced, being 49 % in the 4:1 ratio. The explanation probably comes from the interaction between PVA and PBI, where many chains are mixed and abundant hydrogen bonds are formed between the polymers. This may give rise to less available groups for the interaction with water and a more condense structure where water has more difficulty to penetrate, which is corroborated by the considerably lower thickness increase of the doped blend membranes compared to pristine PBI. However, by further increasing PVA content, the high affinity for water and KOH rises as expected; reaching in the PVA:PBI 8:1 ratio values of water and KOH uptake similar to pristine PBI. The volume swelling also increases, up to 62 % in the mentioned membrane.

In the swelling behaviour presented in Figure 4.16b, length and width of the membranes suffer minor variations compared to the thickness. Pristine PBI shows a contraction of length and width larger than 10 %, while the presence of PVA gives a small expansion of the membranes up to 6 % with the 8:1 ratio.

To investigate the difference of doping with KOH 15 wt.% during 7 days (similar to the other characterizations previously explained), the L-PVA:PBI 4:1 membranes were measured. Since these conditions have been also used in the C-PVA:PBI 4:1 and linear and crosslinked PVA:ABPBI 4:1, these membranes were equally measured. The swelling behaviour results are presented in Table 4.5.

Table 4.5. Swelling behaviour of membranes doped in KOH 15 wt.% aqueous solution 7 days.

Membrane	Volume swelling / %	Thickness swelling / %	Length swelling / %
L-PVA-PBI 4:1	80 ± 5	48 ± 4	9 ± 1
L-PVA-ABPBI 4:1	83 ± 3	18 ± 7	25 ± 5
C-PVA-PBI 4:1 - 0.5 vol. % GA	95 ± 11	50 ± 5	6 ± 3
C-PVA-ABPBI 4:1 - 0.5 vol. % GA	84 ± 12	14 ± 8	27 ± 6

The volume swelling is in the range of 80-90 % in all the membranes. However, the PBI-based membranes and the ABPBI-based membranes show differences in the thickness and length behaviour, being around 49 % and 16 % thickness swelling respectively for PBI and ABPBI-based ones. On the other hand, the increase in length was higher in the PBI-based membranes (around 26 %) than in the ABPBI-based membranes (around 8 %). Compared to the previous results of doping in more concentrated alkali solution, the swelling behaviour is very similar

in the L-PVA:PBI 4:1 membrane, which tells that probably the membrane grows as much as possible in both conditions, even with different KOH and water uptakes as will be later discussed. The anisotropic behaviour (larger increase in thickness direction than in length/width) has been previously reported in PBI membranes by Aili et al. [23] and Zeng et al. [21] and is related with the microstructure of the membranes, which explains the differences between membranes with different polybenzimidazoles. The volume increase obtained in these membranes is higher than those of the pure polymers in literature. Aili et al. [42] obtained a volume increase of 64 % with linear PBI, which is comparable to the 50 % volume increase reported by Diaz et al. [43]. Probably the reason is the blending of the polybenzimidazole polymer with PVA, which in this case allows higher final volume. The effect of quite different swelling behaviour in polybenzimidazole membranes at different alkali concentrations has been also reported by other authors like Linares et al. [19] or Aili et al. [42].

From the comparison with literature, the swelling behaviour of the membranes is considered to be moderate and adequate to be used in the final application.

Regarding the KOH and water uptake of these membranes, the obtained results are presented in Table 4.6 and Figure 4.17.

Table 4.6. KOH and water uptake of the membranes respect to the initial dry weight and final polymer content in the doped membrane. After doping in KOH 15 wt.% solution 7 days.

Membrane	Polymer / %	KOH / %	H_2O / %
L-PVA-PBI 4:1	49 ± 2	1 ± 0.5	50 ± 2
L-PVA-ABPBI 4:1	30 ± 7	1 ± 0.5	69 ± 7
C-PVA-PBI 4:1 - 0.5 vol. % GA	73 ± 6	5 ± 0.5	22 ± 6
C-PVA-ABPBI 4:1 - 0.5 vol. % GA	25 ± 4	8 ± 0.5	67 ± 4

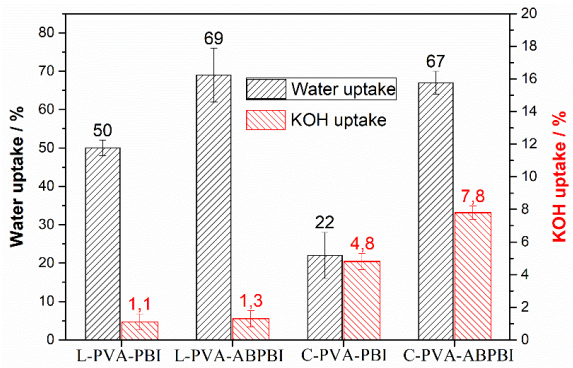

Figure 4.17. Water and KOH uptake of linear and crosslinked PVA:polybenzimidazole 4:1 membranes after doping in KOH 15 wt.% 7 days.

The water uptake of the linear membranes is in the same range, but the ABPBI shows a higher value which probably comes from the more hydrophilic structure. The value of L-PVA:PBI 4:1 is slightly lower than when it was doped with high concentrated KOH solution, but it makes sense since the KOH uptake is much lower and KOH helps to introduce water (solvating the ions) in the membrane. The crosslinked membranes show a different behaviour: the PBI-based membrane reduces greatly the water uptake to a 22 %, while the ABPBI-based one maintains a 67 % similar to its linear membrane. This difference could be related with the homogeneity of the distribution of PVA in the membranes that was previously investigated in the SEM analysis, in such a way that the better homogeneity of the ABPBI-based membranes allowed a better distribution of the crosslinking and thus much lower influence in the absorption of water. The low value of the KOH uptake results is partially explained by the lower concentration of the doping solution. Also some calculation error might influence in the KOH uptake calculation, since it is based in the initial dry weight of the membrane which in the case of linear membranes has changed after the doping and washing (8-13 % loss) while in the crosslinked membranes this effect is not so severe (only around 1 % loss). Even with this uncertainty in the exact KOH uptake, it can be observed that ABPBI tends to absorb also more KOH than PBI-based membranes, which comes from the same structural reason than the water uptake.

These obtained values of KOH and water uptake, independently of the high or low alkali concentration, have demonstrated by the conductivity experiments (except the crosslinked PVA:PBI membrane) to be adequate for the final application. This shows that the interaction of all the parameters (homogeneity, microstructure, KOH and water uptake) play a relevant role in the final conductivity and applicability of these membranes.

2.8 XPS insights of the doping process

XPS measurements were performed to investigate more deeply the doping process of the membranes. The sample used to do it was the L-PVA:PBI 4:1 and the results are presented in the following figures. In Figure 4.18 it can be observed the change in the O 1s spectra with zero, 1 and 6 days of doping in KOH 6 M at room temperature. The spectrum of the not doped sample can be deconvoluted using a single synthetic peak with Gaussian-Lorentzian shape at a binding energy (BE) of 532.5 eV, which can be attributed to the oxygen in the -C-OH bonds of PVA. When the membrane is doped and the doping time increases, this peak becomes broader and a new feature clearly appears in the low binding energy side. These

changes can be attributed to the doping of the sample with KOH. Spectra of the samples after doping can be deconvoluted using two peaks, the first with the previous binding energy of 532.5 eV and the second at 531.2 eV. The second one could be attributed to oxygen in the HO^-K^+ bonds that are formed during the doping process, in good agreement with H. Hou et al. [44]. They proposed a mechanism in which hydrogen bonding was formed between OH^- and -N= in the imidazole ring of PBI, while K^+ goes into the polymer next to OH^- to balance the charge. It is interesting to note that in alkali doped graphene oxide the O 1s spectrum also shows a peak around 531 eV that has been attributed to oxygen in OH^-, therefore supporting the proposed assignation.

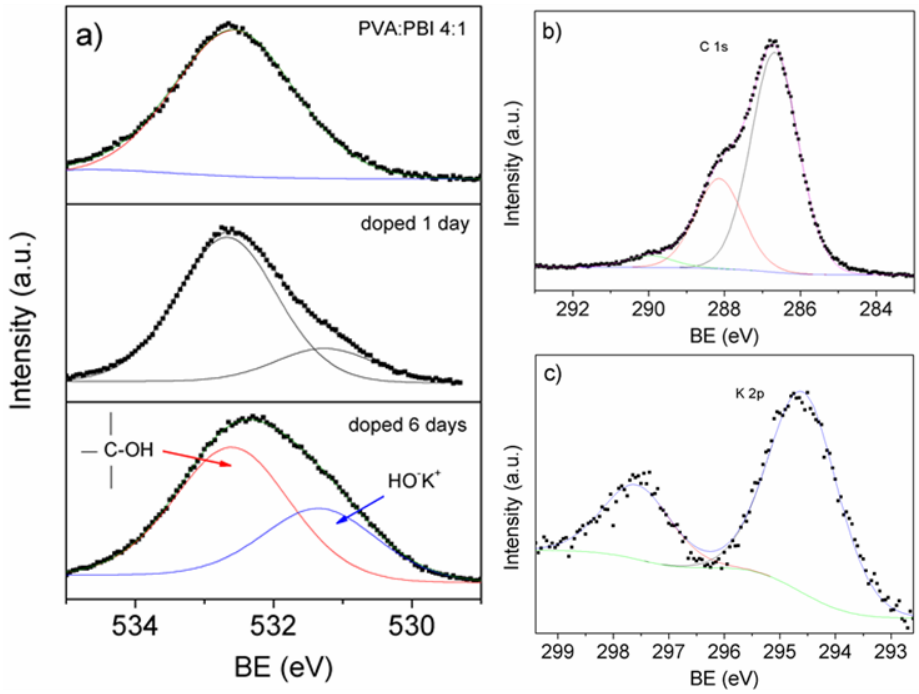

Figure 4.18. XPS spectra of a) Evolution of the O 1s peak measured on the PVA:PBI 4:1 membranes for different doping times in KOH 6 M up to 6 days. The spectrum labelled as 4:1 corresponds to the not doped sample; b) C 1s and c) K 2p spectra measured on the 1 day doped membrane. The synthetic peaks used for deconvolution are also presented.

The N 1s spectrum of membrane PVA:PBI 4:1 is presented in Figure 4.19a. The result can be deconvoluted in two peaks, at 400.4 eV and 398.6 eV, which could be attributed respectively to the nitrogen of amine (-NH-) and imine (=N-) present in the imidazole rings of PBI, based in the results published by other authors [21,45].

The C 1s and K 2p spectra of the sample after 1 day of doping are showed in Figure 4.18b and c respectively. The first was deconvoluted in three synthetic peaks at 285, 286.4 and 287.8 eV. The interpretation is controversial, but there is a general consensus to attribute the peak at binding energy 285 eV (which is used as a reference) to C-C and to C-H bonds [46,47]. In the CN compounds, polarization occurs due to the difference of electronegativity between the atoms of carbon and nitrogen, which leads to a transfer of negative charge from carbon to nitrogen atoms. This effect decreases the binding energy of the N 1s level and increases the binding energy of the C 1s. Since the nature of the bonding between carbon and nitrogen (C-N or C=N) affects the charge transfer effect, the other two peaks can be ascribed to these bonds. The K 2p spectrum shows a doublet with the peak $2p_{3/2}$ at 292.9 eV and a spin-orbit splitting of approximately 3 eV. In literature, the metallic K $2p_{3/2}$ has been reported at a binding energy of 294.6 eV, whereas oxidized and nitrided potassium appears at lower binding energies shifted approximately 1.7 eV [48,49]. Therefore, the peaks in Figure 4.18c were attributed to potassium in both =N-HO-K^+ and -N-K bonds, which are created due to the doping process.

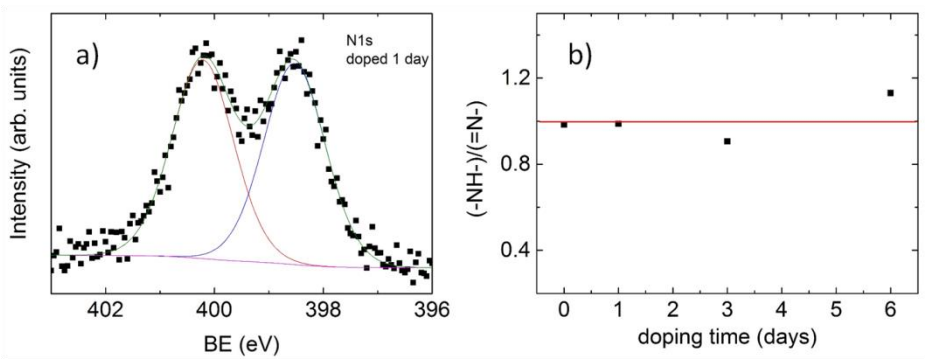

Figure 4.19. a) XPS spectra of the PVA:PBI 4:1 membrane N1s and b) Peak area ratio of N1s related to amine (-NH-) and to imine (=N-) in the imidazole rings as a function of the doping time. The red line of ratio equal to one is given for comparison.

In Figure 4.20a is presented the evolution in the peak area ratio of K 2p/N 1s in function of the doping time. The sensitivity factors provided by the manufacturer to normalize the corresponding peak areas are S_K (4.04) and S_N (1.77). According to the reaction mechanism proposed by Hou et al. [44]/L. Zeng et al. [21] this ratio should remain constant and equal to one. In our results the ratio increases with larger doping time and reaches values far above one, meaning that more K species are incorporated within the blend membrane framework due to the alkali doping process.

The evolution with the doping time of the ratio of amine to imine in the imidazole rings is showed in Figure 4.19b. The ratio remains constant and equal to one, which was the expected result based on the PBI structure; corroborating that the doping process didn't alter the number or the N type of species in imidazole rings of PBI.

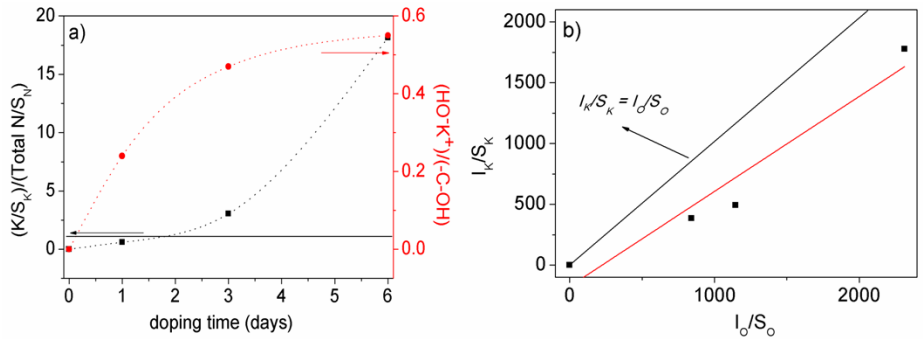

Figure 4.20. a) Evolution of the peak area ratio K 2p/N 1s (left axis) and the peak area ratio of the O 1s of HO^-K^+ bonds to the O 1s of -C-OH bonds of PVA (right axis), as a function of the doping time in KOH 6 M. The peak areas are normalized to the corresponding sensitivity factor (S_K and S_N) and the dotted line is given as a guide for the eye. b) Evolution of the K 2p intensity in function of the oxygen peak intensity at 531.2 eV (black squares). The red line is the experimental data fit to a straight line (slope = 0.78) and the black line represents the expected linear dependence.

The ratio of oxygen from the doping process (in HO^-K^+ bonds) to the oxygen of PVA (in -C-OH bonds) is illustrated in Figure 4.20a (red line and right axis). It can be observed that the ratio tends to saturate when the doping time overcomes 3 days. Again the values are higher than those proposed by H. Hou et al. [44], which was a ratio of 0.036 (1:28 molar, 1:4 weight, PBI:PVA), thus these results also indicate the incorporation of more K species than those expected from that reaction mechanism.

Figure 4.20b shows the evolution of the K 2p intensity as a function of the oxygen peak at 531.2 eV of the O 1s spectrum. The sensitivity factors provided by the manufacturer are S_K (4.04) and S_O (2.85). The experimental results deviate from the expected linear dependence of $I_K/S_K=I_O/S_O$, which could be explained by the incorporation of oxygen in (HO^- species) coming from water, apart from (HO^-K^+), contributing to the peak at 531 eV in the O 1s spectrum or by higher incorporation of OH^- by hydrogen bonds with PVA than K^+.

In conclusion, the XPS served to elucidate that nitrogen atoms of PBI remained unaffected during the doping process as expected, the detection of successful incorporation of OH^- and K^+ in the structure due to the doping and in quantities

much higher than the expected, probably due to the presence of both polymers in the structure and high KOH concentration.

3 Performance in final application

The synthesised membranes are tested in real application electrochemical devices, both in a direct ethanol fuel cell (DEFC) with single cell configuration and in a zero gap liquid alkaline water electrolyser (LAWE), also single cell. It was done in this way to study the membranes without the problems that may appear in a stack, so the final performance of the device due to the different membrane used can be better evaluated. The results for both devices are presented in the following section.

3.1 Direct ethanol fuel cell

The results were obtained using different membranes of linear and crosslinked PVA:polybenzimidazole and commercial PBI membrane (for comparative purpose) as the anion exchange polymer electrolyte, all of them previously doped in KOH aqueous solution. The catalysts used for preparing the electrodes were commercial PtRu/C in the anode and commercial Pt/C in the cathode. The performance measurements were carried out at a temperature of 90 ºC and feeding the fuel cell in the anode with 2 M EtOH / 2 M KOH aqueous solution and in the cathode with pure oxygen gas. The backpressure of the oxygen flow was 0.5 atm (7 psi). The first presented results, in Figure 4.21, are from the different ratios of linear PVA:PBI membranes, which are compared with the commercial PBI. Based on the previous study of better doping time that has been done, each of them was measured after that best doping period in KOH 6 M. The membranes with high content of PVA (6:1 and 8:1) presented some structural problems, making difficult to handle and measure the 6:1 and impossible the 8:1. These problems are probably related with the more heterogeneous microstructure (compared with ABPBI-based ones) and the lower mechanical properties than pure PBI. This problem also produced some crossover of oxygen gas from the cathode to the anode, as observed during the measurements, decreasing the open circuit potential (OCP). This makes that the PVA:PBI 6:1 membrane obtains the

low result of 11 mW cm^{-2} at voltage 220 mV. On the other hand, the enhanced conductivity of the blend membranes allows the membrane of 2:1 ratio to reach 45 mW cm^{-2} (279 mV), near the 53 mW cm^{-2} (260 mV) obtained by the commercial PBI membrane. The best result with this type of membranes is obtained with the PVA:PBI 4:1 ratio, which achieves 76 mW cm^{-2} and potential 310 mV, this result is 43 % better power density than the commercial PBI under the same conditions and thus is considered a very good performance. This membrane gets the compromise between the structural problems of higher PVA quantity with the better conductivity it gives to the electrolyte membrane. The C-PVA:PBI membranes were not tried in the fuel cell, since the lower conductivity values obtained wouldn't allow to reach good performance.

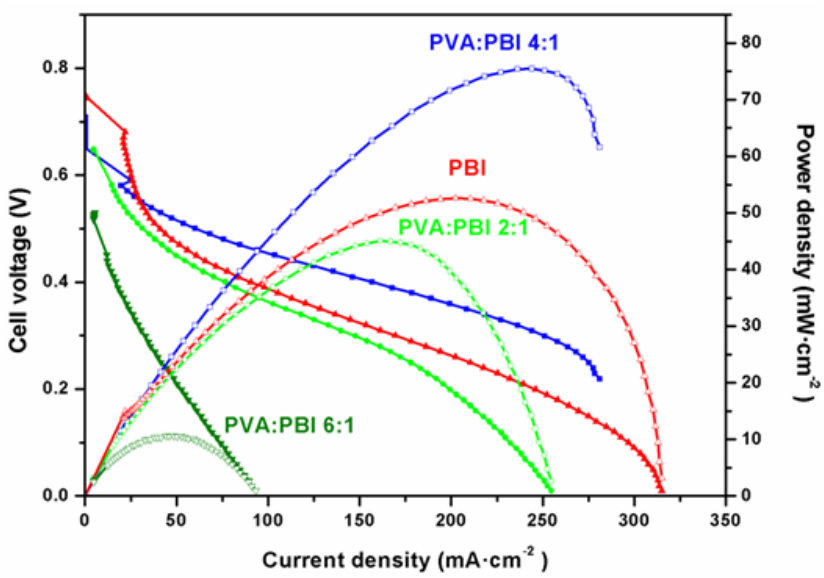

Figure 4.21. Fuel cell polarization and power density curves using L-PVA:PBI membranes of different ratios.

Based in the previous study of best doping time, the doping time of 3 days in 6 M KOH was selected to be used with the linear and crosslinked PVA:ABPBI membranes since it presented very good results and was enough for an adequate doping of the membranes without being too long. The curves obtained with L-PVA:ABPBI membranes are illustrated in Figure 4.22. As it can be observed, the results obtained are considerably higher than those of L-PVA:PBI membranes. The lowest power density value, with the L-PVA:ABPBI 6:1, is 80 mW cm^{-2} (at 338 mV), already higher than the best of L-PVA:PBI ones (76 mW cm^{-2} with 4:1 ratio). The rest of the maximum power density results, from lower to higher are: 88 mW cm^{-2} at 338 mV with PVA:ABPBI 1:1, 102 mW cm^{-2} at 358 mV with PVA:ABPBI 4:1 and 124 mW cm^{-2} at 378 mV with PVA:ABPBI 2:1. These good

results can be explained by the better homogeneity of the microstructure of these membranes, which give a high OCP around 850 mV for most of them, making the polarization curve to start from a higher beginning. Since the activation losses are similar as well as the ohmic resistance (the conductivities were almost equal) the L-PVA:ABPBI membranes are able to reach better power densities than their counterparts. It is worth to note that a similar effect occurs when increasing the PVA content, improving the conductivity but also making worse the structural problems, as corroborated by the lower OCP of the 6:1 ratio. The 124 mW cm^{-2} reached with the L-PVA:ABPBI 2:1 membrane is the highest obtained with this type of blend membranes and reveals and important increase of 2.34 times better than the 53 mW cm^{-2} of the commercial pure PBI membrane under the same conditions.

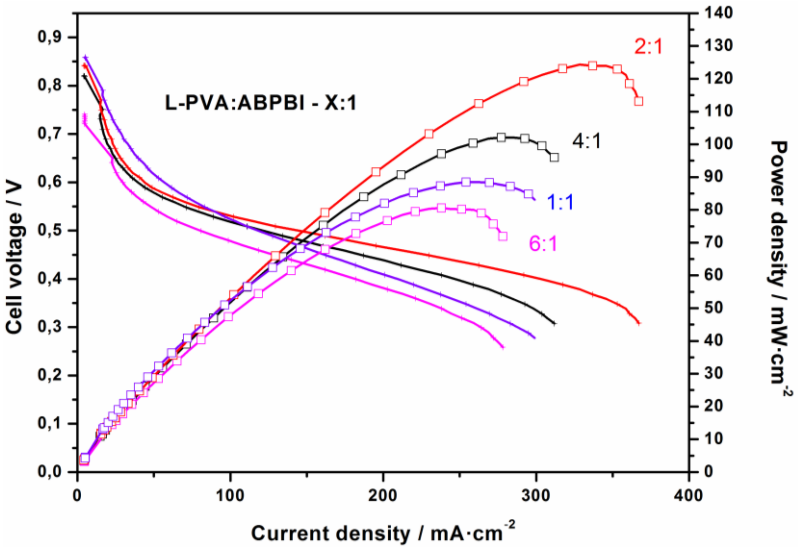

Figure 4.22. Fuel cell polarization and power density curves of L-PVA:ABPBI membranes with different ratios.

Finally the membrane of L-PVA:ABPBI 2:1, that obtained the best result in the previous fuel cell measurements, was tried after crosslinking with GA 0.5 vol.% solution. The result is presented in Figure 4.23. The power density obtained suffers a great decrease to 30 mW cm^{-2} at 268 mV. This occurs probably because the GA occupies many alcohol groups from PVA, making it less conductive. Also, by making the membrane more mechanically resistance to stress, it becomes more fragile and it could happen that micro-cracks are formed during the operation that allow a small fuel or oxidant crossover affecting the OCP, which is lower than in the linear ones. To see if lower GA content could enhance the result, 0.25 and 0.125 vol.% of GA in the crosslinking solution were tried (see Figure 4.23). The

first obtained 93 mW cm^{-2} at 338 mV and the second only 61 mW cm^{-2} at 307 mV. These results suggest that the GA content is optimal around the 0.25 vol.%, not reaching the power density of the best linear membranes but obtaining very good results and probably enhanced long term performance (not investigated in the work of this Thesis).

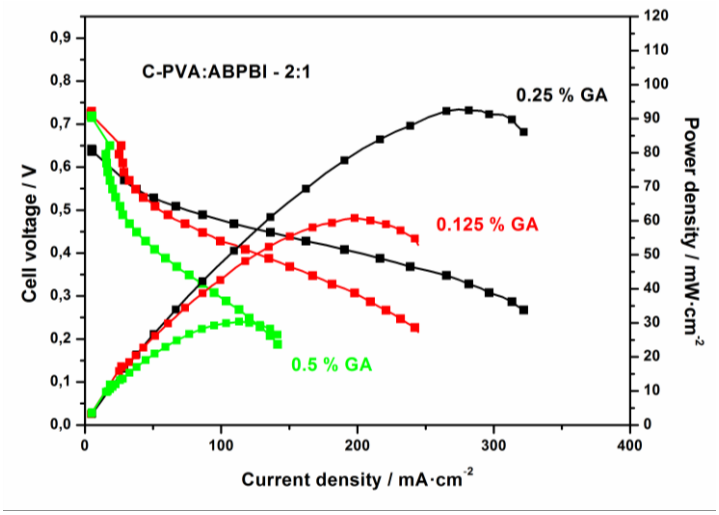

Figure 4.23. Fuel cell polarization and power density curves of C-PVA:ABPBI 2:1 membranes with different % of GA in the crosslinking reaction solution.

It can be concluded that the results in the direct ethanol fuel cell using the synthesised membranes are very good compared with the commercial PBI membrane. L-PVA:PBI 4:1 membrane overcame the power density of PBI but in general the PBI-based membranes presented more structural problems that the ABPBI-based ones. In the PVA:ABPBI membranes the crosslinking hindered the fuel cell performance and an optimum value of GA vol.% was found at 0.25 % while probably improving the long term stability. The linear PVA:ABPBI 2:1 membrane obtained the best result, reaching a power density of 124 mW cm-2 at 378 mV. From the results in literature, experiments with almost similar conditions were done by Hou et al. [50] with a PBI membrane doped in 6 M KOH at 90 ºC and with similar catalysts in a alkaline DEFC, they obtained a good result of 61 mW cm^{-2}, which is the highest in these conditions from one of the latest reviews in PBI based anion exchange membranes for direct ethanol fuel cells [51]. This result is slightly higher than our commercial PBI membrane, but lower than our PVA:polybenzimidazole blend membranes.

3.2 Liquid alkaline water electrolyser

The measurements were done with a single cell liquid alkaline water electrolyser (LAWE) with a zero gap configuration, which was fed with an aqueous 15 wt.% KOH solution and controlled temperature. The electrodes used were of commercial Ni foam and the solid polymer electrolyte membranes were those synthesised in this work. The temperatures and KOH concentration were selected for comparison mainly with previous work and the conditions used in part of the characterization.

To select the membranes with better performance, first the linear PVA:PBI and PVA:ABPBI membranes ratios from 2:1 to 8:1 were tested in the electrolyser at 50 ºC. The results are presented in Table 4.7 summarised and the graphs of the load curves and the chronopotentiometric measurements are illustrated in Figure 4.24 and Figure 4.25 respectively.

Table 4.7. Performance of laboratory electrolysis cell tested with different anion-exchange membranes with circulating 15 wt.% KOH at 50 °C.

Membrane	Current density (mA cm^{-2}) at cell voltage 1.95 V	Cell voltage at 3500 s, applied current density = 200 mA cm^{-2}
L-PVA-PBI 2:1	60	4.0
L-PVA-PBI 4:1	140	2.3
L-PVA-PBI 6:1	140	2.5
L-PVA-PBI 8:1	30	4.0
L-PVA-ABPBI 2:1	30	7,1
L-PVA-ABPBI 4:1	160	2.5
L-PVA-ABPBI 6:1	80	3.4
L-PVA-ABPBI 8:1	40	4.5

An effect of compromise between the better conductivity with higher content of PVA but at the same time more structural problems, similar to the fuel cell measurements, is also observed in the electrolyser. The graphs comparing with the membranes of L-PVA:ABPBI are in the article "Alkali-doped polyvinyl alcohol – Polybenzimidazole membranes for alkaline water electrolysis" made between the group of Argentina and Spain [52]. The membranes with L-PVA:PBI and L-PVA:ABPBI of 2:1 and 8:1 ratios exhibited lower performance than the rest, both in the electrolysis load curves and chronopotentiometric measurements. The membranes L-PVA:PBI 4:1 and 6:1 showed good and similar electrolysis load curves, being the 4:1 ratio slightly better in the chronopotentiometric measurement (2.3 V after 3500 s at 200 mA cm^{-2} compared with the 2.5 V of the 6:1 ratio). In the L-PVA:ABPBI membranes, the 4:1 ratio obtains clearly the best

result, reaching 160 mA cm^{-2} at 1.95 V in the electrolysis load curve and a final voltage of 2.5 V in the chronopotentiometric measurement.

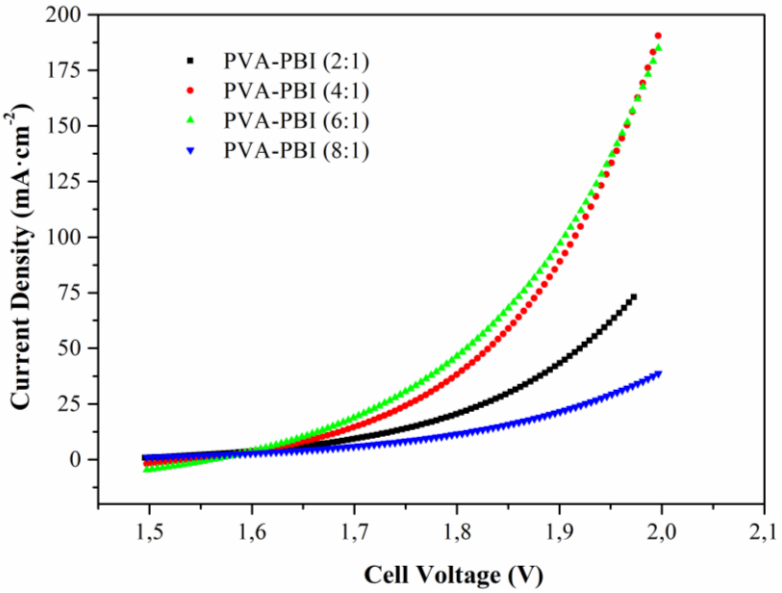

Figure 4.24. LAWE load curves for linear membranes PVA:PBI with ratios from 2:1 to 8:1 in 15 wt.% KOH at 50 ºC.

From these results, the 4:1 ratio, both in L-PVA:PBI and L-PVA:ABPBI membranes, is considered the best and these membranes are selected for further study and for the electrolysis measurements with crosslinked membranes. For the crosslinked membranes, only the PVA:ABPBI 4:1 ratio was studied, since the PVA:PBI one had a very low conductivity performance when crosslinked.

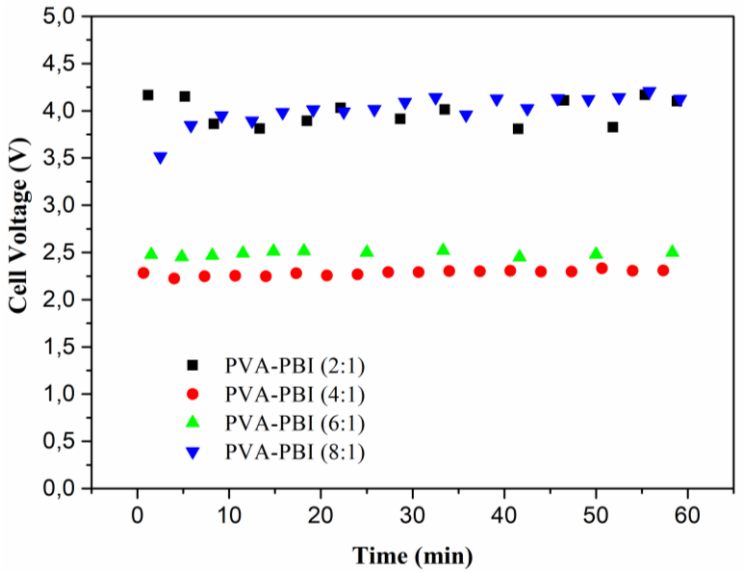

Figure 4.25. Chronopotentiometric curves for membranes L-PVA:PBI with ratios from 2:1 to 8:1 in 15 wt.% KOH at 50 ºC and at constant current of i=200 mA cm^{-2}.

The results of L-PVA:PBI 4:1 at 50 ºC and 70 ºC are presented in Figure 4.26 and the most relevant values are resumed in Table 4.8. The graphs comparing with the membranes of L-PVA:ABPBI are in the previously mentioned article "Alkali-doped polyvinyl alcohol – Polybenzimidazole membranes for alkaline water electrolysis".

The increase of temperature has a beneficial effect in the load curves and the chronopotentiometric measurements, as it was expected due to the improved mobility of the ions and faster electrode kinetics at higher temperature. The increase of the L-PVA:PBI 4:1 membrane is higher than in the L-PVA:ABPBI, reaching the first 430 mW cm^{-2} at 2 V and 70 ºC (very similar to the C-PVA:ABPBI 4:1 at 50 ºC). The C-PVA:ABPBI 2:1 also improves the performance at higher temperature, reaching the maximum value between all the studied membranes: 900 mA cm^{-2} at 70 ºC. Actually this value is extrapolated since the equipment has a current limit of 500 mA cm^{-2}, the same curve obtains a current of 360 mA cm^{-2} at 1.9 V. The chronopotentiometric measurements (in Figure 4.26b) were consistent with the previous results in the load curves, improving with the higher temperature. The voltage values after 60 min obtained by L-PVA:ABPBI 4:1 at 50 at 70 ºC were 2.6 and 2.25 V and by C-PVA:ABPBI 4:1 at 50 at 70 ºC were 2.1 and 1.95 V, respectively. Therefore, the best outcome was obtained by the C-PVA:ABPBI 2:1, which showed a voltage of 1.95 V after 3500 s at 70 ºC.

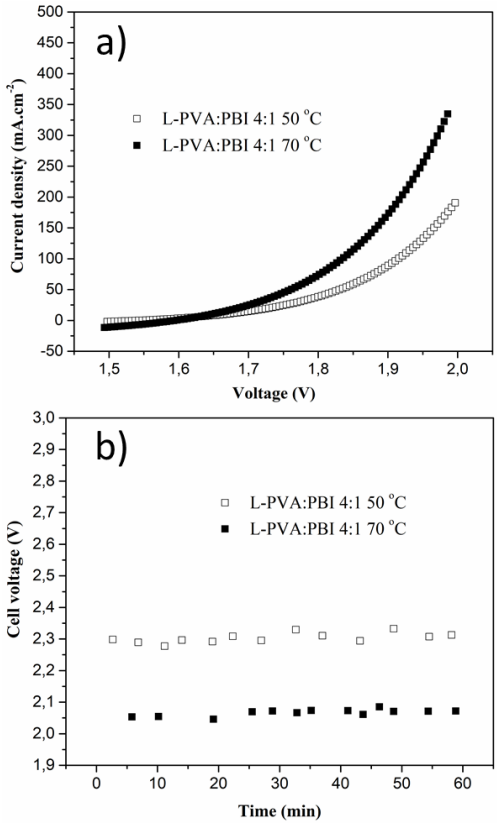

Figure 4.26. a) LAWE load curves for L-PVA-ABPBI 4:1 membranes in 15 wt.% KOH at 50 °C and 70 °C and b) Chronopotentiometric curves in 15 wt.% KOH at 50 °C and 70 °C, i=200 mA cm^{-2}.

It is also interesting to note that in this case the crosslinking has a beneficial effect, not only in the expected long term stability (not studied) but also in the electrolyser performance. This is an important difference with the behaviour observed in the fuel cell, which is probably originated in the differences of the two devices since there is no possibility in this case of reagents crossover.

Membrane	Temperature (°C)	Current density (mA·cm^{-2}) at cell voltage 2 V
L-PVA-PBI 4:1	50	180
L-PVA-ABPBI 4:1	50	220
C-PVA-ABPBI 4:1	50	450*
L-PVA-PBI 4:1	70	430*
L-PVA-ABPBI 4:1	70	290
C-PVA-ABPBI 4:1	70	900*
Zirfon® ***	50	140
Zirfon®	80	~160**
L-ABPBI ***	50	180
C-ABPBI ***	50	160
L-ABPBI ***	70	280
C-ABPBI ***	70	335

Table 4.8. Performance of laboratory electrolysis cell tested with circulating 15 wt.% KOH and different anion-exchange membranes.*=Extrapolated values, **=30 wt.% KOH, from [53], ***=from [43].

The group of Abuin et al. had previously obtained good results with linear and crosslinked ABPBI membranes, better than commercial Zirfon® diaphragm under similar applied conditions [43]. The best performance was obtained with C-ABPBI operating with 15 wt.% KOH solution at 70 ºC (results in Table 4.8). This performance is comparable to the obtained by industrial units, which are typically operated using KOH 6-7 M at 80-90 ºC. Therefore the obtained results with the C-PVA:ABPBI are very promising since they are far superior than commercial porous Zirfon diaphragm and 2.5 times better than the C-ABPBI membranes (which used 3 M KOH at 70 ºC). Even more, the performance of all the studied PVA:polybenzimidazole membranes with 15 wt.% KOH and 50 ºC is higher than the Zirfon diaphragm tested under typical LAWE commercial units (30 wt.% KOH at 80-90 ºC). These are very important results since the milder conditions of alkali concentration and temperature have a relevant enhancement effect of the long term stability of PBI-based membranes as demonstrated by other authors [39].

3.3 Conclusion

In can be resumed that the characterization of the membranes gave important insights of the chemical composition and interactions between the polymers by hydrogen bonds and the deep analysis of the IR and Raman spectra were used to also clearly detect the polymers and the effect of crosslinking. The thermal stability was also certified by TGA analysis. The conductivity measurements gave adequate OH^- ionic conductivity values for most of the PVA:polybenzimidazole membranes, like the 103 mS cm^{-1} or the 70 mS cm^{-1} at 90 ºC with KOH 6 M of L-PVA:PBI 8:1 and 4:1 respectively. Good results are also obtained with 15 wt.% KOH doping solution in both L-PVA:polybenzimidazole 4:1 membranes and ABPBI-based crosslinked ones, reaching 50 mS cm^{-1} in the C-PVA:ABPBI 4:1 with 0.5 vol.% GA solution. The 0.5 vol.% was found the optimal of the studied percentages, since the others gave too low conductivity values. The adequate mechanical properties and the microstructure were also investigated, finding a more homogeneous while weaker microstructure in the ABPBI-based membranes. The water and KOH uptake and swelling behaviour of the membranes was important to understand the changes from the original membranes after the doping process, the anisotropic behaviour was different between the two polybenzimidazole-based types of membranes but the dominant dimension of change was the thickness, which is not so problematic for the final device. The water uptake levels were adequate, being higher in the ABPBI-based membranes than in their counterparts. The XPS gave interesting insights in the doping process, finding no change in the Ns of PBI and high level of K^+ and OH^- in the structure. Finally, the application in the single alkaline direct ethanol fuel has showed very good performances of the synthesised membranes, reaching 76 mW cm^{-2} power density with L-PVA:PBI 4:1, 124 mW cm^{-2} with L-PVA:ABPBI 2:1 and 93 mW cm^{-2} with C-PVA:ABPBI 2:1 at 90 ºC. The zero gap liquid alkaline water electrolyser also obtained very promising performances: 140 and 160 mA cm^{-2} with the L-PVA:PBI and L-PVA:ABPBI 4:1 at 1.95 V and 50 ºC. This was further improved up to 260 mA cm^{-2} at 1.9 V with the C-PVA:ABPBI membrane at 70 ºC, which was calculated to reach 900 mA cm^{-2} at 2 V.

Overall, it can be considered that these blend PVA:polybenzimidazole membranes have some structural problems that can be partially solved by crosslinking and present very good performances, both in alkaline fuel cell and electrolyser; therefore, they are promising electrolytes to be used in these applications.

4 References of the chapter: Blend PVA:polybenzimidazole membranes

[1] G. Merle, M. Wessling, K. Nijmeijer, Anion exchange membranes for alkaline fuel cells: A review, J. Memb. Sci. 377 (2011) 1–35. doi:10.1016/j.memsci.2011.04.043.

[2] G.C. Abuin, P. Nonjola, E. a. Franceschini, F.H. Izraelevitch, M.K. Mathe, H.R. Corti, Characterization of an anionic-exchange membranes for direct methanol alkaline fuel cells, Int. J. Hydrogen Energy. 35 (2010) 5849–5854. doi:10.1016/j.ijhydene.2009.12.128.

[3] J. Hnát, M. Paidar, J. Schauer, J. Žitka, K. Bouzek, Polymer anion selective membranes for electrolytic splitting of water. Part I: Stability of ion-exchange groups and impact of the polymer binder, J. Appl. Electrochem. 41 (2011) 1043–1052. doi:10.1007/s10800-011-0309-9.

[4] J. Hnát, M. Paidar, J. Schauer, J. Žitka, K. Bouzek, Polymer anion-selective membranes for electrolytic splitting of water. Part II: Enhancement of ionic conductivity and performance under conditions of alkaline water electrolysis, J. Appl. Electrochem. 42 (2012) 545–554. doi:10.1007/s10800-012-0432-2.

[5] O.I. Deavin, S. Murphy, A.L. Ong, S.D. Poynton, R. Zeng, H. Herman, J.R. Varcoe, Anion-exchange membranes for alkaline polymer electrolyte fuel cells: Comparison of pendent benzyltrimethylammonium- and benzylmethylimidazolium-head- groups, Energy Environ. Sci. 5 (2012) 8584–8597. doi:10.1108/JPMH-06-2017-0022.

[6] J.R. Varcoe, P. Atanassov, D.R. Dekel, A.M. Herring, M. a. Hickner, P. a. Kohl, A.R. Kucernak, W.E. Mustain, K. Nijmeijer, K. Scott, T. Xu, L. Zhuang, Anion-exchange membranes in electrochemical energy systems, Energy Environ. Sci. 7 (2014) 3135–3191. doi:10.1039/b000000x.

[7] J. Ran, L. Wu, Y. He, Z. Yang, Y. Wang, C. Jiang, L. Ge, E. Bakangura, T. Xu, Ion exchange membranes: New developments and applications, J. Memb. Sci. 522 (2017) 267–291. doi:10.1016/j.memsci.2016.09.033.

[8] C.-C. Yang, S.-J. Lin, Preparation of composite alkaline polymer electrolyte, Mater. Lett. 57 (2002) 873–881. doi:10.1016/S0167-577X(02)00888-1.

[9] A. Lewandowski, K. Skorupska, J. Malinska, Novel poly(vinyl alcohol)-KOH-H2O alkaline polymer electrolyte, Solid State Ionics. 133 (2000) 265–271. doi:10.1016/S0167-2738(00)00733-5.

[10] G.M. Wu, S.J. Lin, C.C. Yang, Preparation and characterization of PVA/PAA membranes for solid polymer electrolytes, J. Memb. Sci. 275 (2006) 127–133. doi:10.1016/j.memsci.2005.09.012.

[11] G. Merle, S.S. Hosseiny, M. Wessling, K. Nijmeijer, New cross-linked

PVA based polymer electrolyte membranes for alkaline fuel cells, J. Memb. Sci. 409–410 (2012) 191–199. doi:10.1016/j.memsci.2012.03.056.

[12] F. Conti, S. Willbold, S. Mammi, C. Korte, W. Lehnert, D. Stolten, Carbon NMR investigation of the polybenzimidazole–dimethylacetamide interactions in membranes for fuel cells, New J. Chem. 37 (2013) 152. doi:10.1039/c2nj40728k.

[13] S. Lai, M. Casu, G. Saba, A. Lai, I. Husu, Solid-State 13 C NMR Study of Poly (vinyl alcohol) Gels, Solid State Nucl. Magn. Reson. 21 (2002) 187–196. doi:10.1006/snmr.2002.0059.

[14] M. Olukman, Ş. Oya, A novel in situ synthesized magnetite containing acrylonitrile and 2-hydroxyethyl methacrylate grafted poly (vinyl alcohol) nanocomposite membranes for pervaporation separation of acetone /, Chem. Eng. Process. Process Intensi Fi Cation. 98 (2015) 60–70.

[15] J. Grobelny, D.M. Rice, F.E. Karasz, W.J. Macknight, High-Resolution Solid-state Carbon-13 Nuclear Magnetic Resonance Study of Polybenzimidazole/Polyimide Blends, Macromolecules. 2139 (1990) 2139–2144.

[16] S. Hu, F. Horii, H. Odani, 1H NMR Study of the Solvation and Gelation in a Poly (vinyl alcohol)/ DMSO-d6 / H20 System, Bull. Inst. Chem. Res. 67 (1989) 5–6.

[17] J.M. Gohil, A. Bhattacharya, P. Ray, Studies On The Crosslinking Of Poly (Vinyl Alcohol), J. Polym. Res. 13 (2006) 161–169. doi:10.1007/s10965-005-9023-9.

[18] S. Panero, P. Fiorenza, M.A. Navarra, J. Romanowska, B. Scrosati, Silica-Added, Composite Poly(vinyl alcohol) Membranes for Fuel Cell Application, J. Electrochem. Soc. 152 (2005) A2400–A2405. doi:10.1149/1.2104207.

[19] R.N. Couto, J.J. Linares, KOH-doped polybenzimidazole for alkaline direct glycerol fuel cells, J. Memb. Sci. 486 (2015) 239–247. doi:10.1016/j.memsci.2015.03.031.

[20] M. Mamlouk, P. Ocon, K. Scott, Preparation and characterization of polybenzimidazole/diethylamine hydrogen sulphate for medium temperature proton exchange membrane fuel cells, J. Power Sources. 245 (2014) 915–926. doi:10.1016/j.jpowsour.2013.07.050.

[21] L. Zeng, T.S. Zhao, L. An, G. Zhao, X.H. Yan, Physicochemical properties of alkaline doped polybenzimidazole membranes for anion exchange membrane fuel cells, J. Memb. Sci. 493 (2015) 340–348. doi:10.1016/j.memsci.2015.06.013.

[22] F. Conti, A. Majerus, D. Noto, C. Korte, Raman study of the polybenzimidazole – phosphoric acid interactions in membranes for fuel cells, Phys. Chem. Chem. Phys. (2012) 10022–10026. doi:10.1039/c2cp40553a.

[23] D. Aili, K. Jankova, J. Han, N.J. Bjerrum, J.O. Jensen, Q. Li, Understanding ternary poly(potassium benzimidazolide)-based polymer

electrolytes, Polymer (Guildf). 84 (2016) 304–310. doi:10.1016/j.polymer.2016.01.011.

[24] C.-K. Yeom, K.-H. Lee, Pervaporation separation of water-acetic acid mixtures through poly(vinyl alcohol) membranes crosslinked with glutaraldehyde, J. Memb. Sci. 109 (1996) 257–265. doi:10.1016/0376-7388(95)00196-4.

[25] L.A. Diaz, G.C. Abuin, H.R. Corti, Water and phosphoric acid uptake of poly [2,5-benzimidazole] (ABPBI) membranes prepared by low and high temperature casting, J. Power Sources. 188 (2009) 45–50. doi:10.1016/j.jpowsour.2008.11.114.

[26] Q. Li, J.O. Jensen, R.F. Savinell, N.J. Bjerrum, High temperature proton exchange membranes based on polybenzimidazoles for fuel cells, Prog. Polym. Sci. 34 (2009) 449–477. doi:10.1016/j.progpolymsci.2008.12.003.

[27] H. Zarrin, M. Fowler, Z. Chen, Highly Anion-Conducting Porous Polymer Electrolyte Membrane for Alkaline Fuel Cells, ECS Trans. 50 (2012) 2083–2089. doi:10.1149/05002.2083ecst.

[28] H. Luo, G. Vaivars, B. Agboola, S. Mu, M. Mathe, Anion exchange membrane based on alkali doped poly(2,5-benzimidazole) for fuel cell, Solid State Ionics. 208 (2012) 52–55. doi:10.1016/j.ssi.2011.11.029.

[29] S.R. Samms, Thermal Stability of Proton Conducting Acid Doped Polybenzimidazole in Simulated Fuel Cell Environments, J. Electrochem. Soc. 143 (1996) 1225. doi:10.1149/1.1836621.

[30] A. Anis, S.M. Al-Zahrani, Sulfonated PVA / PBI based crosslinked composites towards anhydrous proton conductive polymer electrolyte membranes for fuel cells, Int. J. Electrochem. Sci. 7 (2012) 9174–9185. http://www.scopus.com/inward/record.url?eid=2-s2.0-84872869485&partnerID=tZOtx3y1.

[31] C.-P. Liu, C.-A. Dai, C.-Y. Chao, S.-J. Chang, Novel proton exchange membrane based on crosslinked poly(vinyl alcohol) for direct methanol fuel cells, J. Power Sources. 249 (2014) 285–298. doi:10.1016/j.jpowsour.2013.10.117.

[32] J.M. Dodda, P. Bělský, J. Chmelař, T. Remiš, K. Smolná, M. Tomáš, L. Kullová, J. Kadlec, Comparative study of PVA/SiO2 and PVA/SiO2/glutaraldehyde (GA) nanocomposite membranes prepared by single-step solution casting method, J. Mater. Sci. 50 (2015) 6477–6490. doi:10.1007/s10853-015-9206-7.

[33] F. Kursun, I. Nuran, Development of thermo-responsive poly (vinyl alcohol) -g-poly (N-isopropylacrylamide) copolymeric membranes for separation of isopropyl alcohol / water mixtures via pervaporation, J. Ind. Eng. Chem. 41 (2016) 91–104.

[34] L.-Y. Li, B.-C. Yu, C.-M. Shih, S.J. Lue, Polybenzimidazole membranes for direct methanol fuel cell: Acid-doped or alkali-doped?, J. Power Sources. 287 (2015) 386–395. doi:10.1016/j.jpowsour.2015.04.018.

[35] A. Ilie, M. Simoes, S. Baranton, C. Coutanceau, S. Martemianov,

Influence of operational parameters and of catalytic materials on electrical performance of Direct Glycerol Solid Alkaline Membrane Fuel Cells, J. Power Sources. 196 (2011) 4965–4971. doi:10.1016/j.jpowsour.2011.02.003.

[36] K.N. Grew, W.K.S. Chiu, A Dusty Fluid Model for Predicting Hydroxyl Anion Conductivity in Alkaline Anion Exchange Membranes, J. Electrochem. Soc. 157 (2010) B327. doi:10.1149/1.3273200.

[37] L. An, T.S. Zhao, Transport phenomena in alkaline direct ethanol fuel cells for sustainable energy production, J. Power Sources. 341 (2017) 199–211. doi:10.1016/j.jpowsour.2016.11.117.

[38] L. Zeng, T.S. Zhao, L. An, G. Zhao, X.H. Yan, A high-performance sandwiched-porous polybenzimidazole membrane with enhanced alkaline retention for anion exchange membrane fuel cells, Energy Environ. Sci. 8 (2015) 2768–2774. doi:10.1039/c5ee02047f.

[39] D. Aili, K. Jankova, Q. Li, N.J. Bjerrum, J.O. Jensen, The stability of poly(2,2'-(m-phenylene)-5,5'-bibenzimidazole) membranes in aqueous potassium hydroxide, J. Memb. Sci. 492 (2015) 422–429. doi:10.1016/j.memsci.2015.06.001.

[40] R. He, Q. Li, A. Bach, J.O. Jensen, N.J. Bjerrum, Physicochemical properties of phosphoric acid doped polybenzimidazole membranes for fuel cells, J. Memb. Sci. 277 (2006) 38–45. doi:10.1016/j.memsci.2005.10.005.

[41] M. Lim, D. Kim, H. Han, S.B. Khan, J. Seo, Water sorption and water-resistance properties of poly(vinyl alcohol)/clay nanocomposite films: Effects of chemical structure and morphology, Polym. Compos. 36 (2015) 660–667. doi:10.1002/pc.22984.

[42] D. Aili, M.K. Hansen, R.F. Renzaho, Q. Li, E. Christensen, J.O. Jensen, N.J. Bjerrum, Heterogeneous anion conducting membranes based on linear and crosslinked KOH doped polybenzimidazole for alkaline water electrolysis, J. Memb. Sci. 447 (2013) 424–432. doi:10.1016/j.memsci.2013.07.054.

[43] L.A. Diaz, J. Hnat, N. Heredia, M.M. Bruno, F.A. Viva, M. Paidar, H.R. Corti, K. Bouzek, G.C. Abuin, Alkali doped poly (2,5-benzimidazole) membrane for alkaline water electrolysis: Characterization and performance, J. Power Sources. 312 (2016) 128–136. doi:10.1016/j.jpowsour.2016.02.032.

[44] H. Hou, S. Wang, Q. Jiang, W. Jin, L. Jiang, G. Sun, Durability study of KOH doped polybenzimidazole membrane for air-breathing alkaline direct ethanol fuel cell, J. Power Sources. 196 (2011) 3244–3248. doi:10.1016/j.jpowsour.2010.11.104.

[45] W. Lu, G. Zhang, J. Li, J. Hao, F. Wei, W. Li, J. Zhang, Z.-G. Shao, B. Yi, Polybenzimidazole-crosslinked poly(vinylbenzyl chloride) with quaternary 1,4-diazabicyclo (2.2.2) octane groups as high-performance anion exchange membrane for fuel cells, J. Power Sources. 296 (2015)

204–214. doi:10.1016/j.jpowsour.2015.07.048.

[46] M.P. Seah, D. Briggs, eds., Practical surface analysis by Auger and X-ray Photoelectron spectroscopy, John Wiley and Sons Ltd, Chichester, 1983.

[47] J. Hommet, C. Fuchs, E. Fogarassy, F. Le Normand, T. Szörényi, XPS study of pulsed laser deposited CNx films, Phys. Rev. B - Condens. Matter Mater. Phys. 64 (2001) 2354161–23541615. doi:10.1103/PhysRevB.64.235416.

[48] A. Caballero, J.P. Espinós, A. Fernández, L. Soriano, A.R. González-Elipe, Adsorption and oxidation of K deposited on graphite, Surf. Sci. 364 (1996) 253–265. doi:10.1016/0039-6028(96)00659-0.

[49] C.D. Wanger, W.M. Riggs, L.E. Davis, J.F. Moulder, G. E.Muilenberg, eds., Handbook of X-ray Photoelectron Spectroscopy, Perkin-Elmer Corp., Physical Electronics Division, Eden Prairie, Minnesota, 1979.

[50] H. Hou, G. Sun, R. He, Z. Wu, B. Sun, Alkali doped polybenzimidazole membrane for high performance alkaline direct ethanol fuel cell, J. Power Sources. 182 (2008) 95–99. doi:10.1016/j.jpowsour.2008.04.010.

[51] Q.X. Wu, Z.F. Pan, L. An, Recent advances in alkali-doped polybenzimidazole membranes for fuel cell applications, Renew. Sustain. Energy Rev. 89 (2018) 168–183. doi:10.1016/j.rser.2018.03.024.

[52] L.A. Diaz, R.E. Coppola, G.C. Abuin, R. Escudero-Cid, D. Herranz, P. Ocón, Alkali-doped polyvinyl alcohol – Polybenzimidazole membranes for alkaline water electrolysis, J. Memb. Sci. 535 (2017) 45–55. doi:10.1016/j.memsci.2017.04.021.

[53] M.R. Kraglund, D. Aili, K. Jankova, E. Christensen, Q. Li, J.O. Jensen, Zero-Gap Alkaline Water Electrolysis Using Ion-Solvating Polymer Electrolyte Membranes at Reduced KOH Concentrations, J. Electrochem. Soc. 163 (2016) F3125–F3131. doi:10.1149/2.0161611jes.

CHAPTER 5. Membranes of polybenzimidazole-c-PVBC

Membranes of polybenzimidazole-c-PVBC

1 Introduction

Homogeneous membranes with quaternary ammonium groups are one of the most common types of developed anion exchange polymeric membranes. They have the advantage of no phase separation (with the loss of polymer that may present under operation) and the quaternary ammonium groups allow for good conductivity values, being more stable than other groups with fixed positive charges. There are different strategies to obtain the positive quaternary ammonium (QA) groups, depending on the backbone of the polymer and the possible use of side chains and crosslinkers [1]. Polyvinyl benzyl chloride (PVBC) (or the monomer VBC) is a commonly used polymer to synthesise membranes with QA groups due to its high density of -CH_2-Cl bonds that can react with tertiary amines and especially because its structure. In its structure (see Figure 5.1) the CH_2 bound to the quaternary amine (after amination) doesn't have β-hydrogens present and thus cannot undergo Hoffman elimination, which is considered one of the important degradation mechanism with the direct nucleophilic substitution. Due to these reasons PVBC has been widely used in the synthesis of anion exchange membranes by different groups. For example in Scott's group, membranes based mainly in PVBC have been prepared using methylized melamine as crosslinking and quaternizing agent [2], Tuli et al. have prepared block copolymers with polystyrene and PVBC [3], Lu et al. used it as crosslinker and site for quaternizing [4] and in Varcoe's group the VBC monomer is grafted in a previously radiated membrane to create the sites for later quaternization with different amines [5].

In order to investigate the electrolyser and direct ethanol fuel cell application, and based in the previous knowledge about polybenzimidazole-based membranes, the approach of Lu et al. was selected to synthesise the crosslinked polybenzimidazole-c-PVBC membranes (with PBI or ABPBI). In this case, the crosslinking allows to obtain homogeneous membranes, since the polymers are

different and an incorrect crosslinking process causes phase separation as it will be showed. They decided to use 1,4-diazabicyclo [2.2.2] octane (DABCO) (see Figure 5.1) as the tertiary amine to form the QA groups by reaction with PVBC. It was considered a good choice due to the studied good stability of this group in literature. This stability comes from the rigid structure cage, in which the β-hydrogens don't form the anti-periplanar conformation that allows facile Hoffman elimination [6–8]. DABCO has been used in different studies as a crosslinker as well as site of positive QA groups, but since it has been observed that the chemical stability is higher when only one of the nitrogen atoms is quaternized [8,9], the same reaction steps were used, with quaternization step after the membranes crosslinking and casting, to prevent the possibility of DABCO reacting with both nitrogens and the further crosslinking and lower chemical stability it would produce.

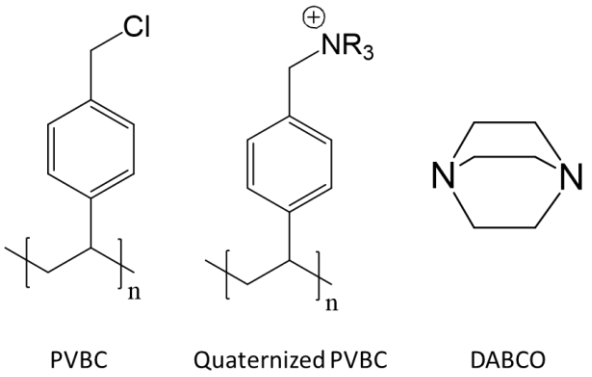

Figure 5.1.Polyvinyl benzyl chloride (PVBC), PVBC quaternized with a generic tertiary amine and 1,4-diazabicyclo [2.2.2] octane (DABCO).

2 Characterization and properties

The membranes characterizations and properties are explained in detail in this section.

In order to facilitate the understanding of the names that will be used in this chapter a breve summary is made here: polybenzimidazole-c-PVBC refers to the crosslinked and casted membrane from these two polymers. For example, "PBI-c-PVBC 1:2" if the molar ratio is double number of mols of PVBC than of PBI.

Moreover, "polybenzimidazole-c-PVBC/Cl" refers to the membrane after the quaternization step, when the Cl^- is the present counter-ion in the QA groups; and "polybenzimidazole-c-PVBC/OH" refers to the membrane after the exchange of Cl^- ions to OH^- ions.

2.1 Synthesis of the membranes

There are 3 main steps in the synthesis of these polybenzimidazole-c-PVBC/Cl membranes: the crosslinking, the casting and the quaternization. The first one is the crosslinking of both polymers to form and homogeneous structure. As it was explained in the experimental chapter, control of the crosslinking conditions as temperature and time are critical to obtain final homogeneous membranes, as it can be observed in Figure 5.2.

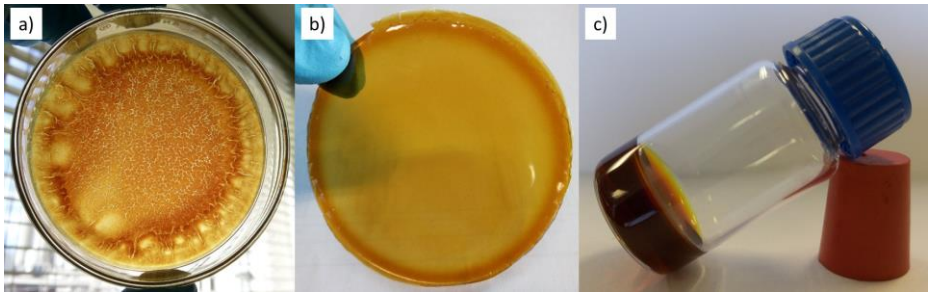

Figure 5.2. Aspect of PBI-c-PVBC 1:1 membranes after a) 1h of crosslinking, b) 24h and c) 72h of crosslinking at 80 ºC. The last one couldn't be placed in a Petri dish and casted since the gelation process was too advanced.

It is clear that at low crosslinking times separation between the polymers is extended (Figure 5.2a) with brown areas mainly from PBI and transparent areas from PVBC. When the time increases, the crosslinking can be detected by the effect of gelation process of the solution: the longer the crosslinking time, the more viscous is the solution. If the crosslinking is too long, the mixture becomes almost solid, as showed in Figure 5.2c, making impossible to place the solution in a Petri dish for the casting. However if an intermediate time is selected, an homogeneous and not too viscous solution can be placed without problem in the Petri dish to obtain homogeneous and flexible membranes after the casting process (Figure 5.2b). It is worth to note that since the crosslinking requires high temperature around 80 ºC to occurs, when the selected time is reached the solution can be naturally cooled to room temperature and used in the following hours without problem. The time at which the solution becomes too viscous

depends on the molar ratio of the polymers, but since with 24h it was found that homogeneous membranes were obtained with all the studied ratios, that was the selected time for crosslinking.

Regarding the casting step, if a vacuum oven is used special care needs to be taken in the applied ramp from ambient pressure to the selected vacuum value. If it is too fast, bubbles are formed in the surface of the solution due to the evaporation of the solvent affecting the final homogeneity of the membrane. The process described in the experimental chapter was adequate to a slow enough casting of these membranes. The thickness of the membranes was controlled with the amount of casting solution deposited in the Petri dish; in this way membranes of thickness around 50 μm were synthesised. Finally, for the quaternization step, the temperature is also necessary to the reaction of PVBC with DABCO and different times may be needed to obtain complete quaternization of the pendant $–CH_2$-Cl groups. In our case it was secured with 3 days in the case of PBI-c-PVBC membranes and 1 day for the ABPBI-c-PVBC membranes. Deep optimization experiments to find the best quaternization time were not performed since the primary need was to ensure complete quaternization, which was corroborated by IR spectroscopy as it will be explained.

The ratios finally used were PBI-c-PVBC 1:2 and 1:3 and ABPBI-c-PVBC 1:2. Some experiments and comparison were also done with 1:1 ratios but since they performed much lower conductivity those were not extensively characterized. Using higher ratios (1:4 for PBI based membranes and 1:3 for ABPBI-based ones) gave membranes too heterogeneous due to the high quantity of PVBC and too brittle to be used. Table 5.1 gives an overview of the used ratios and others to understand the evolution of the different molar and weight relations.

Table 5.1. Membranes with different molar ratios polybenzimidazole:PVBC, the ratio Cl/N in each membrane and the PVBC wt.% in the final sample. All values come from the theoretical calculation based on the molar ratios.

	mols PBI or ABPBI	N atoms per PBI or ABPBI r.u.	mols PVBC	Cl/N	PVBC wt% of membrane
PBI-c-PVBC 1:1	1	4	1	0,25	33,12
PBI-c-PVBC 1:2	1	4	2	0,50	49,76
PBI-c-PVBC 1:3	1	4	3	0,75	59,76
ABPBI-c-PVBC 1:1	1	2	1	0,50	56,80
ABPBI-c-PVBC 1:2	1	2	2	1,00	72,45
ABPBI-c-PVBC 1:3	1	2	3	1,50	79,77

As it can be observed, the Cl/N ratio and the PVBC wt.% advance faster in the ABPBI membrane, due to the smaller monomeric unit and the lower number of nitrogens per mol. The molecular weights used (based in Figures 5.3 and 5.4) are: 308 g mol^{-1} for PBI, 134 g mol^{-1} for ABPBI and 138.5 g mol^{-1} for PVBC.

During the crosslinking step, it is necessary to mention that two different "crosslinking points" can be formed, as described by Lu et al. [4] at the same time: the "single" one between the amine moiety (-NH-) and the $–CH_2Cl$ (non-conducting crosslinking point) and the "double" one when in the same imidazole ring, the (=N-) reacts with a second CH_2Cl forming a delocalized positive charge and thus an imidazolium salt (conductive crosslinking point). These situations and the complete process of the synthesis of the membranes are illustrated in Figure 5.3 and 5.4.

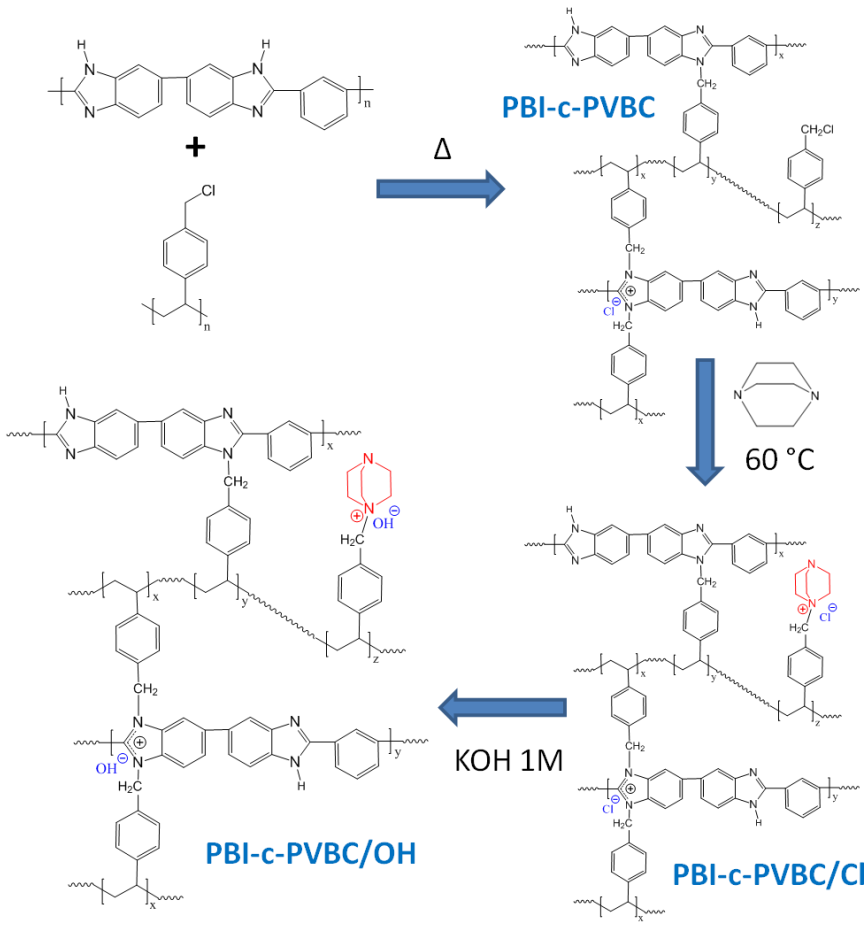

Figure 5.3. Reaction process of the synthesis of membranes, concretely the case of the PBI-c-PVBC. The ABPBI-c-PVBC scheme would be similar but with the ABPBI monomer. The single and double crosslinking points are depicted within the structure.

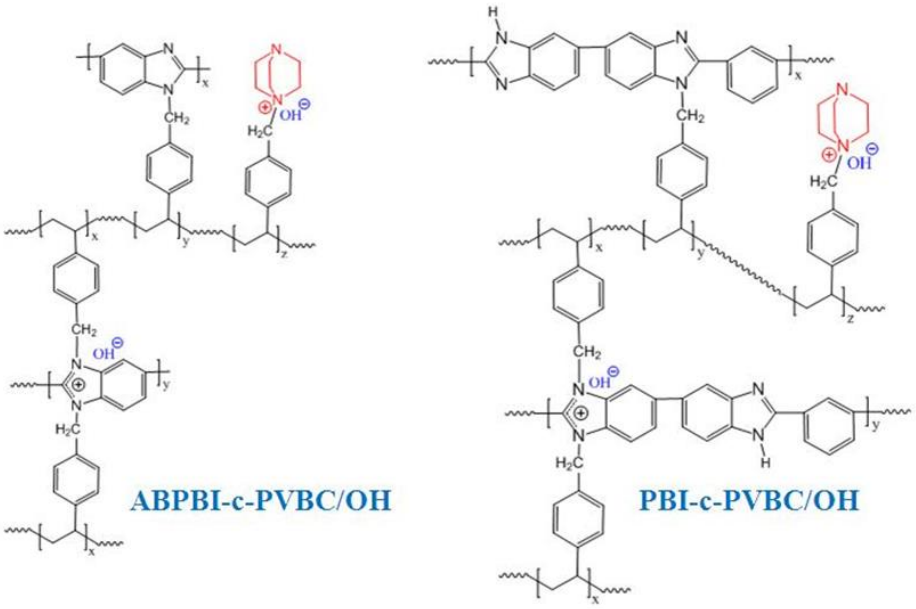

Figure 5.4. Scheme of the final chemical structure of PBI-c-PVBC/OH and ABPBI-c-PVBC/OH membranes.

2.2 IR spectroscopy characterization

The IR spectra of pure PBI, ABPBI, PVBC, DABCO and the synthesised polybenzimidazole-c-PVBC membranes were compared to investigate the presence of the mentioned polymers in the membranes and the correct development of the reactions. The spectra of the crosslinked membranes PBI-c-PVBC 1:2 and ABPBI-c-PVBC 1:2 are showed in Figure 5.5a and b respectively. The most relevant observed bands were at 1265, 709 and 675 cm^{-1} from the CH_2-Cl bonds of PVBC [10], the band at 1288 cm^{-1} from the imidazole ring [11] of PBI/ABPBI and the band at 800 cm^{-1} from the C=C and C=N stretching in plane vibrations (present in PVBC and the polybenzimidazoles).

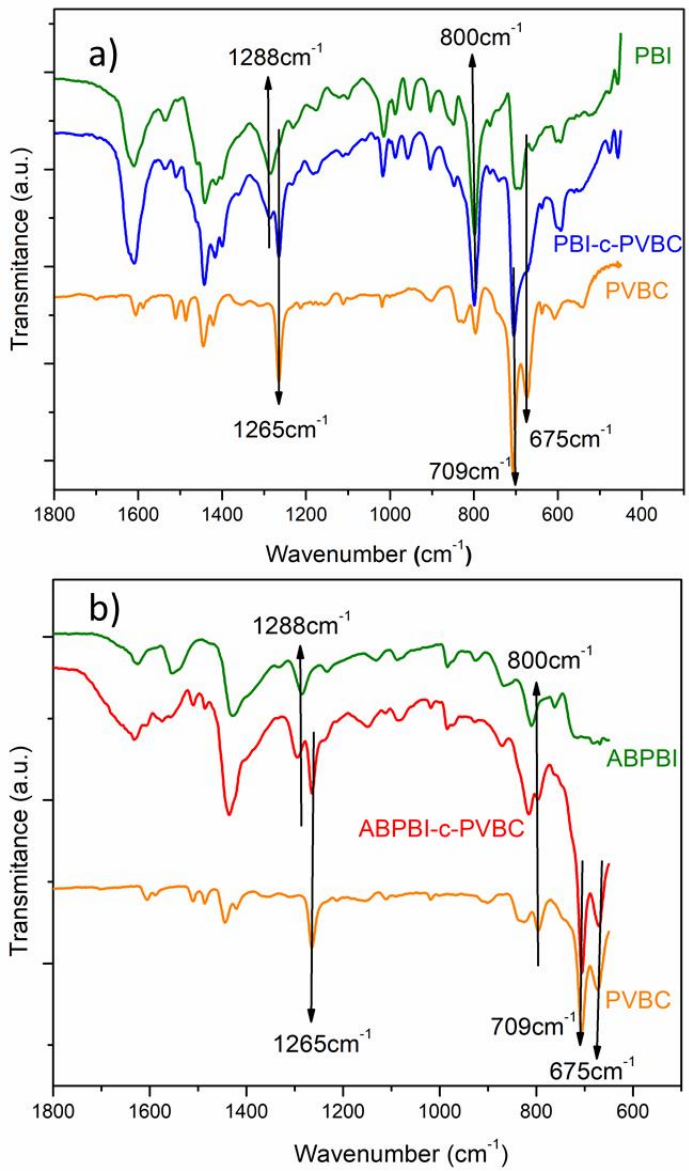

Figure 5.5. IR spectra of the crosslinked polybenzimidazole-c-PVBC, pure PVBC and the corresponding pure polybenzimidazole for a) PBI and b) ABPBI.

Other important peak is located at 2923 cm^{-1} and assigned to the CH_2 vibrations in the PVBC aliphatic chain [12]. This peak is used as a reference to normalize all the spectra to its height when their heights are compared, so they are normalized to the PVBC content. The two ratios of ABPBI-c-PVBC, 1:2 and 1:3, were qualitatively compared and, as it was expected, the signal of the CH_2-Cl at 1265 cm^{-1} increased from the membrane with 1:2 ratio to 1:3 and finally to pure PVBC, since more CH_2 are bonded to Cl and less to N of polybenzimidazole

(same behaviour in the PBI-based membranes). Comparing the 1:2 molecular ratios of both polybenzimidazole-c-PVBC membranes it was observed that the ABPBI-based one presents higher amount of unreacted (not crosslinked) CH_2-Cl, which is logical since it has higher ratio of Cl/N as showed in Table 5.1.

After the reaction with DABCO during the quaternization stage, new bands appear in the spectra of the membranes (see Figure 5.6, ABPBI-c-PVBC/OH, also exchanged to OH^- form) at 1060 cm^{-1} and 1460 cm^{-1}, demonstrating the presence of the amine in the membrane structure. Another relevant change is the disappearance of the band at 1265 cm^{-1} of the CH_2-Cl bond (detail in Figure 5.7), due to the substitution of the Cl by DABCO. This indicates that the quaternization of the non-crosslinked CH_2-Cl groups has been complete.

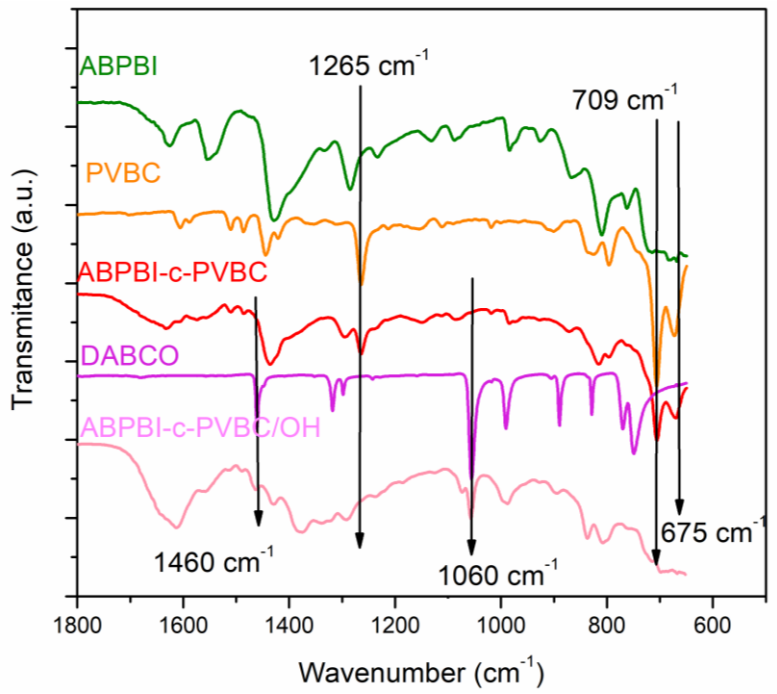

Figure 5.6. FT-IR spectra of ABPBI-c-PVBC membrane just crosslinked and in OH^- form (quaternized) compared to pure ABPBI, PVBC and DABCO.

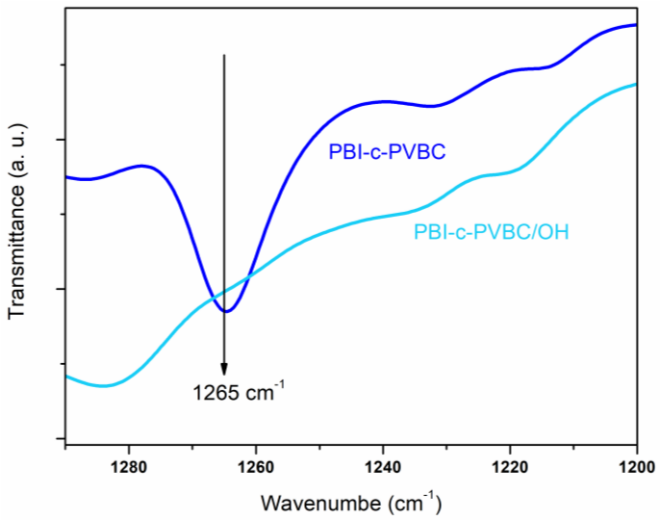

Figure 5.7. Comparison of the CH_2-Cl peak at 1265 cm^{-1} in the PBI-c-PVBC 1:2 membrane just after crosslinking and after being quaternized (in final OH^- form).

Some of the most important IR bands and the assigned bonds are summarised in Table 5.2.

Table 5.2. FT-IR most important signals and their corresponding bonds.

Origin	Band (cm^{-1})	Bond
PBI	800	C=C y C=N
	1288	imidazole rings
PVBC	675	CH_2-Cl
	1265	
	2923	aliphatic CH2
DABCO	1460	CH_2
	1060	NC_3
OH^-	1651	O-H

2.3 X-ray photoelectron spectroscopy (XPS)

In order to provide additional information on the chemical reactions produced during the formation of the anion exchange membrane (AEM), and its subsequent quaternization with DABCO solutions, XPS has been used. The preparation of the membranes involves the mixture of PBI and PVBC according to the molar ratios 1:1, 1:2 and 1:3 leading to PBI-c-PVBC 1:1, 1:2 and 1:3 membranes, respectively. The crosslinked membranes presented similar spectra and the membrane of 1:2 ratio was the sample investigated in the next study in order to understand the quaternization process.

Figure 5.8 shows the N 1s peaks of (a) pristine PBI, (b) pure DABCO, (c) PBI-PVBC 1:2 membrane and (d) PBI-PVBC 1:2 membrane after quaternization with DABCO. As can be observed the single PBI membrane displays two peaks at 400.3±0.3 and 398.7±0.3 eV which are usually attributed to nitrogen of amine (-NH-) and imine (=N-) in the imidazole rings, respectively [13]. The ratio of imine to amine is close to one as expected from the structure of the PBI molecule. The DABCO substrate displays a single broad peak at 402.9 eV (NR_3) since in this case both N atoms of the DABCO molecule are completely equivalents and therefore indistinguishable.

With the formation of the cross-linked membrane PBI-c-PVBC, Figure 5.8c, three peaks are observed at 398.7, 400.3 and 402.9 eV. It is worth noting that although the peaks at 398.7 and 400.3 should still be attributed to imine and amine in the PBI, respectively, the ratio of imine to amine is now 0.6, therefore indicating that at this stage the membrane is not merely a physical mixture of PBI and PVBC but there has been crosslinking between PBI and PVBC. The new peak appearing at 402.9 eV would be related to the nitrogen of the cross-linked species formed. It should be also indicated that the Cl 2p peak (see Figure 5.9) displays a doublet with the Cl $2p_{3/2}$ peak at 200.4 eV and a spin orbit splitting (*sos*) between Cl $2p_{3/2}$-Cl$2p_{1/2}$ of 1.6 eV that is characteristic of covalent Cl species. This is logical since most of the Cl atoms remaining in the membrane after the crosslinking are in the unreacted CH_2-Cl groups of PVBC, so they are covalently bonded.

We have found two possible explanations for the change in the ratio between the peaks at 400.3 eV (amine) and 398.7 (imine). The first one is based in the statement that the crosslinking reaction occurs between the CH_2-Cl groups of PVBC mainly with the imine (=N-) groups in the imidazole rings of PBI. This would explain the reduction of the imine peak respect to the amine one. The

new peak at 402.9 eV would be related with the formed N species (positively charged?). However, this would be contrary to the mechanism explained by Lu et al. [4]. In their mechanism, if only one nitrogen of the imidazolium ring reacts, it would be the amine one (-NH-).

The other explanation we have found is based in the statement that the crosslinking reaction occurs between the CH_2-Cl and the amine (-NH-) group of PBI (contrary to the previous but in agreement with Lu). In this case the peak at 400.3 eV (amine) would increase respect to the peak at 398.7 eV (imine) due to the double crosslinking points formed, which would produce quaternary ammoniums. The quaternary ammonium would present a binding energy around 400.3 eV indistinguishable of the amines. In the NIST XPS database [14] it has been found for example that the N of the quaternary ammonium tetraethylammonium chloride presents a binding energy of 401.4 eV [15]. Obviously it is different from the quaternary ammoniums that could be formed in PBI, but it shows that the binding energy could be in that range. The new peak at 402.9 eV would be related mainly to the crosslinking bond formed. It would be a tertiary amine since the (-NH-) of PBI substitutes the H with the C from -CH_2-Cl of PVBC. This is logical since the N on the tertiary amine of DABCO also appears at that binding energy.

From both explanations there should be present the quaternary ammoniums from the reacted imine (in the first one) or the double crosslinking point (in the second one). Next to this positively charged groups there should be Cl^- counter-ions, but the Cl in ionic state is not observed in the crosslinked membrane, maybe because they are in low amount and thus are not detected.

Quaternization:

Figure 5.8d shows the N 1s of the PBI-PVBC 1:2 membrane after treatment with DABCO. Again, three peaks are observed at 398.7, 400.3 and 402.9 eV. It is interesting to notice that the ratio of imine to amine is now 0.09 and that the peak at 402.9 eV increases its intensity five times with respect to the non-quarternized PBI-PVBC 1:2 membrane. Moreover, as shown in Figure 5.9, the Cl 2p doublet displays a shift from 200.4 eV to 198.8 eV from the non-quaternized membrane (Figure 5.9a) to the quaternized one (Figure 5.9b) revealing a change in the bonding character of Cl atoms from covalent to ionic upon quaternization with DABCO. These last effect is logical since the Cl atoms are now counter-ions of the formed quaternary ammonium groups and the fact that not covalent Cl is detected confirms the total quaternization of the CH_2-Cl groups that didn't react in the crosslinking step (although absence of traces of unreacted PVBC in the quaternized membrane cannot be completely assured).

It was thought that the quaternization step could produce more crosslinking inside the membrane since it involves 60 ºC during 3 days, although it was not expected due to the already conformed structure that wouldn't allow too much mobility of the polymeric chains. A procedure quite similar was performed, immersing the membrane in EtOH at 60 ºC during 3 days (but in absence of DABCO). The XPS of the final membrane was similar to the crosslinked membrane before the process so this effect was discarded.

The observed changes in the ratio between the peaks at 400.3 eV and 398.7 eV are supposed to support the second interpretation previously explained of the reaction mechanism. This means that the peak at 400.3 eV increases in intensity due to the higher amount of quaternary ammonium nitrogens (now coming from the N of DABCO bounded to PVBC). The first proposed mechanism would indicate a reduction of the peak at 398.7 eV, therefore indicating that quaternization strongly enhance the crosslinking reaction and practically exhausts the imine groups. Since the effect of temperature and time was discarded and the DABCO molecules aren't supposed to interact with the nitrogens of PBI this explanation doesn't seem logical.

The observed increase of the peak at 402.9 eV would be produced by the addition of the signal of the tertiary nitrogens from the DABCO molecules over the previous signal produced in the crosslinking. The signals overlap in such a way that they cannot be accurately separated.

More research is being performed to elucidate clearly the reaction mechanism. However, based in these preliminary results, it is proposed that the crosslinking reaction occurs mainly between the CH_2-Cl groups of PVBV and the amine (-NH-) groups of PBI.

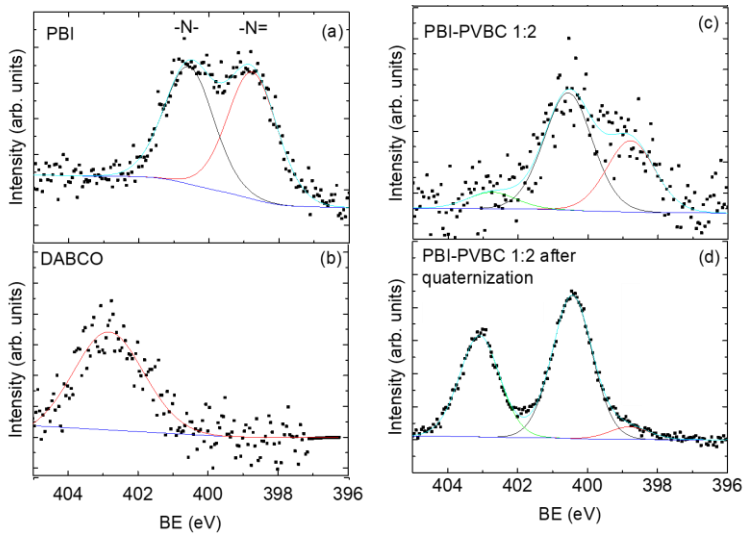

Figure 5.8. XPS N 1s peaks of a) pristine PBI, b) pure DABCO, c) PBI-PVBC 1:2 membrane (crosslinked) and d) PBI-c-PVBC/Cl 1:2 membrane (after quaternization with DABCO).

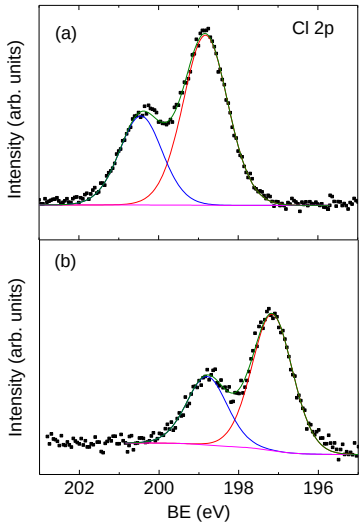

Figure 5.9. XPS Cl 2p peak doublet of a) PBI-PVBC 1:2 membrane (crosslinked) and b) PBI-c-PVBC/Cl 1:2 membrane (after quaternization with DABCO).

2.4 Gel fraction of the membranes

The approximate quantity of polymer that was crosslinked was measured by the gel fraction, immersing the membrane in the original solvent of the polymers at

70 ºC following the steps described in the Experimental chapter. N-methyl pyrrolidone was used with the ABPBI-based membranes and dimethylacetamide with the PBI-based ones. Since the crosslinked chains are much more difficult to dissolve, only the not bounded polymer is taken away from the membrane, reducing its weight. As it can be observed in Figure 5.10, the ABPBI membrane retains a much higher % of the initial mass, meaning that the crosslinking process is more efficient, while the PBI-based membranes show lower gel fraction with the 1:2 ratio higher than the 1:3. In all the cases, after the initial weight loss, the weight is stable and not further loss is measured in the 34 h. Even with the mass loss of the PBI-c-PVBC 1:3, the sample has good appearance and is flexible after the treatment due to the stable structure of the crosslinked membranes.

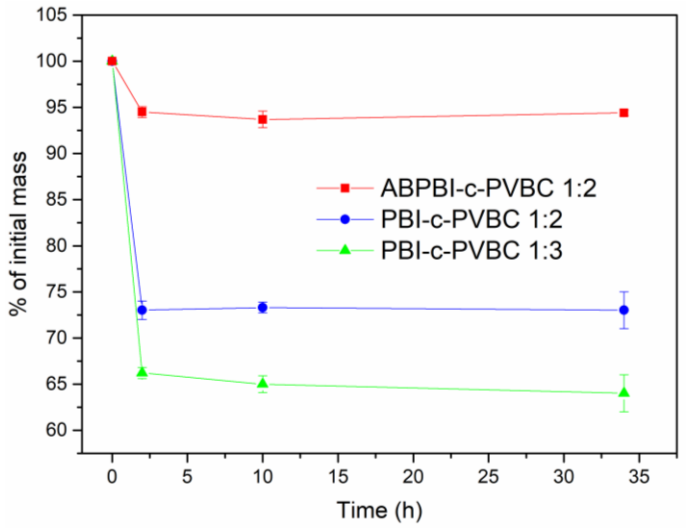

Figure 5.10. Gel fraction measurement of the synthesised membranes.

Our results for the PBI-c-PVBC membranes are lower than those obtained by Lu et al. [4], around 94.5 % of initial mass. This is due to the longer crosslinking time (36 h) they use in their study, which logically entangles more the polymeric chains and thus less polymer is dissolved during the gel fraction measurements. It has to be taken into account that the lower gel fraction obtained in our membranes is not a problem since the polymers are not soluble in aqueous media and thus not polymer loss is expected during operation.

2.5 NMR spectroscopy

The crosslinked membranes were very difficult to dissolve as it has been previously commented, for this reason solid ^{13}C-NMR spectroscopy was used to obtain the spectra of crosslinked and quaternized PBI-based membranes in order to corroborate the adequate synthesis. The results are presented in Figure 5.11.

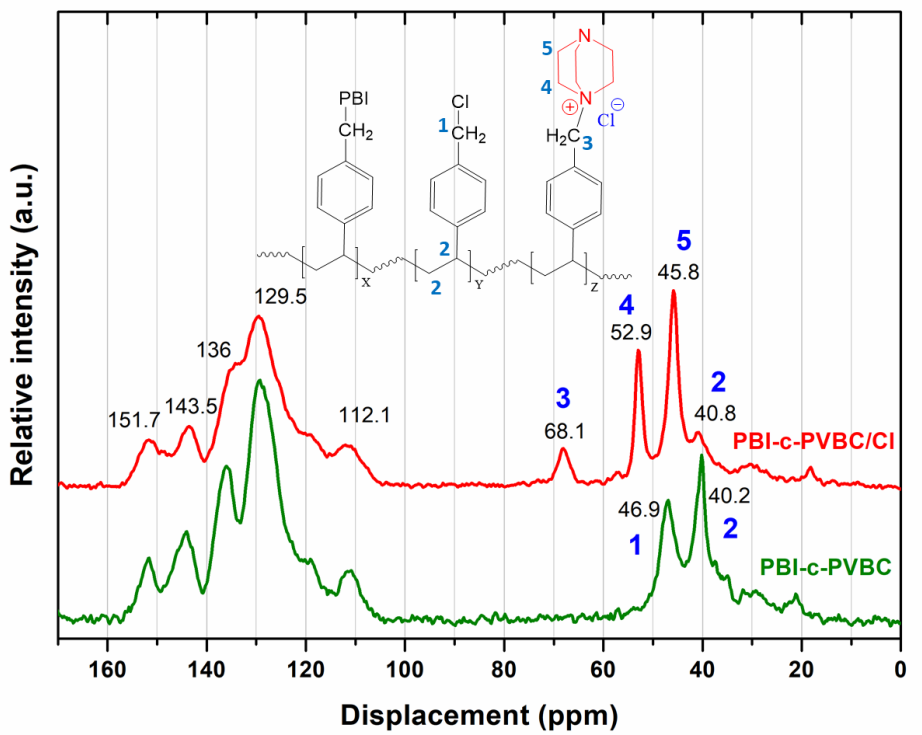

Figure 5.11. Solid ^{13}C-NMR spectra of PBI-c-PVBC and PBI-c-PVBC/Cl 1:1.

The peaks in the range of 100-160 ppm come from the aromatic rings of PVBC and PBI and the imidazole rings of PBI, as it was described in the NMR results of PVA:polybenzimidazole membranes and in literature [12]. The area between 30 and 80 ppm presents interesting changes when the membranes is quaternized: the peak at 46.9 ppm, ascribed to the C bonded to Cl, vanishes and in the same region appear two new peaks at 52.9 and 45.8 ppm. These peaks are ascribed to the C atoms of DABCO next to the quaternary ammonium and to the tertiary ammonium, respectively. This result confirms the quaternization of DABCO only by one nitrogen, as it was intended. A new peak also appears at 68.1 ppm, coming from the C of PVBC bonded to the quaternary ammonium of DABCO instead of to the Cl atom, and thus at higher displacement values. The C of

PVBC bonded to PBI couldn't be clearly distinguished, since it is probably in the broad band in this region. The assignation of the peaks was done according to literature [12,16,17] and the predicted ^{13}C-NMR spectra by the software NMRPredict of MestreNova.

2.6 Surface and cross-section

Scanning electron microscopy (SEM) and Energy dispersive X-ray analysis (EDX) were used to observe the superficial and cross-section microstructure of the membranes and study their chemical composition. The obtained results showed that both PBI and ABPBI-based membranes present a homogeneous structure with no phase separation between the polymers.

The good homogeneity of the membranes is most probably due to the adequate crosslinking between the polymers, preventing the phase segregation that was observed in the PVA:PBI samples.

The detected presence of Cl in the crosslinked membranes came mainly from the Cl atoms in the CH_2-Cl bonds. Thus, it is an indicator of where the PVBC chains are present. For this reason, mapping of the cross-section in the whole area and in line were performed, checking the Cl presence. The results are presented in Figure 5.12.

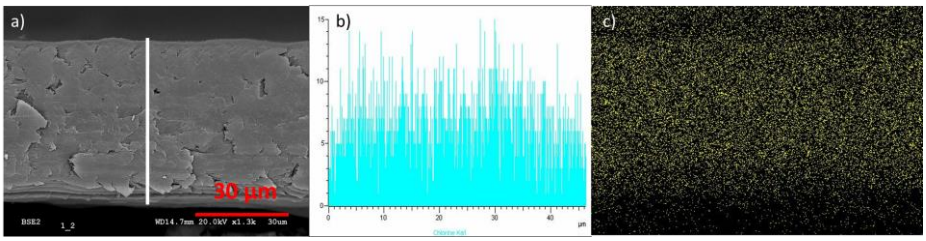

Figure 5.12. a) SEM image of the cross-section of a PBI-c-PVBC 1:3 membrane, with a white line to mark where the line-EDX analysis was performed, b) EDX analysis results of the Cl peak abundancy (left-to-right in the graph corresponds to top-to-bottom in the cross-section) and c) area mapping of the presence of Cl atoms.

The homogeneous distribution of Cl in the cross-section of the membrane confirms the presence of PVBC in the whole area, which is the desired result of the synthesis since heterogeneities in the CH_2-Cl presence would lead to areas with lower quaternary ammonium groups and worse ionic conductivity.

2.7 Thermal stability

Thermogravimetric analysis (TGA) of the membranes was performed by increasing the temperature and measuring the weight decrease as explained in the Experimental chapter. The derivative weight (mass %/time) was calculated from the TGA results and is also presented to see more clearly where the mass loss steps occur. The thermal stability of ABPBI and PBI has been extensively studied. In the case of PBI, it is stable until approximately 500-600 ºC [18,19] and ABPBI shows similarly a very high thermal stability (measured and presented here). The results of pure ABPBI and PVBC, as well as crosslinked polybenzimidazole-c-PVBC membranes are presented in Figure 5.13. ABPBI shows an initial weight loss in the range of 65-250 ºC resulting from the loss of water and maybe some residual solvent, after this loss it is stable until approximately 550 ºC where it starts to degrade (not showed). Regarding PVBC, it is thermally stable until 350 ºC, when the degradation of $–CH_2Cl$ groups starts. At 450 ºC PVBC suffers a new loss step from the degradation of the main chain. The crosslinked membranes show the weight loss of absorbed water and residual solvent below 150 ºC. Rising the temperature, around 200 ºC, there is a new weight loss not present in the curves of the pure polymers. This loss is assumed to be originated by the degradation of the conductive crosslinking points (imidazolium salt formed by double crosslinking of the imidazole ring as explained in the synthesis). In the PBI-c-PVBC membranes this weight loss is around 6-7 % while in the ABPBI-c-PVBC 1:2 membrane it is not observed and in the 1:3 it is only around 2 %. It can be concluded that the PBI-based membranes tend to form more double crosslinking points, which may be explained by the lower density and higher d-spacing of PBI (1.33 g cm^{-3} and 4.05 Å) respect to ABPBI (1.5 g cm^{-3} and 3.3 Å) [20] allowing for more room to attack the imidazolium ring from both sides. The crosslinked membranes also present weight losses around 300-350 ºC, attributed to the degradation of the non-conductive (simple) crosslinking point. In the PBI-c-PVBC 1:2 and 1:3 membranes this losses are respectively around 16 and 20 %, while in the ABPBI-c-PVBC 1:2 and 1:3 membranes are approximately 16 and 21 %. The single crosslinking is thus much more extended than the double one as expected and no relevant differences are presented between the PBI and ABPBI-based membranes, so probably the more dense structure of ABPBI is not so relevant for this process. Logically the membranes with higher amount of PVBC present higher losses from this single crosslinking point. Finally, the non-reacted $–CH_2Cl$ groups degrade around 350-450 ºC.

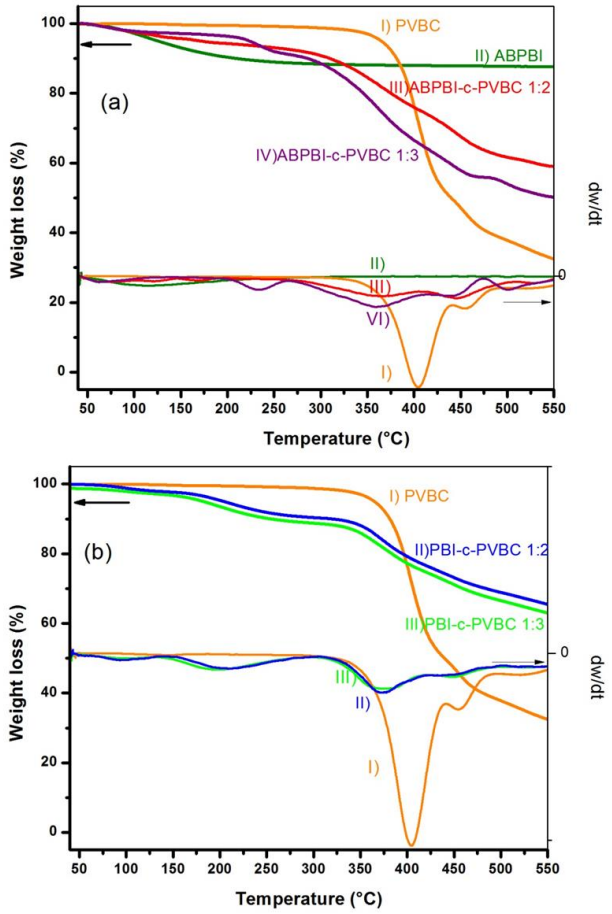

Figure 5.13. TGA thermographs of a) ABPBI-c-PVBC and b) PBI-c-PVBC membranes with different ratios, as well as pure PVBC and ABPBI.

The process of quaternization probably generates an additional stabilization of the structure since the first weight loss around 200 ºC is not observed in the quaternized membranes, see Figure 5.14. The small loss around 120 ºC comes probably from water and residual solvents. The other loss regions are more or less similar to the previous ones, maybe changed by the presence of OH ions in the structure.

These membranes are developed to be used in systems operating at temperatures under 100 ºC. Therefore, besides the structural information extracted, it can be concluded that all of them are thermally stable at that temperatures and thus suitable for the desired applications.

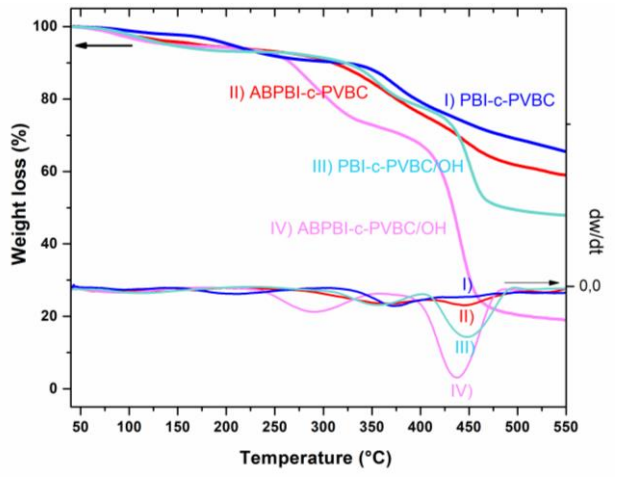

Figure 5.14. TGA thermographs of polybenzimidazole-c-PVBC membranes of 1:2 molar ratio, comparing the degradation of the membranes after the crosslinking and after the quaternization (in OH^- form).

2.8 Mechanical properties

Mechanical tensile tests of PBI-c-PVBC membranes crosslinked and quaternized were measured to have an approximation of their strength and evaluate the effect of quaternization to the membranes. The ABPBI-based membranes were not measured, so it has to be noted that they were more brittle but still could be handled with no trouble to prepare the conformation of membrane electrode assembly in the final device and perform during operation. The results obtained with the PBI-based membranes are illustrated in Figure 5.15.

It can be observed that the results are not very homogeneous, derived from the small differences between the laboratory synthesised membranes. However, it is clear the tendency of higher maximum stress in the crosslinked membranes compared to the quaternized membranes (in Cl^- form).

From the comparison with doped PBI and PVA:PBI 4:1 membranes in Figure 5.15b, it can be concluded that the obtained values are in the same range and thus are adequate to be used in the final device. The PBI-c-PVBC membranes are not yet humidified and doped (in OH^- form), therefore some decrease in maximum stress and increase in total elongation can be expected from the experience with the PVA:polybenzimidazole membranes. Taking into account that these membranes are crosslinked and very homogeneous these changes won't be too large.

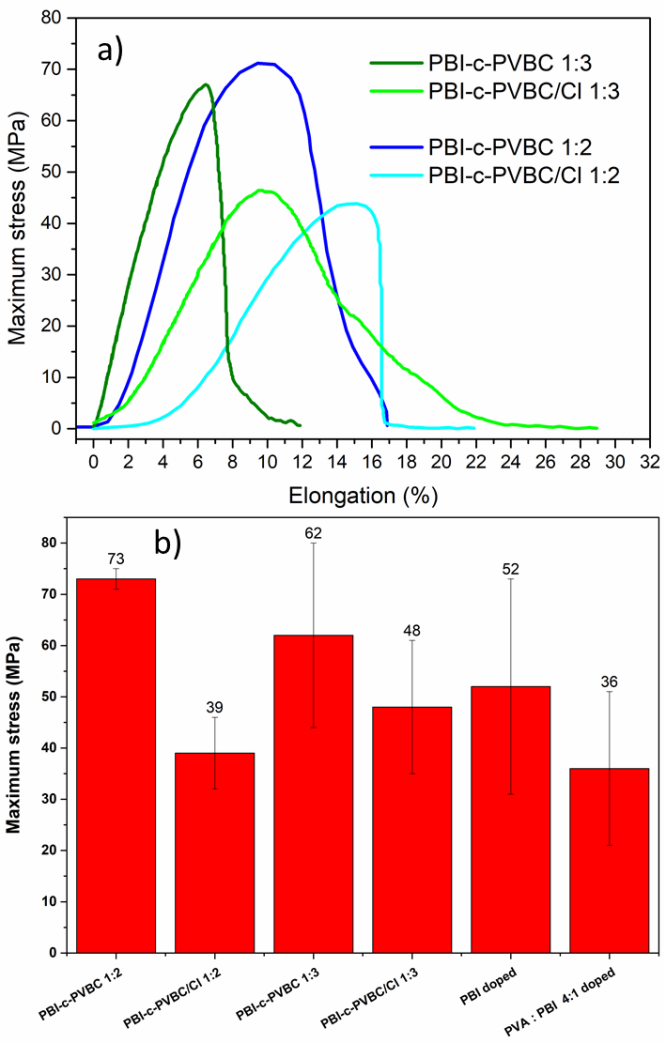

Figure 5.15. a) Tensile strength results (average curve) of the crosslinked and quaternized PBI-c-PVBC membranes and b) maximum stress values of the previous membranes compared with doped PBI and L-PVA:PBI 4:1 membranes in KOH 6 M for 5 and 3 days respectively.

2.9 Water uptake, KOH uptake and swelling behaviour

Once the thermal and mechanical properties had been ensured, the swelling behaviour of the membranes when fully hydrated and incorporating KOH was measured. As previously explained, this is important to understand better how does the membrane behave in conditions closer to the real ones; since an adequate degree of water and KOH uptake help to promote the ionic conductivity but if they are too large the structural properties of the membrane and MEA can be compromised. Calculations were done according to equations 3.10 and 3.11 for the water and KOH uptake respectively (% respect to the initial weight of the membrane). In the case of the polymer %, it is calculated as the polymer mass respect to the weight of the final membranes, which apart of the polymer contains water and KOH. The results are showed in Tables 5.3 and 5.4.

Table 5.3. Polymer wt.%, KOH and water uptake of polybenzimidazole-c-PVBC membranes doped 2 days in KOH 1 M at 25 ºC compared to linear and cross-linked PVA:polybenzimidazole 4:1 membranes and ABPBI membranes. *(doped in KOH ~3 M (15 wt.%)), #(doped in KOH 1.9 M, from [21]).

Membrane	Polymer/ wt.%	KOH/ wt.%	H_2O/ wt.%
PBI-c-PVBC/OH 1:2	68 ± 4	4 ± 1	45 ± 9
PBI-c-PVBC/OH 1:3	65 ± 5	3.5 ± 0.5	52 ± 9
ABPBI-c-PVBC/OH 1:2	62 ± 3	11 ± 7	51 ± 7
L-PVA-PBI *	49 ± 2	1.0 ± 0.5	50 ± 2
L-PVA-ABPBI *	30 ± 7	1.0 ± 0.5	69 ± 7
C-PVA-PBI *	73 ± 6	5.0 ± 0.5	22 ± 6
C-PVA-ABPBI *	25 ± 4	8.0 ± 0.5	67 ± 4
L-ABPBI #	46	16	38
C-ABPBI #	49	17	34

The KOH uptake comes from two contributions, as described by Hao et al. [22]. One is related to the acid-base reaction between the acid groups of the polybenzimidazole membranes forming potassium polybenzimidazolate salt and water. The second comes from the free KOH entering the membrane structure and helps in the OH^- conductivity transport within the membrane. Both can be present without total reaction of the acidic sites in the polybenzimidazoles.

The results show that the KOH uptake of the PBI-based membranes is lower than in the ABPBI-based ones, which is probably related with the different molecular structure since PBI contains hydrophobic aromatic rings. ABPBI materials with different structures (linear and crosslinked) have been reported to present high KOH uptake [21]. However, from the obtained results, not only containing ABPBI, but also the effect of crosslinking (which helps to retain water and KOH) and the presence of quaternary ammonium groups are the factors that lead to the KOH uptake of 11 % of the ABPBI-c-PVBC/OH 1:2 membrane, the highest between the polybenzimidazole-based membranes synthesised in this Thesis.

The water uptake results show more similarity between the different polybenzimidazole-c-PVBC membranes. The PBI-c-PVBC/OH 1:3 membrane has slightly higher water uptake than the 1:2 ratio, probably due to the presence of more hydrophilic quaternary ammonium groups (as will be later confirmed).

The percentage of polymer in all the studied polybenzimidazole-c-PVBC membranes is very similar. It is slightly lower in the ABPBI-c-PVBC/OH membrane due to the higher KOH uptake than the PBI-based membranes and the higher water uptake than the 1:2 one, but the differences are not relevant and all of them have a considerable quantity of polymer in the final membrane.

The complementary results of the swelling behaviour of the membranes are presented in Table 5.4.

Table 5.4. Swelling ratio (SR) measured as VSR (volume SR), TSR (thickness SR) and LSR (length SR) of polybenzimidazole-c-PVBC membranes doped 2 days in KOH 1 M at 25 ºC compared to linear and cross-linked PVA:polybenzimidazole 4:1 membranes. *(doped in KOH ~3 M (15 wt.%)).

Membrane	VSR/%	TSR/%	LSR/%
PBI-c-PVBC/OH 1:2	23 ± 8	9 ± 6	5 ± 2
PBI-c-PVBC/OH 1:3	24 ± 5	5 ± 1	9 ± 2
ABPBI-c-PVBC/OH 1:2	90 ± 10	38 ± 3	21 ± 7
L-PVA-PBI *	80 ± 5	48 ± 4	9 ± 1
C-PVA-PBI *	90 ± 10	50 ± 5	6 ± 3
L-PVA-ABPBI *	83 ± 3	18 ± 7	25 ± 5
C-PVA-ABPBI *	80 ± 10	14 ± 8	27 ± 6

Swelling results of the polybenzimidazole-c-PVBC membranes show important differences between the PBI and ABPBI-based ones. The membrane of ABPBI-c-PVBC/OH presents a higher VSR, especially due to the larger increase in the thickness direction. This is probably related with the higher KOH uptake of these membranes and probably some differences in the microstructure that couldn't be observed by SEM, also derived from the absence of the hydrophobic aromatic ring of PBI. However being high compared to the PBI-c-PVBC membranes, the swelling results of the ABPBI-c-PVBC/OH are in the range of those previously obtained with PVA:polybenzimidazole membranes and thus are within acceptable values to be used in the fuel cell or electrolyser.

2.10 Ion exchange capacity (IEC)

The evaluation of the ion exchange capacity (IEC) was performed to investigate the amount of quaternary ammonium (QA) groups in the different membranes. It was done by exchange of the OH^- ions of the membrane (counter-ions of the QA groups) with Cl^- ions, and titrating the OH^- extracted to the solution, as described in details in the Experimental chapter. The results obtained with the different polybenzimidazole-c-PVBC membranes are presented in Figure 5.16.

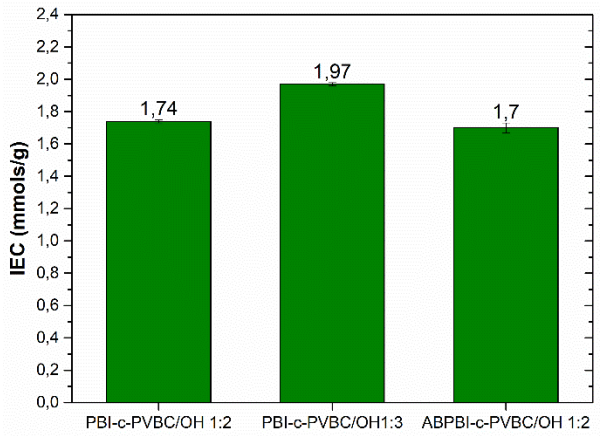

Figure 5.16. IEC values of different polybenzimidazole-c-PVBC membranes.

The values obtained are in the same range, but different from each other. First, both membranes of 1:2 ratio present a similar IEC value. This could look illogical since the Cl/N ratio of the ABPBI-c-PVBC 1:2 is much higher (ratio 1) than in the case of PBI-c-PVBC 1:2 (ratio 0.5, from Table 5.1) and thus much more "free" PVBC CH_2-Cl bonds (that can be quaternized) could be expected.

However, taking into account the high crosslinking degree of ABPBI-c-PVBC 1:2 showed by the gel fraction, probably more CH_2-Cl groups are consumed in the crosslinking compared to the PBI one. It was also estimated that the PBI-based membranes presented more conductive crosslinking points, which could contribute to the higher IEC values. Comparing PBI-c-PVBC/OH 1:2 and 1:3 membranes, the higher IEC value of the second is surely due to the higher amount of PVBC in the membrane which leads to increased abundance of QA groups. These values are lower than the obtained by Lu et al. [4], the longer crosslinking time may give more abundancy of conductive crosslinking points or more retention of KOH within the membrane than is later titrated. Overall the IEC values are very adequate and similar to other membranes with very good performance as anion exchange membranes [5], since values much higher than these may probably lead to excessive water and KOH uptake and structural weakening.

2.11 Ionic conductivity

After measuring the properties required for a good performance in the previous sections and obtaining adequate results, the OH^- ionic conductivity of the prepared membranes was measured after two days of doping in KOH 1 M at 25 ºC at different temperatures and the activation energy values were extracted. The obtained results are illustrated in Figure 5.17.

It is observed that the ABPBI-c-PVBC/OH 1:2 membrane obtains the best values, reaching 48 mS cm^{-1} and 56 mS cm^{-1} at 50 and 90 ºC respectively. The PBI-based membranes also obtain very good values, while not as high as the previous one. The higher conductivity of the ABPBI-based membrane is probably obtained due to the higher KOH uptake and adequate ratio of polybenzimidazole to PVBC, giving rise to a homogeneous structure with suitable channels for the transport of hydroxyl anions and high concentration of them. Also the good amount of quaternary ammonium groups (measured by the IEC) and the presence of the conductive crosslinking points are crucial to obtain these conductivities. In the PBI-based membranes, the higher conductivity of the membrane with 1:3 ratio is surely due to the higher IEC of those membranes.

The obtained conductivity values are not as high as those obtained with the PVA:polybenzimidazole membranes of very high PVA content like 6:1 or 8:1, but those membranes were too mechanically unstable. However, these results are quite similar to those of linear and crosslinked PVA:polybenzimidazole membranes with 2:1 and 4:1 ratios which presented very good performances.

They are also similar to the conductivity obtained in similar membranes by Lu et al. [5].

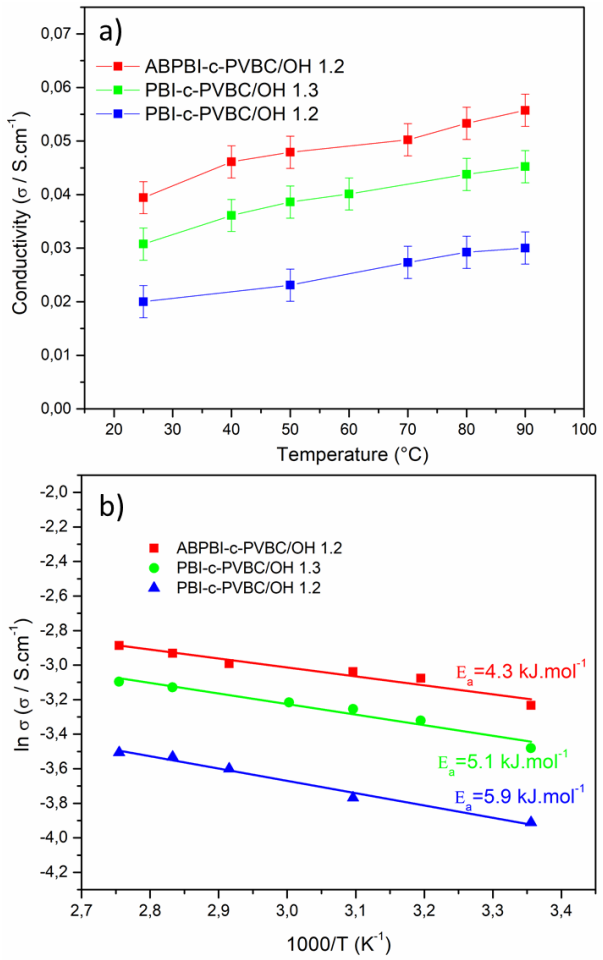

Figure 5.17. a) Ionic OH^- conductivity values of different polybenzimidazole-c-PVBC/OH membranes at increasing temperatures and b) linear fitting of the data to obtain the activation energy (Ea) results.

The increase in temperature produces and increased conductivity due the higher mobility of the hydroxyl anions, similarly to other anion exchange membranes. From the relation of these two parameters, by an Arrhenius relation as equation 3.12 (like in the PVA:polybenzimidazole membranes), the activation energy value is obtained from the slope of the linear fitting, as showed in Figure 5.17b. The obtained values are very similar to those obtained previously with PVA:polybenzimidazole membranes or others in literature [23], meaning that a similar combination of transport mechanisms are involved (e.g. Grotthuss,

diffusion, migration or convection). No relevant differences are either observed between PBI and ABPBI membranes crosslinked with PVBC.

2.12 Durability tests in alkaline and oxidative media

To evaluate the durability of the polybenzimidazole-c-PVBC membranes, two different tests were performed. One of them in alkali media (KOH 1 M solution) at 60 ºC during various days and measuring the conductivity with the increasing time, as well as the IEC, water uptake and swelling behaviour after 20 days. The other was performed in a strong oxidative media (Fenton's reagent) and taking the weight of the membrane each day. In the PBI-based samples FT-IR spectroscopy was also used to investigate the effects produced.

2.12.1 Degradation in alkaline media

Different parameters were used to evaluate the degradation in KOH 1 M at 60 ºC with time, as presented in the following figures.

The change in the OH^- conductivity at 25 ºC during the degradation time is showed in Figure 5.18.

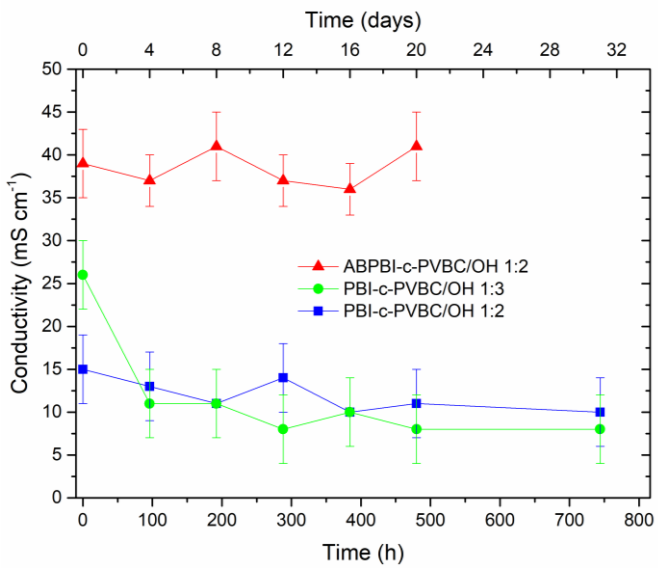

Figure 5.18. Change in the OH^- conductivity at 25 ºC at different degradation times at 60 ºC in KOH 1 M solution. Time zero is considered with the membrane doped as usually after 2 days in KOH 1 M at 25 ºC.

As it can be observed, the membranes of 1:2 ratio maintain the conductivity values in the same range as the original ones, with no indication of relevant degradation. The same behaviour was observed by Lu et al. [4] with similar conductivity values at long degradation test times. The membrane of PBI-c-PVBC/OH 1:3 ratio presents a drop in conductivity in the first 4 days, after which the values are maintained and similar to the PBI-c-PVBC 1:2. This initial effect could be related with the higher IEC of the membrane and thus more QA groups that can be degraded. Even after the 31 days the membranes showed good appearance.

The IEC after 20 days degradation time is compared with the initial one in Figure 5.19. The % of IEC loss of PBI-c-PVBC/OH 1:2, 1:3 and ABPBI-c-PVBC 1:2 are 10 %, 16 % and 7 % respectively.

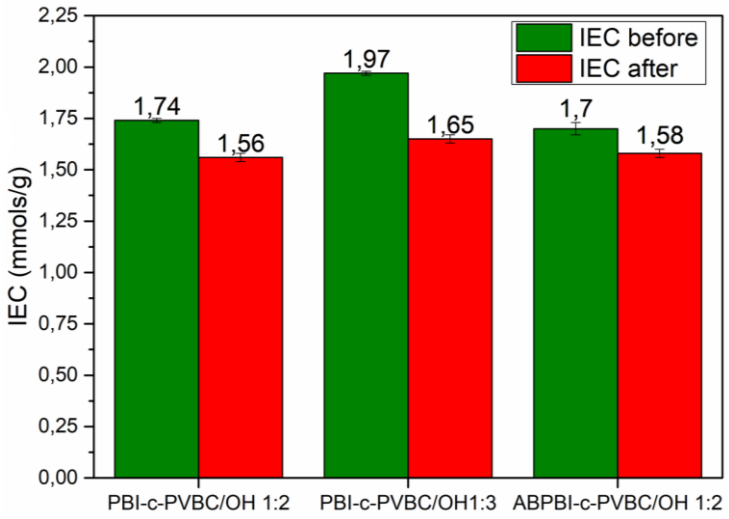

Figure 5.19. IEC values of polybenzimidazole-c-PVBC/OH membranes before (green) and after (red) the alkali durability test.

The obtained values are comparable to other highly alkali stable quaternary ammonium groups like 1-methylpyrrolidine or N-methylpiperidine studied by Ponce et al. [5] and better than the benchmark trimethylamine. The membrane that suffers the highest decrease (PBI-c-PVBC/OH 1:3) is the same that presented the highest IEC before the test, which seems logical. This effect can also explain the decrease in ionic conductivity observed in this membrane.

The water uptake of the membranes before and after the alkali treatment as well as the swelling behaviour are presented in Figure 5.20. The samples were the same that were used for the IEC and only the water uptake was measured (not

including KOH in the membrane), which explains the differences with the previous water uptake results.

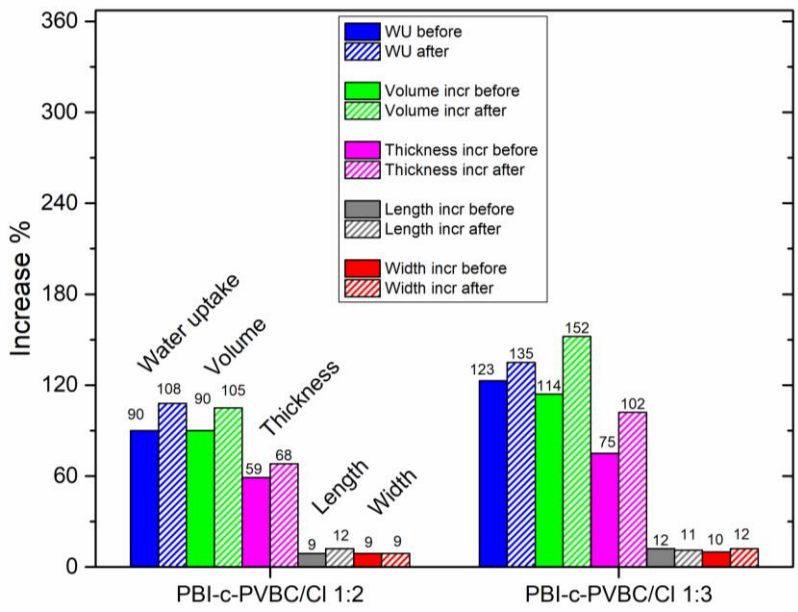

Figure 5.20. Water uptake and swelling behaviour of the polybenzimidazole-c-PVBC/Cl membranes before and after 20 days of alkali treatment at 60 ºC in 1 M KOH solution. The % of increase is referred to the initial parameters of the dry membrane.

In the case of ABPBI-c-PVBC/Cl 1:2, the values (after and before) are for the water uptake (118 and 154 %), volume (275 and 340 %), thickness (82 and 90 %), length (44 and 50 %) and width (43 and 54 %). As it can be observed, the membranes show higher water uptake and the corresponding increased swelling after the alkali durability test than before. This wouldn't make sense considering the IEC values, which are lower after the alkali test and thus there are less hydrophilic QA groups. However, the effect of the temperature during the alkali test (60 ºC) helps to promote the inclusion of water molecules in the membrane structure and this effect is clearly more relevant in these cases than the low decrease in the IEC values. Obtained values of water uptake and swelling increase are high, but still adequate for the membranes to be used in final application as discussed before.

The FT-IR spectra at different days are presented in Figure 5.21. Only some of the days are presented to have a clear picture.

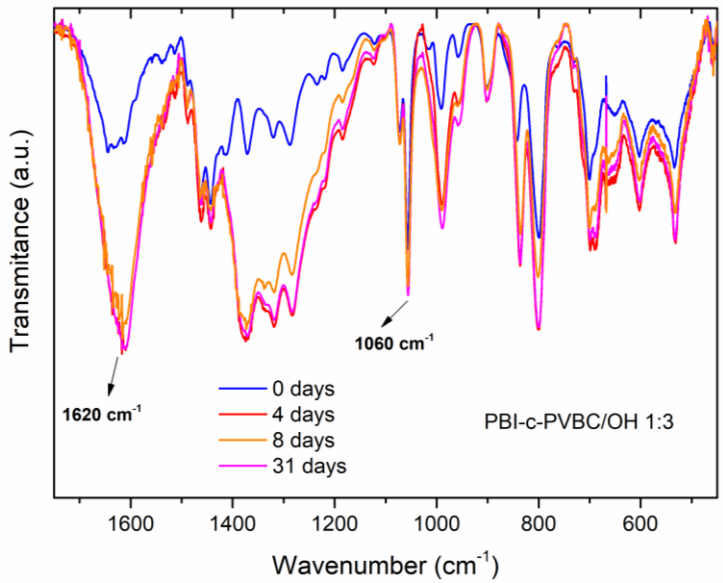

Figure 5.21. FT-IR spectra of the PBI-c-PVBC/OH 1:3 membrane at different days of the durability test. The other membranes presented similar spectra (not showed).

The most relevant changes are the observed incorporation of OH^- ions in the structure by the increase in intensity of the peaks in the area between 1200 and 1400 cm^{-1} and the big broad band at 1600 cm^{-1}, as reported by other authors [5,24]. It is also observed that the peak at 1060 cm^{-1} of the DABCO molecule is still present without relevant decrease after 31 days of alkali durability test, confirming the good stability of the membranes.

2.12.2 Degradation in oxidative media

The membranes have to work in the fuel cells in an oxidative media, since pure O_2 is supplied constantly and some species may be formed in the electrodes like H_2O_2, which is a strong oxidant and can produce hydroxyl ions and radicals that attack the polymeric structure of the membrane [25]. The test was done in an aqueous solution with Fenton's reagent ($4*10^{-6}$ M $FeSO_4$ and 3 wt.% of H_2O_2) at 40 ºC measuring the weight of the samples each day and changing the solution with fresh one. It has to be considered that the conditions of the test are much stronger than the real ones present in the fuel cell under operation and thus it is just an accelerated test to have an idea of the membrane stability in this media. The obtained results are presented in Figure 5.22.

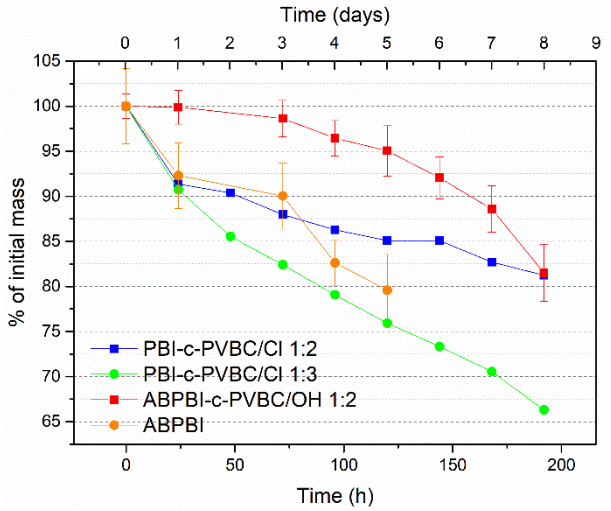

Figure 5.22. Decrease of weight under accelerated durability test in oxidative media of polybenzimidazole-c-PVBC membranes compared to pure ABPBI membrane.

The results show that pure ABPBI membrane suffers a loss around 20 % in 5 days, very similar to the degradation exhibited by PBI in literature [26]. The results of the synthesised polybenzimidazole-c-PVBC membranes are logical attending to the degree of crosslinking that they showed in the gel fraction measurements: the PBI-c-PVBC 1:3 membrane is less crosslinked and thus the chains are more easily attacked and degraded, while the ABPBI-c-PVBC 1:2 shows the best durability in the accelerated test, especially in the first days, finally showing an approximately 19 wt.% decrease at 8 days similar to the PBI-c-PVBC 1:2 membrane.

The final aspect of the membranes after the test is showed in Figure 5.23. It can be observed that the membrane of PBI-c-PVBC 1:2 ratio shows the lowest rupture in pieces, which comes probably from the compromise between the high crosslinking of ABPBI-c-PVBC 1:2 (stiffer) and the high amount of free PVBC in the PBI-c-PVBC 1:3 membrane.

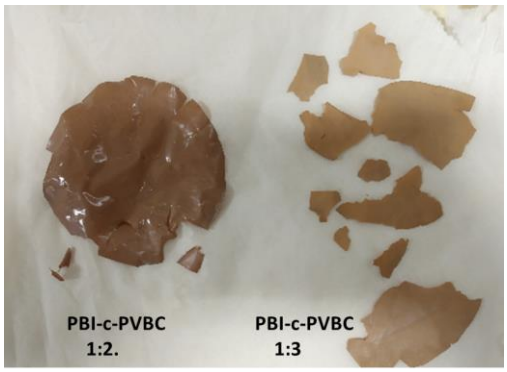

Figure 5.23. Aspect of the polybenzimidazole-c-PVBC membranes after the accelerated oxidative test.

The FT-IR spectra of one of the membranes after the test is presented in Figure 5.24.

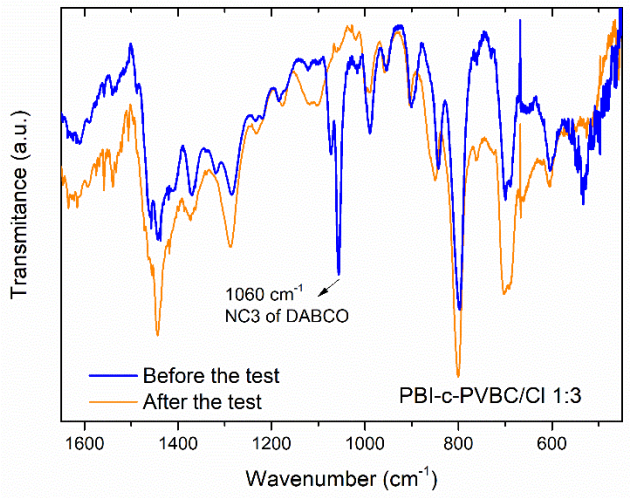

Figure 5.24. FT-IR spectra of the PBI-c-PVBC/Cl membrane before and after the accelerated oxidative degradation durability test.

It shows that the most important change is the disappearance of the band at 1060 cm^{-1} from the DABCO molecules, showing the complete degradation of the quaternary ammonium groups of the membrane under this strong conditions.

Overall, the membranes show a very good stability in alkaline and oxidative media, keeping good conductivity and IEC values after long time alkaline test and presenting similar and better oxidative resistance than the pure polymers.

3 Performance in final application

The membranes of polybenzimidazole-c-PVBC showed very promising and adequate values in the different characterization techniques and properties previously measured and thus it was investigated their performance in the final application devices, similar to the PVA:polybenzimidazole membranes: the alkaline direct ethanol fuel cell (DEFC) and the zero gap liquid alkaline water electrolyser (LAWE).

3.1 Alkaline direct ethanol fuel cell

The measurements in the fuel cell were not easily performed since different problems may happen. One of the most common was that during operation, the membrane may suffer small cracks (even with the good mechanical properties already measured), these cracks can be produced by small errors in the components assembly when the single cell was prepared. Also, small heterogeneities, not perceived by eye, can be weak points in the membrane when the pressure and temperature are applied or simply by degradation of the membranes. This cracks cause mixing of the reactants (oxygen and ethanol) crossover and, depending of the extent, may have a small impact in the open circuit potential (OCP) and on the performance of the fuel cell. In addition, since the membranes are synthesised in the laboratory and the electrodes are handmade (in the spraying process of the ink) differences are most probably present between each measurement. Also the flooding of the electrodes occurring at relatively high current density (when more water is produced) will be never exactly the same between different measurements since it depends greatly on the exact humidification state of each electrode. These reasons explain the differences present between measurements using similar conditions. The same can be applied to the membranes of PVA:polybenzimidazole presented in the previous chapter and the membranes based on ETFE of the next one, while in those based on ETFE the possibility to break is usually lower since they are prepared from a commercial film highly homogeneous and resistant.

In order to test the adequate conditions to measure the membranes, some parameters were kept constant and others were varied. For example the fuel rate of EtOH 2M / KOH 2M (as well and the ratio and concentrations) was kept constant at 1 mL min^{-1}, since from previous optimization experiments

performed in the research group it was found to be adequate. The gas rate of 0.2 slpm of O_2 at the cathode was also maintained due to similar reasons. The temperature of 90 ºC for the final measurements was used in all the samples. At higher temperatures, the ethanol in the water solution starts to evaporate and bubbles of ethanol are formed causing too much convection troubles in the anode side, and if 100 ºC are reached water would also evaporate increasing the mentioned problems. On the other hand, lower temperatures may be beneficial for the long-term durability of the membranes but the mobility of the ions is lower and the electrode kinetics too. Therefore, since these measurements are designed to obtain the power density in short term tests, it was decided to compare all the results at 90 ºC. One of the parameters that was changed was the O_2 backpressure, since it is usually observed that higher pressures yield better performance due to the improved retention of the O_2 molecules in the cathode in the gas diffusion layer and specially in contact with the catalyst layer. However, high pressures tend to break the membrane more easily and increase the O_2 crossover.

In the results presented, the previously fixed conditions were maintained: temperature of 90 ºC, feeding of the anode with EtOH 2M / KOH 2M at 1 mL min^{-1} and the cathode with pure O_2 at 0.2 slpm. The membranes were doped and exchanged in most of the cases with KOH 1 M for 2 days (small variations were performed in the first tests) and the pristine PBI membranes were doped 5 days in KOH 6 M to obtain its optimum doping level (previously studied in the group). The catalysts used for preparing the electrodes were commercial PtRu/C in the anode and commercial Pt/C in the cathode as described in the Experimental chapter.

The results only present membranes of PBI-c-PVBC because the membranes of ABPBI-c-PVBC have not yet been evaluated in the fuel cell.

First, membranes with different PBI:PVBC ratios and under various conditions were tested to elucidate which of them had better performance and the adequate conditions. The results of some of the most representative polarization and power density curves are collected in Table 5.5 and showed in Figure 5.25.

Table 5.5. PBI-c-PVBC/OH membranes of different ratios and the obtained average power density under various O_2 backpressures.

Membrane	Thickness (μm)	Average power density (mW cm^{-2})	Temperature (ºC)	O_2 backpressure (psi)	O_2 backpressure (bar)
PBI-c-PVBC/OH 1:1 a	54	32	90	45	3
PBI-c-PVBC/OH 1:1 b	36	32	90	45	3
PBI-c-PVBC/OH 1:2 a	55	96	90	22	1.5
PBI-c-PVBC/OH 1:2 b	32	70	90	30	2
PBI-c-PVBC/OH 1:2 c	31	53	90	22	1.5
PBI-c-PVBC/OH 1:3 a	38	49	90	15	1
PBI-c-PVBC/OH 1:3 b	79	55	90	15	1

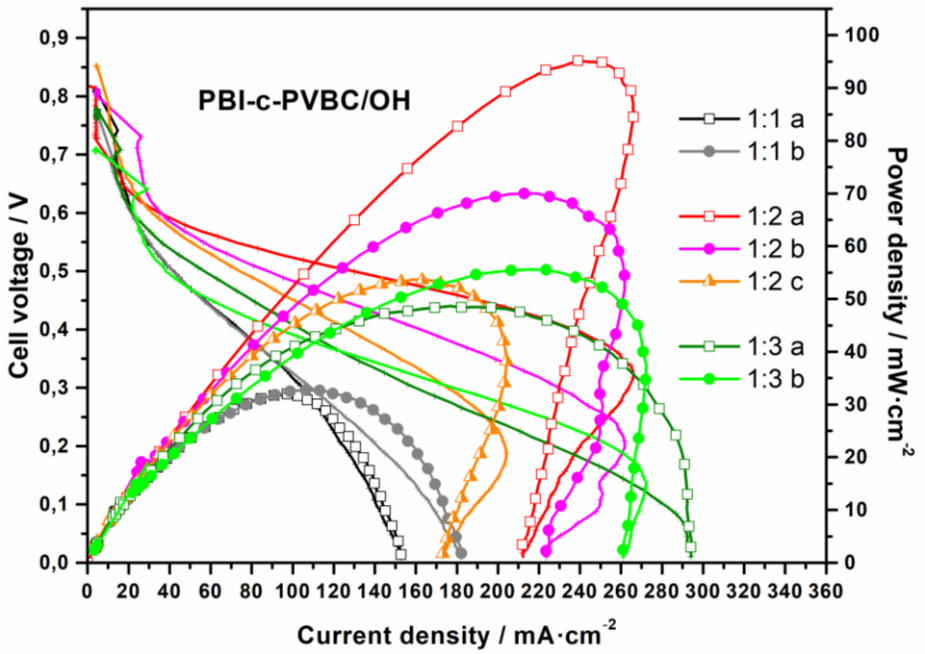

Figure 5.25. Fuel cell polarization and power density curves using PBI-c-PVBC/OH membranes. More details in Table 5.5.

High O_2 backpressure (around 3 bar) was measured with all the membranes, but many of them broke under that conditions. From the results presented in Table 5.5 it is clear that the higher the PVBC content, the lower the maximum pressure it could be applied. Some membranes of 1:2 and 1:3 ratios were measured at higher pressures, but most of them broke and the obtained results were not good. The found trend with PVBC content is consistent since pure PBI is much more resistant than membranes where it is combined with other polymers. The crosslinking of PBI with PVBC helps to have a resistant structure, but it doesn't

reach the resistance of pristine PBI. The data of the membrane's thickness is also showed; it is also an important parameter, since very thick membranes have large ohmic resistance while very thin membranes may break easily and present crossover of the reactants. A good compromise between conductivity and thickness needs to be reached. In these cases it seems that the thickness of the membranes is not the key parameter for determining the result. For example both membranes of 1:1 ratio obtain similar maximum power densities having different thickness and membranes "b" and "c" of 1:2 ratio present different maximum power densities having similar thickness. It looks that the range of thickness is adequate since good results are obtained, but further conclusions couldn't be extracted. The best power density was obtained with the membrane PBI-c-PVBC/OH "a", which reached 96 mW cm^{-2}. It was tried to reproduce this result, but with no success. As it can be observed from the collection of the measures obtained with membranes of 1:2 ratio, it was not easy to control all the parameters to obtain highly reproducible results; so probably one or some of the many parameters that cannot be perfectly controlled allowed to obtain the good result of 96 mW cm^{-2}. From these results, each measurement was performed a few times (at least three) and the result that showed an intermediate power density was considered the average. Overall it was clear that membranes of 1:2 ratio presented better maximum power densities than those with 1:3 ratio and 1:1 ratio (in this order). They also presented good OCP values (around 0.80-0.85 V), similar to those of 1:1 ratio and slightly better than the membranes of 1:3 ratio (0.7-0.8 V). Therefore the ratios of PBI:PVBC 1:2 and 1:3 were selected to continue the investigations. Moreover, since high O_2 backpressures didn't gave specially good results, a backpressure of 0.5 bar (8 psi) was selected for the following experiments. Since quite similar performances were obtained compared to higher pressures, it was kept constant at that value.

The average results using 0.5 bar with membranes of PBI-c-PVBC/OH 1:2 and 1:3 are illustrated in Figure 5.26.

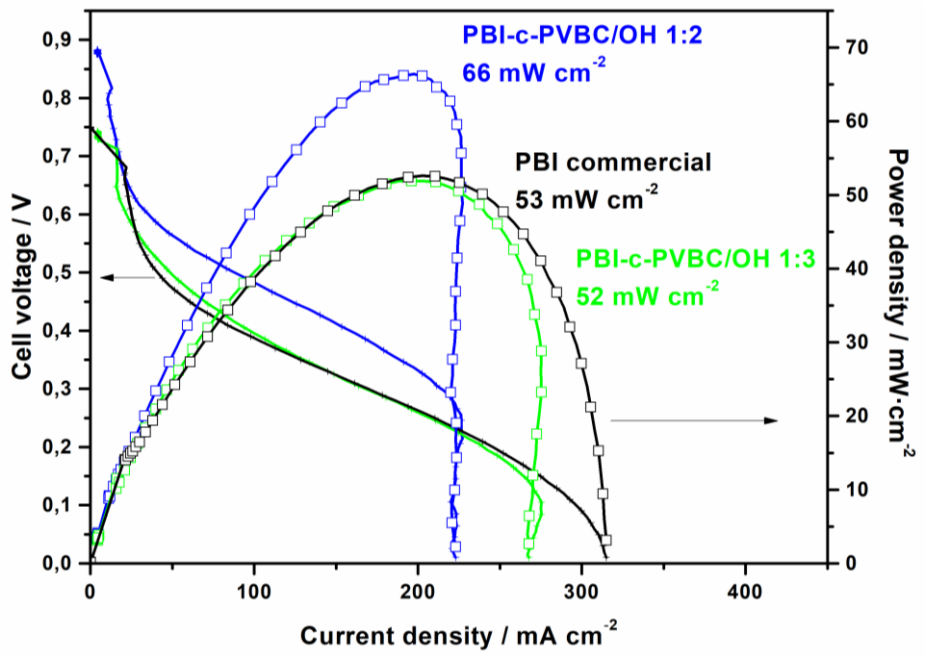

Figure 5.26. Fuel cell polarization and power density curves using PBI-c-PVBC/OH membranes and compared to pristine PBI membrane.

As it can be observed, the PBI-c-PVBC/OH 1:3 membranes show a similar open circuit voltage (OCP) of 750 mV and maximum power density about 53 mW cm^{-2} than the commercial PBI membrane. This can be considered a good result since the homogeneity and the precision in the preparation at the laboratory scale is not comparable to commercial one. The PBI-c-PVBC/OH 1:2 obtains a higher power density than the other two membranes, reaching 66 mW cm^{-2} at 337 mV, 25 % higher than commercial PBI. The reason of the better performance of this membrane is surely the higher OCP, almost 900 mV, that allows a higher overall potential during the curve since the activation and ohmic losses are quite similar. The higher OCP is related with a lower crossover of the reactants through the membrane compared to pristine PBI and PBI-c-PVBC 1:3, acting better as a barrier separator. This effect comes probably from the adequate microstructure of the membrane, which leads to a better structural resistance (as in the oxidant stability test) while showing high conductivity and IEC values like the others. One of the ways of evaluating the structural resistance was the mechanical properties values, as it was observed the membranes of 1:2 and 1:3 ratio showed similar values, however, the higher resistance of the 1:2 membrane was clearly observed in the accelerated degradation test in oxidative media and as it was explained comes from the higher crosslinking in the membrane (higher gel fraction).

Even with power densities not as high as those obtained with the PVA:polybenzimidazole membranes, thanks to the very stable structure and presence of the quaternary ammonium groups this membranes show a good performance in the alkaline direct ethanol fuel cell, with probably much better long-term durability.

Comparing with the state of the art in alkaline fuel cell using ethanol, a review of D. Dekel [27] shows that the best results that have been obtained are around 150-170 mW cm^{-2} maximum power density. However, all those were obtained by variations in the electrodes composition but using the commercial Tokuyama membrane electrolyte. Taking that into account, it can be observed that our synthesised membranes of PBI-c-PVBC are just around 1/2 or 1/3 of those and thus can be considered promising results. Comparing with PBI doped membranes, the recent review of Wu et al. [28] shows that power densities obtained with PBI doped membranes are in the range of 30-120 mW cm^{-2} using different conditions, catalysts and ethanol or KOH concentrations. From the reviewed measurements, the conditions more similar to ours are from Hou et al [29] as commented in the previous chapter. They measure also at 90 ºC, with a PBI membrane of original thickness of 50 μm (quite similar to ours), using EtOH 2 M / KOH 2 M in the anode and pure oxygen in the cathode. The main differences were the 2 bar of oxygen backpressure they use and the composition of the catalysts: Pt-Ru/C (30% Pt, 15% Ru) for the anode and Pt/C (20% Pt) for the cathode (but similar final Pt loading than our measurements). They obtained a power density of 61 mW cm^{-2} at 90 ºC with an OCP of 0.98 V. The OCP is higher than the one obtained by us, probably due to the even more homogeneous structure of pristine PBI. On the other hand, the maximum power density is slightly lower than ours (61 vs 66 mW cm^{-2}), probably due to the better conductivity of the PBI-c-PVBC/OH membranes with quaternary ammonium groups. They provide conductivity value of 18 mS cm^{-1} at room temperature, similar to our values, but no information is given for higher temperatures. Also other parameters like the good KOH and water uptakes of our membranes may contribute. It can be concluded that these membranes are still far from commercial membranes with other chemistries (Tokuyama) but are superior to the commercial PBI membrane measured in our laboratory and in the range of other membranes based on PBI in literature.

3.2 Liquid alkaline water electrolyser

A single cell liquid alkaline water electrolyser (LAWE) with zero gap configuration was used to perform the measurements with the polybenzimidazole-c-PVBC/OH membranes as anion exchange polymeric solid electrolyte. The membranes were previously doped and exchanged (from the Cl^- form) in KOH 1 M solution at 25 ºC for 2 days. The measurements were performed feeding the electrolyser with aqueous 15 wt.% KOH solution at controlled temperature and the electrodes were made of commercial Ni foam.

The obtained polarization and chronopotentiometric curves are illustrated in Figure 5.27. The comparison with the APBBI-c-PVBC/OH 1:2 membranes will be presented in the article "Polybenzimidazole-crosslinked-poly(vinyl benzyl chloride) as anion exchange membrane for alkaline electrolyzers" (actually under review).

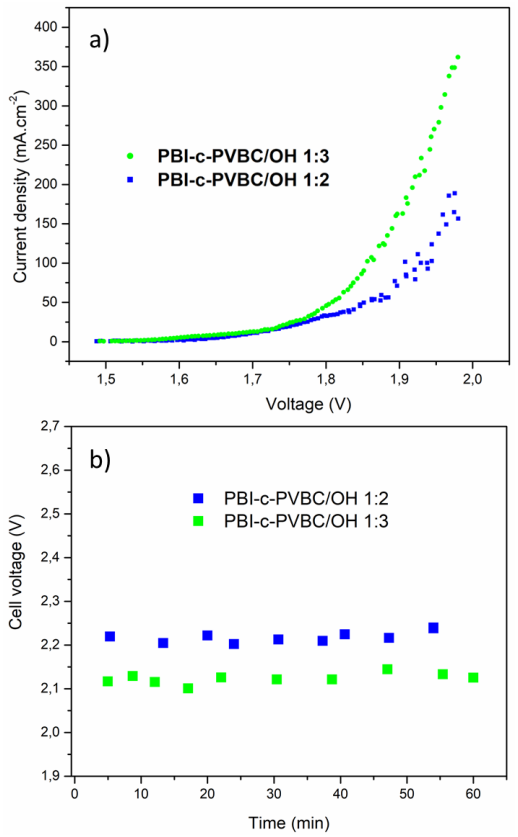

Figure 5.27. Electrolyser performance using the PBI-c-PVBC membranes with KOH 1M solution at 50 ºC. a) Polarization curves and b) chronopotentiometric curves at i=200 mA cm^{-2}.

The results in Figure 5.27a show that PBI-c-PVBC/OH 1:3 (which performance is very similar to ABPBI-c-PVBC/OH 1:2) has better performance than PBI-c-PVBC/OH 1:2, in agreement with the conductivity values previously obtained. The first two obtain a current density of 450 mA cm^{-2} at 2 V and the last (PBI-c-PVBC/OH 1:2) a current density of 225 mA cm^{-2} at the same voltage. These are very good results compared to the commercial Zirfon® porous diaphragm, which obtains 140 mA cm^{-2} at 2 V with circulating KOH 3 M solution [21].

The chronopotentiometric curves are presented in Figure 5.27b. No potential decrease of observed during the test in any of the measured membranes, relating the good stability they have at those conditions. The results are consistent with the linear sweep voltammetry curves, showing that the PBI-c-PVBC/OH 1:2 membranes has the worst performance (higher voltage) at 2.25 V and the 1:3 ratio maintains a lower voltage value (2.1 V). The ABPBI-c-PVBC/OH 1:2 membrane has the best performance with a voltage of 2.05 V.

The results obtained in the electrolyser with the membranes of PVA:polybenzimidazole were also very good. With those membranes, the best performance was obtained with the C-PVA:ABPBI 4:1 membrane (0.5 vol.% GA solution), reaching a current density of 450 mA cm^{-2} at 2 V, similar to the values obtained with polybenzimidazole-c-PVBC/OH membranes. However, in that case the operation conditions were with 2.3 M KOH (higher concentration) and 50 ºC. Therefore, it can be concluded that the polybenzimidazole-c-PVBC/OH membranes obtain better results since they reach similar current densities with lower concentration of the alkali solution, which is an important parameter especially for the long-term durability of the system. These results are higher than others reported in literature using anion exchange membranes with DABCO like for example the study made by Hnát et al. [30], in which they develop films of polystyrene-block poly (ethylene-ran-butylene)-block-polystyrene (PSEBS) functionalized with DABCO (PSEBS-CM-DABCO), using that material as anion exchange electrolyte and catalytic layer binder. They obtained a current density of 150 mA cm^{-2} at 2 V.

A comparison of the performance with industrial LAWEs [21] is presented in Table 5.6.

Table 5.6. Comparison of electrolysis performance of the membranes prepared in this work, other membranes and industrial systems. * comes from [30] and ** comes from [21].

Electrolyzer	Membrane	Circulation of KOH / M	Temperature / ºC	Cell voltage / V	Current density / $mAcm^{-2}$
This work	PBI-c-PVBC/OH 1:2	1	50	2.0	225a
This work	PBI-c-PVBC/OH 1:3	1	50	2.0	450a
This work	ABPBI-c-PVBC/OH 1:2	1	50	2.0	450a
This work	C-PVA-ABPBI	2.3	50	2.0	450
Ref *	PSEBS-CM-DABCO	2.3	40	2.0	150
Ref **	Zirfon®	3	50	2.0	140
Hydrogenics **	Porous diaphragm (PD)	6.7	80-90	1.7	375
Oronzio de Nora **	PD	6.7	80-90	1.8	150
IHT **	PD	6.7	80-90	1.9	200
Teletype **	PD	6.7	80-90	2.2	300
Uralkhimmash **	PD	6.7	80-90	2.3	200

It can be observed that our membranes obtain similar performances using lower alkali concentration in the process. As explained before, this is an important result since the low KOH concentration is very advantageous for the long-term durability of the membranes, electrocatalysts and metal components of the system, as well as reducing possible safety problems.

4 Conclusions

From the development of the research and the obtained results, the following conclusions can be extracted. The synthesis of the crosslinked membranes with polybenzimidazole (PBI and ABPBI) and PVBC has been successfully developed with different molar ratios of the polymers, from 1:1 to 1:3. The synthesised membranes show homogeneous appearance, which has been further confirmed by the SEM and EDX analysis, and present the typical IR bands of the component polymers. The crosslinking of the membranes has been confirmed and characterized using the gel fraction test and the thermogravimetric analysis, finding the formation of the conductive and non-conductive crosslinking points and the higher gel fraction (and crosslinking) of the ABPBI-c-PVB 1:2 membrane respect to the PBI-c-PVBC 1:2 and 1:3 ones.

The quaternization of the crosslinked membranes with DABCO has also been successfully performed, obtaining complete substitution of the Cl atoms bonded to PVBC by DABCO molecules, creating the fixed quaternary ammonium groups. The solid ^{13}C-NMR analysis has also confirmed the reaction of DABCO mainly by only one of the nitrogens, as desired for the superior described alkaline stability of this conformation.

Thermal and mechanical stability of the membranes have also been studied, with good results in both cases, taking note that the ABPBI-based membranes present more rigidity probably due to the higher crosslinking.

The study of the water uptake, KOH uptake and swelling behaviour has given interesting insights of the membranes, confirming the high affinity of ABPBI to water and KOH that causes the higher KOH and water uptakes the ABPBI-based membranes show. Other important factor affecting these parameters are the crosslinking degree and the presence of the hydrophilic quaternary ammonium groups in the membrane structure.

The obtained IEC values are logical with the previous results, and with the KOH uptake support the conductivity measurements, in which the membranes from higher to lower conductivity are: ABPBI-c-PVBC/OH 1:2, PBI-c-PVBC/OH 1:3 and PBI-c-PVBC/OH 1:2. The conductivity values aren't almost affected during the durability test in alkaline conditions, especially in the membranes of 1:2 ratios, which show a very stable conductivity during the 31 days. This test also reveals the higher water uptake and swelling increase at elevated temperature, which is not too large to cause important structural problems. The durability in oxidative media has also been evaluated, showing the good resistance of the membranes to the accelerated degradation test.

Finally, the membranes have been tested in an alkaline direct ethanol fuel cell and a zero gap alkaline water electrolyser. Further research and long-term measurements would be necessary to complete the study of the membranes in these devices. However, from these preliminary results it can be concluded that the membranes show similar or better performance than the commercial references (PBI membrane and Zirfon® diaphragm respectively) and are among the best found in literature.

5 References of the chapter: Membranes of polybenzimidazole-c-PVBC

[1] J.R. Varcoe, P. Atanassov, D.R. Dekel, A.M. Herring, M. a. Hickner, P. a. Kohl, A.R. Kucernak, W.E. Mustain, K. Nijmeijer, K. Scott, T. Xu, L. Zhuang, Anion-exchange membranes in electrochemical energy systems, Energy Environ. Sci. 7 (2014) 3135–3191. doi:10.1039/b000000x.

[2] Y.C. Cao, X. Wu, K. Scott, A quaternary ammonium grafted poly vinyl benzyl chloride membrane for alkaline anion exchange membrane water electrolysers with no-noble-metal catalysts, Int. J. Hydrogen Energy. 37 (2012) 9524–9528. doi:10.1016/j.ijhydene.2012.03.116.

[3] S.K. Tuli, A.L. Roy, R.A. Elgammal, M. Tian, T.A. Zawodzinski, T. Fujiwara, Effect of morphology on anion conductive properties in self-assembled polystyrene-based copolymer membranes, J. Memb. Sci. 565 (2018) 213–225. doi:10.1016/j.memsci.2018.08.028.

[4] W. Lu, G. Zhang, J. Li, J. Hao, F. Wei, W. Li, J. Zhang, Z.-G. Shao, B. Yi, Polybenzimidazole-crosslinked poly(vinylbenzyl chloride) with quaternary 1,4-diazabicyclo (2.2.2) octane groups as high-performance anion exchange membrane for fuel cells, J. Power Sources. 296 (2015) 204–214. doi:10.1016/j.jpowsour.2015.07.048.

[5] J. Ponce-González, D.K. Whelligan, L. Wang, R. Bance-Soualhi, Y. Wang, Y. Peng, H. Peng, D.C. Apperley, H.N. Sarode, T.P. Pandey, A.G. Divekar, S. Seifert, A.M. Herring, L. Zhuang, J.R. Varcoe, High performance aliphatic-heterocyclic benzyl-quaternary ammonium radiation-grafted anion-exchange membranes, Energy Environ. Sci. 9 (2016) 3724–3735. doi:10.1039/C6EE01958G.

[6] D. Stoica, L. Ogier, L. Akrour, F. Alloin, J.F. Fauvarque, Anionic membrane based on polyepichlorhydrin matrix for alkaline fuel cell: Synthesis, physical and electrochemical properties, Electrochim. Acta. 53 (2007) 1596–1603. doi:10.1016/j.electacta.2007.03.034.

[7] C. Iojoiu, F. Chabert, M. Maréchal, N. El Kissi, J. Guindet, J.Y. Sanchez, From polymer chemistry to membrane elaboration: A global approach of fuel cell polymeric electrolytes, J. Power Sources. 153 (2006) 198–209. doi:10.1016/j.jpowsour.2005.05.039.

[8] U.S. Hwang, J.H. Choi, Changes in the electrochemical characteristics of a bipolar membrane immersed in high concentration of alkaline solutions, Sep. Purif. Technol. 48 (2006) 16–23. doi:10.1016/j.seppur.2004.11.014.

[9] B. Bauer, H. Strathmann, F. Effenberger, Anion-exchange membranes with improved alkaline stability, Desalination. 79 (1990) 125–144. doi:10.1016/0011-9164(90)85002-R.

[10] W. Lu, Z. Shao, G. Zhang, Y. Zhao, B. Yi, Crosslinked poly (vinylbenzyl chloride) with a macromolecular crosslinker for anion exchange membrane fuel cells, J. Power Sources. 248 (2014) 905–914. doi:10.1016/j.jpowsour.2013.08.141.

[11] M.M. Cordes, J.L. Walter, Infrared and Raman studies of heterocyclic compounds—II Infrared spectra and normal vibrations of benzimidazole and bis-(benzimidazolato)-metal complexes, Spectrochim. Acta Part A Mol. Spectrosc. 24 (1968) 1421–1435. doi:10.1016/0584-8539(68)80165-5.

[12] R. V. Law, D.C. Sherrington, C.E. Snape, I. Ando, H. Kurosu, Solid-State 13 C MAS NMR Studies of Hyper-Cross-Linked Polystyrene Resins, Macromolecules. 29 (1996) 6284–6293. doi:10.1021/ma951606o.

[13] D. Herranz, R. Escudero-Cid, M. Montiel, C. Palacio, E. Fatás, P. Ocón, Poly (vinyl alcohol) and poly (benzimidazole) blend membranes for high performance alkaline direct ethanol fuel cells, Renew. Energy. 127 (2018) 883–895. doi:10.1007/978-3-642-20487-6.

[14] Nist database XPS, (n.d.). https://srdata.nist.gov/xps/selEnergyType.aspx (accessed June 16, 2019).

[15] Nist XPS tetraethylammonium chloride, (n.d.). https://srdata.nist.gov/xps/XPSDetailPage.aspx?AllDataNo=21035 (accessed June 16, 2019).

[16] N. Fontanals, J. Cortés, M. Galià, R.M. Marcé, P.A.G. Cormack, F. Borrull, D.C. Sherrington, Synthesis of davankov-type hypercrosslinked resins using different isomer compositions of vinylbenzyl chloride monomer, and application in the solid-phase extraction of polar compounds, J. Polym. Sci. Part A Polym. Chem. 43 (2005) 1718–1728. doi:10.1002/pola.20646.

[17] T. Lohar, A. Kumbhar, A. Patil, S. Kamat, R. Salunkhe, Synthesis and characterization of new quaternary ammonium surfactant [C 18 - Dabco][Br] and its catalytic application in the synthesis of spirocarbocycles under ultrasonic condition, Res. Chem. Intermed. 45 (2019) 1639–1651. doi:10.1007/s11164-018-3690-8.

[18] S.R. Samms, Thermal Stability of Proton Conducting Acid Doped Polybenzimidazole in Simulated Fuel Cell Environments, J. Electrochem. Soc. 143 (1996) 1225. doi:10.1149/1.1836621.

[19] M. Mamlouk, P. Ocon, K. Scott, Preparation and characterization of polybenzimidazole/diethylamine hydrogen sulphate for medium temperature proton exchange membrane fuel cells, J. Power Sources. 245 (2014) 915–926. doi:10.1016/j.jpowsour.2013.07.050.

[20] R. Nayak, M. Sundarraman, P.C. Ghosh, A.R. Bhattacharyya, Doped poly (2, 5-benzimidazole) membranes for high temperature polymer electrolyte fuel cell: Influence of various solvents during membrane casting on the fuel cell performance, Eur. Polym. J. 100 (2018) 111–120.

doi:10.1016/j.eurpolymj.2017.08.026.

[21] L.A. Diaz, J. Hnat, N. Heredia, M.M. Bruno, F.A. Viva, M. Paidar, H.R. Corti, K. Bouzek, G.C. Abuin, Alkali doped poly (2,5-benzimidazole) membrane for alkaline water electrolysis: Characterization and performance, J. Power Sources. 312 (2016) 128–136. doi:10.1016/j.jpowsour.2016.02.032.

[22] J. Hao, Y. Jiang, X. Gao, W. Lu, Y. Xiao, Z. Shao, B. Yi, Functionalization of polybenzimidazole-crosslinked poly (vinylbenzyl chloride) with two cyclic quaternary ammonium cations for anion exchange membranes, J. Memb. Sci. 548 (2018) 1–10.

[23] R.N. Couto, J.J. Linares, KOH-doped polybenzimidazole for alkaline direct glycerol fuel cells, J. Memb. Sci. 486 (2015) 239–247. doi:10.1016/j.memsci.2015.03.031.

[24] L. Zeng, T.S. Zhao, L. An, G. Zhao, X.H. Yan, Physicochemical properties of alkaline doped polybenzimidazole membranes for anion exchange membrane fuel cells, J. Memb. Sci. 493 (2015) 340–348. doi:10.1016/j.memsci.2015.06.013.

[25] P. Taylor, Y.S. Kim, K. Lee, Fuel Cell Membrane Characterizations, (2015) 37–41. doi:10.1080/15583724.2015.1011275.

[26] J. Hao, Y. Jiang, X. Gao, F. Xie, Z. Shao, B. Yi, Degradation reduction of polybenzimidazole membrane blended with CeO2 as a regenerative free radical scavenger, J. Memb. Sci. 522 (2017) 23–30. doi:10.1016/j.memsci.2016.09.010.

[27] D.R. Dekel, Review of cell performance in anion exchange membrane fuel cells, J. Power Sources. (2017). doi:10.1016/j.jpowsour.2017.07.117.

[28] Q.X. Wu, Z.F. Pan, L. An, Recent advances in alkali-doped polybenzimidazole membranes for fuel cell applications, Renew. Sustain. Energy Rev. 89 (2018) 168–183. doi:10.1016/j.rser.2018.03.024.

[29] H. Hou, G. Sun, R. He, Z. Wu, B. Sun, Alkali doped polybenzimidazole membrane for high performance alkaline direct ethanol fuel cell, J. Power Sources. 182 (2008) 95–99. doi:10.1016/j.jpowsour.2008.04.010.

[30] J. Hnát, M. Plevová, J. Žitka, M. Paidar, K. Bouzek, Anion-selective materials with 1,4-diazabicyclo[2.2.2]octane functional groups for advanced alkaline water electrolysis, Electrochim. Acta. 248 (2017) 547–555. doi:10.1016/j.electacta.2017.07.165.

CHAPTER 6. Quaternization with N-methyl piperidine

Quaternization with N-methyl piperidine

1 Introduction

The development of stable anion exchange groups both for anion exchange membranes and ionomers is one of the main objectives in order to enhance the performance and durability of alkaline fuel cells and electrolysers. Different positively charged fixed groups have been tried, like quaternary ammoniums (QA), heterocyclic systems (e.g. imidazolium [1,2], benzimidazolium [3], PBI-based [4,5] or with pyridinium [6,7]), guanidinium systems [8,9], P-based systems [10,11], sulfonium groups [12] and metal-based systems [13]. Among them, the QA groups are the most studied and different strategies and chemistries have been investigated: use of benzyltrialkylammoniums (like the well known benzyltrimethylammonium) [14–17], alkyl-bound QAs without benzene rings [18,19] or QAs using biclyclic ammoniums systems based on 1-azabicyclo [2.2.2] octane (quinuclidine, ABCO) [20,21] and 1,4-diazabicyclo [2.2.2] octane (DABCO). The last has been explained in detail in the previous chapter, since it was the selected tertiary amine to form the QA groups in the polybenzimidazole-c-PVBC membranes. A study performed by Marino and Kreuer [22] suggested that the use of aliphatic heterocyclic quaternary ammonium head groups (like benzyl-N-methylpiperidinium) in anion exchange membranes could yield improved alkali stabilities, compared with the commonly used benzyltrimethylammonium head group. Other studies have also reported high alkaline stabilities with head groups like N-alkylpyrrolidinium [23,24] or N-methylmorpholinium [25]. From this point the group of John Varcoe tested the stability and performance of different aliphatic heterocyclic QA head groups linked by a benzene ring to a radiation grafted poly(ethylene-co-tetrafluoroethylene) ETFE polymeric film backbone [26]. From the stability tests performed, they concluded that the best head groups were those with N-methylpiperidine (MPRD) and 1-methylpyrrolidine (MPY) and from the fuel cell performance, the membranes quaternized with MPY obtained the best results.

The same synthesis procedure was used with all the membranes, which is logical since optimization of synthesise parameters for each head group would be very time-consuming, but is not the ideal situation to know the best performance a QA ammonium head group can reach. For this reason, and based in the good preliminary results obtained with N-methylpiperidine (MPRD), the synthesis conditions for the quaternization of the membrane have been optimised in the research related in this chapter. This research has been done first in the anion exchange membrane and then implemented in anion exchange ionomers based in the same starting material (radiated ETFE grafted with VBC). Finally the membranes and ionomers have been tested in a fuel cell using H_2 vs O_2 comparing the performance of different QA head groups in the anion exchange membranes and ionomers.

2 Synthesis

The synthesis of the materials was done following the steps detailed in the Experimental chapter, that are resumed here. First the ETFE films (for the anion exchange membranes, AEM) and powders (for the anion exchange ionomers, AEI) were radiated using a e-beam facility, then stored at -40 ºC until grafting with VBC was performed. The obtained degree of grafting (DoG) in the membranes was 63.7 %, calculated from equation 3.1, and in the powders around 50 %. These are adequate values, because if they were much higher that would lead to excessive IEC.

For the amination step, the procedure was optimised with the amination of the membranes to later use similar conditions in the amination of powders. It was done in this way because, due to the filtration steps with the ionomer powders, the process is less time-consuming than the amination of membranes. The general process of amination with MPRD is showed in Figure 6.1, as well as the structures of MPRD, MPY and TMA.

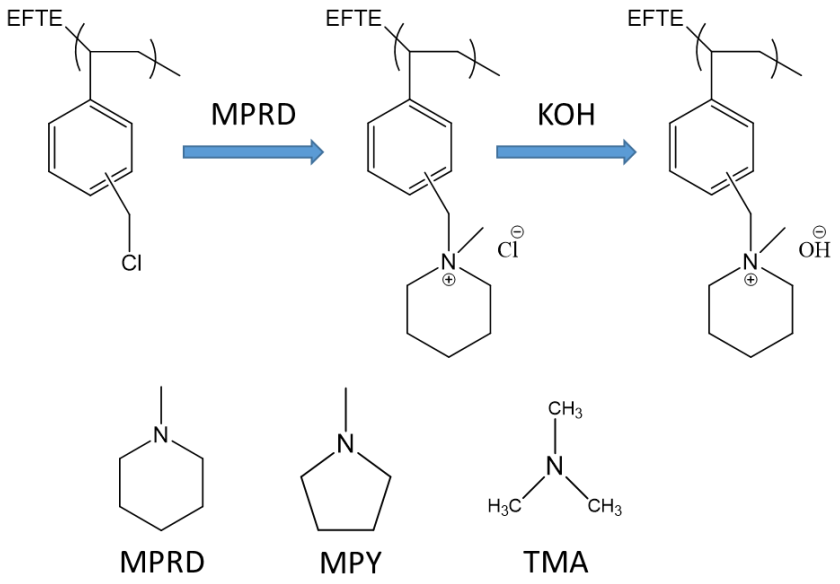

Figure 6.1. Scheme of the process of amination of the VBC-grafted ETFE material with MPRD. It also illustrates the structures of N-methylpiperidine (MPRD), 1-methylpyrrolidine (MPY) and trimethylamine (TMA).

Different temperatures and MPRD % in the aqueous solution were tried, the "%" represents the proportion of amine solution respective to the total aqueous solution used for the amination, so a 15 % means: 15 % of amine from the bottle where it is supplied and 85 % of ultrapure water. The temperatures during the amination and the % were selected based on the previous experience of the group with similar amination processes. In order to decide the final amination conditions, some measurements were performed in the aminated membranes after each procedure. The water uptake, conductivity (of Cl^- ions) at 80 ºC and the ion exchange capacity (IEC) in the Cl^- form were investigated for each of them and compared. The results are presented in Figure 6.2.

The results show that the membranes aminated with very high amount of MPRD in the solution (100 %, so no water is added) present lower water uptake values and conductivity, while those aminated with 15 and 25 % of MPRD show higher values. Especially, the membrane aminated at 70 ºC with 25 % of MPRD presents a high water uptake around 118 %. It was also observed that the membranes with 15 % and 25 % MPRD showed slightly higher IEC values. These effects are probably due to the better penetration of water inside the membrane structure than the pure amine solution, in such a way that the internal pores are bigger after amination with elevated presence of water in the solution, and even higher if the temperature is increased like in the case of 25 % and 70 ºC. Similar water uptake

and conductivity are obtained with the membranes at 60 ºC and 15 and 25 % of MPRD, which makes sense since both of them have an elevated % of water and similar temperature.

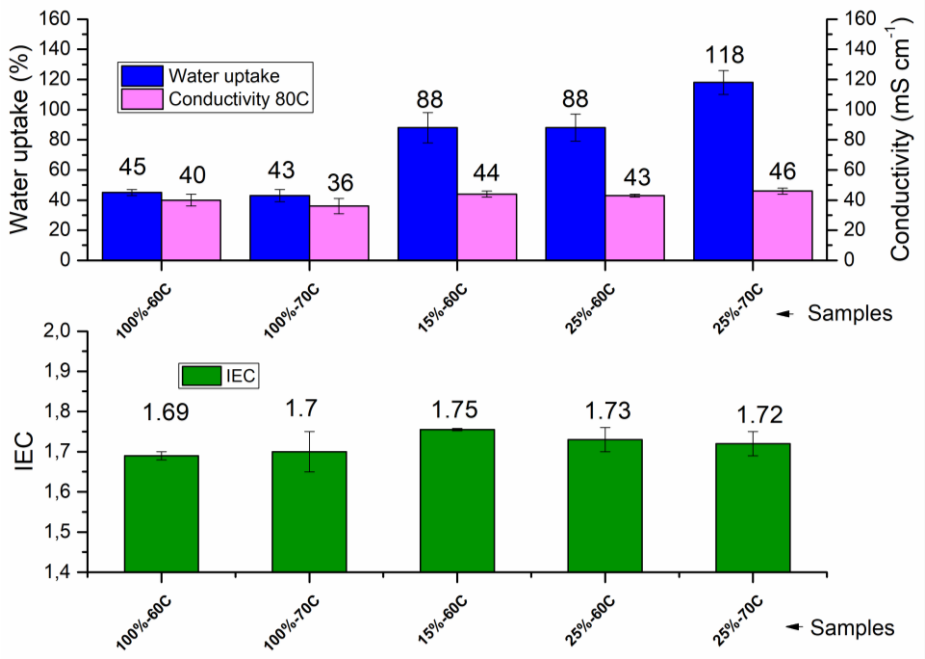

Figure 6.2. Water uptake, conductivity and IEC values of membranes aminated under different conditions of amine % (MPRD) in the aqueous solution and temperature of amination.

The membrane with highest IEC average value is obtained with 15 % of amine in the aqueous solution and temperature of amination of 60 ºC. Curiously, increasing the amount of amine in the solution doesn't increase the obtained IEC and probably, since the amine amount is in excess in all the cases, a higher water content can enhance the dispersion of the amine and the reaction with the CH_2-Cl groups of VBC attached to the ETFE chains. However, as it can be observed the IEC results are very similar between the membranes with low MPRD content in the amination solution.

Further optimization could have been tried but it was decided that the results with the 15 % of MPRD and 60 ºC were already very good due to several reason: the adequate water uptake values, the good IEC results and low temperature (compared with the 70 ºC) and especially the lower amount of MPRD required in the amination solution, which is an important advantage from the cost and the environmental points of view. Therefore, it was chosen to continue the experiments with the membranes aminated under these conditions and to apply

this procedure for the amination of the powders to produce the anion exchange ionomers.

For the synthesis of the ionomers, two different amounts of powders were tried for the grafting step, in order to observe if relevant differences were observed in the final materials. One trial was made with an initial quantity of irradiated ETFE powder of 1.5 g (performed two times) and the other was performed with an initial quantity of 20 g (only one time due to the high amount of material required). Once the grafting process was complete, after following the next steps described in the Experimental part, the powders were aminated with the aqueous solution of 15 % MPRD at 60 ºC during 18 h, same conditions like those used for the membranes. For 1.5 g starting material the solutions of amine were 100 mL (MPRD plus ultrapure water), for 20 g starting material 1 L of total solution was used. The obtained powders were evaluated by measuring the IEC and the results are presented in Figure 6.3.

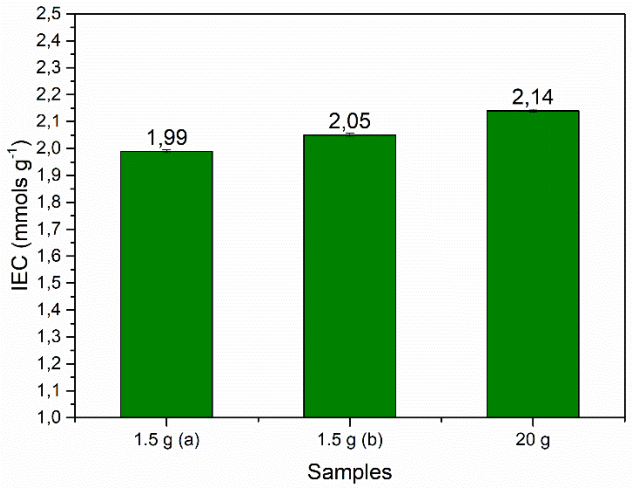

Figure 6.3. IEC values of the synthesised powders using initial quantities of irradiated ETFE material of 1.5 and 20 g for the VBC grafting.

The values of the two samples with 1.5 g are very similar, which reports a good reproducibility of the process. The IEC obtained with the bigger batch of 20 g is higher than those with 1.5 g. It is not clear if the different ratio of powder to solution or the shape of the batch (and thus the convection during stirring) have a relevant role in the better IEC values of the powders from the big batch, but the advantages are clear: higher IEC value, and higher amount of ionomer prepared at the same time, which gives an homogeneous batch to be studied for a long time if needed. For this reason the anion exchange ionomer powder from the batch of 20 g was used in all the subsequent experiments.

3 Characterization and properties

The characterization of the synthesised membranes and ionomers is described in the following sections as well as the relevant properties of the materials.

3.1 Raman spectroscopy

Raman spectroscopy was used to characterize the samples by checking the presence of bands corresponding to the different groups. The spectra of the initial ETFE materials, the grafted ETFE-VBC and the material after amination with MPRD are showed in Figure 6.4. The spectra are the same for ionomers and membranes so they are just reproduced once for each step (initial material, grafted and aminated with ETFE).

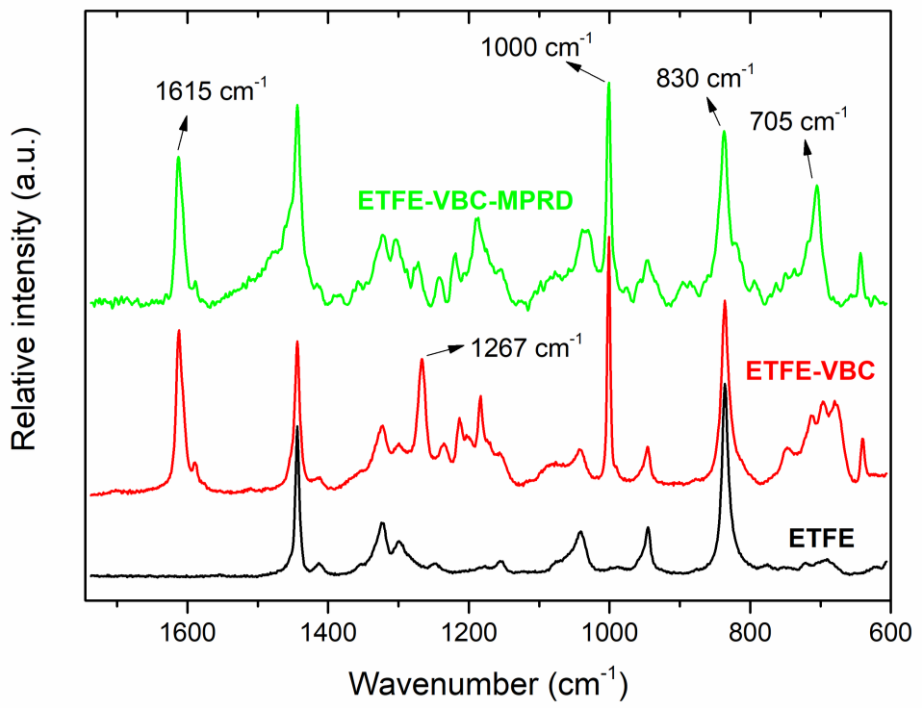

Figure 6.4. Raman spectra of the initial ETFE materials, the VBC-grafted-ETFE and the MPRD aminated final material.

As it can be observed, when the precursor ETFE is grafted new bands appear due to VBC. The most important bands are located at 1615 cm^{-1}, coming from the aromatic ring [27], at 1267 cm^{-1} from the CH_2Cl group [28] and at 1000 cm^{-1}, characteristic of the meta di-substituted phenyl rings [27]. The amination process is confirmed by the absence of the band at 1267 cm^{-1}, since the CH_2Cl groups react with the amines and the Cl is substituted, and the appearance of a sharp band at 705 cm^{-1} coming from the piperidinium group [27].

The spatially-resolved Raman spectro-microscopy (see Figure 6.5) confirmed the successful grafting of the membranes. The analysis was performed in the cross-section of the grafted membrane to study the distribution of the polyvinylbenzyl chloride (PVBC) chains. The colour scale represents the peak area ratio between the band at 1615 cm^{-1} from the PVBC and the band at 830 cm^{-1}, correspondent to the C-F bond of the ETFE backbone.

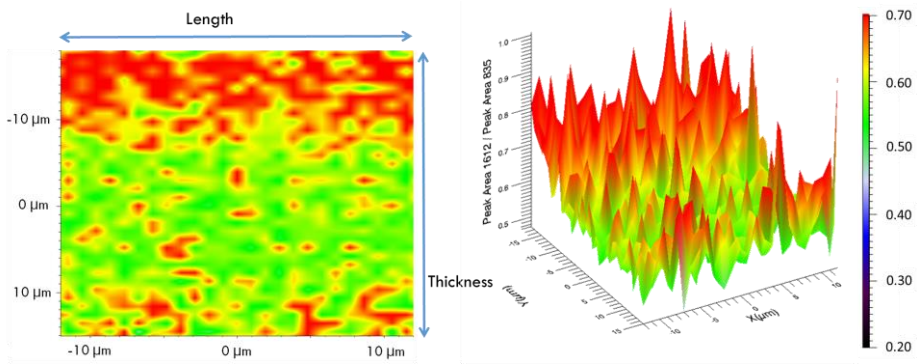

Figure 6.5. Spatially-resolved Raman spectro-microscopy of the cross-section of a VBC-grafted-ETFE membrane.

As it can be observed, the good level of grafting is well distributed in the membrane cross-section, with levels above the 0.50 in the whole area. It is also observed that the top part of the picture (one side of the membrane) has slightly more grafting than the rest. It could be related with the rolling of the membrane in a glass tube to do the grafting, so maybe the external part is a bit more grafted. However, since the grafting level is still high everywhere, it is not a trouble and the membranes are considered in good condition for the amination step.

3.2 SEM and EDX of the ionomers

The superficial aspect of the ionomer powders was investigated with scanning electron microscopy (SEM) and the elemental analysis was obtained by energy dispersive X-ray (EDX) spectroscopy to elucidate the composition of the different features found. The SEM images of the aminated powders (ETFE-VBC-MPRD) are presented in Figure 6.6 and the EDX analysis in Figure 6.7.

The powders were attached to the sample holder by a carbon paint, then the samples were gold coated since they are not electronic conductors. The SEM images in Figure 6.6 show that there is large heterogeneity in the particles sizes and many are agglomerated. The sizes vary from 20 to 100 μm approximately and the agglomeration is probably formed during the synthesis and drying of the powders. After the powders are dried, they undergo a vibromilling process but it isn't completely effective separating the powders as the results show.

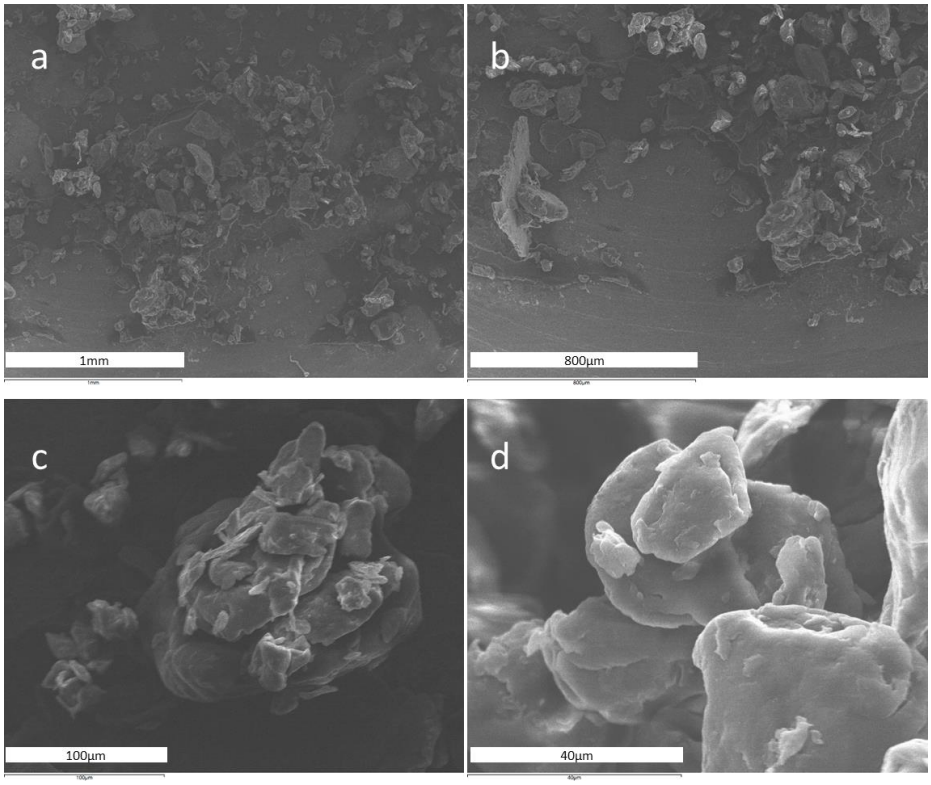

Figure 6.6. SEM images of ETFE-VBC-MPRD powders at a) x50, b) x80, c) x450, and d) x1500 magnifications.

In the EDX analysis presented in Figure 6.7, it can be observed easily the differences between the ionomer particles, the carbon paint and the metallic support were the particles are placed. The ionomer particles can be observed in detail in the images of Figure 6.7a and 6.7d for the zoom into some particles and the general picture (similar images than Figure 6.6). They are clearly different in the EDX analysis due to the high F (fluorine atoms) percentage coming from the ETFE backbone and the presence of Cl (chloride) from VBC. The N (nitrogen) of MPRD is not detected maybe due to the small amount present compared to the other elements. In Figure 6.7b the metallic support can be distinguished by the high content of Al (aluminium) and the presence of Cu (copper), while the carbon paint is analysed in Figure 6.7c with very high content of C (carbon) and presence of O (oxygen).

As it can be observed in Figure 6.8 the powders didn't show that degree of aggregation after de grafting process. The particle size of the grafted powders was in the range of 20-50 μm, very similar to the precursor ETFE powder particles (20-30 μm) [29].

From the above results, it can be concluded that the particles of the aminated ETFE-VBC-MPRD powders are clearly observed and they present a broad range of sizes and some aggregation. The aggregation is mainly formed during the amination and following steps and is not completely avoided with the vibromilling final process.

a)

Element	Weight%	Atomic%
C K	59.80	71.17
N K	0.00	0.00
O K	0.00	0.00
F K	36.11	27.18
Cl K	4.09	1.65
Totals	100.00	

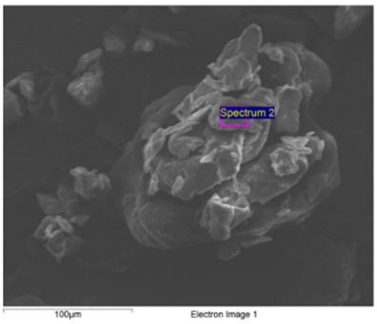

b)

Element	Weight%	Atomic%
C K	27.29	46.94
N K	0.00	0.00
O K	0.00	0.00
F K	0.00	0.00
Al K	66.79	51.14
Cl K	0.00	0.00
Cu L	5.91	1.92
Totals	100.00	

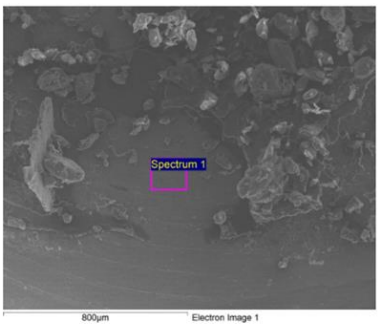

c)

Element	Weight%	Atomic%
C K	89.31	91.75
N K	0.00	0.00
O K	10.69	8.25
F K	0.00	0.00
Cl K	0.00	0.00
Totals	100.00	

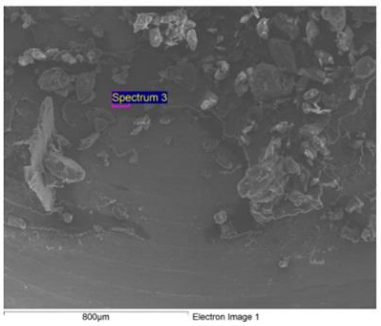

d)

Element	Weight%	Atomic%
C K	62.43	73.80
N K	0.00	0.00
O K	0.00	0.00
F K	32.17	24.04
Cl K	5.40	2.16
Totals	100.00	

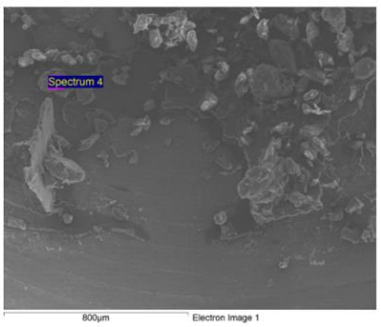

Figure 6.7. EDX analysis of the a) and d) ETFE-VBC-MPRD powders, b) metallic support and c) carbon paint.

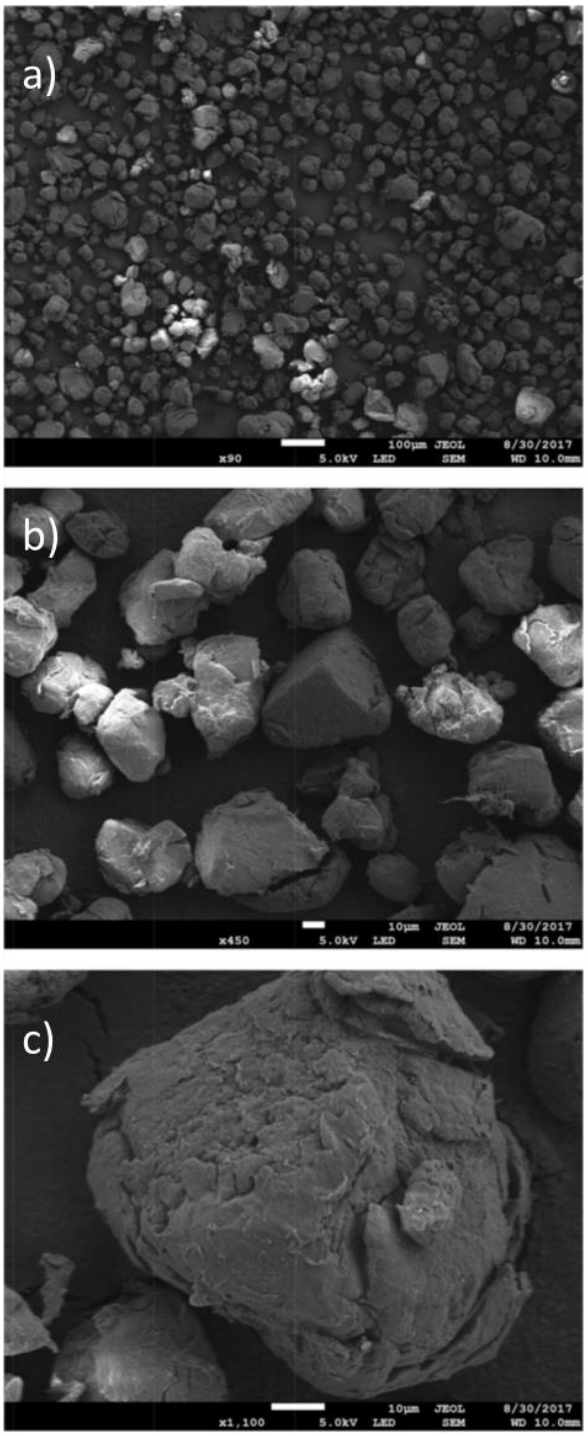

Figure 6.8. SEM images of the grafted ETFE-VBC powders (not aminated) at a) x90, b) x450, and c) x1100 magnifications.

3.3 SEM and EDX of the electrodes

The anion exchange ionomer (AEI) powders aminated with MPRD were incorporated into the electrodes in different weight proportions: 20 and 30 %. The percentage is relative to the total amount of solid mass in the ink prepared, including the metal (Pt or Pt with Ru), carbon, and the AEI. In all cases the loading was 0.4 mgPt cm^{-2} and the catalysts used were commercial Pt/C 40% in the cathode and commercial PtRu/C 50%-25% in the anode. After spraying the ink over the carbon paper used as support and gas diffusion layer, the SEM and EDX analysis were performed. The SEM images are presented in Figure 6.9 and the EDX analysis in Figure 6.10. The elements analysed in all samples were: C, N, O, F, Cl, Ru and Pt. In order to simplify the tables only C, F, Ru and Pt are presented.

In figure 6.9, the different components of the electrodes can be observed. The straight fibres in various directions are the carbon paper fibres and the balls of different sizes are the ionomer particles (order of micrometers size, similar to the previous ones). Both the carbon fibres and the ionomer particles look mostly covered by catalyst (nanometers size). The catalyst layer has a smoother appearance in the case of the cathodes (Pt/C) than in the anodes (PtRu/C), being in the last case like a lot of very small crystals, due to the mixture of Pt and Ru. The ionomer particles are randomly distributed through the surface and by comparing the electrodes with 20 and 30 % of ionomer content it can be observed that the 30 % samples have more particles than the 20 % ones. This makes sense since the loading of the ionomer is higher in those with 30 % and the particles sizes are similar. As it will be observed in the fuel cell measurements, the loading of 20 or 30 % of MPRD ionomer obtained similar high power density results (unlike with other head groups), which can be ascribed to the good water management of the MPRD ionomer, working quite similarly with these percentages. To corroborate the composition of the different components identified in the electrodes the EDX analysis was performed.

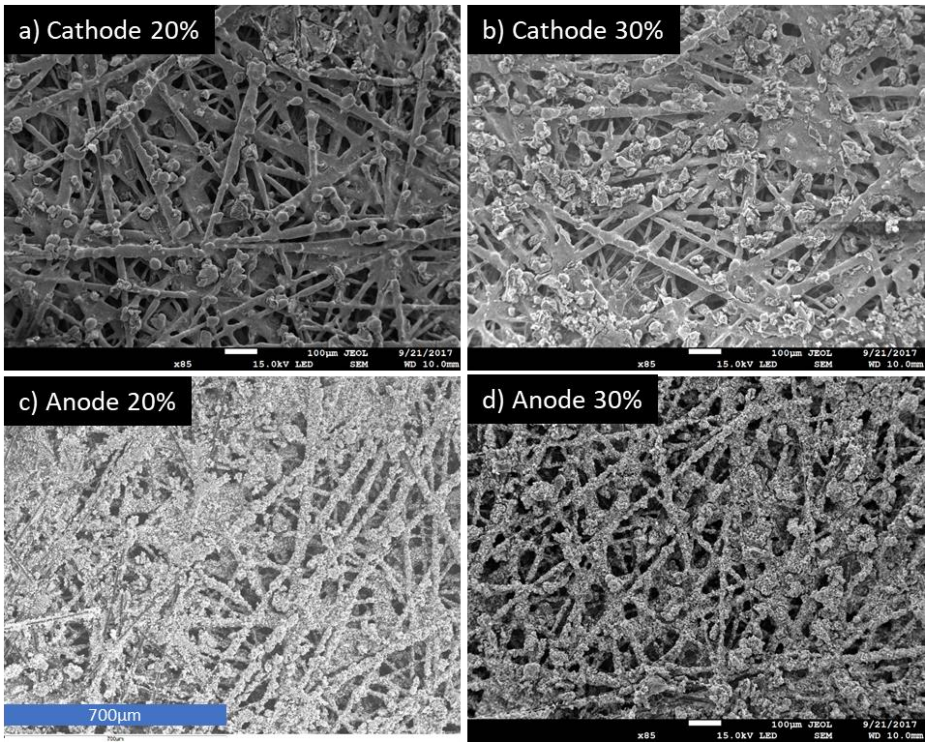

Figure 6.9. SEM images at x85 magnifications of electrodes prepared with carbon paper and sprayed with ink composed of ETFE-VBC-MPRD ionomer and catalyst (Pt/C in cathode and PtRu/C in anode). In a) and c) there is 20% of ionomer and 80% of catalyst and in b) and d) there is 30% of ionomer and 70% of catalyst.

The results of the EDX analysis in Figure 6.10 show clearly the different composition in the studied areas. It can be observed that the catalyst covers most of the surface, like areas 6, 7, 8 of Figure 6.10a or areas 2, 3, 4, 5 of Figure 6.10c. In these cases, the catalyst content (Pt in Figure 6.10c and both Pt and Ru in Figure 6.10a) increase greatly compared to the areas where it is not present as 1, 2, 3, 4, 5 of Figure 6.10a.

The areas without catalyst are carbon paper fibres or ionomer particles not covered. The ionomer particles can be easily differentiated from the high content of F (from the ETFE) like in areas 1, 2, 3 of Figure 6.10a and carbon fibres are characterized by the almost absence of this element and the high content of C like areas 4, 5 of Figure 6.10a.

A good detailed picture and analysis of a partially covered ionomer particle is done in Figure 6.10b. In that particle it is very clear the contrast between the ionomer composition (with F) in the area where is not covered by the catalyst and the other area, covered by the catalyst, with the high content of Pt and Ru.

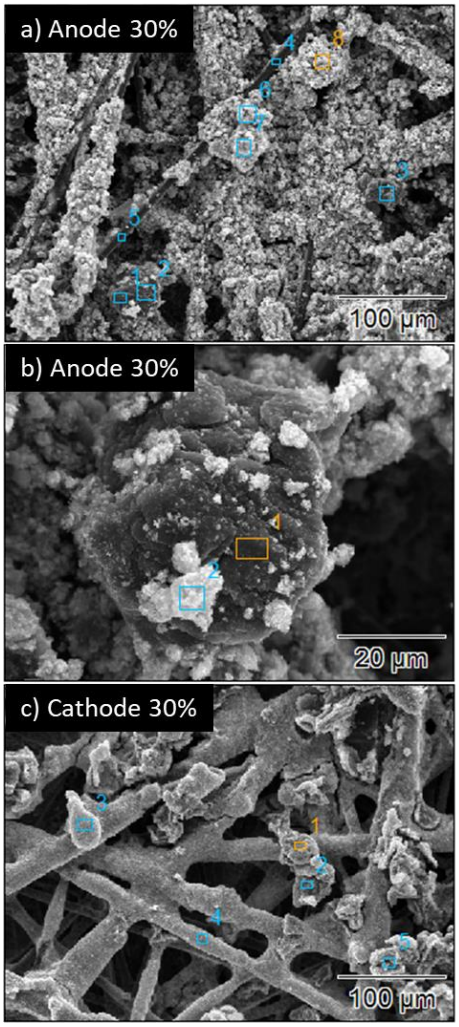

Zone	Elements (atomic %)			
	C	F	Ru	Pt
1	66.8	16.0	0.8	0.7
2	65.2	18.0	1.1	0.8
3	71.0	11.0	1.1	0.7
4	75.0	1.9	0.7	0.9
5	73.9	1.6	0.7	0.6
6	57.5	2.5	16.0	14.3
7	41.2	0.9	25.3	26.5
8	47.9	0.5	19.9	19.2

Zone	Elements (atomic %)			
	C	F	Ru	Pt
1	75.8	7.9	0.3	0.3
2	46.8	3.1	21.6	19.7

Zone	Elements (atomic %)			
	C	F	Ru	Pt
1	78.3	4.0	0.8	3.9
2	74.4	0.7	0.4	16.7
3	83.4	1.2	0.4	7.6
4	76.7	2.2	0.3	7.1
5	71.6	4.1	2.4	8.2

Figure 6.10. EDX analysis of anode and cathode electrodes with 30% of ionomer. a) and c) are at x300 magnifications and b) is at x1500 magnifications.

The electrochemical active areas where the reactions take place are where the catalyst and the ionomer are together, so a higher dispersion and less agglomerated particles could lead to better performance in the fuel cell. For example, in proton exchange membrane (PEM) fuel cells, the Nafion® ionomer is mono-dispersed and it is incorporated as a dispersion in the catalytic layer, allowing to be more uniformly distributed and maximizing the area of contact between the electrocatalyst and the ionomer. The ratio between catalyst and ionomer play a critical role. In the studied cases (20 and 30% of MPRD-ionomer) both results were very good and are probably near the optimal value, but further study would be necessary to check which one is better since the fuel cell performances were very similar.

3.4 Ionic conductivity, water uptake and IEC of the membranes

The synthesised ETFE-VBC-MPRD membranes are compared with membranes prepared in similar conditions and following the same preparation procedure (with changes in the percentages of amine or temperature depending on the head group) [30]. The values of water uptake and IEC are resumed in Table 6.1.

Table 6.1. Water uptake (WU) and Ion exchange capacity (IEC) of the ETFE-VBC-amine membranes with different head groups.

Membrane	Water Uptake (%)	Ion Exchange Capacity (mmol g^{-1})
ETFE-VBC-TMA	62 ± 7	2.03 ± 0.05
ETFE-VBC-MPY	76 ± 7	1.89 ± 0.05
ETFE-VBC-MPRD	85 ± 5	1.72 ± 0.03

The membrane aminated with TMA shows the highest IEC and the lowest WU, followed by the one aminated with MPY and finally the membrane aminated with MPRD shows the highest WU and the lowest IEC. The increasing water uptake of the membranes from using TMA to MPRD is probably related with the highest hydrophilicity of the different head groups, as previously reported [26]. This higher water uptake has been related with the enhanced alkali stability of this head groups, since the higher solvation of the quaternary ammoniums protects them from the OH^- attack.

Usually the IEC of the membrane is directly related to the ionic conductivity, so the membranes with higher IEC present a better conductivity since the abundance of quaternary ammonium groups helps to transport the ions. This explains the conductivity values obtained, presented in Figure 6.11.

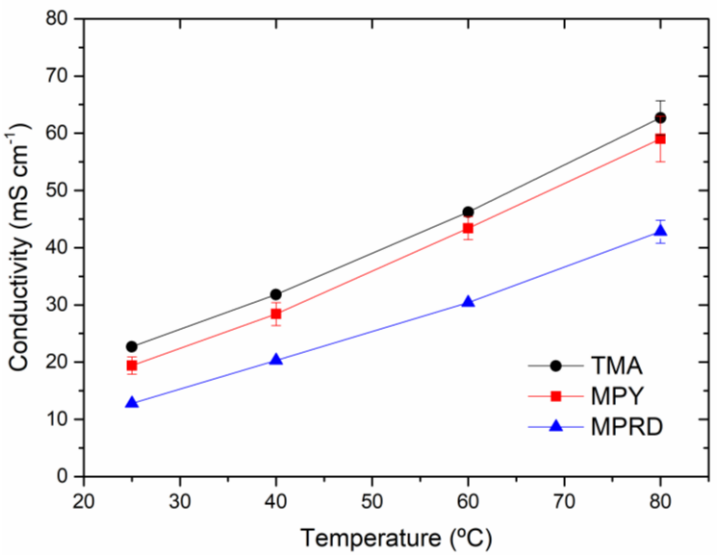

Figure 6.11. In-plane ionic conductivity (Cl^- ions) comparison at different temperatures of the ETFE-based membranes with different head groups to form the quaternary ammonium (QA) groups. Membranes under fully hydration.

The obtained Cl^- conductivity values are very good, in the range of those obtained previously with membranes synthesised from similar ETFE films irradiated and grafted with VBC (but in isopropanol) and aminated with similar amines (but slightly different conditions). It is also important to note that these membranes would present a much higher OH- conductivity, above 100 mS cm^{-1} at high temperatures (70-80 ºC) as it has been reported [26]. The reason is the lower mobility of the Cl^- ion in the aqueous alkaline media, compared to the OH^-.

4 Performance in final application

The synthesised materials were tested in a single cell at 60 ºC using pure H_2 as fuel in the anode side and pure O_2 as oxidant in the cathode side in order to study their performance in the final application. The materials that are going to be compared are the anion exchange membranes (AEMs) and anion exchange ionomers (AEIs) aminated with TMA, MPRD and MPY. The optimization of the synthesis and the results regarding TMA and MPY were performed by the PhD student Ana Laura Gonçalves during her research stay in the University of Surrey in the group of

Professor John Varcoe, while those results involving MPRD membranes and ionomers come mainly from my research during my international stay in that group [30,31].

The study of the different head group chemistries to obtain higher performance and better stabilities in solid ionomers is especially interesting since no reports about this field have been found in the literature.

4.1 Optimization of ionomer (AEI) loading

All the materials presented, based in TMA, MPRD and MPY, present high water uptake behaviour. This is an important factor to consider for the water management in the catalyst layer since electrode flooding could occur. On the other hand, the elevated water absorption may help to avoid electrode drying that decreases the performance and promotes the degradation of the materials, since it has been demonstrated that the OH^- attack is much stronger to the QA groups under low hydration levels. The AEI loading affects the ability to transport ions to the triple-phase boundary region and the water management as previously explained. For this reasons a short optimization study on the amount of AEI loading and its effect in the performance was carried out for each of the ionomers. The studied percentages of ionomer were 20 and 30 % since it was known from previous experience in the group that much higher loadings would probably decrease the final performance. The membrane used as reference benchmark to do these studies was always the ETFE-VBC-TMA.

The results using MPY and TMA powders [30,31] (not showed here) concluded that: for TMA ionomers the best loading was 20 %, it reached 1200 mW cm^{-2} compared with the 650 mW cm^{-2} obtained with 30 %. The last one showed a higher resistance and overpotential at low current densities. For MPY ionomers it was obtained a better result using the 30 % loading (around 1050 mW cm^{-2}) than with 20 % (around 750 mW cm^{-2}). Since the MPY weights more than TMA, more mass of material might be needed to obtain similar amount of QA groups compared to TMA. In any case, since the ionomer load is supposed to mainly affect the behaviour at high current densities more research will be needed in the future to further understand the correlation between loading and the diffusion limitations.

The results with 20 and 30 % of ionomer loading using MPRD ionomer and TMA membrane are presented in Figure 6.12. These ionomers present very good performance (around 1200 mW cm^{-2}) with both loadings, which may be related

with the higher water uptake they present. That may allow an improved water management that facilitates the ion transport and prevents the flooding of the electrodes at high current densities.

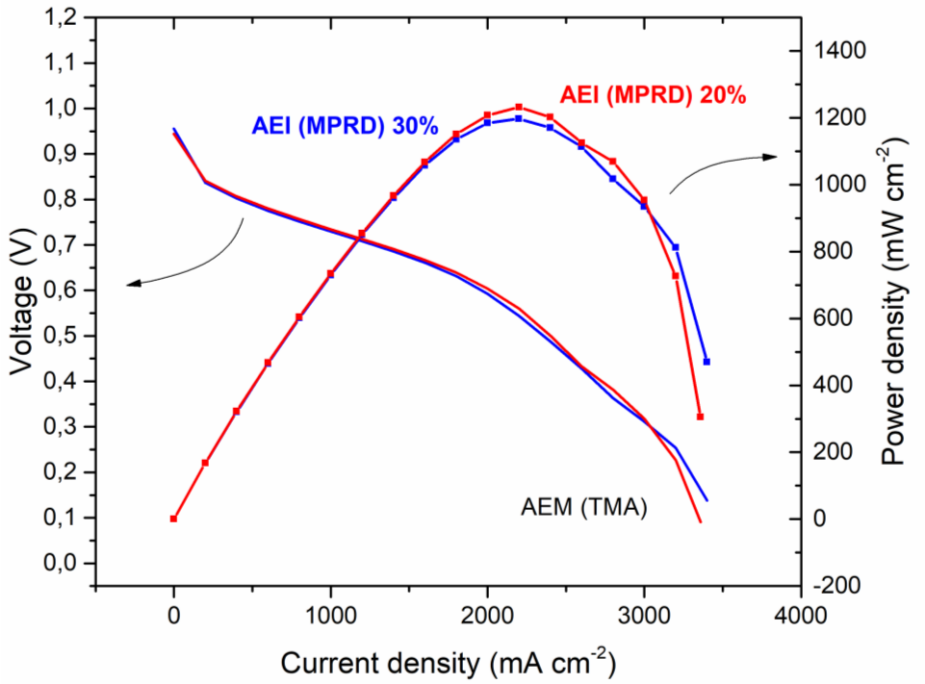

Figure 6.12. Fuel cell polarization and power density curves at 60 ºC with H_2/O_2 using membrane (AEM) of ETFE-VBC-TMA and ionomers (AEI) of ETFE-VBC-MPRD with 20 and 30 % of AEI loading in the both catalyst layers.

From the obtained results, it was decided to use in the rest of the measurements an AEI loading of 20 % in the case of TMA ionomers and 30 % for the MPRD and MPY ionomers.

4.2 Symmetric combinations of head groups in AEMs and AEIs

The study was performed with the idea of combining the different chemistries of the head groups (materials aminated with them) in the membrane and the electrodes, in order to observe if any special combination could obtain an enhanced behaviour in conductivity or water management and thus improve the fuel cell performance. The procedure was to maintain the same head group in both electrodes and make combinations with the membranes and electrodes

chemistries. To name the combinations the following short names were used: "MPRD / TMA / MPRD" would be used for the combination in which the ionomer in anode and cathode is aminated with MPRD and the membrane is aminated with TMA, so the positions in the short name correspond to " ionomer in the anode / membrane / ionomer in the cathode".

From the previous measurements and reports [26] it has been observed that the degree of hydrophilicity of the membranes increases from those aminated with TMA (lower hydrophilicity) to those aminated with MPRD (highest hydrophilicity), with the MPY membranes in between. Since the differences come only from the head group used, the same conclusion can be applied for the ionomers.

The results obtained with all the combinations are summarised in Table 6.2 and most of the combinations done with MPRD are showed in Figure 6.13. For the polarization and power density curves not showed here, the reader is referred to the work of Ana Laura Gonçalves [31].

Table 6.2. Symmetrical combinations of ETFE-VBC membranes and ionomers aminated with different head-groups and their corresponding maximum power densities.

Electrodes	Membrane	Maximum power density (mW cm^{-2})
TMA	TMA	1202
TMA	MPY	1135
TMA	MPRD	1424
MPY	TMA	1140
MPY	MPY	1041
MPY	MPRD	981
MPRD	TMA	1192
MPRD	MPY	1246
MPRD	MPRD	1240

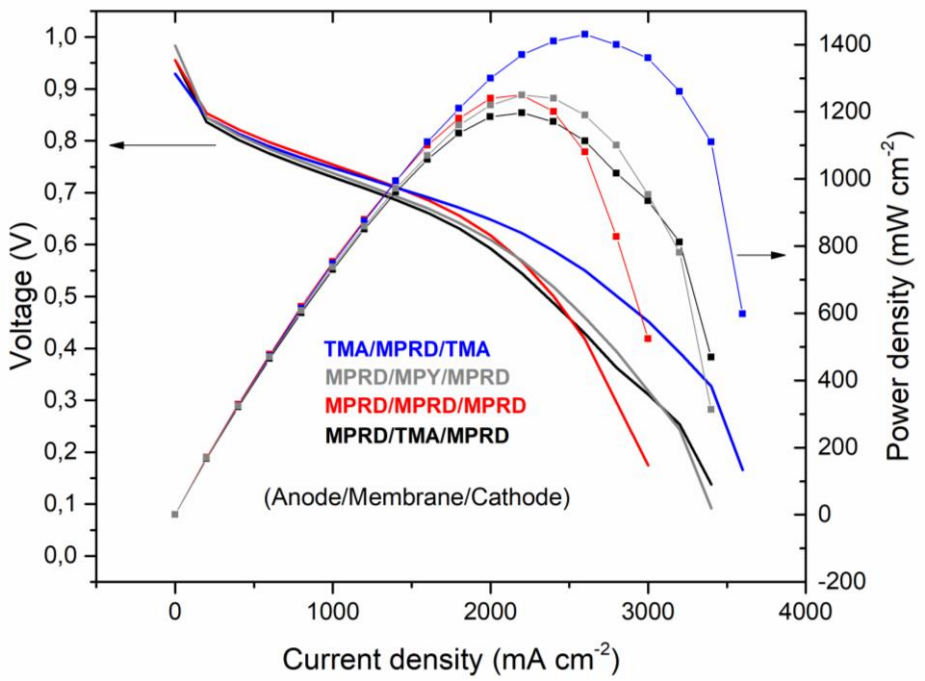

Figure 6.13. Fuel cell polarization and power density curves at 60 ºC with H_2/O_2 using combinations of different head groups in ionomer and membrane. MPRD is used in all the combination, in the blue and red curves in the membrane and in the grey, red and black in the ionomers of the electrodes.

When TMA is used in the electrodes with different membranes (first three lines of Table 6.2) the regions of activation and ohmic polarization overlap and the differences start in the region controlled by diffusion of the reactants at high current density. Here the use of the MPRD membrane allows to reach the highest power density: 1424 mW cm^{-2}, which actually is the highest of all the tested combinations. The result is surprising because that membrane showed the lowest IEC (1.74 mmol g^{-1}) and the lowest conductivity, but it presented a high hydrophilicity, which is probably indicating the relevance of this parameter when these high current densities are achieved. The abundant water produced in the anode when the current is so high causes flooding in the electrodes and the diffusional problems to the reactants to reach the catalytic sites. This combination of MPRD membrane with TMA electrodes shows a much better water management, probably due to the ability of the membrane to take part of that produced water and of the electrode with TMA, more hydrophobic (relatively), to repel the excess water. However further research will be needed to deeply understand the effects taking place. For example the combinations more similar to this one (in terms of hydrophilicity) would be the TMA / MPY / TMA or the MPY / MPRD / MPY and both of them show lower performances.

It is also relevant to note the good performance of the ionomers aminated with MPRD (last three lines of Table 6.2 and all presented in Figure 6.13). In all the cases the maximum power density is around 1200 mW cm^{-2}. Since the values are so near one to each other, no conclusions about which combination is better can be extracted without doubt, as well as with other combinations in the table. The reason is the error margin in the performance on the fuel cells (about 10-20 % in the power density values). This error margin arises from many reasons, the most important are the hand-made preparation of the electrodes, the complexity of the perfect control of all the variables in the system (humidification of the gases, perfect manual conformation of the membrane-electrode assembly..) or the small differences between areas of the synthesised membranes. The last one is probably very small in this case with membranes coming from commercial films with such an optimised treatment procedure, but can be very relevant in the case of laboratory prepared membranes like those presented in the previous chapters.

5 Conclusion

The optimization of the amination step of the membranes with MPRD has been highly effective due to the reduced amount of amine used in the aqueous solution and the relatively low temperature needed. The obtained membranes aminated with MPRD presented good IEC and conductivity values (while lower than with TMA or MPY) and higher water uptake than their counterparts. The synthesis of the ionomers also reported good IEC values as well as the important observation of the slightly better IEC obtained with big batches of 20 g.

The Raman spectroscopy confirmed the good degree of grafting (DoG) and its homogeneity. The ionomer particles were investigated by SEM/EDX, finding the fact that agglomeration occurs during or after the amination. Lowering particle size would be an interesting strategy to optimize results for future studies in order to maximize the triple-phase areas present in the electrode and thus the fuel cell performance. That would need a new optimization of the ionomer loading in the electrodes, since as it has been observed it may play a critical role in the performance.

Finally in the measurements performed in the fuel cell with the synthesised materials, it has been demonstrated the importance of the adequate water management due to the surprising higher results using the materials aminated with MPRD, obtaining however very good performances with all the studied materials.

It can be concluded that the performance of these membranes and ionomers is very promising, also taking into consideration the expected improved long-term durability of the materials with MPRD and MPY. These results are between the best obtained in literature for alkaline membrane fuel cells, only overcome as far as we know by the results obtained by Lianqin et al. [32] (also in the group of Professor John Varcoe) that have reached 2 W cm^{-2} of peak power density using a membrane of low-density polyethylene (LDPE), instead of ETFE, with very low thickness below 30 μm. However, those results have been obtained using the benchmark amination with TMA, so probably they can be further enhanced both in performance and durability if MPRD aminated membranes or ionomers were used.

6 References of the chapter: Quaternization with N-methyl piperidine

[1] X. Yan, S. Gu, G. He, X. Wu, J. Benziger, Imidazolium-functionalized poly(ether ether ketone) as membrane and electrode ionomer for low-temperature alkaline membrane direct methanol fuel cell, J. Power Sources. 250 (2014) 90–97. doi:10.1016/j.jpowsour.2013.10.140.

[2] W. Wang, S. Wang, W. Li, X. Xie, Y. Lu, Synthesis and characterization of a fluorinated cross-linked anion exchange membrane, Int. J. Hydrogen Energy. 38 (2013) 11045–11052. doi:10.1016/j.ijhydene.2013.03.166.

[3] X. Lin, X. Liang, S.D. Poynton, J.R. Varcoe, A. Lien, Novel alkaline anion exchange membranes containing pendant benzimidazolium groups for alkaline fuel cells, J. Memb. Sci. 443 (2013) 193–200. doi:10.1016/j.memsci.2013.04.059.

[4] H.J. Lee, J. Choi, J.Y. Han, H.J. Kim, Y.E. Sung, H. Kim, D. Henkensmeier, E. Ae Cho, J.H. Jang, S.J. Yoo, Synthesis and characterization of poly(benzimidazolium) membranes for anion exchange membrane fuel cells, Polym. Bull. 70 (2013) 2619–2631. doi:10.1007/s00289-013-0978-0.

[5] O.D. Thomas, K.J.W.Y. Soo, T.J. Peckham, M.P. Kulkarni, S. Holdcroft, A stable hydroxide-conducting polymer, J. Am. Chem. Soc. 134 (2012) 10753–10756. doi:10.1021/ja303067t.

[6] K. Matsuoka, S. Chiba, Y. Iriyama, T. Abe, M. Matsuoka, K. Kikuchi, Z. Ogumi, Preparation of anion-exchange membrane by plasma polymerization and its use in alkaline fuel cells, Thin Solid Films. 516 (2008) 3309–3313. doi:10.1016/j.tsf.2007.09.032.

[7] T. Sata, K. Kawamura, K. Matsusaki, Electrodialytic transport properties of anion-exchange membranes prepared from poly(vinyl alcohol), poly(N-ethyl 4-vinylpyridinium salt) and β-cyclodextrin, J. Memb. Sci. 181 (2001) 167–178. doi:10.1016/S0376-7388(00)00507-X.

[8] D.S. Kim, C.H. Fujimoto, M.R. Hibbs, A. Labouriau, Y.K. Choe, Y.S. Kim, Resonance stabilized perfluorinated ionomers for alkaline membrane fuel cells, Macromolecules. 46 (2013) 7826–7833. doi:10.1021/ma401568f.

[9] S.D. Sajjad, Y. Hong, F. Liu, Synthesis of guanidinium-based anion exchange membranes and their stability assessment, Polym. Adv. Technol. 25 (2014) 108–116. doi:10.1002/pat.3211.

[10] X. Yan, S. Gu, G. He, X. Wu, W. Zheng, X. Ruan, Quaternary phosphonium-functionalized poly(ether ether ketone) as highly conductive and alkali-stable hydroxide exchange membrane for fuel cells, J. Memb. Sci. 466 (2014) 220–228. doi:10.1016/j.memsci.2014.04.056.

[11] S. Gu, J. Skovgard, Y.S. Yan, Engineering the van der Waals interaction in cross-linking-free hydroxide exchange membranes for low swelling and high conductivity, ChemSusChem. 5 (2012) 843–848. doi:10.1002/cssc.201200057.

[12] B. Zhang, S. Gu, J. Wang, Y. Liu, A.M. Herring, Y. Yan, Tertiary sulfonium as a cationic functional group for hydroxide exchange membranes, RSC Adv. 2 (2012) 12683–12685. doi:10.1039/c2ra21402d.

[13] Y. Wang, A. Rapakousiou, D. Astruc, ROMP synthesis of cobalticenium-enamine polyelectrolytes, Macromolecules. 47 (2014) 3767–3774. doi:10.1021/ma5007864.

[14] K.D. Kreuer, Ion conducting membranes for fuel cells and other electrochemical devices, Chem. Mater. 26 (2014) 361–380. doi:10.1021/cm402742u.

[15] M.A. Hickner, A.M. Herring, E.B. Coughlin, Anion exchange membranes: Current status and moving forward, J. Polym. Sci. Part B Polym. Phys. 51 (2013) 1727–1735. doi:10.1002/polb.23395.

[16] Y. Wang, J. Qiao, R. Baker, J. Zhang, Alkaline polymer electrolyte membranes for fuel cell applications., Chem. Soc. Rev. 42 (2013) 5768–87. doi:10.1039/c3cs60053j.

[17] O.I. Deavin, S. Murphy, A.L. Ong, S.D. Poynton, R. Zeng, H. Herman, J.R. Varcoe, Anion-exchange membranes for alkaline polymer electrolyte fuel cells: Comparison of pendent benzyltrimethylammonium- and benzylmethylimidazolium-head- groups, Energy Environ. Sci. 5 (2012) 8584–8597. doi:10.1108/JPMH-06-2017-0022.

[18] M. Zhang, H.K. Kim, E. Chalkova, F. Mark, S.N. Lvov, T.C.M. Chung, New polyethylene based anion exchange membranes (PE-AEMs) with high ionic conductivity, Macromolecules. 44 (2011) 5937–5946. doi:10.1021/ma200836d.

[19] H.A. Kostalik, T.J. Clark, N.J. Robertson, P.F. Mutolo, J.M. Longo, H.D. Abruña, G.W. Coates, Solvent processable tetraalkylammonium-functionalized polyethylene for use as an alkaline anion exchange membrane, Macromolecules. 43 (2010) 7147–7150. doi:10.1021/ma101172a.

[20] C. Sollogoub, A. Guinault, C. Bonnebat, M. Bennjima, L. Akrour, J.F. Fauvarque, L. Ogier, Formation and characterization of crosslinked membranes for alkaline fuel cells, J. Memb. Sci. 335 (2009) 37–42. doi:10.1016/j.memsci.2009.02.027.

[21] J. Zhou, K. Joseph, J.M. Ahlfield, D.-Y. Park, P.A. Kohl, Poly(arylene ether) Ionomers with Pendant Quinuclidium Groups and Varying Molecular Weight for Alkaline Electrodes, J. Electrochem. Soc. 160 (2013) F573–F578. doi:10.1149/2.077306jes.

[22] M.G. Marino, K.D. Kreuer, Alkaline stability of quaternary ammonium cations for alkaline fuel cell membranes and ionic liquids, ChemSusChem. 8 (2015) 513–523. doi:10.1002/cssc.201403022.

[23] K.M. Meek, J.R. Nykaza, Y.A. Elabd, Alkaline Chemical Stability and Ion Transport in Polymerized Ionic Liquids with Various Backbones and Cations, Macromolecules. 49 (2016) 3382–3394. doi:10.1021/acs.macromol.6b00434.

[24] F. Gu, H. Dong, Y. Li, Z. Sun, F. Yan, Base stable pyrrolidinium cations for alkaline anion exchange membrane applications, Macromolecules. 47 (2014) 6740–6747. doi:10.1021/ma5015148.

[25] C.G. Morandi, R. Peach, H.M. Krieg, J. Kerres, Novel morpholinium-functionalized anion-exchange PBI-polymer blends, J. Mater. Chem. A. 3 (2015) 1110–1120. doi:10.1039/c4ta05026f.

[26] J. Ponce-González, D.K. Whelligan, L. Wang, R. Bance-Soualhi, Y. Wang, Y. Peng, H. Peng, D.C. Apperley, H.N. Sarode, T.P. Pandey, A.G. Divekar, S. Seifert, A.M. Herring, L. Zhuang, J.R. Varcoe, High performance aliphatic-heterocyclic benzyl-quaternary ammonium radiation-grafted anion-exchange membranes, Energy Environ. Sci. 9 (2016) 3724–3735. doi:10.1039/C6EE01958G.

[27] P.J. Larkin, IR and Raman Spectroscopy: Principles and Spectral Interpretation, Elsevier Science, 2011. doi:10.3390/rel9100297.

[28] J.R. Varcoe, R.C.T. Slade, E. Lam How Yee, S.D. Poynton, D.J. Driscoll, D.C. Apperley, Poly(ethylene-co-tetrafluoroethylene)-Derived Radiation-Grafted Anion-Exchange Membrane with Properties Specifically Tailored for Application in Metal-Cation-Free Alkaline Polymer Electrolyte Fuel Cells, Chem. Mater. 19 (2007) 2686–2693. doi:10.1021/cm062407u.

[29] www.agcce.com/brochurespdfs/sales/FluonGrades.pdf, (n.d.).

[30] A.L. Gonçalves Biancolli, D. Herranz, L. Wang, G. Stehlíková, R. Bance-Soualhi, J. Ponce-González, P. Ocón, E.A. Ticianelli, D.K. Whelligan, J.R. Varcoe, E.I. Santiago, ETFE-based anion-exchange membrane ionomer powders for alkaline membrane fuel cells: a first performance comparison of head-group chemistry, J. Mater. Chem. A. 6 (2018) 24330–24341. doi:10.1039/C8TA08309F.

[31] A.L. Gonçalves Biancolli, Influência dos contaminadores do hidrogênio produzido pela desidrogenação do etanol no desempenho de células a combustível de membranas protônicas e aniônicas, Instituto de Química de São Carlos, 2019. doi:https://doi.org/10.11606/T.75.2019.tde-15042019-104008.

[32] L. Wang, M. Bellini, H.A. Miller, J.R. Varcoe, A high conductivity ultrathin anion-exchange membrane with 500+ h alkali stability for use in alkaline membrane fuel cells that can achieve 2 W cm-2 at 80 °C, J. Mater. Chem. A. 6 (2018) 15404–15412. doi:10.1039/c8ta04783a.

CONCLUSIONS

Conclusions

In this Thesis various anion exchange materials have been synthesised, characterized and finally tested in fuel cells and electrolysers. The anion exchange membranes have been synthesised as: blend membranes with different weight ratios of poly (vinylalcohol) (PVA) (linear and crosslinked) and polybenzimidazole (PBI or ABPBI) (PVA:polybenzimidazole membranes); polybenzimidazole crosslinked with poly (vinylbenzyl chloride) (PVBC) and quaternized with 1,4-diazabicyclo [2.2.2] octane (DABCO) (polybenzimidazole-c-PVBC/OH membranes) and other membranes have been also prepared with ethylene tetrafluoroethylene (ETFE) grafted with VBC and aminated with MPRD. Anion exchange ionomers with similar structure than the last membranes have been also prepared. The main conclusions this study present are the following:

- Homogeneous, resistant and flexible blend membranes were synthesised using polybenzimidazoles and PVA. The prepared membranes presented adequate thermal and mechanical stability.

- The increase in the PVA content enhances the ionic conductivity and reduces the required days of doping but, over a certain point, the structural integrity is compromised.

- Removal of superficial PVA by the alkali solution was observed, which was mostly resolved by with glutaraldehyde (GA).

- Linear and crosslinked membranes presented high performance in direct ethanol fuel cells and zero gap electrolysers. Reaching 124 mW cm^{-2} power density at 90 ºC with the L-PVA:ABPBI 2:1 in the fuel cell and 360 mA cm^{-2} current density at 1.9 V and 70 ºC in the electrolyser.

- Polybenzimidazole-c-PVBC homogeneous membranes were obtained after a crosslinking time of 24 h at 80 ºC. The molar ratios studied range from 1:1 to 1:3. DABCO was successfully used to form the quaternary ammonium groups.

- Different behaviour of the membranes was observed in the water uptake, KOH and swelling ratio with membranes based on PBI or ABPBI. This effect was due to the higher hydrophilicity of ABPBI.

- Adequate ionic conductivity values (OH^-) between 20 and 60 mS cm^{-1} were measured. These performances were mostly unchanged even after 31 days of alkali durability test at 60 ºC in KOH 1M.

- These membranes also presented good ethanol fuel cell and electrolyser performances, superior to the commercial references. Especially promising are the electrolyser results, which obtained current densities of 450 mA cm^{-2} at 2 V with only 50 ºC and 1 M KOH aqueous solution.

- Anion exchange membranes and ionomers based in ETFE and aminated with MPRD were successfully synthesised and the amination procedure optimised.

- Membranes aminated with MPRD showed the lowest IEC and conductivity values when compared with others aminated with TMA and MPY. However, they presented larger water uptake due to the higher hydrophilicity of the QA group with MPRD.

- The improved combination of MPRD membrane with TMA electrodes obtained a power density of 1424 mW cm^{-2} in a fuel cell with H_2 vs O_2 at 60 ºC, one of the best values in literature. This high power density was probably reached thanks to the improved water management by amination with MPRD.

CONCLUSIONES

Conclusiones

Durante esta Tesis varios materiales intercambiadores de iones han sido sintetizados, caracterizados y finalmente evaluados en celda de combustible y electrolizador. Las membranas intercambiadoras de iones sintetizadas han consistido en: membranas formadas por combinación en distintas proporciones de polivinilalcohol (PVA) (lineal y entrecruzado) y polibencimidazol (PBI o ABPBI) (membranas de PVA:polibencimidazol); polibencimidazol entrecruzado con cloruro de polivinilbencilo (PVBC) y cuaternizado con 1,4-diazabiciclo [2.2.2] octano (DABCO) (membranas de polibencimidazol-c-PVBC/OH) y membranas preparadas a partir de etileno tetrafluoroetileno (ETFE) injertadas con VBC y aminadas con MPRD. También se han preparado ionómeros intercambiadores de iones con estructura similar a las últimas membranas. Las conclusiones principales se presentan a continuación:

- Se han sintetizado membranas homogéneas, resistentes y flexibles combinando PVA y los distintos polibencimidazoles. Estas membranas mostraron estabilidad térmica y mecánicas adecuada para su aplicación.

- El incremento de la cantidad de PVA mejora la conductividad iónica y reduce los días necesarios para doparlas, pero a partir de un cierto punto la integridad estructural de las membranas se ve comprometida.

- Se observó que la solución alcalina eliminaba parte del PVA superficial, lo cual fue resuelto entrecruzando el PVA con glutaraldehido (GA).

- Las membranas lineales y entrecruzadas mostraron buenas prestaciones en celda de combustible con etanol y en electrolizador alcalino, alcanzando 124 mW cm^{-2} a 90 ºC con la membrana L-PVA:ABPBI 2:1 en la celda de combustible y 360 mA cm^{-2} a 1.9 V y 70 ºC en el electrolizador.

- Se obtuvieron membranas homogéneas de polibencimidazol-c-PVBC tras un proceso de entrecruzamiento de 24 h a 80 ºC. Se estudiaron proporciones molares en el rango de 1:1 a 1:3 y el DABCO fue usado con éxito para formar los grupos de amonio cuaternario.

- Se observó un comportamiento diferente en la absorción de agua, KOH y cambio de dimensiones con membranas basadas en PBI o en ABPBI. Esto se debe a la mayor hidrofilicidad del ABPBI.

- Se midieron valores de conductividad de OH^- adecuados, entre 20 y 60 mS cm^{-1}. Los cuales permanecieron prácticamente inalterados después de un estudio de degradación de 31 días en KOH 1 M a 60 ºC.

- Estas membranas también presentaron buenas prestaciones en celda de combustible con etanol y en electrolizador alcalino, superiores a las referencias comerciales. Los resultados en electrolizador son especialmente prometedores, ya que se obtuvieron densidades de corriente de 450 mA cm^{-2} a 2 V con solamente 50 ºC y KOH 1 M.

- Se han sintetizado membranas e ionómeros intercambiadores de iones basados en ETFE y aminados con MPRD, optimizando el proceso de aminación.

- Las membranas aminadas con MPRD mostraron los valores más bajos de IEC y conductividad, comparadas con otras aminadas con TMA y MPY. Sin embargo, presentaron los mayores valores de absorción de agua debido a la mayor hidrofilicidad del grupo de amonio cuaternario con MPRD.

- La combinación óptima de membrana con MPRD y electrodos con TMA alcanzó una densidad de potencia de 1424 mW cm^{-2} en una celda de combustible alcalina con H_2 vs O_2 a 60 ºC, uno de los mejores resultados obtenidos en la literatura. Alcanzar esta alta densidad de potencia fue posible probablemente gracias al mejor manejo del agua por la aminación con MPRD.

APPENDIX

APPENDIX

Publications related with this work

- D. Herranz, R. Escudero-Cid, M. Montiel, C. Palacio, E. Fatás, P. Ocón, Poly (vinyl alcohol) and poly (benzimidazole) blend membranes for high performance alkaline direct ethanol fuel cells, Renew. Energy. 127 (2018) 883–895. doi:10.1007/978-3-642-20487-6.
- L.A. Diaz, R.E. Coppola, G.C. Abuin, R. Escudero-Cid, D. Herranz, P. Ocón, Alkali-doped polyvinyl alcohol – Polybenzimidazole membranes for alkaline water electrolysis, J. Memb. Sci. 535 (2017) 45–55. doi:10.1016/j.memsci.2017.04.021.
- A.L. Gonçalves Biancolli, D. Herranz, L. Wang, G. Stehlíková, R. Bance-Soualhi, J. Ponce-González, P. Ocón, E.A. Ticianelli, D.K. Whelligan, J.R. Varcoe, E.I. Santiago, ETFE-based anion-exchange membrane ionomer powders for alkaline membrane fuel cells: a first performance comparison of head-group chemistry, J. Mater. Chem. A. 6 (2018) 24330–24341. doi:10.1039/C8TA08309F.
- D. Herranz, P. Ocón, Benzimidazole as Solid Electrolyte Material for Fuel Cells, Chapter of book: Benzimidazole Its Deriv., Intech Open, 2019. doi:10.5772/intechopen.85430.
- R.E. Coppola, D. Herranz, R. Escudero-Cid, N. Ming, N.B. D'Accorso, P. Ocón, G.C. Abuin, Polybenzimidazole-crosslinked-poly(vinyl benzyl chloride) as anion exchange membrane for alkaline electrolyzers (Under review in J. Memb. Sci.).

- Letter of authors with group of Graciela Abuin of Buenos Aires, Argentina.

Renewable Energy 127 (2018) 883–895

Contents lists available at ScienceDirect

Renewable Energy

journal homepage: www.elsevier.com/locate/renene

Poly (vinyl alcohol) and poly (benzimidazole) blend membranes for high performance alkaline direct ethanol fuel cells

D. Herranz [a], R. Escudero-Cid [a], M. Montiel [a], C. Palacio [b], E. Fatás [a], P. Ocón [a, *]

[a] Departamento de Química Física Aplicada, Universidad Autónoma de Madrid, C/ Francisco Tomás y Valiente 7, 28049, Madrid, Spain
[b] Departamento de Física Aplicada, Universidad Autónoma de Madrid, C/ Francisco Tomás y Valiente 7, 28049, Madrid, Spain

ARTICLE INFO

Article history:
Received 18 October 2017
Received in revised form
29 December 2017
Accepted 4 May 2018
Available online 7 May 2018

Keywords:
Fuel cells
Alkaline
Blend membrane
PBI
PVA
Ethanol

ABSTRACT

A series of poly(vinyl alcohol)-*blend*-poly(benzimidazole) (PVA:PBI) membranes are synthesized with different ratios of PVA and PBI (2:1, 4:1, 6:1 and 8:1) using the casting method. These materials are doped in KOH 6 M solution in order to study their suitability for fuel cell applications. The Infra-red (IR) and Raman spectra confirm the successful doping of the membranes and the dimensional changes due to water and KOH uptakes during the doping are similar to other PBI-based membranes. XPS measurements are performed to evaluate the characteristics of these materials after the doping process. The thermal stability of the membranes is excellent in the range of desired temperatures (below 100 °C) and the conductivity values found are between 10^{-2} and 10^{-1} S cm^{-1}. These results are optimal to consider these membranes as candidates for anion exchange membranes (AEMs) and they are tested in a single cell with ethanol as fuel. The PVA:PBI 4:1 membrane have the best behaviour in fuel cell, reaching a power density of 76 mW cm^{-2}, approximately 50% better than the doped PBI in the same conditions. These important results can be considered highly promising for the future application of these membranes in alkaline polymer electrolyte membrane fuel cells (APEMFC).

1. Introduction

In recent years, polymer exchange membrane fuel cells (PEMFC) are attracting great interest due to the high power densities that are capable of reaching at relatively low temperatures [1–3]. Hydrogen and methanol have been the most common fuels used in these devices but both have certain drawbacks. Hydrogen has problems of production, storage and distribution, and methanol issues due its toxicity [4]. Nowadays, one of the best alternatives to these fuels is the use of ethanol, easy to store and distribute, cheaper and less toxic than methanol. The main advantages are the high energy density of this fuel, in addition to the fact that ethanol is considered a green chemical. It can be produced as a renewable biofuel from the fermentation of biomass in large quantities and, in addition, both ethanol and its final oxidation products are relatively non-toxic.

Direct ethanol fuel cells (DEFC) meet some requirements for a sustainable energy conversion technology, such as high electrical efficiency, easy handling of ethanol, or low operation temperature, and they are attractive power sources for pros electronic devices. However, this technology have important drawbacks as the slow electrode kinetics of ethanol electrooxidation (EOR), the poisoning of catalyst materials and high cost of electrocatalysts [5,6] especially when Nafion® is used as proton exchange electrolyte. Besides, with Pt or Pt alloys nanoparticles a very low conversion is carried out, the C–C bond rupture during the EOR is most likely not occurring and the complete conversion to CO_2 is very low. Nevertheless, the higher pH of alkaline membranes can improve the reaction kinetics of both processes, EOR and ORR (oxygen reduction reaction), with respect to acidic media. It facilitates the use of a range of non-precious metal catalysts in the cathode and in the anode, reducing the dependence of platinum [7–9]. On the other hand, anion exchange membranes present an important decrease of alcohol permeability [10,11]. It is necessary to take into account that the ionic current is now in reverse direction in comparison with proton conducting membranes [12]. These advantages are the main reason to change the common type of PEMFC devices to others with anion exchange membranes as electrolytes. However, the main issue of the improvement of the performance of these fuel cells was the limited development of the anion exchange polymeric membranes (AEM).

* Corresponding author. Department of Applied Physical Chemistry, Sciences Faculty, Universidad Autónoma de Madrid (UAM), C/ Francisco Tomás y Valiente 7, 28049, Madrid, Spain.
E-mail address: pilar.ocon@uam.es (P. Ocón).

https://doi.org/10.1016/j.renene.2018.05.020
0960-1481/

At the present, many groups have made important researches looking for materials capable to exchange anions as well as Nafion® for acid media [13,14]. The main objectives for these membranes for DEFCs applications are to increase the ionic conductivity and to decrease the ethanol permeability trough the electrolyte. Some important groups at membrane research collaborated in one of the more important reviews on this topic in 2014 [12]. This article collects the most representative kind of anion exchange membranes that are being investigated nowadays. The main ways to prepare AEMs according to S. Maurya et al. [15] are: i) by polymerization of monomers [16], ii) by the solution casting method [17] or iii) by the grafting method of conventional polymers [18], and iv) by using composites or blends [19]. Despite all the studies that are being carried out, AEMs are still in an early stage of development, with conductivity values lower than the standard membrane in acid medium, Nafion®. This is related to the lower conductivity of the OH^- anion used in AEMs compared to the H^+ cation used in cation exchange membranes (CEM) [12].

One of the most studied materials for this type of exchange membranes is the polybenzimidazole (PBI) [20–22], but it is necessary to dope it in alkaline medium for several days and, even after this process, its conductivity is still about 10 times lower than Nafion® [23]. Other material that has been used for this application was the polyvinyl alcohol (PVA) [24,25]. This polymer has a hydrophilic nature which is considered as an advantage for some applications but in most cases it becomes a problem because of the high swelling capacity of the membranes in water. To enhance the stability and performance of PVA membranes different modifications have been carried out. The strategy followed in this paper has been to blend it with other polymer, in this case PBI.

In the present research, we report a comparative study of the behaviour of different synthesized blend membranes based on PVA and PBI and the influence of the weight ratio. Specifically, we have prepared a series of PVA:PBI membranes, with different weight ratio of polymers (2:1, 4:1, 6:1 and 8:1), using the casting method. The membranes characterization was performed by: Fourier transform Infra-red spectroscopy (FTIR), Raman spectroscopy and X-ray photoelectron spectroscopy, XPS. The mechanical properties and the ionic conductivity measured by AC impedance technique were determined. Also KOH and water uptake measurements were carried out on the PVA:PBI membranes. In addition, we evaluate the performance and applicability of these materials as solid electrolyte in alkaline membrane direct ethanol fuel cells (AMDEFC).

2. Experimental section

2.1. Materials

The reagents used were poly(2,2′-m-(phenylene)-5,5′-bibenzimidazole) (polybenzimidazole, PBI), powder (BETWEEN, LizenzGMBH) (density 0.7–0.9 dL g^{-1}); polyvinyl alcohol (PVA), hydrolysed, powder of MW89.000–98.000, 99+% (Aldrich); dimethylsulfoxide (DMSO), 99.9%; *N*,*N*-dimethylacetamide (DMAc), 99.5% (Aldrich); and potassium hydroxide (KOH), 85% (Aldrich).

2.2. Synthesis of membranes

A series of PVA:PBI membranes was prepared from solutions of the precursors by using the following weight ratios: 2:1, 4:1, 6:1 and 8:1. A 4.76 wt. % PVA solution was obtained by heating 1 g of PVA in DMSO (20 g) under continuous stirring at 85 °C for 30 min. Similarly, a solution of 3.5 wt. % PBI was obtained by heating 3.5 g of PBI in DMAc (96.5 g) at 80 °C for 48 h. The required amounts of solved PVA and PBI, according to the weight ratio desired, were transferred to glass beakers and stirred for 40 min at 500 rpm at 80 °C.

Then, the solutions were placed in Petri dishes coated with PTFE liners and they were introduced in a vacuum oven (Memmert VO200). The pressure was lowered from room pressure to 10 mbar, and the temperature was maintained at 40 °C. After, the membranes were peeled and stored (see Fig. 1). Commercial PBI membrane of the company Danish Power Systems was used for comparison purposes.

Some membranes were doped in 6 M KOH at different times. Then the membranes were washed and rinsed with Milli-Q water four times, dried with filter paper and stored in sealed plastic bags until been used.

2.3. NMR spectroscopy

High resolution solid-state ^{13}C CP NMR spectra were measured in a Bruker AV-400- WB spectrometer at ambient temperature working at ^{13}C resonance frequency of 100.61 MHz. Spin-lock cross polarization with magic angle sample spinning (CPMAS) were used to obtain the solid state ^{13}C spectra. Samples were hand-compacted into ZrO rotors with Kel-F end caps. All samples were accumulated one night. Chemical shifts were reference relative to the CH_2 signal of adamantane (29.5 ppm) as secondary reference and the TMS (tetramethylsilane) as primary reference.

High resolution liquid ^1H NMR spectra were recorded using a Bruker DRX 500 MHz spectrometer at 298K, with chemical shifts relative to the TMS. The PBI and PVA powders were weighted (10 mg of each), dried in an oven at 110 °C for 15 h and then dissolved in 0.6 mL DMSO-d_6 (deuterated) highly dried separately. The powders PVA were dissolved by heating with a hot-air pistol and agitation with a Vortex machine to achieve complete dissolution. PBI couldn't be completely dissolved using the same methods but the dissolved fraction was enough to clearly color the solution. The spectrum of each one was performed and after 0.4 mL of the PVA solution were mixed with 0.1 mL of the PBI solution, which should give approximately a 4:1 ratio solution. Separately a piece of membrane of 10 mg was partially dissolved in 0.6 mL of DMSO-d_6 highly dried. This liquid phase of the dissolved membrane was used to perform the ^1H NMR spectrum.

2.4. TGA/DSC

Thermal stability of the membranes was studied using the thermogravimetric analysis (TGA) technique (TA Instrument 20). The samples were heated from 25 to 900 °C under nitrogen atmosphere at a rate of 10 °C min^{-1}. The differential scanning calorimetric (DSC) was measured in a TA Instrument 10, under nitrogen atmosphere, heating from 25 to 300 °C at a rate of 10 °C min^{-1} with the samples sealed in aluminium pans.

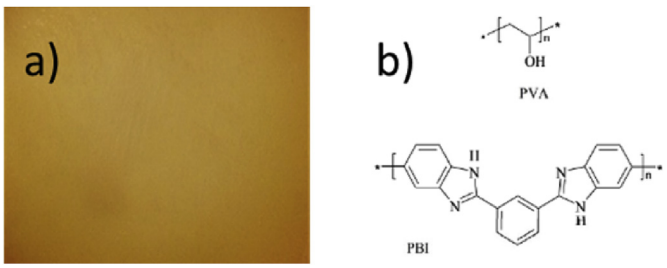

Fig. 1. a) Image of a synthesized PVA: PBI membrane and b) Scheme of the original polymers.

2.5. IR and Raman spectroscopy

The FT-IR/ATR spectra were carried out on a Jasco FT-IR 410 spectrophotometer with an attenuated total reflectance accessory (ATR) between 500 and 4000 cm^{-1} with a resolution of 2 cm^{-1}. The Raman spectra were measured in a Via Raman spectrometer (Renishaw) with an excitation wavelength of 785 nm. The measurements were performed over a range of 100–3500 cm^{-1} employing 10 scans and an exposure time of 10 s per measurement. The sharp silicon line located at 520 cm^{-1} was employed as reference in the Raman shift scale.

2.6. Mechanical properties

Mechanical tensile tests were performed using a MTS® QTest1/L Elite testing machine equipped with a 100 N load cell. Type 4 dumbbell test pieces (according to ISO 37) were tested. The crosshead speed used was 10 mm min^{-1} with an initial width of 2 mm and an initial gauge length of 20 mm. At least 3 pieces were used for each sample.

2.7. SEM/EDX measurements

Morphology of the membranes surface and cross-section was studied with a Hitachi S-300 scanning electron microscope (SEM). The membrane was first placed in a brass holder and sputtered with a thin gold coat under vacuum. The atomic composition was investigated with an INCAxsight (Oxford Instruments) energy-dispersive X-ray spectroscopy (EDX) system equipped in the scanning electron microscope.

2.8. KOH and water uptake

Three pieces of each type of membrane, 2:1, 4:1, 6:1 and 8:1, were cut in rectangular shape of approximately 10 mm × 15 mm. Length, width, thickness, and weight of the samples were accurately measured before drying them in a vacuum oven at 40 °C and 10 mbar for 15 h. Then, they were weighted (W_0) and dimensioned again. After that, the samples were immersed in separate baths of KOH 6 M for the doping process. Each membrane was kept in the bath for the number of days required to achieve the maximum conductivity (PVA:PBI 8:1, 1 day; 6:1, 2 days; 2:1 and 4:1, 3 days). Then, the membranes were dried in the vacuum oven, weighted (W_d) and dimensioned. Water and KOH uptake of the membranes were calculated as follows:

$$\textit{Water uptake}\ (\%) = \frac{W_d - W_{dd}}{W_0} \cdot 100$$

$$\textit{KOH uptake}\ (\%) = \frac{W_{dd} - W_0}{W_0} \cdot 100$$

where W_d, W_{dd} and W_0 are weight of the doped (water + KOH), dried doped (KOH), and dry membranes, respectively.

2.9. XPS measurements

The XPS spectra were measured in an ultrahigh vacuum system (UHV) at a base pressure below 1×10^{-9} mbar using a hemispherical analyzer (SPECS Phoibos 100 MCD-5). The pass energy was 9 eV, giving a constant resolution of 0.9 eV. The Au $4f_{7/2}$, Ag $3d_{5/2}$ and Cu $2p_{3/2}$ lines of reference samples at 84.0, 368.3 and 932.7 eV, respectively, were used to calibrate binding energies. A twin anode (Mg and Al) X-ray source was operated at a constant power of 300 W using Mg Kα radiation ($h\nu = 1253.6$ eV). Although charging was observed due to the insulating character of the samples, this effect was corrected peaking the C 1s band attributed to C–C bonds at 285.0 eV and shifting accordingly all other core levels.

2.10. Conductivity measurements

Through plane ionic conductivity of the membranes was measured using a cell composed of two stainless steel plates. The membrane was sandwiched between two stainless steel electrodes of known area (0.36 cm^2). An AUTOLAB equipment (PGSTAT 302 N) equipped with a Frequency Response Analyzer (FRA) was used to perform the impedance measurements of KOH doped membranes. The applied dc bias voltage was 0 V, and 10 mV rms. Data collected were in the range from 10^6 to 1 Hz. Membrane resistance, R, was calculated from the intercept on the real axis of the Nyquist plot [26]. The conductivity (σ) was calculated as follows:

$$\sigma = \frac{l}{A \cdot R}$$

where l and A are the thickness and the area between the electrodes. The measurements were conducted at 25, 40, 60, 80 and 90 °C. The measurement was carried out in chamber without additional humidification, only the temperature was controlled. Just after the doping process, the membranes were washed with Mili-Q water and superficially dried with filter paper before been sandwiched between the electrodes.

2.11. Performance evaluation of different membranes in single-cell

The membrane-electrode assembly (MEA) was formed with: carbon cloth (LT 1200W ELAT, ETEK), a catalytic layer sprayed on it, and an anion exchange membrane as solid electrolyte. The ink was obtained dispersing Pt/C (Johnson Matthey, 40 wt. %) and PtRu/C (Johnson Matthey, 45 wt. %) at cathode and anode, respectively, with isopropanol, Milli-Q water and Nafion® ionomer (Dupont, 5 wt. %). The final amount of platinum was 1 and 1.33 mg cm^{-2} at cathode and anode, respectively. As electrolyte, synthesized (40–60 μm) PVA:PBI membranes and commercial 50 μm polybenzimidazole (PBI) membrane (Danish Power Systems) were used. All membranes were doped in 6 M KOH solution until their best conductivity was reached. FCTS station (Arbin Instruments) was used and data were collected with MITS-Pro software (Arbin Instruments). Cathode was fed with pure O_2 (Air Liquide) flow rate of 200 ml min^{-1} and atmospheric pressure. Anode was fed with 2 M ethanol in 2 M KOH aqueous solution, with a flow rate of 1 ml min^{-1}, without back pressure, using a peristaltic pump (Dinko Instruments) external to the station. Fuel cell temperature was 90 °C and the area of the MEAs was 4 cm^{-2}.

3. Results and discussion

The membranes were characterized using different techniques and their performance was evaluated.

3.1. ^{13}C and ^{1}H NMR

The NMR study was used the identify the presence of the polymers and the possible interaction between them. Fig. 2a shows the structure of PBI and PVA with numbered C atoms in order to make easier to assign the signals of the solid ^{13}C NMR spectra of Fig. 2b. Assignment of peaks was made according to bibliography [27–30].

For comparison between the spectra of PVA, PBI and PVA:PBI blend, normalization of the intensity of the peaks was used. In the

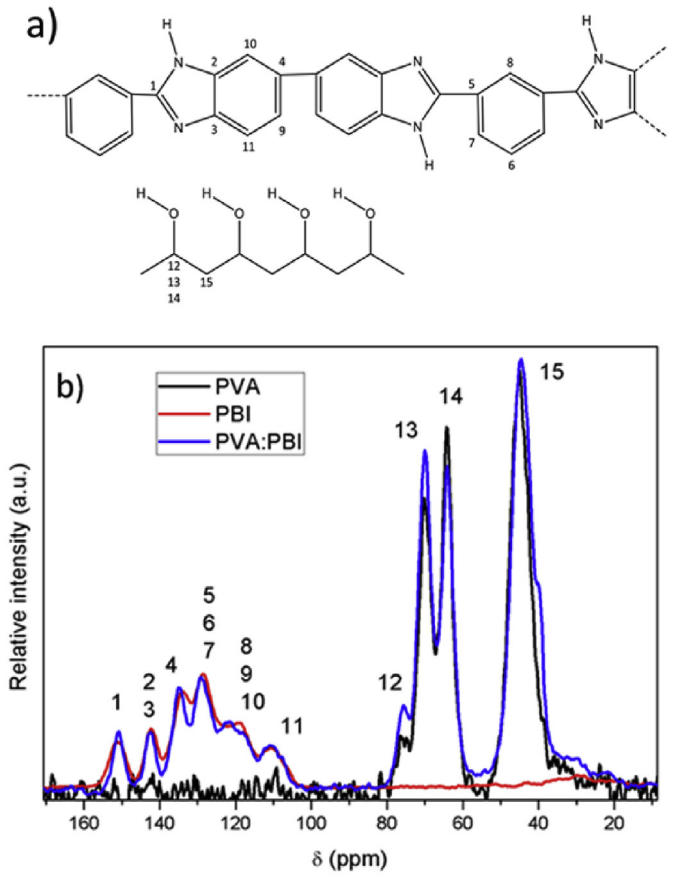

Fig. 2. (a) Structure of PBI and PVA molecules with numbered carbons, (b) Partial ^{13}C NMR spectrum of PVA, PBI and PVA:PBI membranes with numbers of ascribed carbons.

range where PBI signals appear (170-100 ppm), the intensity of the peaks was normalized to the peak at 128.5 ppm (carbons 5,6 and 7). Those carbons belong to the solitary aromatic ring, which probably suffered negligible influence from the mixture with PVA.

In the PVA region (90-30 ppm), normalization was done to the intensity of peak at 45 ppm (carbon 15). This peak is ascribed to the CH_2 of PVA, which shouldn't have significant differences in the mixture with PBI. The peaks 12, 13 and 14 were ascribed to the CHOH carbons whose alcohol group has two, one or none hydrogen bonds formed with neighbours respectively. They are also called isotactic, heterotactic (or atactic) and syndiotactic signals [30]. The differences in the spectra are not very noticeable but it can give some information about the possible presence of interaction between PVA and PBI. The increase of intensity in the 12 and 13 peaks and decrease of the 14 peak in the 4:1 spectrum respect to the single PVA spectrum might mean that hydrogen bonds are being formed with PBI. Also, it is interesting to note that carbon 1 appears with a sharper and taller peak in the 4:1 membrane and carbons 4 and 8, 9, 10 move slightly (2.9 ppm) downfield. All of them, except to 8, belong to the imidazole structure near the nitrogens and so might present this small changes due to the presence of hydrogen bonds with the PVA. The peaks that appear in the PBI spectrum at 227 and 30 ppm, showed in Fig. S1, are the rotational side bands [31].

Liquid ^1H NMR, Fig. 3a, shows the structure of PBI and PVA with the numbered protons assigned to the spectra of Fig. 3b,c and Fig. S2a. The assignment of the peaks was done according to bibliography [32,33]. The chemical shift of the signals related to the corresponding hydrogens and the integration values are given in

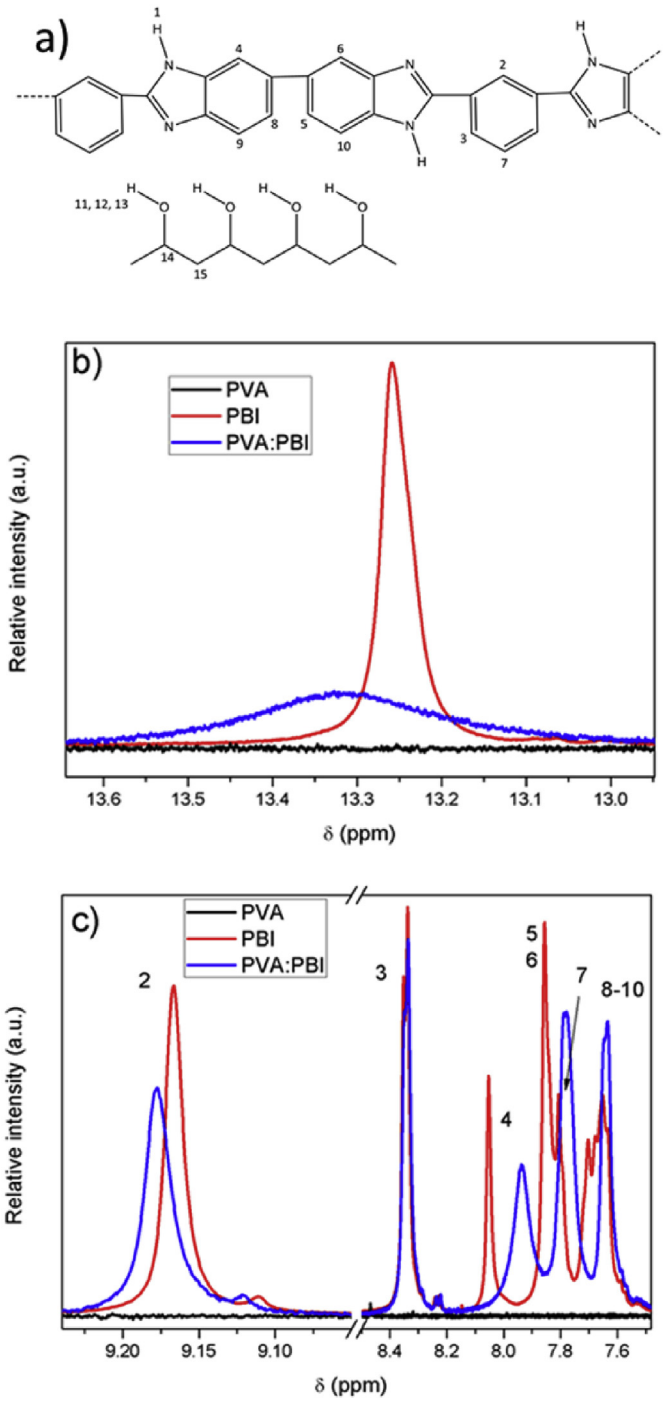

Fig. 3. (a) Structure of PBI and PVA molecules with numbered hydrogens, (b, c) Selected parts of ^1H NMR spectrum of PVA, PBI and PVA:PBI membranes with numbers of ascribed hydrogens.

Table S1. The number of integrated hydrogens correlates perfectly with the hydrogens present in the PVA and PBI monomers.

The comparison of the PBI, PVA and 4:1 mix spectra shows some important changes. It is relevant to note that the interaction between the polymers occurs being both dissolved and it is expected to be more intense when the casting of the membranes is finished and there is further intimate contact between them. The peak at 13.25 ppm (peak 1), in Fig. 3b, ascribed to the N–H proton suffers an important decrease in intensity, expansion of the width and

small shift of 0.06 ppm downfield. We consider this is a clear signal of the interaction of this protons with PVA via hydrogen bonds [33].

Another change that occur in the PBI region, showed with more detail in Fig. 3c, is the slight shift of 0.01 ppm downfield in the peak at 9.16 ppm (peak 2) which is ascribed to the solely proton of the aromatic ring and it might be produced from the effect of forming hydrogen bonds in the two near imidazole rings.

Also in Fig. 3c, relevant differences can be observed in the peaks between 8.1 and 7.6 ppm (peaks 4–10). These peaks are ascribed to the aromatic ring of the benzimidazole and thus is logical to suppose that the aromatic electron cloud will be sensible to the hydrogen bonds established by the NH group. Fig. S2b shows the range in which PVA and solvent signals appear. Peaks not marked come from impurities. Peaks at 3.3 and 2.5 ppm were ascribed to protons of water present in the solution and the DMSO used as solvent respectively, similarly than other works elsewhere [33].

In the PVA region, between 5 and 1 ppm, no great differences can be seen. The peaks at 4.67, 4.47 and 4.22 ppm come from the isotactic, heterotactic and syndiotactic alcohol groups respectively (similar to the signals observed in the ^{13}C spectra). None of them show a shifting of the peak in the 4:1 spectrum but it makes sense since the ratio of reacted PVA (via hydrogen bonds) to unreacted would be so low that the changes are probably neglected by the unreacted signals.

In the PVA region, between 5 and 1 ppm, no great differences can be seen. The peaks at 4.67, 4.47 and 4.22 ppm come from the isotactic, heterotactic and syndiotactic alcohol groups respectively (similar to the signals observed in the ^{13}C spectra). None of them show a shifting of the peak in the 4:1 spectrum but it makes sense since the ratio of reacted PVA (via hydrogen bonds) to unreacted would be so low that the changes are probably neglected by the unreacted signals.

When the spectrum of the dissolved membrane was compared with the spectrum of the mixed PVA and PBI solutions no relevant differences were observed in the described signals.

NMR, and more concretely liquid ^{1}H NMR spectroscopy, has demonstrated to be an accurate technique to identify the interaction between PBI and PVA, showing clearly the formation of a bridge hydrogen bond between these two polymers. This demonstrates that the membrane is not just a physical mix of both polymers but there is chemical interaction between them.

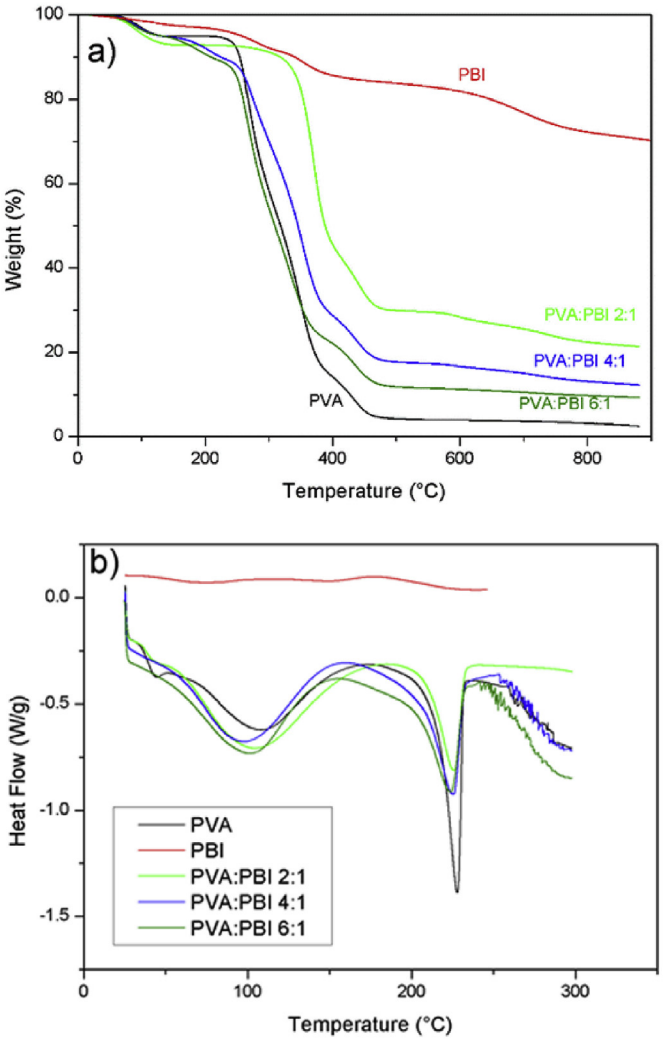

Fig. 4. a) TGA measurements and b) DSC of the blend membranes and pristine PVA and PBI membranes.

3.2. TGA/DSC

In order to know if the synthesized membranes are appropriate to be used as a polymer electrolyte in exchange membrane fuel cells the thermal stability was evaluated. The behaviour of three different blend membranes with 2:1, 4:1 and 6:1 wt ratio of PVA:PBI was measured, in addition to that of PVA and PBI pristine membranes for comparison purposes. The thermal stability of these samples is showed in Fig. 4a. PBI membranes have been broadly studied previously [34–38], revealing that about 10–15 wt. % is lost before reaching 150 °C, due to absorbed water; above 150 °C, no relevant weight loss is observed up to 500 °C, indicating the excellent thermal stability of this polymer. In the range from 500 to 900 °C, another loss of mass occurs (10–15 wt. %), although still most of the original weight remains [39].

Regarding to the pure PVA membrane, three main loss regions are visible in TGA measurements. First, this material loses around 5 wt.% at 96 °C, probably due to the evaporation of absorbed water. The second step, between 200 and 375 °C with sharp decrease around 266 °C, comes from the degradation of the PVA polymer membrane, and an approximate loss of 80 wt.% is observed. This degradation starts with the process known as chain "stripping", which consist on the elimination of water accompanied by the formation of polyene structures. After that, a second loss happens around 350 °C, in which these polyene structures are further converted to low-molecular weight aliphatic products, as described by other authors [40–42]. The third change occurs in the range of 400–500 °C, losing 12 wt. %, owing to the cleavage of C–C backbone of PVA polymer membrane (or so-called carbonation). Finally, the sample gradually degrades until reaching 880 °C, remaining 2.5 wt. % of residual ash.

As Fig. 4a shows, all studied PVA:PBI samples are stable at least up to 250 °C. This value is far superior to the normal PEMFCs operation temperature, around 90 °C, at which these membranes should work. It is also interesting to notice different behaviour between the membranes. In the region from 500 to 850 °C, the degradation of membranes is closely related to the PVA:PBI ratio. Thus, the higher the content of PVA in the membrane the lower remaining residual ash (in weight %) at 850 °C. This result seems logical since PBI still retains most of its original weight in this region, while PVA is almost completely degraded. Partial degradation of PBI in the same range of temperatures is also observed for the membranes with the highest content of PBI (2:1 and 4:1) [39].

The results of the differential scanning calorimetry (DSC) of the membranes are presented in Fig. 4b. The broad endothermic band observed for all samples around 100 °C comes from the evaporation

of water. Pristine PVA and blend membranes present a clear melting transition (T_m) around 228 °C, similar to values reported elsewhere [42,43]. The intensity of the peak at these temperatures is lower for blend membranes, this effect can be attributed to the reduction in crystallinity of PVA due to the mixture with PBI [42]. In summary, although the presence of PBI in blend membranes distorts slightly the PVA crystallinity, all blend membranes are suitable for being used in fuel cells at 90 °C.

3.3. FT-IR and Raman

FTIR and Raman measurements of the membranes were carried out in order to identify the functional groups present in their structures and to obtain information about the possible interaction between PVA and PBI. The recorded spectra of PVA, PBI and PVA:PBI (2:1, 4:1 and 6:1) membranes have been included in Fig. 5.

The FTIR spectrum of PVA membrane shows a very strong broad peak centred at 3270 cm^{-1} for the intermolecular hydrogen bonding and the hydroxyl (O—H) stretching vibration. The C—H asymmetrical and symmetrical stretching vibration occurs at 2940 cm^{-1} and 2910 cm^{-1} respectively, and the transmission peak at 1093 cm^{-1} corresponds to the stretching vibration of C—O of the remaining non hydrolysed vinyl acetate group of the PVA [44]. Another two peaks appear at 1425 cm^{-1} and 1328 cm^{-1} due to —C—H and —O—H bending, in agreement with Panero et al. [45]. The FTIR spectra of the PVA:PBI membranes show the same characteristic transmission peaks of the PVA (see Fig. 5a). On the other hand, the most significant bands observed for the pristine PBI membrane appear in the region 2000-1000 cm^{-1}. These signals are composed of the relatively narrow peaks which can be assigned to the cycle vibrations as well as in plane deformation modes (δ_{NH} and δ_{CN}). Bands derived from aromatic (C=C) and (C=N) stretching modes (ca. 1630 cm^{-1}), in-plane deformation of benzimidazole (1536 cm^{-1} and 1443 cm^{-1}) and breathing mode of the imidazole rings (1289 cm^{-1}) were observed (see Fig. 5a) [35,38]. It is worth noting that PBI characteristic peaks are not clearly visible for the blend membranes in IR.

Regarding the Raman spectra (Fig. 5b), the most relevant information for the blend membranes is obtained from PBI typical signals: 958 (weak), 998 (weak), 1293 (strong), 1447 (medium), 1537 (very strong) and 1592 cm^{-1} (very strong). All membranes containing PBI showed peaks mounted on a high broad band due to fluorescence. Even when the base-line correction was performed, the signal of PBI-based membranes was approximately 20 times stronger than those observed for pristine PVA. For this reason, PVA signals are masked and the Raman spectra of PVA:PBI membranes are so similar to the PBI one. The peaks at 1545 cm^{-1} and 1299 cm^{-1} come from N—H stretching and breathing modes of imidazole rings, respectively [11]. The region between 900 and 1000 cm^{-1} shows different signals assigned to aromatic rings vibrations. IR and Raman spectra have been useful to identify the presence of PVA and PBI in membranes, although a NMR study have been necessary to have further insights in the interaction between the polymers (in section 3.1).

On the other hand, the ionic conductivity of as-synthesized membranes is very low, as it will be discussed in section 3.8, and therefore doping is required to reach adequate conductivity of the ions through the membrane. For this purpose, aqueous solutions of KOH are commonly used in alkaline PEMFCs [35,46]. The effect of doping on membrane structure was analysed using FT-IR and Raman spectroscopy, and the most relevant information is shown in Fig. 6. All blend membranes display similar IR and Raman

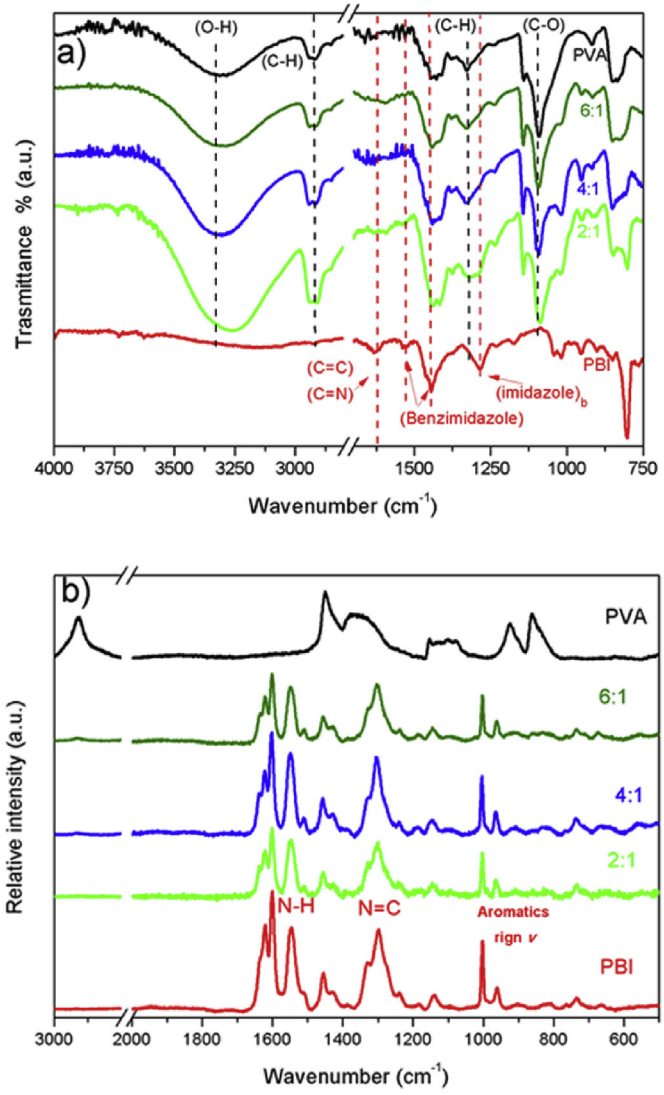

Fig. 5. a) FT-IR/ATR and b) Raman spectra of undoped PBI, PVA and PVA:PBI membranes (2:1, 4:1, 6:1).

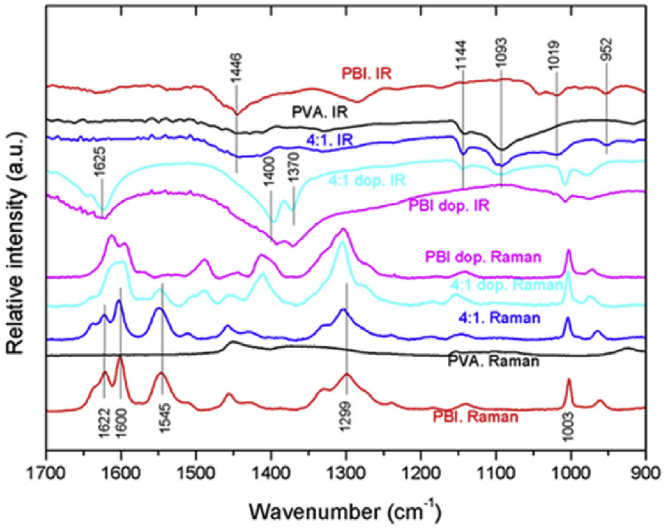

Fig. 6. FT-IR/ATR and Raman spectra of PVA (pristine), PBI (pristine and doped), and PVA:PBI 4:1 (undoped and doped).

spectra, and only slight changes in relative intensities are observed by changing the ratio of polymers. Characteristic peaks observed in the IR spectra at 1144 and 1093 cm^{-1}, from C–O stretching, and at 1019 and 952 cm^{-1}, from the in-plane aromatic C–H bending, reveal the presence of both polymers. Moreover, a signal around 1400 cm^{-1} assigned to the O–H bending mode of the hydroxide (1411 cm^{-1} in Raman and 1397 cm^{-1} in IR) can be observed in all samples, which is a clear indication of the presence of "free KOH" within the membrane structure [35]. Additionally, a strong band at 1625 cm^{-1} (IR) is attributed to the –O–H stretching of the absorbed water [11]. Regarding N-containing groups, a band at 1370 cm^{-1} (IR) might be attributed to free amino moieties coming from the hydrolysis of PBI in a strongly alkaline environment [35]. Moreover, the reaction of NH groups with KOH produces a shift of the C=N stretching vibration to lower energies, giving a broader band around 1600 cm^{-1} in the Raman spectrum. It is worth noting that the signal assigned to N–H stretching of imidazole rings (1545 cm^{-1} in Raman) disappears completely for PBI doped membranes and suffers an important reduction for the PVA:PBI 4:1 ones. This can corroborate the substitution of the acid H^+ of the imidazole rings by K^+ coming from KOH.

3.4. Mechanical properties

In general, before the alkaline doping process in KOH 6 M, PVA:PBI membranes display good mechanical flexibility, light transparent yellow-brown color, and homogeneous appearance (Fig. 1a). In addition, they possess enough consistency to be easily cut into different size and used as solid electrolyte in low temperature fuel cells. Mechanical properties of 2:1 and 4:1 PVA:PBI membranes were investigated, since these blends performed the best results in single cell measurements. The stress vs. elongation graph shows the behaviour of doped and undoped membranes compared to PBI (Fig. 7). Detailed results with averages and standard deviations are in table S2. These results reveal that the resistance of undoped PBI is higher than those of PVA:PBI membranes (2:1, 4:1), whereas blend membranes show similar stress values. On the other hand, the mechanical resistance for doped membranes decreases in all cases. Pristine PBI is reduced to a similar stress value than the undoped blend membranes. Meanwhile, the mechanical strength of doped blend membranes becomes similar for both samples, although the loss is much lower than for PBI.

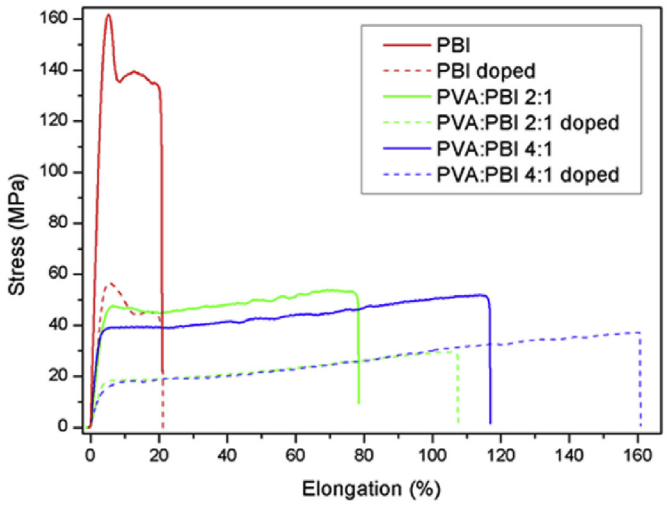

Fig. 7. Stress vs. elongation measurements of pristine PBI and blend PVA:PBI membranes.

Regarding to ductility, the presence of PVA in blend membranes means a clear improvement, and the elongation values observed for these samples, both undoped and doped, are several times larger than for pristine PBI. It was also observed that the ductility was further improved by the doping of the blend membranes while remaining unaffected in the pure PBI doped membrane.

One possible explanation of these results may arise from the process of degradation of the membranes in the strong alkali media. Probably, some bonds are broken in PBI, as was suggested by Linares et al. [35], giving rise to lower modulus and resistance of pristine PBI membranes without significant difference in elongation. In blend membranes, added to the degradation of PBI, small gaps may be formed between PBI chains in the surface and PVA, which would allow larger elongation of the membrane. The results obtained from the mechanical properties of PBI are in good agreement to other results found in literature [11,34] and the values obtained for the PVA:PBI membranes are sufficient to be used as AEMs.

3.5. SEM/EDX

Scanning electron micrographs of the membrane surfaces and cross sections were obtained to investigate the homogeneity of as-synthesized membranes and possible changes after the doping process. The homogeneity of undoped membrane's surface can be observed in Fig. S3. In addition, the mean composition determined by EDX was similar throughout the membrane. After the doping process, differences were observed in the surface of the membrane, especially in those with lower PVA content, Fig. S3. Some circular islands are formed, which are composed mainly by PBI. This composition was deduced from the differences on the N/O ratio: 1.16 in the circular white islands vs. 0.16 in the undoped membrane and the dark zones of the doped membrane. Probably these islands are created due to the removal of superficial PVA during the doping process. However, no tunnel-like forms are observed in the cross-section, therefore it may be just a surface effect, Fig. S3c,d.

3.6. KOH and water uptake

Anion exchange membranes based on PBI are able to absorb water and KOH, undergoing dimensional changes during both alkaline doping and fuel cell measurements. The amount of water and KOH absorbed during the doping is represented in Fig. 8a as weight percentage of the undoped membranes. These values correspond to the optimal doping time for each membrane.

Regarding PBI membranes, they are able to absorb above 85 wt. % of water and around 40 wt. % of KOH. The presence of PVA in blend membranes results in a decrease KOH uptake (32% is the minimum value, for 2:1 membrane) and in water uptake. However, increasing the amount of PVA in the blend, the membrane can absorb more KOH and water (for example PVA:PBI 8:1 reach values of KOH and water uptake similar to pristine PBI).

PVA and PBI show high affinity to water, PVA membranes gain 36% weight in water (water absorbed relative to the dry membrane), which corresponds to 0.9 water molecules per PVA r.u. (repeating unit) as reported by Lim et al. [47]and PBI membranes gain up to 23% in water, which corresponds to 4 water molecules per PBI r.u. [35]. Since PVA gains more water in % of weight than PBI, it should be expected that the addition of PVA to pure PBI would increase the water and KOH absorbed. But as described above, the effect measured in the 2:1 membrane is the opposite. It may be explained by the interaction between PVA and PBI, in which probably many chains are mixed and hydrogen bonds appear between the polymers as explained before. This may give rise to a more condense structure in which water has more difficulty to

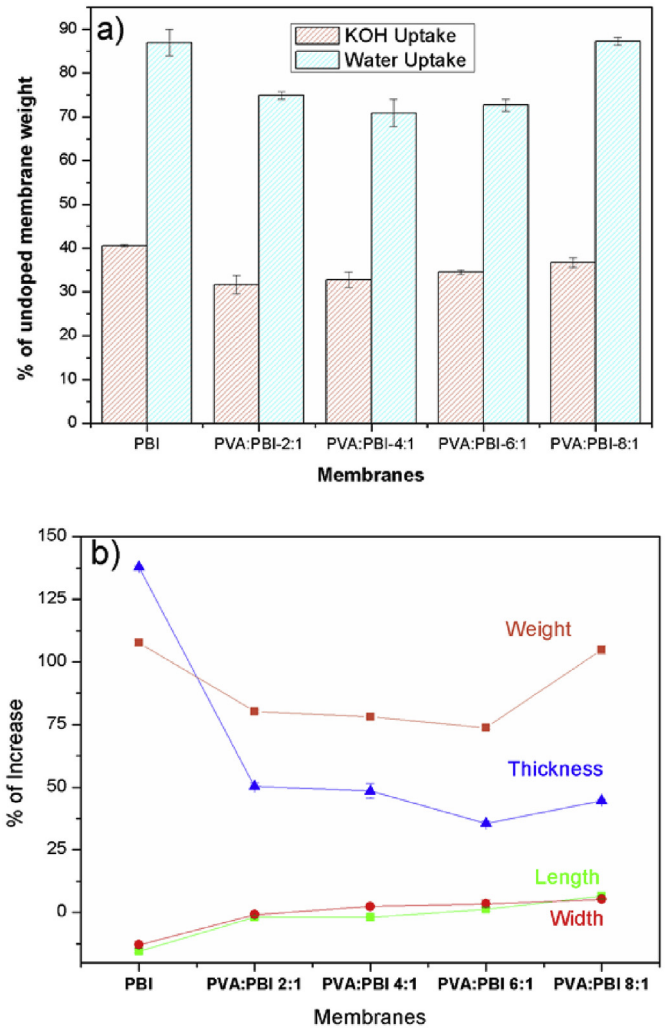

Fig. 8. a) KOH and water absorbed in the membrane due to the doping process. As percentage of the undoped membrane's weight. b) Dimensional changes due to the doping process.

penetrate (as can be observed since the increase of thickness in the blend membranes is significantly lower than in pure PBI) and less available groups for the interaction with water. Opposite to this effect is the fact that PVA gains more water than PBI, so increasing the proportion of PVA increases the water and KOH uptake.

When the membranes are kept in alkaline medium, an increase in the water uptake was observed due to the existence of water molecules solvating the K^+ and OH^- ions that enter the membrane (above 10 molecules of water per r.u. for PBI) [35].

The dimensional changes undergone by membranes during the doping process are depicted in Fig. 8b. Length and width of membranes suffer slight variations as compared to thickness. A contraction of length and width above 10% is observed for PBI, while the presence of PVA favours the expansion of the membranes up to 6% for PVA:PBI 8:1. Nevertheless, for the pristine PBI, a thickness increase of 140% is observed after doping membranes, whereas the expansion of PVA containing membranes is close to 50%.

Expansion of thickness in aqueous alkaline media will be an important factor to take into account when membranes are used to prepare membrane-electrodes assemblies (MEA) for alkaline fuel cells. Thus, in order to avoid the effects of water and KOH uptake during cell operation, it is necessary to dope the membranes before sandwich them between the carbon sheets impregnated with the catalysts.

3.7. XPS measurements

Further information on the chemistry of the membranes and on their behaviour during the doping process can be obtained using XPS. Fig. 9a shows the evolution of the O 1s spectra measured on the PVA:PBI 4:1 sample for different doping times up to 6 days. The spectrum labelled as PVA:PBI 4:1 corresponds to the sample with no doping. This spectrum can be deconvoluted using solely a synthetic peak with Gaussian-Lorentzian shape at 532.5 eV, which could be attributed to oxygen in the –C–OH bonds of the PVA. With increasing doping time, this peak becomes broader and a new feature clearly appears in the low binding energy (BE) side. Such changes can be attributed to the successful doping on the membrane.

Spectra of the doped samples can be properly deconvoluted using two peaks, the first one at the BE indicated above, and the second one at 531.2 eV, which could be attributed to oxygen in the HO–K^+ bonds appearing during the doping process. This results is in good agreement with H. Hou et al. [23], who proposed a mechanism involving hydrogen bonding between OH^- and –N = in the imidazole ring of PBI, while K^+ is introduced in the polymer connected with OH^- to balance the charge during alkaline doping. It should be pointed out that the O 1s spectrum of alkali doped graphene oxide membranes display a peak at around 531 eV that has been also attributed [48] to oxygen in OH^- therefore supporting the assignation proposed above. The N 1s spectrum of PVA:PBI4:1 membrane is shown in Fig. S4. As can be observed, it can be deconvoluted using two peaks at 400.4 eV and 398.6 eV, which could be attributed to the nitrogen of amine (–NH–) and imine (=N–) in the imidazole rings, respectively, in good agreement with previously published results [11,49]. In addition to that, Fig. 9 shows b) the C 1s and c) the K 2p spectra measured on the PVA:PBI 4:1 sample doped 1 day. The C 1s spectrum can be deconvoluted using three synthetic peaks with Gaussian-Lorentzian shape at 285, 286.4 and 287.8 eV. The interpretation of the C 1s spectrum is somewhat controversial. However, there is a general consensus to attribute the peak at 285 eV (used as binding energy reference) to C–C and to C–H bonds [50,51]. In the case of CN compounds, polarization occurs due to the difference of electronegativity between carbon and nitrogen atoms leading to a transfer of negative charge from carbon to nitrogen atoms, which increases the binding energy of the C 1s level and decreases the binding energy of the N 1s level. Since this charge transfer is dependent of the nature of the bonding between carbon and nitrogen [51] (either C–N or C=N), the other two peaks could be attributed to C–N and C=N bonds, respectively. The K 2p spectrum of Fig. 9c is characterized by a doublet with the peak $2p_{3/2}$ at 292.9 eV and a spin-orbit splitting of ~3 eV. The binding energy of metallic K $2p_{3/2}$ has been reported at 294.6 eV whereas oxidized and nitrided potassium appears shifted ~1.7 eV to lower binding energies [52,53]. Therefore, the peak observed in Fig. 9c could be attributed to potassium in both = N–HO^-K^+ and –N–K bonds, which appear during the doping process.

Fig. 10a shows the evolution of K 2p/N 1s peak area ratio as a function of the doping time in days (black lines). Peak areas have been normalized to the corresponding sensitivity factors S_K (4.04) and S_N (1.77) provided by the manufacturer.

As can be observed, this ratio increases with increasing the doping time, however according to the reaction mechanism proposed by H. Hou et al./L. Zeng et al. for the alkaline doping process, this ratio should remain constant an equal to one. Therefore, this behaviour points to the incorporation of more K species within the PVA:PBI 4:1 membrane framework during the alkali doping

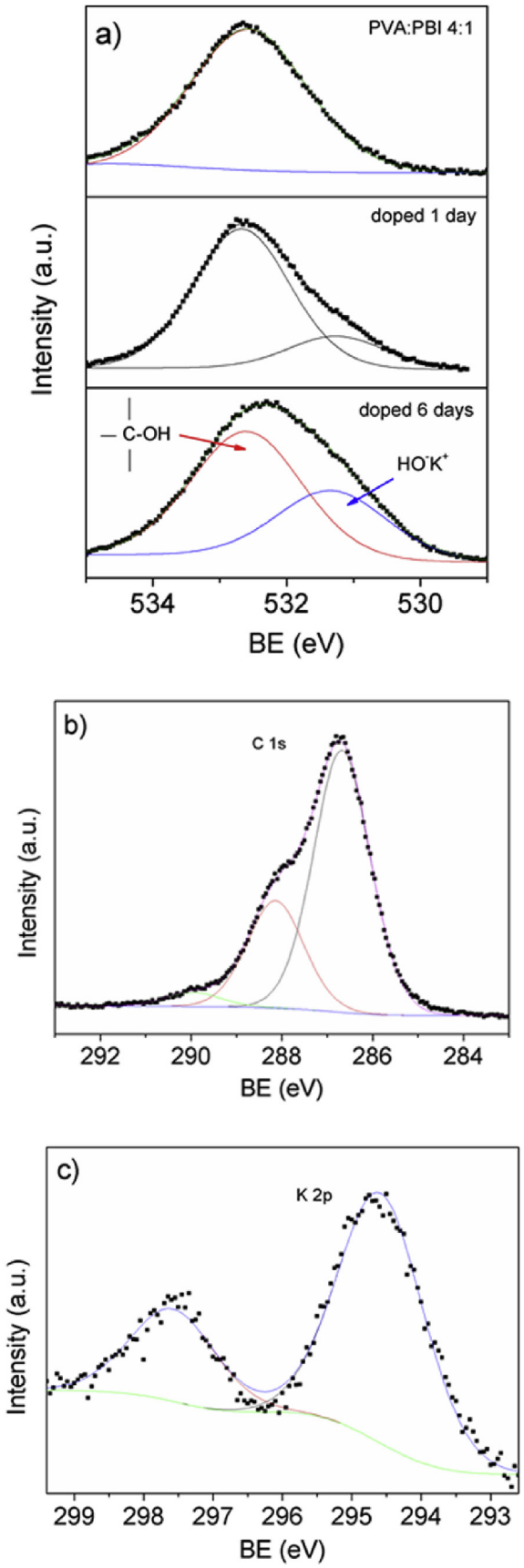

Fig. 9. a) Evolution of the O 1s spectra measured on the PVA:PBI 4:1 sample for different doping times up to 6 days. The spectrum labelled as 4:1 corresponds to the sample with no doping; b) C 1s and c) K 2p spectra measured on the membrane doped 1 day. The synthetic peaks used for deconvolution as explained in the text are also shown.

process, different from the above mentioned reaction mechanism.

Fig. S5 shows the ratio of amine (−NH−) to imine (=N−) in the imidazole rings as a function of the doping time. It can be observed that the ratio remains constant and equal to one, as expected from the structure of the PBI molecule involved in the PVA:PBI 4:1 membrane. This result indicates that the reaction produced during the membrane formation does not alter neither the number, nor the type, of N species of the imidazole rings present in the PBI molecule.

The ratio of oxygen present in the HO−K^+ bonds (appeared during the doping process) to the oxygen in the −C−OH bonds of the PVA molecule, is depicted in Fig. 10a as a function of the doping time (red lines). As can be observed, this ratio tends to saturate for doping times above 3 days. According to the reaction mechanism proposed by H. Hou et al. [23] for the alkaline doping process, a ratio of 0.25 (1:4) should be expected. However, at saturation, the ratio is well above this value, indicating again the incorporation of more K species than expected from the above mentioned reaction mechanism.

The evolution of the K 2p intensity is shown as a function of the intensity of the oxygen peak at 531.2 eV in the O 1s spectrum Fig. 10b (black squares). Intensities (peak areas) have been normalized to the corresponding sensitivity factors S_K (4.04) and S_O (2.85) provided by the manufacturer. Red line in Fig. 10b represents the fit of the experimental data to a straight line (slope = 0.78) whereas the black line represents the expected linear dependence $I_K/S_K = I_O/S_O$. Experimental results of this figure indicate that the oxygen peak at 531 eV in the O 1s spectrum should be composed not only of oxygen in HO−K+ but also of oxygen (HO− species) coming from water which would incorporate within the membrane framework during the alkaline doping process. This incorporation could explain the deviation of experimental data from the above mentioned expected linear dependence $I_K/S_K = I_O/S_O$.

3.8. Conductivity measurements

The ionic conductivity of the blend membranes with progressive doping days was measured and the results were included in Table 1. It was observed that the higher the PVA content of the membrane, the higher the conductivity maximum was reached and the shorter the doping time required to get it. The presence of higher amount of PVA enhances the conductivity, probably due to the abundance of −OH groups in the polymer that helps to absorb water and KOH by hydrogen bonds formation. This effect may produce shorter doping time and make easier the conductivity of ions through the membrane. After reaching the maximum conductivity at certain days of doping, the degradation of the membranes could be due to being maintained in a strong alkaline medium. This was reflected in a decrease in the conductivity of the samples.

The best conductivity values for the different PVA:PBI blend membranes are showed in Table 1. The best performance is observed for PVA:PBI 8:1, which reaches a conductivity of 103 mS cm^{-1} at 90 °C. This value decreases with the decreasing content of PVA in membranes, as observed for 4:1 blend membrane (70 mS cm^{-1} at 90 °C). Thus, pristine PBI shows the lowest value of series (28 mS cm^{-1} at 90 °C, that is 3.6 and 2.5 times less than 8:1 and 4:1 membranes, respectively), which is in the range of conductivities observed by other authors [11,54].

These results clearly reveal that the increment in PVA enhances the ionic conductivity of the membrane.

In order to study the dependence of the OH^- conductivity of the

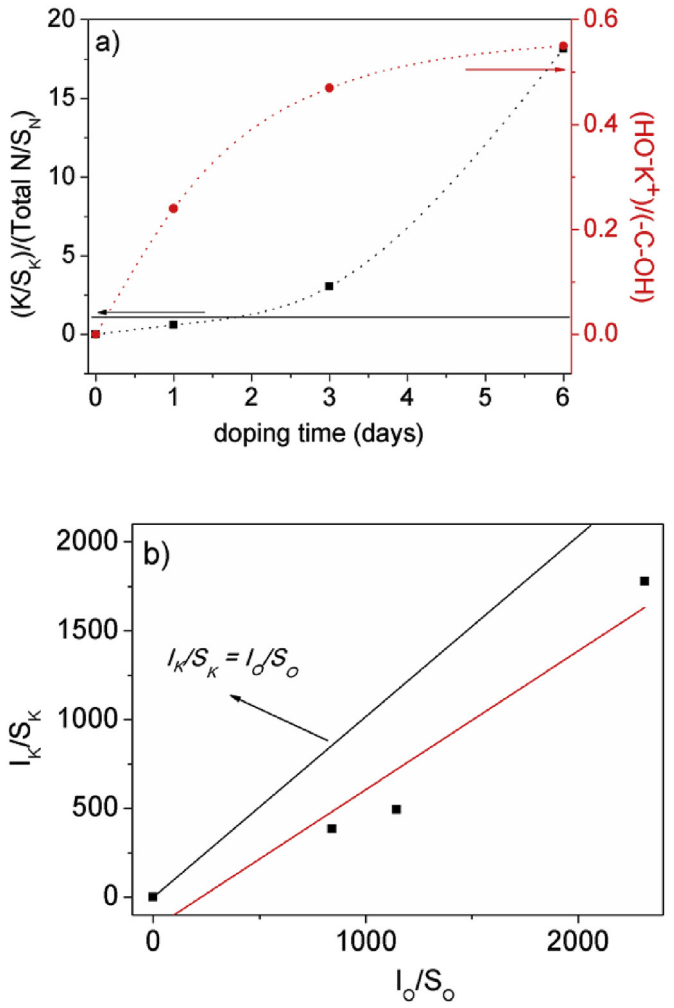

Fig. 10. a) Evolution of the peak area ratio K 2p/N 1s and peak area ratio of the O 1s related to HO^-K^+ bonds to the O 1s related to –C–OH bonds in the PVA molecule as a function of the doping time in days for the PVA:PBI 4:1 membrane. The peak areas have been normalized to the corresponding sensitivity factors S_K and S_N, respectively. The dotted line is given to guide the eye. b) Evolution, during the doping of the PVA:PBI 4:1 membrane, of the K 2p intensity as a function of the intensity of the oxygen peak at 531.2 eV in the O 1s spectrum (black squares). The intensities (peak areas) have been normalized to the sensitivity factors, S_K and S_O, respectively. The red line represents the experimental data fit to a straight line (slope = 0.78), whereas the black line represents the expected linear dependence $I_K/S_K = I_O/S_O$. (For interpretation of the references to colour in this figure legend, the reader is referred to the Web version of this article.)

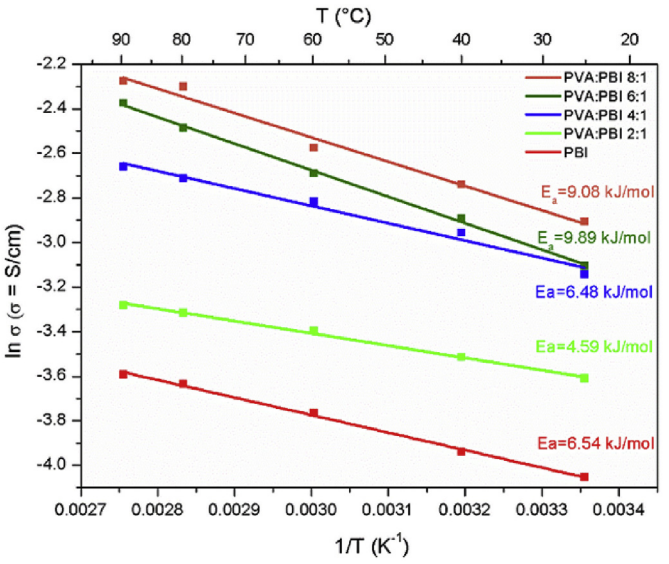

Fig. 11. Activation energy at their corresponding optimum days of doping for all PVA:PBI membranes and pristine PBI membrane.

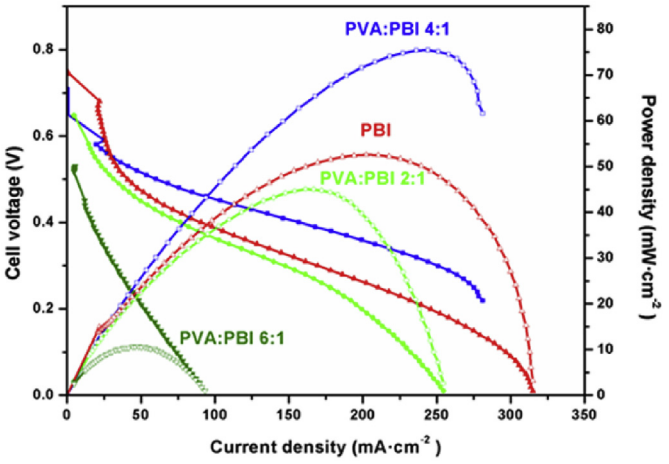

Fig. 12. Polarization and power density curves of PVA:PBI and pristine PBI membranes.

membranes with the temperature and the possible mechanisms behind, the activation energy (E_a) was calculated from the conductivity vs. temperature data. The ionic conductivity of all membranes significantly increases with increasing temperature (25 °C–90 °C) due to the improved mobility of OH^- species within polymeric membranes. The linear fitting of the results presented in Fig. 11allow us to calculate the activation energy following the Arrhenius law. The obtained values are in the range of those previously mentioned from literature, which are consistent with some possible mechanisms for the hydroxyl transportation: Grotthuss mechanism, surface site hopping, diffusion and convention via permeation, and osmotic drag could take place [35,55]. OH^- could diffuse via the hydrogen-bonded network of water molecules, through the formation/breaking of covalent bonds combined with diffusion/migration transport process (vehicular mechanism).

The activation energies are compared at 4 days of doping in KOH 6 M for each membrane in Table 1. The results show that activation energy decreases with the increasing content in PVA, and thus the membranes have lower dependence with the temperature the higher the content of PVA is. The activation energy reported in literature for pristine PBI membrane is 22–23 kJ/mol in KOH 4 mol L^{-1} one week [35]. To conclude, all doped blend membranes present conductivity values higher than 10 mS cm^{-1}, which is considered the limit value for an acceptable polymer electrolyte membrane [38].

3.9. Single cell

After confirming the suitability of blend membranes, single cell measurements with different membranes as electrolytes are carried out to check the final applicability of these materials. Fig. 12 shows the polarization and power density curves of MEAs with different membranes in single direct ethanol fuel cell. The MEA was prepared using commercial Pt-based catalysts as cathode and anode materials, and KOH-doped PVA:PBI and commercial PBI membranes as electrolytes. Performance measurements were

Table 1
Best conductivity (σ) and activation energy (Ea) for each membrane at their optimal doping time and for each membrane at 4 days of doping.

Membrane	σ/mS·cm^{-1} at 90 °C	Ea/kJ·mol^{-1}	Optimal doping time/days	Ea (4 days of doping)/kJ·mol^{-1}
PVA:PBI 8:1	103	9.08	1	8.75
PVA:PBI 6:1	93	9.89	2	9.73
PVA:PBI 4:1	70	6.48	3	12.66
PVA:PBI 2:1	38	4.59	3	13.18
PBI	28	6.54	5	6.47

carried out at 90 °C feeding the fuel cell with 2 M EtOH in 2 M KOH aqueous solution. The backpressure of the oxygen flow was 0.5 atm (7 psi). Doped PVA:PBI membranes present more structural problems than doped standard PBI membranes and they show more O_2 crossover. This problem is more noticeable when the PVA:PBI weight ratio increases, and it becomes impossible to have any measure for PVA:PBI 8:1. Open circuit potentials of different MEAs display the same trend as expected: PBI (744 mV), PVA:PBI 2:1 (647 mV), PVA:PBI 4:1 (651 mV) and PVA:PBI 6:1 (530 mV). As previously was reported (section 3.4), PBI membranes have better mechanical properties than blend membranes PVA:PBI and, according to that, it is not an unexpected result. When the PVA content is increased in blend membranes, the mechanical stability of the membrane is worst. In addition, some crossover of the oxygen from cathode to anode is observed, decreasing the open circuit potential. For example, PVA:PBI 6:1 OCP is 29% worse than standard PBI membrane.

The maximum power density was achieved by PVA:PBI 4:1 (76 mW cm^{-2}) at potential $E_p = 310$ mV, whereas PVA:PBI 2:1 and PVA:PBI 6:1 reach 45 mW cm^{-2} at 279 mV and 11 mW cm^{-2} at 220 mV, respectively. The result obtained in the same operating conditions by PBI, a typical commercial electrolyte for these devices, achieves a maximum power density of 53 mW cm ^{2} at 260 mV.

The best results obtained for the PVA:PBI 4:1 blend membrane as solid electrolyte is 43% better in power density than standard PBI membrane under same conditions. Although other synthesized membranes as 6:1 and 8:1 PVA:PBI presented better ionic conductivity, the single-cell test performances do not show the same trend. PVA:PBI 6:1 membrane presents important issues and it is clearly deteriorated after short times under test conditions presenting after stabilization polarization curve the worst performance. In the case of PVA:PBI 8:1 membranes, which present the best conductivity values, the study of single-cell performance was not possible owing to the O_2 crossover. It was not possible the use of these membranes in real operation conditions in single cell.

These presented results are very promising and demonstrate that incorporating PVA to standard PBI polymer is a good way to improve not only the conductivity but also the final performance in operation conditions in alkaline fuel cell. The PVA polymer increases the conductivity of the final material, whereas the PBI polymer improves the stability and durability of final blend membrane. Nevertheless, both of them possess some drawbacks and it is important to achieve the adequate PVA:PBI ratio in order to avoid them. In this study we demonstrate than a PVA:PBI ratio of 4:1 is the best one in order to have good performance in direct ethanol fuel cell. It demonstrates that PVA:PBI membranes are better anion conductors than membranes based on only PBI.

4. Conclusions

PVA:PBI blend membranes were successfully prepared using the casting method and characterized, demonstrating the presence of both polymers in the final membrane and the interaction between them by hydrogen bonds. The thermal and mechanical stability were also studied and determined to be adequate. The doping process was carefully investigated giving evidence of the successful incorporation of KOH in the structure of the membrane by FTIR, EDX and XPS. XPS was also used to have further relevant information about the relation of the atoms in the doped membranes. Due to the doping, good ionic conductivity values were obtained for the blend membranes, with increasing conductivity as the PVA content in the membranes increased. The high conductivity obtained, with the rest of characterizations were promising of the applicability for alkaline direct ethanol fuel cells, as the single test results corroborate. The PVA:PBI 4:1 membrane had the optimal behaviour in the fuel cell, giving a power density of 76 mW cm^{-2}, approximately 50% higher than the doped PBI in the same conditions. PVA:PBI 6:1 and 8:1 membranes presented better ionic conductivity that 4:1 but the single cell tests do not show same trend. Deterioration after short times appears as big problem. The degradation problem should still be solved and our actual research works in that way, by chemical cross-linking of the membrane. After all we consider that these membranes have promising qualities to be used in alkaline polymeric electrolyte fuel cells for high efficiency conversion of energy.

Acknowledgements

This work has been partially supported by the Spanish Ministry of Economy, Industry and Competitiveness (MINECO) under projects ENE2016-77055-C3-1-R and CTQ2015-68844-REDT, and by the Madrid Regional Research Council (CAM) under project S2013/MAE-2882 (RESTOENE-2).

Appendix A. Supplementary data

Supplementary data related to this article can be found at https://doi.org/10.1016/j.renene.2018.05.020.

References

[1] F. De Bruijn, The current status of fuel cell technology for mobile and stationary applications, Green Chem. 7 (2005) 132–150, https://doi.org/10.1039/b415317k.
[2] G.D. Watt, A new future for carbohydrate fuel cells, Renew. Energy 72 (2014) 99–104, https://doi.org/10.1016/j.renene.2014.06.025.
[3] H. Deng, D. Wang, X. Xie, Y. Zhou, Y. Yin, Q. Du, K. Jiao, Modeling of hydrogen alkaline membrane fuel cell with interfacial effect and water management optimization, Renew. Energy 91 (2016) 166–177, https://doi.org/10.1016/j.renene.2016.01.054.
[4] A. Oliveira Neto, M.J. Giz, J. Perez, E.A. Ticianelli, E.R. Gonzalez, The electrooxidation of ethanol on Pt-Ru and Pt-Mo particles supported on high-surface-area carbon, J. Electrochem. Soc. 149 (2002) A272–A279, https://doi.org/10.1149/1.1446080.
[5] A.N. Geraldes, D. Furtunato da Silva, J.C. Martins da Silva, O. Antonio de Sá, E.V. Spinacé, A.O. Neto, M. Coelho dos Santos, Palladium and palladium–tin supported on multi wall carbon nanotubes or carbon for alkaline direct ethanol fuel cell, J. Power Sources 275 (2015) 189–199, https://doi.org/10.1016/j.jpowsour.2014.11.024.
[6] J.B. Xu, T.S. Zhao, Y.S. Li, W.W. Yang, Synthesis and characterization of the Au-modified Pd cathode catalyst for alkaline direct ethanol fuel cells, Int. J. Hydrogen Energy 35 (2010) 9693–9700, https://doi.org/10.1016/j.ijhydene.2010.06.074.
[7] L. Ma, H. He, A. Hsu, R. Chen, PdRu/C catalysts for ethanol oxidation in anion-

exchange membrane direct ethanol fuel cells, J. Power Sources 241 (2013) 696–702, https://doi.org/10.1016/j.jpowsour.2013.04.051.
[8] S. Carrión-Satorre, M. Montiel, R. Escudero-Cid, J.L.G. Fierro, E. Fatás, P. Ocón, Performance of carbon-supported palladium and palladium-ruthenium catalysts for alkaline membrane direct ethanol fuel cells, Int. J. Hydrogen Energy 41 (2016) 8954–8962, https://doi.org/10.1016/j.ijhydene.2016.04.053.
[9] L. Osmieri, R. Escudero-cid, A.H.A.M. Videla, P. Oc, S. Specchia, Application of a non-noble Fe-N-C catalyst for oxygen reduction reaction in an alkaline direct ethanol fuel cell, Renew. Energy (2017), https://doi.org/10.1016/j.renene.2017.08.062.
[10] J.R. Varcoe, R.C.T. Slade, E.L.H. Yee, S.D. Poynton, D.J. Driscoll, Investigations into the ex situ methanol, ethanol and ethylene glycol permeabilities of alkaline polymer electrolyte membranes, J. Power Sources 173 (2007) 194–199, https://doi.org/10.1016/j.jpowsour.2007.04.068.
[11] L. Zeng, T.S. Zhao, L. An, G. Zhao, X.H. Yan, Physicochemical properties of alkaline doped polybenzimidazole membranes for anion exchange membrane fuel cells, J. Membr. Sci. 493 (2015) 340–348, https://doi.org/10.1016/j.memsci.2015.06.013.
[12] J.R. Varcoe, P. Atanassov, D.R. Dekel, A.M. Herring, M.A. Hickner, P.A. Kohl, A.R. Kucernak, W.E. Mustain, K. Nijmeijer, K. Scott, T. Xu, L. Zhuang, Anion-exchange membranes in electrochemical energy systems, Energy Environ. Sci. 7 (2014) 3135–3191, https://doi.org/10.1039/c4ee01303d.
[13] L. Wang, E. Magliocca, E.L. Cunningham, W.E. Mustain, S.D. Poynton, R. Escudero-cid, M.M. Nasef, J. Ponce-González, R. Bance-souahli, R.C.T. Slade, D.K. Whelligan, J.R. Varcoe, An optimised synthesis of high performance radiation-grafted anion-exchange membranes, Green Chem. 19 (2017) 831–843, https://doi.org/10.1039/c6gc02526a.
[14] N. Benipal, J. Qi, J.C. Gentile, W. Li, Direct glycerol fuel cell with polytetra fl uoroethylene (PTFE) thin film separator, Renew. Energy 105 (2017) 647–655, https://doi.org/10.1016/j.renene.2016.12.028.
[15] S. Maurya, S.-H. Shin, Y. Kim, S.-H. Moon, A review on recent developments of anion exchange membranes for fuel cells and redox flow batteries, RSC Adv. 5 (2015) 37206–37230, https://doi.org/10.1039/c5ra04741b.
[16] T. Sata, M. Tsujimoto, T. Yamaguchi, K. Matsusaki, Change of anion exchange membranes in an aqueous sodium hydroxide solution at high temperature, J. Membr. Sci. 112 (1996) 161–170, https://doi.org/10.1016/0376-7388(95)00292-8.
[17] G.-J. Hwang, H. Ohya, Preparation of anion-exchange membrane based on block copolymers: Part 1. Amination of the chloromethylated copolymers, J. Membr. Sci. 140 (1998) 195–203, https://doi.org/10.1016/S0376-7388(97)00283-4.
[18] J.R. Varcoe, R.C.T. Slade, E. Lam How Yee, S.D. Poynton, D.J. Driscoll, D.C. Apperley, Poly(ethylene-co-tetrafluoroethylene)-Derived radiation-grafted anion-exchange membrane with properties specifically tailored for application in metal-cation-free alkaline polymer electrolyte fuel cells, Chem. Mater. 19 (2007) 2686–2693, https://doi.org/10.1021/cm062407u.
[19] A. Huang, C. Xia, C. Xiao, Z. Lin, Composite anion exchange membrane for alkaline direct methanol fuel cell: structural and electrochemical characterization, J. Appl. Polym. Sci. 100 (2006) 2248–2251, https://doi.org/10.1002/app.23579.
[20] H. Hou, S. Wang, H. Liu, L. Sun, W. Jin, M. Jing, L. Jiang, G. Sun, Synthesis and characterization of a new anion exchange membrane by a green and facile route, Int. J. Hydrogen Energy 36 (2011) 11955–11960, https://doi.org/10.1016/j.ijhydene.2011.06.054.
[21] L. Jheng, S.L. Hsu, B. Lin, Y. Hsu, Quaternized polybenzimidazoles with imidazolium cation moieties for anion exchange membrane fuel cells, J. Membr. Sci. 460 (2014) 160–170, https://doi.org/10.1016/j.memsci.2014.02.043.
[22] B. Xing, O. Savadogo, Hydrogen/oxygen polymer electrolyte membrane fuel cells (PEMFCs) based on alkaline-doped polybenzimidazole (PBI), Electrochem. Commun. 2 (2000) 697–702, https://doi.org/10.1016/S1388-2481(00)00107-7.
[23] H. Hou, G. Sun, R. He, B. Sun, W. Jin, H. Liu, Q. Xin, Alkali doped polybenzimidazole membrane for alkaline direct methanol fuel cell, Int. J. Hydrogen Energy 33 (2008) 7172–7176, https://doi.org/10.1016/j.ijhydene.2008.09.023.
[24] B.P. Tripathi, M. Kumar, V.K. Shahi, Organic-inorganic hybrid alkaline membranes by epoxide ring opening for direct methanol fuel cell applications, J. Membr. Sci. 360 (2010) 90–101, https://doi.org/10.1016/j.memsci.2010.05.005.
[25] J. Fu, J. Qiao, H. Lv, J. Ma, X.-Z. Yuan, H. Wang, Alkali doped poly(vinyl alcohol) (PVA) for anion-exchange membrane fuel cells: ionic conductivity, chemical stability and FT-IR characterizations, ECS Trans. 25 (2010) 15–23, https://doi.org/10.1149/1.3315169.
[26] S.J. Lue, W.T. Wang, K.P.O. Mahesh, C.C. Yang, Enhanced performance of a direct methanol alkaline fuel cell (DMAFC) using a polyvinyl alcohol/fumed silica/KOH electrolyte, J. Power Sources 195 (2010) 7991–7999, https://doi.org/10.1016/j.jpowsour.2010.06.049.
[27] F. Conti, S. Willbold, S. Mammi, C. Korte, W. Lehnert, D. Stolten, Carbon NMR investigation of the polybenzimidazole–dimethylacetamide interactions in membranes for fuel cells, New J. Chem. 37 (2013) 152, https://doi.org/10.1039/c2nj40728k.
[28] S. Lai, M. Casu, G. Saba, A. Lai, I. Husu, Solid-state 13 C NMR study of poly (vinyl alcohol) gels, Solid State Nucl. Magn. Reson. 21 (2002) 187–196, https://doi.org/10.1006/snmr.2002.0059.
[29] M. Olukman, Ş. Oya, A novel in situ synthesized magnetite containing acrylonitrile and 2-hydroxyethyl methacrylate grafted poly (vinyl alcohol) nanocomposite membranes for pervaporation separation of acetone/, Chem. Eng. Process. Process Intensif. 98 (2015) 60–70.
[30] S. Hu, F. Horii, H. Odani, 1H NMR study of the solvation and gelation in a poly (vinyl alcohol)/DMSO-d6/H20 system, Bull. Inst. Chem. Res. 67 (1989) 5–6.
[31] J. Grobelny, D.M. Rice, F.E. Karasz, W.J. Macknight, High-resolution solid-state Carbon-13 nuclear magnetic resonance study of polybenzimidazole/polyimide blends, Macromolecules 2139 (1990) 2139–2144.
[32] M. Olukman, Ş. Oya, A novel in situ synthesized magnetite containing acrylonitrile and 2-hydroxyethyl methacrylate grafted poly (vinyl alcohol) nanocomposite membranes for pervaporation separation of acetone/, Chem. Eng. Process. Process Intensif. 98 (2015) 60–70.
[33] F. Conti, S. Willbold, S. Mammi, C. Korte, W. Lehnert, D. Stolten, Carbon NMR investigation of the polybenzimidazole–dimethylacetamide interactions in membranes for fuel cells, New J. Chem. 37 (2013) 152, https://doi.org/10.1039/c2nj40728k.
[34] Q. Li, J.O. Jensen, R.F. Savinell, N.J. Bjerrum, High temperature proton exchange membranes based on polybenzimidazoles for fuel cells, Prog. Polym. Sci. 34 (2009) 449–477, https://doi.org/10.1016/j.progpolymsci.2008.12.003.
[35] R.N. Couto, J.J. Linares, KOH-doped polybenzimidazole for alkaline direct glycerol fuel cells, J. Membr. Sci. 486 (2015) 239–247, https://doi.org/10.1016/j.memsci.2015.03.031.
[36] H. Zarrin, M. Fowler, Z. Chen, Highly anion-conducting porous polymer electrolyte membrane for alkaline fuel cells, ECS Trans. 50 (2012) 2083–2089, https://doi.org/10.1149/05002.2083ecst.
[37] H. Luo, G. Vaivars, B. Agboola, S. Mu, M. Mathe, Anion exchange membrane based on alkali doped poly(2,5-benzimidazole) for fuel cell, Solid State Ionics 208 (2012) 52–55, https://doi.org/10.1016/j.ssi.2011.11.029.
[38] M. Mamlouk, P. Ocon, K. Scott, Preparation and characterization of polybenzimidzaole/diethylamine hydrogen sulphate for medium temperature proton exchange membrane fuel cells, J. Power Sources 245 (2014) 915–926, https://doi.org/10.1016/j.jpowsour.2013.07.050.
[39] S.R. Samms, Thermal stability of proton conducting acid doped polybenzimidazole in simulated fuel cell environments, J. Electrochem. Soc. 143 (1996) 1225, https://doi.org/10.1149/1.1836621.
[40] A. Anis, S. Al-Zahrani, Sulfonated PVA/PBI based crosslinked composites towards anhydrous proton conductive polymer electrolyte membranes for fuel cells, Int. J. 7 (2012) 9174–9185. http://www.scopus.com/inward/record.url?eid=2-s2.0-84872869485&partnerID=tZOtx3y1.
[41] C.-P. Liu, C.-A. Dai, C.-Y. Chao, S.-J. Chang, Novel proton exchange membrane based on crosslinked poly(vinyl alcohol) for direct methanol fuel cells, J. Power Sources 249 (2014) 285–298, https://doi.org/10.1016/j.jpowsour.2013.10.117.
[42] J.M. Dodda, P. Bělský, J. Chmelař, T. Remiš, K. Smolná, M. Tomáš, L. Kullová, J. Kadlec, Comparative study of PVA/SiO2 and PVA/SiO2/glutaraldehyde (GA) nanocomposite membranes prepared by single-step solution casting method, J. Mater. Sci. 50 (2015) 6477–6490, https://doi.org/10.1007/s10853-015-9206-7.
[43] F. Kursun, I. Nuran, Development of thermo-responsive poly (vinyl alcohol) -g-poly (N-isopropylacrylamide) copolymeric membranes for separation of isopropyl alcohol/water mixtures via pervaporation, J. Ind. Eng. Chem. 41 (2016) 91–104.
[44] J.M. Gohil, A. Bhattacharya, P. Ray, Studies on the crosslinking of poly (vinyl alcohol), J. Polym. Res. 13 (2006) 161–169, https://doi.org/10.1007/s10965-005-9023-9.
[45] S. Panero, P. Fiorenza, M.A. Navarra, J. Romanowska, B. Scrosati, Silica-added, composite poly(vinyl alcohol) membranes for fuel cell application, J. Electrochem. Soc. 152 (2005) A2400–A2405, https://doi.org/10.1149/1.2104207.
[46] P.N. Pintauro, Crosslinked poly(phenylene oxide)-based nanofiber composite membranes for alkaline fuel cells, J. Mater. Chem. A Mater. Energy Sustain. 4 (2015) 132–141, https://doi.org/10.1039/C5TA06209H.
[47] M. Lim, D. Kim, H. Han, S.B. Khan, J. Seo, Water sorption and water-resistance properties of poly(vinyl alcohol)/clay nanocomposite films: effects of chemical structure and morphology, Polym. Compos. 36 (2015) 660–667, https://doi.org/10.1002/pc.22984.
[48] T. Bayer, B.V. Cunning, R. Selyanchyn, T. Daio, M. Nishihara, S. Fujikawa, K. Sasaki, S.M. Lyth, Alkaline anion exchange membranes based on KOH-treated multilayer graphene oxide, J. Membr. Sci. 508 (2016) 51–61, https://doi.org/10.1016/j.memsci.2016.02.017.
[49] W. Lu, G. Zhang, J. Li, J. Hao, F. Wei, W. Li, J. Zhang, Z.-G. Shao, B. Yi, Polybenzimidazole-crosslinked poly(vinylbenzyl chloride) with quaternary 1,4-diazabicyclo (2.2.2) octane groups as high-performance anion exchange membrane for fuel cells, J. Power Sources 296 (2015) 204–214, https://doi.org/10.1016/j.jpowsour.2015.07.048.
[50] J.E. Castle, Practical Surface Analysis by Auger and X-ray Photoelectron Spectroscopy, John Wiley and Sons Ltd, Chichester, 1990, https://doi.org/10.1002/sia.740060611. (Accessed 25 August 2016).
[51] F. Le Normand, J. Hommet, T. Szörényi, C. Fuchs, E. Fogarassy, XPS study of pulsed laser deposited CNx films, Phys. Rev. B 64 (2001), 235416, https://doi.org/10.1103/PhysRevB.64.235416.
[52] A. Caballero, J.P. Espinós, A. Fernández, L. Soriano, A.R. González-Elipe, Adsorption and oxidation of K deposited on graphite, Surf. Sci. 364 (1996) 253–265, https://doi.org/10.1016/0039-6028(96)00659-0.
[53] C.D. Wagner, G.E. Muilenberg, Handbook of X-ray Photoelectron

Spectroscopy, Physical Electronics Division, Perkin-Elmer Corp, Eden Prairie, Minn., 1979.
[54] L.-Y. Li, B.-C. Yu, C.-M. Shih, S.J. Lue, Polybenzimidazole membranes for direct methanol fuel cell: acid-doped or alkali-doped? J. Power Sources 287 (2015) 386–395, https://doi.org/10.1016/j.jpowsour.2015.04.018.
[55] G. Merle, M. Wessling, K. Nijmeijer, Anion exchange membranes for alkaline fuel cells: a review, J. Membr. Sci. 377 (2011) 1–35, https://doi.org/10.1016/j.memsci.2011.04.043.

Electronic supplementary information

Poly (vinyl alcohol) and Poly (benzimidazole) blend membranes for high performance alkaline direct ethanol fuel cells

D. Herranz,[a] R. Escudero-Cid,[a] M. Montiel,[a] C. Palacio,[b] E. Fatás,[a] and P. Ocón[a]

[a]Departamento de Química Física Aplicada, Universidad Autónoma de Madrid, C/ Francisco Tomás y Valiente 7, 28049, Madrid (Spain).

[b]Departamento de Física Aplicada, Universidad Autónoma de Madrid, C/ Francisco Tomás y Valiente 7, 28049, Madrid (Spain).

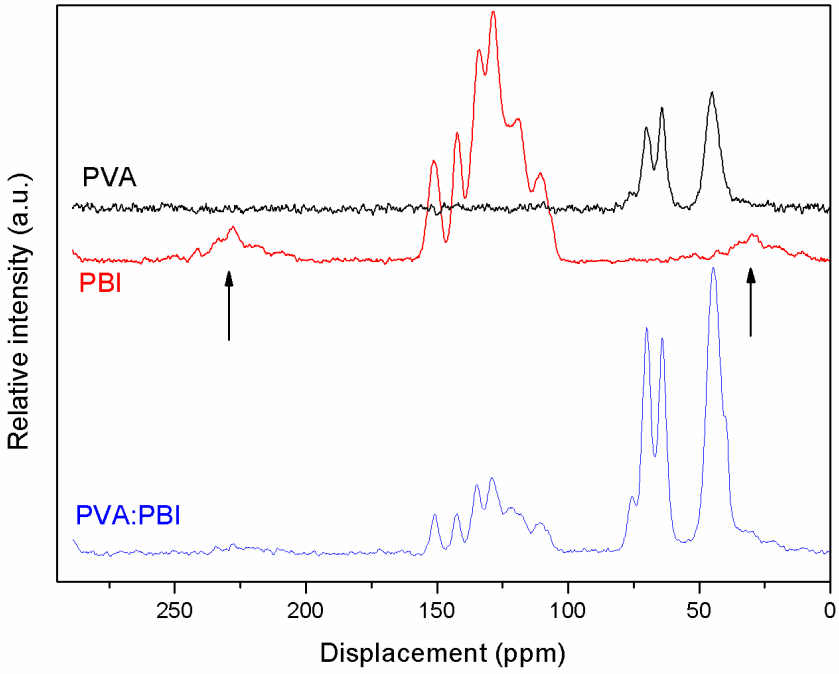

Fig. S1. Complete solid ^{13}C-NMR spectra of PVA, PBI and PVA:PBI membranes. Displacement by offset was done to appreciate them separately. Rotational side bands observed in the PBI spectrum are marked with arrows.

Atom[a]	^{1}H δ (ppm)[b]
1	13.3 (1H)
2	9.16 (1H)
3	8.34 (2H)
4	8.05 (1H)
5, 6	7.85 (2H)
7	7.81 (1H)
8-10	7.70-7.63 (3H)
11-13	4.67-4.22 (1H)
14	3.85 (1H)
15	1.40 (2H)

Table S1. Numbered protons with their respective chemical shift (δ) and integration values. [a]Atom labelling is referred to Fig. 3a. [b] The number of equivalent protons in showed in parenthesis.

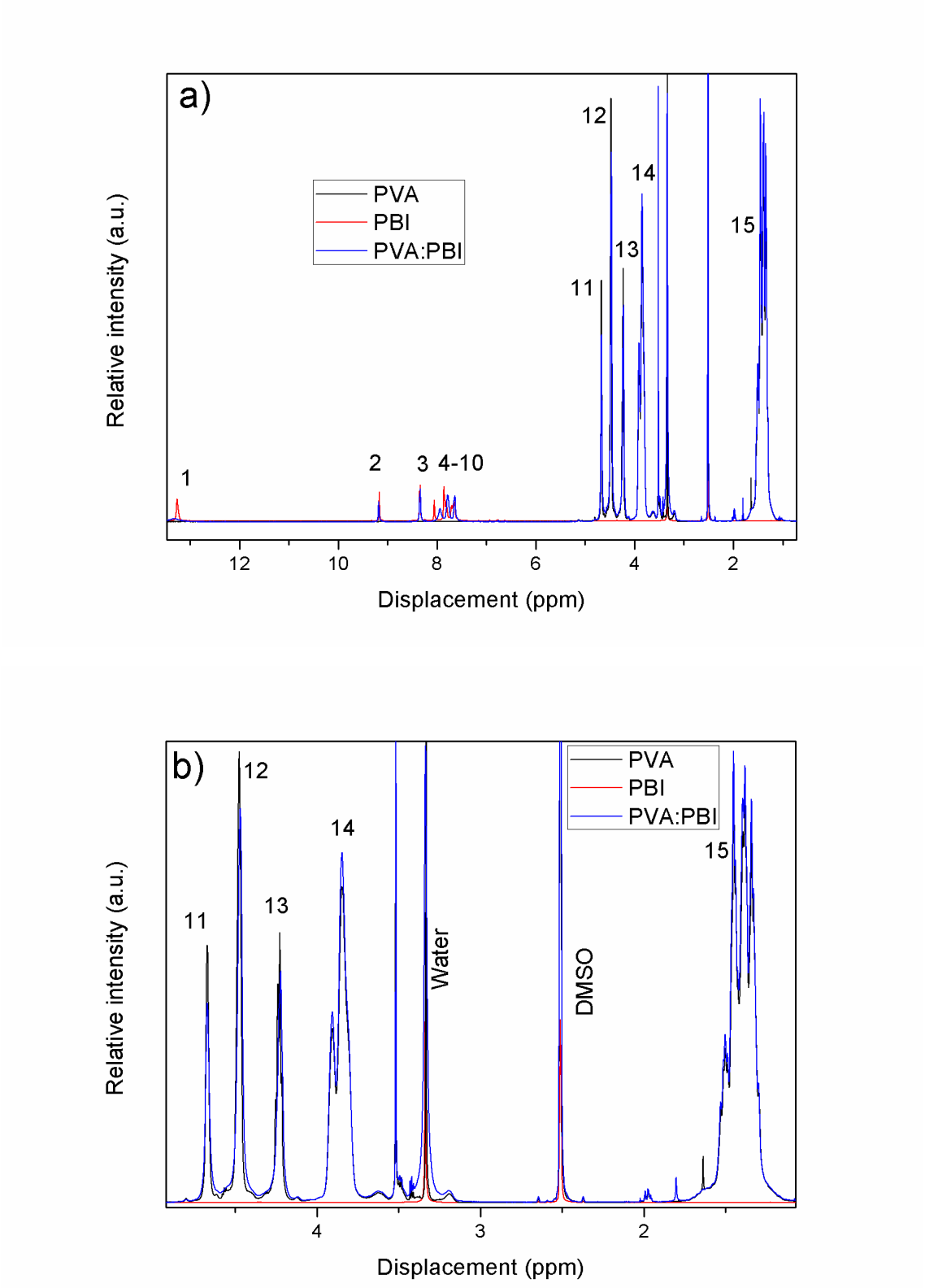

Fig. S2. a) Complete ^{1}H-NMR spectra of PVA, PBI and PVA:PBI solutions in DMSO-d_6, b) partial ^{1}H-NMR spectra showing the peaks of PVA and solvent.

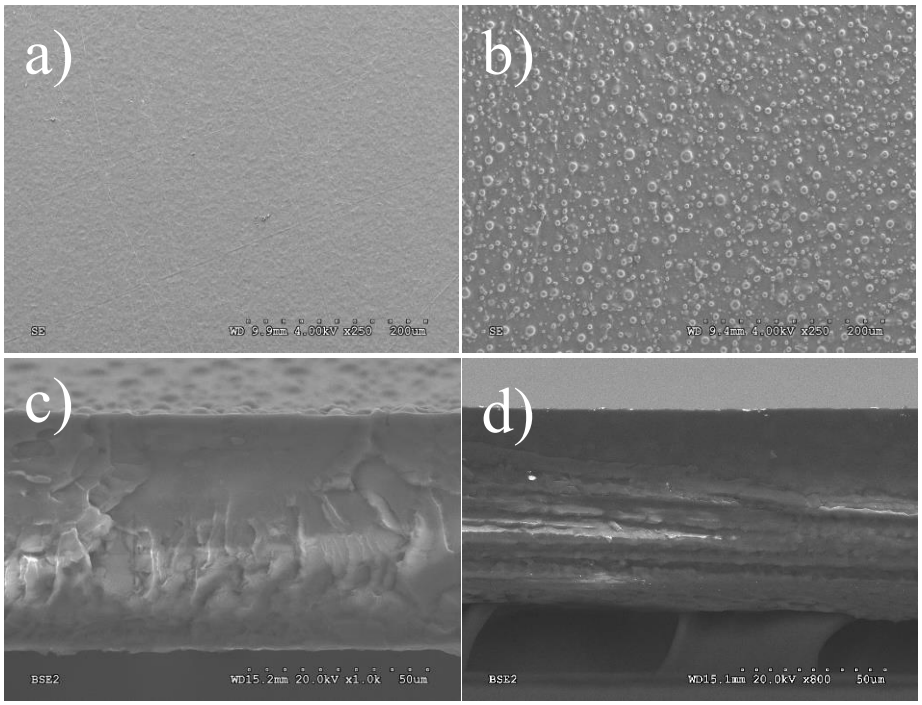

Fig. S3: Scanning electron micrographs of 4:1 PVA:PBI blend membranes (a) surface of undoped membrane, (b) surface of membrane doped in KOH 6M during 3 days, (c) cross-section of membrane doped in KOH 6M during 3 days and (d) cross-section of undoped membrane.

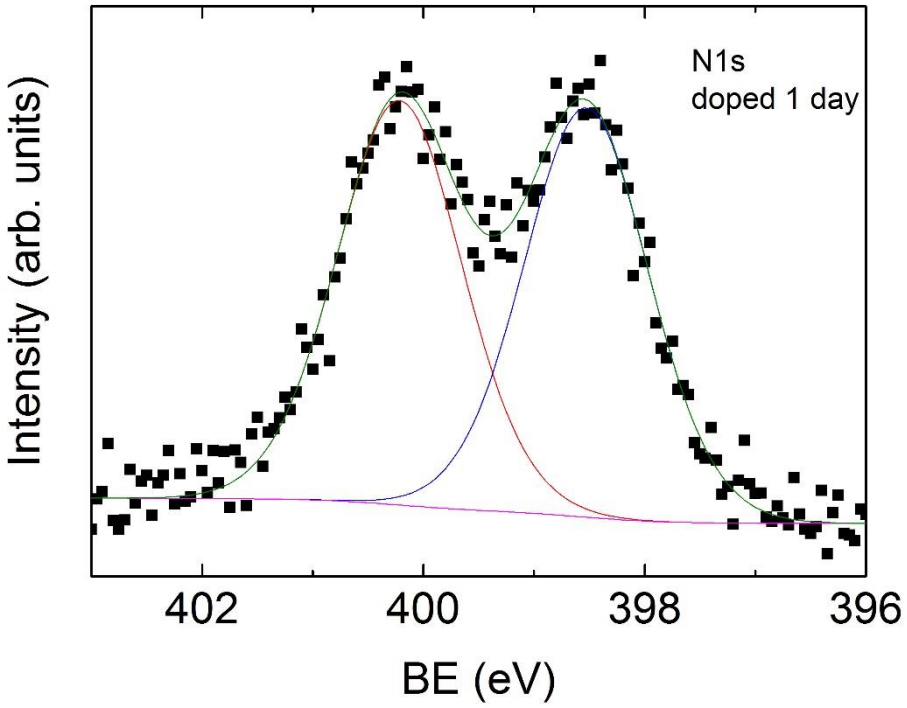

Fig S4. N1s XPS spectrum of the PVA:PBI 4:1 membrane.

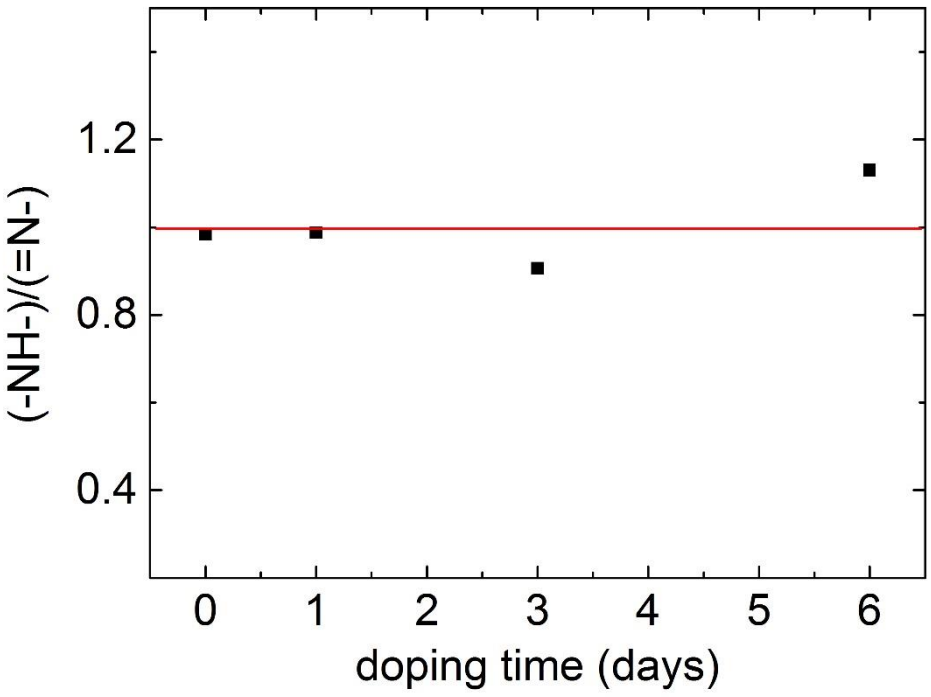

Fig S5. Peak area ratio of N1s related to amine (–NH–) and to imine (=N–) in the imidazole rings as a function of the doping time for the PVA:PBI 4:1 membrane. The line of ratio equals to one is also given for comparison.

Journal of Membrane Science 535 (2017) 45–55

Contents lists available at ScienceDirect

Journal of Membrane Science

journal homepage: www.elsevier.com/locate/memsci

Alkali-doped polyvinyl alcohol – Polybenzimidazole membranes for alkaline water electrolysis

L.A. Diaz[a], R.E. Coppola[a], G.C. Abuin[a,*], R. Escudero-Cid[b], D. Herranz[b], P. Ocón[b]

[a] Instituto Nacional de Tecnología Industrial (INTI), Centro de Procesos Superficiales, Av. General Paz 5445, B1650KNA San Martín, Buenos Aires, Argentina
[b] Universidad Autónoma de Madrid (UAM), Departamento de Química Física Aplicada, C/Francisco Tomás y Valiente 7, 28049 Madrid, Spain

ARTICLE INFO

Keywords:
Anion exchange membranes
PVA
PBI
ABPBI
Water electrolysis

ABSTRACT

We developed an innovative polymer blend system composed of polyvinyl alcohol (PVA) and polybenzimidazole as an anionic membrane for application to zero gap alkaline electrolysers. The challenge was to combine PVA with either poly[2-2′-(m-phenylene)-5-5′-bibenzimidazole] (PBI) or poly (2,5-benzimidazole) (ABPBI) to complement these neutral polymers, which must be doped to conduct, with hydroxyl groups that benefit the OH^- transport mechanism. We studied PVA-PBI and PVA-ABPBI membranes with compositions varying between 2:1 and 8:1, with 4:1 being best ratio. PVA is crosslinked inside PVA-PBI 4:1 and PVA-ABPBI 4:1 membranes with glutaraldehyde (GA) by immersion in a reaction solution with different GA contents ranging from 0.5 vol% to 50 vol% to enhance the stability of the membranes. The chemical stability in a KOH environment, thermal and mechanical properties, surface morphology, swelling, water/KOH sorption, and conductivity of the linear alkali-doped (L-PVA-PBI, L-PVA-ABPBI) and crosslinked (C-PVA-PBI, C-PVA-ABPBI) membranes were analysed. The best results were observed for the C-PVA-ABPBI 4:1 membrane crosslinked in 0.5 vol% GA, which exhibited specific conductivities at 90 °C of 50 mS cm^{-1} and 90 mS cm^{-1} when doped using 15 wt% and 30 wt% KOH, respectively. In short-term electrolysis tests performed with circulated 15 wt% KOH at 50 °C, this membrane exhibited a current density that was twice that of the commercial porous Zirfon® diaphragm (i.e., 300 mA cm^{-2} and 140 mA cm^{-2}, respectively) at a cell voltage of 2.0 V. The performance achieved with the C-PVA-ABPBI membrane in a 15 wt% KOH electrolyte at 70 °C was good (i.e., 360 mA cm^{-2} at a cell voltage of 1.9 V).

1. Introduction

Hydrogen is a viable energy carrier for renewable and sustainable energy and a promising energy conversion technology for intermittent electricity generation from solar cells and windmills. Water electrolysis (WE) is an advantageous process for the production of pure hydrogen that must reduce investment and operational costs to achieve a widespread utilization. The currently employed technologies include proton exchange membrane WE (PEMWE) and liquid alkaline WE (LAWE). LAWE is a well-established technology that consists of nickel electrodes separated by a porous diaphragm and employs a liquid electrolyte (i.e., typically 30 wt% KOH) at 80–90 °C. Although harmful to the materials, the high temperature and electrolyte concentration result in a decrease in the ohmic drop in the cell, which can be operated at voltages ranging from 1.9 to 2.1 V [1–4].

A comparison of the LAWE and PEMWE technologies indicates that PEMWE is advantageous in terms of the electrochemical performance. In addition, LAWE is advantageous in terms of cost savings because PEMWE employs precious metals as catalysts. The zero gap configuration with the porous electrodes attached to an anion-selective membrane, which is also an anion-exchange membrane (AEM), can be a good intermediate alternative. In zero gap cells, the porous electrodes are in contact with both sides of the AEM, reducing the voltage drop as well as the energy requirement for H_2 production. Furthermore, the replacement of the diaphragm and electrolyte-filled gap of LAWE by an ion-conducting membrane allows for a significant reduction in the electrolyte concentration, resulting in a reduction in the corrosive stress of the material in the system and auxiliary devices [4]. The main challenge of this alternative is to identify an anion selective membrane with a satisfactory ionic conductivity as well as sufficient chemical stability under the strongly alkaline environments and elevated temperatures that are employed in these devices. Currently, the operational temperature of an anion-selective membrane is limited to a temperature below 70 °C due to the chemical stability of the functional groups [1]. In fact, an anion-selective membrane capable of achieving low ohmic drops at moderate temperatures and KOH concentrations would be advantageous for avoiding the use of an aggressive media (e.g., concentrated KOH) at high temperatures.

* Corresponding author.
E-mail address: gabuin@inti.gob.ar (G.C. Abuin).

http://dx.doi.org/10.1016/j.memsci.2017.04.021
Received 26 October 2016; Received in revised form 9 April 2017; Accepted 11 April 2017
Available online 15 April 2017
0376-7388/

Many studies have focused on the application of AEMs to fuel cells, especially direct alcohol fuel cells. As proposed by Merle et al., AEMs can be categorized as *heterogeneous membranes*, which are composed of an anion solvating polymer matrix doped with an alkaline hydroxide solution; or *homogeneous membranes*, which are composed of an anion-exchanging polymer [5].

Polymers modified by incorporation of quaternary ammonium groups account for most of the studied homogeneous AEMs [6–8]. These AEMs exhibit good performance in terms of thermochemical stability and conductivity but they suffer from chemical degradation by hydroxide anions that attack the quaternary ammonium groups, progressively reducing their ion-exchange capacity [9].

This problem is avoided in heterogeneous membranes where the anion transport does not depend on functional groups but on the alkali doping solution. Alkali-doped PBI poly[2,2′-(m-phenylene)-5,5′-bibenzimidazole] and PBI-modified polymers are well known materials that are characterized by satisfactory thermochemical and mechanical properties. PBI and ABPBI doped with H_3PO_4 (PA) have been broadly evaluated in PEM fuel cells that were fed with H_2 or alcohol and operated up to 180 °C for high-temperature PEM fuel cells (HT-PEMFC) [10,11]. To a smaller extent, KOH-doped polybenzimidazole membranes have also been evaluated for use in fuel cells. For these membranes, Xing and Savadogo [12] reported room temperature ionic conductivities (IC) of 5 mS cm^{-1} to 20 mS cm^{-1} in H_2 fuel cells. Additional studies have also evaluated this type of membrane in hydrogen and direct alcohol fuel cells [13–16].

For LAWE applications, Aili et al. reported an IC of 20 S cm^{-1} for 3 M KOH-doped PBI membranes at room temperature [17]. When doped in 30 wt% KOH, the crosslinked PBI membranes exhibited better stability than the linear ones in durability tests performed at 85 °C. We reported similar conductivities and promising performances in a zero gap LAWE device with linear and benzoxazine-crosslinked ABPBI membranes [18].

Recently, research efforts have been focused on systemically characterizing the physicochemical properties of polybenzimidazole in alkaline environments. Zeng et al. [19] studied PBI membranes equilibrated in KOH (0–6 M) and proposed a mechanism for the interaction between the doped alkali and the polymer. Aili et al. [20] employed a combination of techniques to study the physicochemical properties of PBI films in aqueous KOH with concentrations ranging from 0 to 50 wt%. Furthermore, Kraglund el al. [21] investigated the influence of the electrolyte concentration on the performance and stability of a PBI membrane in a zero gap alkaline water electrolyser.

Herein, we combined PBI and ABPBI polymers with polyvinyl alcohol (PVA). This poly-hydroxyl polymer (PVA) has a film forming ability and is inexpensive, biodegradable and thermochemically stable. PVA also possesses a good OH^- transport ability based on the hydrophilicity derived from the presence of a considerable number of hydroxyl group pendants on its backbone. In addition, its structure becomes amorphous upon incorporation of KOH, being ionic conductivity mainly localized in the amorphous phase [22]. Some studies have investigated PVA as an anion solvating polymer in pure PVA, blend or composite membranes [5,22].

In the current study, we performed a comparative study of new membranes based on a blend of PBI or ABPBI and PVA. These membranes are interesting for WE applications because PBI/ABPBI have good thermal and mechanical properties, and PVA could contribute to important improvements in conductivity. The aim of this study was to characterize the properties and electrochemical performance of alkali-doped PVA-PBI and PVA-ABPBI membranes in a zero gap electrolyser cell.

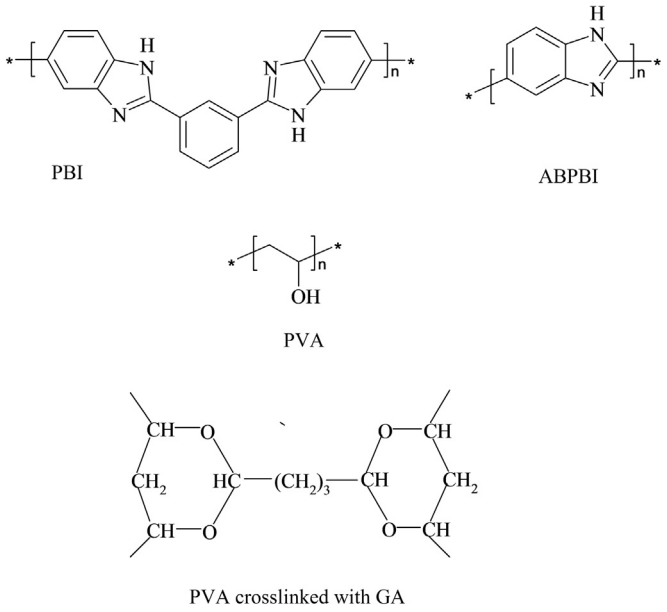

Fig. 1. Chemical structure of the PBI, ABPBI, linear PVA and PVA crosslinked with glutaraldehyde.

2. Experimental

2.1. Materials

3,4-Diaminobenzoic acid (DABA, 97 wt%), polyphosphoric acid (PPA, 85 wt%, Aldrich), PBI powder (BETWEEN, LizenzGMBH), polyvinyl alcohol (PVA, hydrolysed powder with a MW of 89,000–98,000, 99 + %, Aldrich), dimethyl sulfoxide (DMSO, 99.9%, Aldrich), N,N-dimethylacetamide (DMAc, 99.5%, Aldrich), glutaraldehyde (GA, 25% aqueous solution, Aldrich), potassium hydroxide (KOH, 85 wt%, Aldrich), H_2SO_4 (96 wt%, Baker Analysed), HCl (35–36 wt%, Biopack) and ethanol (Merck) were employed in this study. Deionized water was used to prepare the aqueous solutions.

The chemical structures of the PBI, ABPBI and PVA polymers are shown in Fig. 1. The ABPBI polymer was prepared by condensation of the DABA monomer in PPA followed by neutralization, washing, drying and milling according to a previously reported procedure [18]. The intrinsic viscosity of the polymer solution in 96 wt% H_2SO_4 at 30 °C was 2.96 dl g^{-1}, and the averaged molecular weight, which was calculated from the Mark–Houwink equation [23], was 23,200 g mol^{-1}.

2.2. Membrane preparation

The L-PVA-PBI and L-PVA-ABPBI membranes were synthesized using a casting method. A solution of 5 wt% PVA in DMSO was obtained by heating at 85 °C for 30 min under continuous stirring (1 g of PVA in 20 g of DMSO). 3.5 wt% PBI in DMAc was obtained by heating at 80 °C for 48 h (3.5 g of PBI in 96.5 g of DMAc). For the L-PVA-PBI membranes, the appropriate amounts of the PVA/DMSO and PBI/DMAc solutions were transferred to a glass beaker according to the required molar ratio (e.g., 2:1). The mixtures were stirred for 40 min at 500 rpm, placed in Petri dishes coated with a PTFE liner and introduced into a vacuum oven (Memert VO200), where the pressure was lowered from room pressure to 10 mbar. During the entire casting process, the temperature was maintained at 40 °C. Then, the membranes were easily peeled off the PTFE liner and stored in inert plastic bags prior to use.

For the L-PVA-ABPBI membranes, 1 wt% PVA in DMSO was prepared by heating at 80 °C for 30 min under continuous stirring (1 g of PVA in 100 g in DMSO), and then, the solution was cooled to room temperature. ABPBI was dissolved in absolute ethanol/NaOH according to a previously reported procedure [11]. The ethanol solution

contained ca. 1 wt% ABPBI, and 1 wt% NaOH was added for dissolution of ABPBI. The mixture was refluxed at 50 ºC until complete dissolution of ABPBI was achieved.

Based on the desired proportion of L-PVA-ABPBI, the prepared solutions PVA/DMSO and ABPBI/NaOH/ethanol (i.e., amounts corresponding to the desired molar proportion (e.g., 2:1)) were transferred to a glass beaker and gently stirred. Then, the solutions were placed in Petri dishes in an air convection oven (San Jor SE60DF) overnight at 50 °C. Finally, the membranes were removed by immersing them in water and stored in inert plastic bags prior to use.

The C-PVA-PBI and C-PVA-ABPBI crosslinked membranes were prepared according to the procedure reported by Yeom et al. [24]. The dry L-PVA-PBI or L-PVA-ABPBI membrane was heated at 40 °C for 48 h in different reaction solutions containing different amounts the aqueous GA solution, acetone and HCl. The GA solution content in the reaction solution ranged from 0.5 vol% to 50 vol%. The HCl content was maintained at 0.12 vol%. After the process, the membrane was washed several times with DI water and placed in pure water for 24 h at 40 °C to remove any residual HCl and GA followed by drying in an oven overnight at 50 °C.

The L-PVA and L-ABPBI membranes were prepared by casting from solutions containing 1 wt% PVA in DMSO and ABPBI in ethanol/NaOH, respectively. When necessary, the L-PVA and L-ABPBI membranes were subjected to treatment with GA according to the previously described procedure.

For all samples, the membrane thickness ranged from 40 μm to 120 μm (measured with a Mitutoyo Digital Micrometer). The linear and crosslinked PBI and ABPBI membranes were doped in KOH solutions at room temperature.

2.3. Alkaline water electrolysis

A single-cell laboratory water electrolyser with a zero gap configuration [18] was used to test the linear and crosslinked PVA-ABPBI and PVA-PBI membranes. Two 3.61 cm^2 electrodes consisting of Ni foam (Sigma Aldrich, thickness 1.6 mm, bulk density 0.45 g/cm^3, porosity 95%) were directly attached to the membrane surfaces. The active electrode surface area was 4.4 cm^2 in this arrangement. The single cell was fabricated from gold-plated Ni sheets, which were used as current collectors and electrolyte distributors. The cell was inserted in the system as described in [18], and KOH solution was recirculated by a dual head pump. The electrolysis load curves were measured using a cell voltage that ranged from 1.5 V to 2.0 V at 50 °C and 70 °C. In the chronopotentiometric measurements, a constant current density of 200 mA cm^{-2} was applied for 60 min.

2.4. Characterization of crosslinking reactions

Infrared spectroscopy was performed using an FTIR spectrometer (Thermo Scientific Nicolet 6700 FTIR). The IR spectra were recorded for non-doped crosslinked C-PVA-PBI and C-PVA-ABPBI samples to detect changes in the different GA amounts in the crosslinking reaction solution.

In order to assess the crosslinking of the membrane, the gel content test was performed. A weighted sample of membrane was immersed in a DMSO-Ethanol 5:2, with 1 wt% NaOH, at 80 °C). After certain periods of time, the sample was removed, washed, dried and weighted. The ratio of the residual (not dissolved) mass relative to the initial mass of the sample, was identified as the gel fraction, indicative of crosslinking of the membrane.

2.5. Stability in alkaline environment, surface morphology, mechanical and thermal properties

The membrane stability was evaluated in an alkaline environment. The membrane samples were immersed for 7 days in KOH solutions with concentrations ranging from 15 wt% to 30 wt% at 70 °C.

The surface morphology analysis was performed using a FEI QUANTA 250 scanning electron microscope (SEM) on membrane samples sputter coated with Au.

The thermal properties of the linear and crosslinked membranes were studied by thermogravimetric analysis (TG) on a TA Instrument 20. The samples were heated to 900 °C at a heating rate of 10 °C min^{-1} under a nitrogen atmosphere. The weight loss was measured and reported as a function of the temperature. Differential scanning calorimetry (DSC) measurements were performed to investigate the miscibility behaviour of PVA and polybenzimidazole polymers based on analysis of the glass transition temperatures. DSC was measured in a TA Instrument 10, under nitrogen atmosphere doing a heating procedure from −90 to 500 °C at a rate of 10 °C min^{-1} with the samples sealed in aluminium pans.

The mechanical properties were measured with an INSTRON model 3345 testing instrument, at 65% RH and room temperature. The membrane samples, with length 40 mm and width 4 mm, doped in 15 wt% KOH, were pulled at a crosshead speed of 5 mm min^{-1}.

2.6. Swelling, KOH doping level and water sorption

The membrane swelling was calculated based in the thickness, length and width before and after doping of the dry membrane.

The KOH doping level and water content were determined using the following method. Non-doped membrane samples were dried for 12 h at 80 °C under vacuum, weighed to determine the dry weight (w_0), and immersed in a 15 wt% KOH solution. After 7 days, each membrane was removed from the doping solution, and its surface was dried with tissue paper. Next, the sample was weight to obtain the wet weight of the sample (w_s). Then, the samples were dried overnight at 80 °C under vacuum and weighed again (w_d). This weight (w_d) was equivalent to weight of the polymer and KOH, and the water content (w_w) was determined to be $w_w = w_s - w_d$. In addition, the KOH content (w_a) was obtained as follows: $w_a = w_d - w_0$.

Finally, to determine if any polymer was lost in the doping solution, the samples were washed several times in water at 70 °C, dried overnight at 80 °C under vacuum and weighed again. If this weight equals w_0, no polymer loss occurs during the doping process. However, if any polymer loss was observed, it is necessary to determine if this loss occurs during doping or during the washing process.

The IR spectra were employed to determinate the possible PVA dissolution from the membranes during the doping process. For this purpose, PVA-polybenzimidazole membranes were added to 15 wt% KOH for 7 days in stainless steel vessels to avoid organic contamination of the solutions from plastic vessels. After removal of the membrane, the doping solution was neutralized with HCl, and the resulting salt solution was heated at 80 °C until dried. Then, 40 ml of ethanol was added to dissolve the PVA. The mixture was placed in a spin dryer at 500 rpm. Finally, a 10 ml aliquot of the supernatant was transferred to an aluminium container and dried. The infrared spectrum of the resulting solid was recorded.

2.7. Ionic conductivity

The through plane ionic conductivity (σ) of the membranes was determined based on a complex impedance analysis (EIS) in a temperature range from 25 °C to 110 °C. A two-point technique was employed where two stainless steel electrodes were placed in contact with opposite sides of the membrane sample. The samples were introduced to the conductivity cell under wet conditions, and the conductivity measurement was performed immediately. The EIS measurements were carried out with an Autolab PGSTAT 30N coupled to a frequency response analyser (FRA). The frequencies were swept from 100 kHz to 1 Hz, and six points per decade were recorded with an AC signal amplitude of 10 mV around the open circuit potential. Each

membrane sample was washed in DI water to remove the excess KOH solution, dried carefully with tissue paper and sandwiched between two stainless steel electrodes. The membrane conductivity was obtained from the resistance measurement (R) from the intercept of the real axis of the Nyquist plot at high frequencies.

The specific ionic conductivity was calculated as follows:

$$\sigma = \frac{\delta}{RA} \quad (1)$$

where δ (cm) is the thickness of the membrane and A (cm^2) is the active surface area of the sample (0.36 cm^2).

3. Results and discussion

3.1. Selection of PVA-polybenzimidazole ratio

L-PVA-PBI and L-PVA-ABPBI with compositions varying from 2:1 to 8:1 (molar ratio) were prepared using a solution casting method, as described in Section 2.2. Prior to use in the WE cell, the membranes were alkali doped by immersion in 15 wt% KOH aqueous solutions for 7 days at room temperature.

The effect of the PVA-polybenzimidazole ratio on the properties, which will define the behaviour of these membranes in the zero gap configuration LAWE process, is difficult to predict. The LAWE performance is influenced by the membrane conductivity, mechanical properties, permeability, and contact resistance between the membrane and the Ni foam electrodes as well as other properties. Therefore, the water electrolysis experiments performed in the single-cell laboratory water electrolyser with a zero gap configuration described in Section 2.3 were performed first, and based on the load curves (current – cell-potential) and chronopotentiometric results, the best PVA: PBI ratio was selected for subsequent characterizations.

The electrolysis load curves obtained for the L-PVA-PBI and L-PVA-ABPBI membranes with compositions varying from 2:1 to 8:1 (15 wt% KOH, 50 °C) are shown in Fig. 2a and b, respectively, and the chronopotentiometric curves for the same membranes in 15 wt% KOH at 50 °C (i = 200 mA cm^{-2}) are shown in Fig. 3a and b, respectively. In addition, the results are summarized in Table 1. The membranes with L-PVA-PBI and L-PVA-ABPBI compositions of 2:1 and 8:1 exhibited very poor performance for the electrolysis load or chronopotentiometric measurements. The membranes with PVA-PBI compositions of 4:1 and 6:1 exhibited similar good performances according to their electrolysis load curves, where the L-PVA-PBI 4:1 response in the chronopotentiometric measurements was slightly better than the response of PVA-PBI 6:1. As shown in Table 1, after 3500 s at 200 mA cm^{-2}, the cell voltage was 2.3 V for the L-PVA-PBI 4:1 membrane and 2.5 V for the L-PVA-ABPBI 4:1 and L-PVA-PBI 6:1 membranes.

In summary, L-PVA-ABPBI 4:1 exhibited the best performance based on both current – potential and chronopotentiometric measurements.

Based in these results, a PVA: polybenzimidazole ratio of 4:1 provide the best results among the studied ratios, and therefore, the properties of L-PVA-PBI 4:1 and L-PVA-ABPBI 4:1 will be evaluated. When we refer to L-PVA-PBI and L-PVA-ABPBI membranes in subsequent sections, a 4:1 ratio was employed.

3.2. Preparation of crosslinked PVA-polybenzimidazole membranes. IR spectral analysis

Although PVA is an advantageous polymer due to its chemical stability, film forming ability and low cost, it typically requires reinforcement via crosslinking reactions to enhance its mechanical, thermal and chemical stabilities for PEMFC/WE applications [5]. Yeom et al. [24] prepared very stable pure PVA membranes crosslinked with glutaraldehyde by immersing PVA films in acetone with different GA contents 5–50 vol% aqueous solution) using HCl as the catalyst. The membrane prepared with 5 vol% GA exhibited the best performance in the pervaporation separation of acetic acid water mixtures.

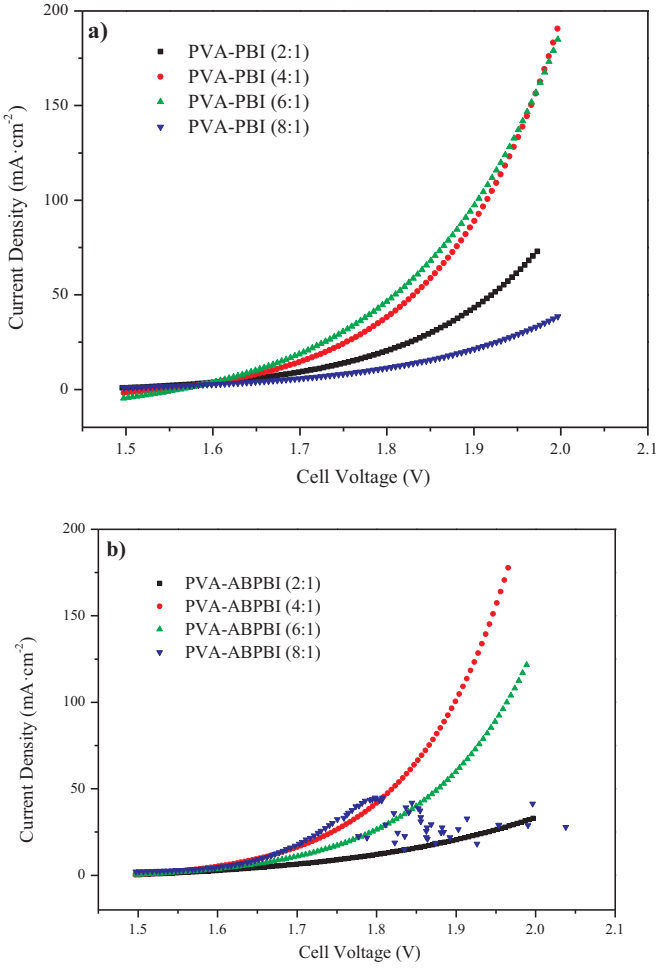

Fig. 2. LAWE load curves for membranes in 15 wt% KOH at 50 °C: **a)** L-PVA-PBI membrane performance between 2:1 and 8:1. **b)** L-PVA-ABPBI membranes performance between 2:1 and 8:1.

It is important to note that the crosslinking process that involves the reaction between GA molecules and hydroxyl pendant groups on the backbone of the PVA polymer can affect the hydrophilic nature of the membrane as well as hydroxyl transport in PVA-based anion conducting membranes.

The C-PVA-PBI 4:1 and C-PVA-ABPBI 4:1 crosslinked membranes were prepared, as described in Section 2.2, with a GA solution content ranging from 0.5 vol% to 50 vol%. Fig. 4a) and S1 show the IR spectra of the C-PVA-ABPBI 4:1 and C-PVA-PBI 4:1 membranes, respectively.

As observed for pure PVA membranes by Yeom and Lee [24], the IR spectra changed as the GA solution content increase as follows:

(i) A decrease in the absorbance of the peak at 3300–3400 cm^{-1} due to the loss of hydroxyl groups from PVA upon reaction with aldehydes (acetylation).
(ii) An increase in the absorbance peaks located at 1720, 2731 and 2866 cm^{-1}, which correspond to aldehyde groups. This change may be related to unreacted GA, which is unlikely due to the membranes being subjected to a several washing processes to remove residual GA. Therefore, this change must be related to monofunctional reactions of GA, where only one of the aldehyde groups of the GA molecule reacts with the PVA chain, and the other group remains unreacted and a pendant on the PVA chain. Yeom and Lee observed this effect in pure PVA membranes [24] and postulated that a monofunctional reaction is favoured when reduction in the chain mobility occurs due to the progress of the

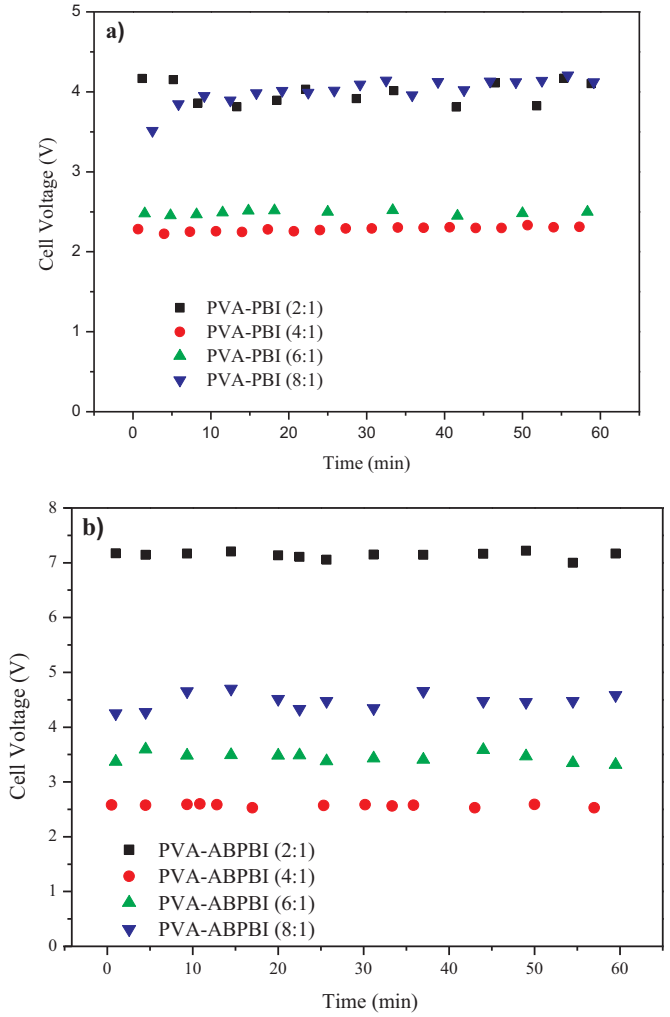

Fig. 3. Chronopotentiometric curves for membranes in 15 wt% KOH at 50 °C, i = 200 mA cm^{2}: **a)** L-PVA-ABPBI membranes and **b)** L-PVA-PBI membranes.

Table 1
Performance of laboratory electrolysis cell tested with different anion-exchange membranes with circulating 15 wt% KOH at 50 °C.

Membrane	Current density (mA cm^{-2}) at cell voltage 1.95 V	Cell voltage at 3500 s, applied current density = 200 mA cm^{-2}
L-PVA-PBI 2:1	60	4.0
L-PVA-PBI 4:1	140	2.3
L-PVA-PBI 6:1	140	2.5
L-PVA-PBI 8:1	30	4.0
L-PVA-ABPBI 2:1	30	7,1
L-PVA-ABPBI 4:1	160	2.5
L-PVA-ABPBI 6:1	80	3.4
L-PVA-ABPBI 8:1	40	4.5

bifunctional crosslinking reaction.

(iii) An increase in the absorbance peaks between 970 and 1385 cm^{-1} due to the formation of acetal carbon-oxygen bonds, which results from a reaction between hydroxyl and aldehyde groups: 2 aldehyde groups from GA with hydroxyl groups from PVA (bifunctional reaction involving crosslinking) or a monofunctional reaction.

An analysis of the IR spectra was carried out to identify the changes.

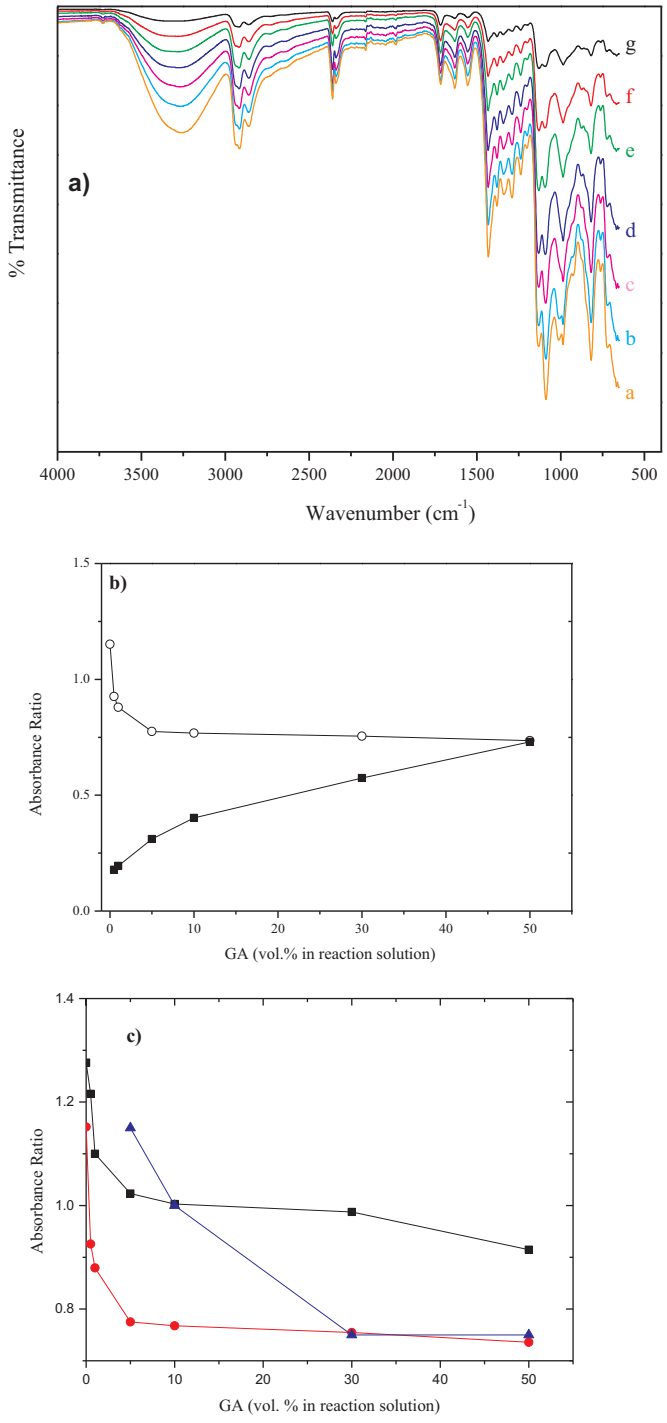

Fig. 4. a) IR spectra of C-PVA-ABPBI 4:1 membranes crosslinked in reaction solution with different GA solution contents: (a) 0 vol% GA, (b) 0.5 vol% GA, (c) 1 vol% GA, (d) 5 vol% GA, (e) 10 vol% GA, (f) 30 vol% GA and (g) 50 vol% GA. **b)** A_{3350}/A_{2940} and A_{1720}/A_{2940} absorbance ratios for (○) hydroxyl and (■) aldehyde groups, respectively, in C-PVA-ABPBI 4:1 membranes crosslinked in a reaction solution with different GA solution contents. **c)** A_{3350}/A_{2940} absorbance ratios for hydroxyl groups in (▲) pure PVA membrane [14], (■) C-PVA-PBI 4:1 membrane and (•) C-PVA-ABPBA 4:1 membrane.

The absorbance ratios of the functional groups with respect to a reference peak were determined (see Fig. 4c). Based on the strategy reported by Yeom and Lee [24], the methylene stretching band at 2940 cm^{-1} was used as the reference peak. The hydroxyl group located at 3350 cm^{-1} and the aldehyde group located at 1720 cm^{-1} were associated with the acetylation and monofunctional reaction of GA, respectively, with A_{3350}/A_{2940} and A_{1720}/A_{2940} absorbance ratios for

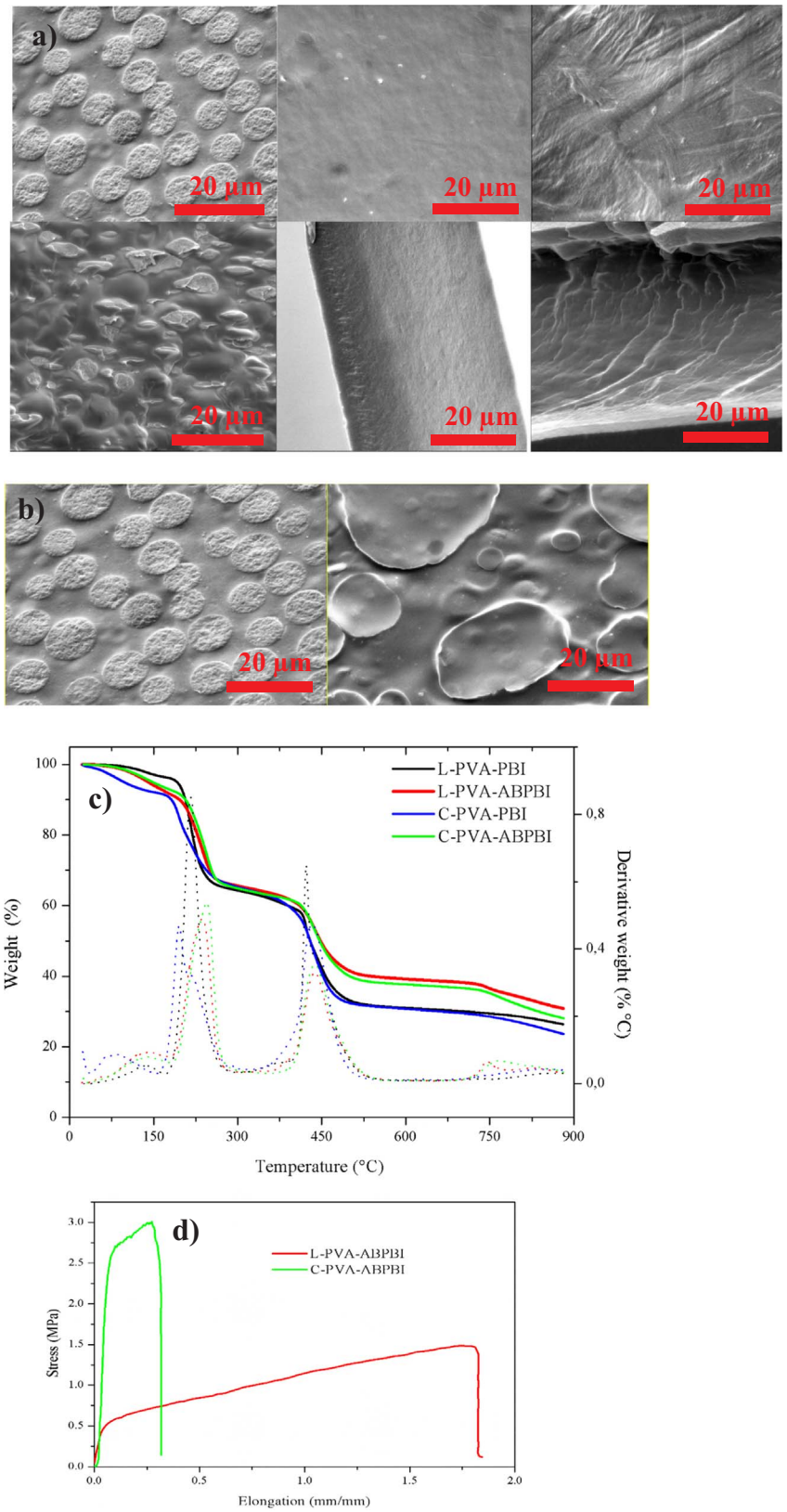

Fig. 5. a) SEM images of surface (upper) and cross-section area (down) from: L-PVA-PBI (left), PVA-ABPBI (centre) and C-PVA-ABPBI (0.5 vol% GA) (right) doped membranes. **b)** Surface SEM images of the L-PVA-PBI membranes as a function of immersion time in a 15 wt% KOH solution: 7 months (left) and 15 days (right). **c)** Thermograms and its normalized DTG derivatives for 15 wt% doped L-PVA-PBI, PVA-ABPBI, C-PVA-PBI (0.5 vol% GA) and C-PVA-ABPBI (0.5 vol% GA). d) Stress-strain curves of L-PVA-ABPBI and C-PVA-ABPBI (0.5 vol% GA) membranes.

the hydroxyl and aldehyde groups, respectively. The peaks assigned to the formation of acetal carbon-oxygen bonds were not selected due to base line issues.

The results in Fig. 4b) indicate that the absorbance ratio for the hydroxyl groups decreases with increasing GA concentration in the reaction solution (acetylation reaction). However, the absorbance ratio corresponding to the monofunctional reaction increases. The trends in the absorbance ratio for the hydroxyl groups in pure PVA, PVA-PBI and PVA-ABPBI membranes are shown in Fig. 4c. The PVA and PVA-ABPBI membranes exhibit a similar trend. Although A_{3350}/A_{2940} in the PVA membrane is higher than that in the PVA-ABPBI membrane, both ratios tend to have the same constant value at GA concentrations in the reaction solution higher than 30 vol%. The absorbance ratio for hydroxyl groups in the PVA-PBI membranes exhibits a different behaviour with the A_{3350}/A_{2940} values being considerably higher than those for the PVA and PVA-ABPBI membranes. This behaviour may be related to the polymer microstructure, which is more compact in the PVA-PBI membranes than in the PVA-ABPBI membranes. This microstructural difference between the PBI and ABPBI membranes has been previously reported [26], and the compact structure of PVA-PBI can hinder GA molecule access to hydroxide sites in PVA.

As shown in the C-PVA-ABPBI 4:1 membrane absorbance ratio curves, the primary change in the absorbance ratio occurs in the range up to 5 vol% GA in the reaction solution, and at the lower GA concentration in the reaction solution (0.5 vol%), a change in the A_{3350}/A_{2940} and A_{1720}/A_{2940} absorbance ratios with respect to the absorbance ratios for the linear PVA-ABPBI 4:1 membrane was observed. Although an increasing crosslinking grade can improve membrane stability, it involves compact structures and consumption of hydrophilic PVA pendant hydroxyl groups, and therefore, a conductivity loss is expected. In fact, the ionic conductivity measurements (Section 3.5) indicate that the best value was obtained for C-PVA-ABPBI (GA concentrations in reaction solutions ranged from 0.5 to 5 vol%) with 0.5 vol% GA, and C-PVA-PBI (IR spectra shown in Fig. S1) completely lost its conductivity even at this GA concentration.

The gel content test performed by immersion in a DMSO-EtOH 5:2, with 1 wt% NaOH, at 80 °C, showed that L-PVA-ABPBI membrane dissolved completely, while C-PVA-ABPBI (GA 0.5 vol%) had a gel fraction of 94% after 30 h (Fig. S2). Due to the crosslinking, the C-PVA-ABPBI (GA 0.5 vol%) membrane could not dissolve even after immersion during 30 h at 80 °C in a DMSO-EtOH solvent in which not crosslinked PVA-ABPBI membrane dissolves immediately.

Finally, because the imidazole/aldehyde reaction has been previously reported [25], we investigated the possible reaction between GA and benzimidazole by comparing the IR spectra of L-ABPBI and the same membrane subjected to the GA crosslinking procedure with 0.5 vol% GA in the reaction solution (i.e., C-ABPBI-GA 0.5 vol%). No differences in the IR spectra were observed (Fig. S3 and Table S1), indicating that no reaction occurred between GA and benzimidazole.

3.3. Chemical stability, surface morphology, mechanical and thermal properties

After immersion for 7 days in a 15 wt% KOH solution at 70 ºC, the L-PVA-PBI membranes with 2:1 and 8:1 compositions became fragile. When the KOH concentration was increased to 18 wt%, the L-PVA-PBI membranes (i.e., 4:1 and 6:1) exhibited the same brittle behaviour after 7 days at 70 ºC. The chemical stability of the C-PVA-PBI membrane was not measured in this study due to its low conductivity values. However, the brittle behaviour was not observed for the linear or (0.5 wt% GA) crosslinked PVA-ABPBI membranes even after immersion for 7 days in 30 wt% KOH at 70 ºC. Regarding pure membranes immersed in KOH solutions in the same conditions, L-ABPBI became fragile after immersion in KOH concentrations higher than 15 wt%; while L-PVA and C-PVA (0.5 wt% GA) didn't change, except for becoming a brownish colour, after immersion even in 30 wt% KOH.

The SEM images (Fig. 5a) show heterogeneities in the front and cross-section view of the L-PVA-PBI membrane, which may be due to a lack of miscibility between the polymers. In contrast, the linear and crosslinked PVA-ABPBI membranes displayed a homogeneous appearance. In Fig. 5b, the heterogeneities of the L-PVA-PBI membrane with different immersion times in 15 wt% KOH solution are compared. The rough aspect of the round-shaped areas on the membrane immersed for 15 days softened in the membrane aged by immersion for 7 month in this solution. This behaviour may be due to polymer loss, which could be evaluated using other methods.

The thermogram profiles (TG) of the L-PVA-PBI, L-PVA-ABPBI, C-PVA-PBI and C-PVA-ABPBI membranes (Fig. 5c) indicate weight loss in two temperature ranges (i.e., 180–280 °C and 380–518 °C). The derivative TG (DTG) peak at T higher than 300 °C is primarily due to thermal decomposition of the polymer backbone. The C-PVA-PBI membrane degrades at lower temperatures that any other membranes. In the DTG profile, the C-PVA-PBI membrane exhibits an onset peak at 100 °C, which his lower than that of C-PVA-ABPBI. It is interesting to note that the “two extreme” DTG behaviours of these two membranes coincide with C-PVA-PBI and C-PVA-ABPBI being the worst and best membranes with regards to conductivity, respectively. Therefore, the conductivity loss of the C-PVA-PBI membrane may be caused by degradation.

The water sorption peaks are typically observed at approximately 100 °C. Therefore, the first peak may be attributed to water sorption. The peak between 150 °C and 250 °C was not observed in pure ABPBI doped with KOH [18], which may be due to PVA decomposition.

The four membranes exhibited sufficient thermal stability for use under WE operating conditions (50–70 °C).

Samples of L-PVA-PBI and L-PVA-ABPBI (non-doped) were tested using DSC to assess the miscibility and compatibility of the systems. The data obtained from the analysis of the endothermic DSC curves, (see Fig. S4), indicated the first endothermic peak, assignable to PVA glass transition temperature (T_g) located at 32.3 °C and 40.7 °C respectively. These values are close to the pristine PVA (39.1 °C) in the same experimental conditions. The second endothermic peak at about 225 °C represents the phase transition temperature (T_m) which was the same than that of pure PVA.

We don’t locate any T_g coming from PBI or ABPBI, that should be located around 425–480 °C. We consider that the endothermic peaks located between 250 °C and 500 °C in Fig. S4 correspond to PVA decomposition. According to this measurement, L-PVA-PBI and L-PVA-ABPBI are heterogeneous blends, because a single Tg between both precursors polymers was not found.

Finally, the stress-strain curves in Fig. 5d demonstrate that the crosslinking of PVA in polymer blend PVA-polybenzimidazole system enhance the mechanical properties of the membrane. C-PVA-ABPBI (0.5 vol% GA) membrane exhibits a tensile stress of 3.0 MPa in contrast with the tensile stress of 1.5 MPa of L-PVA-ABPBI membrane. The elongation at break value of the crosslinked membrane reduces significantly compared with linear one (i.e., 30% and 180%, respectively).

3.4. Swelling, water sorption and KOH doping level

Table 2 shows the swelling results for membranes soaked for 7 days in 15 wt% KOH at 25 °C. The volume swelling varies between 80% and 95% for all studied membranes. However, a different thickness and length swelling behaviour was observed compared the PBI-based membranes (L-PVA-PBI 4:1 and C-PVA-PBI 4:1) and ABPBI based membranes (L-PVA-ABPBI 4:1 and C-PVA-ABPBI 4:1). The thickness of the PBI-based membranes increased 48–50%, and the thickness of ABPBI membranes increased by only 14–18% after doping in 15 wt% KOH. However, the length of the PBI-based membranes increased 6–9% compared to 25–27% for the ABPBI-based membranes. The anisotropic swelling behaviour in the PBI membranes (i.e., swelling ratio in the

Table 2
Swelling behaviour of 15 wt% KOH-doped membranes.

Membrane	Volume swelling/%	Thickness swelling/%	Length swelling/%
L-PVA-PBI 4:1	80 ± 5	48 ± 4	9 ± 1
L-PVA-ABPBI 4:1	83 ± 3	18 ± 7	25 ± 5
C-PVA-PBI 4:1–0.5 vol% GA	95 ± 11	50 ± 5	6 ± 3
C-PVA-ABPBI 4:1–0.5 vol% GA	84 ± 12	14 ± 8	27 ± 6

thickness direction larger than that in the length/width directions) was reported by Aili et al. [20] and Zeng et al. [19]. The excessive and perhaps uneven swelling experienced by linear and crosslinked PVA-PBI membranes is most likely due to the molecular structure of this membranes, which compromises its stability as demonstrated by the results in Section 3.3, and this behaviour could be reflected in the water electrolysis performance measurements. The effect of this characteristic will be evaluated below.

The increase in the volume after doping in the PVA-polybenzimidazole membranes was higher than that of pure polybenzimidazole membranes. Aili et al. [17] obtained a 64% volume increase in linear PBI. This value is comparable to the 50% increase reported by Diaz et al. [18] in L-ABPBI and C-ABPBI. The length and thickness increases were higher in the PBI membranes than in the L-ABPBI and C-ABPBI membranes (10% and 17% for thickness and length swelling, respectively [18]). However, this increase is still moderate, except for the increase in the thickness of the PBI-based membranes.

Considering that the anisotropic swelling observed (Table 2), can be disadvantageous during cell assembly, particularly the excessive swelling in area direction shown by L-PVA-ABPBI and C-PVA-ABPBI membranes, cell assembly tests were performed. At time zero, the membrane sample was extracted from the doping solution, placed between the two cell seals, and exposed to environmental conditions for one hour. During this time, the membrane had no contact with the KOH solution, simulating the cell assembly time interval. After 1 h, the membrane sample was immersed in the doping solution during 1.5 h, and then extracted, in order to check if it recover its initial state (t = 0). Images obtained at time zero, 10 min, 30 min, 45 min and 1 h and 2.5 h are shown at Fig. S5.

Fig. S5 shows that all the membranes keep their dimensions unaffected if the assembly period don't exceed 30 min. At 45 min it can be observed in all the membranes shrinking and swelling zones that will cause inadequate contact between membrane, seals and electrodes.

The KOH solution acts as a plasticizer, so, when the membrane is immersed again in the doping solution, it recovers its initial state. This means that if 30 min were not enough to complete the cell assembly, it is possible to recover the membrane by simple immersion in the doping solution.

The water and KOH uptake were determined for linear and crosslinked PVA-polybenzimidazole membranes after impregnation in KOH 15 wt%. The results are shown in Table 3 and Fig. 6.

In L-PVA-PBI and L-PVA-ABPBI, the water uptake was 50% and 69%, respectively. The same membranes crosslinked with GA 0.5% exhibited a decrease in the water uptake for C-PVA-PBI but not for C-PVA-ABPBI (see Fig. 6), which retains a water uptake 67%. The

Table 3
Polymer, water and KOH contents of 15 wt% KOH-doped membranes.

Membrane	Polymer/%	KOH/%	H_2O/%
L-PVA-PBI 4:1	49 ± 2	1 ± 0.5	50 ± 2
L-PVA-ABPBI 4:1	30 ± 7	1 ± 0.5	69 ± 7
C-PVA-PBI 4:1–0.5 vol% GA	73 ± 6	5 ± 0.5	22 ± 6
C-PVA-ABPBI 4:1–0.5 vol% GA	25 ± 4	8 ± 0.5	67 ± 4

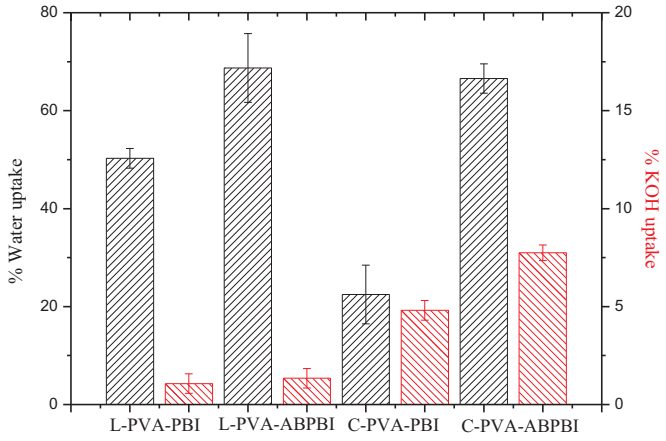

Fig. 6. Water (black) and KOH (red) uptake for the synthesized membranes. (For interpretation of the references to color in this figure legend, the reader is referred to the web version of this article).

reduction in the water uptake in the C-PVA-PBI membrane may be related to the sharp consumption of OH^- groups from PVA, as observed in Fig. 4b, which affects the hydrophilicity of the membrane as noted in Section 3.2.

The KOH uptake can be divided into two contributions as described by Hou [13]. The first contribution is related to the acid–base reaction between the acid sites of the polybenzimidazole membranes and KOH to afford potassium polybenzimidazolate salt and water, and the second contribution is related to KOH entering the membrane structure, which is responsible for the OH^- transport within the membrane. However, the order of the steps is not important because free KOH is available without completing the total reaction with the acidic sites of the polybenzimidazole membranes.

The low KOH content of the L-PVA-PBI 4:1 and L-PVA-ABPBI 4:1 linear membranes may be due to a calculation error. If polymer loss occurred during the doping stage, the calculated KOH uptake (based on the initial polymer weight) would be affected. However, the calculated water uptake (based on the weight difference between doped and dried membrane) would not be affected. This polymer loss may also be due to the structural change observed in the SEM analysis of the L-PVA-PBI membranes.

Differences were observed between the weight of de-doped, washed and dried samples and the weight of the initial dry sample (w_0); linear membranes (8–13 wt% loss) and crosslinked membranes (~1 wt% loss). As it was pointed out in Section 2.6, in order to determine if this loss occurs during doping, IR spectroscopy was employed using the conditions described in Section 2.6. Signals related to PVA were not observed. However, this is not enough to asses that no polymer loss occurs during doping. The absence of PVA signals can be due to limitations related with the detection limit of the IR spectroscopy equipment (10^{-6} mol l^{-1}) or degradation of PVA to lower molecular weight species with different absorption patterns.

Unfortunately, the amount of polymer loss that occurs during the doping stage and washing procedure cannot be distinguished.

3.5. Ionic conductivity (IC)

The ionic conductivities of linear and crosslinked PVA-PBI and PVA-ABPBI membranes doped in 15 wt% KOH in a temperature range from 25 °C to 90 °C are shown in Fig. 7a). The L-PVA-PBI and L-PVA-ABPBI membranes exhibit ionic conductivities of 40–70 mS cm^{-1}, and the conductivities of L-PVA-PBI were slightly higher than those of L-PVA-ABPBI, especially in the 60 and 90 °C range.

The C-PVA-PBI conductivities decreased to values less than 1 mS cm^{-1} at a 0.5 vol% GA concentration in the reaction solution. For the C-PVA-ABPBI membranes, the membranes crosslinked at 0.5 vol

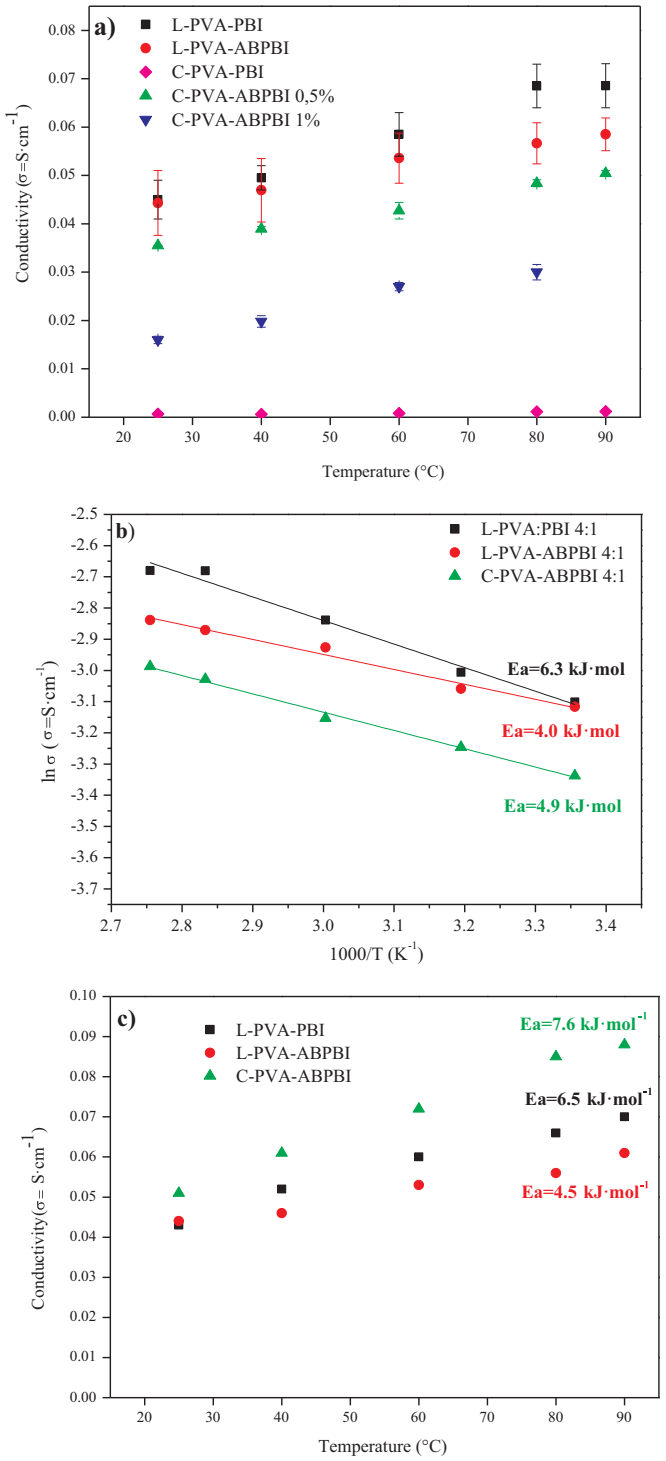

Fig. 7. a) Ionic conductivity of membranes doped in 15 wt% KOH: L-PVA-PBI; L-PVA-ABPBI; C-PVA-ABPBI (0.5 and 1 vol% GA) and C-PVA-PBI (0.5 vol% GA) **b)** Arrhenius plot for membranes doped in 15 wt% KOH: L-PVA-PBI; L-PVA-ABPBI and C-PVA-ABPBI (0.5 vol% GA) **c)** Ionic conductivity of membranes doped in 30 wt% KOH: L-PVA-PBI, L-PVA-ABPBI and C-PVA-ABPBI (0.5 vol% GA).

% GA exhibited conductivities ranging from 25 to 55 mS cm^{-1}, and these values are only slightly lower than those of L-PVA-ABPBI. In addition, the conductivity in membranes crosslinked at 1 vol% GA decreased. The C-PVA-PBI membranes and C-PVA-ABPBI membranes crosslinked at GA concentration higher than 0.5 vol% in the reaction solution exhibited an unacceptable ionic conductivity for the application considered in this study and are not further characterized. C-PVA-ABPBI 4:1 crosslinked with at 0.5 vol% GA are referred to as C-PVA-ABPBI in subsequent sections.

The ionic conductivity of all PVA-polybenzimidazole membranes significantly increased with increasing temperature (25–90 °C) due to the increased mobility of the OH^- species within the polymeric membrane. The ionic conductivity was due to the KOH included in the membranes. The transport mechanism in the anion-exchange membranes is dependent on the relative humidity and temperature similar to the proton transport in Nafion® membranes [27,28]. In the Grotthuss mechanism, diffusion and convection are considered dominant transport mechanisms for OH^- transport through the membrane [5,29]. OH^- can diffuse via the hydrogen-bonded network of water molecules and the formation/dissociation of covalent bonds combined with a diffusion/migration transport process (vehicular mechanism). Insights into the activation energy of the OH^- conduction process can be extracted from the relationship between the conductivity (σ) and temperature by fitting the data to the Arrhenius expression (2):

$$\sigma = \sigma_0 \exp\left(-\frac{E_a}{RT}\right) \quad (2)$$

where E_a is the activation energy for electrical conduction, σ_0 is the maximum electrical conductivity (supposed at infinite temperature), and R is the gas constant.

The studied membranes exhibited similar relationships between the temperature and conductivity (see Fig. 7b), which indicated similar ionic conduction mechanisms. A linear relationship was obtained for the plot of ln conductivity as a function of the inverse temperature. The activation energies for the L-PVA-ABPBI, L-PVA-PBI and C- PVA-ABPBI membranes are 6.3, 4.0 and 4.9 kJ mol^{-1}, respectively, which fall in the range of values that have been obtained for other alkaline membranes. Therefore, the crosslinked PVA/poly(diallyldimethylammonium chloride) membranes that were pre-treated with 1 mol l^{-1} KOH have E_a values of 8–10 kJ mol^{-1} [30], and the PVA/sodium alginate membranes treated with 40 wt% KOH have 7–40 kJ mol^{-1} [31]. However, other alkaline membranes including the PBI membranes impregnated in 4 mol l^{-1} KOH (22–23 kJ mol^{-1}) [32] and ABPBI membranes doped in 1 mol l^{-1} NaOH (13.6–14.2 kJ mol^{-1}) [33] possess higher E_a values.

In agreement with the determined E_a values, several OH^- mechanisms for hydroxyl transport, such as the Grotthuss mechanism, surface site hopping, diffusion and convention via permeation and osmotic drag, may occur. The obtained activation energies were similar for all PVA-polybenzimidazole membranes, even the crosslinked ones. This result indicates that the crosslinking process does not affect the mechanism of hydroxyl transport within the membranes. Finally, all membranes exhibited conductivity values higher than 10^{-2} S cm^{-1}, which is considered the limit for an acceptable polymer electrolyte membrane [31].

In addition, the ionic conductivity (IC) results for L-PVA-PBI, L-PVA-ABPBI and C-PVA-ABPBI doped in 30 wt% KOH are shown in Fig. 7c. The ICs values for the C-PVA-ABPBI membranes are higher than those of the linear PVA-PBI and PVA-ABPBI membranes, which may be due to improved resistance of the crosslinked membranes to chemical degradation compared to that of the linear ones. In addition, a particular molecular structure may allow for a higher KOH penetration capacity in the polymer matrix. The comparison between the conductivity values of C-PVA-PBI doped in 15 or 30 wt% KOH indicates that a higher KOH concentration results in a higher conductivity value. This result may be due to this membrane not being completely doped in the 15 wt% KOH solution.

The ionic conductivities measured in this study at temperatures near 90 °C with a 30 wt% KOH doping solution were similar to those of linear (90 mS cm^{-1}) and crosslinked (60 mS cm^{-1}) PBI membranes measured by Aili et al. [17] and Jheng et al. [34], who reported exhibit ionic conductivity values of 96 mS cm^{-1} for linear PBI under the same conditions. Furthermore, our crosslinked membranes doped at ≈15 wt

% KOH exhibited IC values higher than that reported by Jheng et al. [34] for L-PBI doped at the same KOH concentration.

When doped in 15 wt% KOH, crosslinked membranes exhibited a lower conductivity than linear membranes. Their structures most likely allow for less OH^- mobility. In the C-PVA-PBI membranes, the substantial decrease in the conductivity may be due to the large decrease in water uptake that is related to the compact microstructure of this membrane as well as the consumption of pendant OH^- from PVA, which enhances the hydrophilicity as mentioned in Section 3.2. Water molecules facilitate the Grotthuss mechanism. According to Merle et al. [5], the assumption that the Grotthuss mechanism is primarily responsible for hydroxide transport through the AEM is supported by the Grotthuss behaviour exhibited by hydroxide in aqueous solutions (i.e., OH^- diffuses through the H-bonded network of H_2O molecules through the formation/cleavage of covalent bonds). When doped in 30 wt% KOH, the C-PVA-ABPBI membrane exhibited the best conductivity, which is most likely related to the increase in the KOH uptake.

3.6. Alkaline water electrolysis

The experiment was performed by testing the PVA-polybenzimidazole membranes under LAWE conditions. A single-cell electrolyser with a zero gap configuration, as described in Section 2.3, was fed with a 15 wt% KOH aqueous solution at 50 °C and 70 °C. The I/E polarization curves obtained for the L-PVA-PBI, L-PVA-ABPBI and C-PVA-ABPBI membranes are shown in Fig. 8a). In a previous study [18], we demonstrated that the WE short-term performance of our linear and benzoxazine-crosslinked ABPBI membranes was better than that of the commercial Zirfon diaphragm under the applied conditions. The best performance was observed for C-ABPBI operating with 15 wt% KOH at 70 °C, and this performance is comparable to that of industrial units, which are typically operated with 6–7 M KOH and 80–90 °C.

The results in Table 4 indicate that the performance of the L-PVA-PBI membranes is similar to those of the L-ABPBI and C-ABPBI membranes, and the performance of L-PVA-ABPBI and C-PVA-ABPBI was superior to that of ABPBI (2–3 M KOH, 50 °C) [18]. These results are in agreement with the conductivity results shown in Fig. 7a.

The performance of C-PVA-ABPBI is superior to that of the commercial porous Zirfon® diaphragm, 2.5 times higher than that of the C-ABPBI membranes (3 M KOH, 70 °C) and comparable to industrial units (6–7 M KOH, 80–90 °C) [18]. Furthermore, the performance of all the studied PVA-polybenzimidazole membranes at 15 wt% KOH and 50 °C was superior to that of the Zirfon® diaphragm tested using the typical conditions for LAWE commercial units (30 wt%, 80 °C) [21], which is a very important result. A membrane that allows us to achieve LAWE performances under mild conditions comparable to that of LAWE units with concentrated KOH at high temperatures is advantageous for preventing material corrosion and maintaining long-term membrane stability, as highlighted by Aili et al. [35]. This group demonstrated that L-PBI is stable for up to 200 days in 5 wt% KOH at 88 °C but degrades at higher KOH concentrations.

As expected, the PVA-polybenzimidazole membrane performance improved by increasing the electrolyser operational temperature to 70 °C. In Fig. 8a), the C-PVA-ABPBI throughput significantly improved and reached values of 360 mA cm^{-2} at 1.9 V, even at 15 wt% KOH. To the best of our knowledge, this is currently the most promising result for a zero gap electrolyser. The measurement equipment has a safety current limit of 500 mA cm^{-2}. Therefore, the electric current cuts off at this limit.

Finally, the chronopotentiometric curves for the L-PVA-PBI, L-PVA-ABPBI and C-PVA-ABPBI membranes (15 wt% KOH, 50 °C and 70 °C, i = 200 mA cm^{-2}) are shown in Fig. 8b. The results are consistent with the performance exhibited by the linear sweep voltammetry curves (Fig. 8a), and the best outcomes were achieved by the C-PVA-ABPBI membrane at both working temperatures. In addition, the L-PVA-PBI membrane requires an additional 20 °C to achieve the same perfor-

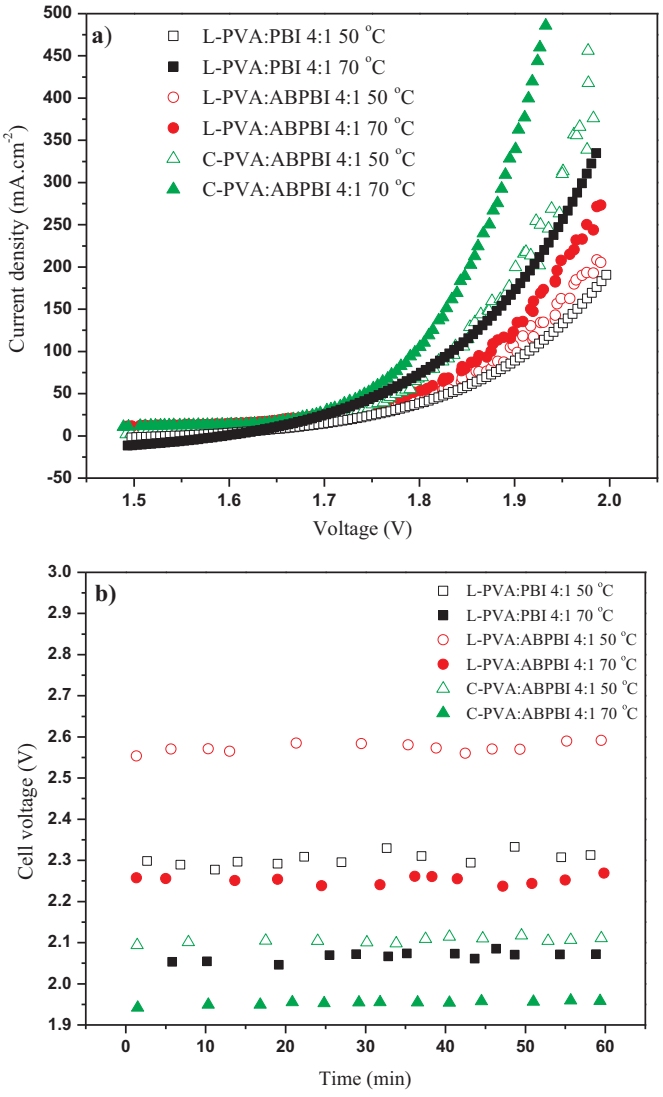

Fig. 8. a) LAWE load curves for membranes in 15 wt% KOH at 50 °C and 70 °C: L-PVA-PBI 4:1; L-PVA-ABPBI 4:1 and C-PVA-ABPBI (0.5 vol% GA) 4:1. **b)** Chronopotentiometric curves for membranes in 15 wt% KOH at 50 °C and 70 °C, i = 200 mA cm^{-2}: L-PVA-PBI 4:1; L-PVA-ABPBI 4:1 and C-PVA-ABPBI (0.5 vol% GA) 4:1.

Table 4
Performance of laboratory electrolysis cell tested with circulating 15 wt% KOH and different anion-exchange membranes.

Membrane	Temperature (°C)	Current density (mA cm^{-2}) at cell voltage 2 V
L-PVA-PBI 4:1	50	180
L-PVA-ABPBI 4:1	50	220
C-PVA-ABPBI 4:1	**50**	**450**[a]
L-PVA-PBI 4:1	70	430[a]
L-PVA-ABPBI 4:1	70	290
C-PVA-ABPBI 4:1	**70**	**900**[a]
Zirfon® [18]	50	140
Zirfon® [21]	80	~160[b]
L-ABPBI [18]	50	180
C-ABPBI [18]	50	160
L-ABPBI [18]	70	280
C-ABPBI [18]	70	335

[a] Extrapolated value.
[b] 30 wt% KOH.

mance as that of C-PVA-ABPBI at 50 °C.

4. Conclusions

PVA: polybenzimidazole membranes (i.e., PVA-PBI and PVA-ABPBI) with compositions varying from 2:1 to 8:1 were prepared and tested in an alkaline water electrolysis cell. Membranes with a PVA: polybenzimidazole ratio of 4:1 exhibited the best electrochemical performance.

To improve the membrane stability, PVA in the membranes was crosslinked by immersion in acetone solutions with various glutaraldehyde compositions. Membranes crosslinked by immersion in a reaction solution containing GA > 0.5 vol% exhibited conductivities that were lower than 1 mS cm^{-1}, and therefore, only membranes crosslinked with GA = 0.5 vol% were considered in this study.

Ionic conductivities up to 75 mS cm^{-1} at 90 °C were achieved by linear PVA-PBI and PVA-ABPBI membranes doped in 15 wt% KOH, and crosslinked PVA-ABPBI membranes exhibited ionic conductivities up to 55 mS cm^{-1} at the same temperature and doping concentration. C-PVA-PBI membranes exhibited conductivities lower than 1 mS cm^{-1}. C-PVA-ABPBI membranes exhibited high ionic conductivities (90 mS cm^{-1}) at 90 °C when doped with 30 wt% KOH, which is similar to that of linear PBI membranes [17,34].

All membranes exhibited a similar behaviour for water and KOH uptake, except for the thickness increase in PBI-based membranes. The thermooxidative stability of the linear and crosslinked membranes was satisfactory, with a decomposition temperature between 300 and 400 °C.

The short-term WE performances of L-PVA-PBI, L-PVA-ABPBI and C-PVA-ABPBI were better than that of a standard Zirfon membrane separator. C-PVA-ABPBI exhibited the best performance at 70 °C and 15 wt% KOH. This result is comparable to that of industrial units operating at KOH concentrations of 6–7 M and 80–90 °C.

Electrolysis cells that work at low KOH concentrations and temperatures are advantageous to ensure the long-term stability of materials in the final application. The durability of PVA-polybenzimidazole membranes under LAWE conditions will be further studied in the future.

Acknowledgments

This work was supported by Centro de Estudios de America Latina (UAM-Banco de Santander) under the project CEAL-AL/2015-24, the Madrid Regional Research Council (CAM) [RESTOENE-2 grant n. S2013/MAE2882] and the Spanish Economy and Competitiveness Ministry. ENE2016-77055-C3-1-R. Author wish to thank Andres Ceriotti for his help in interpreting IR spectra.

Appendix A. Supplementary material

Supplementary data associated with this article can be found in the online version at http://dx.doi.org/10.1016/j.memsci.2017.04.021.

References

[1] M. Paidar, V. Fateev, K. Bouzek, Membrane electrolysis—history, current status and perspective, Electrochim. Acta 209 (2016) 737–756.
[2] M. Wang, Z. Wang, X. Gong, Z. Guo, The intensification technologies to water electrolysis for hydrogen production – a review, Renew. Sustain. Energy Rev. 29 (2014) 573–588.
[3] K. Zeng, D. Zhang, Recent progress in alkaline water electrolysis for hydrogen production and applications, Prog. Energy Combust. Sci. 36 (2010) 307–326.
[4] D. Pletcher, X. Li, Prospects for alkaline zero gap water electrolysers for hydrogen production, Int. J. Hydrog. Energy 36 (2011) 15089–15104.
[5] G. Merle, M. Wessling, K. Nijmeijer, Anion exchange membranes for alkaline fuel cells: a review, J. Memb. Sci. 377 (2011) 1–35.
[6] G.C. Abuin, P. Nonjola, E.A. Franceschini, F.H. Izraelevitch, M.K. Mathe, H.R. Corti, Characterization of an anionic-exchange membranes for direct methanol alkaline fuel cells, Int. J. Hydrog. Energy 35 (2010) 5849–5854.
[7] J. Hnát, M. Paidar, J. Schauer, J. Žitka, K. Bouzek, Polymer anion selective membranes for electrolytic splitting of water. Part I: stability of ion-exchange groups and impact of the polymer binder, J. Appl. Electrochem. 41 (2011) 1043.
[8] J. Hnát, M. Paidar, J. Schauer, J. Žitka, K. Bouzek, Polymer anion-selective membranes for electrolytic splitting of water. Part II: enhancement of ionic conductivity and performance under conditions of alkaline water electrolysis, J. Appl. Electrochem. 42 (2012) 545–554.
[9] K.-D. Kreuer (Ed.), Fuel Cells: Selected Entries from the Encyclopedia of Sustainability Science and Technology, Springer Science + Business Media, New York, 2013.
[10] J. Lobato, P. Cañizares, M.A. Rodrigo, J.J. Linares, G. Manjavacas, Synthesis and characterisation of poly[2,2-(m-phenylene)-5,5-bibenzimidazole] as polymer electrolyte membrane for high temperature PEMFCs, J. Memb. Sci. 280 (2006) 351–362.
[11] L.A. Diaz, G.C. Abuin, H.R. Corti, Methanol sorption and permeability in Nafion and acid-doped PBI and ABPBI membranes, J. Memb. Sci. 411 (2012) 35–44.
[12] B. Xing, O. Savadogo, Hydrogen/oxygen polymer electrolyte membrane fuel cells (PEMFCs) based on alkaline-doped polybenzimidazole (PBI), Electrochem. Commun. 2 (2000) 697–702.
[13] H. Hou, G. Sun, R. He, Z. Wu, B. Sun, Alkali doped polybenzimidazole membrane for high performance alkaline direct ethanol fuel cell, J. Power Sources 182 (2008) 95–99.
[14] A.D. Modestov, M.R. Tarasevich, A.Y. Leykin, V.Y. Filimonov, MEA for alkaline direct ethanol fuel cell with alkali doped PBI membrane and non-platinum electrodes, J. Power Sources 188 (2009) 502–506.
[15] L. Osmieri, R. Escudero-Cid, A.H.A. Monteverde Videla, P. Ocón, S. Specchia, Performance of a Fe-N-C catalyst for the oxygen reduction reaction in direct methanol fuel cell: cathode formulation optimization and short-term durability, Appl. Catal. B Environ. 201 (2017) 253–265.
[16] L. Zeng, T.S. Zhao, L. An, G. Zhao, X.H. Yan, A high-performance sandwiched-porous polybenzimidazole membrane with enhanced alkaline retention for anion exchange membrane fuel cells, Energy Environ. Sci. 8 (2015) 2768–2774.
[17] D. Aili, M.K. Hansen, R.F. Renzaho, Q. Li, E. Christensen, J.O. Jensen, N.J. Bjerrum, Heterogeneous anion conducting membranes based on linear and crosslinked KOH doped polybenzimidazole for alkaline water electrolysis, J. Memb. Sci. 447 (2013) 424–432.
[18] L.A. Diaz, J. Hnát, N. Heredia, M.M. Bruno, F.A. Viva, M. Paidar, H.R. Corti, K. Bouzek, G.C. Abuin, Alkali doped poly (2,5-benzimidazole) membrane for alkaline water electrolysis: characterization and performance, J. Power Sources 312 (2016) 128–136.
[19] L. Zeng, T.S. Zhao, L. An, G. Zhao, X.H. Yan, Physicochemical properties of alkaline doped polybenzimidazole membranes for anion exchange membrane fuel cells, J. Memb. Sci. 493 (2015) 340–348.
[20] D. Aili, K. Jankova, J. Han, N.J. Bjerrum, J.O. Jensen, Q. Li, Understanding ternary poly(potassium benzimidazolide)-based polymer electrolytes, Polymer 84 (2016) 304–310.
[21] M.R. Kraglund, D. Aili, K. Jankova, E. Christensen, Q. Li, J.O. Jensen, Zero-gap alkaline water electrolysis using ion-solvating polymer electrolyte membranes at reduced KOH concentrations, J. Electrochem. Soc. 163 (2016) F3125–F3131.
[22] C.-C. Yang, S.-J. Lin, Preparation of composite alkaline polymer electrolyte, Mater. Lett. 57 (2002) 873–881.
[23] S. Li, J.R. Fried, J. Colebrook, J. Burkhardt, Molecular simulations of neat, hydrated, and phosphoric acid-doped polybenzimidazoles. Part 1: poly(2,2′-m-phenylene-5,5′-bibenzimidazole) (PBI), poly(2,5-benzimidazole) (ABPBI), and poly (*p*-phenylene benzobisimidazole) (PBDI), Polymer 51 (2010) 5640–5648.
[24] C.-K. Yeom, K.-H. Lee, Pervaporation separation of water-acetic acid mixtures through poly(vinyl alcohol) membranes crosslinked with glutaraldehyde, J. Memb. Sci. 109 (1996) 257–265.
[25] M. Schnopp, G. Haberhauer, Highly selective recognition of α-chiral primary organoammonium ions by C_3 -symmetric peptide receptors, Eur. J. Org. Chem. 2009 (2009) 4458–4467.
[26] L.A. Diaz, G.C. Abuin, H.R. Corti, Water and phosphoric acid uptake of poly [2,5-benzimidazole] (ABPBI) membranes prepared by low and high temperature casting, J. Power Sources 188 (2009) 45–50.
[27] E.G. & G.S. (Firm), N.E.T.L. (U.S.), Fuel cell handbook [electronic resource]/EG & G Technical Services, Inc., 7th ed., U.S. Dept. of Energy, Office of Fossil Energy, National Energy Technology Laboratory Morgantown, WV, 2004.
[28] F. Barbir, PEM fuel cells : theory and practice, Elsevier Academic, 2005.
[29] K.N. Grew, W.K.S. Chiu, A. Dusty Fluid, Model for predicting hydroxyl anion conductivity in alkaline anion exchange membranes, J. Electrochem. Soc. 157 (2010) B327–B337.
[30] A. Ilie, M. Simoes, S. Baranton, C. Coutanceau, S. Martemianov, Influence of operational parameters and of catalytic materials on electrical performance of direct glycerol solid alkaline membrane fuel cells, J. Power Sources 196 (2011) 4965–4971.
[31] M. Mamlouk, P. Ocon, K. Scott, Preparation and characterization of polybenzimidzaole/diethylamine hydrogen sulphate for medium temperature proton exchange membrane fuel cells, J. Power Sources 245 (2014) 915–926.
[32] R.N. Couto, J.J. Linares, KOH-doped polybenzimidazole for alkaline direct glycerol fuel cells, J. Memb. Sci. 486 (2015) 239–247.
[33] H. Luo, G. Vaivars, B. Agboola, Shichun Mu, M. Mathe, Anion exchange membrane based on alkali doped poly(2,5-benzimidazole) for fuel cell, Solid State Ion. 208 (2012) 52–55.
[34] L. Jheng, S.L. Hsu, B. Lin, Y. Hsu, Quaternized polybenzimidazoles with imidazolium cation moieties for anion exchange membrane fuel cells, J. Memb. Sci. 460 (2014) 160–170.
[35] D. Aili, K. Jankova, Q. Li, N.J. Bjerrum, J.O. Jensen, The stability of poly(2,2′-(m-phenylene)-5,5′-bibenzimidazole) membranes in aqueous potassium hydroxide, J. Memb. Sci. 492 (2015) 422–429.

Supporting information for

Alkali doped polyvinyl alcohol – polybenzimidazole membranes for alkaline water electrolysis

L. A. Diaz[a], R. E. Coppola[a], G. C. Abuin[a,*], R. Escudero-Cid[b], D. Herranz[b], P. Ocón[b]

[a]Instituto Nacional de Tecnología Industrial (INTI), Centro de Procesos Superficiales, Av. General Paz 5445, B1650KNA, San Martín, Buenos Aires, Argentina.

[b]Universidad Autónoma de Madrid, Departamento de Química Física Aplicada, C/Francisco Tomás y Valiente 7, 28049, Madrid, Spain UAM

Correspondence should be addressed to:

E-mail: gabuin@inti.gob.ar

3.2 Preparation of crosslinked PVA-polybenzimidazole membranes. IR spectra analysis.

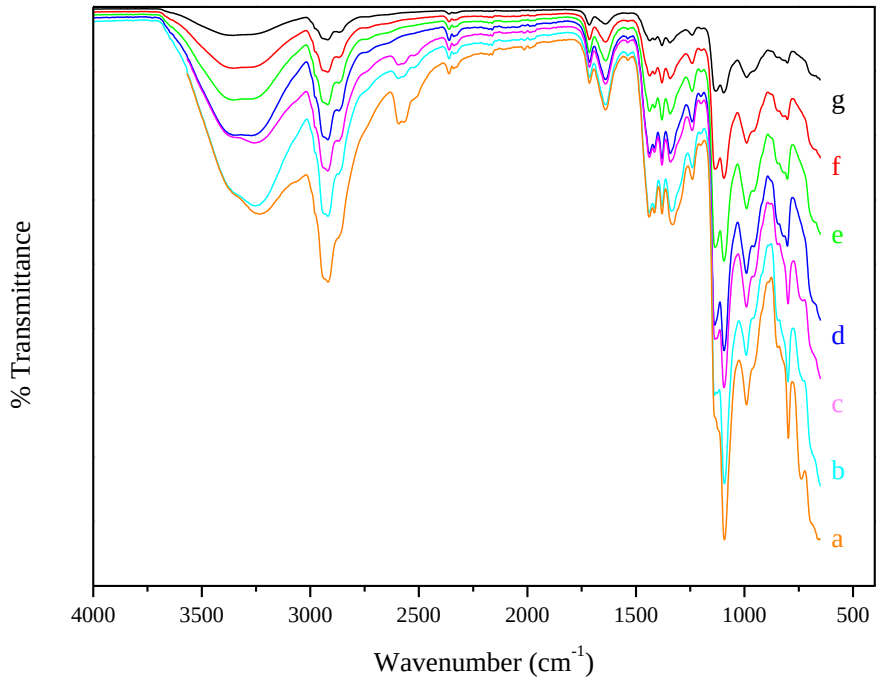

Figure S1: IR spectra of C-PVA-PBI 4:1 membranes crosslinked at different GA solution content in reaction solution. (a) 0 vol. % GA; (b) 0.5 vol. % GA; (c) 1 vol. % GA; (d) 5 vol. % GA; (e) 10 vol. % GA; (f) 30 vol. % GA and (g) 50 vol. % GA.

The IR spectra from C-PVA-PBI membranes shown at Fig. S1 are similar to that from C-PVA-ABPBI shown at Fig. 4 a). IR spectra, with increasing GA solution content, show the following changes.

(i) A decrease in the absorbance of the peak at 3300 - 3400 cm^{-1} due to the loss of the hydroxyl groups from PVA upon reaction with aldehydes (acetylation).

(ii) An increase in the absorbance peaks located at 1720, 2731 and 2866 cm^{-1} related with aldehyde groups.

iii) An increase in the absorbance peaks between 970 and 1385 cm^{-1} assignable to the formation of acetal carbon-oxygen bonds from reaction between hydroxyl and aldehyde groups, may be from 2 aldehyde groups from GA with hydroxyl groups from PVA (bi-functional reaction involving crosslinking), or mono-functional reaction.

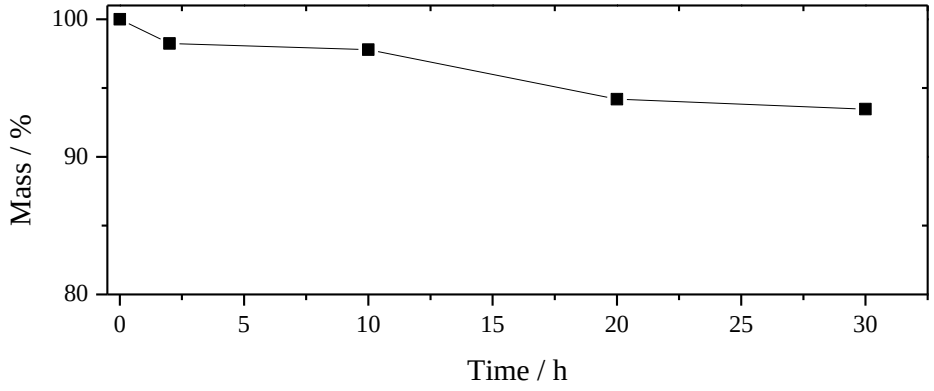

Figure S2: gel fraction of C-PVA-ABPBI-GA 0.5 vol. %

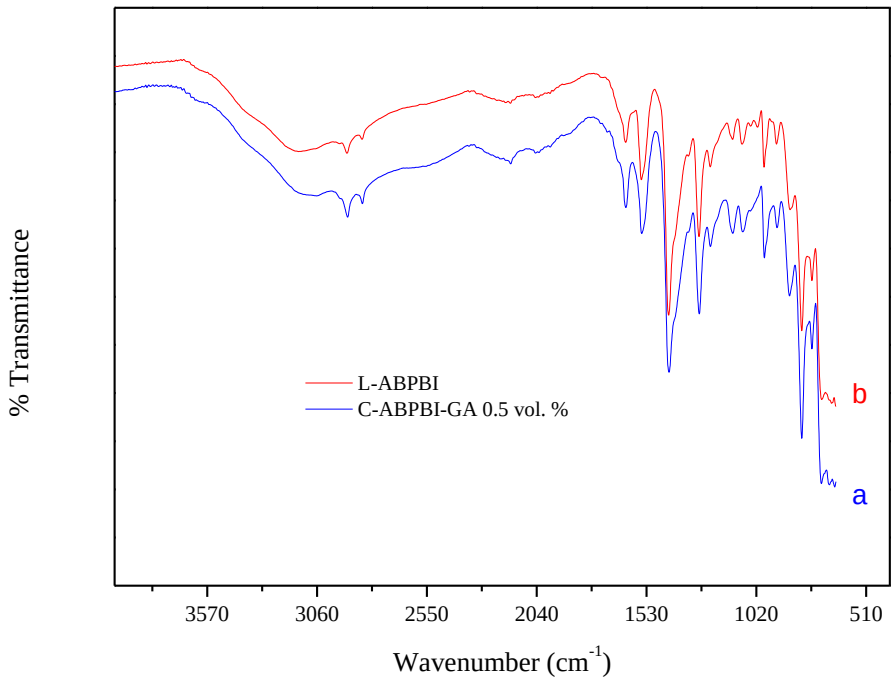

Figure S3: IR spectra of L-ABPBI and C-ABPBI-GA 0.5 vol. %

The IR spectra (whose bands are described in Table S1) show no difference between L-ABPBI and C-ABPBI-GA 0.5 vol. %, so we conclude that there is no reaction between benzimidazole and GA.

Table S1: Infrared Spectra of Polybenzimidazoles [S1].

ABPBI pristine Wevenumber (cm^{-1})	
3360	Free non-hydrogen-bonded N-H stretching.
3120	Associated N-H stretching.
1626	C=C/C=N stretching.
1546	Ring-vibration characteristic of conjugation between benzene and imidazole rings.
1423	In plane deformation of benzimidale rings.
1398	
1284	Breathing mode of the imidazole ring.
1234	In plane C-H deformation.
805	Out-of-plane C-H bending of the benzene rings.

[S1] J.A. Asensio, S. Borrós, P. Gómez- Romero, Proton-Conducting Polymers Based on Benzimidazoles and Sulfonated Benzimidazoles, Journal of Polymer Science: Part A: Polymer Chemistry, Vol. 40, 3703–3710 (2002)

3.3 Chemical stability, surface morphology, mechanical and thermal properties

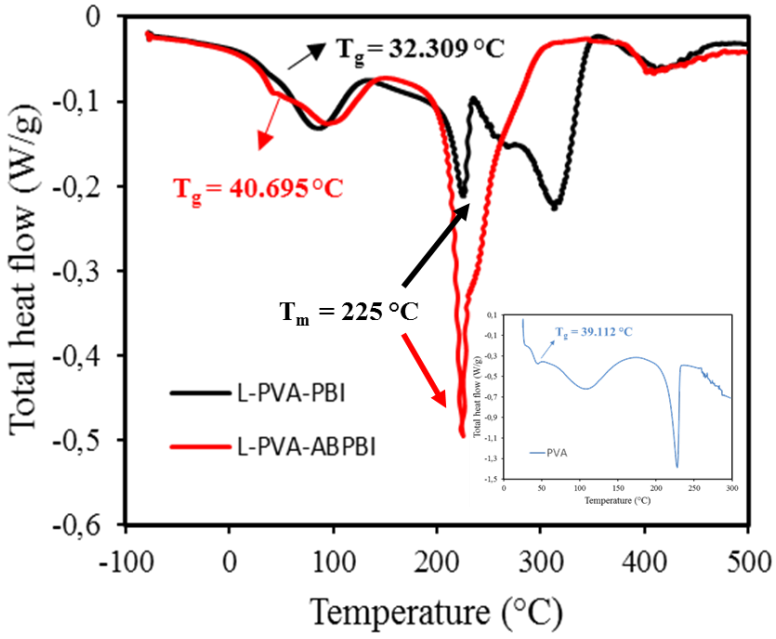

Figure S4: DSC of the L-PVA-PBI, L-PVA-ABPBI and pristine PVA membranes with their glass and melting transition.

3.4 Swelling, water sorption and KOH doping level

Considering that the anisotropic swelling observed (Table 2), can be disadvantageous during cell assembly, particularly the excessive swelling in area direction shown by L-PVA-ABPBI and C-PVA-ABPBI membranes, cell assembly tests were performed.

Table 2: Swelling behavior of 15 wt. % KOH doped membranes.

Membrane	Volume swelling / %	Thickness swelling / %	Length swelling / %
L-PVA-PBI 4:1	80 ± 5	48 ± 4	9 ± 1
L-PVA-ABPBI 4:1	83 ± 3	18 ± 7	25 ± 5
C-PVA-PBI 4:1 - 0.5 vol. % GA	95 ± 11	50 ± 5	6 ± 3
C-PVA-ABPBI 4:1 - 0.5 vol. % GA	84 ± 12	14 ± 8	27 ± 6

Several pictures were taken to evaluate the effect of the asymmetric swelling ratio in the length/width direction of alkaline doped L-PVA-ABPBI, C-PVA-ABPBI and L-PVA-PBI membranes at the cell assembly period.

Assembly test: at time zero, the membrane sample was extracted from the doping solution, placed between the two cell seals, and exposed to environmental conditions for one hour. During this time, the membrane had no contact with the KOH solution, simulating the cell assembly time interval. After 1 h, the membrane sample was immersed in the doping solution during 1.5 h, and then extracted, in order to check if it recover its initial state (t = 0). Images obtained at time zero, 10 min, 30 min, 45 min and 1 h and 2.5 h are shown at Figure S3.

Figure S3 shows that all the membranes keep their dimensions unaffected if the assembly period don’t exceed 30 min. At 45 min it can be observed in all the membranes shrinking and swelling zones that will cause inadequate contact between membrane, seals and electrodes.

The KOH solution acts as a plasticizer, so, when the membrane is immersed again in the doping solution, it recovers its initial state. This means that if 30 min were not enough to complete the cell assembly, it is possible to recover the membrane by simple immersion in the doping solution.

L-PVA-ABPBI

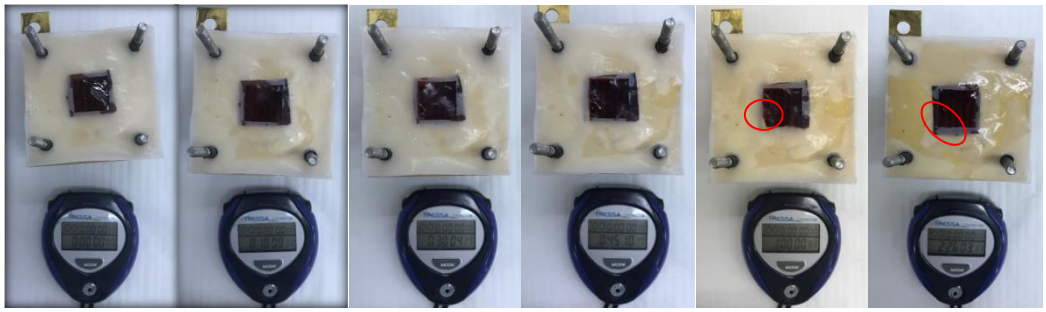

C-PVA-ABPBI

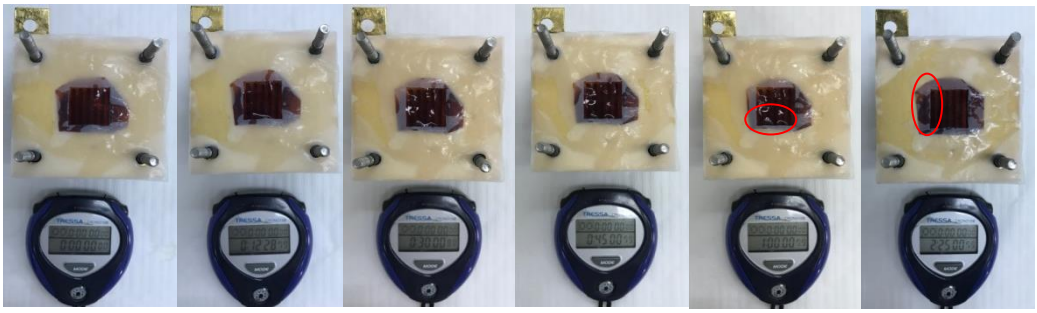

L-PVA-PBI

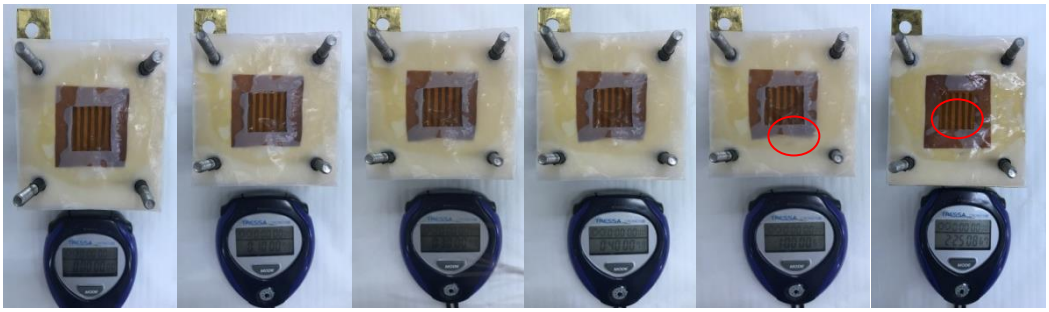

Figure S5: Cell assembly tests, from left to right: t = 0, t = 10 min, t = 30 min, t = 45 min, t = 1 h and t = 2.5 h

Journal of Materials Chemistry A

PAPER

View Article Online
View Journal

Cite this: DOI: 10.1039/c8ta08309f

ETFE-based anion-exchange membrane ionomer powders for alkaline membrane fuel cells: a first performance comparison of head-group chemistry†

Ana Laura Gonçalves Biancolli, [ad] Daniel Herranz, [cd] Lianqin Wang, [d] Gabriela Stehlíková, [ed] Rachida Bance-Soualhi, [d] Julia Ponce-González, [d] Pilar Ocón, [c] Edson A. Ticianelli, [a] Daniel K. Whelligan, [d] John R. Varcoe *[d] and Elisabete I. Santiago [bd]

In the last few years, the development of radiation-grafted powder-form anion-exchange ionomers (AEI), used in combination with anion-exchange membranes (AEM), has led to the assembly of AEM-based fuel cells (AEMFC) that routinely yield power densities ranging between 1–2 W cm^{-2} (with a variety of catalysts). However, to date, only benzyltrimethylammonium-type powder AEIs have been evaluated in AEMFCs. This study presents an initial evaluation of the relative AEMFC power outputs when using a combination of ETFE-based radiation-grafted AEMs and AEIs containing three different head-group chemistries: benzyltrimethylammonium (TMA), benzyl-*N*-methylpyrrolidinium (MPY), and benzyl-*N*-methylpiperidinium (MPRD). The results from this study strongly suggest that future research should focus on the development and *operando* long-term durability testing of AEMs and AEIs containing the MPRD head-group chemistry.

Received 27th August 2018
Accepted 29th October 2018

DOI: 10.1039/c8ta08309f

rsc.li/materials-a

Introduction

Fuel cells are considered an efficient and clean energy conversion technology, which can offer superior energy efficiencies to conventional technologies, such as combustion engines. Such devices have been considered promising, due to the ability to directly convert chemical energy (provided from a fuel, *e.g.* H_2) into electrical energy, with wide applicability in mobile (transportation), portable, and stationary systems.[1,2]

In the class of low-temperature fuel cells, alkaline fuel cells (AFC) have regained relative importance due to the development of high-performance anion-exchange membranes (AEM). The main advantages of an anion-exchange membrane fuel cell (AEMFC) over current proton exchange membrane fuel cells (PEMFC) are: (i) lower activation overpotential at the cathode promising the use of non-Pt-group catalysts, (ii) a less corrosive environment allowing the use of cheaper metallic components, (iii) reduced gas and alcohol crossover, and (iv) alternate water management.[3,4] AEMs are ionomeric polymers, in the same way as the proton exchange membranes used in PEMFCs, but where hydroxyl ions (OH^-) are ionically bound to polymer-bonded (positively charged) quaternary ammonium groups, which form the anion conducting network.[5]

Despite the improvements in the development of AEMs, AEMFCs have (until recently) presented poorer performances in comparison to the more well-stablished PEMFCs. One of the reasons for this is associated with the inferior OH^- conductivity of many AEMs in comparison to H^+ conduction in PEMs; this often lead to the use of AEMs with higher IECs (ion exchange capacity), leading to the risk of additional mechanical instabilities.[6] This poor AEMFC performance is also due to the unavailability of suitable anion-exchange ionomer (AEI) candidates, which are needed to impart OH^- conducting in the catalyst layers of the electrodes (more on this later). The chemical, thermal and mechanical stabilities of AEMs is strongly dependent on the nature of the (anion conducting) functional groups and also the backbone chain. Besides temperature, the main cause of degradation of various anion conducting groups and polymer chains is the alkalinity of the medium (high pH), a problem that is especially severe in materials containing lower hydration levels.[7,8] AEMs are formed

[a]Instituto de Química de São Carlos, Universidade de São Paulo, São Carlos, Brazil
[b]Instituto de Pesquisas Energéticas e Nucleares – IPEN-CNEN/SP, São Paulo – SP, Brazil
[c]Departamento de Quimica Fisica Aplicada, Universidad Autonoma de Madrid, Madrid, Spain
[d]Department of Chemistry, The University of Surrey, Guildford GU2 7XH, UK. E-mail: j.varcoe@surrey.ac.uk
[e]Department of Inorganic Chemistry, Faculty of Natural Sciences, Comenius University, 84215 Bratislava, Slovakia

† Electronic supplementary information (ESI) available: Additional SEM, EDX and fuel cell data in support of the main article. See DOI: 10.1039/c8ta08309f

using a variety of backbones, including non-fluorinated, partially fluorinated or fully fluorinate polymers, such as poly(ethylene), polysulfones, poly(phenylene oxide)s (PPO), poly(phenylene)s, polybenzimidazoles (PBI), and modified poly(ethylene-*co*-tetrafluoroethylene) (ETFE). The covalently-linked side-chain quaternary ammonium cationic groups are responsible for conduction of the anions (OH^-).

Such side-chains can be incorporated onto the backbone of polymer precursors by copolymerization of monomers using the radiation-grafting technique, which allows the use of pre-fabricated polymeric films, leading to facile AEMs production.[9] The desired objective of radiation-grafting is to create active sites on the polymer chains onto which grafted polymer side-chains can be attached (when placed in contact with suitable monomers). A major advantage of this technique is that materials with different head-group chemistries can be synthesised from the same precursor polymer electrolytes with similar ion-exchange capacities (as an aside, this is demonstrated by the data presented in Fig S1 in the ESI† related to the development of different imidazolium-based radiation-grafted AEMs). However, other modifications induced by polymer irradiation can occur, including undesirable scission of the backbone chain (producing mechanically weaker materials), formation of covalent cross-links, and the introduction of (reactive) unsaturated chemical groups.[10]

Radiation-grafted anion-exchange polymer electrolytes have been prepared by using both simultaneous-(mutual)-irradiation or pre-irradiation induced grafting methods. In general, the simultaneous method results in the production of undesired, un-grafted homopolymers, while polymers with lower degrees of grafting are typically produced with the pre-irradiation method (often then requiring higher radiation doses that will result in more polymer damage).[11]

The lack of optimised gas diffusion electrodes (GDE) for the MEA (membrane-electrode assembly), which combine ionic and electronic conductivity with efficient transport of reactants, products and water in the three-phase boundary, has impeded development of high-performance AEMFCs.[12] In this context, the AEI plays an essential role on the GDE's catalyst layer (CL), with active participation in the ion transport to and from the surfaces of the electrocatalysts.[13,14] The AEIs, often supplied in solution or dispersion form, combine the role of binder and OH^- ion conductor in the CL.[15] Similar to the AEMs, the main requirements for the use in GDE are the combination of high ion conductivity and stability in alkaline media, especially in the cathode where dry out leads to reduced conductivity and durabilities.[16–18] The development of AEIs is much more early stage (*cf.* AEMs) due to the difficulty of formulating dispersions or ionomer solutions without deterioration of their chemical properties. AEI concepts based on both cross-linked and uncross-linked polymers have been proposed,[12,19–23] but their performances in AEMFCs is still poor compared to the perfluorosulfonic acid (PFSA) ionomers used in PEMFCs. Advances in AEI development are desperately required.

In 2014, Poynton *et al.* first reported the use of a powdered AEI in AEMFCs.[24] The AEI powder was prepared by the radiation-grafting of VBC (vinylbenzyl chloride) monomer onto ETFE powders followed by functionalisation with trimethylamine to form the quaternary ammonium forms, which can then be directly used within the CLs. Subsequently, this AEI powder has been used in combination with optimised AEMs leading to impressive AEMFC performances;[25–29] this demonstrates that ionomer powders can be effectively incorporated into CLs, opening up new opportunities for high performance AEMFCs.

In this context, this article describes the synthesis and characterization of irradiated ETFE-based AEI powders (Scheme 1) that have been functionalised with three different cationic head-groups (previously only studied for radiation-grafted AEMs[30] and not for AEI powders): benzyltrimethylammonium (TMA), benzyl-*N*-methylpyrrolidinium (MPY), or benzyl-*N*-methylpiperidinium (MPRD). This study will evaluate these three different types of AEI powder with respect of AEMFC power outputs (alongside their corresponding functionalised AEMs). The results from this study can then be used to direct future (time intensive and expensive) *operando* durability studies with down-selected head-group chemistry options. The effect of using different batches of VBC-grafted ETFE (in electrode fabrication) and repeat electrodes (with the same AEI powder batch) are also evaluated.

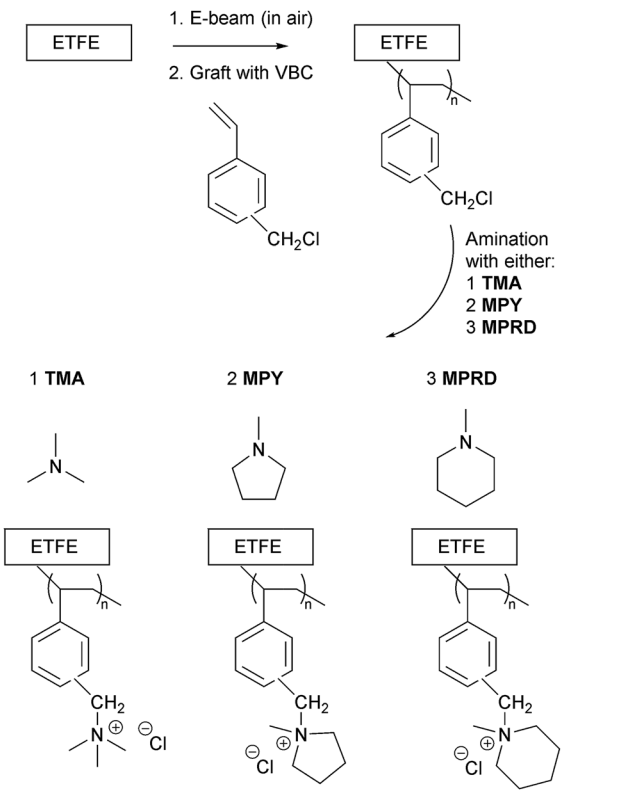

Scheme 1 An outline of the synthesis of the radiation-grafted anion-exchange membranes (AEM, formed by modification of ETFE films) and powder anion-exchange ionomer (AEI, formed from ETFE powders). These are designated AEM(TMA), AEM(MPY), AEM(MPRD), AEI(TMA), AEI(MPY), and AEI(MPRD) in this article. These Cl^- anion forms can be converted to other anion forms (*e.g.* OH^-) *via* an appropriate ion-exchange procedure (see Materials and methods section).

Table 1 A summary of the reaction conditions used to synthesise the AEMs in this study along with key properties of the final AEMs in their Cl^- forms (*in italics*). Error bars indicate sample standard deviations of measurements conducted on $n = 3$ different samples of each AEM

	AEM(TMA)	AEM(MPY)	AEM(MPRD)
Radiation dose	30 kGy	40 kGy	40 kGY
VBC concentration	5% vol.	5% vol.	5% vol.
Graft time/temp.	16 h at 70 °C	16 h at 70 °C	16 h at 70 °C
Amination solution (aq.) concentration	45% vol.	50% vol.	15% vol.
Amination time	24 h	16 h	18 h
Amination temp.	Room temp.	70 °C	60 °C
IEC/mmol g^{-1}	*2.05 ± 0.05*	*2.09 ± 0.08*	*1.73 ± 0.03*
σ/mS cm^{-1}[a]	*46.1 ± 0.2*	*43.3 ± 3.1*	*30.8 ± 1.2*
WU (%)[b]	*67 ± 7*	*121 ± 5*	*84 ± 8*
$t_{hyd}/\mu m$[c]	*56 ± 3*	*70 ± 2*	*55 ± 2*
$t_{dehyd}/\mu m$[d]	*45 ± 2*	*47 ± 2*	*43 ± 2*
TPS (%)[e]	*24*	*49*	*28*
IPS (%)[f]	*16*	*31*	*18*

[a] The in-plane Cl^- anion conductivity of the AEMs in water at 60 °C from 4-probe electrochemical impedance spectroscopy data. [b] Gravimetric water uptakes at room temperature. [c] Hydrated AEM thickness at room temperature. [d] Dehydrated AEM thickness at room temperature. [e] Through-plane swelling $(=100 \times (t_{hyd} - t_{dehyd})/t_{dehyd})$.[29] [f] In-plane swelling $(=100 \times A_{hyd} - A_{dehyd})/A_{dehyd}$ where A is membrane area.

Materials and methods

Preparation of anion-exchange membranes (AEM)

This work involved the synthesis of radiation-grafted AEMs based on ETFE polymer films (Nowofol, 25 μm thick), which were electron-beamed in presence of air (4.5 MeV Dynamatron Continuous Electron Beam Unit, STERIS Synergy Health, South Marston, UK) with absorbed doses controlled by the number of passes (10 kGy per pass).[24,28] The ETFE films were exposed to a 30 or 40 kGy absorbed dose and stored at −40 °C before grafting.

The e-beam-treated ETFE films (13 × 13 cm) were immersed in aqueous mixtures containing 5% vol. vinylbenzyl chloride monomer (VBC, Sigma-Aldrich product code 338729, 97% purity, mixture of 3- and 4-isomers, no prior removal of the 700–1100 ppm nitromethane or 50–100 ppm *tert*-butylcatechol inhibitors) and 1% vol. 1-octyl-2-pyrrolidone dispersant (Sigma-Aldrich) in glass vessels. After the grafting mixtures were purged with N_2 (2 h) the vessels were sealed and heated at 70 °C for 16 h. After grafting was complete, the films were removed and washed multiple times with toluene to remove excess unreacted VBC and any traces of VBC homopolymer that may be present. The resulting intermediate VBC-grafted films were subsequently dried at 70 °C for 5 h in a vacuum oven.

The VBC-grafted films were then aminated with three different amines by immersion in aqueous solutions of various concentrations for various durations (exact conditions summarised in Table 1). The amines used were trimethylamine (TMA), *N*-methylpyrrolidine (MPY) and *N*-methylpiperidine (MPRD). After amination, the resulting crude AEMs (predominantly in the Cl^- anion forms) were washed multiple times with ultrapure water (UPW). They were then ion-exchange to the pure

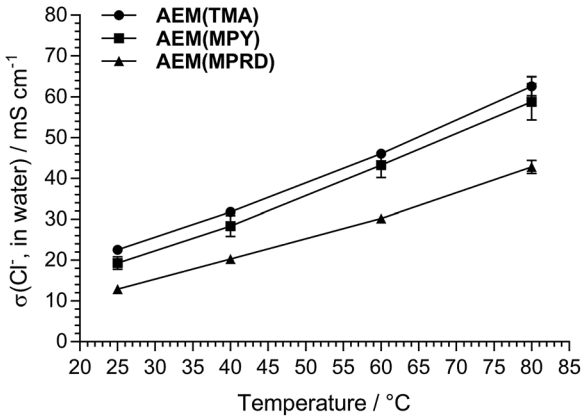

Fig. 1 A relative comparison of the Cl^- anion conductivities of the AEMs used in this study (fully hydrated in water, 4-probe electrochemical impedance spectroscopy data).

Table 2 A summary of the reaction conditions used to synthesise the powder AEIs in this study along with their IECs in the Cl^- anion form (*in italics*). Error bars indicate sample standard deviations of measurements conducted on $n = 3$ different samples of each AEI

	AEI(TMA)	AEI(MPY)	AEI(MPRD)
Radiation dose	100 kGy	100 kGy	100 kGy
VBC concentration	5% vol.	5% vol.	5% vol.
Graft time/temp.	24 h at 60 °C	24 h at 60 °C	24 h at 60 °C
Amination solution (aq) concentration	45% vol.	50% vol.	15% vol.
Amination time	24 h	16 h	18 h
Amination temp.	Room temp.	50 °C	60 °C
IEC/mmol g^{-1}	*2.01 ± 0.01*	*1.90 ± 0.02*	*1.99 ± 0.01*

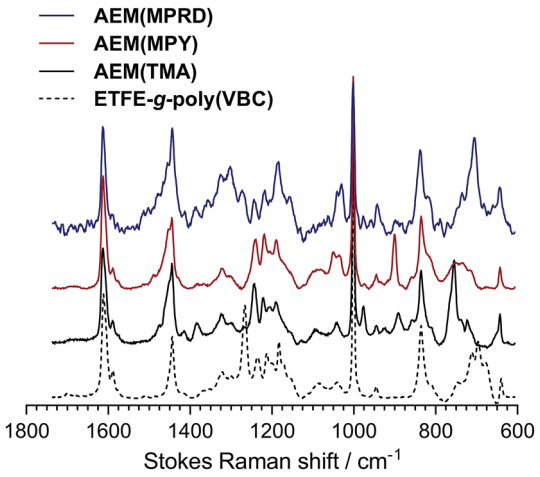

Fig. 2 The Raman spectra for the (pre-aminated) VBC-grafted ETFE-film (ETFE-*g*-poly(VBC)) and the three AEMs synthesised for this study (if viewing in black and white, the legend items are in same order as the spectra). Laser $\lambda = 785$ nm.

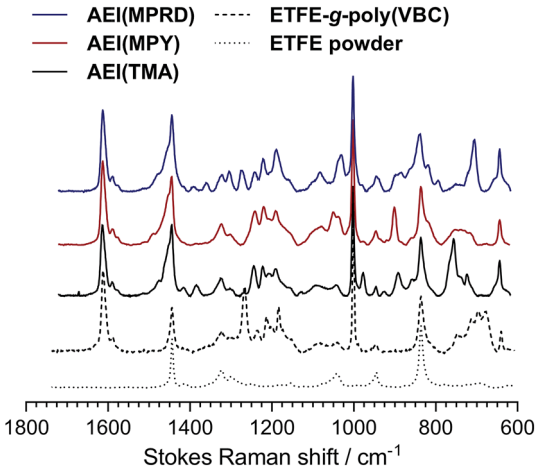

Fig. 3 The Raman spectra for the precursor (pre-irradiated) ETFE powder, the (pre-aminated) VBC-grafted ETFE-powder (ETFE-*g*-poly(VBC)) and the three AEIs synthesised for this study (if viewing in black and white, the order of the AEIs in the legend is in the same order as the spectra). Laser $\lambda = 785$ nm.

Cl^- anion forms *via* immersion in aqueous NaCl (1 mol dm^{-3}) overnight at room temperature (with at least 2 changes of solution during this time). The final Cl^- form AEMs were obtained after rigorous washing in UPW at room temperature (ensuring no Na^+ co-ions and no excess Cl^- counter ions were present, such that the only Cl^- counter ions present were those charge balancing the positive charges on the grafted polymer chains). All AEMs were stored in UPW until required.

Characterisation of the AEMs

The AEMs were characterised in the Cl^- forms using the routine procedures detailed in ref. 29 (without modification): these include the measurement of ion-exchange capacity (IEC), 4-probe (in-plane) conductivities in water, and gravimetric water uptakes. These key properties are summarised in Table 1. We note that the AEMs swell more in the thickness direction than in the in-plane direction: this is important for future long-term mechanical durabilities when operated in AEMFCs. Raman spectra of the VBC-grafted ETFE-films and the final AEMs were collected using Renishaw InVia Raman Spectrometer (laser $\lambda =$ 785 nm) equipped with CCD and Leica microscope.

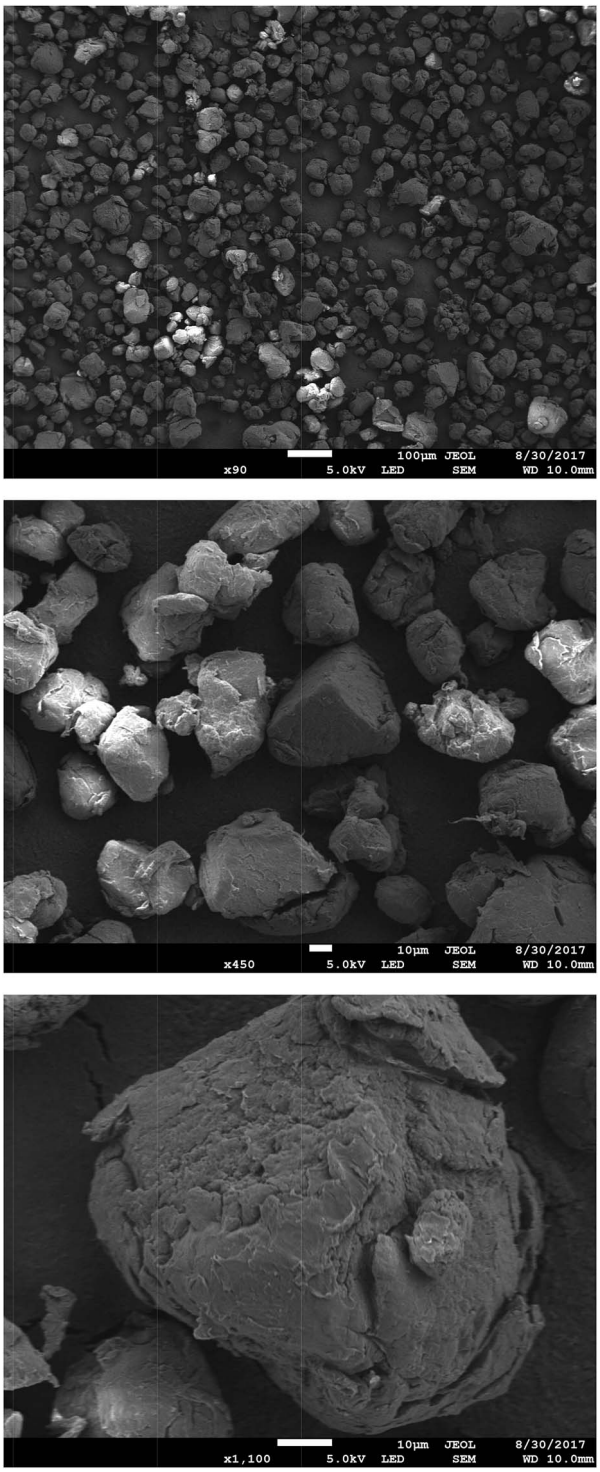

Fig. 4 SEM micrographs of the (pre-aminated) VBC-grafted ETFE powders at ×90, ×450, and ×1100 magnifications (from top to bottom).

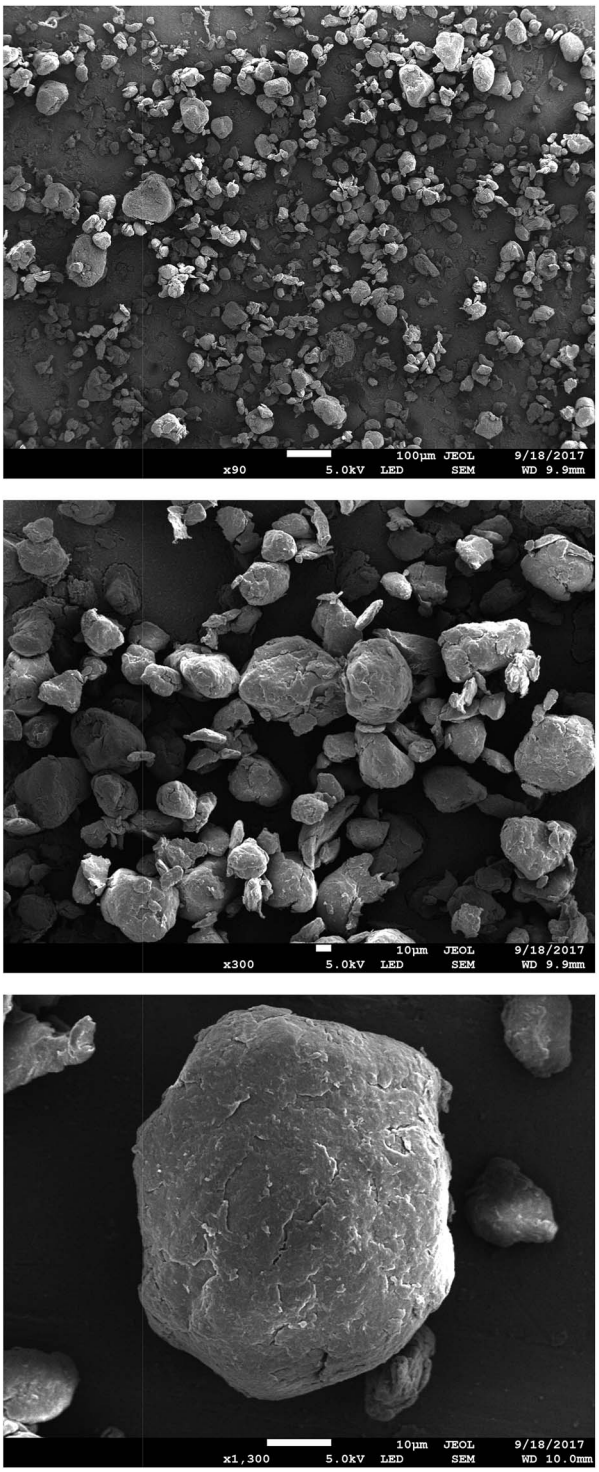

Fig. 5 SEM micrographs of AEM(TMA) at ×90, ×300, and ×1300 magnifications (from top to bottom).

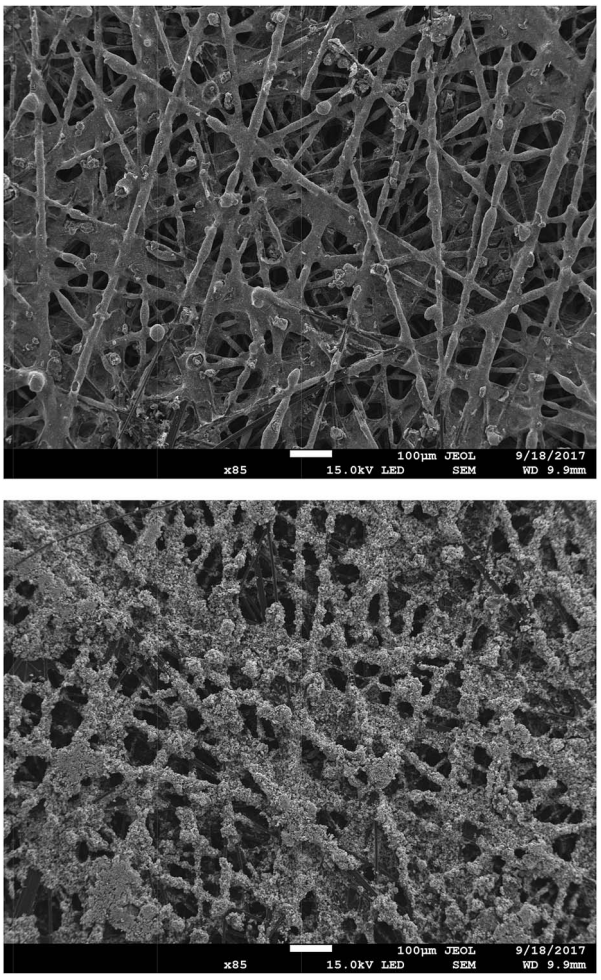

Fig. 6 SEM micrographs (×85 magnification) of an exemplar Pt/C cathode (top) and PtRu/C anode (bottom) containing AEM(TMA) at a loading of 20% wt.

Preparation and initial characterisation of the powder anion-exchange ionomers (AEI)

The methodology for synthesising the radiation-grafted ETFE-based powder AEIs was similar to that used for producing the AEMs above. These procedures will not be repeated in detail; however, modifications are highlighted in the following text.

The ETFE powders (Fluon® Z-8820X, AGC Europe, particle diameters 20–30 μm) were irradiated in air to an absorbed dose of 100 kGy using the same electron-beam facility. The e-beamed powders (up to 20 g per batch) were grafted using aqueous grafting solutions with the conditions summarised in Table 2. The resulting intermediate VBC-grafted powders were recovered by filtration, washed with toluene and subsequently dried at 50 °C for 5 h in a vacuum oven. The AEI powders when then aminated using the conditions summarised in Table 2. After ion-exchange to the pure Cl^- anion forms and thorough washing with UPW (additional filtration steps needed to recover the modified powders) the final AEI powders were then dried in a vacuum oven at 50 °C overnight before being subjected to ball milling for 8 h to achieve deagglomeration of the powder particles. The IECs of the powder AEIs were recorded using exactly the same method that was used for the AEMs.[29] Raman spectra of the ETFE precursor powder, the VBC-grafted powders and the final powder AEIs were collected using the same Renishaw InVia Raman spectrometer as used with the AEMs.

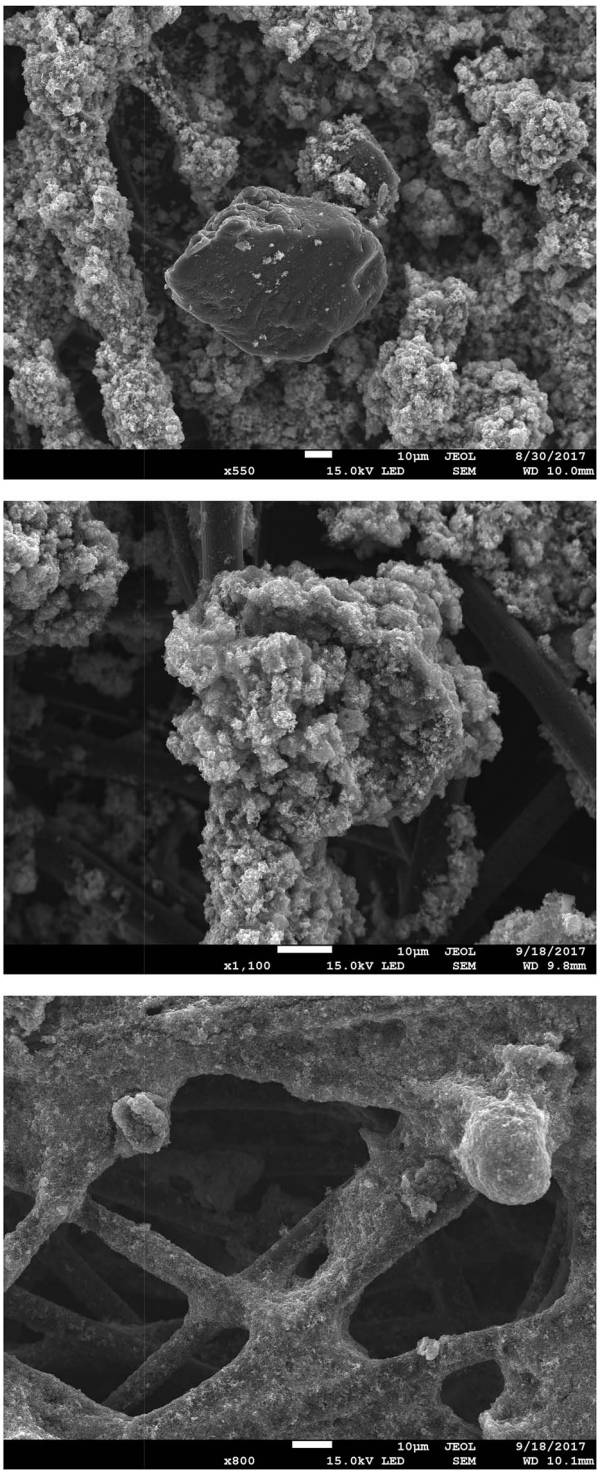

Fig. 7 SEM micrographs of: (top) an uncoated AEI(MPY) particle in a PtRu electrode (×550); (middle) a coated AEI(MPY) particle in a PtRu electrode (×1100); and (bottom) the coating of AEI(MPY) particles in a Pt/C electrode (×800).

Scanning electronic microscopy (SEM) and energy-dispersive X-ray spectroscopy (EDX) of the powder AEIs

The powder AEIs (and the electrodes fabricate from them – see next section) were evaluated morphologically using SEM. A small amount of each AEI (and the grafted precursor) was deposited onto a sample holder using epoxy resin and subsequently coated with Au film (9 nm thickness). The Field Emission Scanning Electron Microscopy (FE-SEM) images, and the associated EDX elemental (C, N, O, Cl, F, Pt and Ru) data, were obtained using a JEOL JSM-7100F instrument.

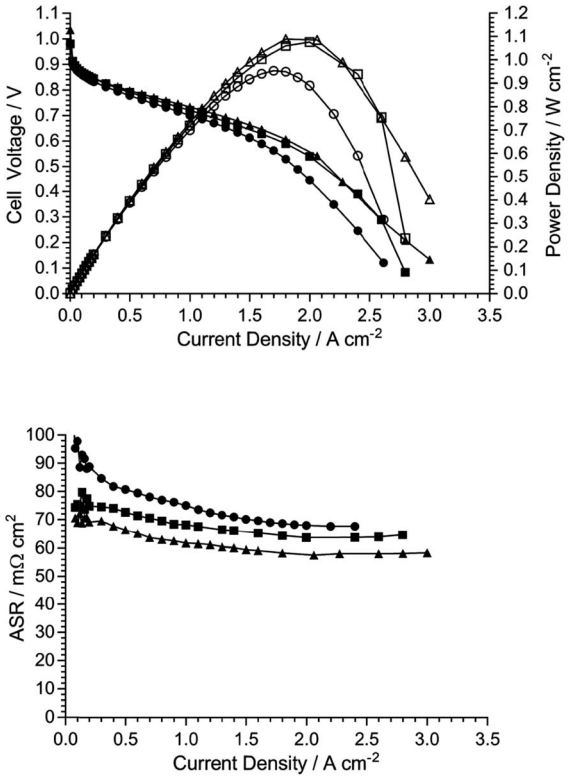

Fig. 8 AEMFC fuel cell performances at 60 °C (H_2 anode gas and O_2 cathode gas, both supplied unpressurised with dewpoint temperatures of 55 °C) with three repeated MEA fabrications, each containing the same TMA-based AEM (IEC = 2.05 mmol g^{-1}) and the same TMA-based AEI (synthesised in a single batch with an IEC = 1.94 mmol g^{-1}). PtRu/C anodes and Pt/C cathodes were used (containing 20% wt AEI and 0.40 ± 0.03 mg cm^{-2} Pt loadings).

Electrode and membrane-electrode assembly (MEA) fabrication

The catalysed gas diffusion electrode (GDE) method was used for fabricating the AEMFC electrodes. For each cathode GDE, Pt/C (Alfa Aesar, Johnson Matthey HiSPEC 4000, 40% wt Pt) and AEI powder (20% wt of the total solid mass for AEI(TMA) and 30% wt for AEI(MPY) and AEI(MPRD)) were mixed together with 1 mL of water and 9 mL of propan-2-ol. This cathode catalyst ink was homogenised in ultrasound for 30 min, sprayed onto a Toray TGP-H-60 carbon paper gas diffusion layer (GDL, non-teflonated), and then dried in air. For the anode GDEs, PtRu/C (Alfa Aesar, Johnson Matthey HiSPEC 12100, 50% wt Pt and 25% wt Ru) catalyst was used as the catalyst. The geometric areas of all GDEs were 5.0 cm^2 and the Pt loadings for all anodes and cathodes were 0.40 ± 0.03 mg_{Pt} cm^{-2}.

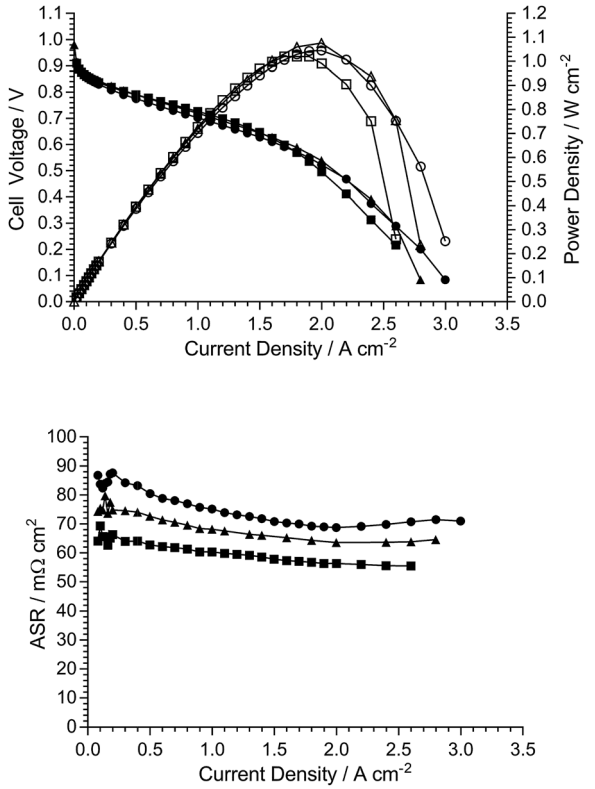

Fig. 9 AEMFC fuel cell performances at 60 °C (H_2 anode gas and O_2 cathode gas, both supplied unpressurised with dewpoint temperatures of 55 °C) with three MEAs fabricated using the same TMA-based AEM (IEC = 2.05 mmol g^{-1}) but with three different batches of TMA-based AEI (IECs ranging between 1.82 and 1.94 mmol g^{-1}). PtRu/C anodes and Pt/C cathodes were used (containing 20% wt AEI and 0.40 ± 0.03 mg cm^{-2} Pt loadings).

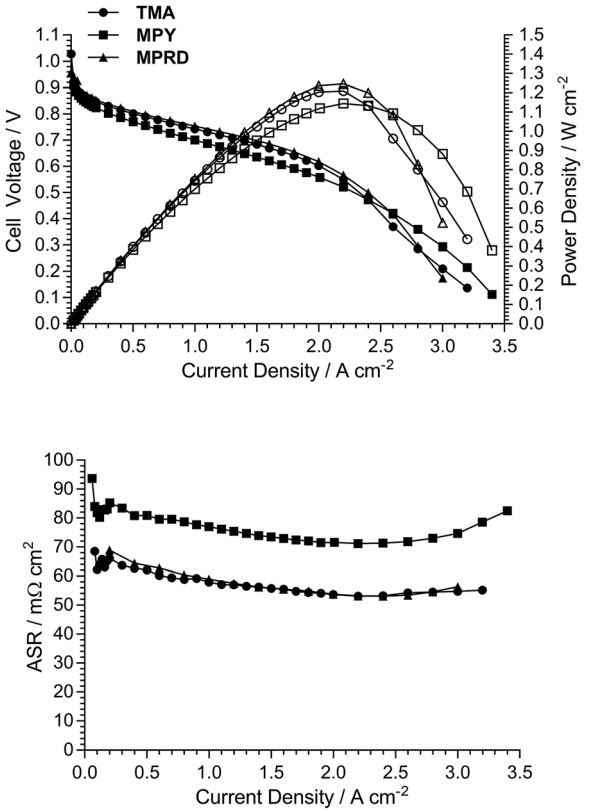

Fig. 10 AEMFC fuel cell performances at 60 °C (H_2 anode gas and O_2 cathode gas, both supplied unpressurised with dewpoint temperatures of 60 °C) with three different chemistry MEAs (convention = AEI_{anode}/AEM/$AEI_{cathode}$): (1) AEI(TMA)/AEM(TMA)/AEI(TMA); (2) AEI(MPY)/AEM(MPY)/AEI(MPY); and (3) AEI(MPRD)/AEM(MPRD)/AEI(MPRD). PtRu/C anodes and Pt/C cathodes were used (containing 20% wt AEI loading with AEI(TMA) and 30% wt AEI loading with AEI(MPY) and AEI(MPRD), along with 0.40 ± 0.03 mg cm^{-2} Pt loadings).

Prior to MEA assembly, the electrodes and AEM under test were immersed in aqueous KOH (1 mol dm^{-3}) for 1 h, followed by thorough washing with UPW (to remove excess K^+ and OH^- ions). Each membrane-electrode assembly (MEA) was assembled by placing the anode, cathode, and AEM (4 cm × 4 cm), to be tested together, between two graphite plates machined with serpentine type distribution channels (the 5 cm^2 fuel cell fixture used was supplied by Scribner Associates, USA) and applying a torque of 5.5 N m. It is important to note that unlike with PEMFCs, no prior hot-pressing was used to produce the MEAs: the MEAs hot-press *in situ* on fuel cell start-up.

Anion-exchange membrane fuel cell (AEMFC) testing

The H_2/O_2 AEMFC tests of each MEA fabricated were conducted using an 850C fuel cell test station (Scribner Associates, USA). All AEMFC tests were conducted at 60 °C with 1 dm^3 min^{-1} gas supplies. The exact test conditions used for each test are detailed in the relevant figure captions. All gases were supplied without back-pressurisation. The AEMFCs were "activated" *via* operation at 0.5 V until a steady current was achieved (min. 1 h). Polarisation curves were collected in galvanostatic mode. *In situ* area specific resistances (ASR) were collected using the 850C's internal current interrupt method.

Results and discussion

Initial AEM and AEI characterisation

As stated before, and to aid routine characterisations,[11] we always conduct initial analyses of our AEMs (for select properties) in the Cl^- anion forms before they have been exposed to any extreme pH environments (that may subtly change their properties) and to eliminate CO_2-derived interferences processes (that will change OH^- forms of AEMs to CO_3^{2-}/HCO_3^- forms). As such, our standard procedure for performance testing means we only convert the AEIs and AEMs into the OH^- forms immediately before device testing (see AEMFC testing description above).

The IECs for the Cl^- anion form AEMs and AEIs are reported in Tables 1 and 2, respectively. The IECs of the powder AEIs were similar, while the IEC of AEM(MPRD) was slightly lower than for AEM(TMA) and AEM(MPY). This contributed towards the lower conductivity profile of AEM(MPRD) across all application relevant temperatures (Fig. 1). Our previous study of thicker ETFE-based AEMs made using TMA, MPY, and MPRD (from the radiation-grafting of 50 μm ETFE as opposed to the 25 μm used in this study) showed that MPRD-based radiation-

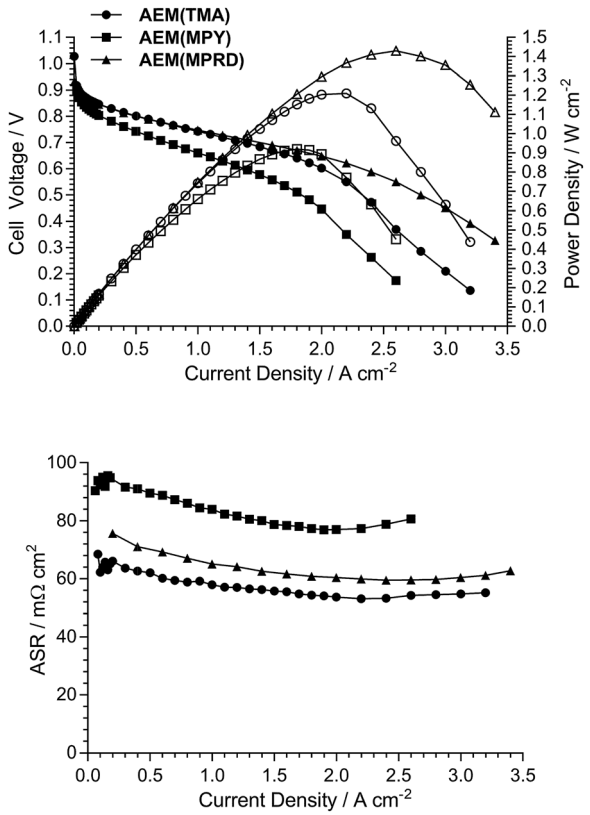

Fig. 11 AEMFC fuel cell performances at 60 °C (H_2 anode gas and O_2 cathode gas, both supplied unpressurised with dewpoint temperatures of 60 °C) of MEAs containing AEI(TMA) in all electrodes along with the AEMs given in the legend. PtRu/C anodes and Pt/C cathodes were used (containing 20% wt AEI loadings and with 0.40 ± 0.03 mg cm^{-2} Pt loadings).

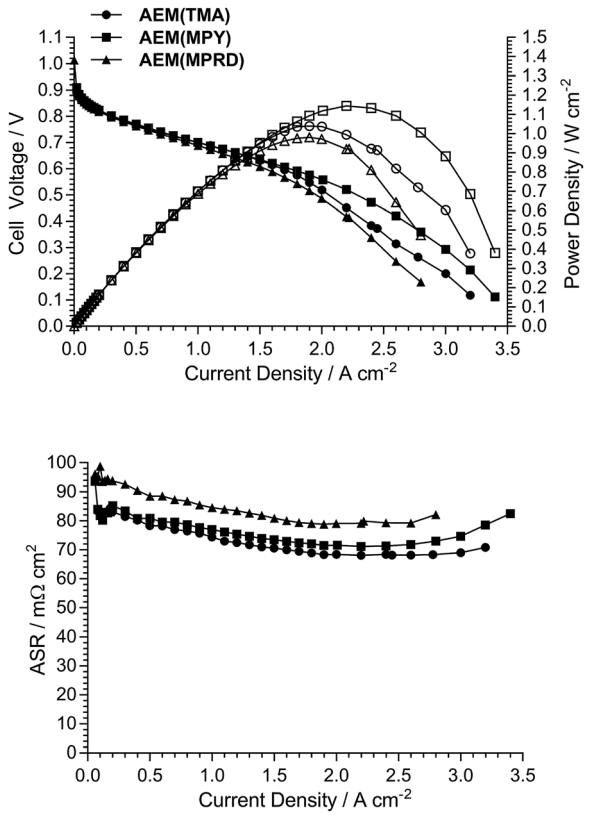

Fig. 12 AEMFC fuel cell performances at 60 °C (H_2 anode gas and O_2 cathode gas, both supplied unpressurised with dewpoint temperatures of 60 °C) of MEAs containing AEI(MPY) in all electrodes along with the AEMs given in the legend. PtRu/C anodes and Pt/C cathodes were used (containing 30% wt AEI loadings and with 0.40 ± 0.03 mg cm^{-2} Pt loadings).

grafted AEMs intrinsically present much higher water-uptakes compared to TMA- and MPY-based AEMs.[30] The use of a lower IEC for AEM(MPRD) in this study was intended to prevent an excessive water uptake and swelling, which would have led to an AEM with undesirably low mechanical properties[11] (it is the AEM, not the AEI, that is required for safe H_2 and O_2 gas separation characteristics inside the AEMFCs).

The Raman spectra of the AEMs are presented in Fig. 2. These spectra confirm successful synthesis as they precisely match those previously reported for the thicker ETFE-based radiation-grafted AEMs.[30] Key features include the characteristic peak at 1267 cm^{-1} in the pre-aminated VBC-grafted ETFE films, which derives from the presence of the $-CH_2Cl$ groups on the poly(VBC) grafted chains. The disappearance of this peak in the spectra of each of the AEMs indicates successful amination (conversion of the $-CH_2Cl$ groups into the various quaternary ammonium groups). Amination is confirmed by the appearance of characteristic peaks at 756 cm^{-1}, 901 cm^{-1} and 705 cm^{-1} due to the presence of the quaternary ammonium head-groups for AEM(TMA), AEM(MPY), AEM(MPRD), respectively. All spectra contain peaks at *ca.* 1612 cm^{-1} (aromatic ring vibrations), 1001 cm^{-1} (due to the *meta*-disubstituted aromatic ring component of the grafted poly(VBC) chains), and 835 cm^{-1} (due to the presence of ETFE $-CF_2-$ groups). The Raman spectra of the ETFE-based radiation-grafted powder AEIs are highly similar with all the above-mentioned features (Fig. 3). This, alongside the measurable IECs, confirms successful synthesis of the powder AEIs.

SEM and EDX analysis of the powder AEIs and electrodes

Fig. 4 presents SEM micrographs of the VBC-grafted ETFE powder before it was reacted with the amines. The powder particles show irregular morphology with particle diameters generally in the range 20–50 μm. The precursor ETFE powder particles range from 20–30 μm.[31] This shows that grafting did not have an excessive effect on powder particle sizes. On amination with TMA (and subsequent ball milling) the inhomogeneity in particle shape and size (ranging 10–70 μm) increases as shown in Fig. 5. Large inhomogeneities were also observed for AEI(MPY) and AEI(MPRD) (Fig. S2 in the ESI†).

The powder AEIs were incorporated into cathodes (containing Pt/C electrocatalyst) and anodes (containing PtRu/C). 20% wt ionomer was used in the AEI(TMA) electrodes, while 30% wt ionomer was used with AEI(MPY) and AEI(MPRD). These loadings were from AEMFC test optimisation studies (see later). SEM micrographs of sample areas of an electrode of each

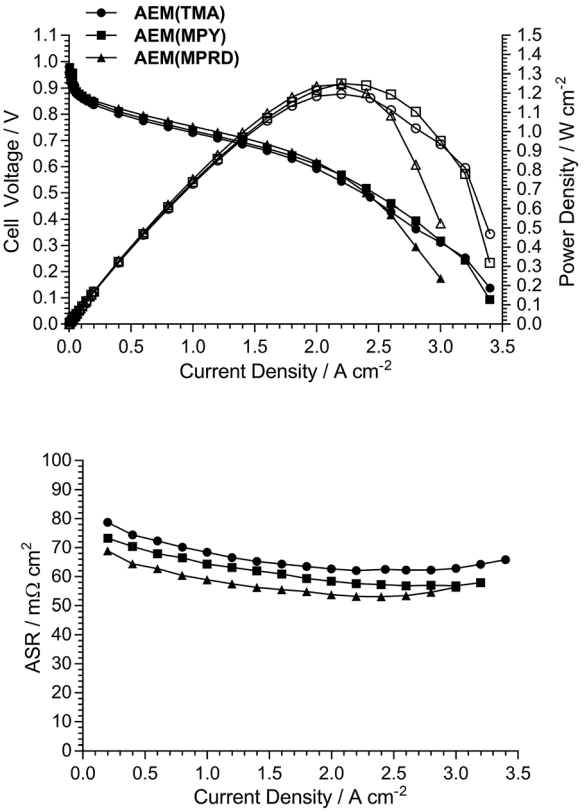

Fig. 13 AEMFC fuel cell performances at 60 °C (H_2 anode gas and O_2 cathode gas, both supplied unpressurised with dewpoint temperatures of 60 °C) of MEAs containing AEI(MPRD) in all electrodes along with the AEMs given in the legend. PtRu/C anodes and Pt/C cathodes were used (containing 30% wt AEI loadings and with 0.40 ± 0.03 mg cm^{-2} Pt loadings).

type are presented in Fig. 6 (for AEI(TMA)) and Fig. S3 in the ESI† (for all powder AEIs). As the powder AEIs are μm-sized but the electrocatalysts are nanoparticles (<100 nm in size) these micrographs cannot give much of a visual indication of the exact morphology of the Pt and PtRu electrocatalyst particles. However, the AEI particles clearly form a denser coverage with the AEI(MPY)- and AEI(MPRD)-containing electrodes (due to the higher ionomer loadings used). A rougher morphology is seen for the PtRu/C-containing anodes compared to the Pt/C-containing cathodes (with all three AEIs). As no microporous layer (MPL) was used (with this class of powder AEI, the use of an MPL appears to lead to lower AEMFC performances) the polymer-catalyst agglomerates are attached directly onto the carbon-fibres of the Toray carbon-paper GDL (with a degree of penetration into the GDL).

On closer inspection, there is evidence of both the Pt/C and PtRu/C catalysts coating the AEI particles and the carbon-fibres of the Toray paper electrodes (Fig. 7 shows some higher magnification SEM micrographs of sample areas of AEI(MPY) containing electrodes). There is also evidence of a proportion of AEI particles (and carbon-fibres) that are not coated with electrocatalyst. Fig. S4–S6 (in the ESI†) show the EDX analysis of different regions on several exemplar electrodes. This EDX

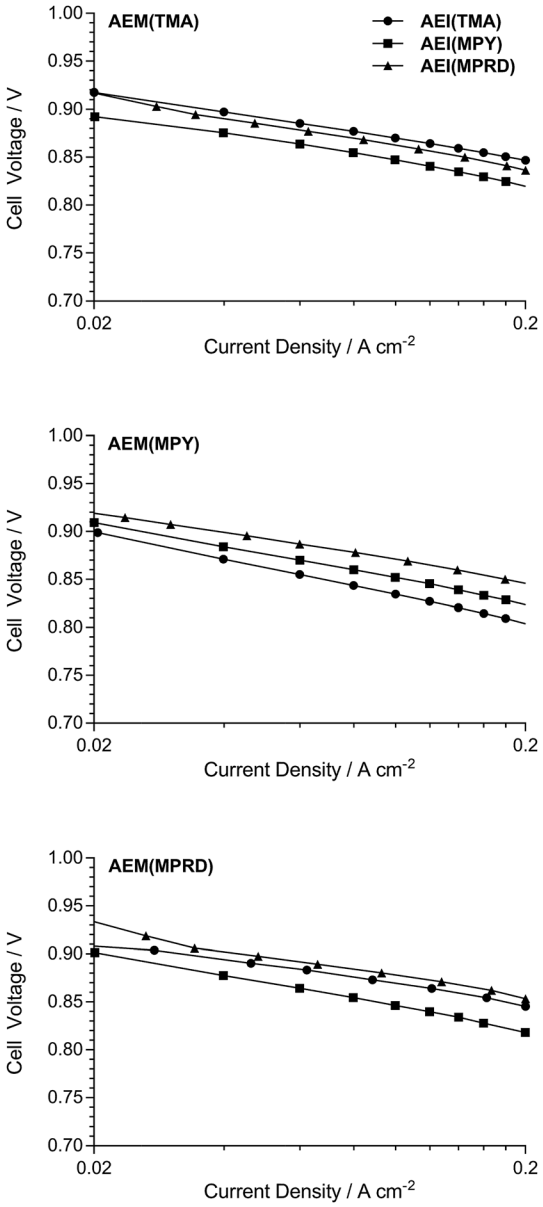

Fig. 14 Cell potential *vs.* $\log_{10}$(current density) plots for the data extracted from Fig. 11–13 between 0.02 and 0.2 A cm^{-2}.

analysis confirms that the electrodes contain a poor distribution of C (from the Toray paper and the carbon-support of the electrocatalysts), F (from the AEI), and metals (Pt and Ru).

The morphology of these AEMFC electrodes is clearly different to that found in PEMFC based electrodes, which contain uniform distributions of ionomer and electrocatalyst.[32] However, numerous studies have proven that these AEMFC electrodes (containing TMA-based radiation-grafted powder AEIs) can produce high AEMFC power performances.[11,25–27,29,33]

AEMFC test data (repeatability)

As the electrodes are hand sprayed, and before investigation of the effect of the different quaternary ammonium chemistries, initial experiments were conducted to evaluate the repeatability

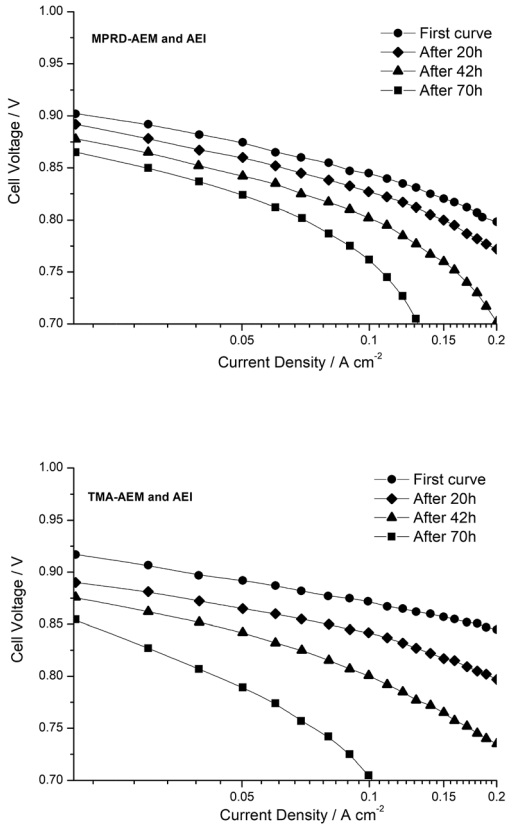

Fig. 15 Changes in the quasi-Tafel plots extracted from H_2/O_2 AEMFC tests at 60 °C, with MPRD-(top) and TMA (bottom) MEAs, both before and after cell discharge at 0.70 V for increasing periods of time (PtRu/C anodes and Pt/C cathodes).

of electrode preparation. Two types of repeatability tests were conducted: (1) Fig. 8 shows the AEMFC fuel cell performances of three repeat MEAs fabricated using the same TMA-based AEM and powder AEI (from a single batch), and (2) Fig. 9 shows the AEMFC fuel cell performances of three MEAs fabricated using the same TMA-based AEM and three different batches of powder AEIs fabricated using the same synthetic protocol.

As can be seen from this data, there is a small amount of variation in peak power density: mean = 1.04 W cm^{-2} and sample standard deviation = 0.05 W cm^{-2} (range = 0.95–1.09 W cm^{-2}) across the $n = 5$ tests conducted (one of the performance curves in Fig. 9 is common with a curve in Fig. 8). As expected, due to the hand fabrication nature of the MEAs, the main differences in performance were due to variances in mass-transport limitations (in the high current density region); variances in electrocatalytic performances (low current density region) and ohmic losses (medium current density region) were less significant. Considering the above, and to aid the relative comparison of AEM/AEI chemistries in AEMFC performance tests (discussed in the next section), the criterion used for the purpose of this study was that MEAs were deemed to have varied in AEMFC performance if their peak power performances were different by >0.10 W cm^{-2}.

AEMFC test data (chemistries)

Fig. 10 presents AEMFC test data with three different MEAs where the AEI and AEM in each MEA contain the same quaternary ammonium chemistry (*e.g.* an MEA containing AEI(TMA) in both electrodes along with AEM(TMA)). It is clear that changing the quaternary ammonium chemistry did not lead to significant differences in AEMFC performance with the use of MEAs in this configuration (containing only one quaternary ammonium chemistry per MEA). Note that 30% wt of ionomer was used with the AEI(MPY)- and AEI(MPRD)-containing MEAs, while 20% wt ionomer was used with the AEI(TMA)-containing MEA, in response to initial studies of AEI loading with each chemistry (Fig. S7–S9 in the ESI†). These loadings are used throughout the rest of this study.

Subsequent experiments involved the comparison of electrodes fabricating using each AEI in MEAs containing the different AEMs. Note this study only considers MEAs that contain the same AEI in each electrode: a study into the use of MEAs containing different AEIs in each electrode is planned for the future. Fig. 11 shows the data collected with MEAs containing AEI(TMA)-based electrodes. The variances in peak power densities are large with the use of the different AEM chemistries. The MEA containing AEM(MPRD) yielded the highest power density (of this entire study): 1.43 W cm^{-2} (at 2.6 A cm^{-2}, ASR = 60 mΩ cm^2). The differences in performances were primarily due to differences in *in situ* ohmic losses and mass transport losses. Considering that AEM(MPRD) had the lowest *ex situ* conductivity, this result is surprising; this highlights the importance of recording *in situ* performances in AEMFC tests, which suggest, here, that AEM(MPRD) has faster water transport characteristics that lower mass transport losses.

Fig. 12 and 13 show the analogous AEMFC test data using electrodes containing AEI(MPY) and AEI(MPRD), respectively. The relative differences in performances with the three different AEM chemistries is less clear cut when using these cyclic-quaternary-ammonium-based powder AEIs (peak power densities ranged from 0.99 to 1.25 W cm^{-2} over the $n = 6$ experiments presented). The performance variations were again primarily due to differences in mass transport losses. The most interesting (take home) finding was that the AEI(MPRD)-based electrodes were particularly insensitive to the AEM chemistry used and produced the highest peak power densities of the cyclic-quaternary ammonium-based AEIs.

Fig. 14 shows quasi-Tafel-plots (extracted from the data presented in Fig. 11–13), comparing the fuel cells responses for each AEM combined with each AEI. These results show that the Tafel lines are all generally parallel indicating that Tafel slopes do not significantly vary with AEI chemistry (with the same catalysts used in all cases). This implies that the reaction mechanisms and rate determining steps (for both the hydrogen oxidation reaction on PtRu/C and the oxygen reduction reaction on Pt/C) are not being affected by the different AEI chemistries in any major way. This behaviour is consistent with the high local OH^- anion concentration in both the anode and cathode environments that may surpass any specific activity effects due to the AEI chemistry. However, the consistently high cell

potentials observed with the use of AEI(MPRD) in the electrodes indicates that this AEI generally leads to better electrocatalysis; this could either be due to an enhanced number of active sites or an increase in exchange current densities for one or both reactions.

Initial *in situ*, short-term stability testing

The *ex situ* alkali stability tests for TMA-, MPY- and MPRD-AEMs have been reported previously.[30] Due to the higher hydration levels related to the MPY and MPRD head-group chemistries, these exhibited higher alkali stabilities compared to the benchmark TMA chemistry (*e.g.* 17–18% loss in IEC when treated in aqueous KOH (1 mol dm^{-3}) for 28 d at 80 °C compared to 30% loss for the TMA-based AEM).

However, besides leading to promising fuel cell performances, MPRD-based polymer electrolytes need to be more stable under *operando* conditions. As an initial move towards this, we conducted comparative, short-term AEMFC tests with the TMA- and MPRD-based MEAs (each MEA contained the same chemistry in all polymer electrolyte components). Fig. 15 presents the quasi-Tafel plots for these two fuel cells: data was collected immediately after cell start up, and then after 20, 42 and 70 h of AEMFC discharge at 0.7 V and at 60 °C (88% and 92% RH for the H_2 anode and the O_2 cathode respectively).

In all cases the low current density (catalyst activation) region showed a decay in performance as a function of AEMFC discharge time, which relates to a loss of catalyst activity or electrochemical active area (ECSA). For the MPRD-MEA (Fig. 15a), this loss was *ca.* 37 mV between the initial performance and that observed after 70 h of cell discharge: in contrast this loss was 70 mV for the TMA-MEA (Fig. 15b). Large changes in ECSA have recently been reported for a Pt/C catalyst in aqueous NaOH (0.1 mol dm^{-3}) alkaline electrolyte during accelerated cyclic voltammetric stress tests at 25 °C:[34] after 150 cycles (100 mV s^{-1}, between 0.1 to 1.23 V, total test duration of 1 h) a loss of 60% ECSA was observed. This prior observation indicates that catalyst degradations contribute towards the changes in performances reported in Fig. 15, which highlights the need to develop catalysts with stabilities tailored towards operation in AEMFCs.

After several days of AEMFC discharge time, the quasi-Tafel plots tended to curve down at higher current densities (but still at current densities that are below those that cause diffusion limitations): this is characteristic of an increase in ohmic losses, which may be due to a combination of detachment of catalyst from the C-supports,[34] and degradation of the anion-exchange polymer electrolyte components. Several prior works have stressed the difficulties in achieving optimized water balance in AEMFCs;[25,35–37] the drying out of part of the MEAs in AEMFCs risks AEM/AEI degradation. The use of AEM(MPRD), as already discussed, facilitates better water management and consequently the rate of ohmic resistance increase would be expected to be lower than with the use of AEM(TMA), which is observed in the data presented in Fig. 15.

Overall, the *operando* voltage decays observed in Fig. 15 cannot be wholly attributed to AEI or AEM degradation. This scenario further highlights that more effort is required to determine the predominant source of *operando* stability. Considering issues with accessing test equipment and the length of time that such experiments take, such testing can only be rigorously conducted once suitable AEI-AEM combinations are identified. The results reported in this study represent the first step towards achieving this.

Conclusions and future directions

This study involved the development of ETFE-based radiation-grafted anion-exchange ionomer (AEI) powders containing different head-group chemistries made using trimethylamine (TMA), *N*-methylpyrrolidine (MPY), and *N*-methylpiperidine (MPRD) amination agents. These AEIs were used to form membrane electrode assemblies (MEA) containing anion-exchange membranes (AEM) with the same chemistries. The resulting anion-exchange membrane fuel cell (AEMFC) performance tests on these MEAs showed that all the head-group chemistries yielded excellent AEMFC performances at 60 °C. The key finding of this study was that the MPRD-based materials showed particularly notable characteristics related to the power outputs of the AEMFCs.

Our previous study on ETFE-based radiation-grafted AEMs containing the TMA-, MPY-, and MPRD-based chemistries showed that MPRD-containing (and MPY-containing) materials have higher alkali stabilities (when hydrated) compared to TMA-based materials.[30] The combination of this prior finding with the AEMFC findings in this study strongly suggests that further detailed investigation of MPRD-based radiation-grafted AEMs and AEIs is warranted. However, as recently discovered (subsequent experiments that were chronologically conducted after those presented in this paper), replacing the ETFE-based AEMs with LDPE-AEMs leads to more mechanically robust AEMs (it is the mechanical weakness of the ETFE-based AEMs that limits AEMFC testing to 60 °C).[38] We are now investigating the use of these powder AEIs in combination with LDPE-based AEMs (including MPRD versions); now that the highest performing AEI- and AEM-chemistry has been identified, these studies involving the more robust LDPE-based AEMs will include *in situ* durability testing at 80 °C (not achievable with ETFE-based AEMs).

Author contributions

Most of the test results were collected by ALGB, who also synthesised and characterised AEI(TMA) and AEI(MPY), with assistance from EIS (whose preliminary experiments on AEI synthesis and loadings guided this study). The MPRD-based materials were synthesised and characterised by DH. AEM(TMA) and AEM(MPY) materials were produced and characterised by LQW and RBS, respectively. EAT assisted with the data collection and analyse for Fig. 14 and 15. The choice of head-group chemistry was directed by JPG's work and guidance. GS's results were essential in justifying the use of the radiation-grafted method for this study (Fig. S1†). All other authors made contributions towards project direction, data analysis and

manuscript preparation. JRV was responsible for overall project supervision and made a substantial contribution towards the drafting of the article.

Conflicts of interest

There are no conflicts to declare.

Acknowledgements

The research was funded by the Engineering and Physical Sciences Research Council (EPSRC grants EP/M014371/1, EP/M022749/1, and EP/M005933/1). ALGB's exchange was funded by FAPESP grants 2016/13277-9 and 2015/09210-3, while EIS' exchange was funded by FAPESP grants 2015/23621-6, 2014/09087-4 and 2014/50279-4. DH's student-exchange was funded by a PDIF Short Stay Scholarship of the Autonomous University of Madrid. GS' 2015 exchange was funded by the ERASMUS+ work placement scheme.

References

1 P. P. Kundu, V. Sharma and Y. G. Shul, *Crit. Rev. Solid State Mater. Sci.*, 2007, **32**, 51–66.
2 Z. P. Cano, D. Banham, S. Ye, A. Hintennach, J. Lu, M. Fowler and Z. Chen, *Nat. Energy*, 2018, **3**, 279–289.
3 *Fuel Cell Systems Explained*, ed. J. Larmine and A. Dick, 2nd edn, John Wiley & Sons, 2003.
4 T. Zhou, R. Shao, S. Chen, X. He, J. Qiao and J. Zhang, *J. Power Sources*, 2015, **293**, 946–975.
5 A. Brouzgou, A. Podias and P. Tsiakaras, *J. Appl. Electrochem.*, 2013, **43**, 119–136.
6 J. Pan, C. Chen, L. Zhuang and J. Lu, *Acc. Chem. Res.*, 2012, **45**, 473–481.
7 B. Gupta and G. Scherer, *Chimia*, 1994, **48**, 127–137.
8 U. Lappan, U. Geißler, U. Gohs and S. Uhlmann, *Macromolecules Materials and Engineering*, 2009, **294**, 510–515.
9 M. Mamlouk, J. A. Horsfall, C. Williams and K. Scott, *Int. J. Hydrogen Energy*, 2012, **37**, 11912–11920.
10 L. Gubler, *Adv. Energy Mater.*, 2014, **4**, 1300827.
11 L. Wang, J. J. Brink, Y. Liu, A. M. Herring, J. Ponce-González, D. K. Whelligan and J. R. Varcoe, *Energy Environ. Sci.*, 2017, **10**, 2154–2167.
12 X. Gao, H. Yu, J. Jia, J. Hao, F. Xie, J. Chi, B. Qin, L. Fu, W. Song and Z. Shao, *RSC Adv.*, 2017, **7**, 19153–19161.
13 J. R. Varcoe, R. C. T. Slade and E. Lam How Yee, *Chem. Commun.*, 2006, 1428–1429.
14 D. Yang, H. Yu, G. Li, Y. Zhao, Y. Liu, C. Zhang, W. Song and Z. Shao, *J. Power Sources*, 2014, **267**, 39–47.
15 J. R. Varcoe, P. Atanassov, D. R. Dekel, A. M. Herring, M. A. Hickner, P. A. Kohl, A. R. Kucernak, W. E. Mustain, K. Nijmeijer, K. Scott, T. Xu and L. Zhuang, *Energy Environ. Sci.*, 2014, **7**, 3135–3191.
16 S. Gu, R. Cai, T. Luo, Z. Chen, M. Sun, Y. Liu, G. He and Y. Yan, *Angew. Chem., Int. Ed.*, 2009, **48**, 6499–6502.
17 J. Pan, C. Chen, L. Zhuang and J. Lu, *Acc. Chem. Res.*, 2012, **45**, 473–481.
18 J. Pan, S. Lu, Y. Li, A. Huang, L. Zhuang and J. Lu, *Adv. Funct. Mater.*, 2010, **20**, 312–319.
19 L. Zeng and T. S. Zhao, *Electrochem. Commun.*, 2012, **34**, 278–281.
20 L. Zeng, T. S. Zhao, L. An, G. Zhao, H. X. Yan and C. Y. Jung, *J. Power Sources*, 2015, **275**, 506–515.
21 M. S. Shin, Y. J. Byun, Y. W. Choi, M. S. Kang and J. S. Park, *Int. J. Hydrogen Energy*, 2014, **39**, 16556–16561.
22 Y. Leng, L. Wang, M. A. Hickner and C. Y. Wang, *Electrochim. Acta*, 2015, **152**, 93–100.
23 L. Sun, J. Guo, J. Zhou, Q. Xu, D. Chu and R. Chen, *J. Power Sources*, 2012, **202**, 70–77.
24 S. D. Poynton, R. C. T. Slade, T. J. Omasta, W. E. Mustain, R. Escudero-Cid, P. Ocón and J. R. Varcoe, *J. Mater. Chem. A*, 2014, **2**, 5124–5130.
25 T. J. Omasta, L. Wang, X. Peng, C. A. Lewis, J. R. Varcoe and W. E. Mustain, *J. Power Sources*, 2018, **375**, 205–213.
26 T. J. Omasta, A. M. Park, J. M. LaManna, Y. Zhang, X. Peng, L. Wang, D. L. Jacobson, J. R. Varcoe, D. S. Hussey, B. S. Pivovar and W. E. Mustain, *Energy Environ. Sci.*, 2018, **11**, 551–558.
27 L. Wang, J. J. Brink and J. R. Varcoe, *Chem. Commun.*, 2017, **53**, 11771–11773.
28 J. Ponce-González, I. Ouachan, J. R. Varcoe and D. K. Whelligan, *J. Mater. Chem. A*, 2018, **6**, 823–827.
29 L. Wang, E. Magliocca, E. L. Cunningham, W. E. Mustain, S. D. Poynton, R. Escudero-Cid, M. M. Nasef, J. Ponce-González, R. Bance-Souahli, R. C. T. Slade, D. K. Whelligan and J. R. Varcoe, *Green Chem.*, 2017, **19**, 831–843.
30 J. Ponce-Gonzalez, D. K. Whelligan, L. Wang, R. Bance-Soualhi, Y. Wang, Y. Peng, H. Peng, D. C. Apperley, H. N. Sarode, T. P. Pandey, A. G. Divekar, S. Seifert, A. M. Herring, L. Zhuang and J. R. Varcoe, *Energy Environ. Sci.*, 2016, **9**, 3724–3735.
31 www.agcce.com/brochurespdfs/sales/FluonGrades.pdf, accessed 2018-08-14.
32 S. J. Normile, D. C. Sabarirajan, O. Calzada, V. de Andrade, X. Xiao, P. Mandal, D. Y. Parkinson, A. Serov, P. Atanassov and I. V. Zenyuk, *Materials Today Energy*, 2018, **9**, 187–197.
33 L. Wang, M. Bellini, H. A. Miller and J. R. Varcoe, *J. Mater. Chem. A*, 2018, **6**, 15404–15412.
34 A. Zadick, L. Dubau, N. Sergent, G. Berthoméand and M. Chatenet, *ACS Catal.*, 2015, **5**, 4819–4824.
35 A. Serov, I. V. Zenyuk, C. G. Arges and M. Chatenet, *J. Power Sources*, 2018, **375**, 149–157.
36 S. Gottesfeld, D. R. Dekel, M. Page, C. Bae, Y. Yan, P. Zelenay and Y. S. Kim, *J. Power Sources*, 2018, **375**, 170–184.
37 D. R. Dekel, S. Willdorf, U. Ash, M. Amar, S. Pusara, S. Dhara, S. Srebnik and C. E. Diesendruck, *J. Power Sources*, 2018, **375**, 351–360.
38 L. Wang, J. J. Brink, Y. Liu, A. M. Herring, J. Ponce-Gonzalez, D. K. Whelligan and J. R. Varcoe, *Energy Environ. Sci.*, 2017, **10**, 2154–2167.

Electronic supplementary information (ESI)

ETFE-based anion-exchange membrane ionomer powders for alkaline membrane fuel cells: a first performance comparison of head-group chemistry

Ana Laura Gonçalves Biancolli,[a,d] Daniel Herranz,[c,d] Lianqin Wang,[d] Gabriela Stehlíková,[e,d] Rachida Bance-Soualhi,[d] Julia Ponce-González,[d] Pilar Ocón,[c] Edson A. Ticianelli,[a] Daniel K. Whelligan,[d] John R. Varcoe,[d] and Elisabete I. Santiago [b,d]

This document provides additional data in support of the main article.

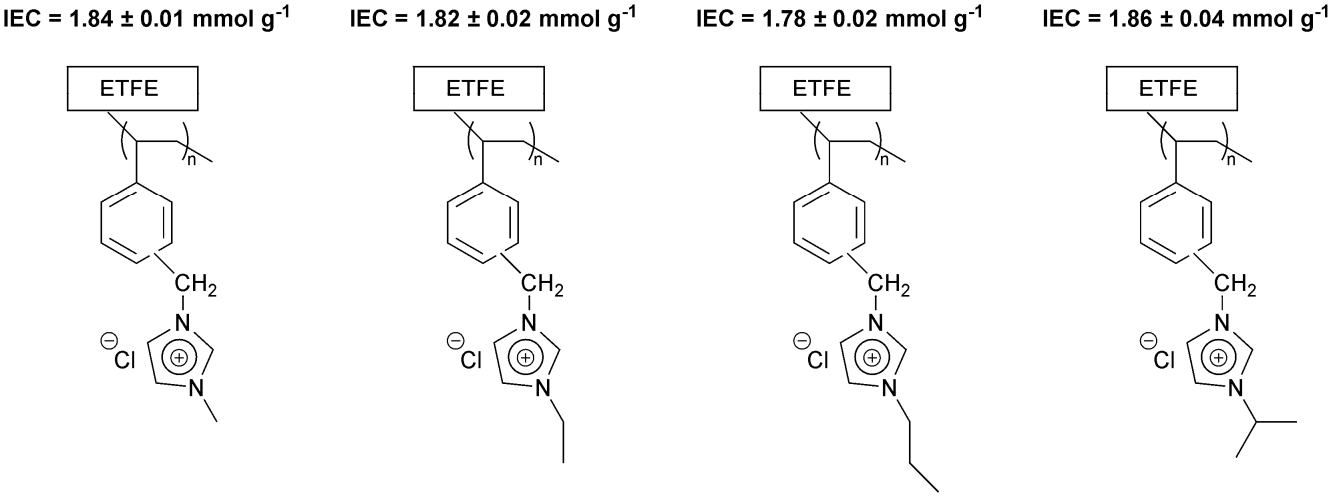

Fig. S1 A series of imidazolium-type anion-exchange membranes (AEM) that were synthesised from the same batch of radiation-grafted VBC-grafted ETFE that was then reacted with a variety of imidazole amination reagents (1-methylimidazole, 1-ethylimidazole, 1-propylimidazole, 1-isopropylimidazole, respectively). All of these AEMs exhibited a Cl^- anion conductivity ($\sigma_{Cl,hydrated}$, 4-probe, in water, room temperature) of 18 mS cm^{-1}. This data is included to demonstrate the lab-scale advantage of using the radiation-grafted technique, where AEMs with different cationic (anion-exchange group) chemistries can be synthesised with similar ion-exchange capacities (IEC) and conductivities.

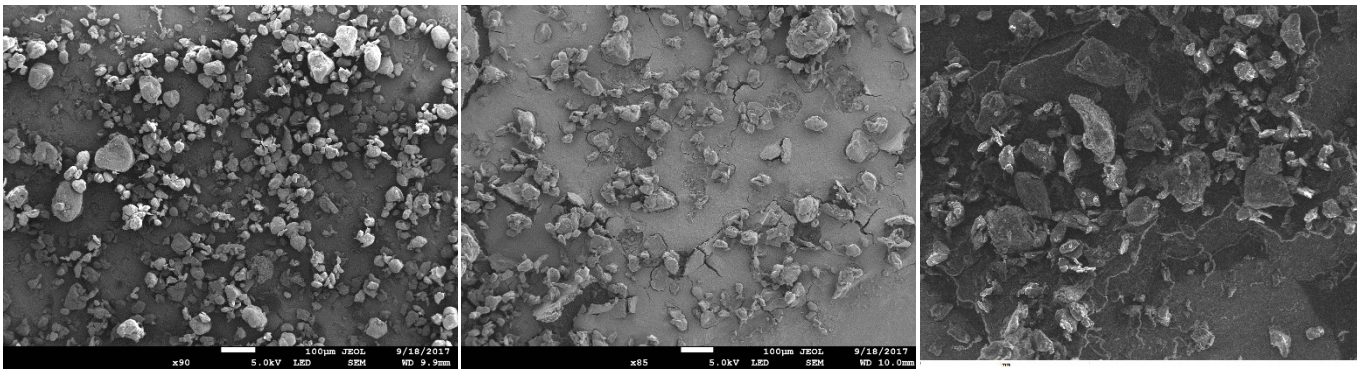

Fig. S2 (left to right) SEM micrographs of **AEI(TMA)** at ×90, **AEI(MPY)** at ×85, and **AEI(MPRD)** at ×90 magnification. Image manipulation involved contrast level adjustment only for visual clarity. Note the **AEI(MPRD)**-containing electrode was studied using a Hitachi S-3200N SEM instrument.

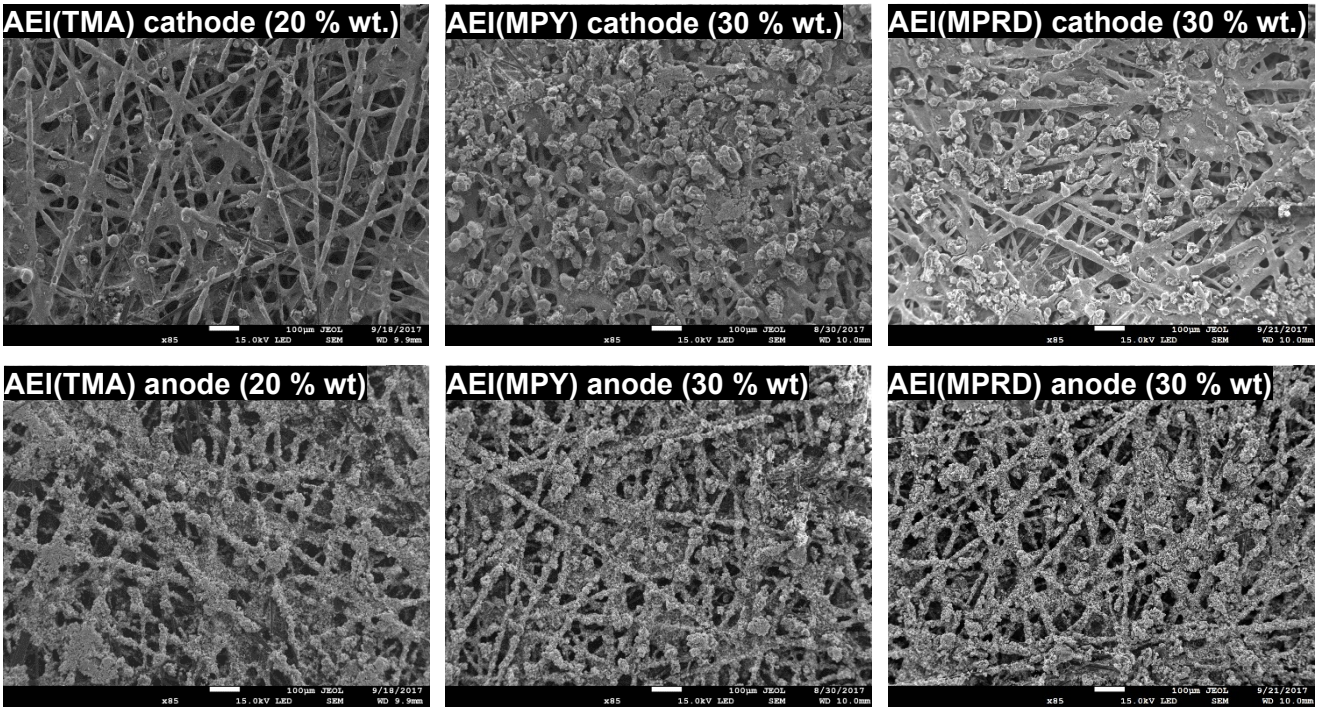

Fig. S3 SEM micrographs (×85 magnification) of exemplar PtRu/C anodes and Pt/C cathodes containing the different powder AEIs.

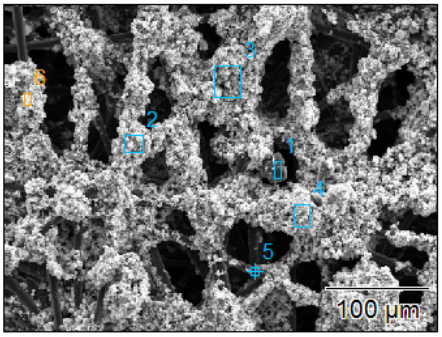

Area	C (%)	F (%)	Ru (%)	Pt (%)
1	35.3	44.7	3.3	6.5
2	4.0	0.0	29.9	61.8
3	4.7	0.1	29.0	63.1
4	4.6	0.0	31.2	61.2
5	60.5	0.2	1.6	3.5
6	10.4	0.1	29.9	55.7

Fig. S4 EDX analysis of sample points of a **AEI(TMA)**-containing PtRu/C anode. Other elements (*e.g.* N, O, Cl) were also analysed (not shown in the table). All percentages are % wt.

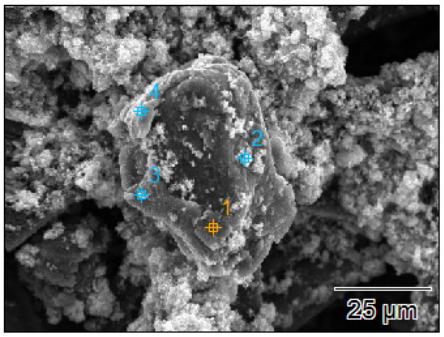

Area	C (%)	F (%)	Ru (%)	Pt (%)
1	69.2	7.7	-	2.4
2	9.3	1.2	37.8	51.6
3	4.4	2.3	44.8	46.7
4	72.4	7.9	-	-

Fig. S5 EDX analysis of sample points of a **AEI(MPY)**-containing PtRu/C anode. Other elements (*e.g.* N, O, Cl) were also analysed (not shown in the table). All percentages are % wt.

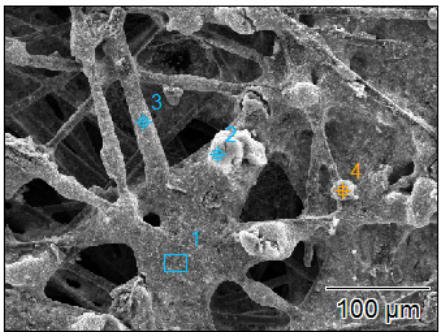

Area	C (%)	F (%)	Pt (%)
1	27.1	0.3	67.2
2	36.5	0.1	58.9
3	29.9	0.1	64.7
4	27.9	0.0	64.6

Fig. S6 EDX analysis of sample points of a **AEI(MPY)**-containing Pt/C cathode. Other elements (*e.g.* N, O, Cl) were also analysed (not shown in the table). This data suggests a more uniform coverage of the Pt/C catalyst (compared to the PtRu/C anodes analysed in Figs. S4 and S5 above). All percentages are % wt.

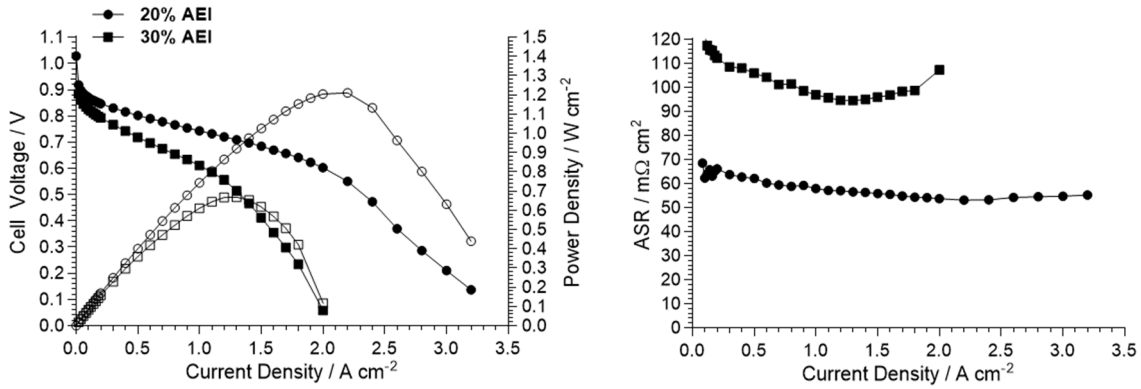

Fig. S7 AEMFC fuel cell performances at 60 °C (H_2 anode gas and O_2 cathode gas, both supplied unpressurised with dewpoint temperatures of 60 °C) with **AEI(TMA)/AEM(TMA)/AEI(TMA)**-based MEAs containing either 20 or 30 % wt. AEI loadings. PtRu/C anodes and Pt/C cathodes were used (with 0.40 ± 0.03 mg cm^{-2} Pt loadings). These two specific AEI loadings were selected in response to anecdotal evidence collected over a number of initial [unpublished] experiments.

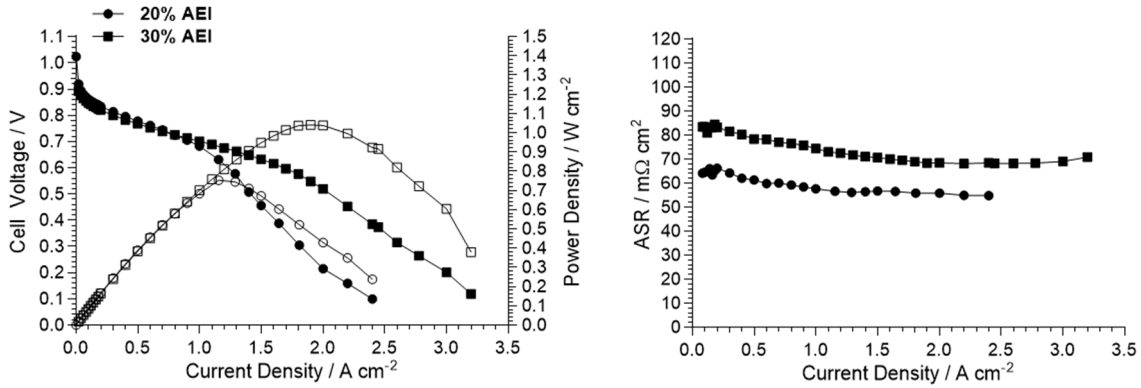

Fig. S8 AEMFC fuel cell performances at 60 °C (H_2 anode gas and O_2 cathode gas, both supplied unpressurised with dewpoint temperatures of 60 °C) with **AEI(MPY)/AEM(TMA)/AEI(MPY)**-based MEAs containing either 20 or 30 % wt. AEI loadings. PtRu/C anodes and Pt/C cathodes were used (with 0.40 ± 0.03 mg cm^{-2} Pt loadings).

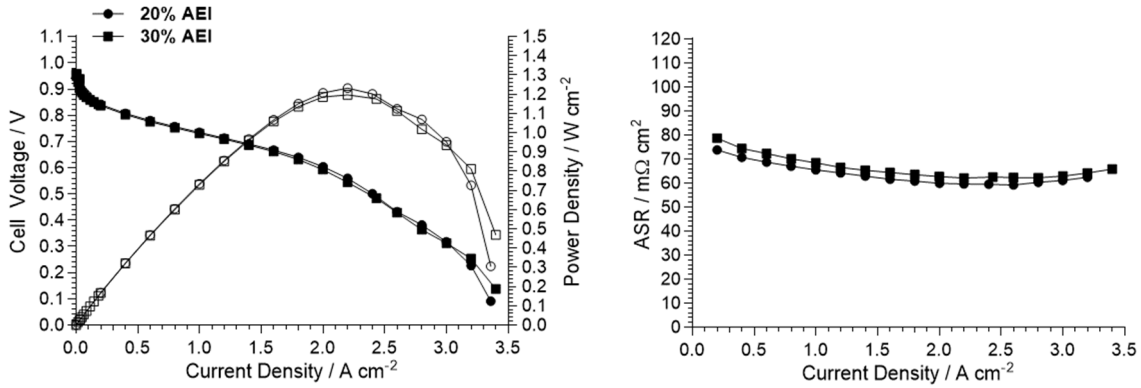

Fig. S9 AEMFC fuel cell performances at 60 °C (H_2 anode gas and O_2 cathode gas, both supplied unpressurised with dewpoint temperatures of 60 °C) with **AEI(MPRD)**/**AEM(TMA)**/**AEI(MPRD)**-based MEAs containing either 20 or 30 % wt. AEI loadings. PtRu/C anodes and Pt/C cathodes were used (with 0.40 ± 0.03 mg cm^{-2} Pt loadings).

Chapter

Benzimidazole as Solid Electrolyte Material for Fuel Cells

Daniel Herranz and Pilar Ocón

Abstract

This chapter is focused in the application of benzimidazole, mainly in the form of poly[2,2′-(*m*-phenylene)-5,5′-bisbenzimidazole] (PBI) and poly(2,5-benzimidazole) (ABPBI), in the fuel cell technology. A short introduction is given of the fuel cell principles, explaining both the theory and the high importance of this technology. PBI and ABPBI are used in a certain type of fuel cells: the polymer electrolyte fuel cells and are key materials in the composition of some of the electrolyte membranes used. Commercially available membranes composed of PBI are indicated in order to give an overview of their potential performance. The synthesis of the polymers is explained. Moreover, the preparation of the different kinds of membranes, both in proton exchange membrane fuel cells (PEMFCs) and anion exchange membrane fuel cells (AEMFCs) is studied. A deep description is given about the properties that make this family of compounds so interesting for the fuel cell technology as well as an how these polymers have been characterized with the corresponding analysis. The comparison with other ion exchange membranes is also discussed. Special attention will be given to the state of the art of different kinds of PBI/ABPBI fuel cell electrolyte membranes, in which our group and others are working nowadays.

Keywords: polybenzimidazole, electrolyte, fuel cells, proton exchange membrane, anion exchange membrane

1. Introduction

Benzimidazole and its family can be used in the energy world easily in the form of polymers, since these materials have the possibility to create designed structures for many applications. The fuel cells and electrolyzers are emerging technologies with wonderful potential. In these technologies, an electrolyte is needed to separate two electrodes where electrochemical reactions occur. The separation must be physical and electrical, but the electrolyte allows the ionic conduction of ions in order to close the circuit (so the current goes through the external circuit and can be used) and to make possible the continuity of the reactions at the electrodes. Here is where benzimidazoles (in the form of polybenzimidazole, e.g.) play a key role, in the conformation of a solid polymer electrolyte membrane, alone or with other chemical materials.

But, what is a fuel cell? What do we understand for membranes in this field? Fuel cells are electrochemical devices that convert directly the chemical energy of the reagents into electrical energy and side-products via an electrochemical

reaction. This process allows theoretical efficiencies as high as 80% [1], which is a wonderful advantage compared to the thermal machines limited thermodynamically by the Carnot cycle. There are many types of fuel cells, the most relevant are alkaline fuel cells (AFCs), polymer electrolyte membrane fuel cells (PEMFCs), phosphoric acid fuel cells (PAFCs), molten carbonate fuel cells (MCFCs), and solid oxide fuel cells (SOFCs).

Polymer electrolyte membrane fuel cells have as principal characteristics the low operation temperature (<120°C), high power density, and easy scale-up, making them a promising technology for power generation. Their main application fields are backup power, portable power, distributed generation, and transportation [1]. It is relevant to note the role of transition energy technology, since they can play an important function in the near future in order to overcome the fossil fuel depletion and mitigate the climate change. The reason is that fuels like hydrogen or alcohols, which are produced by unsustainable ways, could be produced with renewable energies. An example of this is the actual production of hydrogen mainly from catalytic reforming of methane and just some from electrolysis [2]. The hydrogen can be produced from electrolysis powered with electricity coming from renewables. This should be done when production is higher than the demand, allowing to store chemically the energy and later use it when needed with a PEMFC; this is known as the "hydrogen economy system." It is also possible to accumulate energy in short-chain alcohols like methanol or ethanol and use them to power PEMFCs [3, 4], mainly used in the portable applications. A great advantage of this technology is the low pollution associated with the process. For example, when hydrogen is used as fuel, the only products are electricity and water. The potential of PEMFCs is really promising but still drawbacks as high cost (mainly from the expensive catalysts based in Pt) and low durability have to be overcome for a general commercialization [1].

In PEMFCs one of the most important components is the polymeric ion exchange membrane (IEM) that works as an electrolyte. It has to be an electrical insulator to force the produced electrons to go through the external circuit, it also has to avoid the mixture of the reagents supplied in anode and cathode, and it is responsible of the adequate ionic conductivity of the ions traveling through it. Depending on the ion movement, two types of IEMs can be distinguished: anion exchange membranes (AEMs), where the ionic charge carriers are the hydroxide ions (OH^-) that travel from cathode to anode, and cation exchange membranes (CEMs) where generally the proton ion (H^+) moves from anode to cathode in the fuel cell. For that reason, the last ones are also called proton exchange membranes (PEMs). The AEMs are used in alkaline media and the others in acid media. The proton exchange membrane fuel cells (PEMFCs) have been historically more used because of the discovery of the Nafion® membrane that has good ionic conductivity and durability and has been the standard so far [5]. The higher mobility of the H^+ ion compared to OH^- in aqueous media has also been a relevant factor [6]. The alkaline media in the other hand does not have a standard membrane and presents relevant advantages that have produced high interest in the last years. Some of them are the faster electrochemical kinetics in the alkaline media, possible absence of noble metals as catalysts, minimized corrosion problems, and cogeneration of electricity and valuable chemicals [7].

Independently of the media, membranes are expected to have good ionic conductivity, long-term chemical and electrochemical stability, adequate mechanical strength, good moisture control, low fuel or oxygen crossover, and production costs compatible with intended application [5, 6].

In the FCs, the active materials (fuel and oxidant) are continuously fed and extracted. The fuel cell, **Figure 1**, is made up of two electrodes: the anode, where the

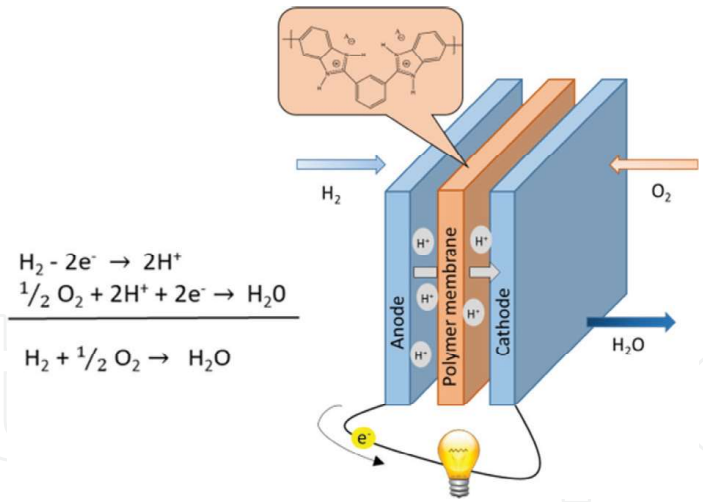

Figure 1.
Polymer exchange membrane fuel cell working with H_2 and O_2.

fuel is oxidized, and the cathode, where the oxidant (O_2) is reduced. It also involves an electrolyte, which acts as an ionic conductor and electrical insulator. The electrons obtained in the anode are addressed directly to the cathode through the external circuit, generating an electric current directly usable. In addition, the protons produced in the anode go through the electrolyte, up to the cathode to reduce O_2, generating water as the only product of the reaction. The reaction is exothermic and has a value of $\Delta H^0_r = -285.83$ kJ/mol for H_2O (l) and − 241.862 kJ/mol for H_2O (v). Although this is a spontaneous reaction, it needs to be catalyzed to be operational, since the kinetics of the process is too slow otherwise.

At atmospheric pressure, the maximum potential difference obtained by the fuel cell will be determined by the difference of energy between the initial and final state of the system. The Gibbs free energy variation of the process, ΔG, can be calculated from the operation temperature (T) and changes with both enthalpy (ΔH) and entropy (ΔS) of the reaction. Under standard conditions

$$\Delta G^0 = \Delta S^0 - T\,\Delta S^0 \tag{1}$$

and the maximum potential difference, obtained in the fuel cell, $E^0_{theoric}$, will be

$$E^0 = \frac{-\Delta G^0}{nF} = 1.23V \tag{2}$$

where n is the number of electrons exchanged and F is Faraday's constant. At 298 K and 1 atm, $\Delta G^0 = -237.340$ J/mol and therefore $E^0 = 1.23$ V. For an operating temperature of 80°C, the values of ΔH and ΔS change, but slightly, and the decrease in ΔG will be mainly due to the temperature, resulting in a theoretical potential difference of 1.18 V approximately. However, in practice this potential, called the open circuit potential, is significantly lower than this potential value, usually less than 1 V. This suggests that some losses appear in the fuel cell even when no external current is generated. The potential difference of the fuel cell in operation, that is, when the current is passing through the system, $E_{fuel\ cell\ (I)}$, will be given by the sum of thermodynamic or reversible value (I = 0), minus the anode and cathode activation overvoltage and the ohmic losses or overvoltage. The electrode kinetics was represented by the Butler-Volmer equation, the mass transport process was described by the multicomponent Stefan-Maxwell equations and Fick's law, and the

ionic and electronic resistances are described by Ohm's law. The $E_{\text{fuel cell (I)}}$ value could be obtained by

$$E_{fuel\ cell\ (I)} = E_{Reversible\ (I=0)} - \eta_{activation} - \eta_{ohmic} \tag{3}$$

The losses considered are in relation to the activation overvoltages, and they are dependent on the kinetics of the processes involved and therefore directly related to the goodness of catalyst used for the process. Thus, $\eta_{\text{activation}}$ is related directed with both the oxidation kinetic reaction and the reduction kinetic reaction of the reagent involved in the catalysts surface materials. The $\eta_{\text{activation}}$ for an H_2/O_2 fed in PEMFC will come mainly determined by the slow kinetics of oxygen reduction reaction (ORR) on the catalyst material in comparison to H_2 oxidation, while $\eta_{\text{activation (transport)}}$ is the consequence of material transport. This overpotential considers the combination of the flow of reactants and products in the fuel cell. The polarization from concentration gradients occurs when a reactant is rapidly consumed at the electrode by the electrochemical reaction so that gradients are established. The η_{ohmic} = iR will be due to the combination of resistors provided by internal/external electrical contacts and ionic resistance due to ion motion through the membrane. Therefore, the fuel cell when current is not zero has an $E_{\text{fuel cell(I)}}$ expression like this:

$$E_{fuel\ cell\ (I)} = E_{rever\ (I=0)} - \frac{RT}{\alpha_c} ln\left(\frac{i}{i_{0,c}}\right) - \frac{RT}{\alpha_a} ln\left(\frac{i}{i_{0,a}}\right) - \frac{RT}{\alpha_c} ln\left(\frac{i_{I,c}}{i_{I,c} - i}\right) - \frac{RT}{\alpha_a} ln\left(\frac{i_{I,a}}{i_{I,a} - i}\right) \tag{4}$$

$$E_{rev\ (I=0)} = 1.229 - \left(8.5 \times 10^{-4}\right)(T - 298.15) + \left(4.308 \times 10^{-5}\right)T[\ln(P_{H2}) + 0.5\ln(P_{O2})] \tag{5}$$

being i_{oc}, α_c, i_{Lc} and i_{oa}, α_a, i_{La} the exchange current density, transfer coefficient, and limit current density of the cathodic and anodic processes, respectively [8]. The polarization curve of the device can be found in **Figure 2**, where the different losses mentioned above are indicated.

It was previously stated that the ion exchange polymer membrane is electrically insulator and practically impermeable to reactant gases, but some small amount of mainly H_2 will crossover from anode to cathode. Hydrogen that permeates through the membrane does not participate in the electrochemical reaction on the anode

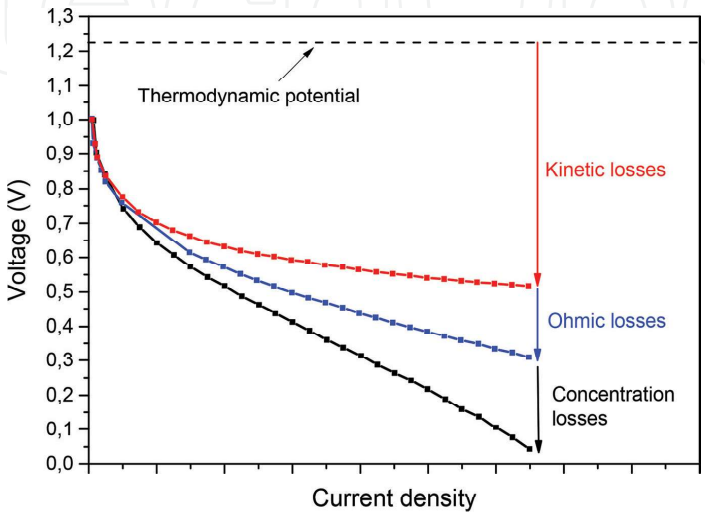

Figure 2.
Polarization curves with voltage losses of a fuel cell.

side. Each hydrogen molecule on the cathode side reacts with oxygen on the surface of the catalyst resulting in two fewer electrons in the generated current that travels through the external circuit and thus in a reduction of cathode and the overall fuel cell potential. These losses are not big in fuel cell operation, but when the fuel cell is at open circuit potential or at very low current densities, this situation may have a dramatic effect on fuel cell potential. At least, all these losses have to be taken into account when the device works and have a lot to do with good fuel cell performance.

2. Synthesis of polybenzimidazole materials

Polybenzimidazoles are synthesized by the repetitive reaction of aromatic amino groups with carboxyl groups using a 1:2 molar ratio by the process of step-grow polymerization [9]. Usually the monomer reagents are a diacid and a tetra-amine, like the example in **Figure 3**. There are many polybenzimidazoles but the ones that have presented better application and have been more studied are poly(2,2′-(*m*-phenylene)-5,5′-bibenzimidazole), known as PBI, and poly(2,5-benzimidazole), known as ABPBI. Both were first synthesized by Vogel and Marvel in 1961 [10]. For PBI the synthesis was a two-step process with an intermediate prepolymer that prevented the production of high molecular weight polymer. Cho et al. [11, 12] discovered a process with 3,3′,4,4′-tetraaminobiphenyl (TAB) and isophthalic acid (IPA) to do the synthesis in a single step obtaining high molecular weight, in the presence of catalyzers and at temperatures higher than 350°C. It is important to know the molecular weight of the polymer, which is obtained by the measurement of the inherent viscosity (IV, in dLg^{-1}) of the polymer dissolved in concentrated sulfuric acid. For membrane application, usually casted from solution, it is interesting to have high molecular weight in order to achieve mechanically stable membranes that can support higher doping and thus obtain better ionic conductivity. The previously described method of Vogel and Marvel and Cho et al. can be classified in the heterogeneous molten/solid state synthesis [13, 14]. The other synthesis method used is the homogeneous solution synthesis, using solvents as polyphosphoric acid (PPA) [15]; this method allows to use moderate temperature and more stable monomers and is excellent to synthesize linear high molecular weight polymers at laboratory or small batch scale. These advantages make this synthesis method the most commonly used. Another example of solvent is Eaton's reagent, a mixture of phosphorus pentoxide (P2O5) and methanesulfonic acid (MSA) proposed by Eaton et al. [16], which has low viscosity making it suitable for the homogeneous solution synthesis and the acid washing after it [17, 18]. A shorter reaction time with high molecular weight has been obtained using homogeneous solution microwave-assisted synthesis recently, both for PBI and ABPBI [14].

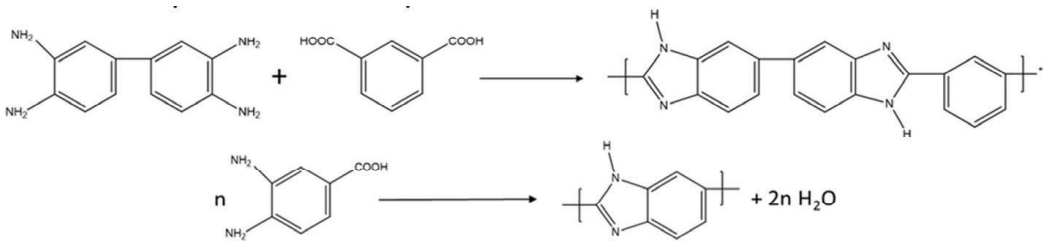

Figure 3.
Example synthesis of (top) poly(2,2′-(m-phenylene)-5,5′-bibenzimidazole), abbreviated as PBI, and (bottom) poly(2,5-benzimidazole) (ABPBI).

ABPBI is synthesized from a single monomer, (3,4-diaminobenzoic acid) (DABA), which as the advantages of being less expensive, commercially available, and non-carcinogenic. The scheme is shown in **Figure 3**. Different syntheses have been done by the homogeneous solution method in PPA or Eaton's reagent, and inherent viscosity values as high as 7.33 have been reached, as reported by Li et al. by using recrystallized DABA [19]. This is essential for the direct casting of ABPBI membranes since it has been suggested by Asensio and Gómez-Romero that values of at least 2.3 dL g^{-1} are necessary to cast good membranes [13].

In the case of ABPBI, since there is only a monomer, its purity is not as critical as in PBI; however, the use of high purity monomer produces polymers of high molecular weight [20]. Since polybenzimidazoles have to be doped in order to become ionic conductors, two methods are used to prepare the membranes: direct casting from the polymerization solution, as the work developed by Asensio et al. [21], or dissolving the previously synthesized polymer and then doing the casting of the membrane. The casting process consists in the formation of a thin film by the deposition of the polymer by evaporation of the solvent in the solution. To solubilize PBI or ABPBI, usually strong bases or acids are needed; only a few organic solvents can also do it; one of them is the N,N-dimethylacetamide (DMAc) [13, 22]. There is also an alternative way to cast ABPBI membranes from a mixture of NaOH and ethanol [23].

3. Properties of the materials and characterization

The structure of polybenzimidazoles has a good degree of flexibility and chemical and thermal resistance compared to other polymers with more single bonds in their main chain between aromatic units. The presence of aromatic units in the main chain to have higher thermal stability than the aliphatic analogs is also important [9]. In order to characterize polybenzimidazoles, one of the most important parameters is the molecular weight of the polymer, which will be highly related to the final membranes properties. The common way to obtain the molecular weight is by measurement of the intrinsic viscosity of the polymer (η_{IV}) at a certain temperature (normally 25–30°C). From the plotting of the specific viscosity (η_{sp}) as function of the polymer concentration, the intrinsic viscosity is calculated extrapolating to zero concentration. A simpler measurement process was proposed to do the calculation with a single-point method using Eq. (6), where C is the polymer concentration in a concentrated acid like 96 wt% H_2SO_4:

$$\eta_{IV} = (\eta_{SP} + 3\ln(1 + \eta_{SP}))/4C \tag{6}$$

The protocol test is to calculate the η_{sp} of a polymer solution 5 g L^{-1} in concentrated sulfuric acid at 30°C using an Ubbelohde viscometer. From the η_{IV} value, the average molecular weight is calculated with the Mark-Houwink- Sakurada expression:

$$\eta_{IV} = K * M_W^{\alpha} \tag{7}$$

where the Mark-Houwink constants depend on the molecular weight range and distribution. Values often used for this constants are K = 1.94 × 10^{-4} dL g^{-1}, and α = 0.791, obtained from Buckley et al. by light scattering measurements. Other solvents as formic acid or MSA can also be used to measure the viscosity of polybenzimidazoles [14].

There are various techniques in order to investigate the structure of polybenzimidazoles. Nuclear magnetic resonance is very powerful for pure organic

compounds or the repeating unit of a polymer. Solvents that can be used include deuterated dimethyl sulfoxide (DMSO- d_6) and deuterated sulfuric acid (D_2SO_4). The most commonly used to record ^{1}H-NMR spectra is DMSO-d_6 because with D_2SO_4, the fast exchange interaction with the proton in the imine of the imidazole rings (-NH-) causes the chemical shift of that hydrogen to be often indiscernible [24]. ^{1}H-NMR PBI characteristic signals in DMSO-d_6 are at 13.2 (2H), 9.1 (1H), 8.3 (2H), and 8.0–7.6 (7H) ppm, the first of them attributed to the imidazole protons and the others to the aromatic protons [25, 26]. IR and Raman spectroscopy are also used, mainly to identify different functional groups and obtain or corroborate the chemical structure of the polymers [24, 27, 28]. In PBI, the IR spectrum region from 2000 to 4000 cm^{-1} is interesting since N–H stretching modes occur in this range, showing three typical bands at 3415, 3145, and 3063 cm^{-1}. The broad band around 3145 cm^{-1} has been attributed to the stretching vibrations of N–H groups self-associated by hydrogen bonds, and the peak at 3145 cm^{-1} is assigned to the N–H groups stretching vibration. In the region from 1630 to 1500 cm^{-1}, the peaks observed come from the vibration of C=C and C=N bonds [27]. In the Raman spectra of PBI, the most significant absorption band comes from the benzene ring vibration and is located around 1000 cm^{-1} [28]. For the measurement of the Raman spectra, it is relevant to use an excitation wavelength of 785 nm (red laser) since it gives much less fluorescence than the 532 nm (green laser) [29]. Because the structure and functional groups are the same, ABPBI presents the same IR peaks than PBI, as reported by Asensio et al. [30]. They also investigated the bands appearing when the polymer membrane is doped with phosphoric acid: in the N–H stretching zone, they found the evolution of nitrogen protonation by the acid, and in the medium and high doped samples, the broad band of N^+–H vibration becomes stronger, while the nonassociated imidazole protons decreases. In polybenzimidazoles doped with alkaline media for anion conductivity purposes, the structure changes are also clearly identified. Aili et al. [31] investigated PBI with different degrees of KOH doping and found that in the IR spectra, at KOH concentrations higher than 15 wt.%, the N–H stretching band at 3415 cm^{-1} disappear as well as the broad band around 3100 cm^{-1} of shelf-associated hydrogen bonded N–H groups. They concluded that the IR data indicated the predominance of the deprotonated form of PBI with KOH concentrations of the bulk solution around 15–20 wt.%. In the ^{1}H-NMR spectrum the signal at 13.3 ppm of the N–H proton disappeared at high bulk KOH concentration, and most signals from the aromatic protons showed upfield shift compared to pristine PBI, indicating complete ionization. This full ionization of the polymer releases the extensive intermolecular hydrogen bonding allowing for high swelling behavior and water and KOH uptake and therefore enhanced ion conductivity. This study corroborates the knowledge that the introduction of species that interact with imidazole groups by hydrogen bonding decreases the intermolecular polybenzimidazole cohesion, causing a strong plasticizing effect observed in the great decay of the tensile strength and enhanced elongation at break when the doping level increases, especially when full ionization of the polymer is reached. Using an even higher concentration doping solution, they found that a higher crystallinity structure was obtained, as observed by XRD, mechanical test, and swelling behavior measurements. X-ray photoelectron spectroscopy (XPS) is also a helpful technique for the characterization of polybenzimidazoles, concretely for the capacity to distinguish the oxidation states of the elements present and allow their quantification in the surface of the membrane [29]. Other fundamental measurements usually performed on the synthesized membranes are the determination of the ionic conductivity, the swelling behavior with water and in acidic/alkaline media, or the thermogravimetric analysis (TGA). In conclusion, a full set of characterization analysis have been studied and are used

to identify and test the properties of the synthesized polybenzimidazoles and the membranes prepared with them.

4. Commercial availability

There have been different companies relevant in the fuel cell membrane field, probably the most known one is DuPont for developing the Nafion® membrane made of a sulfonated tetrafluoroethylene-based fluoropolymer-copolymer with excellent thermal and mechanical stability as well as high proton conductivity in low-temperature fuel cells. Companies like Solvay, Gore, and others have also commercialized membranes with this chemistry. This membrane has been the standard for fuel cells used in low-temperature and acidic media, but at temperatures higher than 100°C, Nafion® performance drops dramatically due to the lower hydration level. It is in these conditions where membranes made of polybenzimidazoles have shown good performance and promising applicability, and production for commercialization has occurred. BASF Fuel Cell (formerly PEMEAS Fuel Cell), a part of one of the larger chemistry industries, has developed a product line about a membrane electrode assembly (MEA) based in a PBI membrane, Celtec® [32, 33]. These MEAs optimal operation conditions are between 120 and 180°C, doped in phosphoric acid. They have shown relevant advantages working as high temperature PMFCs, like high tolerance to fuel gas impurities such as CO (up to 3%), H_2S (up to 10 ppm), NH_3, or methanol, no humidification required, far simpler system due to elimination of water, and a less complex reformer technology. In addition, several advantages can be obtained for the electrocatalysis, but it is necessary to be especially careful at the high stability toward corrosion needed to ensure long fuel cell lifetimes, apart from high activity for the oxidation of the fuels and the oxygen reduction reaction. Other companies that commercialize PBI- and PBI-based membranes are "PBI Performance Products" with their Celazole® PBI PEM [22, 34] and Danish Power Systems with their Dapozol® membranes and MEAs [35]. Membranes based on PBI are of high applicability as it can be observed, both for the fuel cell technology in development and also for other applications as carbon capture, pervaporation dehydration processes, or electrochemical hydrogen separation, among others.

5. Proton exchange membrane fuel cells (PEMFCs)

Polybenzimidazole (PBI) as ionic exchange membrane can be used as proton exchange if the material is doped with phosphoric acid (H_3PO_4), sulfuric acid (H_2SO_4), and nitric acid (HNO_3) solvent media. The PBI has benzimidazole units in the polymer chain and bears the pKa = 5.5 that is responsible for the weak acid character, and they have excellent oxidative and thermal stability [36]. The acid molecules penetrate the membranes during doping process, due to the acid-base interaction between them and gradually swelling of PBI membrane. Therefore, PBI can be easily doped with different types of strong acids, which act as predominant protonation through the PBI membranes.

In these circumstances, the material can work as solid electrolyte in a fuel cell in temperature range between 100 and 200°C, overcoming the dehydration problem that the Nafion® membrane has in operation condition at around 100°C and in consequence the dramatically reduction of its proton conductivity, presenting a near zero electro-osmotic drag [37]. High temperature makes HT-PEMFC more tolerant to impurities in feed gases (CO, e.g.) and simplifies elimination of waste

heat with a simpler cooling system. If the fuel cell is working with reformed natural gas as a power source, the device does not require humidification of reactants due to the simple water management; that is why all these features greatly simplify design of HT-PEMFC stack [38].

In the PBI/H_3PO_4 system, the polybenzimidazole acts not only as a matrix polymer but also as proton acceptor [39]. For HT-PEMFCs, PBI/H_3PO_4 is considered a reasonably successful solid electrolyte because the excellent conductivity and thermochemical stability. Phosphoric acid has been widely employed as an anhydrous proton conductor because of its high proton conductivity, low cost, and thermal stability. At temperatures above 150°C, the dehydration of the acid occurs and yields pyrophosphoric acid or higher oligomers, which exhibit worse proton conductivity. On the other hand, the long-running operation leads to the release and dilution of H_3PO_4 from the membranes, which results in a loss of the acid into the fuel cell gas/vapor exhaust streams, the decrease of membrane ionic conductivity, and thus a lower fuel cell performance occurs. The high proton conductivity of the membranes was proved only when the polymer holds a large excess of phosphoric acid [40]. The optimum doping level was around 5 moles H_3PO_4 per PBI repeat unit, where a compromise between conductivity and mechanical properties was achieved.

A thick membrane is not usually advantageous because it is mainly responsible for the large ohmic polarization and modest power performance of HT-MEA. However, approx. 100 μm has been implemented with the intention of improving their mechanical properties [41]. The acid doping is an essential process, but it softens the PBI membrane, causing membrane ripping in MEA fabrication. The mechanical stability of the doped PBI membrane can be improved by lowering the H_3PO_4 doping level; however, the proton conductivity is reduced [42].

The problems of HT-PEMFCs operating at temperatures up to 100°C are not solved yet and demonstrate the necessity of research on new and more satisfactory alternatives. In this context, the ionic liquids (ILs) have been used as nonaqueous and low-volatility proton carriers in replacement of aqueous electrolytes. The protic ILs for example are able to transport protons due to their acid-base character and their capability to form complex or intermolecular hydrogen bonds [43] even in nonaqueous conditions. This type of materials tries to overcome the formation of unstable materials in the operating conditions and then to improve the performance of the PEMFC at high temperatures. The first research team working in this subject was Watanabe and colleagues, who identified the potential electroactive use of ILs in fuel cell reactions [44]. Sometimes, polymer phase substrate and the IL result in nonhomogeneous and unmanageable membranes when both components are integrated together. In general, ILs and polymers dissolved in a common solvent and later are casted as a film. In this way hybrid membranes are obtained, and the materials may be studied once the solvent has been removed. PBI-based hybrid membranes holding ILs are examples of this methodology. Greenbaum et al. [45] demonstrated that the composite gel-type membranes obtained from H_3PO_4 and aprotic hydrophilic IL, namely, 1-propyl-3-methylimidazolium dihydrogen phosphate [PMI][H_2PO_4] and PBI, can be operated as ion exchange membrane up to 150°C in a PEMFC. The composite membranes were homogeneous and both chemically and thermally stable with wide temperature range. Nevertheless, phase separation occurred when mixing the 1-ethyl-3-methylimidazolium triflate [EMI][Tf] or 1-ethyl-3-methylimidazolium bis(trifluoromethanesulfonyl)imide [EMI][TFSI] ILs with H_3PO_4 and PBI, resulting in homogeneous membranes. Schauer et al. [46] investigated the use of aprotic ionic liquid 1-butyl-3-methylimidazoliumtrifluoromethanesulfonate [BMIM][TfO] and protic ionic liquid 1-ethylimidazoliumtrifluoromethanesulfonate [EIM][TfO] to prepare membranes with several different

polymers: a polybenzimidazole derivative with benzofuranone (PBI-O-Ph), Udel®-type polysulfone (Udel® PSU), and poly(vinylidene fluoride-co-hexafluoropropene) fluoroelastomer. The proton conductivity of the membranes was a function of the temperature and the ionic liquid amount in the membrane and the polymeric matrix itself. For PBI-O-Ph-based membranes, the conductivity was very low up to 90°C. Wang et al. [47] studied the PBI/IL composite membranes where the IL was 1-hexyl-3-methylimidazolium trifluoromethanesulfonate [HMI][Tf], an organosoluble fluorine ionic liquid. The ionic conductivity reached a value as high as 1.6×10^{-2} S cm^{-1} at 250°C under anhydrous conditions, and the results depended on temperature and IL content. The IL [HMI][Tf] works simultaneously as plasticizer and ion carrier. On the other hand, the major drawback related to the IL addition is a loss of membranes' mechanical properties, resulting in a good solid electrolyte to carry out the functions of HT-PEMFC at temperature > 200°C.

In many cases imidazolium salts are the most investigated as ILs in these applications; composite membranes with good specific conductivity have been found for their application as electrolytes in PEMFCs; however low performances (maximum power densities of around 1 mW cm^{-2} [48]) have been obtained.

Another example of composite hybrid membranes is the use of PBI as matrix and the diethlyaminebisulfate/sulfate IL, [DE][SH], in different compositional ratios, PBI/[DE][SH_x], as was published by Ocón et al. [49]. In this case, the composite membranes were obtained using a solution casting method. The interaction between the IL and the PBI was analyzed by FTIR spectroscopy. The imine group from the imidazole ring of PBI composite membranes showed no evidence of protonation, and consequently, the interaction between the IL and PBI was weak, remaining free inside of the PBI structure and allowing for the ionic conduction. The mechanical properties and tensile stress of pristine PBI was deteriorated dramatically on increasing the IL content, despite the fact that the conductivity values were very acceptable for the described application. For demanding fuel cell operation conditions, such as 200°C, and low humidity conditions, the PBI/[DE][SH_x] membranes exhibited acceptable ionic conductivity values, higher than 0.01 S cm^{-1}. In addition to high proton conductivity in anhydrous environment, which is an indispensable condition for potential HT-PEMFC membrane candidates, other requisites must also be fulfilled: barrier to the reagent gases, thermal and dimensional stability under operating conditions, electrochemical stability under reducing and oxidizing potentials, and compatibility with the electrocatalyst. In this particular case, low open-circuit voltage (OCV) of the cell, 0.8 V, was obtained. This suggests a mixed potential, although no crossover was detected in the experiments. The authors suggested that kinetic complication could show up like additional oxidation and reduction reactions simultaneously with the corresponding oxygen reduction reaction (ORR) and hydrogen oxidation reaction (HOR), respectively; furthermore, the poisoning effect of the H_2S generated at the anode should not be ignored.

On the other side, the beneficial effect on the decrease of the IL viscosity was observed in the performance of the fuel cell. The optimum performance was obtained with no limiting current, being the maximum current density ca. 70 mA cm^{-2} and 13.5 mW cm^{-2}, using 100% relative humidity at 80°C. At temperature higher than 80°C, the system starts to dehydrate, whereas the IL viscosity increases and the proton diffusion was hindered. The performance at 150°C wasn't good showing clear evidences of the system dehydration at temperatures beyond 80°C. The migration of the IL from anode to cathode was demonstrated in *postmortem* analysis of PBI/[DE][SH_x] composite-based electrodes. The IL went out of the composite membrane, and in consequence the cell resistivity increased by a factor of six times after polarization measurements.

It is necessary to keep in mind that the requirements of cell lifetime vary for different applications, that is, 5000 h for cars, 20,000 h for buses, and 40,000 h for stationary application with continuous operation [43]. This means that the development of ionic exchange membranes with a long operating life is a challenge to develop.

6. Anion exchange membrane fuel cells (AEMFCs)

Many electrochemical systems use ion exchange membranes, such as fuel cells, electrolyzers, or redox flow batteries. Traditionally cation exchange membranes have been used in these systems due to the idea that anion exchange membranes had too low conductivity and stability. However, in the last years, many advances have been made, and anion exchange membranes (AEMs) are demonstrating to have performances comparable to acid ones, showing promising application in several technologies [2]. These membranes conduct negatively charged ions like OH^- or Cl^- and usually have positive-charged groups in the polymer structure, which could be directly present in the polymer backbone or more commonly fixed to it by extended side chains of varying lengths and chemistries. Varcoe et al. [2] investigated a deep review about the different chemistries of polymer backbones and head groups and their current state of research. The use of alkaline media, compared to acid media, has some advantages like the better electrochemical kinetics of the oxygen reduction reaction (ORR). This allows the possibility of using non-noble metals in the electrocatalysts reducing the fuel cell system cost. Other advantages are the minimized corrosion problems and the cogeneration of electricity and valuable chemicals [7, 50]. Compared to classical alkaline fuel cells (AFCs) where the electrolyte is in aqueous phase, the use of AEMs solves the carbonation problems and the difficulties of the liquid electrolyte management. The fuels commonly used in anion exchange membrane fuel cells (AEMFCs) are hydrogen and alcohols. Hydrogen is the common fuel in commercialization and research and gives the higher power densities. On the other hand, alcohols like methanol or ethanol have the advantages of easier handle, store, and transport and can be acquired from abundant biomass, which is environmentally friendly considering the process is carbon-neutral.

Among all the polymers available and tested for AEMFCs, polybenzimidazoles have demonstrated good applicability, and the most commonly used and studied are PBI and ABPBI. Some of their advantages remain in the properties previously described, as excellent thermal stability, which allows to use them at higher temperatures, superior mechanical properties that can withstand the performance conditions, and the presence of amine and imine groups which form strong hydrogen bonding interactions and can be further functionalized. The great stability properties have also encouraged many studies combining polybenzimidazoles with other polymers, creating blend or crosslinked membranes with excellent performances. Membranes based on polybenzimidazoles alone or with other polymers have also demonstrated low alcohols crossover, making them adequate electrolytes in alcohol fuel cells. In the alkaline media, the pristine form of PBI can be equilibrated in aqueous solutions of alkali metal hydroxides forming homogeneous systems with the hydroxide salt and water dissolved in the polymer matrix. These materials have shown high ion conductivity and great chemical stability at low alkali concentrations and have been tested as anion-conducting electrolytes in fuel cells with hydrogen or alcohol and in water electrolyzers. In order to understand the physical and chemical properties of polybenzimidazoles in alkaline media, Aili et al. have made a study with thin films of PBI in aqueous KOH solution with concentrations

from 0 to 50 wt.% [31]. They observed by the EDS cross-sectional maps that the dissolved KOH is evenly distributed in the electrolyte membrane. The polymer has strong water affinity through hydrogen bonding with the imidazole groups, absorbing around the water molecules per repeating unit (r.u.), and KOH forms various hydrated complexes when dissolved in water. The degree of ionization of the polymer is determined by the position of the acid-base equilibrium presented in **Figure 4**. They observed that it depends on the KOH concentration as was expected, increasing the KOH content per PBI r.u. with the higher concentration of the bulk solution, reaching 2.6 KOH molecules/r.u. at bulk concentration of 25 wt.%.

A similar trend was observed for the water molecules, reaching more than 20 H_2O molecules/r.u. at KOH concentration around 20–25 wt.% in the bulk solution. In the polymer phase, the number of water molecules per KOH decreased while increasing the bulk solution concentration, showing a concentrating effect of KOH in the polymer. They did the measurements by titration and gravimetrically, getting consistent results that corroborate previous knowledge. They also observed the anisotropic swelling behavior of the polymer at different KOH concentrations that had been previously reported and performed X-ray diffraction (XRD) measurements to explain it. The explanation they found was that the increasing of surface area and thickness up to 15 wt.% concentration was due to the uptake of water and KOH, but further increasing the concentration leads to full ionization of the polymer, breaking many of the hydrogen bonds and separating the layered structure. This separation is easier in the interlayer dimension than in the intra-layer one, causing high thickness increase and area decrease. When KOH bulk solution concentration reached 50 wt.%, sharp peaks appeared in the XRD and were attributed to a crystalline phase of a poly(potassiumbenzimidazolide) hydrate with a symmetric and highly regular structure with crystallite size in the range of 70–120 nm. These crystalline peaks were vanished after washing in water until neutral pH. They also observed that the previously described effect of the introduction of water and KOH that disturbs the polymer hydrogen bonding of imidazole groups affected the mechanical properties, causing great decay in the tensile strength and enhanced elongation at break. When full ionization of the polymer was reached, at 20–25 wt. %, more than 200% elongation at break and 0.3 GPa elastic modulus were obtained, which compared with the 80% elongation at break and 3.0 GPa in pure water, showing the great differences. The IR measurements showed clearly that the chemical environment of the benzimidazole moieties changed greatly from the

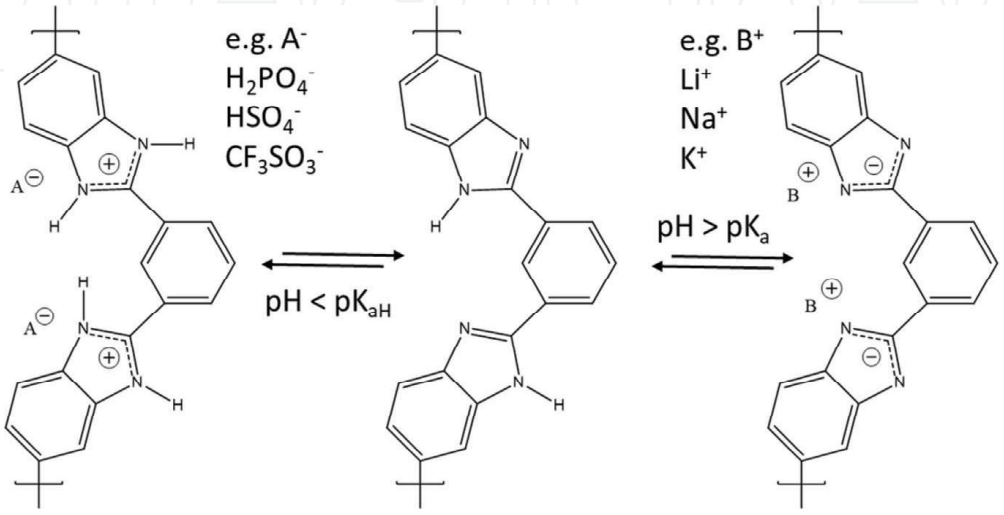

Figure 4.
Scheme showing the amphoteric nature of PBI in acidic (left) and alkaline (right) environments.

dissociation of the acidic proton. The result was that the deprotonated form of PBI predominates when the KOH concentration of the bulk solution is around 15–20%.

In order to discuss the different membranes based on polybenzimidazoles, the classification of anion exchange membranes made by Merle et al. will be useful [6]. Membranes are classified in three main groups: heterogeneous membranes, interpenetrating polymer networks, and homogeneous membranes. The heterogeneous membranes are composed by an anion exchange material embedded in an inert compound and can be divided in ion-solvating polymers if the inert compound is a salt or hybrid membranes in it is an inorganic segment. Polybenzimidazoles alone or blended with other polymers would fall into the category of ion-solvating polymers. The interpenetrating polymer network is a combination of two polymers in which one or both are synthesized or crosslinked in the presence of the other without any covalent bonds between them. The homogeneous membranes are composed only by the anion exchange material, forming a one-phase system, where the cationic charges are covalently bonded to the polymer backbone. Mobile counter ions are associated with the ionic sites to preserve the electroneutrality of the polymer. Examples of the cationic sites are the quaternary ammonium (QA) groups commonly used in AEMs. Depending on the production method and the starting materials, homogeneous membranes are divided into three types: (co) polymerization of monomers, modification into a polymer, and modification on a preformed film.

Alkali-doped PBI was investigated by Xing et al. for use in AEMFCs [51]. They obtained very interesting results, like conductivity as high as 9×10^{-2} S cm^{-1} at 25° C, higher than 2×10^{-2} S cm^{-1} of a H_2SO_4-doped PBI membrane, or the similar performance in hydrogen/oxygen fuel cells with alkali-doped PBI membrane and Nafion®117 membrane. Since that pioneering work, extensive attention has been paid to the alkali-doped PBI membranes, and thus great progress has been made. However, relevant issues are still remaining such as alkali leakage, fuel permeability, and mechanical stability. The single-cell performance of alkali-doped PBIs has been extensively studied with various fuels [52], such as hydrogen, methanol, ethanol, ethylene glycol, glycerol, formate, and borohydrides.

Using hydrogen as fuel, Zarrin et al. [53] have developed a stable and highly ion-conductive porous membrane doped with KOH. They found enhanced ionic conductivity by introducing the porosity in the membrane and obtained around twice better cell performance and conductivity compared with a commercial Fumapem® FAA membrane. Moreover, the KOH-doped PBI membrane maintained the ionic conductivity after 14 days of stability test, far more than the 3 h of the commercial one. The peak power density obtained with the porous PBI membrane of porosity 0.7 was 72 mW cm^{-2}, better than the 41 and 45 mW cm^{-2} obtained with a dense PBI membrane and the commercial FAA membrane, respectively. This better performance was demonstrated to be ascribed to the fact that the porous structure offered a higher ion transport rate through the membrane. One of the previously mentioned issues is the gradual alkali leakage during the cell operation. To solve it Zeng et al. [54] synthesized a sandwiched porous PBI membrane doped with KOH. The pore-forming method rendered numerous sponge-like walls and interconnected macropores, improving the interaction between the PBI and the doping alkali, indicating that both anionic conductivity and alkali retention could be enhanced by this method. Using this sandwiched porous PBI membrane doped with KOH in an AEMFC, they obtained an open-circuit voltage (OCV) of 1.0 V and a peak power density of 544 mW cm^{-2} at 90°C, which was higher than using the conventional membrane structure. They also investigated the durability of the fuel cell at a constant current density of 700 mW cm^{-2} and found that the conventional fuel cell had a dramatic voltage drop after short operation time, which was ascribed

to the progressive release of the alkali solution. On the other hand, the sandwiched porous membranes performed with improved stability; the voltages reduced gradually to 0.1 V and remained there for another 25 h approximately. They explained that the performance enhancement was attributed to the retarding in the release of the alkali solution from the sponge-shaped wall, maintaining the high conductivity of the membrane. However, finally the leakage occurred, but as the authors indicated, the membrane could be reused after doping with KOH solution again.

Another approach was that used by Lu et al. [55]. They used PBI to react with poly(vinylbenzyl chloride) (PVBC), a polymer commonly used by other groups as for example Varcoe et al. in their grafted PTFE membranes [56, 57]. PVBC has the advantage of reacting with the imidazole rings of PBI creating a crosslinking connection with remaining -CH_2Cl groups unreacted that can be later functionalized as desired. For the functionalization of these groups, they decided to use the diamine 1,4-diazabicyclo (2.2.2) octane (DABCO), a very stable amine in alkaline media especially when only one of the two nitrogen is quaternized as previously reported [2, 6]. This method had the advantage that quaternization is done in the already casted membrane so it can be ensured that only one of the nitrogens react with PVBC obtaining the stability desired. Thanks to the good mechanical properties of PBI, they obtained membranes with good flexibility and strength both in dry conditions and saturated in water as well as high hydroxide conductivity (>25 mS cm^{-1} at room temperature) and superior chemical stability in alkaline environment. They tested the membrane in the H_2/O_2 fuel cell obtaining a peak power density of 230 mW cm^{-2} at 50°C and performed stability test, which showed high durability both in the constant current and continuous open-circuit voltage.

In addition to being used as an anion exchange membrane, alkali-doped PBI can work as ionomer, serving as ion-conductive pathway in the catalyst layer as well as a binder. Matsumoto et al. [58] developed a well-structured electrocatalyst for AEMFCs composed of carbon nanotubes (CNT), KOH-doped PBI ionomer, and platinum nanoparticles. This allowed them to obtain highly effective diffusivity and improved electrochemical activity, and they obtained a peak power density of 256 mW cm^{-2} at 50°C when tested in a H_2/O_2 fuel cell.

For fuel cells running on methanol, Hou et al. [59] tested a direct methanol fuel cell with a KOH-doped PBI membrane and observed that when a mixed solution of 2.0 M methanol and 2.0 M KOH was used as fuel, the OCV was around 1.0 V, and the peak power density was 31 mW cm^{-2} at 90°C. Wu et al. [60] prepared a membrane of KOH-doped PBI with CNT nanocomposites and obtained maximum power densities of 67 mW cm^{-2} and 104 mW cm^{-2} at 60 and 90°C, respectively, with a fuel composition of 2.0 M methanol + 6.0 M KOH and humidified oxygen. Li et al. [61] worked with pristine PBI membrane synthesized by solution casting method and treated it separately with 2.0 M H_3PO_4 and 6.0 M KOH to prepare a PEM and an AEM, respectively. They also studied several parameters of the structure design and operating parameters. They found that the conductivity of the KOH-doped PBI membrane was higher than the phosphoric acid membrane, 21.6 and 7.9 mS cm^{-1}, respectively. They also obtained a higher peak power density with the KOH-doped PBI membrane, 117.9 mW cm^{-2} at 90°C, than with the acid one, 46.5 mW cm^{-2}. They even reached a peak power density of 158.9 mW cm^{-2} at 90°C when using free-microporous layer electrodes and tripled the fuel flow rate.

In fuel cells running on ethanol, Hou et al. [62] developed a KOH-doped PBI membrane and found that with fuel composition of 2.0 M ethanol +2.0 M KOH, they obtained OCV of 0.92 V and maximum power density of 42.9 mW cm^{-2} at 75°C and 0.97 V and 60.9 mW cm^{-2} at 90°C. Modestov et al. [63] fabricated a membrane electrode assembly (MEA) employing non-platinum electrocatalysts and a KOH-doped membrane. In the anode they used a mixed solution of 3.0 M KOH

+2.0 M ethanol as fuel, while in the cathode they used air flow. With these conditions and at temperature of 80°C, a peak power density of 100 mW cm^{-2} was obtained at a voltage of 0.4 V. It was also found that by operating the fuel cell with pure oxygen, the current density was improved by 10%. Also using ethanol as fuel, recently Herranz et al. [29] tested the fuel cell performance of membranes synthesized with PBI and poly(vinyl alcohol) (PVA) with different weight ratios. PVA alcohol groups interacted with PBI by hydrogen bonding as well as allowing enhanced conductivity of the hydroxyl anion through the membranes. The increasing content in the PVA blend membrane leads to higher conductivities but if excessive could bring structural problems since PBI demonstrated to be essential for the membrane integrity. PVA:PBI 4:1 membrane obtained the best performance with a peak power density of 76 mW cm^{-2} at 90°C, 50% higher than a pristine KOH-doped PBI tested in the same conditions.

ABPBI has also been widely investigated for AEMs synthesis and application. Luo et al. [64] synthesized ABPBI and prepared the pristine membranes by the solution casting method. They studied the conductivity of the membranes at various alkali doping levels. They found high conductivity values for the membranes as 2.3×10^{-2} S cm^{-1} at 25°C and 7.3×10^{-2} S cm^{-1} at 100°C in the ABPBI membrane with alkali doping level of 0.37. They also founded the membranes have great thermal stability and excellent chemical stability, demonstrated by maintaining the conductivity values in alkaline media at 100°C for more than 1000 h.

Other alcohols and fuels have also been tested in AEMFCs using polybenzimidazoles in the membrane structure, showing promising results [65, 66]. Overall, the applicability and interest of benzimidazoles as AEMs are actual and will continue to increase due to their excellent properties.

7. Conclusions

Polybenzimidazoles have been deeply studied in the last decades, and great advancements have been done in their synthesis, making them economical materials with excellent thermal and mechanical properties as well as high chemical resistance in acidic and alkaline media. Their special structure with imidazole moieties and high intermolecular hydrogen bonding make them excellent materials to be used and ion exchange membranes for fuel cells. They can be used alone or in combination with other polymers or compounds, like the ionic liquids, as has been demonstrated many times. With them, it is possible to reach performances similar to other fuel cells and allow the application at higher temperatures, with all the benefits that implies. In the acidic media temperatures in the range of 120–200°C are used with good performances and easier water management, but still issues like structural stability with high doping level have to be solved. In order to help with the conductivity, ionic liquids have been investigated because of their nonaqueous and low-volatility properties as proton carriers. Interesting developments have been done but further research is necessary. In the alkaline media, their application has also attracted great interest. The ionization of the structure has been clearly identified at certain doping levels and the plasticizing effects it has. Pristine polybenzimidazole membranes have been directly doped with alkali solutions obtaining very good conductivity values, and other strategies like crosslinking with other polymers or synthesis of blend membranes have reported also promising results. The fuel cell performance is not yet as good as in the acidic media, but good results around 100 mW cm^{-2} have been obtained. Commercialization of membranes and MEAs based on PBI shows the potential they have, and research continues nowadays to develop them even more and better understand

the possibilities of these wonderful materials in the fuel cell technology and the energy applications.

Acknowledgements

The authors want to acknowledge the Spanish Ministry of Economy Industry and Competitiveness (MINECO) project ENE2016-77055-C3-1-R and to Madrid Regional Research Council (CAM) project P2018/EMT-4344 (BIOTRES-CM).

Conflict of interest

The authors declare that they have no conflict of interest.

Nomenclature

PBI	Poly[2,2′-(*m*-phenylene)-5,5′-bisbenzimidazole]
ABPBI	Poly(2,5-benzimidazole)
PEMFCs	Proton exchange membrane fuel cells. Also used for general polymer electrolyte membrane fuel cells
AEMFCs	Anion exchange membrane fuel cells
IEM	Ion exchange membrane
AEMs/CEMs	Anion/cation exchange membranes
ORR	Oxygen reduction reaction
IV	Inherent viscosity
PPA	Polyphosphoric acid
MEA	Membrane electrode assembly
ILs	Ionic liquids
OCV	Open-circuit voltage
QA	Quaternary ammonium

Author details

Daniel Herranz and Pilar Ocón*
Department of Applied Physic Chemistry, University Autonomous of Madrid, Madrid, Spain

*Address all correspondence to: pilar.ocon@uam.es

References

[1] Wang Y, Chen KS, Mishler J, Cho SC, Adroher XC. A review of polymer electrolyte membrane fuel cells: Technology, applications, and needs on fundamental research. Applied Energy. 2011;**88**:981-1007. DOI: https://doi.org/10.1016/j.apenergy.2010.09.030

[2] Varcoe JR, Atanassov P, Dekel DR, Herring AM, Hickner MA, Kohl PA, et al. Anion-exchange membranes in electrochemical energy systems. Energy & Environmental Science. 2014;**7**:3135-3191. DOI: https://doi.org/10.1039/b000000x

[3] Corti HR, Gonzalez ER. Direct Alcohol Fuel Cells. Dordrecht: Springer; 2014. DOI: https://doi.org/10.1007/978-94-007-7708-8

[4] Zakaria Z, Kamarudin SK, Timmiati SN. Membranes for direct ethanol fuel cells: An overview. Applied Energy. 2016;**163**:334-342. DOI: https://doi.org/10.1016/j.apenergy.2015.10.124

[5] Smitha B, Sridhar S, Khan AA. Solid polymer electrolyte membranes for fuel cell applications—A review. Journal of Membrane Science. 2005;**259**:10-26. DOI: https://doi.org/10.1016/j.memsci.2005.01.035

[6] Merle G, Wessling M, Nijmeijer K. Anion exchange membranes for alkaline fuel cells: A review. Journal of Membrane Science. 2011;**377**:1-35. DOI: https://doi.org/10.1016/j.memsci.2011.04.043

[7] Pan ZF, An L, Zhao TS, Tang ZK. Advances and challenges in alkaline anion exchange membrane fuel cells. Progress in Energy and Combustion Science. 2018;**66**:141-175. DOI: https://doi.org/10.1016/j.pecs.2018.01.001

[8] O'Hayre RP, Cha S-W, Colella W, Prinz FB. editors. In: Fuel Cell Fundamentals. Hoboken, New Jersey: John Wiley & Sons; 2006. DOI: https://doi.org/10.1002/9781119191766

[9] Ebewele RO. Polymer Science and Technology. Vol. 74. Boca Raton, New York: CRC Press LLC; 1985. DOI: https://doi.org/10.1016/0025-5416(85)90434-3

[10] Vogel H, Marvel CS. Polybenzimidazoles, new thermally stable polymers. Journal of Polymer Science. 1961;**50**:511-539. DOI: https://doi.org/10.1002/pol.1961.1205015419

[11] Choe E. Catalysts for the preparation of Polybenzimidazoles. Journal of Applied Polymer Science. 1994;**53**:497-506. DOI: https://doi.org/10.1002/app.1994.070530504

[12] Choe EW. Single-stage melt polymerization process for the production of high molecular weight polybenzimidazole. US patent. 1982;**4**(312):976

[13] Li Q, Jensen JO, Savinell RF, Bjerrum NJ. High temperature proton exchange membranes based on polybenzimidazoles for fuel cells. Progress in Polymer Science. 2009;**34**:449-477. DOI: https://doi.org/10.1016/j.progpolymsci.2008.12.003

[14] Yang J, He R, Aili D. Synthesis of Polybenzimidazoles. High Temperature Polymer Electrolyte Membrane Fuel Cells. Switzerland: Springer; 2016. DOI: https://doi.org/10.1007/978-3-319-17082-4_7

[15] Iwakura Y, Uno K, Imai Y. Polyphenylenebenzimidazoles. Journal of Polymer Science. 1964;**2**:2605-2615. DOI: https://doi.org/10.1002/pol.1964.100020611

[16] Eaton PE, Carlson GR, Lee JT. Phosphorus pentoxide-methanesulfonic

acid. Convenient alternative to polyphosphoric acid. The Journal of Organic Chemistry. 1973;**38**:4071-4073. DOI: https://doi.org/10.1021/jo00987a028

[17] Kim H, Cho SY, An SJ, Eun YC, Kim J, Yoon H, et al. Synthesis of poly (2,5-benzimidazole) for use as a Fuel-cell membrane. Macromolecular Rapid Communications. 2004;**25**:894-897. DOI: https://doi.org/10.1002/marc.200300288

[18] Jouanneau J, Mercier R, Gonon L, Gebel G. Synthesis of sulfonated polybenzimidazoles from functionalized monomers: Preparation of ionic conducting membranes. Macromolecules. 2007;**40**:983-990. DOI: https://doi.org/10.1021/ma0614139

[19] JS W, MH L. S RF. High temperature membranes. In: W V, A L, HA G, editors. Handbook of Fuel Cells. Vol. 3. United States: John Wiley & Sons Ltd. 2003. pp. 436-446

[20] Asensio JA, Borro S, Gómez-Romero P. Polymer electrolyte fuel cells based on phosphoric acid-impregnated poly(2,5-benzimidazole) membranes. Journal of the Electrochemical Society. 2004;**151**:304-310. DOI: https://doi.org/10.1149/1.1640628

[21] Asensio JA, Borrós S, Gómez-Romero P. Proton-conducting membranes based on poly (2,5-benzimidazole) (ABPBI) and phosphoric acid prepared by direct acid casting. Journal of Membrane Science. 2004;**241**:89-93. DOI: https://doi.org/10.1016/j.memsci.2004.03.044

[22] Fishel KJ, Gulledge AL, Pingitore AT, Hoffman JP, Steckle WP, Benicewicz BC. Solution polymerization of polybenzimidazole. Journal of Polymer Science, Part A: Polymer Chemistry. 2016;**54**:1795-1802. DOI: https://doi.org/10.1002/pola.28041

[23] Litt M, Ameri R, Wang Y, Savinell R, Wainwright J. Polybenzimidazoles/phosphoric acid solid polymer electrolytes: Mechanical and electrical properties. Materials Research Society Symposium Proceedings. 1999;**548**:313-323. DOI: https://doi.org/10.1557/PROC-548-313

[24] He RH, Sun BY, Yang JS, Che QT. Synthesis of poly[2,2′-(m-phenylene)-5,5′-bibenzimidazole] and poly(2,5-benzimidazole) by microwave irradiation. Chemical Research in Chinese Universities. 2009;**25**:585-589

[25] Yang J, He R, Che Q, Gao X, Shi L. A copolymer of poly[2,2′-(m-phenylene)-5,5′-bibenzimidazole] and poly(2,5-benzimidazole) for high-temperature proton-conducting membranes. Polymer International. 2010;**59**:1695-1700. DOI: https://doi.org/10.1002/pi.2906

[26] Conti F, Willbold S, Mammi S, Korte C, Lehnert W, Stolten D. Carbon NMR investigation of the polybenzimidazole–dimethylacetamide interactions in membranes for fuel cells. New Journal of Chemistry. 2013;**37**:152. DOI: https://doi.org/10.1039/c2nj40728k

[27] Musto P, Karasz FE, MacKnight WJ. Hydrogen bonding in polybenzimidazole/polyimide systems: A Fourier-transform infra-red investigation using low-molecular-weight monofunctional probes. Polymer. 1989;**30**:1012-1021. DOI: https://doi.org/10.1016/0032-3861(89)90072-4

[28] Li Q, He R, Berg RW, Hjuler HA, Bjerrum NJ. Water uptake and acid doping of polybenzimidazoles as electrolyte membranes for fuel cells. Solid State Ionics. 2004;**168**:177-185. DOI: https://doi.org/10.1016/j.ssi.2004.02.013

[29] Herranz D, Escudero-Cid R, Montiel M, Palacio C, Fatás E, Ocón P. Poly

(vinyl alcohol) and poly (benzimidazole) blend membranes for high performance alkaline direct ethanol fuel cells. Renewable Energy. 2018;**127**:883-895. DOI: https://doi.org/10.1007/978-3-642-20487-6

[30] Asensio JA, Borrós S, Gómez-Romero P. Proton-conducting polymers based on benzimidazoles and sulfonated benzimidazoles. Journal of Polymer Science, Part A: Polymer Chemistry. 2002;**40**:3703-3710. DOI: https://doi.org/10.1002/pola.10451

[31] Aili D, Jankova K, Han J, Bjerrum NJ, Jensen JO, Li Q. Understanding ternary poly(potassium benzimidazolide)-based polymer electrolytes. Polymer. 2016;**84**:304-310. DOI: https://doi.org/10.1016/j.polymer.2016.01.011

[32] Mader J, Xiao L, Schmidt TJ, Fuel B, Ave V. Polybenzimidazole/acid complexes as high-temperature membranes. Advances in Polymer Science. 2008;**216**:63-124. DOI: https://doi.org/10.1007/12

[33] BASF Proton-Conductive Membrane. Available from: https://www.basf.com/global/en/who-we-are/organization/locations/europe/german-companies/BASF_New-Business-GmbH/our-solutions/proton-conductive-membrane.html [Accessed: February 10, 2019]

[34] PBI Products. Celazole PBI. Available from: https://pbipolymer.com/markets/membrane/ [Accessed: February 10, 2019]

[35] Danish Power Systems High Temperature PEM Fuel Cells. Available from: http://daposy.com/fuel-cells [Accessed: February 10, 2019]

[36] Wainright JS, Wang J-T, Weng D, Savinell RF, Litt M. Acid-doped Polybenzimidazoles: A new polymer electrolyte. Journal of the Electrochemical Society. 1995;**142**:L121-L123. DOI: https://doi.org/10.1149/1.2044337

[37] Weng D, Wainright JS, Landau U, Savinell RF. Electro-osmotic drag coefficient of water and methanol in polymer electrolytes at elevated temperatures. Journal of the Electrochemical Society. 1996;**143**:1260-1263. DOI: https://doi.org/10.1149/1.1836626

[38] Chandan A, Hattenberger M, El-Kharouf A, Du S, Dhir A, Self V, et al. High temperature (HT) polymer electrolyte membrane fuel cells (PEMFC)—A review. Journal of Power Sources. 2013;**231**:264-278. DOI: https://doi.org/10.1016/j.jpowsour.2012.11.126

[39] Kreuer KD, Fuchs A, Ise M, Spaeth M, Maier J. Imidazole and pyrazole-based proton conducting polymers and liquids. Electrochimica Acta. 1998;**43**:1281-1288. DOI: https://doi.org/10.1016/S0013-4686(97)10031-7

[40] Ma Y-L, Wainright JS, Litt MH, Savinell RF. Conductivity of PBI membranes for high-temperature polymer electrolyte fuel cells. Journal of the Electrochemical Society. 2004;**151**:A8-A16. DOI: https://doi.org/10.1149/1.1630037

[41] Vielstich W, Lamm A, Gasteiger HA, editors. In: Handbook of Fuel Cells: Fundamentals, Technology, Applications. United States: John Wiley & Sons, Ltd.; 2009

[42] Aili D, Allward T, Alfaro SM, Hartmann-Thompson C, Steenberg T, Hjuler HA, et al. Polybenzimidazole and sulfonated polyhedral oligosilsesquioxane composite membranes for high temperature polymer electrolyte membrane fuel cells. Electrochimica Acta. 2014;**140**:182-190. DOI: https://doi.org/10.1016/j.electacta.2014.03.047

[43] Wu J, Yuan XZ, Martin JJ, Wang H, Zhang J, Shen J, et al. A review of PEM

fuel cell durability: Degradation mechanisms and mitigation strategies. Journal of Power Sources. 2008;**184**: 104-119. DOI: https://doi.org/10.1016/j.jpowsour.2008.06.006

[44] Susan MABH, Noda A, Mitsushima S, Watanabe M. Brønsted acid–base ionic liquids and their use as new materials for anhydrous proton conductors. Chemical Communications. 2003;**3**:938-939. DOI: https://doi.org/10.1039/b300959a

[45] Ye H, Huang J, Xu JJ, Kodiweera NKAC, Jayakody JRP, Greenbaum SG. New membranes based on ionic liquids for PEM fuel cells at elevated temperatures. Journal of Power Sources. 2008;**178**:651-660. DOI: https://doi.org/10.1016/j.jpowsour.2007.07.074

[46] Schauer J, Sikora A, Plíšková M, Mališ J, Mazúr P, Paidar M, et al. Ion-conductive polymer membranes containing 1-butyl-3-methylimidazolium trifluoromethanesulfonate and 1-ethylimidazolium trifluoromethanesulfonate. Journal of Membrane Science. 2011;**367**:332-339. DOI: https://doi.org/10.1016/j.memsci.2010.11.018

[47] Wang JTW, Hsu SLC. Enhanced high-temperature polymer electrolyte membrane for fuel cells based on polybenzimidazole and ionic liquids. Electrochimica Acta. 2011;**56**:2842-2846. DOI: https://doi.org/10.1016/j.electacta.2010.12.069

[48] Che Q, He R, Yang J, Feng L, Savinell RF. Phosphoric acid doped high temperature proton exchange membranes based on sulfonated polyetheretherketone incorporated with ionic liquids. Electrochemistry Communications. 2010;**12**:647-649. DOI: https://doi.org/10.1016/j.elecom.2010.02.021

[49] Mamlouk M, Ocon P, Scott K. Preparation and characterization of polybenzimidzaole/diethylamine hydrogen sulphate for medium temperature proton exchange membrane fuel cells. Journal of Power Sources. 2014;**245**:915-926. DOI: https://doi.org/10.1016/j.jpowsour.2013.07.050

[50] Vijayakumar V, Nam SY. Recent advancements in applications of alkaline anion exchange membranes for polymer electrolyte fuel cells. Journal of Industrial and Engineering Chemistry. 2019;**70**:70-86. DOI: https://doi.org/10.1016/j.jiec.2018.10.026

[51] Xing B, Savadogo O. Hydrogen/oxygen polymer electrolyte membrane fuel cells (PEMFCs) based on alkaline-doped polybenzimidazole (PBI). Electrochemistry Communications. 2000;**2**:697-702. DOI: https://doi.org/10.1016/S1388-2481(00)00107-7

[52] Wu QX, Pan ZF, An L. Recent advances in alkali-doped polybenzimidazole membranes for fuel cell applications. Renewable and Sustainable Energy Reviews. 2018;**89**: 168-183. DOI: https://doi.org/10.1016/j.rser.2018.03.024

[53] Zarrin H, Jiang G, Lam GY-Y, Fowler M, Chen Z. High performance porous polybenzimidazole membrane for alkaline fuel cells. International Journal of Hydrogen Energy. 2014;**39**: 18405-18415. DOI: https://doi.org/10.1016/j.ijhydene.2014.08.134

[54] Zeng L, Zhao TS, An L, Zhao G, Yan XH. A high-performance sandwiched-porous polybenzimidazole membrane with enhanced alkaline retention for anion exchange membrane fuel cells. Energy & Environmental Science. 2015; **8**:2768-2774. DOI: https://doi.org/10.1039/c5ee02047f

[55] Lu W, Zhang G, Li J, Hao J, Wei F, Li W, et al. Polybenzimidazole-crosslinked poly(vinylbenzyl chloride) with quaternary 1,4-diazabicyclo (2.2.2) octane groups as high-performance anion exchange membrane for fuel cells.

Journal of Power Sources. 2015;**296**:204-214. DOI: https://doi.org/10.1016/j.jpowsour.2015.07.048

[56] Herman H, Slade RCT, Varcoe JR. The radiation-grafting of vinylbenzyl chloride onto poly (hexafluoropropylene-co-tetrafluoroethylene) films with subsequent conversion to alkaline anion-exchange membranes: Optimisation of the experimental conditions and characterisation. Journal of Membrane Science. 2003;**218**:147-163. DOI: https://doi.org/10.1016/S0376-7388(03)00167-4

[57] Poynton SD, Slade RCT, Omasta TJ, Mustain WE, Escudero-Cid R, Ocón P, et al. Preparation of radiation-grafted powders for use as anion exchange ionomers in alkaline polymer electrolyte fuel cells. Journal of Materials Chemistry A. 2014;**2**:5124-5130. DOI: https://doi.org/10.1039/c4ta00558a

[58] Matsumoto K, Fujigaya T, Yanagi H, Nakashima N. Very high performance alkali anion-exchange membrane fuel cells. Advanced Functional Materials. 2011;**21**:1089-1094. DOI: https://doi.org/10.1002/adfm.201001806

[59] Hou H, Sun G, He R, Sun B, Jin W, Liu H, et al. Alkali doped polybenzimidazole membrane for alkaline direct methanol fuel cell. International Journal of Hydrogen Energy. 2008;**33**:7172-7176. DOI: https://doi.org/10.1016/j.ijhydene.2008.09.023

[60] Wu JF, Lo CF, Li LY, Li HY, Chang CM, Liao KS, et al. Thermally stable polybenzimidazole/carbon nano-tube composites for alkaline direct methanol fuel cell applications. Journal of Power Sources. 2014;**246**:39-48. DOI: https://doi.org/10.1016/j.jpowsour.2013.05.171

[61] Li L-Y, Yu B-C, Shih C-M, Lue SJ. Polybenzimidazole membranes for direct methanol fuel cell: Acid-doped or alkali-doped? Journal of Power Sources. 2015;**287**:386-395. DOI: https://doi.org/10.1016/j.jpowsour.2015.04.018

[62] Hou H, Sun G, He R, Wu Z, Sun B. Alkali doped polybenzimidazole membrane for high performance alkaline direct ethanol fuel cell. Journal of Power Sources. 2008;**182**:95-99. DOI: https://doi.org/10.1016/j.jpowsour.2008.04.010

[63] Modestov AD, Tarasevich MR, Leykin AY, Filimonov VY. MEA for alkaline direct ethanol fuel cell with alkali doped PBI membrane and non-platinum electrodes. Journal of Power Sources. 2009;**188**:502-506. DOI: https://doi.org/10.1016/j.jpowsour.2008.11.118

[64] Luo H, Vaivars G, Agboola B, Mu S, Mathe M. Anion exchange membrane based on alkali doped poly(2,5-benzimidazole) for fuel cell. Solid State Ionics. 2012;**208**:52-55. DOI: https://doi.org/10.1016/j.ssi.2011.11.029

[65] Couto RN, Linares JJ. KOH-doped polybenzimidazole for alkaline direct glycerol fuel cells. Journal of Membrane Science. 2015;**486**:239-247. DOI: https://doi.org/10.1016/j.memsci.2015.03.031

[66] Zeng L, Zhao TS, An L, Zhao G, Yan XH. Physicochemical properties of alkaline doped polybenzimidazole membranes for anion exchange membrane fuel cells. Journal of Membrane Science. 2015;**493**:340-348. DOI: https://doi.org/10.1016/j.memsci.2015.06.013

Polybenzimidazole-crosslinked-poly(vinyl benzyl chloride) as anion exchange membrane for alkaline electrolyzers

R.E. Coppola[a], D. Herranz[b], R. Escudero-Cid[b], N. Ming[b], N.B. D'Accorso[c,d], P. Ocón[b], G.C. Abuin[a]

a. Instituto Nacional de Tecnología Industrial (INTI), Departamento de Almacenaje de Energía, Av. General Paz 5445, B1650KNA, San Martín, Buenos Aires, Argentina.

b. Departamento de Química Física Aplicada, Universidad Autónoma de Madrid, C/ Francisco Tomás y Valiente 7, 28049, Madrid, Spain.

c. Universidad de Buenos Aires, Facultad de Ciencias Exactas y Naturales, Departamento de Química Orgánica, Buenos Aires, Argentina

d. CONICET- Universidad de Buenos Aires, Centro de Investigaciones en Hidratos de Carbono (CIHIDECAR), Buenos Aires, Argentina

Corresponding author: pilar.ocon@uam.es (P.Ocón); gabuin@inti.gob.ar (G.Abuin)

Abstract:

Zero-gap liquid alkaline water electrolyzers have great potential for hydrogen production. In order to enhance their actual performance, one of the key components to investigate is the anionic exchange membrane that allows the conduction of anions between the electrodes. This paper reports the preparation and characterization of membranes composed of a polybenzimidazole, either poly (2, 5-benzimidazole) (ABPBI) or poly [2-2′-(m-phenylene)-5-5′-bibenzimidazole] (PBI), crosslinked with different ratios of poly (vinylbenzyl chloride) (PVBC), forming highly thermally stable and homogeneous films. Quaternization of these films with 1, 4-diazabicyclo (2.2.2) octane (DABCO) followed by immersion in an alkaline solution lead to the introduction of quaternary ammonium groups and hydroxide anions respectively. Adequate thermal stability is observed in the temperature range of application (below 100 ºC). Measurements of KOH and water and related swelling reflect the higher absorption capacity of ABPBI based membranes relative to PBI based ones. ABPBI-c-PVBC/OH 1:2 membranes at 50 ºC are characterized by high ionic conductivity values (48 $mS \cdot cm^{-1}$), reaching 450 $mA \cdot cm^{-2}$ at cell voltage 2 V; much better than our previous studies and the commercial porous Zirfon® diaphragm, which obtains 140 mA cm^{-2} under similar conditions. In conclusion, these membranes are promising candidates as anion exchange membranes for zero-gap alkaline water electrolyzers.